MEMBRANE PROCESSES IN ERYTHROID DEVELOPMENT AND RED CELL LIFE TIME

EDITED BY: Giampaolo Minetti, Eitan Fibach and Anna Rita Migliaccio
PUBLISHED IN: Frontiers in Physiology

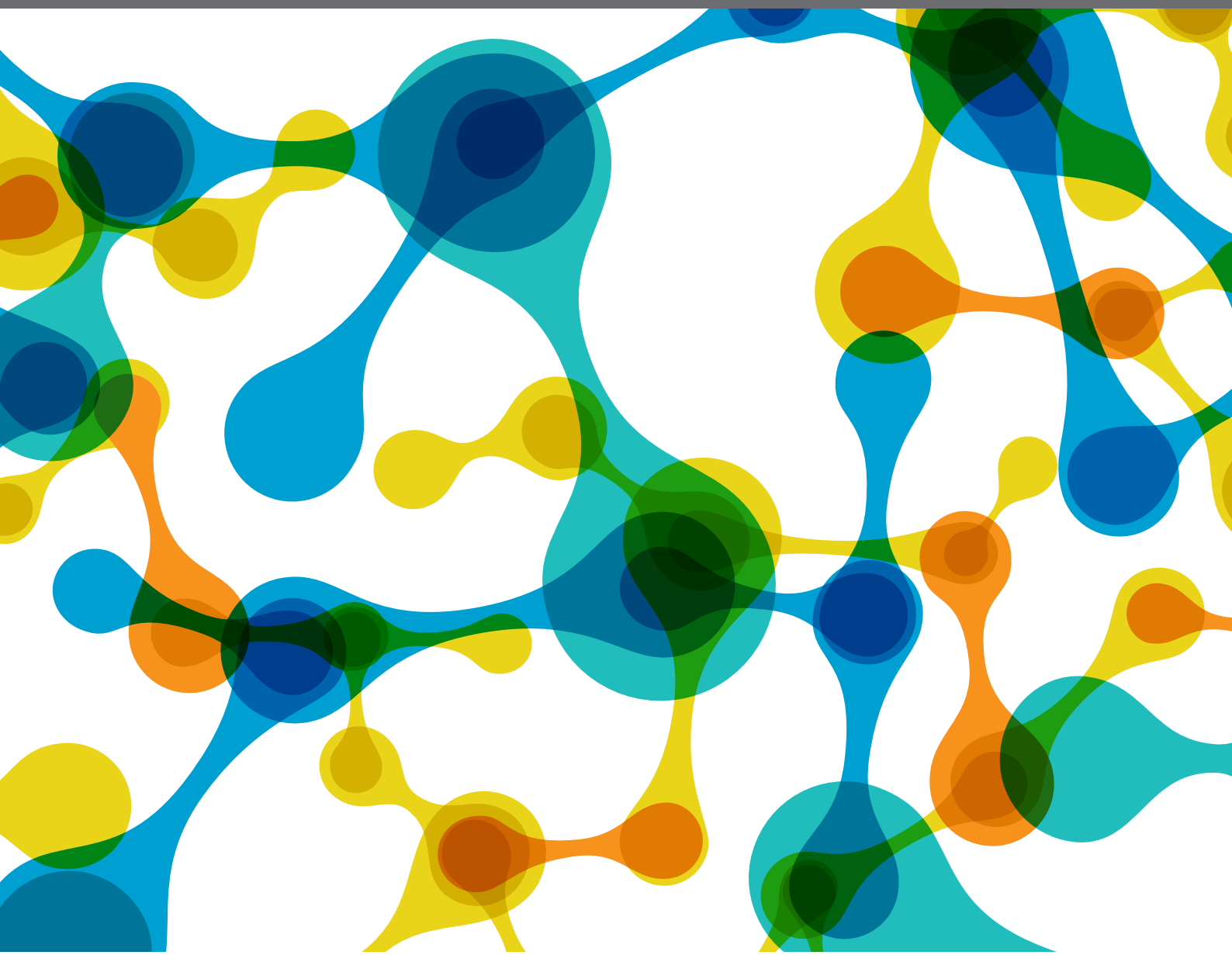

frontiers Research Topics

frontiers

ISSN 1664-8714
ISBN 978-2-88966-630-0
DOI 10.3389/978-2-88966-630-0

About Frontiers

Frontiers is more than just an open-access publisher of scholarly articles: it is a pioneering approach to the world of academia, radically improving the way scholarly research is managed. The grand vision of Frontiers is a world where all people have an equal opportunity to seek, share and generate knowledge. Frontiers provides immediate and permanent online open access to all its publications, but this alone is not enough to realize our grand goals.

Frontiers Journal Series

The Frontiers Journal Series is a multi-tier and interdisciplinary set of open-access, online journals, promising a paradigm shift from the current review, selection and dissemination processes in academic publishing. All Frontiers journals are driven by researchers for researchers; therefore, they constitute a service to the scholarly community. At the same time, the Frontiers Journal Series operates on a revolutionary invention, the tiered publishing system, initially addressing specific communities of scholars, and gradually climbing up to broader public understanding, thus serving the interests of the lay society, too.

Dedication to Quality

Each Frontiers article is a landmark of the highest quality, thanks to genuinely collaborative interactions between authors and review editors, who include some of the world's best academicians. Research must be certified by peers before entering a stream of knowledge that may eventually reach the public - and shape society; therefore, Frontiers only applies the most rigorous and unbiased reviews.
Frontiers revolutionizes research publishing by freely delivering the most outstanding research, evaluated with no bias from both the academic and social point of view. By applying the most advanced information technologies, Frontiers is catapulting scholarly publishing into a new generation.

What are Frontiers Research Topics?

Frontiers Research Topics are very popular trademarks of the Frontiers Journals Series: they are collections of at least ten articles, all centered on a particular subject. With their unique mix of varied contributions from Original Research to Review Articles, Frontiers Research Topics unify the most influential researchers, the latest key findings and historical advances in a hot research area! Find out more on how to host your own Frontiers Research Topic or contribute to one as an author by contacting the Frontiers Editorial Office: frontiersin.org/about/contact

MEMBRANE PROCESSES IN ERYTHROID DEVELOPMENT AND RED CELL LIFE TIME

Topic Editors:
Giampaolo Minetti, University of Pavia, Italy
Eitan Fibach, Hadassah Medical Center, Israel
Anna Rita Migliaccio, Icahn School of Medicine at Mount Sinai, United States

Citation: Minetti, G., Fibach, E., Migliaccio, A. R., eds. (2021). Membrane Processes in Erythroid Development and Red Cell Life Time. Lausanne: Frontiers Media SA. doi: 10.3389/978-2-88966-630-0

Table of Contents

frontiers in Physiology

EDITORIAL
published: 18 February 2021
doi: 10.3389/fphys.2021.655117

Editorial: Membrane Processes in Erythroid Development and Red Cell Life Time

Giampaolo Minetti[1]*, *Anna Rita Migliaccio*[2,3] and *Eitan Fibach*[4]

[1] Laboratories of Biochemistry, Department of Biology and Biotechnology "L. Spallanzani," University of Pavia, Pavia, Italy, [2] Biomedical and Neuromotorial Sciences, Alma Mater Studiorum University, Bologna, Italy, [3] Myeloproliferative Neoplasm Research Consortium, New York, NY, United States, [4] Department of Hematology, Hadassah Medical Center, Jerusalem, Israel

Keywords: cultured red blood cells, reticulocyte maturation, red blood cell aging, membrane rafts, exosomes, vesiculation, autophagy, cholesterol

Editorial on the Research Topic

Membrane Processes in Erythroid Development and Red Cell Life Time

Despite the intense research on erythroid development of the past years, many questions are still open concerning the red blood cell (RBC) life cycle: the maturation of the reticulocyte (retic), a process that for its complexity is now defined terminal erythroid maturation, and RBC senescence and death. Although for subject and methodology the papers included in this Research Topic are very diverse, they all represent a snap-shot of the most relevant questions of RBC physiology being addressed at the moment.

When published, in 1986, "The Reticulocyte," a book by Samuel Mitja Rapoport, represented a thorough perusal of the currently available literature and own work, set the basis for, and stimulated the systematic investigations that followed. The book was seminal, one can find there the seeds of all the important avenues that retic investigators undertook in the years to come. The idea that ATP-ubiquitin-dependent processes control the breakdown of selected retic proteins was there (Ciechanover's discovery of ubiquitin in rabbit retics dated back to only a few years earlier). So were the concepts, although still in their embryonic stage, of autophagic mechanisms for the degradation of mitochondria, and of vesicular trafficking for the selective release of plasma membrane proteins (e.g., the transferrin receptor, TfR) and lipids in the form of vesicles (now called exosomes). In the years to follow, significant advancements have been made in the understanding of erythroid and retic maturation in the marrow. Among other issues that have remained rather unexplored is the question of the relation between the maturation of retics and the aging of RBCs. The importance of this question was stressed by Rapoport in the concluding remarks of his book (Rapoport, 1986). Understanding of the mechanisms underlying retic production, release, and maturation is a key to successful production of RBCs from discarded (sometimes molecularly engineered) stem cells for transfusion purposes. The perfection of the techniques for *ex vivo* production of retics may also be useful for research, for instance to obtain retics from other mammals, such as the horse, which have no circulating retics (Kämpf et al.). This brings us to articles in this series that reveal new aspects of retic maturation in health and disease.

Retics are generated by enucleation of the orthochromatic erythroblast and go through a maturation process in which four stages have been identified: from R1 retics in the bone marrow,

Edited and reviewed by:
Guizouarn Helene,
Centre National de la Recherche Scientifique (CNRS), France

***Correspondence:**
Giampaolo Minetti
minetti@unipv.it

Specialty section:
This article was submitted to Red Blood Cell Physiology, a section of the journal Frontiers in Physiology

Received: *18 January 2021*
Accepted: *26 January 2021*
Published: *18 February 2021*

Citation:
Minetti G, Migliaccio AR and Fibach E (2021) Editorial: Membrane Processes in Erythroid Development and Red Cell Life Time. Front. Physiol. 12:655117. doi: 10.3389/fphys.2021.655117

with detectable RNA and TfR, through the circulating R2 and R3, to the most mature R4, having no TfR left in the membrane and only residual RNA inside. One of the main unsolved problems is the terminal maturation of circulating, R2 retics. Much more is known regarding the enucleation and R1 maturation since these processes are largely spontaneous and can be recapitulated *in vitro*, albeit less efficiently than *in vivo*. These highly complex events are prone to perturbation by defects in any of the intracellular processes with which they are coordinated. This is nicely illustrated by the article of Flatt et al., who used a loss-of-function approach to show how, in subjects with Southeast Asian Ovalocytosis band 3 variant, retic maturation is deranged from the very stage of enucleation on to the retic maturation, due to band 3 misfolding that impacts on the internal quality control, vesicular trafficking and autophagy mechanisms.

Terminal maturation of retics is mostly played at the plasma membrane. Evolutionary pressure has evidently selected for the progressive biogenesis and stabilization of a unique lipid bilayer-membrane skeleton complex that characterizes the mammalian biconcave discocyte. In addition to its physiological advantage, membrane stability and robustness render mature RBCs suitable for biotechnological applications and *ex vivo* manipulations that make them drug-carriers, or cellular therapeutics, as illustrated in the article by Rossi et al.

To reduce its size, the R1 retic releases significant amounts of its plasma membrane and most of the TfR as exosomes, which also appear to be enriched in membrane rafts; autophagy operates the dismantling of mitochondria and other organelles, and ATP/ubiquitin/proteasome-mediated proteolysis takes care of the removal of selected unneeded intracellular proteins. Different investigators contributing to this Research Topic conclude that membrane lipids play a key role in the proliferation and maturation process of erythroid precursors (Zingariello et al., Bernecher et al., Minetti et al.). Cultured, but also *in vivo* produced, retics suffer from membrane stability problems, possibly because of the lower deformability of a more spherical cell and a still immature connectivity between the bilayer and the membrane skeleton. Yet, from Bernecker et al.'s article, we learn that cultured retics display a severe cholesterol deficiency, which the authors directly connect with an even higher osmotic fragility displayed by these cells with respect to natural retics. In fact, the defect can be almost completely corrected by lipid supplementation during culturing, which brings the cholesterol content in the membrane to near normal levels. Conversely, cholesterol depletion, with methyl-ß-cyclodextrin, renders normal mature RBCs osmotically fragile.

Zingariello et al. also discuss in their paper the cholesterol deficiency of cultured retics and highlight the importance of lipid composition of the culture medium that, by optimizing cholesterol bioavailability, increases both the yield and the maturation of retics. This sheds light on the long-known problem that dexamethasone (a glucocorticoid receptor agonist added to culture media for sustaining the first proliferative phase of erythroid development) decreases the efficiency of enucleation *in vitro*. It was previously observed that the enucleation rate dramatically increased when cultured human erythroblasts were injected into an immune-deficient host (mouse). This suggested that dexametasone induced a defect in the composition of the membrane, in particular of the lipid moiety, which could be reverted once the cells were infused into the host, from which they evidently acquired the missing component(s). The present study (Zingariello et al.) indeed shows that supplementation of the culture medium with the proper formulation of light-density (LDL) and very-light-density (VLDL) lipoprotein, two physiological cholesterol carriers, increases the proliferation rate and prevents the autophagic death of erythroid precursors.

Yet another article from Minetti et al., reports on the profound rearrangement of membrane lipids in the maturation of circulating R2 retics. Starting from the established fact that membrane rafts are selectively lost from the membrane of maturing R1 retics (being enriched in the membrane of the released exosomes), the authors hypothesize that rafts may also be lost in the maturation of R2 retics. However, by comparing the lipid composition of pure R2 retics with that of the membrane of mature RBCs from the same donors, the authors find the exact opposite. Those lipids that are typical of membrane rafts, cholesterol and sphingolipids, are actually enriched in the membrane of mature RBCs. Protein markers of rafts behave differently depending on protein type: whereas flotillins appear to be lost by R2 retics, stomatin maintains the same levels. The conclusions that authors draw from these data are twofold. First, membrane rafts must be heterogeneous, with different raft classes bearing different protein composition. The heterogeneous nature of rafts cannot be appreciated when they are all together isolated as detergent-resistant-membrane. Second, the finding fits perfectly with the concept, first proposed by this research group, that rafts serve the purpose of additional anchoring sites for the bilayer to the membrane skeleton in mature RBCs. The association is probably mediated by a direct lipid-skeleton interaction, as no protein anchor and the corresponding anchoring site(s) in the membrane skeleton have been identified so far (band 3 and glycophorins are completely absent in membrane rafts).

Another result of this work is that band 3 and spectrin are partially lost as R2 retics mature. This is not trivial, since the exosomes with which presumably most of the excess membrane is lost by R1 retics are completely devoid of band 3, glycophorins and membrane skeletal proteins. This also shows that the two phases of retic maturation occur by two completely different mechanisms, where R1 maturation is largely spontaneous whereas R2 maturation is not; it requires the intervention of other organs (spleen, liver, endothelium). Moreover, the hypothesized continuum (Minetti et al., 2018) from retic maturation to RBC senescence that proceeds from large irregularly shaped retics to progressively smaller and yet still biconcave discocytes to the last day of RBC life, still holds, although it appears to be sustained by different mechanisms.

Concerning the latter issue, a connection can now be made between retic maturation and RBC aging. The same research group has recently observed that, contrary to what is generally

believed, i.e., that human RBCs lose membrane, as they age, in the form of spectrin-free vesicles, they may actually lose portions of lipid bilayer and membrane skeleton simultaneously (Ciana et al., 2017). If confirmed, this result would again point to non-spontaneous processes driving the changes that RBCs undergo from their R2 retic stage to the last day of RBC circulatory life. The discussion around the issue of vesiculation of RBCs *in vivo* has been boosted by the theoretical elaboration by Asaro et al. They propose that under the particular flow conditions that RBCs face when they transit from the splenic red pulp through the slits in the endothelium that lines the venous sinuses, vesicles may be released by a process of "infolding." Interestingly, the model can be tuned to predict the formation of both skeleton-free and skeleton-containing vesicles. A more refined model from the same group includes an active role possibly played by splenic endothelial cells in facilitating/inducing the release of vesicles via tethering under the peculiar splenic flow conditions (Asaro et al., 2020). Given the plethora of interactions that RBCs experience with other cell types, and that are extensively reviewed in the article by Pretini et al., this aspect cannot be excluded from theoretical models. Attempts to reproduce a mechanical splenic action to induce maturation of cultured retics to biconcave discocytes (Moura et al., 2018), have so far failed. Yet, it would be of paramount importance to experimentally test the theoretical model described above to verify whether a properly set microfluidic system could be tuned to actually produce vesicles with or without membrane-skeletal proteins. If sufficient amounts of vesicles could be produced with this method, they could be easily probed for the presence or absence of membrane skeleton proteins (e.g., spectrin). Along this line, it must be also admitted that a purely mechanical remodeling may not work on cultured retics because they are different from their native counterpart. That these retics have impaired osmotic resistance, linked to cholesterol deficiency in their membrane, has been shown only recently by the above-mentioned work of Bernecker et al. Finding better culturing conditions would be the starting point for verifying if and to what extent shear forces could be sufficient to convert cultured retics into discocytes.

As said, solving the problem of how circulating retics or mature RBCs lose membrane is important for shedding light on the properties of the senescent RBC and the mechanisms of its clearance from the circulation (Kaestner and Minetti, 2017). A strain of mice is described, which express a red fluorescent protein in the erythroid lineage, producing red fluorescent RBCs. This technique proved useful in applications such as intravital microscopy, 3D-shape analysis, and transfusion experiments, with the possibility, therefore, to study RBC aging *in vivo*. Concerning this subject, Bernhardt et al. draw attention to the two vexed issues: is there any increase in intracellular free $Ca2^{+}$ and in phosphatidylserine (PS) exposure in old RBCs? This topic is paradigmatic of situations where different results are obtained when working with RBC in bulk or with single cells, or populations of cells selected according to e.g., cell age. Moreover, intrinsic difficulties in the methods of measuring intracellular free Ca^{2+} have rendered even more difficult to reach consensus. Authors try to reconcile conflicting data from two sets of experiments aimed at correlating RBC density (age) with PS exposure. They conclude, on the one hand, that conflicting results make the increased intracellular Ca^{2+} with aging elusive. On the other hand, more consistent reports exist that allow concluding that PS exposure does not change with cell age. Thus, probably, the variation of the free intracellular Ca^{2+} concentration does not exceed 10 μM, which appears to be the threshold for scramblase activation (inducing PS exposure) and flippase inactivation (blocking the energy-dependent translocation of PS from the outer to inner membrane leaflet) (Bernhardt et al.).

As discussed throughout the Research Topic, membrane shedding, in the form of microvesicles, plays a key role in erythroid cells. Partial disturbance of the membrane-cytoskeleton linkage and increased intracellular Ca^{2+} content are considered to be mechanisms underlying the process, but it is questionable whether they constitute the primary initiating steps. In a review by Fibach, he summaries some data-based and hypothetical possibilities that await experimental confirmation regarding the interaction between membrane shedding and the redox system. The latter depends on the equilibrium between oxidants and antioxidants—excess oxidants results in oxidative stress, which affects many cellular components, including the membrane. Oxidative stress may initiate membrane shedding by indirect effect on the membrane-cytoskeleton and the Ca^{2+} content. RBCs undergo changes in both their redox system and membrane shedding throughout their life—from birth—their production in the bone marrow, to death—aging in the peripheral blood and clearance in the reticuloendothelial system, serving specific roles at each stage. Both processes are disturbed in diseases affecting RBCs, such as the hereditary and acquired hemolytic anemias (i.e., thalassemia, sickle cell anemia, and autoimmune hemolytic anemia). Antioxidants may represent an important therapeutic modality.

Together with articles collected in other topics on RBCs (Kaestner and Bogdanova, 2018), we hope that this Research Topic, focused on the membrane of retics and RBCs, will contribute to the wealth of knowledge that has accumulated over the past years in the Red Blood Cell Physiology section of Frontiers. For this, we thank all the contributors, with whom we share the same curiosity and enthusiasm in investigating this fascinating cell type.

AUTHOR CONTRIBUTIONS

GM wrote the first draft and edited the revisions. AR revised and contributed new concepts to the editorial. EF significantly edited and improved the final version.

FUNDING

Work generated within the Dipartimenti di Eccellenza programme (2018–2022) of the Italian Ministry of Education, University and Research (MIUR) Dept. of Biology and Biotechnology L. Spallanzani, University of Pavia (to GM).

REFERENCES

Asaro, R. J., Zhu, Q., and MacDonald, I. C. (2020). Tethering, evagination, and vesiculation via cell-cell interactions. *Biomech. Model. Mechanobiol.* doi: 10.1007/s10237-020-01366-9. [Epub ahead of print].

Ciana, A., Achilli, C., Gaur, A., and Minetti, G. (2017). Membrane remodelling and vesicle formation during ageing of human red blood cells. *Cell. Physiol. Biochem.* 42, 1127–1138. doi: 10.1159/000478768

Kaestner, L., and Bogdanova, A. (2018). Editorial: the red cell life-cycle from erythropoiesis to clearance. *Front. Physiol.* 9:1537. doi: 10.3389/fphys.2018.01537

Kaestner, L., and Minetti, G. (2017). The potential of erythrocytes as cellular aging models. *Cell Death Differ.* 24, 1475–1477. doi: 10.1038/cdd.2017.100

Minetti, G., Achilli, C., Perotti, C., and Ciana, A. (2018). Continuous change in membrane and membrane-skeleton organization during development from proerythroblast to senescent red blood cell. *Front. Physiol.* 9:286. doi: 10.3389/fphys.2018.00286

Moura, P. L., Hawley, B. R., Mankelow, T. J., Griffiths, R. E., Dobbe, J. G., Streekstra, G. J., et al. (2018). Non-muscle myosin II drives vesicle loss during human reticulocyte maturation. *Haematologica* 103, 1997–2007. doi: 10.3324/haematol.2018.199083

Rapoport, S. M. (1986). *The Reticulocyte*. Boca Raton, FL:CRC Press.

Conflict of Interest: The authors declare that the research was conducted in the absence of any commercial or financial relationships that could be construed as a potential conflict of interest.

frontiers in Physiology

ORIGINAL RESEARCH
published: 16 November 2018
doi: 10.3389/fphys.2018.01607

Erythrocyte Aging, Protection via Vesiculation: An Analysis Methodology via Oscillatory Flow

Robert J. Asaro[1]*, *Qiang Zhu*[1] and *Pedro Cabrales*[2]

[1] Department of Structural Engineering, University of California, San Diego, San Diego, CA, United States, [2] Biological Engineering, University of California, San Diego, La Jolla, CA, United States

We demonstrate that erythrocyte deformations, specifically of a type as occur in splenic flow (Zhu et al., 2017), and of the type that promote vesiculation can be caused by simple, yet tailored, oscillatory shear flow. We show that such oscillatory shear flow provides an ideal environment to explore a wide variety of metabolic and biochemical effects that promote erythrocyte vesiculation. Deformation details, typical of splenic flow, such as *in-folding* and implications for membrane/skeleton interaction are demonstrated and quantitatively analyzed. We introduce a theoretical, essentially analytical, vesiculation model that directly couples to our more complex numerical, multilevel, model that clearly delineates various fundamental elements, i.e., sub-processes, that are involved and mediate the vesiculation process. This analytical model highlights particulary important vesiculation precursors such as areas of membrane/skeleton disruptions that trigger the vesiculation process. We demonstrate, using flow cytometry, that the deformations we experimentally induce on cells, and numerically simulate, do not induce lethal forms of cell damage but do induce vesiculation as theoretically forecasted. This, we demonstrate, provides a direct link to cell membrane/skeletal damage such as is associated with metabolic and aging damage. An additional noteworthy feature of this approach is the avoidance of artificial devices, e.g., micro-fluidic chambers, in which deformations and their time scales are often unrepresentative of physiological processes such as splenic flow.

Keywords: vesiculation, oscillatory flow, oxidative damage, erythrocyte vesicles, self protection

OPEN ACCESS

Edited by:
Giampaolo Minetti,
University of Pavia, Italy

Reviewed by:
Thomas Podgorski,
UMR5588 Laboratoire Interdisciplinaire de Physique (LIPhy), France
Giovanna Tomaiuolo,
Università degli Studi di Napoli Federico II, Italy
Othmane Aouane,
Helmholtz Institute Erlangen-Nürnberg, Germany

***Correspondence:**
Robert J. Asaro
rasaro@san.rr.com

Specialty section:
This article was submitted to Red Blood Cell Physiology, a section of the journal Frontiers in Physiology

Received: *27 June 2018*
Accepted: *25 October 2018*
Published: *16 November 2018*

Citation:
Asaro RJ, Zhu Q and Cabrales P (2018) Erythrocyte Aging, Protection via Vesiculation: An Analysis Methodology via Oscillatory Flow. Front. Physiol. 9:1607. doi: 10.3389/fphys.2018.01607

1. INTRODUCTION AND BACKGROUND

Without a nucleus, a mature erythrocyte (or RBC) contains a cytosol enclosed within a highly flexible cell membrane. This composite membrane, consisting of a lipid bilayer supported by a membrane skeleton, is essential to its structural integrity and stability. The basic picture is that of a skeleton created from junctional complexes (JCs) bound to each other via head-to-head associations of spectrin (Sp), which is anchored to the fluidic lipid bilayer at linkage sites (Mohandas and Evans, 1994; Mohandas and Gallager, 2008; Lux, 2015). RBCs possess one of the best characterized molecular architectures among all cell types and are thus often chosen as a model system to study various functions of cells, especially those that involve mechanical behavior and response. A particularly intriguing process that erythrocytes exhibit is vesiculation, during which part of the phospholipid bilayer separates from the skeleton and the rest of the membrane to create a vesicle (Peng et al., 2010; Zhu et al., 2017). The occurrence of vesiculation depends

on the magnitude of the skeleton-bilayer dissociation stress—that develops during deformation - as well as the strength of the skeleton-bilayer connectivity—which may be compromised during the aging process as discussed below. To date there is incomplete knowledge about the detailed process or physiological significance of vesiculation although evidence has mounted as to its role in erythrocyte aging (Fox et al., 1991; Schwarz-Ben Meir et al., 1991; Glaser et al., 1994; Willekens et al., 2003b; Hattangadi and Lodish, 2007; Bosman et al., 2012; Zhu et al., 2017). Herein we present a novel methodology for a coupled experimental-theoretical study of human erythrocyte vesiculation.

Our recent studies have demonstrated the strong prospects for human erythrocyte vesiculation during flow through the spleen (Zhu et al., 2017). Our numerical simulations, along with our underlying analysis of skeleton-membrane interactions provided vital insight into the coupling of the RBC aging process with metabolic processes that occur during the aging process. These aging processes include, among others, denaturing of hemoglobin, including such occurring via oxidative damage, and binding of denatured Hb to the skeleton-membrane attachment sites causing disruption of the skeleton-membrane attachment (Willekens et al., 2003a,b; Bosman et al., 2012). Erythrocyte aging, involving vesiculation, in turn involves processes such as oxidative stress (ROS) and other reactive stresses such as involves, *inter alia*, nitrates (NOS), phenyldrazine, Ca^{2+} uptake, or Cd. **Figure 1** illustrates examples of various key steps of oxidative stress and damage via ROS (Low et al., 1985; Fox et al., 1991; Nagababu and Rifkind, 2000; Cao et al., 2009; Rifkind and Nagababu, 2013; Mohanty et al., 2014). Such effects can be readily explored via our developed methodology as they contribute to vesiculation (Willekens et al., 2003a; Cao et al., 2009; Rifkind and Nagababu, 2013; Mohanty et al., 2014; Zhu et al., 2017).

In the context of splenic flow, our simulations led to a description of what is most likely required to induce vesiculation during splenic flow and provided a paradigm that, in fact, supported the view that erythrocyte vesiculation, including vesiculation during splenic flow, may be a *self-protective* mechanism (Willekens et al., 2003b; Bosman et al., 2012; Zhu et al., 2017). In this context, self-protection involves the elimination of *removal molecules* such as denatured Hb as well as phosphatidylserine (PS) and IgG that are known to be associated with cell removal (Willekens et al., 2003b; Bevers and Williamsonl, 2010; Wieschhaus et al., 2012; Kostova et al., 2015; Bevers and Williamson, 2016; Bevers et al., 2017). Our results, in addition, revealed that as vesiculation occurs, presumably in younger deformable cells, and hemoglobin concentration increases and membrane area decreases, the prospects for vesiculation decreases; hence the self-protective mechanism may be effectively shut off with aging. This is closely linked with a loss in cell deformability that is often related to a loss in cell viability. In addition, our methods should be expected to shed new light on the effects of oxidative damage, caused by reactive oxidative species (ROS), on the vesiculation process (Hattangadi and Lodish, 2007; Marinkovic et al., 2007). Thus, the continued study of the vesiculation process is warranted as it appears so closely tied to cell aging, to cell viability, and cell death. Particularly important is to directly link vesiculation to the vital factors of aging, such as those associated with oxidative damage and a methodology to confirm the various hypotheses of the mechanisms involved.

1.1. Background on Extracellular Vesicles: viz. Microvesicles (MV's)

The extracellular space of multicellular organisms contains a variety of species including, *inter alia*, metabolites, ions, proteins, polysaccharides, *etc*. and also a large number of mobile membrane bound vesicles that have been collectively referred to as *extracellular vesicles* (EV's) (Morel et al., 2010; György et al., 2011; Raposo and Stoorvogel, 2012). There are ongoing attempts at classification of EV's where distinctions are based on, for example, size, constituency, and mechanisms of formation (Morel et al., 2010; György et al., 2011; Raposo and Stoorvogel, 2012; Alaarg et al., 2013). For example, *exosomes* are generally placed in a size range with diameters <100 nm whereas *microvesicles* (MV's) are generally placed in the diameter range of 100-1,000 nm. Moreover, exosomes are generally created intracellularly and excreted, whereas MV's are formed through budding from the bilipid membrane. Exceptions, however, may exist as we note, for example, the report by Booth et al. (2006) of exosomes being in the size range 50-100 nm budding from T cells. Herein we focus on what we call (following e.g., Morel et al., 2010; György et al., 2011; Raposo and Stoorvogel, 2012; Alaarg et al., 2013), MV's budded from erythrocyte membranes, and generally expected to be in the size range 100–250 nm. Our analysis, however, does not preclude budded vesicles in a size range <100 nm, yet probably not smaller than 40-50nm as discussed below.

MV formation is associated with structural alterations of the bilipid membrane and a host of factors that disrupt erythrocyte skeleton-membrane attachment (Lutz et al., 1977; Willekens et al., 2003a,b; Morel et al., 2010; György et al., 2011; Bosman et al., 2012; Raposo and Stoorvogel, 2012; Alaarg et al., 2013). This we specifically address herein. Causes of disruption include, *inter alia*, various forms of oxidative damage associated with aging (Willekens et al., 2003a,b; Hattangadi and Lodish, 2007; Bosman et al., 2012), nitrite induced stress, i.e., NOS (Nagababu and Rifkind, 2000; Cao et al., 2009; Rifkind and Nagababu, 2013), excess Ca^{2+} uptake (Allan and Mitchell, 1977; Dodson et al., 1987; Pasquet et al., 1996; Bratosin et al., 2001; Chunyi et al., 2001; Klarl et al., 2006), and ATP depletion (Lutz et al., 1977). Association of increased MV production with diseases such as hemolytic anemias has been reported and discussed (Alaarg et al., 2013). Moreover, although we demonstrate that imposed deformation on cells, such as occurs e.g., in splenic flow, can indeed promote vesiculation the known phenomenology shows that intense imposed deformations are not required for budded vesicles to form. Indeed, Fox et al. (1990, 1991) have shown that disruption of the actin based JC of the skeleton promotes microvesiculation without imposed shear deformation. In addition, Schwarz-Ben Meir et al. (1991) and Glaser et al. (1994) have shown that calpain (Ca^{2+}-dependent thiol protease) binds to, and degrades, band 3 that is a major erythrocyte membrane attachment protein for the skeleton; this

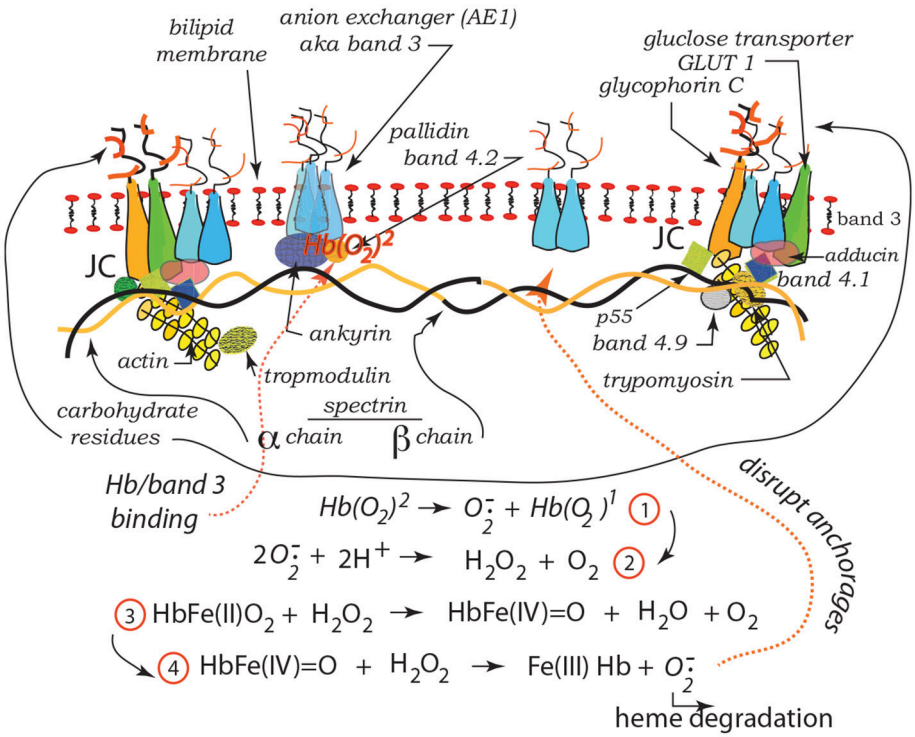

FIGURE 1 | Hb binding to band 3. ROS reactions leading with Hb to degraded heme and binding and disruption of band 3 skeleton anchorage (Low et al., 1985; Nagababu and Rifkind, 2000; Cao et al., 2009; Rifkind and Nagababu, 2013; Mohanty et al., 2014). The JC complex is described in section 2 in detail.

leads to membrane loss via vesiculation. These two studies were particularly concerned with aging, not just of the red blood cell, but of people over 70 years of age in whom the effects were accelerated. Still again, Kostova et al. (2015) have recently discussed how the Ca^{2+} ionophore ionomycin provides an effective pathway, due to membrane disruption, to vesiculation. Wieschhaus et al. (2012) report of the effects of increased Ca^{2+} uptake in degrading attachment proteins such as band 3, 4.1, and ankyrin in the presence of calpain-1 and consequently reducing cell deformability. These, among other observations, provide a basis for our model of budding that begins with localized, i.e., small 20–40 nm, sections of the membrane whose attachments to the skeleton have been disrupted. *Specifically, we study herein how vesiculation can be explored using a remarkably simple imposed oscillatory shear flow that allows for readily tailored modes and intensities of deformation.*

Finally, we note that microvesicles budded from erythrocytes are typically characterized by exposure of PS on their outer bilayer leaflet (Dasgupta et al., 2009; Bevers and Williamsonl, 2010; Bevers and Williamson, 2016; Bevers et al., 2017). Hence translocation of PS from the inner-to-outer leaflets may be viewed as a part of the vesiculation process or, in fact, a contributor to vesiculation. Two possible pathways for a PS translocation role are: (i) it induces a shape change involving initial curvature of the membrane out from the skeleton (Sheetz and Singer, 1974), and/or (ii) that it acts as an energy source as does skeletal deformation (Sheetz and Singer, 1974; Bevers and Williamson, 2016). Lipid asymmetry represents stored free energy, given the work required to create it against a steep concentration gradient, that can be made available to induce deformation and aid the vesiculation process as described below in section 4.2. Also as we show in section 4.3, pre-curvature provides a "boost" in the membranes bulging process by which a vesicle forms. This view is supported by Bevers et al. (2017), who demonstrated that in RBCs affected by Scott's syndrome microvesiculation was diminished in frequency (see also Lhermusier et al., 2011). Dasgupta et al. (2009) studied microvesiculation in mice treated with lactadherin and showed a lactadherin deficiency led to increased numbers of microvesicles at steady state.

1.2. Background on Recent Theoretical Innovations

Our simulations (Zhu et al., 2017) of erythrocyte flow through simulated venous-like slits of the spleen were performed with a hierarchical model that followed the cell's deformation process in detail. Noteworthy is that this model considers the cell membrane and skeleton separately and explicitly accounts for the lateral mobility of the skeleton's attachment trans-membrane proteins through the membrane. Hence during deformation, the areal density of skeletal attachments may change, viz. decrease due to large areal deformation of the skeleton, and thereby weaken the overall skeleton-membrane attachment as described in detail elsewhere (Peng et al., 2010; Zhu et al., 2017). However,

as the trans-membrane attachment proteins have finite (but documented) mobility, the process of changing skeletal density has its own time scale that operates within the deformation's time scale; this too was predicted (see Zhu et al., 2017 and its discussion of the results of Peng et al., 2010, 2011; Peng and Zhu, 2013). Now, in this we find that deformation processes in splenic flow, such as what we have dubbed *in-folding*, produce a "tension" (dubbed *negative pressure* in Zhu et al., 2017) between the skeleton and membrane that can promote separation that leads to vesiculation (Zhu et al., 2017). However, a key feature of this is that the time scales of splenic flow are such that large changes (decreases) in the areal density of attachment points are unlikely (Zhu et al., 2017). Hence the vital role of attachment disruption via, e.g., binding of denatured Hb, is required. *That is, since areal density reduction of attachments does not occur in time during splenic flow deformation restructuring, it must occur by metabolically induced disruption of anchorage points.*

Our simulations were quite detailed as to what was required with respect to such disruptions to cause separation. But to study vesiculation by inducing erythrocyte flow through artificial slits (as can be made by pores or slits in commercial filters can be) however, problematic. For example, flow through artificial slits in the splenic range of 1 μm generally leads to cell damage and fragmentation under very different time scales. This brings us to the following novel discovery, prospect and proposal.

We have found, that under certain ranges of frequency and shear amplitudes, simple oscillatory shear flow causes cell deformations whose characteristics (e.g., magnitude of shear deformation and even in-folding) and time scales are comparable to those in splenic flow, and thereby may induce vesiculation. This provides the prospect of following vesiculation without the use of artificial slits or resorting to deformation methods such as micro-pipette aspiration — that, as it happens, we have already shown can cause vesiculation but whose time scales are quite unlike those of splenic flow. Hence we have discovered the prospect of studying vesiculation in an open environment, devoid of artificial structure, e.g., the slits or pores of man-made filters, in which control of chemistry is readily achievable. This is now illustrated by way of past and new results specific to our modeling in sections 3 and 4.

2. OVERVIEW OF THE SIMULATION MODEL AND RESULTS

One of the most severe physiological deformations a RBC sustains occurs inside the spleen, where it "squeezes" through slits as narrow as 0.6 micron (Chen and Weiss, 1973; Mebius and Kraal, 2005; Lux, 2015; Zhu et al., 2017). Under this extreme condition the cell undergoes dramatic shear variations, including a novel deformation mode called *infolding* discovered in recent computational studies (Freund, 2013; Salehyar and Zhu, 2016; Zhu et al., 2017). The mechanical loads on the cell membrane include the external loads (traction and normal stress) from the external/internal fluids, and the internal stresses within the membrane itself. Hereby the internal stresses are categorized into two parts, *viz.* in-plane and out-of-plane. The in-plane stresses contain an isotropic component, a shear component, and friction between the skeleton and the bilayer. The out-of-plane stress is the normal interaction stress between the skeleton and the bilayer that either pulls them together (association) or pushes them apart (dissociation). No prestress in the skeleton is considered so that the stress-free state of the cell coincides with its natural biconcave state. The membrane thus possesses shape memory.

The model we use is based on a multiscale multi-physics framework as described in detail elsewhere (Zhu et al., 2007, 2017; Zhu and Asaro, 2008; Peng et al., 2010, 2011; Peng and Zhu, 2013). As illustrated in **Figure 2**, this approach includes three models at different scales: in the complete cell level (Level III) the membrane is modeled as two layers of continuum shells using the finite element method; the constitutive properties of the inner layer (the membrane skeleton) are obtained from a 3D molecular-detailed JC model (Level II); the mechanical properties of Sp, including its folding/unfolding reactions (Bustamante et al., 1994; Lee and Discher, 2001; Zhu and Asaro, 2008), are obtained with a stress-strain model based on Arrhenius equation (Level I). The fluid-cell interaction is mathematically formulated within a low-Reynolds number Stokes/Oseen flow framework and solved using a boundary-element method (for details see **Appendix**).

As demonstrated in **Figure 3A** (Salehyar and Zhu, 2016; Zhu et al., 2017), under certain conditions right after the cell passes through the slit a part of its membrane bends inward to form a concave region on its rear surface. Our model also illustrates that due to the increased surface curvature and skeletal energy density, infolding usually coincides with significantly increased dissociation stress between the skeleton and the lipid bilayer. The values of stress we found are orders of magnitude higher than those in normal conditions such as in a steady shear flow field (Zhu et al., 2017).

Further examination shows that in addition to splenic flow, infolding may happen in other scenarios, e.g., in an oscillatory shear flow field. As shown in **Figure 3B**, when a RBC is put in a shear flow field with sinusoidally varying

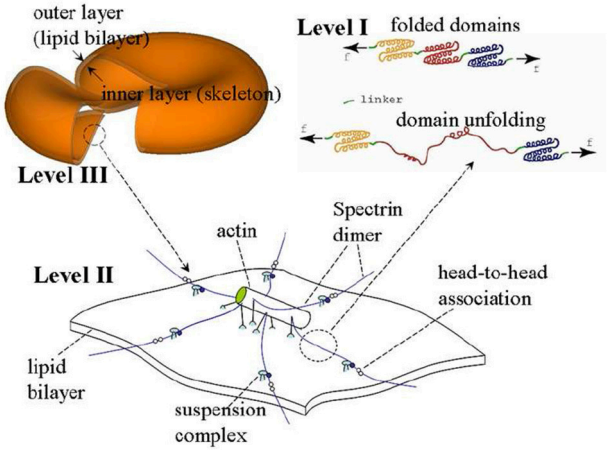

FIGURE 2 | A sketch of the multiscale RBC model.

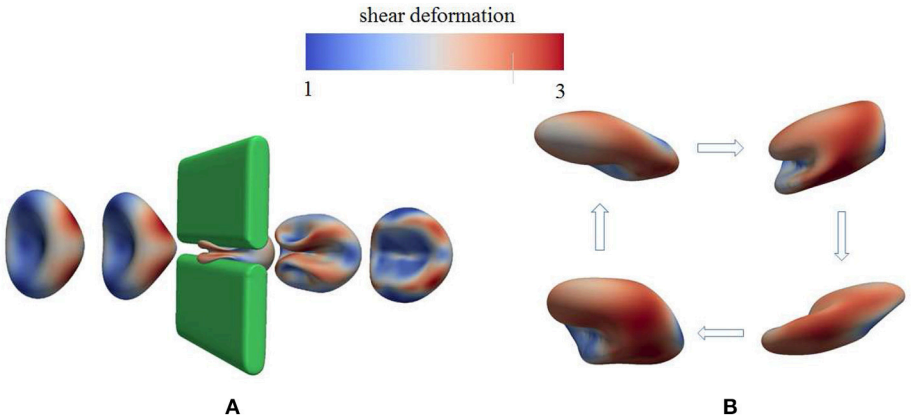

FIGURE 3 | Occurrence of membrane infolding in **(A)** splenic flow (Salehyar and Zhu, 2016) and **(B)** oscillatory shear flow. In **(B)** the cytosolic/medium viscosity ratio was 1; the average shear stress applied to the cell was in the range $\bar{\tau} \sim 6Pa$. The peak shear rate is 1,000 s^{-1}, and the frequency is 67 Hz. In both figures the color contour corresponds to shear deformation χ (see section 3.2 for the definition of χ) of the skeleton with the value ranging from 1 (in blue) to 3 (in red). $\chi = \lambda_1/\lambda_2$ with $\lambda_i, i = 1, 2$ being the principal skeletal stretches (see section 3.2).

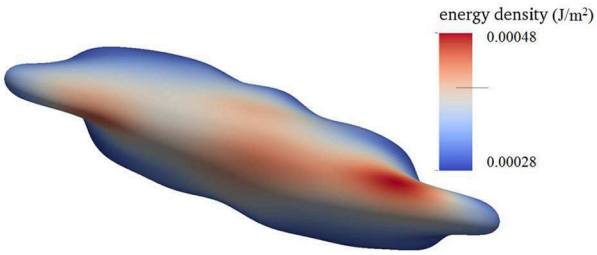

FIGURE 4 | Contours of skeleton energy density, χ, in an oscillatory shear flow field. The shear rate was σ =2,000s^{-1} at a frequency of 100 Hz. The cytosolic/medium viscosity ratio was equal to 1; the average shear stress applied to the cell was in the range $\bar{\tau} \sim 12Pa$. Areas in red color are judged to be those with a high probability for vesiculation (see section 4.4).

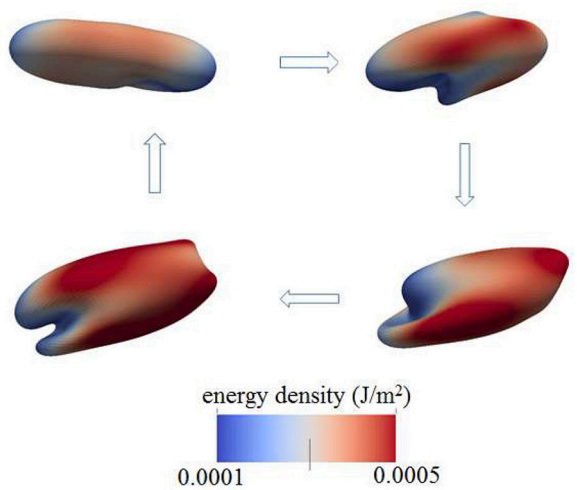

FIGURE 5 | Contours of skeleton energy density, χ, in an oscillatory shear flow field. The shear rate was $\sigma = 5{,}000s^{-1}$ at a frequency of 67 Hz. The cytosolic/medium viscosity ratio is 5; the average shear stress applied to the cell was in the range $\bar{\tau} \sim 6Pa$. The energy densities range from about 1×10^{-4}Jm^{-2} (blue) – 5×10^{-4}Jm^{-2} (red).

shear strength and direction, it undergoes similar infolding behavior, resulting in increased skeleton-bilayer dissociation stress inside the membrane. Indeed, our simulations suggest that within the range of parameters achievable in laboratory conditions, this dissociation stress in oscillatory shear flows attains levels comparable to splenic flow and may thus contribute to vesiculation (see also **Figure 7**). Meanwhile, the deformations of the cell remain moderate so that the risk of cell bursting is minimal.

2.1. Examples of Oscillatory Flow

Figure 4 shows a snapshot of the deformed cell subject to a shear flow field characterized by frequency 100 Hz with a shear rate $\sigma = 2{,}000s^{-1}$. The contours shown are for skeleton deformation energy density as so labeled with the insert. We note that in this case the maximum skeleton energy density is nearly 5×10^{-4}Jm^{-2} and is located on **Figure 10** as point "a"; this is used in later discussion of vesiculation in section 4.4.

Still another case is shown is shown in **Figure 5** where in this case the shearing rate is well above physiological rates and is set at $\sigma = 5{,}000s^{-1}$; the frequency of flow was 67 Hz. This case differs from those also shown, i.e., in **Figures 3**, **4**, **6** in that a higher viscosity is prescribed for the cell interior. In this case, the contours are of skeleton shear deformation and like those for **Figures 3**, **6** the area deformations are just above unity. That means that the maximum skeletal energy density is near to point "b," close to point "a," of **Figure 10**.

2.2. Additional Perspective on Oscillatory Shear Flow

We believe this ability to tailor deformation via oscillatory flow presents a novel methodology for probing the metabolic effects

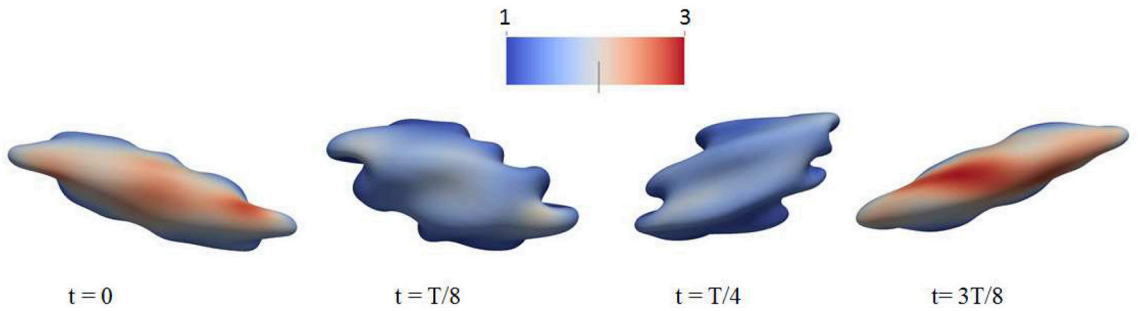

FIGURE 6 | Deformation of a red blood cell in a strong high-frequency oscillatory shear flow field. The amplitude of the shear flow is 2,000 s^{-1} and the frequency is 100 Hz. The cytosolic/medium viscosity ratio was equal to 1; the average shear stress applied to the cell was in the range $\bar{\tau} \sim 12Pa$. The color contour shows the shear deformation χ of the skeleton. Areas in red color are judged to be those with a high probability for vesiculation (see section 4.4). $\chi = 1$ (blue) to 3 (red).

of membrane/skeleton degradation that defines aging. For this reason we have run additional simulations to investigate the response of red blood cells to strong oscillatory shear flows. This has uncovered additional interesting phenomena. For example, in **Figure 6** we plot the deformation of a cell to a sinusoidally varying shear flow of 100 Hz and peak shear rate of 2,000 s^{-1}. It is seen that the cell undergoes complicated deformations with multiple infolded regions on its membrane. These regions are characterized by large curvature as well as significant dissociation stress between the cytoskeleton and the lipid bilayer. Indeed, our simulations indicate that in cases like these the dissociation stress reaches levels of $\mathcal{O}(100)$Pa, comparable to the level that can be reached as the cell passes through inter-endothelial slits in a spleen (Zhu et al., 2017). This provides evidence that, in terms of skeleton-bilayer dissociation, an oscillatory flow field is able to create conditions similar to the physiological conditions of splenic flow.

Furthermore, we carefully monitored maximal areal deformations of the lipid bilayer during these processes and note that even under extreme conditions, such as the case of **Figure 6**, they were only $\sim 1 - 2\%$; this is significantly smaller than the approximate areal strain of 10% a cell can sustain under dynamic (i.e., impact) conditions (Li et al., 2013). It is also at, or below, the somewhat lower values in the range 2–3% found under different deformation conditions (Leverett et al., 1972; Sandza et al., 1974; Sutera and Mehrjardi, 1975; Evans et al., 1976; Sutera et al., 1977; Daily et al., 1984; Watanabe et al., 2006; Wantanbe et al., 2007; Meram et al., 2013; Hashimoto, 2014; McNamee et al., 2016; Horobib et al., 2017). We thus conclude that pressure-induced cell bursting due to large area deformation of the bilayer is not likely to occur in these conditions as discussed further in section 4.5 along with additional detail and perspective.

2.3. Vesiculation Forecasts With Oscillatory Flow

Based on the analysis of our next section, based in turn on our simulation results of cell deformations presented in this section, we suggest that areas shaded in red and zones of infolding as shown, for example, in **Figure 7** are most probable vesiculation sites. The areas in red generally experience skeletal

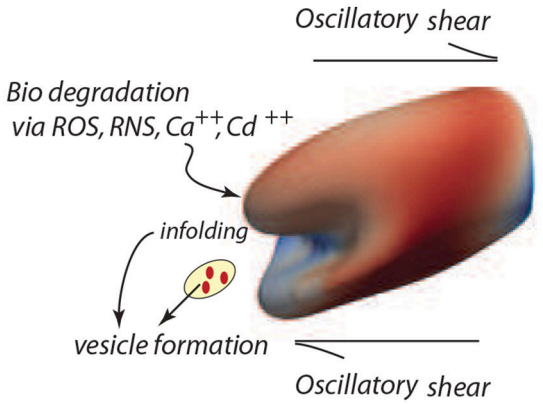

FIGURE 7 | Degradation of the cell's membrane/skeleton attachment structure induces vesiculation under the deformations of oscillatory shear flow as in the case of **Figure 3B** (upper right frame).

energy densities in the range $\epsilon_0 \sim 3 - 5 \times 10^{-4}\text{Jm}^{-2}$ and shear stresses in the range $\bar{\tau} \sim 5 - 10$Pa that as discussed in sections 3, 4.4, and 4.5 promote vesiculation.

3. PROSPECTS FOR VESICULATION

The model developed herein focuses on the mechanisms of vesiculation as a natural, essential, mechanistic component of the erythrocyte aging process. However, in a more general context the focus is on cellular aging *per se*, and on the role of oxidative stress and other biochemical stress on aging (Iuchi et al., 2007; Pandey and Rizvi, 2010, 2011; Mohanty et al., 2014). Such aging effects are manifest in at least two ways, viz. a weakening of the skeletal/bilayer connection as measured by γ and in the size of the initial skeletal/bilayer separation. The particular contribution here is that we provide a detailed, quite specific, yet quite simple, mechanistic pathway by which erythrocyte aging occurs and by which erythrocytes are removed. This process involves a general metabolic aging via ROS and other biochemical activity and in this way its analysis provides still another clue as to the

effects of biochemical activity on the aging process (Dröge, 2002; Rattan, 2006; Harman, 2009; Tsuda, 2010). Our unique approach follows vesiculation as promoted by biochemical aging and the imposition of splenic-like deformations using our novel tool of oscillatory shear flow as illustrated in **Figure 7**.

3.1. Vesiculation Model

Imagine that initially a quite localized circular patch of membrane, of radius ℓ_0, separates from the skeleton, as in the bottom most figure, **Figure 8Ai**. We can imagine that this occurs due to the binding of Hb (Willekens et al., 2003a,b; Bosman et al., 2012), or by oxidative damage (Rifkind and Nagababu, 2013; Mohanty et al., 2014), or other forms of biochemically induced damage (Allan and Mitchell, 1977; Low et al., 1985; Nagababu and Rifkind, 2000; Cao et al., 2009), as noted above. This induces a bulging out and some curvature - also note that if there is a negative (i.e., separating) pressure this will also contribute to an initial curvature as sketched in the next upward figure - call this curvature $\mathcal{C}_0$ as indicated in **Figure 8Aii**. We address this in more detail below.

The initial bleb, or "blister," may propagate due to (i) a negative pressure induced by membrane/skeleton deformation as appears in our simulations (Zhu et al., 2017), (ii) additional binding of Hb or translocation of anionic lipids such as PS (Sheetz and Singer, 1974) leading to additional curvature caused fueled by biochemical energy, and (iii) the release of skeletal energy attached to the membrane following more intense skeletal deformation. Later we suggest a potentially important contribution arising from stored chemical energy associated with the asymmetry in lipid composition between the leaflets of the bilayer. Let us define ϵ_0 as the elastic energy stored in the skeleton per unit area - this energy is released as the membrane separation spreads. This energy indeed depends on the deformation state as discussed in section 3.2. In a simple sense, the skeleton exerts a kind of "pinching action" on the membrane causing membrane/skeleton separation. The effect of skeletal deformation has been considered in several studies, e.g., those concerned with erythrocyte shape (Waugh, 1996; Lim et al., 2002; Mukhopadhyay et al., 2002) and vesiculation (Li and Lykotrafitis, 2015). In these citepd studies of minimum energy erythrocyte shapes (Lim et al., 2002; Mukhopadhyay et al., 2002) the same skeletal deformation that we consider here actually acts to inhibit budding, in their case to form echinocytes. In these studies skeletal energy was not estimated as we do by simulating actual cell deformations. This view is entirely consistent with ours, except that here we explicitly account for release of skeletal energy as membrane/skeleton separation occurs.

Note the geometric factors $\ell(t)$ and $h(t)$, where ℓ is the current radius of the membrane separation and h is the height of the bulging membrane; here t may be viewed as a "time like parameter" marking the progression of the process (see **Figure 8Aii**). Vesiculation occurs soon after $h \to \ell$ as discussed below. Note also, that there is the "work of adhesion" that must be done to de-bond the area of the membrane still attached to the skeleton; this called γ (per unit area); this has been discussed at length in the context of splenic vesiculation (Zhu et al., 2017). It is important to note that the membrane considered in **Figure 8A** is not open, i.e., finite, but is considered part of the overall cell's closed membrane. As budding occurs, additional membrane is drawn in as the vesicle's membrane area increases; this process requires the additional work of membrane/skeleton separation, γ, described below.

Now, for perspective, note that the bending energy of a spherical vesicle is simply $8\pi\kappa_b$, independent of its radius; κ_b is the membrane's bending modulus. On the other hand, the elastic energy stored in a circular membrane/skeleton patch of radius ℓ is

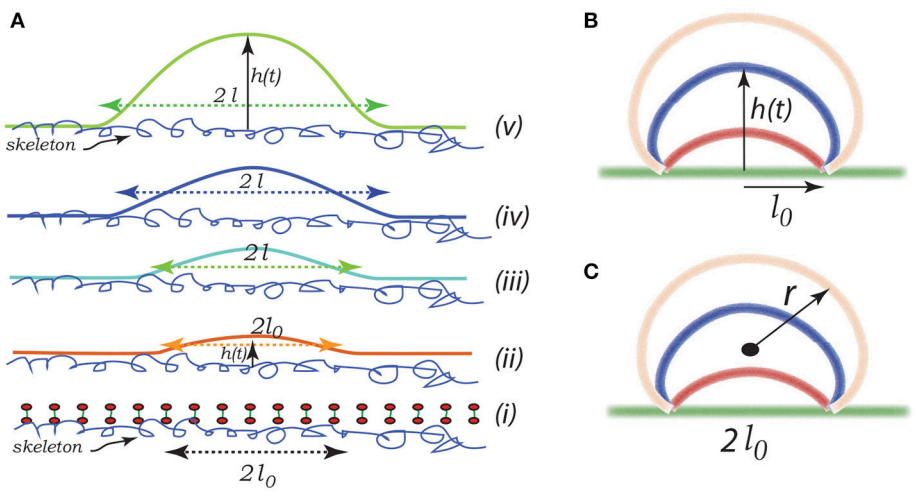

FIGURE 8 | Schematic of a budding vesicle. In **(Aii)** we illustrate a pre-curvature as discussed in the text. From **(Aiii** to **Av)** we have progressing membrane bulging leading to vesiculation. **(B,C)** depict a model expansion analyzed below. Vesiculation begins within a damaged membrane/skeleton area of diameter $2\ell_0$. Driven by release of stored skeletal energy a bulge forms and possibly grows as in **(B,C)** where the energy pathway is given in **Figure 11**. The final stage of pinching-off and vesicle release in illustrated in **Figure 12**.

$\pi \ell^2 \epsilon_0$. This would seem to set a lower limit to the size of a vesicle that may form, i.e., we need

$$\pi \ell^2 \epsilon_0 \geq 8\pi \kappa_b \;\; \rightsquigarrow \;\; \ell_{crit} \geq 2\sqrt{2}\{\frac{\kappa_b}{\epsilon_0}\}^{1/2}. \tag{1}$$

We next discuss the skeletal energy, i.e., ϵ_0, and then the debonding energy γ.

3.2. Skeleton Stored Energy

As shown in **Figure 9**, we consider a single JC consisting of six spectrin dimers (Sp), numbered 1 to 6. In its undeformed state the length of each Sp is Ł$_0$ so that the area covered by this hexagon is $A_0 = \frac{3\sqrt{3}}{2} L_0^2$. We now consider a case in which the JC is stretched in x direction by a factor of λ_1 and in y direction by a factor of λ_2 ($\lambda_1 \geq \lambda_2$), the corresponding area deformation is $\psi = \lambda_1 \lambda_2$ and the shear deformation is $\chi = \lambda_1/\lambda_2$. In the deformed state the lengths of the Sp become L_i ($i = 1, \cdots, 6$).

Invoking the Worm Like Chain (WLC) model (Weiner, 1983; Zhu et al., 2007) the strain energy stored in the i-th Sp is Zhu et al. (2007)

$$\phi_i = \frac{k_B T}{p} \left(\frac{3L_i^2 - 2Ł_i^3/L_c}{L_c - L_i} \right), \tag{2}$$

where k_B is the Boltzmann constant. T is the temperature. L_c and p are the contour length and persistence length of Sp, respectively. In the following example we choose $L_c = 144$ nm, $L_0 = 40$ nm, and $p = 0.8$ nm. The strain energy density is then calculated as $\sum_{i=1}^{6} \phi_i/(\psi A_0)$.

We note additionally that the erythrocyte skeleton is in a deformed state while attached to the cell's membrane "at rest," i.e., without imposed deformations. This is revealed clearly in the observations of Vertessy and Steck (1989) and Shen et al. (1986) who observed skeletal shrinkage in Triton X-100 membranes. Such collapse of released membrane skeletons was reported by Levin and Korenstein (1991) and Truvia et al. (1998) in their studies of membrane fluctuations. In such studies skeletal contractions were at least on the order of a factor of 2.

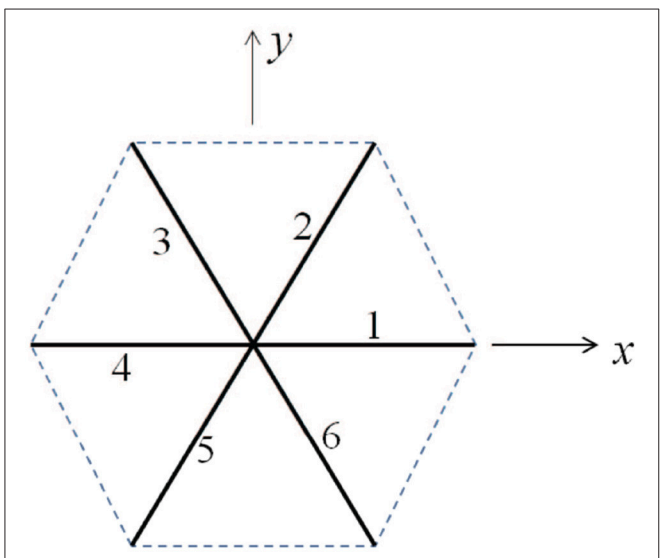

FIGURE 9 | Simplified sketch of a junctional complex consisting of six Sps. The initial length of the JC spokes are taken as $L_0 = 40$ nm here.

3.3. Skeletal Energy Density vs. Deformation Modes, ϵ_0

In **Figure 10** we present contours of ϵ_0 as it depends of the deformation parameters $\chi = \lambda_1/\lambda_2$ (representing shear deformation) and $\psi = \lambda_1 \lambda_2$ (representing area deformation), where λ_1 and λ_2 are principal in-plane stretches and by definition $\lambda_1 > \lambda_2$. We note that, within the range of deformations explored, we find $\epsilon_0 \sim \mathcal{O}(3 - 8 \times 10^{-4})\text{Jm}^{-2}$.

We note this range would lead using Equation (1) to minimal separated membrane patch and hence vescile sizes in the range

$$\begin{aligned} 31.8\text{nm} \lesssim \ell_{crit} \lesssim 51.6\text{nm} \\ 63\text{nm} \lesssim 2\ell_{crit} \lesssim 106\text{nm} \end{aligned} \tag{3}$$

This is indeed a relevant, albeit lower, size range as noted, for example, by measured size ranges for vesciles formed during splenic flow (Bosman et al., 2012). It is also noteworthy that this areal size scale is comparable to that covered by a JC unit as depicted in **Figure 9**. This provides a basis for the comment made above in section 1.1 that vesicles with diameters less than, say, 40–50 μm are unlikely. For example, a membrane patch with a area of πr_{m}^2 would produce a vesicle of diameter $r_{\text{v}} \sim 0.5 r_{\text{m}}$ as follows from the membrane's area incompressibility, *i.e.* $\pi r_{\text{m}}^2 = 4\pi r_{\text{v}}^2$ for a spherical vesicle.

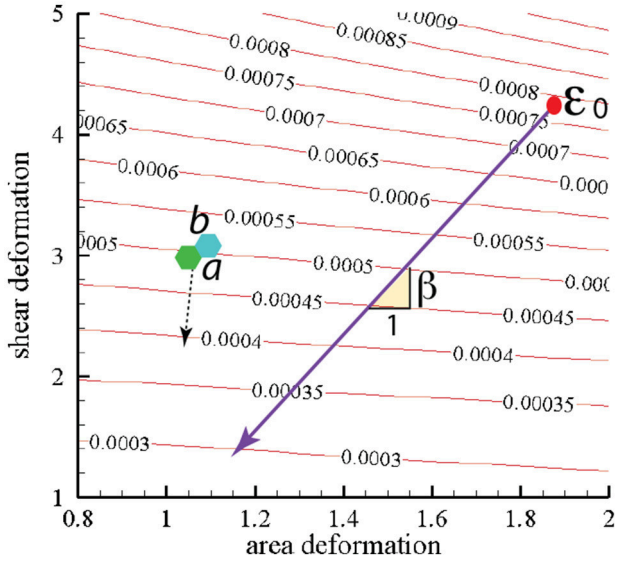

FIGURE 10 | Stored skeletal energy density in units of Jm^{-2} vs. deformation mode. The heavy line indicates a possible path of reduced skeletal area and shear deformation. The points labeled "a" and "b" correspond to maximum energy densities achieved in simulations that are described in section 4. The broken line arrow suggests an energy path aiding promoting vesiculation.

3.4. Work of Membrane/Skeleton Adhesion, γ

Estimates for the work required to separate the membrane from the skeleton have been reviewed and analyzed recently by Zhu et al. (2017). Their analysis was based on experimental data measured for experiments on the formation of tethers. The results are somewhat tentative, yet would estimate γ to be of order $\gamma \sim \mathcal{O}(1 \times 10^{-4})\text{Jm}^{-2}$. This order is noteworthy when compared to our simulated range of the stored elastic energy in the skeleton, *viz.* $\epsilon_0 \sim \mathcal{O}(3 - 8 \times 10^{-4})\text{Jm}^{-2}$. This implies that if $(\epsilon_0 - \gamma) < 0$ this combination represents a driving force for vesiculation, although this assumes that as an area element of membrane/skeleton separates all of the stored elastic energy is released.

The heavy line in **Figure 10** drawn at slope β represents a possible deformation path taken by the skeleton during its release from the membrane during a vesiculation process as discussed below.

3.5. Vesiculation Simulations

Here we consider a simple scenario of spherical cap-like bud emerging from an initially flat membrane/skeleton section. The cap initiates from a circular patch, or raft, of radius l_0 as shown in **Figures 8(Aii,iii)** and expands as a growing spherical cap with height $h(t)$ and a fixed cord $2\ell_0$. As the cap expands in area it draws in lipid bilayer and requires additional area of skeleton/membrane interface to separate.

Let the cap be of a sphere of radius $r(t)$. The emerging cap's area is $\mathcal{A}_{\text{cap}}(t) = \pi(h^2 + \ell_0^2)$ and its radius is such that $2r(t) = (h^2+\ell_0^2)/h$; of course this means that as $h \to \infty$, $2r \to h$. Also let ℓ be defined as the radius of a circular raft of membrane/skeleton with area of the spherical cap bud of **Figures 8B,C**. Hence the change in the area of skeleton/membrane area separated upon the cap's growth is $\delta\mathcal{A}_{\text{ske}} = \delta(\pi\ell^2)$. But the change in the cap's area is $\delta\mathcal{A}_{\text{cap}} = \delta\{\pi(h^2 + \ell_0^2)\}$. Since the membrane is incompressible, $\mathcal{A}_{\text{ske}} = \mathcal{A}_{\text{cap}}$, and thus $\ell\delta\ell = h\delta h$ and $\partial\ell/\partial h = h/\ell$.

Now the change in energy stored in the skeleton that is currently in the cap is

$$\epsilon^{\epsilon} = \Delta\mathcal{E} = \epsilon_0\Big\{\frac{\pi l_0^2}{\pi(h^2 + \ell_0^2)} - 1\Big\}\pi\ell^2, \tag{4}$$

and this leads, upon differentiation with respect to h noting $\partial\ell/\partial h = h/\ell$, to $\delta\epsilon^{\epsilon} = -2\pi h\epsilon_0\delta h$.

Next we note that as $\delta\mathcal{A}_{ske} = 2\pi h\delta h$ from above that the work expended in membrane/skeleton separation is $\delta\epsilon^{\gamma} = 2\pi\gamma h\delta h$.

The energy of bending in the cap is given as

$$\epsilon^{\kappa} = \frac{1}{2}\kappa_b\kappa^2\mathcal{A}_{\text{cap}}, \tag{5}$$

with κ taken as the mean curvature given by

$$\kappa = \frac{4h}{h^2 + \ell_0^2}. \tag{6}$$

With Equation (6) we have

$$\epsilon^{\kappa} = 8\pi\kappa_b\frac{h^2}{h^2 + \ell_0^2}. \tag{7}$$

Note that as $h \to \infty$, $\epsilon^{\kappa} = 8\pi\kappa_b$ as expected. This yields upon differentiation

$$\delta\epsilon^{\kappa} = 16\pi\kappa_b\frac{h\ell_0^2}{(h^2 + \ell_0^2)^2}\,\delta h. \tag{8}$$

Taken together we have

$$\begin{aligned}\delta\epsilon &= \delta\epsilon^{\kappa} + \delta\epsilon^{\gamma} + \delta\epsilon^{\epsilon}\\ &= 16\pi\Big\{\frac{h\kappa_b\ell_0^2}{(h^2 + \ell_0^2)^2} - \frac{1}{8}h\zeta\Big\}\delta h,\end{aligned} \tag{9}$$

with, as above, $\zeta = \epsilon_0 - \gamma$. To resolve this we may write $h = \alpha\ell_0$ and obtain

$$\delta\epsilon = 16\pi\Big\{\frac{\alpha\kappa_b}{(\alpha^2 + 1)^2} - \frac{1}{8}\alpha\ell_0^2\zeta\Big\}\delta\alpha. \tag{10}$$

Upon reintegrating Equation (10) we obtain

$$\epsilon = 8\pi\Big\{\kappa_b\Big[1 - \frac{1}{1 + \alpha^2}\Big] - \frac{1}{8}\alpha^2\ell_0^2\zeta\Big\}. \tag{11}$$

3.5.1. Simulation Results

Let us take $\zeta = \tilde{\zeta} \times 10^{-4}\text{Jm}^{-2}$, with $\tilde{\zeta} = 1 - 4$. Also take $\kappa_b = \tilde{\kappa} \times 10^{-19}$J, with $\tilde{\kappa} = 1 - 1.5$. Finally take $\ell_0 = \tilde{\ell} \times 10^{-8}m$, with $\tilde{\ell} = 1 - 4$; this puts ℓ_0 in the range $10\text{nm} \leq \ell_0 \leq 40\text{nm}$. With these definitions and values Equation (11) becomes

$$\epsilon = 8 \times 10^{-19}\pi\Big\{\tilde{\kappa}\Big[1 - \frac{1}{1 + \alpha^2}\Big] - \frac{1}{80}\alpha^2\tilde{\ell}^2\tilde{\zeta}\Big\}. \tag{12}$$

3.6. Vesiculation: *Pinching-Off* as the Final Stage

The final stages of vesicle release may go as depicted in **Figure 12**. Here expansion continues as h increases along a downward slope of a ϵ *vs.* $\alpha(h)$ curve. At some stage the "bridge," ℓ_0, may itself retreat as the bud becomes more compliant with increasing radius, $r = (h^2 + \ell_0^2)/2h$. As the angle θ defined in **Figure 12** decreases, the bending stresses in at the junction of the bud and bilayer main body increase and eventually rupture the bilayer. Spectrin may be retained within the vesicle, e.g., bound to Hb (Snyder et al., 1985), and/or released into the medium so as to remove skeletal proteins from the cell in rough proportion to lost membrane area in the vesicle as suggested by Ciana et al. (2017b). Resealing on the membrane is favored, of course, as is reattachment of the skeleton to the membrane.

As for estimates of vesicle size, we may proceed as follows. Consider as a first example **Figure 11A**; here the activation barrier is crossed at $\alpha \sim 1.2(\tilde{\zeta} = 4)$ or $\alpha \sim 2(\tilde{\zeta} = 1)$ with $\tilde{\ell} = 2$ and $\tilde{\kappa} = 1.5$. Now analysis of **Figure 12** shows that

$$\theta = \tan^{-1}\frac{2\alpha}{\alpha^2 - 1}, \tag{13}$$

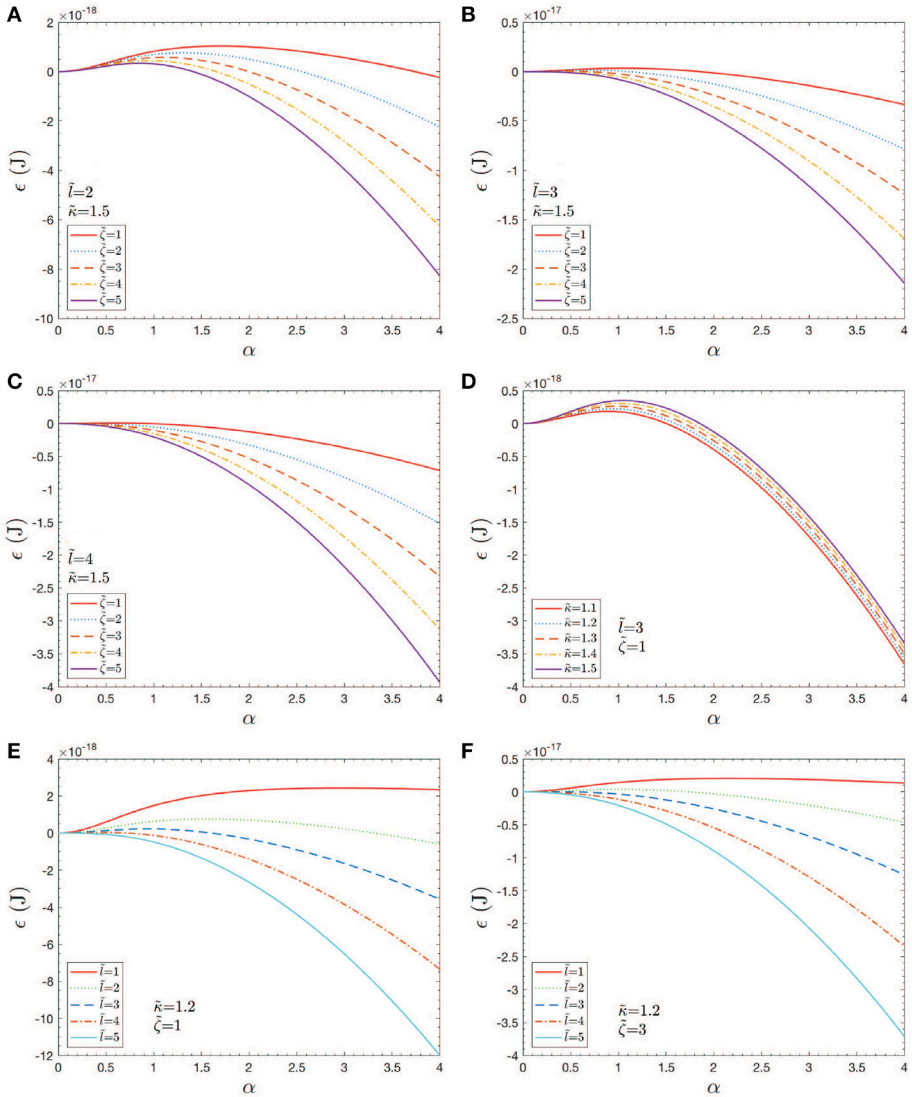

FIGURE 11 | Case studies of total energy, ϵ vs. $h = \alpha\ell_0$. Note that an $\ell_0 = 40$nm ($\tilde{\ell} = 4$) would correspond to an initial skeletal/membrane separation covering about one JC unit. The parameters in the cases shown in **(A–F)** are listed within the figure.

and hence if θ reduces so that $\theta \to \theta_{\rm crit}$,

$$\frac{2\alpha_{\rm crit}}{\alpha_{\rm crit}^2 - 1} \to \theta_{\rm crit}. \tag{14}$$

Let us take, to explore the numerology, $\theta_{crit} = \pi/8$; this yields $\alpha_{crit} \approx 5$. At this stage we would have $h_\nu \approx 5 \times 2 \times 10^{-8}$m = 100nm. On the other hand if $\tilde{\ell} = 4$, as in **Figure 11C**, we would find $h_\nu \sim 200$nm.

As a purely geometric criterion, Equation (14) would effectively define the length scale ℓ_0 as the mediator of vesicle formation (at least vesicle size). Yet the vanishing of ΔG_{act} that depends also on κ_b, ϵ_0 and γ as well as on ℓ_0 all play vital roles. However, it may be judged, that as long as $\Delta G_{\rm act} \to 0$, ℓ_0 may be judged as a (the) prime determinant of vesiculation. Of course, the very factors that influence γ as well as ϵ_0, and possibly even κ_b are involved in causing an ℓ_0 in the first place. With the numerology used here we find that predominantly vesicles are expected in the size range 100nm $\lesssim h_\nu \lesssim$ 200nm; however, vesicles as small as $h_\nu \sim 40 - 50$nm are possible if sufficient driving energy, ϵ_0 is available.

Finally we discuss the release of a severed bud, i.e., its closing to a spherical vesicle. The question is: once free, does the bud completely fold or revert to a flat disc with an exposed edge? This question is depicted in **Figure 13**. The severed bud ("B") is depicted in **Figure 13b** and it may revert to a planar disc of area "A" as in **Figure 13a** or close to a vesicle ("V") as in **Figure 13c**. The bud and the flat circular patch, however, possess an "edge," Γ, with energy γ_s measured in units Jm^{-1} and which provides a driving force to close the bud or, if insufficient, fold a flat patch as in "A".

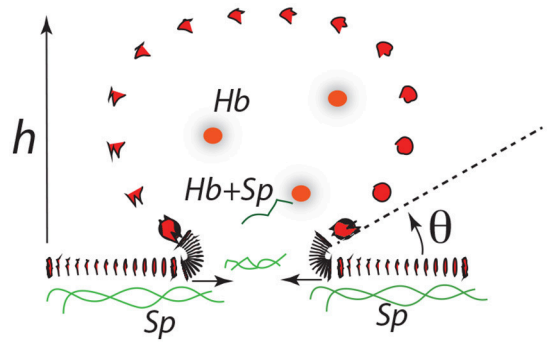

FIGURE 12 | A budding vesicle of height h formed off an initial skeletal/membrane separation of radius ℓ_0. The angle θ is the inclination of the vesicle membrane as it just leaves off the cell's membrane body. Note that as θ is reduced the curvature at that location increases dramatically.

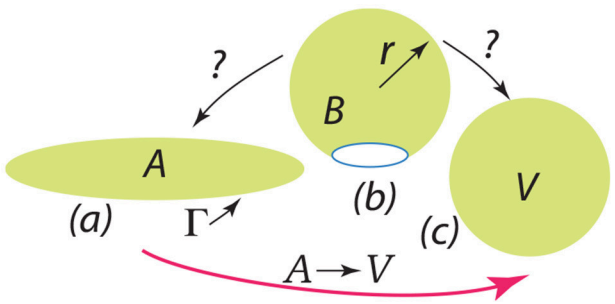

FIGURE 13 | The depiction should be interpreted as follows: a bud ($\mathcal{B}$) is released as in **(b)** and may revert to a flat patch ($\mathcal{A}$) as in **(a)** or may close to form a spherical vesicle ($\mathcal{V}$) as in **(c)**.

The issue of the folding of an initially flat patch was considered by Helfrich (1974), and later by Fromherz (1983), and here we list a key result as phrased by Hu et al. (2012) who developed an approach based on these results for estimating values for the key parameters. In Equation 15 $\mathcal{E}$ is the energy along the path given by curve $\mathcal{A} \rightarrow \mathcal{V}$ in **Figure 13**.

$$\frac{\mathcal{E}(\xi,\eta)}{4\pi(2\kappa_b+\kappa_g)} = \tilde{\mathcal{E}} = \xi + \eta\{\sqrt{1-\xi}-1\}, \text{ with}$$
$$\xi = (\frac{\mathcal{R}}{r})^2,\ \eta = \frac{\gamma_s \mathcal{R}}{2\kappa_b+\kappa_g}, \text{ and } \mathcal{R} = (\frac{\mathcal{A}}{4\pi})^{1/2}. \tag{15}$$

Here ξ is a parameter that measures the progress along path $\mathcal{A} \rightarrow \mathcal{B} \rightarrow \mathcal{V}$ where $\xi = 0$ represents the initial flat patch of membrane of area $\mathcal{A}$ and $\xi = 1$ a full spherical vesicle of radius R (whose area is equal to $\mathcal{A}$). The modulus κ_b has already been defined and κ_g is the so-called Gaussian modulus (Helfrich, 1974; Fromherz, 1983; Hu et al., 2012) ($\kappa_g \approx -\kappa_b$). Now as noted by Hu et al. (2012) - and is readily verified - the path $\mathcal{A} \rightarrow \mathcal{B} \rightarrow \mathcal{V}$ displays an activation barrier if $\eta < 2$ at $\xi_{\text{act}} = 1-(\eta/2)^2$; this amounts to $\Delta\tilde{\mathcal{E}}_{\text{act}} = (1-\eta/2)^2$. With this, our question is: as per **Figure 13b**, does the $\mathcal{B}$ revert to $\mathcal{A}$ or proceed to vesicle $\mathcal{V}$ after the driving energy supplied by, *inter alia*, ϵ_0 and ΔG_{mix} has been expended?

To make use of these results we use representative values for κ_b, κ_g, and γ_s provided by Hu et al. (2012); in particular we take $\kappa_{\text{b}} \sim 10^{-19}$J, $\kappa_{\text{g}} \sim -0.9\kappa_{\text{b}}$, and $\gamma_{\text{s}} \sim 3kT\text{nm}^{-1} \approx 1.2 \times 10^{-11}\text{Jm}^{-1}$. Then with our defined geometry we find

$$\mathcal{R} = \{\frac{\mathcal{A}}{4\pi}\}^{1/2} = \frac{1}{2}\sqrt{\alpha^2+1}\ell_0,\ \ \eta = 0.55\tilde{\ell}\sqrt{\alpha^2+1}, \text{ and}$$
$$\xi_{\text{act}} = 1 - 0.076\,(\alpha^2+1)\,\tilde{\ell}^2,\ \text{ with }\ \ell_0 = \tilde{\ell}\times 10^{-8}\text{m}. \tag{16}$$

Now if at the point of bud severing α were in the range, say, $\alpha \geq 2$ and $\tilde{\ell} \geq 2$ we would judge that $\eta \gtrsim 2.6$. In such cases no activation barrier would exist (from a flat disc) to form a closed vesicle. If, on the other hand, $\tilde{\ell}$ were modest in size, say $\tilde{\ell} \sim 1$ and $\alpha \lesssim 2$ at budding then $\eta \lesssim 1.22$ and a barrier would exist to form a closed vesicle. In such cases one might suspect that severed bud would revert back to a flat disc, i.e., a "membrane fragment" as are often found.

4. DISCUSSION OF VESICULATION SIMULATION RESULTS OF SECTION 3

The results shown in **Figures 11A–F** provide an initial assessment of the key parameters, $\kappa_b, \zeta = \epsilon_0 - \gamma$, and ℓ_0. These are, in turn, affected by metabolic and biochemical influences as discussed above. Now given the magnitudes of the activation barrier, ΔG_{act} as indicated in **Figure 11D**, we expect vesiculation to essentially require $\Delta G_{\text{act}} \rightarrow 0$; we thereby take this as a possible criterion for vesicle release. For example, **Figures 11A,D** clearly indicate the effects of high values of κ_b and/or small initial membrane/skeleton separation ℓ_0 in inhibiting vesiculation; the effect of ℓ_0 is noteworthy. This perhaps obvious result is nontrivial as it suggests that the initial "triggering event" may have a mediating effect on the eventual size of the vesicle released, as opposed to the details of progression of skeleton/membrane separation and ongoing membrane bulging. **Figures 11B,C,F** support this view as they show that, even at modest-to-high values of κ_b and low values of ζ, ΔG_{act} may effectively vanish if ℓ_0 is at least as large as a typical JC complex, viz. if $\ell_0 \sim 40-50$nm.

Next, we note that the magnitude of κ_b (Harmandaris and Deserno, 2000; Hu et al., 2012), the bending modulus, clearly plays a role in setting the height of ΔG_{act}, and even determining if $\Delta G_{act} \geq 0$. In general, κ_b depends on membrane thickness and also on the bilayer membrane's lipid composition, including the lipid composition asymmetry. Here we introduce **Figure 14**, taken from Zwaal et al. (1997) that helps explain these issues. Yet, the prospect for vesiculation is also determined by the relative magnitudes of the terms ϵ_0 and γ given in Equation (11) and (12) via $\zeta = \epsilon_0 - \gamma$. We continue to discuss the prospects for $\Delta G_{\text{act}} \rightarrow 0$ below. For now we note that Equation (12) reveals an activation barrier at $\alpha^2 = \sqrt{80/\mu} - 1$ with $\mu = \tilde{\ell}^2\tilde{\zeta}/\tilde{\kappa}$. This shows, after substitution into Equation (12), that if $\mu/80 < 1$ an activation barrier exists with $\Delta G_{act} > 0$; conversely, we have that

$$\mu/80 = \tilde{\ell}^2\tilde{\zeta}/\tilde{\kappa} \geq 1 \tag{17}$$

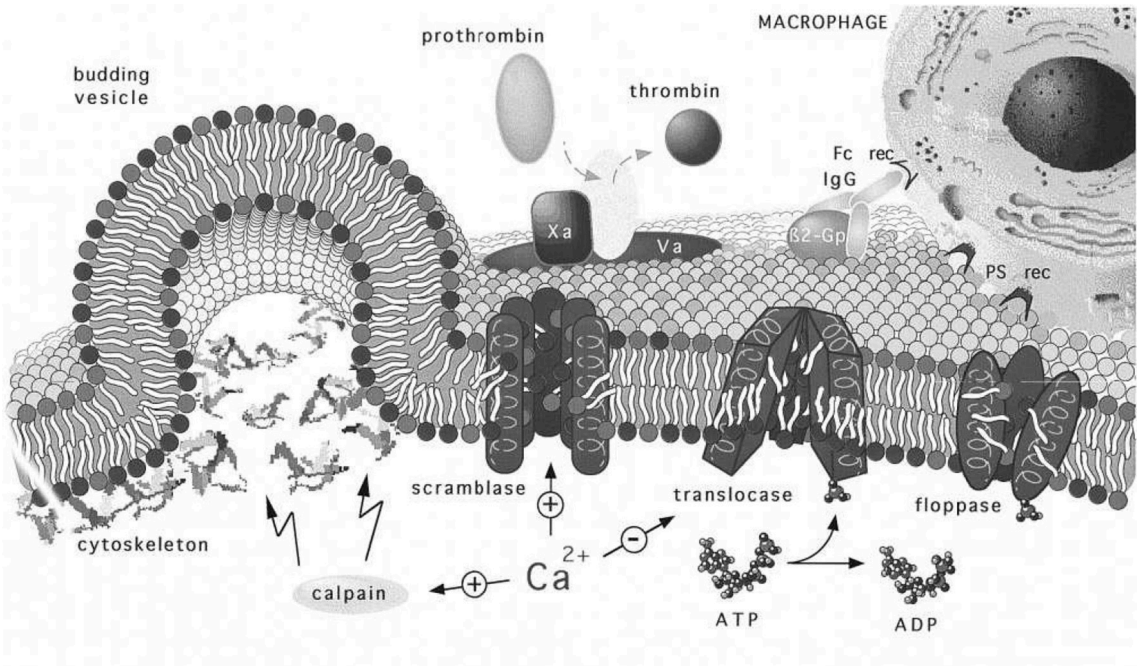

FIGURE 14 | Regulation and physiology of membrane phospholipid asymmetry and vesiculation, taken from Zwaal et al. (1997). The effects of Ca^{2+} uptake on phospholipid randomization and on calpain activation that facilitates blebbing and release of PS exposing vesicles are addressed. We use the figure to also illustrate the geometry of a budding vesicle and to highlight how large curvatures develop and lead to pinching off of the vesicle bud. Note also that the large tensile strains in the membrane may increase the kinetics of randomization that initiates before vesiculation (Zwaal et al., 1997).

implies that, once initiated, a bud will spontaneously grow.

Now the roles of calpain and Ca^{2+} uptake in vesiculation have been already discussed and are referred to in **Figure 14**. We take the depiction of budding as shown there to represent a stage in any of our **Figure 11** but along a downward slope of a ϵ *vs.* $\alpha(h)$ curve; note the curvatures at such stages, most particularly at the sites where the bud meets the membrane body. As such stages we envision that phospholipid asymmetry has been lost (or partially lost) and that the membrane is under considerable tension at what is to be the "pinching off" sites located as just referred to above. This is addressed in more detail below as we suggest how vesiculation is completed, but after a relevant diversion concerning the spectrin skeleton.

4.1. Disposition of Skeletal Proteins During Vesiculation

A question arises suggested by the Zwaal-Schroit depiction of **Figure 14** as well as by **Figure 12** below, viz. *what happens to the spectrin contained in the released skeleton?* It has been reported that shed vesicles (MV's) are deficient in skeletal proteins, viz. spectrin (Lutz et al., 1977; Dumaswala and Greenwalt, 1984; Knowles et al., 1997; Willekens et al., 2003a,b; Bosman et al., 2012) and this has suggested that spectrin may remain in the cells. Ciana et al. (2017a,b) have, however, recently shown that the cells that shed vesicles, *in vivo*, lose spectrin in rough proportion to their membrane area; no data was presented on the spectrin content of the shed vesicles, however. The fact is that the number of vesicles found in venous blood is orders of magnitude too low to account for the cell membrane lost. This means that vesicle membrane is recycled without entering general circulation, i.e., presumably within the organ where the vesicle forms. Yet Snyder (Snyder et al., 1985) had already shown that vesicles shed from "young cells" (i.e., cells so classified by their low density) contained "Hb-spectrin complexes" suggesting that spectrin was also shed into vesicles in at least some amounts. Hence we speculate that spectrin may indeed be lost to either the medium and/or retained within shed vesicles along with Hb as is repeatedly reported. In fact, examining either **Figures 14**, **12** or Figure 2 of Alaarg et al. (2013) suggests that, since the pinching off process produces very large local deformations, the skeleton would bed severed and retained within the vesicle or the medium of the organ producing vesicle. As many reports of spectrin deficient vesicles are those produced *in-vitro* we discuss this further and will suggest, in the Discussion, that our oscillatory shear methods be utilized to study the character of vesicles produced via our splenic-like deformations. This logically leads us to more detailed consideration of γ and ϵ_0.

4.2. Biochemical Energetics

As noted in section 3 most prominently, and elsewhere, attachment between the skeleton and membrane can be reduced by a number of biochemical and metabolic causes. Hence we realize that although imposed deformations that increase ϵ_0 will stimulate vesiculation, e.g., during splenic flow or under our conditions of oscillatory shear flow, even modest states of

deformation are sufficient to induce the process. An intriguing possibility is that the free energy released by losing phospholipid concentration asymmetry may provide some of the required energy associated with ϵ_0. This remains to be explored, but here we make a simple estimate of such a contribution to test the idea's viability. The fact is that significant metabolic free energy is expended in creating lipid concentration asymmetry (Zwaal et al., 1997; Fadeel and Xue, 2009; Bevers and Williamson, 2016) and we wonder what portion of it may be available to perform the work of vesiculation.

We take a simple view and consider the primary lipids that "mix" in a final state of symmetry from an initial state of asymmetry between the outer and inner bilayer leaflets to be grouped into 2 groups. Let group #1 consist of sphingomyelin and phosphstidylcholine (initially located on the outer leaflet) and group #2 contain phosphatidylethanolamine, phosphatidylserine, and phosphatidylnositol (initially on the inner leaflet). We will call the molecular fraction of either group "x" since we assume a perfect solution within the leaflets.

We use the well known relation for the entropy of mixing for a perfect solution, viz.

$$\Delta g_{mix} = -nk\{x\ln x + (1-x)\ln(1-x)\}, \tag{18}$$

where, in context, n is the total number of lipids in a leaflet, k is Boltzman's constant, and x is either group #1's or #2's molecular fraction. We use Equation (18) to compute

$$\Delta S_{mix} = \Delta g_{\rm sym} - \Delta g_{\rm asym}, \tag{19}$$

and note that the free energy change, just associated with perfect mixing, is $\Delta G_{a\to s} = -T\Delta S_{mix}$; we will take $T = 300$ K. We take for n, the number of lipids per leaflet, $1.4\times10^{18}m^{-2} \leq n \leq 1.5\times10^{18}m^{-2}$ (White and King, 1985; Giang and Schick, 2014) (this being computed from the average area per lipid, $a \sim 0.68 - 0.70\text{nm}^2$) and $kT \sim 4\times10^{-21}J$. For $\times$ we take $x \sim 0.74$ (Zwaal et al., 1997; Fadeel and Xue, 2009). These numbers yield $\Delta G_{\rm mix} \sim -(6.7-7.2)\times10^{-4}\text{Jm}^{-2}$, which is in the range of ϵ_0, a primary driving force for vesiculation (see **Figure 10**). Even if a portion of this stored free energy were made available it could drive vesiculation. For perspective, we recall that the standard free energy of hydrolysis of ATP is in the range $\Delta G^{\circ}_{\rm ATP} \sim -(11-13)$kcal/mole $\sim -(7.5-9)\times10^{-20}$J/ATP (Alberts et al., 2002). Hence one ATP per $10^2 - 10^3$ lipids could fuel vesiculation. We note Beleznay et al. (1994) and Zachowski (1993) report that transport of lipids such as PS consumes about one ATP per lipid, i.e., an order of magnitude larger than we estimate for $\Delta G_{\rm mix}$ per lipid - as such lipid transport must have a substantial activation barrier, this seems quite reasonable. *Interactions and association of PS with spectrin have been documented* (An et al., 2004a,b; Grzybek et al., 2006) *and those may be disrupted during membrane/skeletal separation, promoting translocation.*

Thus for the above reasons we expect reductions in γ and increases in ℓ_0 are prime contributors to, and even mediators of, vesiculation. A simple view would be that the skeletal energy density, ϵ_0, would be augmented by $-\Delta G_{a\to s}$ as a prime driver of vesiculation. As imposed deformations, i.e., ϵ_0, have the prospect of promoting the process as we explore next regarding imposed oscillatory shear flows in the specific context of the above vesiculation model prospects. Finally we address the "pinching off" process that releases the vesicle.

4.3. Pre-curvature and Biochemically Induced Curvature

Returning to **Figure 11**, we recognize that when $\Delta G_{\rm act} > 0$ we are typically in scenarios where $\alpha \lesssim 1 - 1.5$ yet if we began the process at, say $\alpha \gtrsim 1.5$ in most cases ΔG_{act} would vanish. We thereby ask about the effects of pre-curvature, or spontaneous curvature, as may arise, for example, by the expected trends to randomize the lipid concentration between the inner and outer leaflets (Zwaal et al., 1997). As noted Sheetz and Singer (1974) anionic molecules such as PS that are known to partition to the outer leaflet with vesiculation will indeed tend to cause crenation, i.e., outward budding (see also Deuticke, 1968). Just above we have shown that the thermodynamic driving force for this can be, indeed, substantial. A simple analysis of such induced curvature might go as follows. Simply consider Equation (7), the bending energy, and equate it to a portion of the free energy of mixing $\Delta G_{\rm mix}$; call this portion $\Delta\tilde{G}_{\rm mix}$. This yields

$$8\pi\kappa_b\frac{h^2}{h^2+\ell_0^2} = -\Delta\tilde{G}_{\rm mix}, \tag{20}$$

or

$$|\Delta\tilde{G}_{mix}| = 8\frac{\alpha^2}{(\alpha^2+1)^2}\frac{\kappa_b}{\ell_0^2}. \tag{21}$$

For some numerology, take $\alpha = 1$, $\kappa_b = 10^{-19}$J and recall the definition of $\tilde{\ell}$ to obtain

$$|\Delta\tilde{G}_{mix}| = 2\frac{10^{-3}}{\tilde{\ell}^2} = \begin{cases} 5\times10^{-4}, & \tilde{\ell}=2 \\ 2.2\times10^{-4}, & \tilde{\ell}=3 \\ 1.25\times10^{-4}, & \tilde{\ell}=4, \text{ etc.} \end{cases} \tag{22}$$

Hence we may envision that in all the cases shown in **Figure 11**, taken as examples, ΔG_{act} may be driven to near zero. Now the reader will notice that as we take ℓ_0 larger and larger, the required $\Delta\tilde{G}_{mix}$ reduces, eventually as $\Delta\tilde{G}_{mix} \sim 1/\alpha^2$.

These arguments also demonstrate that the effects of the cell membrane's natural curvature are quite modest due to the much larger curvatures involved in creating a budding vesicle; that is, the cell's surface appears to be relatively flat compared to the emerging vesicle.

4.4. Vesiculation in Oscillatory Flow: Final Analysis

Taken together, the results herein and those of sections 2 and 3 would support a scenario such as this: imagine a deformation state such as represented by points "a" or "b" of **Figure 10** that can arise from the simulations we described. Now imagine an augmentation of the associated $\epsilon_0 \sim 5\times10^{-4}\text{Jm}^{-2}$ of order, say $-\Delta G_{a\to s} \sim \mathcal{O}(2-3\times10^{-4}\text{Jm}^{-2})$. This places the total prime vesiculation driving force at $\sim 7-8\times10^{-2}\text{Jm}^{-2}$, that according

to the result scenario's of **Figure 11** could very probably produce vesiculation.

A further assessment of vesiculation prospects with the examples of **Figures 4–6** could go as follows. Consider the vesiculation simulations as, say, in **Figure 11**. From **Figure 11C**, for example, looking at the contours of energy density we would conclude that if there were regions—call them *aged regions*—where skeletal/membrane disruptions had occurred over areas of, say, $\tilde{\ell} \geq 3$ the probability of vesiculation at regions where $\tilde{\zeta} \geq 2$ would be quite high; at regions where $\tilde{\zeta} \geq 4$ vesiculation would be judged to be nearly assured. This follows since in this case $\Delta G_{act} \rightarrow 0$. Hence, in **Figure 6** we would conclude that at any region displaying a red color we expect vesiculation to occur in cells containing aged areas where $\tilde{\ell} \gtrsim 3-4$. In **Figure 4** which also displays deformation states quite similar to those developed in splenic flow (Zhu et al., 2017) we would likewise focus on those regions in the lower-right foreground. Note, here we take $\gamma = 1 \times 10^{-4}\text{Jm}^{-2}$ (Zhu et al., 2017) and that the red areas display $\tilde{\zeta} \geq 3$. On the other hand, the case shown in **Figure 3B** displays somewhat reduced levels of stored energy, i.e., $\tilde{\zeta} \lesssim 3$ and hence we judge that vesiculation may require larger aged areas involving, say $\tilde{\ell} \gtrsim 4-5$.

Similar case studies can be made and from such we could well conclude that during splenic flow — as closely replicated by our oscillatory flow - vesiculation is highly probable providing aged regions exist covering nearly the area of a single JC unit (i.e., corresponding to $\tilde{\ell} \sim 3-4$). This would surely classify the spleen as an effective filter as expected — it might also support the notion that the majority of such *self-protection vesicles* are produced *in vivo* in such flow conditions, e.g., in the spleen and elsewhere where such deformations are imposed.

4.5. Shear Induced Erythrocyte Membrane Trauma

Given the flexibility and inherent time and rate dependence of RBC deformation, it is unsurprising that cell damage induced by imposed shear displays a complex phenomenology. For perspective *vis-à-vis* oscillatory shear, as we have presented it, we briefly review some background. We begin by noting that the physiological range of shear stress imposed upon the RBC is often put in the range of $\bar{\tau} \sim 5-10\text{Pa}$ (Meram et al., 2013); it is hence noteworthy that our forecasted average shear stresses presented herein for oscillatory flow are in that range. However, as explained early on by Leverett et al. (1972), the question of membrane rupture depends not only on stress level but also on the time of exposure suggesting perhaps "creep-like" damage mechanisms are operative. Moreover, stressing rate is important (Li et al., 2013) and in the case of cyclically imposed stresses, both frequency and amplitude are important (Watanabe et al., 2006; Wantanbe et al., 2007; Hashimoto, 2014; McNamee et al., 2016); this suggests that even wave form for periodic stressing would likely be still another factor. In fact, patterns using stress (flow) bursts coupled to pauses (i.e., hold times) have been employed (McNamee et al., 2016; Horobib et al., 2017). Nevertheless, when stresses are imposed for long times ($\gtrsim$ 60 min) a critical shear stress to induce cell lysis in the range $\tau_{\text{crit}} \sim 150Pa$ has been quoted (Leverett et al., 1972); other reports place this higher at $\tau_{\text{crit}} \sim 250Pa$ (Sutera and Mehrjardi, 1975). Yet—and this is important!—in a study involving exposure to shear stresses $\tau \sim$ 10Pa, but for 2 h, it was found that such exposed cells were recognized and sequestered by rabbit spleens (Sandza et al., 1974). That is, such cells were sequestered and removed during splenic flow. Here we may speculate that although such exposure was *sublethal* (i.e., did not cause bursting, cell distortion, or other residual damage), it did induce *cell removal processes*, perhaps vesiculation. Note that the time to induce possible vesiculation in Sandza et al. (1974) was unknown, but the stress level at $\tau \sim$ 10Pa is just at the levels we forecast for oscillatory flow as in the case of **Figure 5**. Finally, we note that human splenic flow passage times are $< 1s$ (MacDonald et al., 1987; Zhu et al., 2017). Given that multiple passages may be involved, we take the stress protocol to involve multiple passes with durations of, say 0.02-1 s; these to employ shear stress levels of $\tau \sim 5-10\text{Pa}$. In oscillatory flow we would suggest frequencies in the range $\nu \sim 1-50\text{Hz}$.

We also note that our simulations methods can be used to analyze the deformations experienced by RBC's subject to all the flow patterns imposed in the studies cited above, and can thereby be used to assess potential damage, lethal or sublethal, that may be caused. Moreover, it is possible to include interactions between cells and/or cells and structural features such a channel walls so that more quantitative assessments can be made of possible influences they may have on cell response.

5. SUPPORTING EXPERIMENTAL EVIDENCE

To confirm the effects of oscillatory flow as we have described them and to assure that our proposed imposed deformations do not cause lethal damage to a significant population of cells we used flow cytometry to explore the process of vesiculation and possible fragmentation following typical programs of shear. We imposed both modest and somewhat severe deformations to more completely explore the extent of possible cell damage via fragmentation and vesiculation. We suggest below, however, that in exploring aging induced vesiculation only the more modest deformations we have described be imposed. For example, an oscillatory frequency of 10 Hz appears to be reasonable since it coincides with the typical duration (0.1 sec) of slit passage in splenic flows (MacDonald et al., 1987). The shear stress on the cell depends on both the applied shear rate and the viscosity of the surrounding fluid. To match the typical shear deformation of the skeleton in splenic flow (the area deformation is negligibly small) this stress should be 5–10 Pa as described in section 4.5 and by the various plots of deformation in oscillatory flow we have included.

5.1. Materials and Methods

5.1.1. Blood Samples and Reagents

Adsol (Fenwal Laboratories, Deerfield, IL) preserved and leukoreduced red cell units were purchased from the San Diego Blood Bank (San Diego, CAI). Glycophorin A-PE, Annexin V FITC, and annexin V-binding buffer concentrate were purchased

from BD Pharmingen (San Jose, CA). Flow Cytometry Absolute Counting Standard microbeads (6–7 μm) were purchased from Bangs Laboratories, Inc. (Fishers, IN). Megamix, a blend of monodisperse fluorescent beads of three diameters (0.5, 0.9, and 3 μm) was purchased from BioCytex (American Diagnostic, Hauppauge, NY, United States).

5.1.2. Oscillatory Shear

The steady and oscillatory shear conditions were applied on a stress-controlled shear rheometer (T.A. Instruments, model AR-G2), with a cone-plate of 60 mm diameter and 1° of angle, and with a plate-plate geometry of 60 mm diameter and a gap of 100 μm. The shear flows are imposed with a duration of 1–2 s, and repeated for multiple cycles, and carried out at 37°C.

5.1.3. Isolation and Purification of Red Cell Vesicles From Shear RBC Suspension

Isolation of vesicles from the RBCs suspensions were completed by high-speed centrifugation as previously described (Kriebardis et al., 2008). Briefly, 1-mL aliquots were removed and centrifuged at 2,000 g at 4°C. The supernatant was centrifuged once again to ensure the absence of any RBCs and immediately filtered through sterile 0.8 mm pore size syringe-driven nitrocellulose filter units (Millipore, CA, United States). The supernatant was ultra-centrifuged at 37,000 g at 4°C for 1 hour, and the pellet of vesicles was resuspended in PBS and ultra-centrifuged twice under the same conditions.

5.1.4. Quantitation of Micro-Vesicles Using Flow Cytometry

Red cell vesicle analysis and enumeration was obtained using a FACS Aria flow cytometer (BD Biosciences, San Jose, CA, United States). To confirm the formation of vesicles after imposed shear, the side scatter and forward scatter events from size calibration beads (0.5, 0.9, 3, and 7.6μm,) was compared to the side scatter and forward scatter events of a small volume of supernatant and erythrocytes of blood centrifugated at 2,000 g at 4°C (**Figure 15A**). These results were used to determine the resolution of the instrument, and to confirm the presence of vesicles and smaller cell fragments as the amount of imposed shear deformation increased (**Figure 15A**). The size range was confirmed and corrected by spiking a blood sample with calibration beads to establish the effect of the calibration beads' higher index of refraction on size relative to membrane vesicles (lower size threshold than membrane vesicles) (Yuana et al., 2011). Purified vesicles from RBC suspensions were labeled with glycophorin A-PE and annexin V FITC at ice temperature and protected from light. Red cell vesicles were discriminated by size and further defined as CD235a-PE and Annexin V positive event. Vesicle counts were calculated by adding a predetermined number of calibration beads to each blood sample, and from the nominal number of beads added per volume of sample a total number of vesicles was calculated.

5.2. Results

Two-color flow cytometric analysis, employing a combination of antiglycophorin A and Annexin-V-FITC, has demonstrated that shear deformations induce vesiculation as theoretically forecasted herein. Flow cytometry results are shown in **Figure 15**, where size is one of the key factors defining these events. Flow cytometry allowed us to obtain information on the morphology (size and granularity) of vesicles formed due to imposed shear, as evidenced by the forward scatter and side scatter of vesicles compared to calibration beads of appropriate diameters (**Figure 15A**). Forward scatter properties were used as an estimate of size, and side scatter properties were used as an estimate of particle shape. Forward and side scatter events from size calibration beads were used to resolve the instrument sensitivity and detection range. **Figure 15A** shows that the sub-population of vesicles increased with shear deformation as forecasted. Examination of the top-left scatter plot in **Figure 15A** indicates that 0.2 μm is the lower limit of detection for the beads. Vesicles are defined as membranous vesicles of arbitrary size from 0.2 to 1.0 μm. In contrast to RBCs, vesicles derived from RBCs may expose negatively charged phospholipids toward their surface. Living cells, however, employ energy-dependent mechanisms to actively shift negatively charged phospholipids to the inner membrane leaflet as discussed in section 4.2. Flow cytometric observation allows for the determination of the fraction of vesicles that bind annexin V, which suggests exposure of negatively charged phospholipids. **Figure 15B** shows that the fractions of glycophorin A positive and exposed PS vesicles (observations in the upper right quadrant) increased with shear deformation. Fluorescence events from antiglycophorin A and Annexin-V-FITC showed that the erythrocyte vesicles that expose PS, also had a high expression of glycophorin A.

Moreover, these results prove that oscillatory shear flows do not damage a significant portion of the RBC's. As an example, the results in **Figure 15** indicate that after a protocol of 100 cycles, of shear rate $\sigma = 200s^{-1}$, at 100 Hz we found the number of vesicles to be $\mathcal{O}(10^4)$. As this protocol corresponds, based on the deformations experienced by the cells, to approximately 10,000 *in-vivo* splenic slit passages for each cell we would expect that given our 10^7 cells this would have resulted in a number of vesicles of $\mathcal{O}(4.8 - 6.5 \times 10^9)$ *in-vivo*. In this we assumed that *in-vivo* a vesicle is produced at a rate of approximately 2–2.71 per day per cell (Willekens et al., 2003b; Ciana et al., 2017b). Hence as this expected *in-vivo* vesicle count is clearly much larger than our result of $\mathcal{O}(10^4)$ we conclude our methods do not induce spurious cell damage or unexpected vesiculation. In terms of *in-vivo* splenic passages the deformation histories experienced by cells in this protocol would have occurred over about 250 days (if cell deformations outside of the spleen are not considered), or more than twice of a cell's average lifetime. Thus, a reason for the difference is that cells would not be expected to metabolically age during as they would *in-vivo* in the quite short durations of our tests. Additionally, we imposed somewhat more severe deformations (shear rate amplitude 2,000 s^{-1} at 50 Hz and with 100 cycles with durations of 2 s) to further explore the extent of possible cell damage. The basic hemologic parameters demonstrate that the majority of the cells (> 95%) survive the treatment.

Vesicle counts found per microliter of plasma were as follows: 217 for our control with no-shear and 986, 23,034, and 46,026

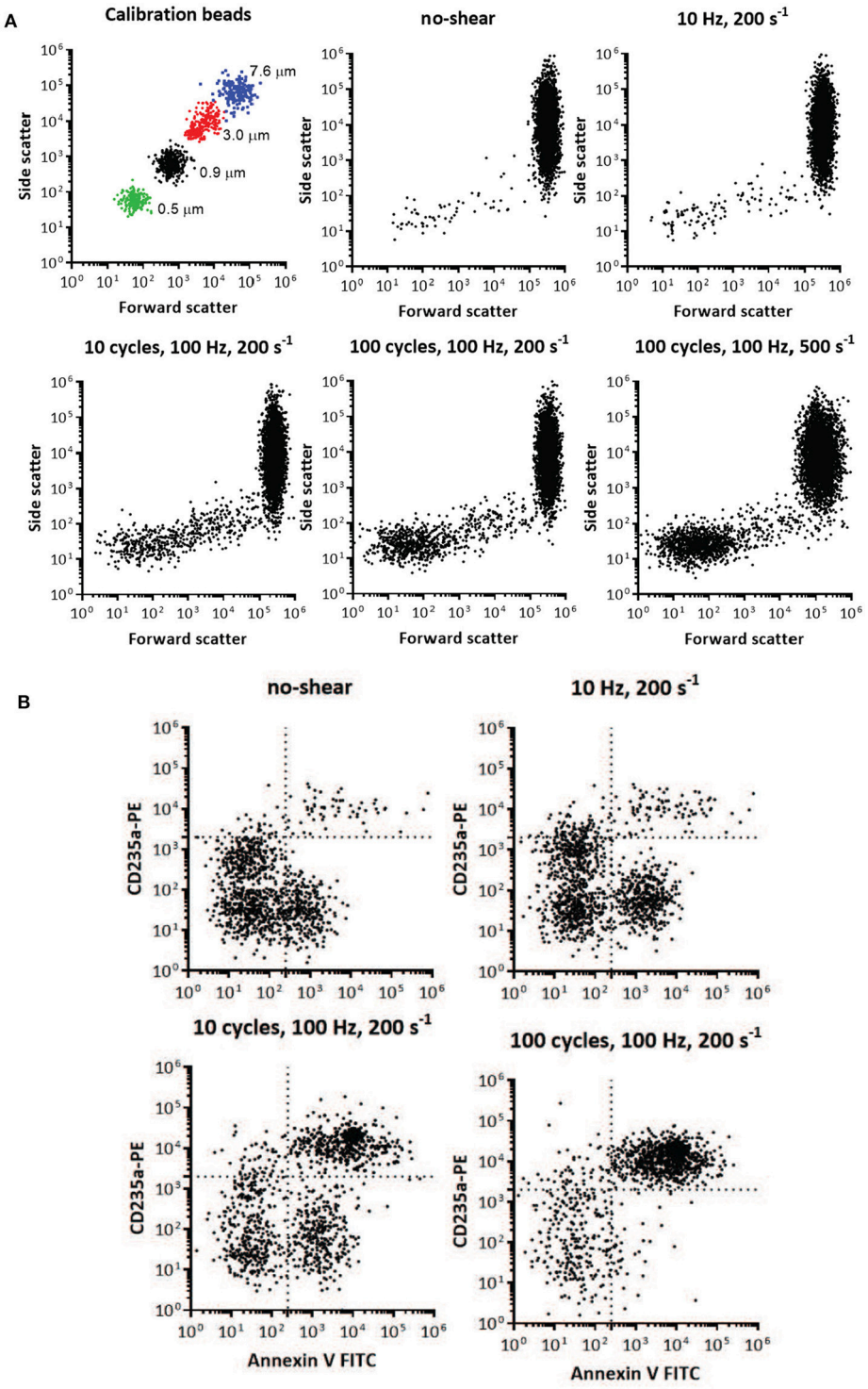

FIGURE 15 | Flow cytometry identification of presence and size of RBC vesicles based on the light scatter parameters and quantification of RBC vesicles based on marker for phospholipid PS and glycophorin A (CD235A) using flow cytometry. **(A)** Light scatter results using side scatter (SSC) as the indicator of shape and forward scatter (FSC) the indicator of size. Top left panel shows light scatter parameters of the mixture of standard calibration beads (7.6, 3, 0.9, and 0.5 μm). Other panels show light scatter parameters of the blood samples before mechanical shear (no-shear), and after being subjected to different frequencies, cycles, and degrees of oscillatory shear. Inspection of the scatter from the calibrated beads and the blood subjected to mechanical shear indicates the increasing presence of vesicles below 1 μm in size. Direct size comparison cannot be made between beads and vesicles, since beads have a higher index of refraction, and therefore lower size threshold, than vesicles (Lacroix et al., 2010; Yuana et al., 2011). **(B)** Flow cytometry analysis of RBC vesicles extracted from blood before oscillatory shear (no-shear), and after being subjected to different frequencies and number of cycles of oscillatory shear. Only events positive to anti-CD235a and Annexin V were defined as RBC vesicles (Kriebardis et al., 2008). The number of calibration beads was counted to determine the absolute number of RBC vesicles. The number of cells was approximately 10^7.

for the cases of 1 cycle at 10 Hz, 10 cycles at 100 Hz and 100 cycles at 100 Hz, all with a shear rate of $\sigma = 200\text{s}^{-1}$, respectively. The number of 217 vesicles per μl of plasma is consistent with and helps confirm previous such findings, e.g., those of Willekens et al. (2003b) who reported the range 61-308 with an average of 169 vesicles per μl of plasma.

Measurements have shown that the volume rate of blood flowing through 100gms of spleen is approximately 170 ml/min/100 gms (Oguro et al., 1993). Assuming the spleen weighs, on average, 150gms and the body contains 4.5l of blood we estimate that the splenic passage rate of a typical erythrocyte is about 80 per day. However, not all these passages involve passages through the venous slits of the red pulp; in fact depending on mammalian species and degree of health versus diseased states, up to 90% of the blood flow may bypass the filtration beds of the red pulp (Schmidt et al., 1993; Cesta, 2006). Thus, the precise rate of erythrocyte passage through the venous slits is difficult to specify and here we make the assumption of 50%. Hence we arrive at an estimate for, discussion sake, of $\sim$ 40 slit transits per cell per day. We thereby envision they undergo a pulsed-like deformation with a frequency of say $\nu_f \sim \mathcal{O}(0.0005)$Hz. Hence we suggest that our lower frequency test protocols are more appropriate for studies of age induced vesiculation. Now the most severe deformation occurs within a time scale of 0.1 s. A realistic deformation protocol would thus be to subject cells to one oscillation cycle, pause for 2160s, start a second cycle, and repeat that for $\sim 40 \times 120 \sim 4,800$ times (as a cell does in typical circulation). As this may not be practical, we believe the approach we use, i.e., subject a population of cells to high frequency oscillatory flow for 1–2 s and repeat for $\mathcal{O}(10 - 100)$ cycles is an attractive, viable alternative; this is consistent with physiological deformation time scales as discussed in section 4.5. Indeed, we also suggest that lower shear rates such as $\sigma = 200 - 500\text{s}^{-1}$ be explored as we have done.

6. CONCLUDING DISCUSSION

To illustrate the versatility of our proposed methods, we revisit the discussion of section 4.1 concerning the disposition of skeletal proteins, viz. spectrin, during vesiculation. As noted there, Ciana et al. (2017b,a) have shown that cells that shed vesicles *in-vivo* lose spectrin in proportion to their loss of membrane; this makes sense given the cell's need to maintain a functional mechanical membrane/skeleton structure. Now consider the *in-vitro* experimental findings of e.g., Knowles et al. (1997) who induced vesiculation via micro-pipette aspiration. Indeed, (i) skeleton/membrane separation, (ii) membrane vesicle ejection, and (iii) skeleton retraction back into the cell, were all observed. Hence, these vesicles were indeed deficient in spectrin and we speculate also in anchoring proteins. This process was successfully simulated and explained by simulation with an earlier version of our computational models (Peng et al., 2010). In short, what we found in Peng et al. (2010) was that the deformations and their time scales cause very significant skeletal restructuring at regions of eventual vesiculation. This was due to the viscous drag of anchoring proteins (viz. band 3 and glycophorin C/JC) and results in very large ($\sim$ 80–90%) reductions in areal densities of skeleton anchoring sites. This, combined with the large disassociation stresses at the aspiration's tip, causes the membrane to "tear away," or rather "pull away," from the cell and skeleton where the latter retracts back into the cell. But we later showed that such a scenario does not occur during splenic flow due to the very different time scales and hence reductions in anchoring density must occur otherwise (Zhu et al., 2017) . That is, during *in-vivo* splenic flow, there is not time for mechanically driven reductions in anchoring density. This explains the important role our analysis parameter ℓ_0 plays in deciding the progress of vesiculation. Indeed, if ℓ_0 were very large, say $\ell_0 \gtrapprox 40 - 80$nm, as it may well be in *in-vitro* experiments, vesiculation would readily occur via a different pathway as suggested by Ciana et al. (2017b,a). Since our methods are designed to reproduce both the deformation histories, with the appropriate time scales, as occur in splenic flow, we suggest that the character of vesicles produced in oscillatory flow be examined with various degrees of membrane/skeleton disruption.

We add that as far as the effects of viscosity and viscosity ratios is concerned, that the hydrodynamic load on the cell depends on the frequency of oscillatory shear flow as well as the amplitude of the shear stress, $\eta_1\sigma$; here η_1 is the viscosity of the outside medium and σ is the amplitude of the shear flow. Numerical algorithms work more efficiently when the ratio $\eta_2/\eta_1 = 1$ with η_2 being the cell viscosity. For that reason simulations were often performed with $\eta_2/\eta_1 = 1$ with the understanding that has little effect as long as the amplitude of the shear stress, $\eta_1\sigma$, is unchanged. This correlation has been confirmed by simulations with viscosity ratios in the range $1 \leq \eta_2/\eta_1 \leq 7$. This observation is most useful when exploring a large parameter space as mentioned above. Our previous work provides much further detail as to the broader range of numerical methods (see e.g., Peng et al., 2010, 2011).

The focus herein has been on oscillatory shear flow states that produce splenic-like conditions of deformation, stress distributions around the cell, and their respective time scales. It would be of interest, however, to more systematically explore a wider range of scenarios involving various conditions of frequency, shear rate amplitude, and cell/medium viscosity. In this manner we may explore the potential effects of time scales that may allow, for example, skeletal restructuring to occur. This is a large, yet interesting, topic of future research.

The scenarios presented just above, along with all the results and analysis of section 4 support the view that vesiculation can be driven by either metabolically, or mechanically (i.e., imposed deformation), induced energetics. In either case a reduction in skeletal/bilayer binding, (i.e., aging induced reductions in γ), although not strictly required, are strongly causative influences that promote vesiculation. This view is consistent with our earlier conclusions in Zhu et al. (2017). Purely mechanically driven vesiculation is unlikely under physiological conditions since such large separating stresses are unlikely to develop. Exceptions are, for example, flow in aspiration as demonstrated by Peng et al. (2010), where we have noted the time scales as well as the severe deformations were sufficient to effectively reduce

γ by dynamically restructuring the skeleton that reduces the areal density of attachment points. However, such restructuring does not occur during splenic flow or our oscillatory flow introduced herein (Zhu et al., 2017) due to the inherently shorter time scales in these types of flow. Indeed, our modeling described in section 3 defined a key parameter, ℓ_0, that represented a membrane/skeleton area damaged by metabolic and/or biochemical means that played a strong role, if not mediated, the vesiculation process. The importance of such damaged membrane zones has been recently emphasized (Leal et al., 2018).

This view is consistent with the fact that although a given RBC transits the spleen on the order of 40 times per day, such cells only produce about 2.71 vesicles per day (Ciana et al., 2017b). *Hence vesiculation, even under conditions of large deformations, should be viewed as a rather improbable event!* An efficient way to generate vesicles systematically in laboratory conditions is to process vast number of cells simultaneously, which happens to be the advantage of our oscillatory flow device.

We have noted that the prime driving force for vesiculation in our model is ϵ_0, the skeleton's elastic energy, may be augmented by $-\Delta G_{a\to s}$, or at least by some part of it. This free energy is released upon a transition to a more symmetric lipid leaflet composition. But on the one hand, the kinetics for lipid flipping is not normally large and thus times scales are a question. Yet, as inner leaflet lipids like PS are exposed on vesicles, it appears that flipping does indeed occur during vesiculation; it is possible that the normally slow kinetics of lipid flipping is increased by membrane deformation. But this will alter the membrane energetics due to, e.g., non-local bending energy as well as through the pre-curvature energy term (Miao et al., 1994; Waugh, 1996; Lim et al., 2002; Mukhopadhyay et al., 2002; Bozic, et al.); specifically, it relates to, for example, how one assesses the terms involving ΔA_0 in the cited works. Hence, this question awaits future detailed study.

It was noted that RBCs of those affected by Scott's syndrome display a decreased rate of vesiculation (Bevers and Williamson, 2016; Bevers et al., 2017). Indeed, Rosing et al. (1985) reported that the syndrome originates from a defective scramblase activity that suppresses PS exposure on the outer membrane leaflet. Hence these observations may support the idea that a loss in lipid asymmetry may play a direct role in promoting vesiculation as suggested above and in section 4.2.

We add that our approach allows for a thorough study of the effects of not only cytosol viscosity but also medium, or plasma, viscosity that will effect the forces and deformations experienced by the cell during a given imposed flow (Williams and Morris, 1980; Chien, 1987; Tuvia et al., 1997; Pozrikidis, 2005; Freund et al., 2012; Freund, 2013; Zhu et al., 2017). Effects of altered viscosity, including plasma viscosity, have been associated with a variety of dysfunctions and disease (e.g., Késmárky et al., 2008; Sapmaz et al., 2011; Toprak et al., 2012). In general, with increased plasma viscosity deformations, and the associated ϵ_0, will be augmented and hence so will the prospect for vesiculation. Hence our approach offers novel prospects for pursuing such lines of future inquiry.

We herein introduced a novel theoretical/simulation approach to subject cells to *tailored* shear deformations that, mimic, and expand on the types of deformations that promote vesiculation (Zhu et al., 2017). This clearly suggests an experimental plan, based on these findings, that would subject erythrocytes to biochemical stress including, e.g., oxidative, nitrite (NOS), and Ca^{2+} uptake stress, *inter alia*, so as to induce "aging damage," e.g., disruptions to the cell's skeleton/bilayer membrane and to follow the resulting course of promoted vesiculation as influenced by carefully tailored modes of deformation with varying shapes and intensity. The findings presented in sections 3.1 and 4 demonstrate that such an approach is viable and would clearly provide novel insights into the aging/vesiculation process.

Finally we add that, aside from the existence of non-biological walls that typically are part of flow chambers, our methods involve no artificial structures and naturally subject large numbers of cells to our tailored deformations. We demonstrate how splenic flow induced deformations can be produced and thereby provide conditions to study events such as age induced vesiculation. Our methods may also provide a valuable compliment observations made within micro fluidic devices (e.g., Deplaine et al., 2011; Picot et al., 2015) provided these can be fabricated with splenic-like slits with dimensions $\leq$ 1.5μm and through which red cells can actually flow through and not simply become "jammed"; such behavior involves deformations and time scales quite unlike splenic flow and is hence nonrepresentative. Moreover, although of use in visualizing individual passage through even sub-micron artificial slits (Gambhire et al., 2017), micro-fluidic chambers do not naturally deal with the very large number of cells required for vital statistical studies; recall that, *in-vivo*, vesiculation is a quite rare event, occurring roughly 1 in every 15 splenic passages.

AUTHOR CONTRIBUTIONS

RA and QZ wrote the manuscript and performed the analysis and simulations. PC contributed to the experimental portions of the research.

REFERENCES

Alaarg, A., Schiffelers, R. M., van Solinge, W. W., and van Wijk, R. (2013). Red blood cell vesiculation in hereditary hrmolytic anemia. *Front. Physiol.* 4:365. doi: 10.3389/fphys.2013.00365

Alberts, B., Johnson, A., Lewis, J., Raff, M., Roberts, K., and Walter, P. (2002). *The Cell*, New York, NY: Garland Science.

Allan, D., and Mitchell, R. H. (1977). Calcium ion-dependent diacylglyerol accumulation in erythrocytes is associated with microvesiculation but not with efflux of potassium ions. *Biochem. J.* 166, 495–499.

An, X., Guo, G., and Mohandas, N. (2004b). Phosphatidylserine binding sites in red blood cell spectrin. *Blood Cells Mol. Dis.* 32, 430–432. doi: 10.1016/j.bcmd.2004.02.001

An, X., Guo, G., Sum, H., Morrow, J., Gratzer, W., and Mohandas, N. (2004a). Phosphatidylserine binding sites in erythroid spectrin: location and implications for membrane stability. *Biochemistry* 43, 310–315. doi: 10.1021/bi035653

Beleznay, Z., Zachowski, A., Devaux, P. F., Navazo, M. P., and Ott, P. (1994). ATP-dependent aminophospholipid translocation in erythrocytes vesicles-stochiometry of transport. *Biochemistry* 32, 3146–3149. doi: 10.1021/bi00063a029

Bevers E. M. and Williamson, P. L. (2016). Getting to the outer leaflet: physiology of phosphatidylserine exposure at the plama membrane. *Physiol. Rev.* 96, 605–645. doi: 10.1152/physrev.00020.2015

Bevers, E. M., Wiedmer, T., Comfurius, P., Shattil, S. J., Weiss, H. J., Zwaai, R. F. A., et al. (2017). Defective Ca^{2+}-induced microvesiculation and deficient expression of procoagulant activity in erythrocytes from a patient with a bleeding disorder: a study of the red blood cells of Scott Syndrome. *Blood* 79, 380–388.

Bevers, E. M., and Williamson, P. L. (2010). Phospholipid scramblase: an update. *FEBS Lett.* 584, 2724–2730. doi: 10.1016/j.febslet.2010.03.020

Booth A. M., Fang, Y., Fallon, J. K., Yang, J. M., Hildreth, J. E. K., and Gould, S. J. (2006). Exosomes and HIV Gag bud from endosome-like domains of the T cell plasma membrane. *J. Cell Biol.* 172, 923–935. doi: 10.1083/jcb.200508014

Bosman, G., Willekens, F. L. A., and Weere, J. M. (2012). "Erythocyte senesecence," in *Erythrocytes, phusiology and pathophysiology*, eds F. Land and M. Föller (London: Imperial College Press).

Bozic, B., Svetina, S., Žekš, B., and Waugh, E. E. (1992). Role of lamellar membrane structure in tether formation from bilayer vesicles. *Biophys. J.* 61, 963–973. doi: 10.1016/S0006-3495(92)81903-3

Bratosin, D., Estaquier, J., Petit, F., Arnoult, D., Quatannens, B., Tissier, J. P., et al. (2001). Programmed cell death in mature erythrocytes: a model for investigating death effector pathways operating in the absence of mitochondria. *Cell Death Differ.* 8, 1143–1156. doi: 10.1038/sj.cdd.4400946

Bustamante, C., Marko, J. F., Siggia, E. D., and Smith, S. (1994). Entropic elasicity of λ-phage DNA. 1994. *Science* 265, 1599–1600.

Cao, Z., Bell, J. B., Mohanty, J. G., Nagababu, E., and Rifkind, J. . (2009). Nitrite enhances hypoxic ATP synthesis and release of ATP into the vasculature: a new mechanism for nitrite-induced vesiculation. *Am. J. Physiol. Heart Circ. Physiol.* 2009, H1494–H503. doi: 10.1152/ajpheart.01233.2008

Cesta, M. F. (2006). Normal structure, function, and histology of the spleen. *Taxicol. Pathol.* 34, 455–465. doi: 10.1080/01926230600867743

Chen, L. T., and Weiss, L. (1973). The role of the sinus wall in the passage of erythrocytes through the spleen. *Blood* 41, 529–537.

Chien, S. (1987). Red cell deformability and its relevance to blood flow. *Annu. Rev. Physiol.* 49, 177–192. doi: 10.1146/annurev.ph.49.030187.001141

Chunyi, W., Yanjun, Z., and Weibo, K. (2001). The influence of calcium ions and A23187 on microrheological characteristics of erythrocytes by new model ektacytometry. *Clin. Hemorheol. Microcirc.* 24, 19–23.

Ciana, A., Achilli, C., Gaur, A., and Minetti, G. (2017b). Membrane remodeling and vesicle formation during ageing of human red blood cells. *Cell Physiol. Biochem.* 42, 1139–1152. doi: 10.1159/000478769

Ciana, A., Achilli, C., and Minetti, G. (2017a). Spectrin and other membrane-skeletal components in human red blood cells of different age. *Cell Physiol. Biochem.* 42, 1127–1138. doi: 10.1159/000478768

Daily, B., Elson, E. L., and Zahalak, G. I. (1984). Determination of the elastic compressibility modulus of the erythrocyte membrane. *Biophys. J.* 45, 671–682. doi: 10.1016/S0006-3495(84)84209-5

Dasgupta, S. K., Abdel-Monem, H., Niravath, P., Le, A., Bellera, R. V., Langlois, K., et al. (2009). Lactadherin and clearance of platelet-derived microvesicles. *Blood* 113, 1332–1339. doi: 10.1182/blood-2008-07-167148

Deplaine, G., Safeukui, I., Jeddi, F., Lacoste, F., Brousse, V., Perrot, S. et al. (2011). The sensing of poorly deformable red blood cells by the human spleen can be mimicked *in vitro*. *Blood* 117, e88–e99. doi: 10.1182/blood-2010-10-312801

Deuticke, B. (1968). Transformation and restoration of biconcave shape of human erythrocytes induced by amphiphilic agents and changes in ionic environment. *Biochem. Acta* 163, 494–500. doi: 10.1016/0005-2736(68)90078-3

Dodson, R. A., Hinds, T. R., and Vincenzi, F. F. (1987). Effects of calcium and A23187 on deformability and volume of human red blood cells. *Blood Cells* 12, 555–564.

Dröge, W. (2002). Free radicals in the physiological control of cell function. *Physiol. Rev.* 82, 47–95. doi: 10.1152/physrev.00018.2001

Dumaswala, U. J., and Greenwalt, T. J. (1984). Human erythrocytes shed exotic vesicles *in vivo*. *Transfusion* 24, 490–492. doi: 10.1046/j.1537-2995.1984.24685066807.x

Evans, E. A., Waugh, R., and Melnik, L. (1976). Elastic area compressibility modulus of red cell membrane. *Biophys. J.* 16, 585–595. doi: 10.1016/S0006-3495(76)85713-X

Fadeel B., and Xue, D. (2009). The ins and outs of phosphlipid asymmetry in the plasma membrane: roles in health and disease. *Crit. Rev. Mol. Biochem.* 44, 264–277. doi: 10.1080/10409230903193307

Fox, J. B., Austin, C. D., Boyles, J. K., and Stefen, P. K. (1990). Role of membrane in preventing the shedding of procoagulant-rich microvesicles from the platlet plasma membrane. *J. Cell Biol.* 111, 483–493. doi: 10.1083/jcb.111.2.483

Fox, J. B., Austin, C. D., Reynolds, C. C., and Stefen, P. K. (1991). Evidence that agonist-induced activation of calpain causes the shedding of procoagulant-containing microvesicles from the membrane of aggregating platelets. *J. Biol. Chem.* 266, 13289–13295.

Freund, J. (2013). The flow of red blood cells through a narrow spleen-like slit. *Phys. Fluids* 25:110807. doi: 10.1063/1.4819341

Freund, J. B., Goetz, J. G., Hill, K. L., and Vermont, J. (2012). Fluid flows in development: functions, features and biophysical principles. *Development* 139, 1229–1245. doi: 10.1242/dev.073593

Fromherz, P. (1983). Lipid-vesicle structure: size controlled by edge-active agents. *Chem. Phys. Lett.* 94, 259–266. doi: 10.1016/0009-2614(83)87083-3

Gambhire, P., Atwell, S., Iss, C., Bedeu, F., Ozerov, I., Badens, C. et al. (2017). High aspect ratio sub-micrometer channels using wet etching: application to the dynamics of red blood cell transiting through biomimetic splenic slits. *Small* 13:1700967. doi: 10.1002/smll.201700967

Giang, H., and Schick, M. (2014). How cholesterol could be drawn to the cytoplasmic leaf of the plasma membrane by phosphatidylethanolmine. *Biophys. J.* 107, 2337–2344. doi: 10.1016/j.bpj.2014.10.012

Glaser, T., Schwarz-Benmeir, N., Barnoy, S., Barak, S., Eshar, Z., and Kosower, N. S. (1994). Calpain (Ca^{2+}-dependent thiol protease) in erythrocytes of young and old individuals. *Proc. Natl. Acad. Sci. U.S.A.* 91, 7879–7883. doi: 10.1073/pnas.91.17.7879

Grzybek, M., Chorzalska, A., Bok, E., Hryniewicz-Jankowska, A., Czogalla, A., Diakowski, W., et al. (2006). Spectrin-phospholipid interactions existence of multiple binding sites? *Chem. Phys. Lipids* 141, 133–141. doi: 10.1016/j.chemphyslip.2006.02.008

György, B., Szabó, T. G., Pásztói, M., Pál, Z., Misják, P., Aradi, B., et al. (2011). Membrane vesicles, current state-of-the-art: emerging role of extracellular vesicles. *Cell Mol. Life Sci.* 68, 2667–2688. doi: 10.1007/s00018-011-0689-3

Harman, D. (2009). Origin and evolution of the free radical theory of aging: a brief personal history. *Biogerontology* 10, 773–781. doi: 10.1007/s10522-009-9234-2

Harmandaris, V. A. and Deserno, M. (2000). A novel method for mesuring the bending rigidity of model lipid membranes by simulating ththers. *J. Chem. Phys.* 125:204905. doi: 10.1063/1.2372761

Hashimoto, S. (2014). Detect of sublethal damage with cyclic deformation of erythrocyte in shear flow. *Sys. Cyb. Info.* 12, 41–46.

Hattangadi, S. M., and Lodish, H. F. (2007). Regulation of erythrocyte lifespan: do reactive oxygen species set the clock? *J. Clin. Inves.* 117980, 2075–2076. doi: 10.1172/JCI32559

Helfrich, W. (1974). The size of bilayer vesicles generated by sonification. *Phys. Lett. A* 50, 115–116. doi: 10.1016/0375-9601(74)90899-8

Horobib, J. T., Sabapathy, S., and Simmonds, M. J. (2017). Repetitive supra-physiological shrear stress impairs red blood cell deformability and induces hemolysis. *Artif. Organs* 41, 1017–1025. doi: 10.1111/aor.12890

Hu, M., Briguglio, J. J., and Deserno, M. (2012). Determining the Gaussian curvature modulus of lipid membranes in simulations. *Biophys. J.* 102, 1403–1410. doi: 10.1016/j.bpj.2012.02.013

Iuchi, Y., Okada, F., Onuma, K., Onada, T., Asao, H., and Kobayashi, M. (2007). Elevated oxidative stress in erythrocytes due to a SOD1 deficiency causes anaemia and triggers autoantibody production. *Biochem. J.* 402, 219–227. doi: 10.1042/BJ20061386

Késmárky, G., Kenyeres, P., Rabai, M., and Toth, K. (2008). Plasma viscosity: a forgotten variable. *Clin. Hemorheol. Microcirc.* 39, 243–246. doi: 10.3233/CH-2008-1088

Klarl, B., Lang, P. A., Kempe, D. S., Niemoeller, O. M., Akel, A., Sobiesiak, M., et al. (2006). Protein kinase C mediates erythrocyte "programmed cel death" following glucose depletion. *Am. J. Cell Physiol.* 290, C244–C253. doi: 10.1152/ajpcell.00283.2005

Knowles, D. W., Tilley, L., Mohandas, N., and Chasis, J. A. (1997). Erythrocyte membrane vesiculation: model for the molecular mechanism of protein sorting. *Proc. Natl. Acad. Sci. U.S.A.* 94, 12969–12974. doi: 10.1073/pnas.94.24.12969

Kostova, E. B., Beuger, B. M., Klei, T. R. L., Halonen, P., Lieftink, C., Beijersbergen, R., et al. (2015). Identification of signaling cascades involved in red blood cell shrinkage and vesiculation. *Biosci. Rep.* 35, 1–16. doi: 10.1042/BSR20150019

Kriebardis, A. G., Antonelou, M. H., Stamoulis, K. E., Economou-Petersen, E., Margaritis, L. H., and Papassideri, I. S. (2008). RBC-derived vesicles during storage: ultrastructure, protein composition, oxidation, and signaling components. *Transfusion* 48, 1943–1953. doi: 10.1111/j.1537-2995.2008.01794.x

Lacroix, R., Robert, S., Poncelet, P., and Dignat-George, F. (2010). Overcoming limitations of microparticle measurement by flow cytometry. In Seminars in thrombosis and hemostasis 36, 807–818. doi: 10.1055/s-0030-1267034

Leal, J. K. F., Adabo-Hermans, M. J. W., and Bosman, G. J. C. M. (2018). Red blood cell hemeostasis: mechanisms and effects of microvesicle generation in health and disease. *Font. Physiol.* 9:703. doi: 10.3389/fphys.2018.00703

Lee, J. C. M., and Discher, D. E. (2001). Deformation-enhanced fluctuations in the red cell skeleton with theoretical relations to elasticity, connectivity, and spectrin unfolding. *Biophys. J.* 81, 3178–3192. doi: 10.1016/S0006-3495(01)75954-1

Leverett, L. B., Hellum, J. D., Alfrey, C. P., and Lynch, E. C. (1972). Red blood cell damage by shear stress. *Biophys. J.* 12, 257–273. doi: 10.1016/S0006-3495(72)86085-5

Levin, S., and Korenstein, R. (1991). Membrane fluctuations in erythrocytes are linked to MgATP dependent dynamic assembly of the membrane skeleton. *Biophys. J.* 60, 733–737. doi: 10.1016/S0006-3495(91)82104-X

Lhermusier, T., Chap, H., and Payrastre, B. (2011). Platelet membrane phospholipid asymmetry: from the characterization of a scramblase activity to the identification of an essential protein mutated in Scott syndrome. *J. Thrombosis Haemotasis* 9: 1883–1891. doi: 10.1111/j.1538-7836.2011.04478.x

Li, F., Chan, C. U., and Ohi, C. D. (2013) Yield strength of human erythrocyte membranes to impulsive stretching. *Biophys. J.* 105, 872–879. doi: 10.1016/j.bpj.2013.06.045

Li, H., and Lykotrafitis, G. (2015). Vesiculation of healthy and defective red blood cells. *Phys. Rev. E* 92:012715-1. doi: 10.1103/PhysRevE.92.012715

Lim, G., Wortis, M., and Mukhopadhyay, R. (2002). Stomatcyte-discocyte-echinocyte sequence of the human red blood cell: evidence for the bilayer-couple hypothesis fron membrane mechanics. *Proc. Natl. Acad. Sci. U.S.A.* 99, 16766–16769. doi: 10.1073/pnas.202617299

Low, P. S., Waugh, S. M., Zinke, K., and Drenekhahn, D. (1985). The role of denaturation and band 3 clustering in red blood cell aging. *Science* 227, 531–533. doi: 10.1126/science.2578228

Lutz, H. U., Liu, S. H., and Palek, J. (1977). Release of spectrin-free vesicles from human erythrocytes during ATP depletion. *J. Cell Biol.* 73, 548–560. doi: 10.1083/jcb.73.3.548

Lux, S. E. (2015). Anatomy of the red blood cell membrane skeleton: unanswered questions. *Blood* 127, 187–199. doi: 10.1182/blood-2014-12-512772

MacDonald, I. C., Ragan, D. M., Schmidt, E. E., and Groom, A. C. (1987). Kinetics of red blood cell passage through interendothrlial slits into venous sinuses in rat spleen, aqnalyzed by *in vivo* microscopy. *Macro. Vas. Res.* 33, 118–134.

Marinkovic, D., Zhang, X., Yalcin, S., Luciano, J . P., Brugnara, C., Huber, T., et al. (2007). Foxo3 is required for the regulation of oxidative stress in erythropoiesis. *J. Clin. Inves*. 117, 2133–2144. doi: 10.1172/JCI31807

McNamee, A. P., Tansley, G. D., Sabapathy, S., and Simmonds, M. J. (2016). Biphasic impairment of erythrocyte deformability in response to repeated, short duration exposures of supraphysiological subhaemolytic shear stress. *Biorheology* 53, 137–149. doi: 10.3233/BIR-15108

Mebius, R., and Kraal, G. (2005). Structure and function of the spleen. *Nat. Rev.* 5, 606–616. doi: 10.1038/nri1669

Meram, E., Yilmaz, B. D., Bas, C., Atac, N., and Yalcin, O. (2013). Shear stress-induced improvement of red blood cell deformability. *Bioreheology* 50, 165–176. doi: 10.3233/BIR-130637

Miao, L., Seifert, U., Wortis, M., and Dŏbereiner, H. G. (1994). Budding transitions of fluid-bilayer vesicles: the effect of area-difference elasticity. *Phys. Rev. E* 49, 5289–5407. doi: 10.1103/PhysRevE.49.5389

Mohandas, N., and Gallager, P. G. (2008). Red cell membrane: past, present, and future. *Blood* 112, 3939-3948. doi: 10.1182/blood-2008-07-161166

Mohandas, N. E., and Evans, E. (1994). Mechanical properties of the red cell membrane in relation to molecular structure and genetic defects. *Annu. Rev. Biophys. Biomol. Struct.* 23, 787–818. doi: 10.1146/annurev.bb.23.060194.004035

Mohanty, J. G., Nagababu, E., and Rifkind, J. M. (2014). Red blood cell oxidative stress inpairs oxygen delivery and induces red blood cell againg. *Font. Physiol.* 5:84. doi: 10.3389/fphys.2014.00084

Morel, O., Jessel, L., Freyssinet, J. M., and Toti, F. (2010). Cellular mechanisms underlying the formation of circulating microparticles. *Arterioscler. Thromb. Vasc. Biol.* 31, 15–36. doi: 10.1161/ATVBAHA.109.200956

Mukhopadhyay, R., Lim, G., and Wortis, M. (2002). Echincyte shapes: bending, stretching, and shear determine spicule shape and spacing. *Biophys. J.* 82, 1756–1772. doi: 10.1016/S0006-3495(02)75527-6

Nagababu, E., and Rifkind, J. M. (2000). Reaction of hydrogen peroxide with ferrymemoglobin: superoxide production and heme degradation. *Biochemistry* 39, 12503–12511. doi: 10.1021/bi992170y

Oguro, A., Taniguchi, H., Tanaka, H., Miyata, K., Inaba, T., Nakahashi, H., et al. (1993). *Ann. Nucl. Med.* 7, 245–250. doi: 10.1007/BF03164705

Pandey, K. B., and Rizvi, S. I. (2010). Markers of oxidative stress in reythrocytes and plasma during aging in humans. *Oxidative Med. Cell. Longevity* 3, 2–12. doi: 10.4161/oxim.3.1.10476

Pandey, K. B., and Rizvi, S. I. (2011). Biomarkers of oxidative stress in red blood cells. *Biomed. Pap. Med. Fac. Univ. Palacky Czeh. Rep*. 155, 131–136. doi: 10.5507/bp.2011.027

Pasquet, J. M., Dachary-Prigent, J., and Nurden, A. T. (1996). Calcium influx is a determining factor of calpain activation and microparticle formation in platelets. *Eur. J. Biochem.* 239, 647–654. doi: 10.1111/j.1432-1033.1996.0647u.x

Peng, Z, Asaro, R. J., and Zhu, Q. (2011). Multiscale modeling of erythrocytes in Stokes flow. *J. Fluid Mech.* 686, 299–337. doi: 10.1017/jfm.2011.332

Peng, Z., Asaro, R. J., and Zhu, Q. (2010). Multiscale simulation of erythrocyte membrane. *Phys. Rev. E.* 81:031904. doi: 10.1103/PhysRevE.81.031904

Peng, Z., and Zhu, Q. (2013). Deformation of the erythrocyte cytoskeleton in tank treading motions. *Soft Matter.* 9, 7617–7627. doi: 10.1039/c3sm50895a

Picot, J., Ndour, P. A., Lefevre, S. D., El Nemer, W., Tawfik, H., Galimand, J., et al. (2015). A biomimetric microfluidic chip to study the circulation and mechanical retention of red blood cells in the spleen. *Am. J. Hematol.* 90, 339–345. doi: 10.1002/ajh.23941

Pozrikidis, C. (1992). *Boundary Integral and Singularity Methods for Linearized Viscous Flow*. New York, NY: Cambridge University Press.

Pozrikidis, C. (2005). Axisymmetric motion of a file of red blood cells through capillaries. *Phys. Fluids* 17:031503. doi: 10.1063/1.1830484

Raposo, G., and Stoorvogel, W. (2012). Extracellular vesicles: exosomes, microvesicles and friends. *J. Cell Biol.* 200, 373–383. doi: 10.1083/jcb.201211138

Rattan, S. I. S. (2006). Theories of aging: genes, proteins and free radicals. *Free Radical Res.* 40, 1230–1238. doi: 10.1080/10715760600911303

Rifkind, J. M., and Nagababu, E. (2013). Hemoglobin redsox reactions and red blood cell aging. *Antioxid. Redox Signal.* 18, 2274–2283. doi: 10.1089/ars.2012.4867

Rosing, J., Bevers, E. M., Comfurius, P., Hemker, H. C., van Dieijen, G., Weiss, H. J., et al. (1985). Impaired factor X and prothrombin activation associated with decreased phospholipid exposure in platelets from a patient with a bleeding disorder. *Blood* 65, 1557–1561.

Salehyar, S., and Zhu, Q. (2016). Deformation and internal stress in a red blood cell as it is driven through a slit by an incoming flow. *Soft Matter.* 12, 3156–3164. doi: 10.1039/c5sm02933c

Sandza, J. G., Clark, R. E., Weldon, C. S., and Sutera, S. P. (1974). subhemolytic trauma of erythrocytes; recognition and sequestration by the spleen as a function of shear. *Trans. Am. Soc. Artif. Organs* 2, 457–462.

Sapmaz, T., Saba, C., Haberal, A., Toktamis, M., Cakmak, and Cicek, D. (2011). Fibriogen-albumin ratio: an intriguing relationship for assessing trombosis risk and suspicious effect on blood viscosity. *Int. Cardiovasc. Res. J.* 5, 153–154. doi: 10.5812/icrj.4418

Schmidt, E. E., MacDonald, I. C., and Groom, A. C. (1993). Comparative aspects of splenic microcirculatory pathways in mammals: the region boardering the white pulp. *Scanning Miscrosc.* 7, 613–628.

Schwarz-Ben Meir, N., Glazer, T., and Kosower, N. S. (1991). Band 3 protein degradation by calpain is enhanced in erythrocytes of old people. *Biochem. J.* 275, 47–52. doi: 10.1042/bj2750047

Sheetz, M. P., and Singer, S. J. (1974). Biological membranes as bilayer couples. a molecular mechanism of drug-erythrocyte interactions. *Proc. Natl. Acad. Sci. U.S.A.* 71, 4457–4461. doi: 10.1073/pnas.71.11.4457

Shen, B. W., Josephs, R., and Steck, T. L. (1986). Ultrastructure of the intact skeleton of the human erythrocyte membrane. *J. Cell Biol.* 102, 997–1006. doi: 10.1083/jcb.102.3.997

Snyder, L. M., Fairbanks, G., Trainor, J., Fortier, N. L., Jacobs, J. B., Leb, L. et al. (1985). Properties and characterization of vesicles released by young and old human red cells. *Br. J. Haematol.* 59, 513–522. doi: 10.1111/j.1365-2141.1985.tb07338.x

Sutera, S. P. (1977). Flow-induced trauma to blood cells. *Circ. Res.* 41, 2–8.

Sutera, S. P., and Mehrjardi, M. H. (1975). Deformation and fragmentation of human RBC in turbulent shear slow. *Biophys. J.* 15, 1–10. doi: 10.1016/S0006-3495(75)85787-0

Toprak, S. K., Tek, I., Krakus, S., Gok, N., and Karson, N. (2012). Demir eksikliği gorulen reaktif trombositoz plazma viskozitesini etkilermi? *Turk. J. Hematol.* 29, 248–253. doi: 10.5505/tjh.2012.13008

Truvia, S., Levin. S., Bitler, A., and Korenstein, R. (1998). Mechanical fluctuations of the membrane-skeleton are dependent on F-actin ATPases in human erythrocytes. *J. Cell Biol.* 141, 1551–1561. doi: 10.1083/jcb.141.7.1551

Tsuda, K. (2010). Oxidative Stress and Membrane Fluidity of Red Blood Cells in Hypertensive and Normotensive Men An Electron Spin Resonance Investigation. *Int. Heart J.* 51.2, 21–124. doi: 10.1536/ihj.51.121

Tuvia, S., Almagor, A., Bitler, A., Levin, S., Korenstein, R., and Yedgar, S. (1997). Cell membrane fluctuations are regulated by medium macroviscosity: evidence for a metabolic driving force. *Proc. Natl. Acad. Sci. U.S.A.* 94, 5045–5049.

Vertessy, B. G., and Steck, T. L. (1989). Elasticity of the human red cell membrane skeleton: effects of temperature and denaturants. *Biophys. J.* 55, 255–262.

Wantanbe, N., Arakawa, Y., Sou, A., Kataoka, H., Ohuchi, K., Fujimoto, T., et al. (2007). Deformability of human red blood cells exposed to a uniform shear stress as measured by a cyclically reversing shear flow generator. *Physiol. Meas.* 28, 531–545. doi: 10.1088/0967-3334/28/5/007

Watanabe, N., Kataoka, H., Yasuda, T., and Takatani, S. (2006). Dynamic deformation and recovery response of red blood cells to a cyclically reversing shear flow: effects of frequency of cyclically reversing shear flow and shear stress level. *Biophys. J.* 91, 1984–1998. doi: 10.1529/biophysj.105.060236

Waugh, R. (1996). Elastic energy of curvature-driven bump formation on red blood cell membrane. *Biophys. J.* 70, 1027–1035. doi: 10.1016/S0006-3495(96)79648-0

Weiner, J. H. (1983). *Statistical Mechanics of Elasticity.* Mineola, NY: Dover.

White, S. H., and King, G. I. (1985). Molecular packing and area compressibility of lipid bilayers. *Proc. Natl. Acad. Sci. U.S.A.* 82, 6532–6536.

Wieschhaus, A., Kahn, A., Zaidi, A., Rogalin, H., Hanada, T., Liu, F., et al. (2012). Calpain-1 knockout reveals broad effects on erythrocyte deformability and physiology. *Biochem. J.* 448, 141–152. doi: 10.1042/BJ20121008

Willekens, F. L. A, B., Bregt-Roerdinkholder, Y. A., Groenen-döpp, H. J., Bos, G., JCGM Bosman, A. G., van den Bos, A. J., et al. (2003a). Haemoglobin loss from erythrocytes *in vivo* results from spleen-facilitated vesiculation. *Blood* 101, 747–751. doi: 10.1182/blood-2002-02-0500

Willekens, F. L. A., Werre, J. M., Groenen-Döpp, Y. A. M., Roerdinkholder-Stoelwinder, B., de Pauw, B., and Bosman,G. J. (2003b). Erythrocyte vesiculation: a self-protective mechanism? *Br. J. Haematol.* 141, 549–556. doi: 10.1111/j.1365-2141.2008.07055.x

Williams, A. R., and Morris, D. R. (1980). The internal viscosity of the human erythrocyte may determine its lifespan *in vivo*. *Scand. J. Haematol.* 24, 57–62. doi: 10.1111/j.1600-0609.1980.tb01318.x

Yuana, Y., Bertina, R. M., and Osanto, S. (2011). Pre-analytical and analytical issues in the analysis of blood microparticles. *Thromb. Haemost.* 106, 396–408. doi: 10.1160/TH10-09-0595

Zachowski, A. (1993). Phospholipids in animal eukaryotic membranes. transverse asymmetry and movement. *Biochem. J.* 294, 1–14.

Zhao, H., Isfahania, A., Olsonc, L., and Freund, J. (2010). A spectral boundary integral method for flowing blood cells. *J. Comput. Phys.* 229, 3726–3744. doi: 10.1016/j.jcp.2010.01.024

Zhu, Q., and Asaro, R. (2008). Spectrin folding *vs*. unfolding reactions and RBC membrane stiffness. *Biophys. J.* 94, 2529–2545. doi: 10.1529/biophysj.107.119438

Zhu, Q., Salehyar, S., Cabrales, P., and Asaro, R. J. (2017). Prospects for human erythrocyte skeleton-bilayer dissociation during splenic flow. *Biophys. J.* 113, 900–912. doi: 10.1016/j.bpj.2017.05.052

Zhu, Q., Vera, C., Asaro, R., Sche, P., and Sung, L. A. (2007). A hybrid model for erythrocyte membrane: a single unit of protein network coupled with lipid bilayer. *Biophys. J.* 93, 386–400. doi: 10.1529/biophysj.106.094383

Zwaal, R. F. and Schroit, A. J. (1997). Pathophysiologic implications of membrane asymmetry in blood cells. *Blood* 89, 1121–1132.

Conflict of Interest Statement: The authors declare that the research was conducted in the absence of any commercial or financial relationships that could be construed as a potential conflict of interest.

APPENDIX

Mathematical Formulation for Fluid-Cell Interactions

The fluid-cell interaction is mathematically formulated within a low-Reynolds number Stokes/Oseen flow (Pozrikidis, 1992) so that at any point $\mathbf{x}_0$ on the surface of the cell ($\mathbf{x}_0 \in \Gamma_c$) the velocity $\mathbf{v}$ is given as

$$\begin{aligned}\mathbf{v}(\mathbf{x}_0) = & \frac{2}{1+\Lambda}\bar{\mathbf{v}}(\mathbf{x}_0) \\ & - \frac{1}{4\pi\eta_1(\Lambda+1)}\iint_{\Gamma_c}\mathbf{G}(\mathbf{x},\mathbf{x}_0)\cdot\Delta\mathbf{t}(\mathbf{x})d\Gamma(\mathbf{x}) \\ & + \frac{1-\Lambda}{4\pi(1+\Lambda)}\text{⨍⨍}_{\Gamma_c}\mathbf{v}(\mathbf{x})\cdot\mathbf{T}(\mathbf{x},\mathbf{x}_0)\cdot\mathbf{n}(\mathbf{x})d\Gamma(\mathbf{x}), \quad \text{(A1)}\end{aligned}$$

where $\bar{\mathbf{v}}$ is the undisturbed flow velocity. The viscosity ratio $\Lambda \equiv \eta_2/\eta_1$ (η_1 and η_2 are the viscosities of the external fluid and the internal fluid, respectively). $\Delta\mathbf{t}$ is the difference between the traction in the outside surface of the cell membrane and the traction in the inside surface of the membrane. ⨍⨍ denotes the principal value integration. The matrix $\mathbf{G}$ contains the Green's function for velocity G_{ij}, and the matrix $\mathbf{T}$ contains the Green's function for stress T_{ijk}. We have

$$G_{ij}(\mathbf{x},\mathbf{x}_0) = \frac{\delta_{ij}}{|\mathbf{x}-\mathbf{x}_0|} + \frac{(x_i - x_{0_i})(x_j - x_{0_j})}{|\mathbf{x}-\mathbf{x}_0|^3}, \quad \text{(A2)}$$

and

$$T_{ijk}(\mathbf{x},\mathbf{x}_0) = -6\frac{(x_i - x_{0_i})(x_j - x_{0_j})(x_k - x_{0_k})}{|\mathbf{x}-\mathbf{x}_0|^5}, \quad \text{(A3)}$$

where δ_{ij} is Kronecker's delta.

In this study $\bar{\mathbf{v}}$ is chosen to be a linear shear flow with zero velocity at the centroid of the cell. The shear rate of this flow varies sinusoidally in time with amplitude σ. Numerically, Equation A1 is solved with a boundary-element approach (Peng et al., 2011). By discretizing the cell surface into quadruple elements, Equation A1 is rewritten as

$$\mathsf{v} = \bar{\mathsf{v}}_c - \mathsf{S}_{cc}\mathsf{q}_c + \mathsf{D}_{cc}\mathsf{v}, \quad \text{(A4)}$$

where the global velocity vector v includes velocities at all collocation points on the cell surface and $\bar{\mathsf{v}}_c$ contains the undisturbed velocities at these points. The matrices S_{cc} and D_{cc} are influence matrices representing the second term and the third term on the righthand side of Equation A1, respectively. In general cases, an iterative algorithm is applied to solve Equation A1. In the special case when $\Lambda = 1$, however, the term $\mathsf{D}_{cc}\mathsf{v}$ vanishes so that no iteration is needed and the computational efficiency is greatly enhanced.

We use 6,000 boundary elements on the cell surface, which guarantee numerical stability and accuracy even in cases with extreme cell deformations such as infolding (Peng and Zhu, 2013; Salehyar and Zhu, 2016; Zhu et al., 2017) (indeed, in most cases a coarser mesh with 2,000 elements is sufficient for accuracy but it may lead to instability in scenarios with large membrane curvature). With a time step of 3×10^{-6} second it takes a few hours to run the time integration up to 1 second in a 2.4 GHz workstation with 8 processors.

A modified version of Equation A1 (Zhao et al., 2010) was applied to solve the splenic flow problem demonstrated in **Figure 3A**. That version involves solid boundaries, where no-slip/no-flux boundary conditions are imposed. Besides, the configuration shown in **Figure 3A** is periodic in all three directions so that different forms of Green's functions (G_{ij} and T_{ijk}) are used (Salehyar and Zhu, 2016).

frontiers in Physiology

ORIGINAL RESEARCH
published: 04 April 2019
doi: 10.3389/fphys.2019.00281

Dexamethasone Predisposes Human Erythroblasts Toward Impaired Lipid Metabolism and Renders Their *ex vivo* Expansion Highly Dependent on Plasma Lipoproteins

*Maria Zingariello[1], Claudio Bardelli[2], Laura Sancillo[1], Fiorella Ciaffoni[3], Maria Luisa Genova[2], Gabriella Girelli[4] and Anna Rita Migliaccio[2]**

[1] Unit of Microscopic and Ultrastructural Anatomy, Department of Medicine, University Campus Bio-Medico, Rome, Italy, [2] Department of Biomedical and NeuroMotor Sciences, Alma Mater Studiorum University, Bologna, Italy, [3] Core Facilities – Istituto Superiore di Sanità, Rome, Italy, [4] Centro Trasfusionale, Sapienza University of Rome, Rome, Italy

Cultures of stem cells from discarded sources supplemented with dexamethasone, a synthetic glucocorticoid receptor agonist, generate cultured red blood cells (cRBCs) in numbers sufficient for transfusion. According to the literature, however, erythroblasts generated with dexamethasone exhibit low enucleation rates giving rise to cRBCs that survive poorly *in vivo*. The knowledge that the glucocorticoid receptor regulates lipid metabolism and that lipid composition dictates the fragility of the plasma membrane suggests that insufficient lipid bioavailability restrains generation of cRBCs. To test this hypothesis, we first compared the expression profiling of erythroblasts generated with or without dexamethasone. This analysis revealed differences in expression of 55 genes, 6 of which encoding proteins involved in lipid metabolism. These were represented by genes encoding the mitochondrial proteins 3-Hydroxymethyl-3-Methylglutaryl-CoA lyase, upregulated, and 3-Oxoacid CoA-Transferase1 and glycerol-3-phosphate acyltransferase1, both downregulated, and the proteins ATP-binding cassette transporter1 and Hydroxysteroid-17-Beta-Dehydrogenase7, upregulated, and cAMP-dependent protein kinase catalytic subunit beta, downregulated. This profiling predicts that dexamethasone, possibly by interfering with mitochondrial functions, impairs the intrinsic lipid metabolism making the synthesis of the plasma membrane of erythroid cells depend on lipid-uptake from external sources. Optical and electron microscopy analyses confirmed that the mitochondria of erythroblasts generated with dexamethasone are abnormal and that their plasma membranes present pebbles associated with membrane ruptures releasing exosomes and micro-vesicles. These results indicate that the lipid supplements of media currently available are not adequate for cRBCs. To identify better lipid supplements, we determined the number of erythroblasts generated in synthetic media supplemented with either currently used liposomes or with lipoproteins purified from human plasma [the total lipoprotein fraction (TL) or its high (HDL), low (LDL) and very low (VLDL) density lipoprotein components]. Both LDL and VLDL generated numbers of erythroid cells 3-2-fold greater than that observed in controls. These greater numbers were associated with 2–3-fold greater

OPEN ACCESS

Edited by:
Giampaolo Minetti, University of Pavia, Italy

Reviewed by:
Marieke Von Lindern, Sanquin Research, Netherlands
Asya Makhro, University of Zurich, Switzerland

***Correspondence:**
Anna Rita Migliaccio
annarita.migliaccio@unibo.it;
annarita.migliaccio@mssm.edu

Specialty section:
This article was submitted to Red Blood Cell Physiology, a section of the journal Frontiers in Physiology

Received: *25 January 2019*
Accepted: *04 March 2019*
Published: *04 April 2019*

Citation:
Zingariello M, Bardelli C, Sancillo L, Ciaffoni F, Genova ML, Girelli G and Migliaccio AR (2019) Dexamethasone Predisposes Human Erythroblasts Toward Impaired Lipid Metabolism and Renders Their ex vivo Expansion Highly Dependent on Plasma Lipoproteins. Front. Physiol. 10:281. doi: 10.3389/fphys.2019.00281

amplification of erythroid cells due both to increased proliferation and to resistance to stress-induced death. In conclusion, dexamethasone impairs lipid metabolism making *ex vivo* expansion of erythroid cells highly dependent on lipid absorbed from external sources and the use of LDL and VLDL as lipid supplements improves the generation of cRBCs.

Keywords: erythropoiesis, lipid metabolism, dexamethasone, *ex vivo* expansion, transfusion products

INTRODUCTION

The progress recently made in the development of culture conditions that allow generating great numbers of cultured red blood cells (cRBCs) from discarded stem cell sources is prompting numerous studies aimed to validate these cells as alternative transfusion products (Anstee et al., 2012; Bouhassira, 2012; Migliaccio et al., 2012). Several investigators are currently addressing the numerous challenges encountered in bringing cRBCs into the clinic. The proof-of-principle in animal models was provided in 2008 by the Nakamura laboratory which indicated that transfusion of *ex vivo* generated erythroblasts protects mice from lethal hemolytic anemia (Hiroyama et al., 2008). Giarratana et al. (2011) provided the first proof-of-concept in man by demonstrating that autologous cRBCs generated from mobilized $CD34^{pos}$ cells survive for approximately 30 days *in vivo*. The Douay study also defined good manufacturing practice (GMP) conditions and minimal safety criteria of cRBCs for transfusion (Giarratana et al., 2011; Clinicaltrials.gov, 2012). Additional steps forward were represented by the demonstration that these cells express normal levels of blood group antigens and remain viable after cryopreservation for at least 8 years. Furthermore, these cells may also be generated from discarded buffy coats from blood donations with rare blood phenotypes collected under GMP conditions using media composed by clinical grade reagents of human origin and may be exchanged among laboratories across countries without loss of viability (reviewed in Zeuner et al., 2012).

The development of culture conditions allowing generating great numbers of cRBCs was pioneered by Dr. Fibach who was the first to divide the cultures into two phases (Fibach et al., 1989): the first phase (proliferation) induces hematopoietic stem/progenitor cells to generate morphologically recognizable erythroblasts; the second phase maturation sustains terminal maturation and enucleation generating cRBCs. The two phases are promoted by two different sets of stimuli. In the first phase, the signaling supporting more efficiently proliferation mimics stress erythropoiesis. These conditions were devised by exploiting the knowledge that, *in vivo*, recovery from acute anemia requires activation of the stress pathway controlled by the glucocorticoid receptor that confers to erythroid progenitors the ability to self-replicate (von Lindern et al., 1999; Dolznig et al., 2006; Zhang et al., 2013). Cultures that mimic the stress pathway are therefore stimulated with hematopoietic cytokines (stem cell factor, SCF; interleukin-3, IL-3; and erythropoietin, EPO) in combination with synthetic agonists of the glucocorticoid receptor (either hydrocortisone or dexamethasone, Dex) (Migliaccio et al., 2002; Giarratana et al., 2005; Leberbauer et al., 2005). Maturation is scanty in proliferation cultures. To promote maturation, cells generated after 12–15 days of proliferation cultures are transferred to the second phase culture stimulated with EPO where the cells mature in 7–10 days.

For reasons only partially known, erythroblasts generated with Dex mature in great numbers *in vivo* when transfused into immune-deficient hosts but enucleate with low efficiency when transferred in maturation cultures (Neildez-Nguyen et al., 2002). This challenge was first addressed by the discovery that maturation of erythroblasts into cRBCs is greatly improved by the presence of a feeder layer (Neildez-Nguyen et al., 2002). Since the feeder cells are often of animal original, these conditions are poorly suited for production of clinical grade products. Following studies discovered that feeder cells may be replaced by mifepristone, an antagonist of the glucocorticoid receptor, and plasmanate, a clinical grade derivative of human plasma (Miharada et al., 2006). In addition, enucleation rates may be further improved, reaching approximately 90%, by supplementing the maturation cultures with unfractionated human plasma and thyroid hormone (van den Akker et al., 2010; Masiello et al., 2013). These observations suggest that enucleation *in vitro* is promoted by inhibition of the glucocorticoid receptor signaling, activation of signaling from the thyroid hormone receptor and by components still to be identified present in human plasma. While genetic studies in mice have clarified that the thyroid hormone receptor exerts a pivotal role in the regulation of terminal erythroid maturation (Tanabe et al., 2007), the roles exerted in this process by the glucocorticoid receptor and by human plasma are still poorly understood.

The observation that survival of cRBCs *in vivo* (30 days) is inferior to that expected for young cells (120 days) (Giarratana et al., 2011) suggests that even under the best enucleation conditions developed up to now, cRBCs are fragile. Since the fragility of RBCs is greatly dependent on the physical-chemical properties of their plasma membrane, including fluidity, which are in turn regulated by its lipid composition (Brewer, 1980; An and Mohandas, 2008; Pollet et al., 2018), we hypothesized that the presence of Dex impairs the lipid metabolism of erythroid cells making the biosynthesis of their membranes extremely dependent on lipid uptake from lipoproteins present in human plasma and supplemented in the culture medium.

The plasma membrane of erythroid cells, as that of all the other cell types, consists of a lipid-bilayer attached to the cytoskeleton by integral membrane proteins (Mohandas and Gallagher, 2008). Approximately half of the mass of a RBC is represented by lipids (primarily phospholipids and non-esterified cholesterol) the balanced composition of which has been demonstrated to

confer resistance to sheer stress in the circulation (Brewer, 1980; An and Mohandas, 2008; Pollet et al., 2018). *In vivo*, erythroblasts obtain their lipids either by biosynthesis or by absorption from their natural carriers, the circulating lipoproteins, present in plasma (van den Broek et al., 2017). In culture, erythroblasts may synthesize their lipids from fatty acids carried by albumin and absorb lipids by uptake either from lipoproteins present in fetal bovine serum (FBS) or from synthetic liposomes composed by bovine or human albumin, egg cholesterol and soybean lecithin (Migliaccio and Migliaccio, 1987). Therefore, the lipid composition, and integrity, of the plasma membrane of cultured erythroblasts depends both on the efficiency of the intrinsic cell biosynthetic pathways of the cell and on the presence in the media of lipid carriers suited for optimal absorption (Huang et al., 2018). To a surprise, in spite of the well-established effects exerted by glucocorticoids on lipid metabolism in other systems (Patel et al., 2014), studies to clarify lipid metabolism in erythroid cells and how it is affected by glucocorticoid receptor agonists are scanty.

The "research question" of this study was to clarify the effects exerted by lipid supplements during all the stages of erythroid maturation from progenitor cells down to mature cells using multiple end-points. The aim of this question was to formulate a culture media containing lipid supplements designed for erythroid cells. We hypothesized that the use of this media would allow generating greater numbers of human erythroblasts in proliferation culture. These erythroblasts would also have greater potential for terminal maturation. To address this research question, we first compared the expression profiling of erythroblasts generated with and without Dex. Next we evaluated the morphology of the plasma membranes and of the mitochondria of proerythroblasts generated with Dex and lastly we performed a comprehensive analysis of the effects exerted by various lipid supplements on the number and quality of the erythroid cells generated in culture. The results obtained indicate that Dex impairs the metabolism and membrane homeostasis of the erythroblasts making their expansion and maturation exquisitely dependent from lipids uptake from exogenous sources.

MATERIALS AND METHODS

Human Specimens and Cell Preparation

Plasma and buffy-coats from whole blood donations were discarded material provided from Centro Trasfusionale, University of La Sapienza to be used in experiments performed at Istituto Superiore Sanità. The consent form of the Centro Trasfusionale includes consent to the use of the donation for research. Since specimens were provided as de-identified material, the study was considered non-human subject research by the ethical committee of Istituto Superiore Sanità. Buffy-coats were subjected to mononuclear cell (MNC) separation by Ficoll-Paque (Sigma, St. Louis, MO, United States) centrifugation, cryopreserved in Iscove's modified Dulbecco's medium (IMDM, Gibco-Invitrogen, Carlsbad, CA, United States), FBS (50% vol/vol, Sigma) and dimethylsulphoxide (10% vol/vol, Sigma) and stored in liquid nitrogen.

Purification of Lipoproteins From Human Plasma

Plasma pools of normolipidemic donors were separated into total (TL), high-density (HDL), low-density (LDL) and very low-density (VLDL) lipoprotein fractions by flotation in a series of three centrifugations in which the density (ρ) of the plasma was progressively increased by adding powder KBr according to the procedure established by Havel et al. (1955) (**Supplementary Figure S1A**). The amount of KBr to be added was calculated using the Radding and Steinberg formula (Radding and Steinberg, 1960):

$$X_{KBr} = \frac{V \times (\rho_f - \rho_i)}{1 - 0.312 \times \rho_f}$$

where:

X_{KBr} = amount of KBr in grams

V = volume of plasma sample in mL

ρ_f = final (desired) density to which the solution is to be adjusted

ρ_i = initial density of the solution to be adjusted

the numerical factor 0.312 = partial specific volume of KBr.

Briefly, plasma was divided into two aliquots, one of which was brought to ρ = 1.21g/mL, then centrifuged. The top fraction, containing TL, was collected while the bottom one discarded. The second plasma aliquot was centrifuged without addition of KBr. In this case, the top fraction, containing the VLDL, was stored while the bottom one was brought to ρ = 1.063 g/mL and centrifuged again. The top fraction of this second centrifugation, containing the LDL, was stored while the bottom one was brought to ρ = 1.21 g/mL and centrifuged again. The top fraction of this third centrifugation, containing the HDL, was stored while the bottom one was discarded. All centrifugations were performed at 40,000 rpm (Beckman L-70 ultracentrifuge, 60-TI rotor), at 8°C for 18 h. The fractions were made tissue culture grade by two sequential dialyses, one against H_2O (to remove KBr) and the other one against Iscove Modified Dulbecco's Medium (IMDM) (to balance their osmolarity), sterilized by filtration through a 0.45 μm filter and stored at −20°C. Possible lipid and protein losses induced by the dialysis and filtration processes were documented by determining the protein and lipid content of the tissue culture grade fractions. Quantitative analysis of the apolipoprotein composition of the individual lipoprotein fractions was performed by gel electrophoresis followed by Coomassie or Silver staining (Thermo Scientific, Rockford, IL, United States) (**Supplementary Figure S1B**) and densitometric scanning (**Supplementary Figure S1C**) (Chapman, 1986). Cholesterol and triglycerides were determined by commercially available enzymatic assays (cat. R1120 and R1373, BPC BioSed srl, Castelnuovo di Porto, Italy). The extent of loss was calculated by comparing the apoprotein/lipid enrichment ratio of each fraction with that reported in the literature (**Supplementary Table S2**) (Chapman, 1986). Although, as predicted, the composition of the tissue culture grade fractions is significantly different from that predicted by the literature, some specificity in protein and lipid composition was observed. In particular, Fraction 1 (i.e., purified VLDL) is rich in Apolipoprotein (Apo) B100, A1

and C1-3 and expresses a cholesterol/triglyceride ratio of 0.36. Fraction 2 (purified LDL) contains ApoB100 with traces of A1, A2, and C2-3, shows a protein/lipid ratio of 4.5 and contains approximately three times more cholesterol than triglycerides (cholesterol/triglycerides ratios = 2.83). Fraction 3 (purified HDL) contains ApoB100, A4, A1, A2, C1 and traces of E and human serum albumin (HSA). The cholesterol/triglycerid ratio of this fraction is similar to that of Fraction 2 (2.5 vs. 2.8).

Ex vivo Expansion of Human Erythroblasts

MNC (10^6 cells/mL) were cultured under human erythroid massive amplification (HEMA) conditions in the presence of human SCF (10 ng/mL, Amgen, Thousand Oaks, CA, United States), EPO (3 U/mL, Janssen, Raritan, NJ, United States), IL-3 (1 ng/mL, PeproTech, Rocky Hill, NJ, United States), Dex and estradiol (both 10^{-6}M, Sigma Aldrich, Saint Luis, MO, United States). The culture media was represented by IMDM supplemented with either FBS ($HEMA^{ser}$) (Migliaccio et al., 2002), or clinical grade components mostly of human origin ($HEMA^{def}$) (Migliaccio et al., 2010) (**Supplementary Figure S2**). The components of $HEMA^{def}$ are deionized HSA (10% v/v, Baxter International Inc., Deerfield, IL, United States), human iron saturated transferrin (TRF), recombinant human insulin (Merck KGaA, Darmstadt, Germany), β-mercaptoethanol, sodium pyruvate, nucleosides, trace elements and L-glutamine (all from Sigma-Aldrich). Sources of lipids were represented by either home-made (HM) liposomes composed by HSA, cholesterol (400 μg/mL, Cat. No. C3045, Sigma-Aldrich) and soybean lecithin (1.2 mg/mL, Cat. No. P3644, Sigma-Aldrich), or culture-grade lipids from commercial sources or lipoprotein fractions purified from human plasma described above. The commercial lipids investigated were: A: Lipids Cholesterol Rich from adult bovine serum (Cat. L-4646); B: Fatty Acid Supplement (Cat F7050); C: Lipid Mixture (Cat. L-0288) (all from Sigma-Aldrich), D: Chemically defined Lipid Concentrate (Cat. 11905-031, Gibco Invitrogen, Carlsbad, CA, United States) and E: commercial tissue culture grade LDL (Cat. LP2-2MG, Sigma). LDL-Sigma contain more lipids (78–80% vs. 18%) but less proteins (22–20% vs. 82%) than HM-LDL (**Supplementary Table S3**). Cultures were incubated at 37°C in a fully humidified 5% CO_2 atmosphere and the cells analyzed every 2–4 days up to days 18 of culture. A list of the end-points analyzed in this study and their biological implications is provided in **Supplementary Table S1**.

Determinations of Cell Numbers, Viability and Phenotype

Cell numbers and viability were determined by microscopic evaluation of cells stained with trypan blue (Boston Bioproducts, Ashland, MA, United States) in a Burker chamber. The maturation state was assessed by flow cytometry on the basis of CD235a (glycophorin A) and CD36 (the thrombospondin receptor) expression using the phycoerythrin (PE)–conjugated CD36 and allophycocyanin (APC)-conjugated CD235a antibodies, or appropriate isotype controls (all from BD-Pharmigen, San Diego, CA, United States) (Migliaccio et al., 2011). Maturation stages were confirmed by visual examination of cytocentrifuged smears (Cytospin 3, Shandon, Astmoor, United Kingdom) (Chapman, 1986). Dead cells were excluded by Sytox Blue staining (0.002 mM, Molecular Probes). Fluorescence was measured with a FACS Aria and data were analyzed with the FlowJo software (Tree Star, Inc., Ashland, OR, United States). Sensitivity to autophagic death was determined by Acridine Orange (AO) staining (Fluka Biochemika, Buchs, Switzerland), as described (Migliaccio et al., 2011).

Colony Forming Assay

MNC (10^5 cells/plate) were cultured in semisolid media under conditions resembling either $HEMA^{ser}$ or $HEMA^{def}$ (cf. previous sections). $HEMA^{ser}$ cultures were represented by a commercial semisolid methylcellulose assay containing FBS (30% v/v, MethoCult Stem Cell Technology, Inc., Vancouver, BC, Canada). $HEMA^{def}$ cultures were represented by a home-made methylcellulose assay in which FBS is replaced by deionized human serum albumin (HSA) and HSA-adsorbed cholesterol (final concentrations, 2×10^{-4} mol/L), iron-saturated transferrin (5×10^{-7} mol/L), insulin (1.7×10^{-6} mol/L), nucleosides (10 μg/mL each), sodium pyruvate (10^{-6} mol/L) and L-glutamine (2×10^{-3} mol/L), as previously described (Migliaccio and Migliaccio, 1987). All the cultures were stimulated with human SCF (100 ng/mL), IL-3 (10 ng/mL), GM-CSF (10 ng/mL), G-CSF (100 ng/mL) and EPO (5 U/ml), as described (Masiello et al., 2013). Plates were incubated at 37°C in a fully humidified incubator containing 5% CO_2. Colonies were scored after 8 (colony forming unit-granulocytic erythroid, CFU-E) and 14 (burst forming unit-erythroid, BFU-E, colony forming unit-granulo-monocytic, CFU-GM and colony forming unit-granulocyte, eythroid, megakaryocyte and monocyte, CFU-GEMM) days according to standard morphological criteria (Masiello et al., 2013).

Proliferation Assay

Cell proliferation was assessed by the 3-(4,5-dimethylthiazol-2-yl)-2,5-diphenyltetrazolium bromide (MTT) assay as described (Falchi et al., 2015) where the MTT assay was validated as an index of erythroblast proliferation by careful correlations between MTT values and increased cells numbers detected by visual cell counting. Briefly erythroblasts (5×10^5cells/100 μL/well) were plated in triplicate wells of a 96-well microtitre flat-bottomed plate in the absence or presence of increasing concentrations of commercially available lipid supplements or individual lipoprotein fractions and cultured for 72 h at 37°C in a humidified incubator with 5% CO_2 in air. Ten μL of MTT [5mg/mL] were then added to each well and incubated at 37°C in a humidified atmosphere for additional 4hrs. The solution was removed and the resulting formazan salts dissolved with Sorensen's Glycine Buffer (0.1M Glycine plus 0.1M NaCl in PBS). Optical densities were measured at 540 nm in the VICTOR3^{TM} microplate reader (Perkin Elmer, Waltham, MA, United States) and expressed as absorbance (ABS) values.

Expression Profiling by Microarray Analyses

The expression profile of human erythroblasts generated at days 10 in HEMA^{ser} with or without Dex was previously published (Hricik et al., 2013). The list of differentially expressed genes was manually searched for those involved in lipid metabolism.

Statistical Analysis

Results are presented as Mean (±SD) of at least three separate experiments, unless stated otherwise. Statistical analysis was performed by paired *t*-test and ANOVA (Origin 6.0 for Windows, Microcal Software, Inc., Northampton, MA, United States) and considered statistically different with a $p < 0.05$.

RESULTS

The Expression Profiling of Erythroblasts Generated in the Presence of Dex Predicts Altered Lipid Metabolism

Given the great role played by glucocorticoids in the development of fatty liver disease (Woods et al., 2015), most of what is known on the effects of these hormones on lipid metabolism has been obtained in liver using holistic experimental models. These studies have indicated that glucocorticoids promote the availability of cholesterol indirectly, by increasing the production of VLDL by liver cells, and that of triglycerids directly, by promoting their *ex novo* synthesis by the cells (Bagdade et al., 1976). By contrast, there is little information on the role played by glucocorticoids in the control of lipid metabolism in erythroid cells.

To clarify the genes targeted by Dex in erythroid cells, in a previous study we compared the expression profiling of erythroblasts generated by days 10 in HEMA^{ser} with and without Dex (Hricik et al., 2013). We chose days 10 because this time point contained great numbers of erythroblasts in the process of switching from a proliferation to a maturation mode (Migliaccio et al., 2011), allowing us to detect targets affecting both processes. This study has revealed that erythroblasts generated with and without Dex differ in the expression of only 55 genes (Hricik et al., 2013). By manual analyses, we discovered that six of the differentially expressed genes (approximately 10%) are involved in lipid metabolism, three of which at the mitochondria level (**Table 1**).

Dex activates and inhibits, respectively, the expression of HMGCL and OXCT1, which are synergistically involved in the terminal stages of lipid degradation and in the ketogenic pathway in mitochondria (Fu et al., 2010; Fukao et al., 2014), and increases the expression of ABCA1, which encodes a cholesterol efflux pump (Litvinov et al., 2018). Dex also activates HSD17B7, which encodes an enzyme of the cholesterol biosynthetic pathway (Marijanovic et al., 2003), and decreases the expression of PRKACB, the signaling mediator of several metabolic processes, and of GPAM, the gene that codes for rate-limiting enzyme (GPAT1) of the glycerolipid biosynthetic pathway (Wendel et al., 2009; Søberg and Skålhegg, 2018).

These results suggest that Dex impairs the overall cell metabolism, including lipid metabolism, making the membrane homeostasis of these cells, and possibly additional functions, particularly dependent on lipids up taken from exogenous sources.

Numerous Erythroblasts Generated in the Presence of Dex Present Morphological Evidence of Plasma Membrane and Mitochondria Fragility

To assess whether possible impairment of lipid metabolism may affect the quality of the plasma membrane, we first compared by optical microscopy the morphology of erythroblasts generated by days 10 in the presence and absence of Dex (**Figure 1A** and results not shown). These observations revealed

TABLE 1 | Genes encoding proteins controlling lipid metabolism that are differentially expressed on erythroid cells obtained from adult sources in cultures stimulated with and without Dex.

		Gene symbol	Fold Change	*p*-value	Name	Function
Effects of Dex	Activation	HMGCL	+1.55	2.15E-0.5	3-Hydroxymethyl-3-Methylglutaryl-CoA Lyase	Mitochondrial enzyme involved in the ketogenic pathway
		ABCA1	+2.18	1.71E-0.5	ATP-binding cassette, sub-family A, member 1	Mediator of cholesterol efflux
		HSD17B7	+1.49	1.55E-0.5	Hydroxysteroid 17-Beta Dehydrogenase 7	Postsqualene Enzyme of Cholesterol Biosynthesis
	Inhibition	OXCT1	−1.51	4.50E-0.5	3-Oxoacid CoA-Transferase 1	Mitochondrial enzyme involved in the ketogenic pathway
		GPAM	−1.38	2.03E-0.5	Glycerol-3 Phosphate Acyltransferase, Mitochondrial	Rate limiting enzyme of triacylglycerol biosynthesis
		PRKACB	−1.14	6.19E-0.5	Protein Kinase CAMP-Activated Catalytic Subunit Beta	Mediator of cAMP signaling in several metabolic processes, including in the regulation of lipid metabolism

Symbols of the genes activated (positive fold change) and inhibited (negative fold change) by Dex.

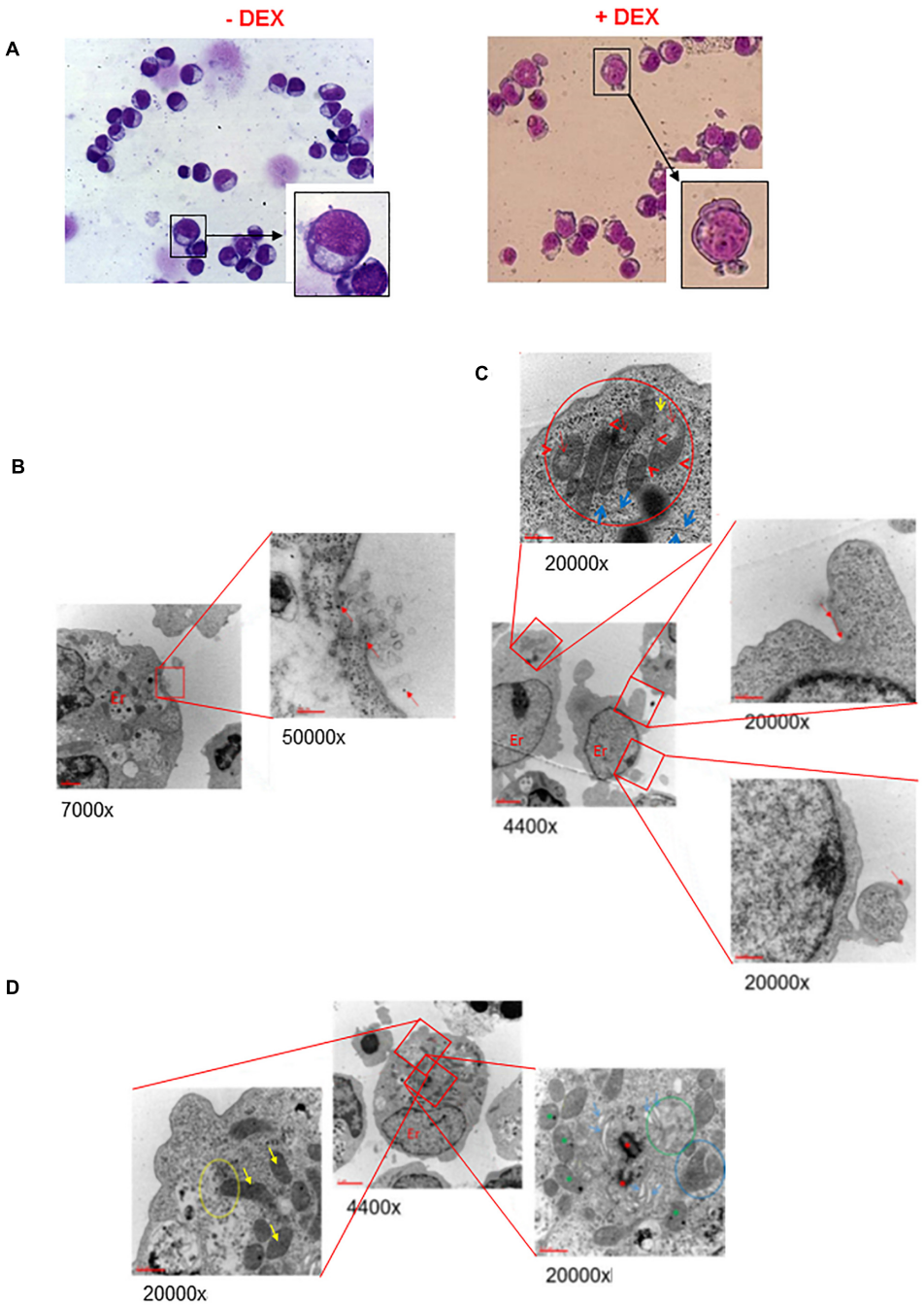

FIGURE 1 | *Ex vivo* generated erythroblasts present morphological evidence of plasma and mitochondrial membrane damage. **(A)** The erythroblasts plasma membrane presents numerous pebbles. May-Grunwald-staining of representative cytospin preparations of erythroblasts from days 10 HEMA^{def} culture obtained with and without Dex, as indicated. Representative pro-erythroblasts are shown at higher magnifications in the inserts. Original magnification 40X. **(B,C)** The membrane pebbles present ultrastructural features associated with exosome and micro-particle release. Electron microscopy analyses of the pebbles on the plasma membrane of representative pro-erythroblasts from days 10 HEMA^{def} with Dex. **(B)** At greater magnification, the pebble, probably a multivesicular body, shows eruption of the plasma membrane with extrusion of exosomes and free ribosomes (red arrows). **(C)** At greater magnification, the pebble shows the presence of membrane leaking (red arrows) and release of micro-particles (panel of the bottom). Greater magnification of this pro-erythroblast (panel on the top) also shows the localization of the mitochondria at a pole of the cytoplasm, the mitochondria body. In addition, the mitochondria present morphological sign of distress (red circle) while the cisterns of the surrounding rough endoplasmic reticulum present numerous traits deprived of ribosomes (blue arrows). **(D)** The mitochondria from erythroblasts cultured with Dex present several abnormalities of the crest membranes. Electron microscopic analyses of a representative pro-erythroblast showing at greater magnification that the mitochondria present several crest abnormalities (reduction in number, diameter larger than normal and membrane ruptures). Only the most external mitochondria (yellow circle) appears partially fused with a phagosome (yellow arrow, bottom left panel). The panel on the right shows fusion among mitochondria (blue circle). Red asterisks indicate centrioles and green asterisks autophagy vesicles. Original magnifications are indicated below each panel.

that cultures with Dex contain greater numbers of erythroid cells presenting alterations of their membrane resembling protrusions or pebbles than those without Dex. In the case the pro-erythroblasts, easily recognizable on smears by their typical morphology and larger size (>30 μm) (Insert in **Figure 1A**), the frequency of cells presenting pebbles was 14 ± 5% in HEMA^{ser} and 23 ± 7% in HEMA^{def} ($p < 0.05$), respectively.

The fine structure of the membrane abnormalities was defined by electron microscopy analysis of erythroblasts expanded in HEMA^{def}, a condition considered superior for generating cRBCs because it sustains levels of amplification 10-times greater than HEMA^{ser} (Migliaccio et al., 2010). Also this analysis was focused on cells with the ultrastructural characteristics of pro-erythroblasts obtained at days 10 of culture. These studies provided evidence that the membrane pebbles are associated with two different types of ultrastructural abnormalities. The first abnormality resembles a burst bubble of plasma membrane with leakage of intracytoplasmic material, as well as of exosomes (<20 nm in diameter) in the environment, a clear indication of membrane fragility, that possibly originated from nearby multivesicular bodies (Raposo and Stoorvogel, 2013) (**Figure 1B**). The second abnormality resembles micro-vesicles ranging in diameter from 105 to 3500 nm (with an average of 1410 ± 877 nm) being released in the environment (**Figure 1C**).

These results indicate that pro-erythroblasts generated with Dex are prone to express membrane abnormalities leading to exosome and microvesicle release, a feature that in RBCs has been reported associated with conditions of cellular distress (Raposo and Stoorvogel, 2013; Leal et al., 2018).

Electron microscopy analysis also allowed us to monitor the plasma membrane of the mitochondria (**Figures 1C,D**). In pro-erythroblasts, mitochondria are localized at a pole of the cytoplasm forming a structure that we define mitochondrial body (top panel in **Figure 1C**). Most, if not all, of the mitochondria are abnormal in morphology with reduced and enlarged internal crests (top panel in **Figures 1C,D**). Only a minority of them, mostly those located in the periphery of the mitochondrial body, appears engulfed into autophagic vesiscles in preparation of the mitophagic degradation that leads to formation of reticulocytes (Moras et al., 2017).

These results provide morphological evidence suggesting that, during erythroid maturation, mitochondria lose their metabolic functions, including those involved in lipid biosynthesis, at the pro-erythroblast stage before the formation of the mitophagic vesicles required for terminal maturation and that these processes may be affected by Dex.

Commercial Lipid Supplements and Lipoproteins Purified From Human Plasma Improve Short-Term Proliferation of Human Erythroblasts in Culture

The morphological data presented above (**Figure 1**) suggest that the plasma membrane abnormalities of erythroblasts generated under current culture conditions are possibly influenced by insufficient and/or not appropriate lipid supplementation in the culture media.

To begin assessing the role exerted by lipid supplementation on *ex vivo* erythroblast expansion, we first determined the level of short-term proliferation of these cells under HEMA^{ser} and HEMA^{def} conditions supplemented either with lipid formulations commercially available or with lipoprotein fractions purified from human plasma (**Figure 2**).

Both under HEMA^{ser} and HEMA^{def} conditions, commercially available supplements sustain levels of proliferation similar (chemically defined lipid concentrate from Gibco), or greatly inferior (see the toxicity exerted by the Fatty Acid Supplement cat L-0288 from Sigma), to those observed in controls (**Figure 2A**). By contrast, all the lipoprotein fractions (regardless of the concentration used) sustain levels of erythroblast proliferation similar to controls in HEMA^{ser}, which already contain bovine lipoproteins provided by FBS (**Figure 2B**). Of note, TL, HDL and VLDL sustain erythroblast proliferation similar to control in HEMA^{def}, that does not contain any additional lipid supplement while LDL significantly increases erythroblast proliferation with respect to controls in a concentration dependent fashion with maximal effects observed at 20–40 μg/mL.

These results indicate that while none of the commercially available lipid supplements is capable to improve proliferation of human erythroblasts above controls, the lipoproteins purified from human plasma, and in particular LDL, which is the fraction with the greatest protein content (**Supplementary Table S2**), may represent a better source of lipids than HM liposomes in HEMA^{def}.

LDL Increases the Number of BFU-E-Derived Colonies Generated in Semisolid Media Under Both HEMA^{def} and HEMA^{def} Conditions

To start assessing the effect of lipid supplementation on erythroid differentiation, we first enumerated the number of hematopoietic colonies generated in semisolid assay by MNC from normal blood donors under HEMA^{ser} and HEMA^{def} conditions supplemented with lipoproteins purified from human plasma (**Table 2**). In these, as well in all the other experiments described from now on, lipoprotein fractions were tested at a concentration of 20 μg/mL. These experiments tested also commercially available LDL for comparison.

Both TL in HEMA^{ser} and all the lipoprotein fractions in HEMA^{def} have modest, although significant, effects on the growth of CFU-GM-derived colonies while do not improve the growth of GFU-GEMM-derived colonies (**Table 2**). By contrast, LDL (by 30%) and VLDL (by approximately 100%) significantly increase the numbers of BFU-E-derived colonies generated in HEMA^{ser} (78 ± 8 and 112 ± 15 vs. 57 ± 9, $p < 0.01$) while LDL increase (by 1.5-fold) that of BFU-E-derived colonies in HEMA^{def} (64 ± 8 vs. 38 ± 5, $p < 0.05$). To be noted that the commercial LDL does not improve colony growth neither in HEMA^{ser} not in HEMA^{def}.

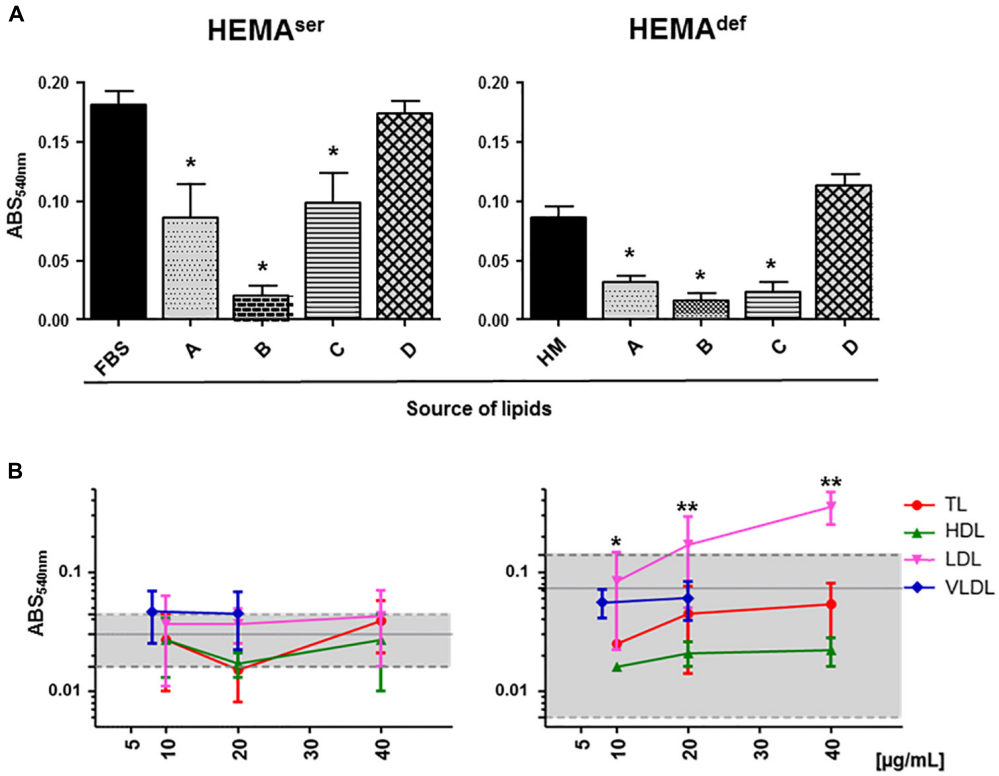

FIGURE 2 | Plasma lipoproteins increase short-term proliferation of human erythroblasts in HEMA^{def}. **(A)** MTT proliferation assay of days 6 erythroblasts cultured for 4 days under HEMA^{ser} (left panel) or HEMA^{def} (right panel) conditions in the presence of commercially available lipid preparations. Source of lipids: **(A)** Lipids Cholesterol Rich from adult bovine serum (Cat. L-4646, Sigma-Aldrich); **(B)** Fatty Acid Supplement (Cat. F7050, Sigma-Aldrich); **(C)** Lipid Mixture (Cat. L-0288, Sigma-Aldrich) and **(D)** Chemically defined Lipid Concentrate (Cat. 11905, Gibco). In control cultures, the source of lipids was FBS (HEMA^{ser}) or home-made liposomes (HM, HEMA^{def}) designed to achieve maximal erythroblast amplification in chemically defined culture conditions (31) (see Materials and Methods for further details). Results are expressed as absorbance (ABS) at 540 nm and are presented as Mean (±SD) of three experiments performed in triplicate, each one with a different donor. Results statistically different from the corresponding controls ($p \leq 0.01$, by paired *t* test) are indicated by *. **(B)** MTT proliferation assay of days 6 erythroblasts cultured for 4 days in the presence of increasing concentrations of lipoproteins purified from human plasma as described in **Supplementary Figure S1**. Controls were represented either by FBS (HEMA^{ser}) or home-made liposomes (HEMA^{def}) and are indicated by the gray areas. Results are presented as Mean (±SD) of three experiments performed in triplicate. In HEMA^{def}, results obtained with LDL are statistically different from the corresponding controls with $p \leq 0.05$ (*) at 10 µg/mL and $p \leq 0.01$ (**) at 20 and 40 µg/mL (by paired *t* test).

These results indicate that the LDL (and to some extent VLDL) fraction purified from human plasma increases the number of BFU-E induced to form erythroid colonies in semisolid cultures.

Both LDL and VLDL Increased the Number of Erythroblasts Generated in Liquid Culture by Adult MNC Under HEMA^{def} Conditions

To further explore in some detail the effects exerted by the lipoprotein fractions, we also evaluated the levels of erythroblast expansion in liquid culture supplemented with these preparations (**Figure 3**). In HEMA^{ser}, the various lipoprotein fractions investigated do not improve the overall fold increase (fold-increase ∼20–40 by days 14–17 in the presence of all supplements). By contrast, both LDL and VLDL increase by 3-fold the total number of erythroblasts generated by days 14–17 under HEMA^{def} conditions (Fold Increase 95 ± 10 and 64 ± 14 vs. 27 ± 6, $p < 0.01$–0.05, respectively for LDL and VLDL compared to control value at the same time point) (**Figure 3** and **Table 3**). On note, the commercial LDL generates erythroblasts in numbers similar to controls.

Both LDL and VLDL Increase the Expansion of Erythroid Progenitors in HEMA^{def}

To clarify the mechanisms underlying the increased erythroblast expansion observed in HEMA^{def} supplemented with LDL and VLDL, we evaluated the effect exerted over time by the various lipoprotein supplements on the number of hematopoietic progenitor cells in liquid culture. Hematopoietic progenitor cells were determined by culturing aliquots harvested from the liquid cultures at days 3, 5, 7, 10, and 14 under semisolid conditions and then scoring the number and type of colonies generated by these cell aliquots (**Figure 4**).

TABLE 2 | Effects of lipoproteins purified from human plasma on the number of colonies generated by human MNC in semisolid cultures under HEMA^{ser} and HEMA^{def} conditions.

HEMA^{ser}	BFU-E	CFU-GM	CFU-GEMM	Total
Control	57 ± 9	22 ± 12	0.5 ± 0.4	79 ± 19
TL	64 ± 15	16 ± 9 $P \leq 0.05$	0.1 ± 0.3	80 ± 21
HDL	47 ± 17	17 ± 5	0.1 ± 0.3	61 ± 20
LDL	78 ± 8 $p \leq 0.01$	25 ± 12	0.3 ± 0.5	104 ± 19 $p \leq 0.01$
VLDL	112 ± 15 $p \leq 0.01$	29 ± 21	0.3 ± 0.3	142 ± 30 $p \leq 0.01$
LDL Sigma	61 ± 10	20 ± 15	0	81 ± 23
HEMA ^{def}	**BFU-E**	**CFU-GM**	**CFU-GEMM**	**Total**
Control	38 ± 5	16 ± 6	0.8 ± 0.6	55 ± 9
TL	40 ± 3	19 ± 8 $p \leq 0.05$	0.7 ± 0. 6	60 ± 11
HDL	33 ± 3	17 ± 8 $p \leq 0.05$	0.3 ± 0. 3	50.3 ± 10
LDL	64 ± 8 $p \leq 0.05$	18 ± 5 $p \leq 0.05$	1.2 ± 0.8	83 ± 12 $p \leq 0.05$
VLDL	48 ± 9	18 ± 7 $p \leq 0.05$	0.5 ± 0.4	67 ± 15
LDL Sigma	43 ± 5	18 ± 8 $p \leq 0.05$	0.2 ± 0.2	60 ± 13

Commercially available LDL were analyzed for comparison. Results are presented as number of colonies per 10^5 MNC and are expressed as Mean (±SD) of at least three separate experiments performed in duplicate. Values statistically different from controls are indicated by oval circles.

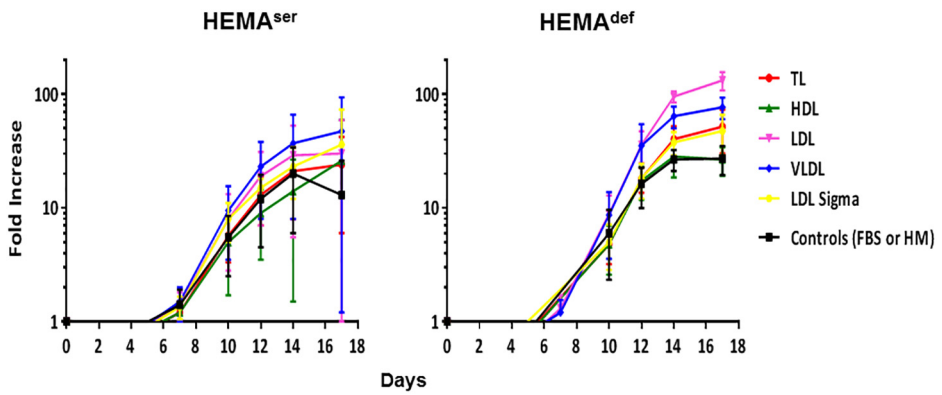

FIGURE 3 | LDL and VLDL significantly increase the numbers of erythroblasts generated in HEMA^{def}. Total number of cells, expressed as Fold Increase (FI), generated over time in HEMA^{ser} **(left)** and HEMA^{def} **(right)** supplemented with lipoproteins purified from human plasma (TL, red; HDL, green; LDL, pink; VLDL, blue, all at 20 μg/mL). Results are compared with those obtained with FBS alone (HEMA^{ser}), home-made liposomes (HEMA^{def}) (controls, black) or LDL from a commercial source (Cat. L-0288 from Sigma, yellow). Results are presented as Mean (±SD) of four experiments each one with a different donor. In HEMA^{ser}, the experimental points are not statistically different from controls. In HEMA^{def}, LDL at days 14 ($p = 0.008$) and days 17 ($p = 0.013$) and VLDL at days 14 ($p = 0.004$) and days 17 ($p = 0.029$) are statistically different from the corresponding controls. Commercial LDL is statically different only at days 3 ($p = 0.012$).

TABLE 3 | Summary of the effects induced by the various lipoprotein fractions on the end-points used to assess the efficiency of erythroid expansion.

	Erythroid Expansion (Day 14)		Progenitor recruitment (Day 0)		Progenitor expansion (Day 10)		Erythroblast proliferation (Day 10)	
	Fold Increase		BFU-E/10^5 MNC**		Tot CFU/Culture ($x10^3$)		ABS 540nm ($x10^2$)	
	$HEMA^{ser}$	$HEMA^{def}$	$HEMA^{ser}$	$HEMA^{def}$	$HEMA^{ser}$	$HEMA^{def}$	$HEMA^{ser}$	$HEMA^{def}$
Control	20 ± 14	27 ± 6	57 ± 9	38 ± 5	n.d.	542 ± 54	3.0 ± 1.4	7.3 ± 6.7
TL	21 ± 13	40 ± 12	64 ± 15	40 ± 3	n.d.	764 ± 216	1.5 ± 0.7	4.5 ± 3.2
HDL	14 ± 12	28 ± 10	47 ± 17	33 ± 3	n.d.	620 ± 100	1.7 ± 0.4	2.1 ± 0.5
LDL	29 ± 23	95 ± 10 $p \leq 0.01$	78 + 8 $p < 0.01$	64 + 8 $p < 0.05$	n.d.	756 ± 104 $p \leq 0.01$	3.7 ± 1.2	17.1 ± 12.1 $p \leq 0.05$
VLDL	37 ± 29	64 ± 14 $p < 0.05$	112 ± 15 p < 0.01	48 ± 9	n.d.	1064 ± 292 $p \leq 0.05$	4.5 ± 1.3	6.1 ± 2.2
LDL Sigma	23 ± 11	38 ± 9	61 ± 10	43 ± 5	n.d.	680 ± 84	n.d.	7.9 ± 4.4

*Results are presented as Mean (±SD) of three experiments performed in triplicate. Experiments were performed in parallel analyzing the same donor under $HEMA^{ser}$ and $HEMA^{def}$ conditions (three separate donors per experimental point). Total colony forming units, CFU total number of colonies generated in semisolid cultures (see **Table 2** and **Figures 2–4, 6** for further detail).*

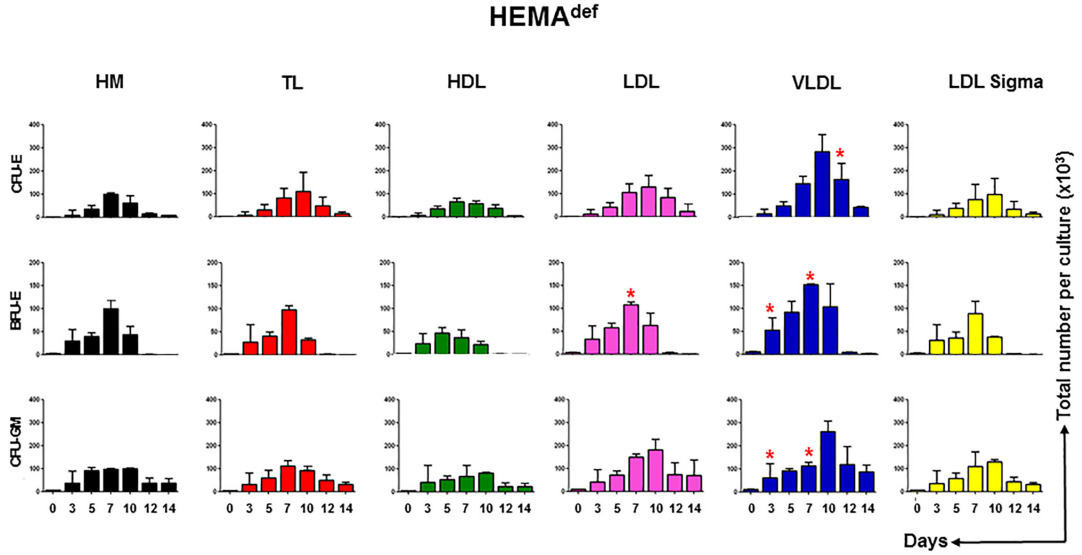

FIGURE 4 | LDL and VLDL increase the expansion of erythroid progenitors under $HEMA^{def}$ conditions. Number of progenitor cells able to generate erythroid (BFU-E and CFU-E) and myeloid (CFU-GM) colonies present over time in $HEMA^{def}$ supplemented with either home-made liposomes (HM) or with TL, HDL, LDL or VLDL (all at 20 μg/mL). Results are expressed as number of progenitor cells per culture and are presented as Mean (±SD) of four experiments each one with a different donor. See legend of **Figure 2** for further detail. Values statistically different ($p < 0.05$ by paired *t*-test) with respect to the corresponding data obtained with HM are indicated by *. Values obtained with LDL-Sigma are not statistically different neither from those obtained with HM nor from those observed with LDL.

In cultures supplemented with HM liposomes, the number of BFU-E and CFU-E progressively increases and then declines reaching the maximum by days 7. In these cultures, BFU-E are barely detectable by days 12. In cultures supplemented with TL and HDL and with commercial LDL, the number of erythroid progenitors increases over time with amplitude and kinetics similar to that observed in controls. By contrast, in cultures supplemented with LDL and VLDL, the maximal levels of amplification of progenitor cells of all types is significantly greater than in controls and the numbers of CFU-E (and CFU-GM) reach their peak at days 10 instead than at days 7.

These results suggest that improved and prolonged expansion of hematopoietic progenitor cells contributes to the greater numbers of erythroblasts observed in $HEMA^{def}$ supplemented with LDL and VLDL.

Erythroblasts Generated in the Presence of VLDL Are Resistant to Death by Autophagy Induced by Growth Factor Deprivation (GFD)

One of the factors limiting erythroblast expansion in HEMA is represented by the great number of cells that die by

autophagy at the end stage of the culture (Migliaccio et al., 2011). To further investigate the mechanism that underlay the improved erythroblast expansion observed in the presence of selected lipid supplements, we assessed the susceptibility to death of erythroblasts generated *ex vivo* in HEMA^{def} supplemented with HM liposomes or with VLDL. Sensitivity to death was determined using as surrogate marker the frequency of erythroblasts undergoing autophagy [identified by Acrydin Orange (AO) staining] following 4 h of GFD, as described (Migliaccio et al., 2011).

A great number (23%) of erythroblasts generated in the presence of HM liposomes became positive to AO staining after GFD (**Figure 5**). By contrast, only 2% of erythroblasts generated with VLDL became AO positive after GFD, an indication that they are resistant to GFD-induced death. Interestingly, the cytoplasm of erythroblasts generated with VLDL also contain fewer vacuoles and their plasma membranes contain less pebbles than erythroblasts generated with HM (14 ± 6 vs. 23 ± 7, $p < 0.05$) (see also the morphological analyses presented in **Figure 5**).

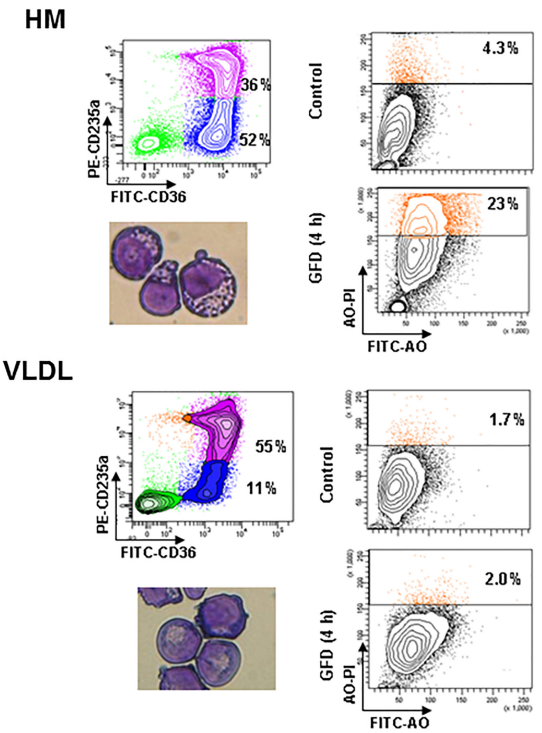

FIGURE 5 | Erythroblasts generated in the presence of VLDL are resistant to autophagic death induced by growth factor deprivation. The panels on the left present the flow cytometry and morphological analyses of erythroblasts generated by days 10 in HEMA^{def} supplemented either with HM liposomes or with VLDL (20 μL/mL). The panels on the right compare the frequency of Acrydine Orange (AO) positive cells, as indication of autophagic death, of the two populations when cultured for 4 h with (Control) or without growth factors (growth factor deprived, GFD). Results are representative of those obtained in two separate experiments.

All the Lipoprotein Fractions From Human Plasma Increase the Level of Terminal Erythroid Maturation Observed by Days 17 in HEMA^{def}

In spite of the presence of Dex, erythroblasts in the proliferation phase eventually progress to terminal maturation. Therefore, to assess the effects of lipid supplementation on the efficiency of terminal erythroid maturation, the maturation profile expressed by erythroblasts generated over time under HEMA^{ser} and HEMA^{def} supplemented with the various lipoprotein fractions was assessed (**Figure 6**). These studies exploited the fact that profiling for CD36/CD235a expression divides human erythroblasts into three maturation classes corresponding respectively to pro-erythroblasts (CD36^{pos}CD235a^{neg} cells); basophilic-erythroblasts (CD36^{pos}CD235a^{high} cells); and poly-chromatophilic/orthochromatic erythroblasts (CD36^{neg}CD235a^{high} cells) (Falchi et al., 2015). The transition from basophilic- to ortho-erythroblasts is also associated with a dramatic reduction in size (from 24 to 19 μm) recognizable by forward/side scatter analyses.

According to our results, in HEMA^{ser}, the cells progress along the maturation pathway with the same kinetics irrespective of the lipids used as supplement (**Figure 6A** and results not shown). Mature erythroblasts (CD36^{pos}CD235a^{high}) represent approximately 12–16% of the population by days 7 while all the erythroblasts express the mature CD36^{neg}CD235a^{high} phenotype by days 17. By days 17, the frequency of non-erythroid cells in HEMA^{ser} is high (46%). Since non-erythroid cells do not proliferate in HEMA (Migliaccio et al., 2002), the relative increase of this population over time is a further indication of the great rates of death of erythroblasts at the end stage of HEMA (Migliaccio et al., 2011). The addition to HEMA^{ser} of any of the lipoprotein fractions tested in this study does not affect the kinetics of the maturation process but increases the frequency of mature erythroblasts, which reaches 30-50% by days 17, an indication that the presence of lipoproteins increases survival of mature erythroblasts.

The kinetics of erythroblast maturation in HEMA^{def} is visible different than that observed in HEMA^{ser} (**Figure 6B** and results not shown). In control cultures, immature CD36^{pos}CD235a^{neg} erythroblasts are detected with a frequency (30%) significantly greater than that observed in HEMA^{ser} (12%) by days 7 and the majority of the cells remains immature until days 17 when this population still represents 70% of the cells. Conversely, by days 17 mature erythroblasts represent only 27% of the cells. A great difference between HEMA^{ser} and HEMA^{def} is represented by the frequency of non-erythroid cells which are barely detectable in HEMA^{def}, an indication of better erythroblast survival. Of note, the replacement of the HM liposomes with the lipoprotein fractions does not affect the kinetics of erythroblast maturation but doubles the frequency of mature erythroblasts detected in HEMA^{def} by days 17 (40–60% vs. 27%) (**Figure 6B** and results not shown).

To further define the maturation stage of erythroid cells obtained by days 17 in HEMA^{def} supplemented with HM, TL and VLDL, the cells in the CD36^{low}/CD235a^{high} gate were reanalyzed for forward scatter (FSC) and side scatter (SSC), two parameters

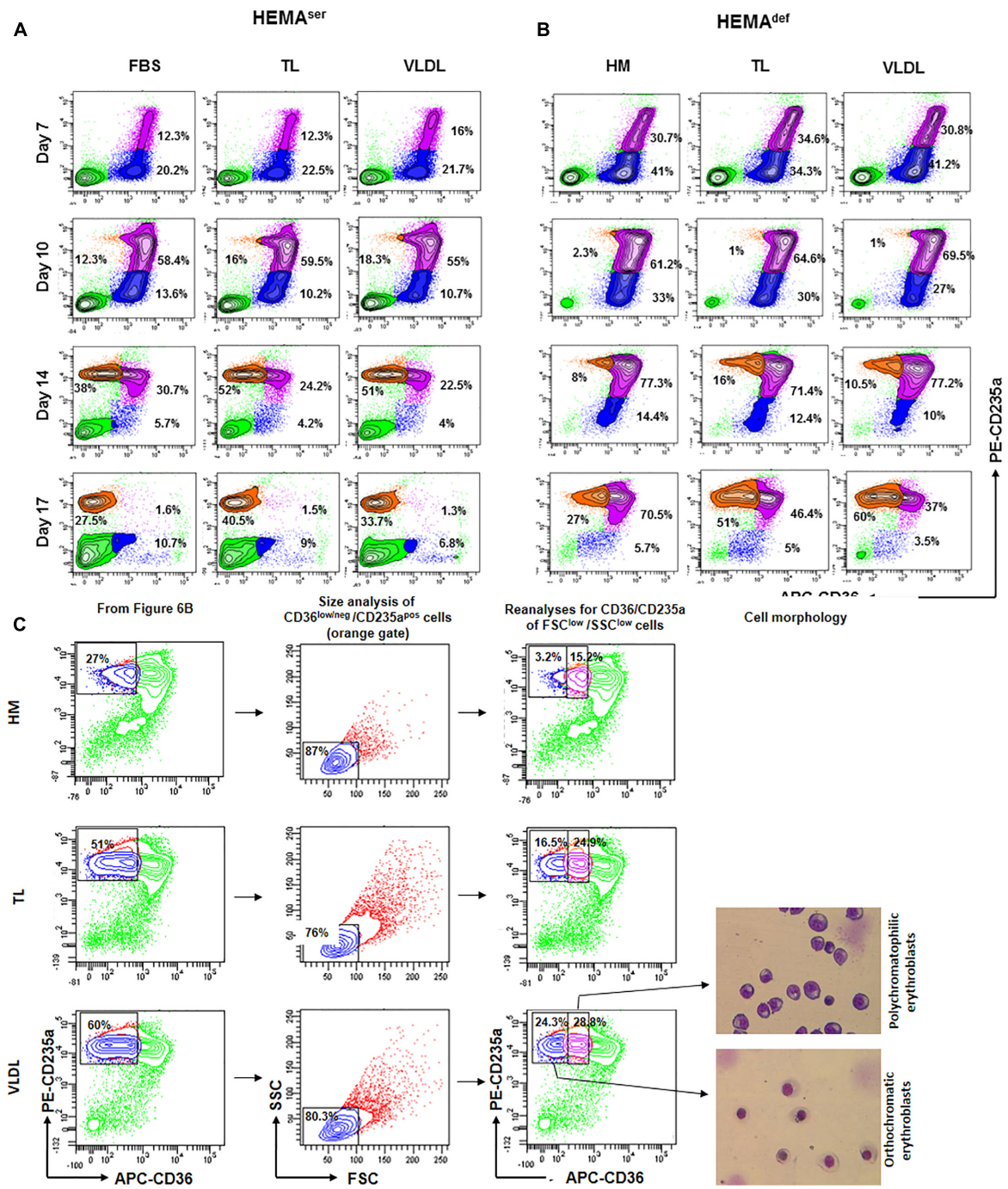

FIGURE 6 | All the lipoprotein fractions increase terminal erythroid maturation under HEMA^{def} conditions. Contour plots for CD36 and CD235a expression obtained by FACS of erythroblasts generated over time in HEMA^{ser} **(A)** and HEMA^{def} **(B)** supplemented with TL and VLDL. Cells obtained with FBS or with HM liposomes were analyzed as control. Similar results were observed in cultures supplemented with HDL, LDL and LDL-Sigma (results not shown). Analyses for CD36/CD235a expression identifies five populations corresponding respectively to lymphocytes (CD36^{neg}CD235a^{neg} cells, bright green); pro-erythroblasts (CD36^{pos}CD235a^{neg} cells, blue); basophilic-erythroblasts (CD36^{pos}CD235a^{high} cells, purple); and polychromatophilic/orthochromatic (CD36^{neg}CD235a^{high} cells, orange) erythroblasts. The frequencies of pro-erythroblasts, basophilic and poly/orthochromatic erythroblasts are indicated within the quadrants. Results are representative of those obtained in two separate experiments. **(C)** Contour plot for forward scatter (FSC) and side scatter (SSC) of the days 17 cells in the CD36$^{low/neg}$/CD235a^{pos} gate of **Figure 6B**. The cells were then re-analyzed for CD36/CD235a expression, sorted and stained with May-Grunwald Gimsa. The numbers inside the panels indicate the frequency of the cells in the different gates. This analysis allows discriminating between erythroid cells at the polychromatophilic and orthochromatic stage. Only results obtained in the HM, TL, and VLDL group are presented. The results obtained with TL and VLDL are representative of those obtained with HDL, LDL, and LDL-Sigma.

which provide indication for size and cytoplasm granularity. The events in FSC^{low}/SSC^{low} gate were then re-analyzed for CD36/CD235a expression and sorted for morphological analyses by May-Grunwald staining (**Figure 6C**). These analyses indicate that in all the experimental groups the mature cells are small in size. However, the mature gate in the HM group contains mostly polychromatophilic erythroblasts while those in the TL and VLDL groups contain both polychromatophilic and orthochromatic erythroblasts in a 50:50 ratio, these results indicate that lipoproteins improve terminal erythroid maturation in $HEMA^{def}$.

DISCUSSION

The conditions used to generate cRBCs for the first-in-man transfusion, as $HEMA^{ser}$, contain FBS (Giarratana et al., 2005) and are not suited to produce cRBCs for multiple transfusions because it can be predicted that, as observed with other cellular products produced with FBS (Selvaggi et al., 1997; Tuschong et al., 2002), will trigger immunological reactions against bovine proteins when transfused into patients. Therefore, the formulation of clinical grade conditions depleted of FBS represents one of the major challenges in designing the manufacturing process of cRBCs (Migliaccio et al., 2012). To address this challenge, we formulated $HEMA^{def}$, a media in which FBS is replaced with clinical grade HSA that sustains erythroblast expansion in proliferation cultures at levels 10-fold greater than those observed with $HEMA^{ser}$ (Migliaccio et al., 2010). However, an important drawback of $HEMA^{def}$ is represented by the source of lipids which is represented by HM liposomes generated by sonicating clinical grade HSA with egg-derived cholesterol and soybean lecithin. Given the known intolerance to both products existing in the human population, $HEMA^{def}$ may not be indicated to produce cRBCs for the general population.

To formulate clinically more suited culture conditions, we determined *ex vivo* expansion of erythroblasts in $HEMA^{def}$ formulated either with commercial lipid supplements or with HM lipoprotein fractions purified from human plasma. Parallel experiments were conducted in $HEMA^{ser}$ for comparison. Our results demonstrate that all the commercially available lipid supplements tested in this study, including LDL from Sigma, generated erythroblasts in numbers inferior to those sustained by HM liposomes (**Figure 2**). By contrast, supplementation of $HEMA^{def}$ with either LDL or VLDL purified in house from fresh human plasma supports the generation of erythroblasts in numbers significantly greater (2–3-times) than those generated by HM liposomes (**Table 3**).

LDL and VLDL fractions increase the numbers of erythroblasts generated in culture through mechanisms targeting both the erythroid progenitor and precursor cells (**Table 3**). At the progenitor level, they significantly increase the number of cells recruited to mature (**Table 2**) and their expansion in liquid culture (**Figure 4**). At the precursor level, they increase proliferation rates (**Figure 2**) and resistance to autophagic death (**Figure 5**). By contrast, all the lipoprotein fractions tested, including commercial LDL from Sigma, increased the levels of terminal erythroid maturation observed at days 17 (**Figure 6**), suggesting that lipoproteins are the factors responsible for improving the enucleation rates in maturation cultures supplemented with human plasma reported by previous studies (van den Akker et al., 2010; Masiello et al., 2013). Although enucleation was not formally investigated in the present manuscript, the observation that cells generated with LDL and VLDL matured readily into ortho-chromatic erythroblasts by days 17 (**Figure 6**) suggests that these cells, by exhibiting high enucleation rates, represent a better source than erythroblasts expanded with current culture media to generate cRBCs in differentiation cultures.

Several events concurred in determining the greater erythroid output observed in proliferation cultures supplemented with lipoproteins. The data presented in this paper provide some clue on the biochemical mechanisms that may underlie some of these events which are summarized in **Figure 7**.

By expression profiling, erythroblasts generated with and without Dex show differences in only 55 genes, six of which involved in lipid metabolism (**Table 1**). More specifically, ABCA1, which encodes a cholesterol efflux pump

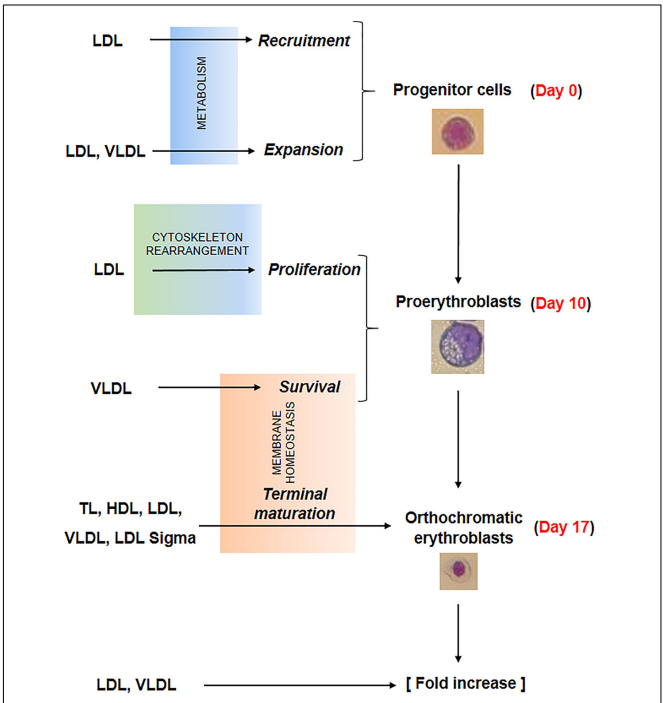

FIGURE 7 | Summary of the effects exerted by the lipoprotein fractions investigated in this study on erythroid differentiation. Recruitment and expansion in liquid culture of the erythroid progenitor cells was improved by LDL and LDL/VLDL, respectively, probably by mechanisms targeting cell metabolism. LDL increased also the proliferation of days 10 proerythroblasts, probably by mechanisms involving rearrangement of the cytoskeleton. Lastly the survival and terminal maturation of the proerythroblasts was favored by LDL and by all the lipoprotein fractions, respectively through mechanisms involving improvement of membrane homeostasis. All these biological effects contributed to the greater erythroid expansion observed in $HEMA^{def}$ supplemented with lipoproteins, expecially when the lipoproteins were represented by LDL and VLDL.

(Litvinov et al., 2018), and HSD17B7, which is involved in cholesterol biosynthesis (Marijanovic et al., 2003), are activated in erythroblasts generated with Dex, suggesting that Dex may promote cholesterol biosynthesis but overall makes these cells cholesterol deficient because of higher efflux rates. Furthermore, Dex inhibits expression of GPAM that encodes an enzyme involved in the synthesis of phosphatidic acid (Wendel et al., 2009), a precursor of TG, suggesting that Dex impairs lipid metabolism in erythroid cells making their membrane biosynthesis highly dependent on lipid absorbed from exogenous sources. Although this interpretation is in partial contrast to other experimental systems such as adipocytes (Lee et al., 2018), the reason of this difference may relay on the specific biological functions exerted by Dex during stress erythropoiesis where it allows the production of greater number of cRBCs by inhibiting terminal maturation and promoting proliferation. In fact, in addition to promoting self-replication (Migliaccio et al., 2002; Zhang et al., 2013), Dex may retain erythroblasts in proliferation by a novel mechanism involving a direct blocking of terminal erythroid maturation through down-modulation of GPAM and, consequently, lower content of phosphatidic acid, the signaling molecule that activates the cytoskeleton rearrangement and the vesicle trafficking (Ferraz-Nogueira et al., 2014; Nguyen et al., 2016) required for this process (see **Figure 7**).

Our data suggest that lipoproteins reduce the susceptibility of pro-erythroblasts to death induced by growth factor starvation and facilitate their terminal maturation by improving membrane homeostasis. In fact, extensive morphological analyses of erythroblasts generated with Dex indicate that these cells present severe abnormalities of the plasma and mitochondrial membranes suggesting that the lipid bioavailability under current culture conditions is insufficient. The plasma membrane abnormalities came in the forms of pebbles associated with exosome and micro-vesicle formation. Release of micro-vesicles by RBCs involves disturbance of the membrane/cytoskeleton interaction (Leal et al., 2018) and is triggered by Ca^{+2} and protein kinase C activation (Nguyen et al., 2016). The effects of micro-vesicle release on the life span of RBCs *in vivo* are controversial: it may increase, by eliminating hemoglobin precipitates, the life span of sickle RBCs but may decrease that of normal RBCs stored for transfusion (D'Alessandro et al., 2015; Leal et al., 2018). We predict that the membrane abnormalities presented by cRBCs may contribute to reduce their life span *in vitro* and possibly *in vivo* (Giarratana et al., 2005). By argument, we infer that these abnormalities are the direct consequences of cholesterol insufficiency. In fact, the inhibitory function of scramblase activity exerted by cholesterol promotes the phospholipid asymmetry of the membrane that preserves the shape and promotes survival of the erythrocytes (Arashiki et al., 2016). Therefore, by reducing the cholesterol content, Dex may increase the scramblase activity reducing phospholipid asymmetry (and integrity) of the membranes. Genetic evidences for the importance of cholesterol for membrane biosynthesis and RBC survival *in vivo* also exists. Patients with Smith-Lemli-Opiz syndrome which is associated with loss of function mutations in the gene encoding cholesterol biosynthesis DHCR7-7-dehydrocholesterol reductase have low levels of cholesterol and are anemic (Jira et al., 2003). In addition, patients with a rare inherited syndrome leading to synthesis of plant sterols instead than cholesterol experience hemolytic anemia (Wang et al., 2014).

In the mitochondria, membrane abnormalities were observed at the level of the crests and are so severe that predict reduced mitochondrial functions with consequent impaired cell metabolism. They were presented by the majority of the mitochondria independently from their inclusion into autophagic vesicles. Therefore, it is unlikely that these abnormalities were caused by the lytic enzymes in the autophagosomes (Betin et al., 2013). Since phosphatidic acid is also a precursor for cardiolipin, the key phospholipid of the internal mitochondrial membranes controlling their functional integrity, bioenergetics and apoptosis (Paradies et al., 2014; Ikon and Ryan, 2017; Mårtensson et al., 2017), we propose that the membrane abnormalities of the mitochondria observed in erythroblasts generated with Dex are due to reduced cardiolipid content as a consequence of GPAM down-regulation.

Red blood cells express a variety of apolipoprotein receptors, in primis the receptor for ApoA1 and B as demonstrated by the hypocholesterolemia and reduced levels of circulating ApoA1 and B expressed by patients with the acquired erythrocytosis Polycythemia Vera (Fujita et al., 2012). Given the great number of RBCs present in the circulation, these receptors are efficient lipid scavengers contributing to maintain the lipid content of the plasma within physiologic levels preventing atherosclerosis and kidney malfunctions (Wahl et al., 2016; Saraf et al., 2017; Vuorio et al., 2018). The effects on erythroblast expansion sustained by VLDL and LDL described in this study suggests that, in addition to exerting scavenger functions, the lipoprotein receptors expressed by erythroid cells tune lipid availability to prevent possible membrane abnormalities due to impairment of lipid metabolism induced by Dex in RBCs produced under conditions of erythroid stress.

The observation that all the lipoprotein fractions promote terminal maturation while only LDL and VLDL promote erythroblast expansion suggests that the effects exerted by lipoproteins on hematopoietic stem/progenitor cells are mediated by mechanism(s) at least partially different from that exerted during terminal maturation (regulators of lipid bioavailability). These mechanism(s) may be represented by improvement of the overall deficient metabolism caused by Dex (**Figure 7**) and/or by still to be identified signaling functions exerted by specific protein component of LDL and VLDL. Although further studies are necessary to clarify possible signaling functions of the individual lipoproteins, recent evidences support this hypothesis by indicating that lipoproteins control directly the proliferation of hematopoietic stem/progenitor cells. This proliferation is inhibited by cholesterol bound-HDL through activation of ABCA1 (Yvan-Charvet et al., 2010), a gene found by us activated by Dex (**Table 1**), while it is promoted by LDL through a mechanism still to be identified (Yvan-Charvet et al., 2010; Feng et al., 2012; Seijkens et al., 2014). These observations may explain why erythroblast expansion is not affected by the presence of HDL and TL, which contain both HDL and LDL, but it is promoted by LDL. Further studies are necessary to clarify the

mediators of the effects of LDL on the proliferation of erythroid progenitors and how these mediators interact with the control exerted by HDL/ABCA1 pathway regulated by Dex.

CONCLUSION

Overall, the results discussed in this paper highlight the importance of further studies on lipid metabolism and mitochondrial function in erythroblasts and how they are regulated by Dex to increase our understanding on how to improve the functions of RBCs generated *in vivo* under condition of stress. They also demonstrate a novel beneficial effect of LDL and VLDL on recruitment and expansion of erythroid progenitor and precursor cells in the proliferation phase of $HEMA^{def}$, indicating that media formulated with supplements which include clinical grade VLDL and/or LDL will allow the generation of greater numbers of cRBCs that will possible survive longer *in vivo* for transfusion.

AUTHOR CONTRIBUTIONS

MZ, CB, LS, and FC performed the experiments, analyzed the data, and wrote the manuscript. GG provided buffy coats from regular blood donations and wrote the manuscript. MLG revised the data and wrote the manuscript. AM designed the experiments, reviewed the data, and wrote the manuscript. All the authors have read the final version of the manuscript and concur with its content.

FUNDING

This study was supported by grants from the National Cancer (P01-CA108671) and Heart, Lung and Blood (1R01-HL116329) Institute and Associazione Italiana Ricerca Cancro (AIRC 17608).

ACKNOWLEDGMENTS

Mr. Hricik and Dr. Martelli are gratefully acknowledged for performing, respectively, microarray analyses and flow cytometry evaluations. Dr. Rosa Alba Rana is gratefully acknowledged for encouragement and support.

SUPPLEMENTARY MATERIAL

The Supplementary Material for this article can be found online at: https://www.frontiersin.org/articles/10.3389/fphys.2019.00281/full#supplementary-material

FIGURE S1 | Characterization of the lipoprotein fractions purified from human plasma investigated in the study. **(A)** Diagram of the purification scheme indicating the series of ultracentrifugations used for lipoprotein fractionation. ρ indicates the density of the original plasma or of infranates prepared for ultracentrifugation and is expressed as g/mL. **(B)** Commassie blue and silver staining of the proteins contained in the various lipoprotein fractions separated by gel electrophoresis. The numbers on the top indicate the amount of protein loaded. The position of the molecular weight markers is indicated in kDa on the left while the identity of the bands (predicted on the basis of their size) is indicated by arrows with the corresponding labels (Chapman, 1986). **(C)** Densitometric profile of the bands present in the lanes of the gel stained with Silver presented in **(B)**.

FIGURE S2 | Design of the experiments used to evaluate the effects of lipid supplementation on erythroblasts expansion under $HEMA^{def}$ and $HEMA^{ser}$ conditions. As summarized in **Supplementary Table S1**, end-points of these experiments were represented by expansion of erythroid (liquid cultures, **Figure 3**) and progenitor (semisolid cultures, **Figure 4**) cells over time and short-term proliferation (**Figure 2**), ability to progress along the terminal maturation pathway (**Figure 5**) and resistance to stress-induced autophagic death (**Figure 6**).

TABLE S1 | list of the end-points analyzed in our study and of their corresponding biological implications.

TABLE S2 | Protein and lipid content of the lipoprotein fractions purified from human plasma used in the study. The expected protein/lipid and CH/TG ratios in each fraction on the basis of published data.

TABLE S3 | Comparison of the composition of the home made and Sigma LDL fractions.

REFERENCES

An, X., and Mohandas, N. (2008). Disorders of red cell membrane. *Br. J. Haematol.* 141, 367–375. doi: 10.1111/j.1365-2141.2008.07091.x

Anstee, D. J., Gampel, A., and Toye, A. M. (2012). Ex-vivo generation of human red cells for transfusion. *Curr. Opin. Hematol.* 19, 163–169. doi: 10.1097/MOH.0b013e328352240a

Arashiki, N., Saito, M., Koshino, I., Kamata, K., Hale, J., Mohandas, N., et al. (2016). An unrecognized function of cholesterol: regulating the mechanism controlling membrane phospholipid asymmetry. *Biochemistry* 55, 3504–3513. doi: 10.1021/acs.biochem.6b00407

Bagdade, J. D., Yee, E., Albers, J., and Pykalisto, O. J. (1976). Glucocorticoids and triglyceride transport: effects on triglyceride secretion rates, lipoprotein lipase, and plasma lipoproteins in the rat. *Metabolism* 25, 533–542.

Betin, V. M., Singleton, B. K., Parsons, S. F., Anstee, D. J., and Lane, J. D. (2013). Autophagy facilitates organelle clearance during differentiation of human erythroblasts: evidence for a role for ATG4 paralogs during autophagosome maturation. *Autophagy* 9, 881–893. doi: 10.4161/auto.24172

Bouhassira, E. E. (2012). Concise review: production of cultured red blood cells from stem cells. *Stem Cells Transl. Med.* 1, 927–933. doi: 10.5966/sctm.2012-0097

Brewer, G. J. (1980). Inherited erythrocyte metabolic and membrane disorders. *Med. Clin. North Am.* 64, 579–596.

Chapman, M. J. (1986). Comparative analysis of mammalian plasma lipoproteins. *Methods Enzymol.* 128, 70–143.

Clinicaltrials.gov (2012). *Clinicaltrials.gov*. Available at: https://www.clinicaltrials.gov/ct2/show/NCT00929266

D'Alessandro, A., Kriebardis, A. G., Rinalducci, S., Antonelou, M. H., Hansen, K. C., Papassideri, I. S., et al. (2015). An update on red blood cell storage lesions, as gleaned through biochemistry and omics technologies. *Transfusion* 55, 205–219. doi: 10.1111/trf.12804

Dolznig, H., Grebien, F., Deiner, E. M., Stangl, K., Kolbus, A., Habermann, B., et al. (2006). Erythroid progenitor renewal versus differentiation: genetic evidence for cell autonomous, essential functions of EpoR, Stat5 and the GR. *Oncogene* 25, 2890–2900. doi: 10.1038/sj.onc.1209308

Falchi, M., Varricchio, L., Martelli, F., Masiello, F., Federici, G., Zingariello, M., et al. (2015). Dexamethasone targeted directly to macrophages induces macrophage niches that promote erythroid expansion. *Haematologica* 100, 178–187. doi: 10.3324/haematol.2014.114405

Feng, Y., Schouteden, S., Geenens, R., Van, Duppen V, Herijgers, P., Holvoet, P., et al. (2012). Hematopoietic stem/progenitor cell proliferation and differentiation is differentially regulated by high-density and low-density lipoproteins in mice. *PLoS One* 7:e47286. doi: 10.1371/journal.pone.0047286

Ferraz-Nogueira, J. P., Díez-Guerra, F. J., and Llopis, J. (2014). Visualization of phosphatidic acid fluctuations in the plasma membrane of living cells. *PLoS One* 9:e102526. doi: 10.1371/journal.pone.0102526

Fibach, E., Manor, D., Oppenheim, A., and Rachmilewitz, E. A. (1989). Proliferation and maturation of human erythroid progenitors in liquid culture. *Blood* 73, 100–103.

Fu, Z., Runquist, J. A., Montgomery, C., Miziorko, H. M., and Kim, J. J. (2010). Functional insights into human HMG-CoA lyase from structures of Acyl-CoA-containing ternary complexes. *J. Biol. Chem.* 285, 26341–26349. doi: 10.1074/jbc.M110.139931

Fujita, H., Hamaki, T., Handa, N., Ohwada, A., Tomiyama, J., and Nishimura, S. (2012). Hypocholesterolemia in patients with polycythemia vera. *J. Clin. Exp. Hematop.* 52, 85–89. doi: 10.3960/jslrt.52.85

Fukao, T., Mitchell, G., Sass, J. O., Hori, T., Orii, K., and Aoyama, Y. (2014). Ketone body metabolism and its defects. *J. Inherit. Metab. Dis.* 37, 541–551. doi: 10.1007/s10545-014-9704-9

Giarratana, M. C., Kobari, L., Lapillonne, H., Chalmers, D., Kiger, L., Cynober, T., et al. (2005). Ex vivo generation of fully mature human red blood cells from hematopoietic stem cells. *Nat. Biotechnol.* 23, 69–74. doi: 10.1038/nbt1047

Giarratana, M. C., Rouard, H., Dumont, A., Kiger, L., Safeukui, I., Le Pennec, P. Y., et al. (2011). Proof of principle for transfusion of in vitro-generated red blood cells. *Blood* 118, 5071–5079. doi: 10.1182/blood-2011-06-362038

Havel, R. J., Eder, H. A., and Bragdon, J. H. (1955). The distribution and chemical composition of ultracentrifugally separated lipoproteins in human serum. *J. Clin. Invest.* 34, 1345–1353. doi: 10.1172/JCI103182

Hiroyama, T., Miharada, K., Sudo, K., Danjo, I., Aoki, N., and Nakamura, Y. (2008). Establishment of mouse embryonic stem cell-derived erythroid progenitor cell lines able to produce functional red blood cells. *PLoS One* 3:e1544. doi: 10.1371/journal.pone.0001544

Hricik, T., Federici, G., Zeuner, A., Alimena, G., Tafuri, A., Tirelli, V., et al. (2013). Transcriptomic and phospho-proteomic analyzes of erythroblasts expanded in vitro from normal donors and from patients with polycythemia vera. *Am. J. Hematol.* 88, 723–729. doi: 10.1002/ajh.23487

Huang, N. J., Lin, Y. C., Lin, C. Y., Pishesha, N., Lewis, C. A., Freinkman, E., et al. (2018). Enhanced phosphocholine metabolism is essential for terminal erythropoiesis. *Blood* 131, 2955–2966. doi: 10.1182/blood-2018-03-838516

Ikon, N., and Ryan, R. O. (2017). Cardiolipin and mitochondrial cristae organization. *Biochim. Biophys. Acta Biomembr.* 1859, 1156–1163. doi: 10.1016/j.bbamem.2017.03.013

Jira, P. E., Waterham, H. R., Wanders, R. J., Smeitink, J. A., Sengers, R. C., and Wevers, R. A. (2003). Smith-Lemli-Opitz syndrome and the DHCR7 gene. *Ann. Hum. Genet.* 67(Pt 3), 269–280. doi: 10.1046/j.1469-1809.2003.00034.x

Leal, J. K. F., Adjobo-Hermans, M. J. W., and Bosman, G. J. C. G. M. (2018). Red blood cell homeostasis: mechanisms and effects of microvesicle generation in health and disease. *Front. Physiol.* 9:703. doi: 10.3389/fphys.2018.00703

Leberbauer, C., Boulm, F., Unfried, G., Huber, J., Beug, H., and Mullner, E. W. (2005). Different steroids co-regulate long-term expansion versus terminal differentiation in primary human erythroid progenitors. *Blood* 105, 85–94. doi: 10.1182/blood-2004-03-1002

Lee, R. A., Harris, C. A., and Wang, J. C. (2018). Glucocorticoid receptor and adipocyte biology. *Nucl. Receptor Res.* 5:101373. doi: 10.32527/2018/101373

Litvinov, D. Y., Savushkin, E. V., and Dergunov, A. D. (2018). Intracellular and plasma membrane events in cholesterol transport and homeostasis. *J. Lipids.* 2018:3965054. doi: 10.1155/2018/3965054

Marijanovic, Z., Laubner, D., Moller, G., Gege, C., Husen, B., Adamski, J., et al. (2003). Closing the gap: identification of human 3-ketosteroid reductase, the last unknown enzyme of mammalian cholesterol biosynthesis. *Mol. Endocrinol.* 17, 1715–1725.

Mårtensson, C. U., Doan, K. N., and Becker, T. (2017). Effects of lipids on mitochondrial functions. *Biochim. Biophys. Acta Mol. Cell Biol. Lipids.* 1862, 102–113. doi: 10.1016/j.bbalip.2016.06.015

Masiello, F., Tirelli, V., Sanchez, M., van den Akker, E., Gabriella, G., Marconi, M., et al. (2013). Mononuclear cells from a rare blood donor, after freezing under good manufacturing practice conditions, generate red blood cells that recapitulate the rare blood phenotype. *Transfusion* 54, 1059–1070. doi: 10.1111/trf.12391

Migliaccio, A. R., Whitsett, C., Papayannopoulou, T., and Sadelain, M. (2012). The potential of stem cells as an in vitro source of red blood cells for transfusion. *Cell Stem Cell* 10, 115–119. doi: 10.1016/j.stem.2012.01.001

Migliaccio, G., Di Pietro, R., di Giacomo, V., Di Baldassarre, A., Migliaccio, A. R., Maccioni, L., et al. (2002). In vitro mass production of human erythroid cells from the blood of normal donors and of thalassemic patients. *Blood Cells Mol. Dis.* 28, 169–180. doi: 10.1006/bcmd.2002.0502

Migliaccio, G., Masiello, F., Tirelli, V., Sanchez, M., Varricchio, L., Whitsett, C., et al. (2011). Under HEMA conditions, self-replication of human erythroblasts is limited by autophagic death. *Blood Cells Mol. Dis.* 47, 182–197. doi: 10.1016/j.bcmd.2011.06.001

Migliaccio, G., and Migliaccio, A. R. (1987). Cloning of human erythroid progenitors (BFU-E) in the absence of fetal bovine serum. *Brit. J. Hemat.* 67, 129–133.

Migliaccio, G., Sanchez, M., Masiello, F., Tirelli, V., Varricchio, L., Whitsett, C., et al. (2010). Humanized culture medium for clinical expansion of human erythroblasts. *Cell Transplant.* 19, 453–469. doi: 10.3727/096368909X485049

Miharada, K., Hiroyama, T., Sudo, K., Nagasawa, T., and Nakamura, Y. (2006). Efficient enucleation of erythroblasts differentiated in vitro from hematopoietic stem and progenitor cells. *Nat. Biotechnol.* 24, 1255–1256. doi: 10.1038/nbt1245

Mohandas, N., and Gallagher, P. G. (2008). Red cell membrane: past, present, and future. *Blood* 112, 3939–3948. doi: 10.1182/blood-2008-07-161166

Moras, M., Lefevre, S. D., and Ostuni, M. A. (2017). From erythroblasts to mature red blood cells: organelle clearance in mammals. *Front. Physiol.* 8:1076. doi: 10.3389/fphys.2017.01076

Neildez-Nguyen, T. M., Wajcman, H., Marden, M. C., Bensidhoum, M., Moncollin, V., Giarratana, M. C., et al. (2002). Human erythroid cells produced ex vivo at large scale differentiate into red blood cells in vivo. *Nat. Biotechol.* 20, 467–472. doi: 10.1038/nbt0502-467

Nguyen, D. B., Ly, T. B., Wesseling, M. C., Hittinger, M., Torge, A., Devitt, A., et al. (2016). Characterization of microvesicles released from human red blood cells. *Cell Physiol. Biochem.* 38, 1085–1099. doi: 10.1159/000443059

Paradies, G., Paradies, V., De Benedictis, V., Ruggiero, F. M., and Petrosillo, G. (2014). Functional role of cardiolipin in mitochondrial bioenergetics. *Biochim. Biophys. Acta* 1837, 408–417. doi: 10.1016/j.bbabio.2013.10.006

Patel, R., Williams-Dautovich, J., and Cummins, C. L. (2014). Minireview: new molecular mediators of glucocorticoid receptor activity in metabolic tissues. *Mol. Endocrinol.* 28, 999–1011. doi: 10.1210/me.2014-1062

Pollet, H., Conrard, L., Cloos, A. S., and Tyteca, D. (2018). Plasma membrane lipid domains as platforms for vesicle biogenesis and shedding? *Biomolecules* 8:94. doi: 10.3390/biom8030094

Radding, C. M., and Steinberg, D. (1960). Studies on the synthesis and secretion of serum lipoproteins by rat liver slices. *J. Clin. Invest.* 39, 1560–1569. doi: 10.1172/JCI104177

Raposo, G., and Stoorvogel, W. (2013). Extracellular vesicles: exosomes, microvesicles, and friends. *JCB* 200, 373–383. doi: 10.1083/jcb.201211138

Saraf, S. L., Shah, B. N., Zhang, X., Han, J., Tayo, B. O., Abbasi, T., et al. (2017). APOL1, α-thalassemia, and BCL11A variants as a genetic risk profile for progression of chronic kidney disease in sickle cell anemia. *Haematologica* 102, e1–e6. doi: 10.3324/haematol.2016.154153

Seijkens, T., Hoeksema, M. A., Beckers, L., Smeets, E., Meiler, S., Levels, J., et al. (2014). Hypercholesterolemia-induced priming of hematopoietic stem and progenitor cells aggravates atherosclerosis. *FASEB J.* 28, 2202–2213. doi: 10.1096/fj.13-243105

Selvaggi, T. A., Walker, R. E., and Fleisher, T. A. (1997). Development of antibodies to fetal calf serum with arthus-like reactions in human immunodeficiency virus-infected patients given syngeneic lymphocyte infusions. *Blood* 89, 776–779.

Søberg, K., and Skålhegg, B. S. (2018). The Molecular Basis for Specificity at the Level of the Protein Kinase a Catalytic Subunit. *Front. Endocrinol.* 9:538. doi: 10.3389/fendo.2018.00538

Tanabe, O., Shen, Y., Liu, Q., Campbell, A. D., Kuroha, T., Yamamoto, M., et al. (2007). The TR2 and TR4 orphan nuclear receptors repress Gata1 transcription. *Genes Dev.* 21, 2832–2844. doi: 10.1101/gad.1593307

Tuschong, L., Soenen, S. L., Blaese, R. M., Candotti, F., and Muul, L. M. (2002). Immune response to fetal calf serum by two adenosine deaminase-deficient patients after T cell gene therapy. *Hum. Gene Ther.* 13, 1605–1610. doi: 10.1089/10430340260201699

van den Akker, E., Satchwell, T. J., Pellegrin, S., Daniels, G., and Toye, A. M. (2010). The majority of the in vitro erythroid expansion potential resides in CD34(-) cells, outweighing the contribution of CD34(+) cells and significantly increasing the erythroblast yield from peripheral blood samples. *Haematologica* 95, 1594–1598. doi: 10.3324/haematol.2009.019828

van den Broek, I., Sobhani, K., and Van Eyk, J. E. (2017). Advances in quantifying apolipoproteins using LC-MS/MS technology: implications for the clinic. *Expert Rev. Proteomics* 14, 869–880. doi: 10.1080/14789450.2017.1374859

von Lindern, M., Zauner, W., Mellitzer, G., Steinlein, P., Fritsch, G., Huber, K., et al. (1999). The glucocorticoid receptor cooperates with the erythropoietin receptor and c-Kit to enhance and sustain proliferation of erythroid progenitors in vitro. *Blood* 94, 550–559.

Vuorio, A., Watts, G. F., and Kovanen, P. T. (2018). Lipoprotein(a) as a risk factor for calcific aortic valvulopathy in heterozygous familial hypercholesterolemia. *Atherosclerosis* 281, 25–30. doi: 10.1016/j.atherosclerosis.2018.11.040

Wahl, P., Ducasa, G. M., and Fornoni, A. (2016). Systemic and renal lipids in kidney disease development and progression. *Am. J. Physiol. Renal Physiol.* 310, F433–F445. doi: 10.1152/ajprenal.00375.2015

Wang, Z., Cao, L., Su, Y., Wang, G., Wang, R., Yu, Z., et al. (2014). Specific macrothrombocytopenia/hemolytic anemia associated with sitosterolemia. *Am. J. Hematol.* 89, 320–324. doi: 10.1002/ajh.23619

Wendel, A. A., Lewin, T. M., and Coleman, R. A. (2009). Glycerol-3-phosphate acyltransferases: rate limiting enzymes of triacylglycerol biosynthesis. *Biochim. Biophys. Acta* 1791, 501–506. doi: 10.1016/j.bbalip.2008.10.010

Woods, C. P., Hazlehurst, J. M., and Tomlinson, J. W. (2015). Glucocorticoids and non-alcoholic fatty liver disease. *J. Steroid Biochem. Mol. Biol.* 154, 94–103. doi: 10.1016/j.jsbmb.2015.07.020

Yvan-Charvet, L., Pagler, T., Gautier, E. L., Avagyan, S., Siry, R. L., Han, S., et al. (2010). ATP-binding cassette transporters and HDL suppress hematopoietic stem cell proliferation. *Science* 328, 1689–1693. doi: 10.1126/science.1189731

Zeuner, A., Martelli, F., Vaglio, S., Federici, G., Whitsett, C., and Migliaccio, A. R. (2012). Concise review: stem cell-derived erythrocytes as upcoming players in blood transfusion. *Stem Cells* 30, 1587–1596. doi: 10.1002/stem.1136

Zhang, L., Prak, L., Rayon-Estrada, V., Thiru, P., Flygare, J., Lim, B., et al. (2013). ZFP36L2 is required for self-renewal of early burst-forming unit erythroid progenitors. *Nature* 499, 92–96. doi: 10.1038/nature12215

Conflict of Interest Statement: The authors declare that the research was conducted in the absence of any commercial or financial relationships that could be construed as a potential conflict of interest.

frontiers in Physiology

BRIEF RESEARCH REPORT
published: 19 June 2019
doi: 10.3389/fphys.2019.00753

The Evolution of Erythrocytes Becoming Red in Respect to Fluorescence

*Laura Hertz[1], Sandra Ruppenthal[1], Greta Simionato[2,3], Stephan Quint[3], Alexander Kihm[3], Asena Abay[3], Polina Petkova-Kirova[1], Ulrich Boehm[4], Petra Weissgerber[4], Christian Wagner[3,5], Matthias W. Laschke[6] and Lars Kaestner[2,3]**

[1] Institute for Molecular and Cell Biology, Saarland University, Homburg, Germany, [2] Theoretical Medicine and Biosciences, Saarland University, Homburg, Germany, [3] Experimental Physics, Saarland University, Saarbrücken, Germany, [4] Center for Molecular Signaling (PZMS), Institute for Pharmacology, Saarland University, Homburg, Germany, [5] Physics and Materials Science Research Unit, University of Luxembourg, Luxembourg City, Luxembourg, [6] Institute for Clinical and Experimental Surgery, Saarland University, Homburg, Germany

Very young red blood cells, namely reticulocytes, can be quite easily recognized and labeled by cluster of differentiation antibodies (CD71, transferrin receptor) or by staining remnant RNA with thiazol orange. In contrast, age specific erythrocyte labeling is more difficult in later periods of their life time. While erythrocytes contain band 4.1 protein, a molecular clock, so far it has not been possible to read this clock on individual cells. One concept to track erythrocytes during their life time is to mark them when they are young, either directly *in vivo* or *ex vivo* followed by a transfusion. Several methods like biotinylation, use of isotopes or fluorescent labeling have proved to be useful experimental approaches but also have several inherent disadvantages. Genetic engineering of mice provides additional options to express fluorescent proteins in erythrocytes. To allow co-staining with popular green fluorescent dyes like Fluo-4 or other fluorescein-based dyes, we bred a mouse line expressing a tandem red fluorescent protein (tdRFP). Within this *Brief Research Report*, we provide the initial characterisation of this mouse line and show application examples ranging from transfusion experiments and intravital microscopy to multicolour flow cytometry and confocal imaging. We provide a versatile new tool for erythrocyte research and discuss a range of experimental opportunities to study membrane processes and other aspects of erythrocyte development and aging with help of these animals.

Keywords: mouse model, transfusion, fluorescent protein, intravital microscopy, imaging

OPEN ACCESS

Edited by:
Eitan Fibach,
Hadassah Medical Center, Israel

Reviewed by:
Giel Bosman,
Radboud University Nijmegen, Netherlands
James Palis,
University of Rochester, United States

***Correspondence:**
Lars Kaestner
lars_kaestner@me.com

Specialty section:
This article was submitted to Red Blood Cell Physiology, a section of the journal Frontiers in Physiology

Received: *15 March 2019*
Accepted: *31 May 2019*
Published: *19 June 2019*

Citation:
Hertz L, Ruppenthal S, Simionato G, Quint S, Kihm A, Abay A, Petkova-Kirova P, Boehm U, Weissgerber P, Wagner C, Laschke MW and Kaestner L (2019) The Evolution of Erythrocytes Becoming Red in Respect to Fluorescence. Front. Physiol. 10:753. doi: 10.3389/fphys.2019.00753

INTRODUCTION

We face many scenarios in erythrocyte research where we need to label erythrocytes. This might be in the context of determining a particular cell shape (Quint et al., 2017), transfusion experiments (Dholakia et al., 2015) or following cell age (Wang et al., 2013). There are numerous strategies available to label erythrocytes based on small molecular dyes (Haugland, 2002), antibodies (Pepe, 1968) or fluorescent proteins (Jung, 2011). Especially the latter one has particular advantages such as high biocompatibility due to cell internal translation, permanent expression and specific subcellular localization (Kaestner et al., 2014). Fluorescent proteins have proved to be useful tools to label cells (Stearns, 1995), to follow protein function (Lipp et al., 2014) or to construct biosensors (Kaestner et al., 2018). Most transgenic approaches in mammals were performed in mice making them the currently most widely used animal model. Considering the wide range of

colors of fluorescent proteins (Shaner et al., 2004) and the great variety of available promoters (Chen et al., 2011), little attention has been paid to erythrocytes. Several attempts have been made to generate mice with ubiquitous expression of fluorescent proteins, e.g., Fink et al. (2010) but to our best knowledge, this has not yet led to efficient fluorescent erythrocyte labeling. However, there are several studies of primitive erythroid cells with a green fluorescent protein (GFP) fused to the ε-globin, e.g., Lucitti and Dickinson (2006), Isern et al. (2008). The use of GFP has, especially in comparison to red fluorescent proteins, numerous disadvantages, such as spectral overlap of excitation and emission with the absorption spectrum of hemoglobin (Kaestner et al., 2006), decreased penetration depth for *in vivo* investigations (Bozhanova et al., 2018) or spectral overlap with some of the most popular fluorescent biosensors, such as Ca^{2+} indicators (Lipp and Kaestner, 2014). Therefore, we set out to genetically label erythrocytes with red fluorescence in mice.

MATERIALS AND METHODS

Mice

Permissions

All animal experiments were performed according to the Guide for the Care and Use of Laboratory Animals published by the U.S. National Institutes of Health and approved by the local governmental animal protection committee (approval numbers 02/2015, 06/2015 and 27/2018).

Breeding

Mice were kept under a standard light/dark cycle with food and water *ad libitum* in a specific pathogen-free animal facility. *Rosa26-tdRFP* mice were previously described (Luche et al., 2007) and kindly provided by Hans Jörg Fehling (Ulm University, Germany). Animals with an activated *Rosa26-tdRFP* allele (*R26-tdRFP-CMV*) were generated by crossing homozygous *Rosa26-NEO-STOP-tdRFP* mice with a heterozygous ubiquitous CMV-Cre deleter strain carrying a huCMV-Cre transgene on the X-chromosome (Schwenk et al., 1995). The resulting heterozygous *R26-tdRFP-CMV* offspring was then crossed *inter se* to obtain homozygous *R26-tdRFP-CMV* mice for analysis. Homozygous *R26-tdRFP-CMV* animals were obtained at expected Mendelian frequencies and did not show any obvious phenotypic abnormalities. The homozygous *R26-tdRFP-CMV* mice were fertile and exhibited robust red fluorescence in erythrocytes.

Erythrocyte Mass Parameters and Indices

Analysis of the erythrocyte mass parameters and indices was performed using a fully automated hematology analyzer (VetScan HM5, Abaxis, Union City, CA, United States). Blood was collected from *R26-tdRFP-CMV* mice with homozygous RFP expression ($RFP^{+/+}$) and $RFP^{-/-}$ siblings.

Transfusions

For transfusion experiments blood was collected from wild type (C57BL/6 mice, Charles River Laboratories, Saint-Constant, QC, Canada) and *R26-tdRFP-CMV* mice by puncture of the heart (final bleeding after 1.5% isoflurane inhalation anesthesia). Wild type erythrocytes were stained using the membrane dye PKH67 (Sigma-Aldrich, St. Louis, MO, United States). Cells were washed three times in 0.9% NaCl solution and incubated for 5 min at room temperature under rotation with PKH67 (1:200 dilution). Quenching of remaining dye was done by addition of 2% bovine serum albumin (BSA) in phosphate buffered solution (PBS) and the cells were washed again three times in 0.9% NaCl solution.

Stained wild type erythrocytes and erythrocytes from *R26-tdRFP-CMV* mice were mixed and a volume of 200 µl was retro-orbitally injected into wild type C57BL/6 mice (Charles River Laboratories, Saint-Constant, QC, Canada). The survival rate of transfused erythrocytes was analyzed by flow cytometry for 1 month. For this purpose, 10 µl blood samples of transfused mice were collected by puncture of the tail vein. The first sample was taken within 5 min after transfusion and the measured value used for normalization of the data. Analysis of the data was done using GraphPad Prism (GraphPad, La Jolla, CA, United States).

In vivo Imaging Experiments

Animals

In vivo experiments were performed in 12- to 14-week old male C57BL/6 mice with a body weight of 24–26 g. The animals were bred and housed in open cages in the conventional animal husbandry of the Institute for Clinical and Experimental Surgery (Saarland University, Germany) in a temperature-controlled environment under a 12 h/12 h light-dark cycle and had free access to drinking water and standard pellet food (Altromin, Lage, Germany).

Dorsal Skinfold Chamber Model

Red blood cell passage of small capillaries was analyzed in the dorsal skinfold chamber model, as previously described (Danielczok et al., 2017). For chamber implantation, mice were anaesthetized by i.p. injection of ketamine (75 mg/kg body weight; Ursotamin®; Serumwerk Bernburg, Bernburg, Germany) and xylazine (15 mg/kg body weight; Rompun®; Bayer, Leverkusen, Germany). Subsequently, two symmetrical titanium frames (Irola Industriekomponenten GmbH & Co. KG, Schonach, Germany) were implanted on the extended dorsal skinfold of the animals in a stepwise procedure, as previously described (Laschke and Menger, 2016). Within the area of the observation window, one layer of skin was completely removed in a circular area of ∼15 mm in diameter. The remaining layers (striated skin muscle, subcutaneous tissue and skin) were finally covered with a removable cover glass. To exclude alterations of the microcirculation due to the surgical intervention, the mice were allowed to recover for 48 h after implantation.

In vivo Microscopy

In vivo microscopic analyses were performed as previously described (Brust et al., 2014). In detail, the mice were anaesthetized and a fine polyethylene catheter (PE10, 0.28 mm internal diameter) was inserted into the *carotid artery* to apply RFP-labeled erythrocytes. Then, the animals were put in lateral decubital position on a Plexiglas pad and the dorsal skinfold

chamber was attached to the microscopic stage of an upright microscope (ECLIPSE Ci-L; Nikon, Tokyo, Japan) equipped with a 40×, NA 0.8, water immersion objective and a LED array (pE300ultra, CoolLED, Andover, United Kingdom) attached to a fluorescein isothiocyanate (FITC) filterset (excitation 465–495 nm, emission 515–555 nm). Up to 0.5 ml of RFP-expressing erythrocytes were transfused immediately before the imaging experiments. The microscopic images were recorded using a CMOS video camera (Prime 95B, Photometrics, Tucson, AZ, United States) connected to a PC at an acquisition speed of 415 images per second.

Trajectory Analysis

The recorded video sequence was analyzed using a single particle tracking algorithm, as previously described (Bächer et al., 2018). Hereby, the intensity profile of each frame was adjusted to have both the top and bottom 1% of all pixels saturated, correcting for changes in illumination and exposure time. With the aid of a tailored MATLAB script, all spherical (round) objects were detected and interconnected among all frames by cross-correlating consecutive images. We derived the respective trajectories by combining the coordinates of all classified erythrocytes over the whole video sequence.

Single Cell Analysis

Bone Marrow Preparation

For the isolation of bone marrow, two mice were sacrificed by an overdose of anesthetics. The femurs and tibias were carefully excised and bone marrow cells were obtained by flushing the bones with cold Tyrode solution containing (in mM): 35 NaCl, 5.4 KCl, 10 glucose, 1 $MgCl_2$, 1.8 $CaCl_2$ and 10 HEPES, pH 7.4. Cells were stained with Hoechst 33258 solution (Sigma-Aldrich, St. Louis, MO, United States) at a final concentration of 10 μg/ml and a TER-119 antibody (Biolegend, San Diego, CA, United States) at 2 μg/ml in PBS at room temperature for 20 min. Cells were washed once before imaging (see below).

Blood Sample Preparation

Blood samples of wild type and *R26-tdRFP-CMV* mice were collected by puncture of the tail vein. Ten μl of blood were diluted in 1 ml Tyrode solution. Erythrocytes were washed three times via centrifugation at 2,500 × *g* for 3 min. The supernatant was discarded each time and the cells resuspended in Tyrode solution.

Confocal Imaging

Bone marrow cells or erythrocytes were suspended in PBS, 0.1% BSA and placed between two glass slides spaced by 20 μm polystyrene beads for imaging on top of a 100× objective of an inverted microscope (Nikon ECLIPSE Ti, Tokyo, Japan). A diode or solid state laser (405, 488, and 561 nm, Nikon LU-NV Laser Unit) was used as a light source for imaging. Z-stack scanning was realized with 300 nm step of piezo motor of a confocal spinning disk (CSU-W1, Yokogawa Electric Corporation, Tokyo, Japan), scanning from top to bottom for a 20 μm *z*-range. Image sequence was acquired by recording with a digital camera (Orca-Flash4.0 Hamamatsu Photonics, Hamamatsu City, Japan). Confocal slices were processed using ImageJ (Wayne Rasband, NIH, United States). 3D-rendering was performed with Vision4D (Arivis, Rostock, Germany).

Flow Cytometry

Fluo-4 (Thermo Fisher Scientific, Waltham, MA, United States) loading of blood samples was done for 1 h at 37°C at a concentration of 5 μM followed by one more washing step. Flow cytometer experiments were performed using a FACSAria III (Becton Dickinson, Franklin Lakes, NJ, United States). Analysis of the data was done using FlowJo 10.4.2 (FlowJo LLC, Ashland, OR, United States).

Statistics

For all statistical analyses the Gaussian distribution of the dataset was checked by the Kolmogorov–Smirnov test. For data with Gaussian distribution the mean value ± the standard deviation was plotted. Testing for significant differences was performed with a paired *t*-test. All graph presentations and statistical tests were performed in GraphPad Prism (GraphPad Software, La Jolla, CA, United States).

RESULTS AND DISCUSSION

Generating Mice With Red Fluorescent Erythrocytes

To generate a mouse model with fluorescently labeled erythrocytes, we aimed for three major properties: (i) the fluorescent protein should emit in the red spectral range for reasons already outlined in the introduction; (ii) the fluorescent protein should be strongly expressed as mature erythrocytes are lacking a transcriptional and translational machinery; and (iii) the fluorescent protein should be cytosolic in order to leave the cell membrane undisturbed. *R26-tdRFP* mice encode the untargeted (and therefore cytosolic) red fluorescent protein (RFP) tandem construct tdimer2(12) (Campbell et al., 2002) under control of the *ROSA26* locus and therefore seems to fulfil all defined criteria. To activate RFP expression in erythrocytes, *R26-tdRFP* mice were crossed with a CMV-Cre line (Schwenk et al., 1995), leading to ubiquitous Cre recombinase – and thus RFP – expression. The breeding scheme is depicted in **Figure 1A**. Heterozygous mice from the F1 generation were crossed *inter se* to generate *R26-tdRFP-CMV* mice with a homozygous expression of RFP. While homozygous *R26-tdRFP-CMV* pups showed 100% red fluorescent erythrocytes, heterozygous *R26-tdRFP-CMV* mice expressed a rather inhomogeneous pattern (**Figure 1B**) and were therefore not used for further investigations. RFP-negative control mice did not display red fluorescence. The tdRFP is ubiquiously expressed in all organs as exemplified in **Supplementary Figure S1**. Compared to (Luche et al., 2007), which describes the initial generation and characterization of the *Rosa26-tdRFP* mouse, our results revealed bright fluorescence in erythrocytes isolated from homozygous *R26-tdRFP-CMV* mice (**Figure 1C**).

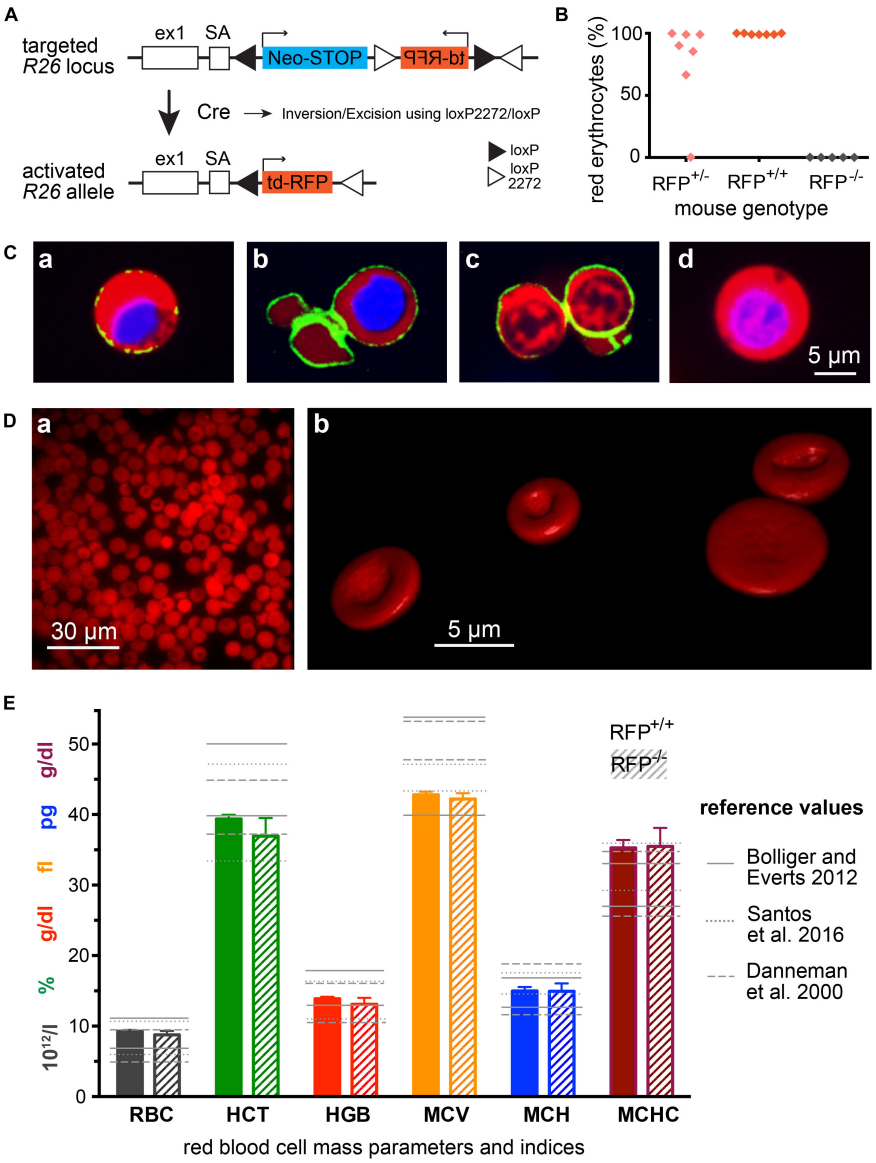

FIGURE 1 | Mice with RFP erythrocytes. **(A)** Genetic strategy to generate *R26-tdRFP-CMV-Cre* mice. Mice expressing Cre recombinase under control of the cytomegalovirus (CMV) promoter were bred to *R26-tdRFP* mice carrying a *loxP*-flanked *tdRFP* gene in the *ROSA26* locus. *R26-tdRFP-CMV-Cre* mice ubiquitously express tdRFP controlled by the *ROSA26* promoter. **(B)** Percentage of red fluorescent erythrocytes in $RFP^{+/+}$ (homozygous), $RFP^{+/-}$ (heterozygous) and $RFP^{-/-}$ (negative) mice. Each point represents an individual mouse. **(C)** Confocal images of cells from the bone marrow of *R26-tdRFP-CMV-Cre* mice. Beside the RFP fluorescence, the nuclei were stained with Hoechst dye (depicted in blue). Additionally a Ter119-FITC antibody was used to visualize the erythropoietic cells, **(Ca)** proerythroblast, **(Cb)** erythroblast, and **(Cc)** reticulocyte. For comparison we display a non-erythropoietic cell, and **(Cd)** from the bone marrow. **(D)** Images of RFP erythrocytes, **(Da)** epi-fluorescence microscopy of a population of erythrocytes, and **(Db)** 3D-rendered individual erythrocytes out of a z-stack of confocal images. **(E)** Erythrocyte mass parameters and indices. Displayed are the parameters erythrocyte count (RBC), haematocrit (HCT), haemoglobin (HGB), mean cellular volume (MCV), mean cellular haemoglobin (MCH), and mean cellular haemoglobin concentration (MCHC). The columns depict mean values and error bars represent the standard deviation out of 5 $RFP^{+/+}$ and 5 $RFP^{-/-}$ mice. The reference values are taken from Danneman et al. (2000), Bollinger and Everds (2012), and Santos et al. (2016).

Properties of Mice With Red Fluorescent Erythrocytes

We did not detect any obvious phenotypic differences in *R26-tdRFP-CMV* mice, except for the red fluorescence, when compared to wild type C57BL/6 mice. We imaged erythropoietic precursor cells from the bone marrow as outlined in **Figure 1C**. The translational more active cells that still contain a nucleus (**Figures 1Ca,b**) show a stronger expression of tdRFP compared to reticulocytes (**Figure 1Cc**). However, the erythrocytes showed a homogeneous red fluorescence as exemplified in **Figure 1Da** and the fluorescent protein was expressed at levels high enough to allow for confocal imaging of *z*-stacks and consecutive

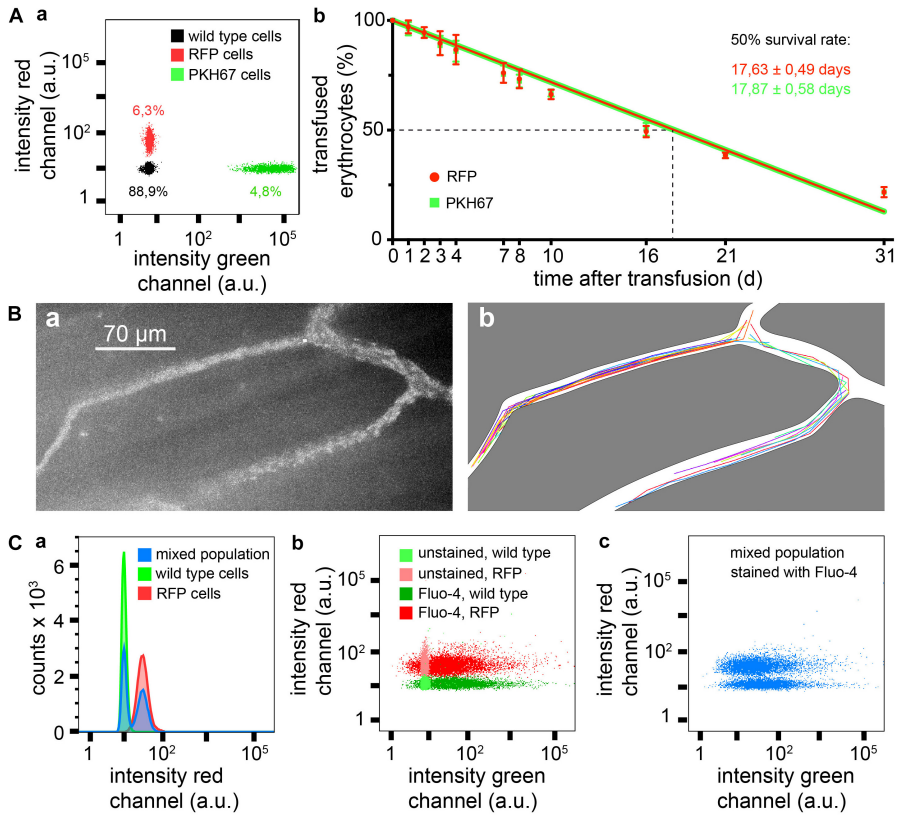

FIGURE 2 | Measurements based on RFP erythrocytes. **(A)** Survival of transfused erythrocytes, **(Aa)** flow cytometric sample measurement immediately after transfusion showing 6.3% of RFP cells and 4.8% of PKH67 stained cells, and **(Ab)** statistical analysis of four transfusions over a time period of 1 month, RFP and PKH67 stained erythrocytes were simultaneously transfused in the same mouse to face identical conditions. **(B)** Intravital imaging of transfused RBCs, **(Ba)** maximal intensity projection of a time series of images, and **(Bb)** trajectories of individual erythrocytes from the same image stack as shown in Ba. **(C)** Flow cytometry of Fluo-4 loaded erythrocytes from $RFP^{+/+}$ and $RFP^{-/-}$ mice, **(Ca)** histograms of red fluorescence of $RFP^{-/-}$ and $RFP^{+/+}$ erythrocytes and of a mixed population (simulating transfusion), **(Cb)** dot plot for red vs. green fluorescence of Fluo-4 stained and unstained $RFP^{+/+}$ and $RFP^{-/-}$ erythrocytes, and **(Cc)** dot plot for red *vs.* green fluorescence of a Fluo-4 stained mixed population of RFP and wild type erythrocytes (simulating transfusion).

3D-redering as shown in **Figure 1Db** (see also **Supplementary Video 1**), demonstrating that RFP expression is sufficient for fluorescence-based cell shape analysis.

Since we designed the mouse line for erythrocyte research, we next analyzed erythrocyte mass parameters and indices and plotted them in **Figure 1E** in comparison with text book values for laboratory mice in general (Danneman et al., 2000; Bollinger and Everds, 2012) as well as for a particular investigation on C57BL/6 mice (Santos et al., 2016). Except for MCHC all values were within the reference range. However, since MCV is on the lower end of the range and haemoglobin concentration (HGB) rather high, it is not surprising that MCHC is at the upper range or slightly above. The reason is that in the used device (VetScan HM5) the MCHC is calculated out of the MCV and the HGB using the following formula: $MCHC = HGB/n \times MCV$ (VetScan HM5, 2018), with n being the number of RBCs per volume. HGB is measured photometrically at 540 nm and MCV is the average volume of RBCs derived from the RBC histogram. Considering the differences even in the ranges in-between textbooks, we conclude that erythrocytes of *R26-tdRFP-CMV* mice are within the physiological variation. Importantly, erythrocytes from $RFP^{+/+}$ mice were not different when compared to those of $RFP^{-/-}$ mice demonstrating the RFP itself does not influence the integrity of the parameters' measurement procedure/principle.

Transfusion Experiments With Red Fluorescent Erythrocytes

To test the transfusion ability of erythrocytes isolated from *R26-tdRFP-CMV* mice we wanted to compare the survival of these cells after transfusion with cells fluorescently labeled with the PKH67 dye (green fluorescence), a marker that proved to be successful in previous transfusion experiments in mice (Wang et al., 2013). To enable a direct comparison under identical conditions both RFP erythrocytes and PKH67 labeled erythrocytes were simultaneously transfused into the same mouse. **Figure 2Aa** depicts a flow cytometric analysis measurement of a blood sample after transfusion. **Figures 2Ab** shows the time course of 1 month of the erythrocyte survival after transfusion. There was no difference between RFP erythrocytes and PKH67 labeled ones. The half life of the transfused

erythrocytes was 17.63 ± 0.49 days for RFP and 17.87 ± 0.58 days for PKH67 labeled cells. Considering that the mean erythrocyte life span varies between different mouse strains in the range of 38–42.5 days and also taking into consideration that the random destruction can vary between 0.6 and 1.3% of erythrocytes per day (Horky et al., 1978), our results are in the same range as reported in previous studies where, e.g., for the popular biotinylation a half life of 20.5 ± 2.1 days was determined (Dholakia et al., 2015).

Taken together, these data demonstrate that the RFP mice are suited as erythrocyte donors for transfusion experiments. If reticulocytosis is induced in these donor mice, the reticulocytes can easily reach counts of 30% (Wang et al., 2013). If then reticulocytes are enriched, for example by using CD71-coated magnetic beads, a pure reticulocyte preparation can be transfused and such, membrane processes or other aspects of erythrocyte development and aging can be investigated, either directly *in vivo* (see below) or by blood sampling at defined time points.

In vivo Measurements of Transfused Red Fluorescent Erythrocytes

Erythrocyte properties in flow and in particular in the circulation differ from erythrocytes in stasis. This starts with cell shape (Kihm et al., 2018) but also applies to Ca^{2+} handling (Danielczok et al., 2017) and other parameters. To investigate erythrocytes *in vivo*, the model of the dorsal skinfold chamber has proven to be a useful tool (Menger et al., 2002). **Figure 2B** provides a proof of principle experiment demonstrating that the fluorescence intensity of the RFP cells is sufficient for this kind of investigations. A single particle tracking algorithm was applied to extract the trajectories of individual cells, which can be used to investigate flow properties of erythrocytes (Bächer et al., 2018). In addition to **Figure 2B** we provide **Supplementary Video 2** at a different magnification to illustrate the experimental opportunities.

Flow Cytometry With Additional Fluorescent Labeled Red Fluorescent Erythrocytes

Fluorescein-based dyes are very popular for antibody labeling as well as for functional biosensors. For the special but very important purpose of measuring Ca^{2+} homeostasis in erythrocytes, the fluorescein-based Ca^{2+} indicator Fluo-4 is the only serious option (Kaestner et al., 2006). Therefore we took Fluo-4 as an example to demonstrate that RFP and Fluo-4 together work well in erythrocytes. **Figure 2C** shows flow cytometric measurements of wild type and RFP erythrocytes loaded with Fluo-4, in separate measurements as well as in a mixed population, demonstrating a clear differentiation of the two populations and the lack of crosstalk between Fluo-4 and RFP.

SUMMARY

We generated a novel mouse strain to robustly label erythrocytes with red fluorescence. We demonstrate that the RFP fluorescence intensity in erythrocytes is sufficient for a range of applications in erythrocyte research such as 3D-shape analysis (**Figure 1Db** and **Supplementary Video 1**), transfusion experiments (**Figures 2A,Ba**), intravital microscopy (**Figure 2B** and **Supplementary Video 2**) and fluorescence multiplexing (**Figures 2Aa,C**).

DATA AVAILABILITY

All datasets generated for this study are included in the manuscript and/or the **Supplementary Files**.

ETHICS STATEMENT

All animal experiments were performed according to the Guide for the Care and Use of Laboratory Animals published by the U.S. National Institutes of Health and approved by the local governmental animal protection committee (approval numbers 02/2015, 06/2015, and 27/2018).

AUTHOR CONTRIBUTIONS

LK and LH defined the study, planned the experiments, interpreted the data, and drafted the manuscript. PW, SR, and UB designed the experimental animal study. LH, ML, GS, AK, AA, PP-K, and SQ performed the data acquisition and analysis. ML, CW, PW, and UB critically revised the manuscript. All authors listed have made a substantial, direct and intellectual contribution to the work, and approved it for publication.

FUNDING

This study was supported by the European Seventh Framework Program under grant agreement number 602121 (CoMMiTMenT, LK), the European Framework "Horizon 2020" under grant agreement number 675115 (RELEVANCE, CW and LK), and the Deutsche Forschungsgemeinschaft (DFG) Sonderforschungsbereich SFB894 (PW and UB).

ACKNOWLEDGMENTS

We acknowledge the support by the Deutsche Forschungsgemeinschaft (DFG, German Research Foundation) and Saarland University within the funding programme Open Access Publishing.

SUPPLEMENTARY MATERIAL

The Supplementary Material for this article can be found online at: https://www.frontiersin.org/articles/10.3389/fphys.2019.00753/full#supplementary-material

REFERENCES

Bächer, C., Kihm, A., Schrack, L., Kaestner, L., Laschke, M. W., Wagner, C., et al. (2018). Antimargination of microparticles and platelets in the vicinity of branching vessels. *Biophys. J.* 115, 411–425. doi: 10.1016/j.bpj.2018.06.013

Bollinger, A. P., and Everds, N. (2012). "Hematology of the mouse," in *The Laboratory Mouse*. ed. H. J. Hedrich (London: Taylor & Francis), 331–334.

Bozhanova, N. G., Baranov, M. S., Baleeva, N. S., Gavrikov, A. S., and Mishin, A. S. (2018). Red-Shifted aminated derivatives of gfp chromophore for live-cell protein labeling with lipocalins. *Int. J. Mol. Sci.* 19:3778. doi: 10.3390/ijms19123778

Brust, M., Aouane, O., Thiébaud, M., Flormann, D., Verdier, C., Kaestner, L., et al. (2014). The plasma protein fibrinogen stabilizes clusters of red blood cells in microcapillary flows. *Sci. Rep.* 4:4348. doi: 10.1038/srep04348

Campbell, R. E., Tour, O., Palmer, A. E., Steinbach, P. A., Baird, G. S., Zacharias, D. A., et al. (2002). A monomeric red fluorescent protein. *Proc. Natl. Acad. Sci. U.S.A.* 99, 7877–7882. doi: 10.1073/pnas.082243699

Chen, C.-M., Krohn, J., Bhattacharya, S., and Davies, B. (2011). A Comparison of exogenous promoter activity at the ROSA26 locus using a phic31 integrase mediated cassette exchange approach in mouse ES cells. *PLoS One* 6:e23376–e23378. doi: 10.1371/journal.pone.0023376

Danielczok, J. G., Terriac, E., Hertz, L., Petkova-Kirova, P., Lautenschläger, F., Laschke, M. W., et al. (2017). Red blood cell passage of small capillaries is associated with transient Ca2+-mediated adaptations. *Front. Physiol.* 8:979. doi: 10.3389/fphys.2017.00979

Danneman, P. J., Suckow, M. A., and Brayton, C. (eds) (2000). "Important biological features," in *The Laboratory Mouse*. (Boca Raton: CRC Press), 1–20.

Dholakia, U., Bandyopadhyay, S., Hod, E. A., and Prestia, K. A. (2015). Determination of RBC Survival in C57BL/6 and C57BL/6-Tg(UBC-GFP) Mice. *Comp. Med.* 65, 196–201.

Fink, D., Wohrer, S., Pfeffer, M., Tombe, T., Ong, C. J., and Sorensen, P. H. B. (2010). Ubiquitous expression of the monomeric red fluorescent protein mcherry in transgenic mice. *Genesis* 48, 723–729. doi: 10.1002/dvg.20677

Haugland, R. P. (2002). *Handbook of Fluorescent Probes and Research Products*, 9 Edn. Eugene: Molecular Probes.

Horky, J., Vácha, J., and Znojil, V. (1978). Comparison of life span of erythrocytes in some inbred strains of mouse using 14C-labelled glycine. *Physiol. Bohemoslov.* 27, 209–217.

Isern, J., Fraser, S. T., He, Z., and Baron, M. H. (2008). The fetal liver is a niche for maturation of primitive erythroid cells. *Proc. Natl. Acad. Sci. U.S.A.* 105, 6662–6667. doi: 10.1073/pnas.0802032105

Jung, G. (ed.) (2011). *Fluorescent Proteins I*. Heidelberg: Springer.

Kaestner, L., Scholz, A., Tian, Q., Ruppenthal, S., Tabellion, W., Wiesen, K., et al. (2014). Genetically encoded Ca2+ indicators in cardiac myocytes. *Circ. Res.* 114, 1623–1639. doi: 10.1161/CIRCRESAHA.114.303475

Kaestner, L., Tabellion, W., Weiss, E., Bernhardt, I., and Lipp, P. (2006). Calcium imaging of individual erythrocytes: problems and approaches. *Cell Calcium* 39, 13–19. doi: 10.1016/j.ceca.2005.09.004

Kaestner, L., Zeug, A., and Tian, Q. (2018). "Optogenetic tools in the microscopy of cardiac excitation-contraction coupling," in *Microscopy of the Heart*. eds L. Kaestner and P. Lipp (Cham: Springer), 97–117. doi: 10.1007/978-3-319-95304-5_5

Kihm, A., Kaestner, L., Wagner, C., and Quint, S. (2018). Classification of red blood cell shapes in flow using outlier tolerant machine learning. *PLoS Comp. Biol.* 14:e1006278. doi: 10.1371/journal.pcbi.1006278

Laschke, M. W., and Menger, M. D. (2016). The dorsal skinfold chamber: a versatile tool for preclinical research in tissue engineering and regenerative medicine. *eCM* 32, 202–215. doi: 10.22203/eCM.v032a13

Lipp, P., Hui, X., Reither, G., and Kaestner, L. (2014). Multi-channel imaging of cellular signaling: interplay of Ca2+ and conventional protein kinase C. *Cold Spring Harb. Protoc.* 2014, 1180–1183. doi: 10.1101/pdb.prot077024

Lipp, P., and Kaestner, L. (2014). Detecting calcium in cardiac muscle: fluorescence to dye for. *AJP: Heart Circ. Physiol.* 307, H1687–H1690. doi: 10.1152/ajpheart.00468.2014

Luche, H., Weber, O., Nageswara Rao, T., Blum, C., and Fehling, H. J. (2007). Faithful activation of an extra-bright red fluorescent protein in "knock-in" Cre-reporter mice ideally suited for lineage tracing studies. *Eur. J. Immunol.* 37, 43–53. doi: 10.1002/eji.200636745

Lucitti, J. L., and Dickinson, M. E. (2006). Moving toward the light: using new technology to answer old questions. *Pediatr. Res.* 60, 1–5. doi: 10.1203/01.pdr.0000220318.49973.32

Menger, M. D., Laschke, M. W., and Vollmar, B. (2002). Viewing the microcirculation through the window: some twenty years experience with the hamster dorsal skinfold chamber. *Eur. Surg. Res.* 34, 83–91. doi: 10.1159/000048893

Pepe, F. A. (1968). Analysis of antibody staining patterns obtained with striated myofibrils in fluorescence microscopy and electron microscopy. *Int. Rev. Cytol.* 24, 193–231. doi: 10.1016/s0074-7696(08)61400-x

Quint, S., Christ, A. F., Guckenberger, A., Himbert, S., Kaestner, L., Gekle, S., et al. (2017). 3D tomography of cells in micro-channels. *Appl. Phys. Lett.* 111:103701. doi: 10.1063/1.4986392

Santos, E. W., Oliveira, D. C., de Hastreiter, A., Silva, G. B. D., Beltran, J. S., de, O., et al. (2016). Hematological and biochemical reference values for C57BL/6, Swiss Webster and BALB/c mice. *Braz. J. Vet. Res. Anim. Sci.* 53, 138–145. doi: 10.11606/issn.1678-4456.v53i2p138-145

Schwenk, F., Baron, U., and Rajewsky, K. (1995). A cre-transgenic mouse strain for the ubiquitous deletion of loxP-flanked gene segments including deletion in germ cells. *Nucleic Acids Res.* 23, 5080–5081. doi: 10.1093/nar/23.24.5080

Shaner, N. C., Campbell, R. E., Steinbach, P. A., Giepmans, B. N. G., Palmer, A. E., and Tsien, R. Y. (2004). Improved monomeric red, orange and yellow fluorescent proteins derived from *Discosoma* sp. red fluorescent protein. *Nat. Biotechnol.* 22, 1567–1572. doi: 10.1038/nbt1037

Stearns, T. (1995). Green fluorescent protein. The green revolution. *Curr. Biol.* 5, 262–264.

VetScan HM5 (2018). *Hematology System Original User's Manual*. Union City, CA: Abaxis Inc.

Wang, J., Wagner-Britz, L., Bogdanova, A., Ruppenthal, S., Wiesen, K., Kaiser, E., et al. (2013). Morphologically homogeneous red blood cells present a heterogeneous response to hormonal stimulation. *PLoS One* 8:e67697. doi: 10.1371/journal.pone.0067697

Conflict of Interest Statement: The authors declare that the research was conducted in the absence of any commercial or financial relationships that could be construed as a potential conflict of interest.

frontiers in Physiology

ORIGINAL RESEARCH
published: 17 July 2019
doi: 10.3389/fphys.2019.00893

Aging Markers in Equine Red Blood Cells

Sandra Kämpf[1,2†], Elena Seiler[1†], Jolanta Bujok[1,3], Regina Hofmann-Lehmann[4], Barbara Riond[4], Asya Makhro[1] and Anna Bogdanova[1,5]*

[1]Red Blood Cell Research Group, Vetsuisse Faculty, Institute of Veterinary Physiology, University of Zurich, Zürich, Switzerland, [2]Vetsuisse Faculty, University of Bern, Bern, Switzerland, [3]Institute of Animal Physiology, Wrocław University of Environmental and Life Sciences, Wrocław, Poland, [4]Clinical Laboratory, Vetsuisse Faculty, University of Zurich, Zürich, Switzerland, [5]The Zurich Center for Integrative Human Physiology (ZIHP), Zürich, Switzerland

Detection of hematopoietic activity in horses is a challenge due to the lack of cells carrying reticulocyte markers such as RNA remnants or CD71 in the circulation. In this study, we fractionated equine red cells according to their density and analyzed the cells forming low (L), medium (M), and high (H) density fractions for markers of aging such as membrane loss, oxidation, and alterations in the intracellular free Ca^{2+} levels. Cells forming L and M fraction were highly heterogeneous in projected areas and shapes, and had higher propensity to swell in response to hypo-osmotic challenge than the cells from the H fraction. The densest cells were deprived of band 3 protein compared to the cells within L or M fraction. Furthermore, the equine red cells from the H fraction were hyper-oxidized compared to the cells within M and L fractions as follows from an increase in autofluorescence characteristic for oxidized damaged hemoglobin and from thiol oxidation as detected using monobromobimane. The lightest cells showed lower free thiol content compared to the red blood cells from the M fraction, but did not contain oxidized hemoglobin. Finally, the majority of red blood cells forming L, M, and H fraction prominently differed from each other in intracellular free Ca^{2+} levels and its distribution within the cells. Based on the obtained findings, we suggest that intraerythrocytic Ca^{2+} levels and its subcellular distribution, eosin-5-maleimide binding test for band 3 abundance, and autofluorescence of cells along with the changes in red blood cell indices, distribution width and creatine levels may become potential markers of regenerative erythropoiesis in horses. Validation of the power of these potential markers of red cell aging is pending.

Keywords: horse red blood cells, aging, senescence, calcium, membrane loss

OPEN ACCESS

Edited by:
Giampaolo Minetti, University of Pavia, Italy

Reviewed by:
John Stanley Gibson, University of Cambridge, United Kingdom
Mauro Magnani, University of Urbino Carlo Bo, Italy

***Correspondence:**
Anna Bogdanova
annab@access.uzh.ch

[†]These authors have contributed equally to this work

Specialty section:
This article was submitted to Red Blood Cell Physiology, a section of the journal Frontiers in Physiology

Received: *30 April 2019*
Accepted: *27 June 2019*
Published: *17 July 2019*

Citation:
Kämpf S, Seiler E, Bujok J, Hofmann-Lehmann R, Riond B, Makhro A and Bogdanova A (2019) Aging Markers in Equine Red Blood Cells. Front. Physiol. 10:893. doi: 10.3389/fphys.2019.00893

INTRODUCTION

Equine red blood cells (RBCs) are surviving in the circulation for as long as 140–150 days (Carter et al., 1974) being exposed to shear stress, oxidation, and hyperthermia associated with high physical activity of these animals. Multiple attempts to detect reticulocytes (RNA-positive cells or cells carrying transferrin receptor) in peripheral blood of horses failed even in the studies, where stress erythropoiesis was induced by phlebotomy, administration of phenylhydrazine, or erythropoietin administration (Lumsden et al., 1975a,b; Shull, 1981; Radin et al., 1986; Cooper et al., 2005). Two possible reasons for that include (1) maturation of reticulocytes in

bone marrow, and (2) facilitated clearance of surface markers such as transferrin receptor from the circulating young cells. Indeed, although transferrin receptor was not detected on the surface of circulating cells, it was recently found in the exosomes (vesicles) isolated from equine blood plasma (Rout et al., 2015). Stimulation of *de novo* RBC production in horses was associated with an increase in heterogeneity reflected in an increase in red cell distribution width (RDW), and in most cases, with an increase in mean corpuscular volume (MCV) (Lumsden et al., 1975a,b; Radin et al., 1986; Cooper et al., 2005; Singh et al., 2007; McKeever et al., 2016). Detection of RBC life-span in horses in which stress erythropoiesis was induced by phlebotomy or erythropoietin administration, revealed a trend to faster clearance of cells produced upon stimulation of their *de novo* production (Lumsden et al., 1975a,b).

The changes in RDW and MCV alone are insufficient as self-standing markers of upregulated hematopoietic activity as these parameters are variable among different breeds of horses, their age, and physical activity. Moreover, they show inter-laboratory variability and depend on the hematological analyzer used (Lording, 2008; Bauer et al., 2012; Satue et al., 2012). Regenerative erythropoiesis is only diagnosed when proven by the examination of bone marrow aspirates (Schalm, 1975, 1981; Lording, 2008; Grondin and Dewitt, 2010). However, contamination of bone marrow aspirates with peripheral blood makes such diagnosis prone to artefactual readouts (Schalm, 1975).

Based on our extensive knowledge of human RBC aging, we have undertaken an attempt to identify a set of possible markers of RBC aging (density, redox state, membrane loss, morphometry, Ca^{2+} levels, and compartmentalization). Along with the changes in RBC indices, this set of markers would be robust and reliable to complement or replace bone marrow aspirate cytology. Aging of healthy human RBC is associated with a gradual membrane loss and increase in RBC density. The existence of RBC fractions of low (L), medium (M), and high (H) density in horse blood was earlier on reported by Wu et al. (1983), and related to the creatine concentration, and, therefore, to the RBC age. We have adapted the measurements of such age-related parameters as intracellular Ca^{2+}, band 3 protein abundance, and responsiveness to osmotic challenge, as well as intracellular reduced thiol content (Piccinini et al., 1995; Bogdanova et al., 2013; Lutz and Bogdanova, 2013; Ciana et al., 2017a,b) for detection by means of flow cytometry. This technique is often applied for detection of clinically relevant parameters in hematological laboratories.

MATERIALS AND METHODS

Equine heparinized blood samples from 19 horses were obtained from Clinical Laboratory of the Vetsuisse Faculty, University of Zurich. The samples were collected by veterinary practitioners as a part of diagnostic workup and sent to the laboratory for routine diagnostic purposes. Leftovers of the samples were used, and no additional blood volume was collected for the current study. No ethical approval was necessary for this study in compliance with the Swiss regulations. Blood samples were processed for analysis, less than 12 h after blood withdrawal. Human blood samples were collected from ten young male adults (elder than 18 years old) within the study on neocytolysis (DFG-SNF, # 320030E_180227). All participants gave their written informed consent prior to the study onset. The study protocol was approved by the Ethics committee of the Medical Department of the University of Heidelberg (S-066/2018). Blood was collected by the authorized medical practitioner at the Medical Department and immediately transported by couriers to the processing site at the University of Zurich at constant temperature no longer than 5 h, where it was immediately processed. Blood was fractionated on Percoll gradient and Ca^{2+} levels were detected in fractions using flow cytometry and fluorescence microscopy as stated elsewhere (Makhro et al., 2017).

RBCs were pelleted and washed three times with the plasma-like medium of the following composition (in mM) 140 NaCl, 4 KCl, 0.75 $MgSO_4$, 10 glucose, 0.015 $ZnCl_2$, 0.2 glycine, 0.2 Na-glutamate, 0.1 arginine, 0.6 glutamine, 0.2 alanine, 20 HEPES – imidazole (pH 7.4 at room temperature), and 0.1% bovine serum albumin. This medium was used throughout this study along with the phosphate buffer (PBS).

Separation of Equine Red Blood Cells According to Their Density Using Centrifugation in Percoll Density Gradient

Percoll (GE Healthcare Life Sciences) was mixed with 10X PBS (1.37 M NaCl, 27 mM KCl, 100 mM Na_2HPO_4, 17.6 mM KH_2PO_4, pH 7.2–7.4 at room temperature) in proportion 9:1 to obtain isotonic Percoll solution. RBC suspension in 1X PBS was carefully layered on top of 13 ml of Percoll solution and spun using Sorwall Lynx 4,000 Centrifuge (Thermo Fisher Scientific) equipped with A22-24x16 rotor at 10,000 ×*g* for 40 min at 30–33°C. Distribution of RBCs into low (L), medium (M), and high (H) density fractions was recorded photographically and cells forming these fractions were then harvested and washed three times from Percoll using the plasma-like medium. Thereafter, RBCs were re-suspended in the same medium to a 40–50% Hct were prepared on and used for further studies (flow cytometry, microscopy, or RBC membrane isolation).

Morphological Characterization and Ca^{2+} levels in Red Blood Cells Forming L, M, and H Fractions Using Fluorescence Microscopy

An aliquot of RBC suspension (1 µl) was added to 1 ml of plasma-like medium supplemented with 2 mM $CaCl_2$ and 2 µM fluo-4AM (Thermo Fischer Scientific) and incubated for 1 h in the darkness. Thereafter, the samples were transferred into the imaging chambers and the bright field images were taken with the Axiovert 200M fluorescent microscope (Carl Zeiss Jena GmbH, Jena, Germany) equipped with x100 oil objective along with images of Fluo-4 fluorescence. All measurements were performed in triplicates, for each sample, 10 fields were imaged. Images were analyzed using CellFinder software [copyright of Maxim Makhinya (Makhro et al., 2017)].

In a separate set of experiments, RBCs loaded with Fluo-4 were re-suspended in Ca^{2+}-free medium and Ca^{2+} uptake following administration of $CaCl_2$ (from 1 M stock solution to reach the final concentration of 1.8 mM) was monitored over 12 min. Bright field and fluorescence images were taken for the same field every minute and kinetics of morphological alterations and Ca^{2+} levels in RBCs responding to Ca^{2+} administration was analyzed using the CellFinder software (for details, see Makhro et al., 2017).

Flow Cytometry

RBCs suspension of ~40–50% hematocrit was prepared in plasma-like medium and 2 µl aliquot of it was mixed with 1 ml of the plasma-like medium containing the following fluorophores: acridine orange (BD Retic-Count™), annexin conjugated with eFluo-450 (eBioscience/Affymetrix at Thermo Fisher Scientific), fluo-4 AM (2 µM), and monobromobimane (10 µM). Separate samples without staining were used to detect autofluorescence of RBCs in all channels (excitation at 488, 635, and 405 nm), which was used as a background reference as well as for estimation of hemoglobin oxidation. The cells were incubated with fluorophores for 1 h in the darkness.

In addition, 5 µl of RBC suspension were incubated in 50 µl of $CaCl_2$-containing plasma-like medium containing 0.5 mg/ml eosin 5-maleimide (EMA, Merck KGaA, Darmstadt, Germany) for 1 h in the darkness. The excess of EMA was then washed away during triple washing in plasma-like medium (30 s, 3,000 ×*g*), and the cells were finally re-suspended in 1 ml of the same medium.

Fluorescence from the fluorochromes was detected using Gallios flow cytometer (Becton Coulter, Indianapolis, IN, USA) equipped with 525/30 BP, 669/20 BP, and 450/50 BP filters. Recordings from 100,000 cells per sample were analyzed using Kaluza analysis software (Beckman Coulter Life Sciences, Indianapolis, IN, USA).

Mechano-sensitive Ca^{2+} uptake by equine RBCs was confirmed by us in a preliminary set of experiments and monitored in fractions as a time course over 2–5 min by flow cytometry. RBCs pre-loaded with fluo-4 were stimulated to swell by mixing of cell suspension in isotonic buffer with distilled water (2:1). Response to acute decrease in osmolarity from 330 to 220 mOsm was recorded as a change in side scatter and the alteration in Ca^{2+}-dependent fluorescence of Fluo-4 fluorochrome.

Band 4.1a:b Ratio

Membranes were isolated from the cells forming L, M, and H fraction and proteins separated on the SDS PAGE gel with the subsequent visualization using Coomassie blue staining. Images of the gels were taken using a $CoolSNAP_{cf}$ camera (Photometrics, Tucson, AZ, USA) equipped with Sigma 50 mm 1:2.8 DC MACROD objective (Hama GmbH & Co KG, Monheim, Germany). Image analysis was performed using MCID image analysis software package for gel densitometry. Identity of equine protein(s) forming a double-band corresponding in electrophoretic mobility to the human band 4.1 was assessed using mass spectrometry.

Mass Spectrometry

Gel bands corresponding to the band 4.1a and b were carefully harvested, cut into small pieces, and washed two times with 100 µl 100 mM NH_4HCO_3/50% acetonitrile, and one time with 50 µl acetonitrile alone. All three supernatants were discarded. The proteins were then digested using 10 µl trypsin (5 ng/µl in a buffer containing 10 mM Tris and 2 mM $CaCl_2$, pH 8.2) in 30 µl of the same Tris-$CaCl_2$ buffer for 30 min at 60°C in a microwave. Supernatant was then removed, and gel pieces extracted one time with 150 µl 0.1% TFA/50% acetonitrile. All supernatants were combined and dried. Samples were dissolved in 20 µl 0.1% formic acid and transferred to autosampler vials for LC/MS/MS. About 3 µl (samples 1, 3, 7, and 9) or 5 µl (2, 4, 5, 6, 8, and 10) were injected and analyzed. Database searches were performed by using the Mascot (SwissProtr, all species; Trembl, mammalian) and PEAKS (*de novo* sequencing and search against a database containing the sequences of *Equus caballus* extracted from the NCBI database) search programs and search results were summarized in Scaffold matrix.

Statistics

Statistical module of SigmaPlot v.13 was used for analysis of variance and differences. It included characterization of the normality of distribution (Shapiro-Wilk test) with the following choice of parametric or nonparametric analysis tools. Wilcoxon signed rank test and the Repeated Measures ANOVA on Ranks was used in majority of cases. For more details, see Figure legends.

RESULTS

Separation of Horse Red Blood Cells Into Fractions of Low, Medium, and High Density

Best results for human RBC separation were obtained using PBS-based isosmotic Percoll solution with the density of 1.1126 kg/L (**Figure 1A**). Optimal conditions for successful separation of horse equine RBC into L, M, and H fractions (**Figure 1A**) were achieved on the self-forming PBS-based isosmotic Percoll density gradient of higher density of 1.124 kg/L. The differences in density between the species reflected the higher mean cells hemoglobin concentration (MCHC) and the smaller cell size as follows from the mean cell volume (MCV) and the RBC diameter of horse cells compared to those of humans (**Table 1**). Clearly separated, L, M, and H fractions of equine and human RBCs (**Figure 1A**) were harvested and the cells forming them stained for RNA as a reticulocyte marker. Whereas in equine L fraction of equine RBCs, only 0.54 ± 0.14% were positive for RNA (**Figure 1B**), human L fraction contained 29.5 ± 11.2% of cells positive for RNA (**Figure 1C**).

Bright-field images of equine RBCs from whole blood (**Figure 2A**) as well as of cells forming L, M, and H fractions were obtained (**Figure 2B**). The images were analyzed and the cellular projected areas and anisotropy (ellipticity) were obtained. In agreement with earlier reports (Lording, 2008), equine RBCs had less pronounced central pallor, compared to the human cells (**Figure 2A**).

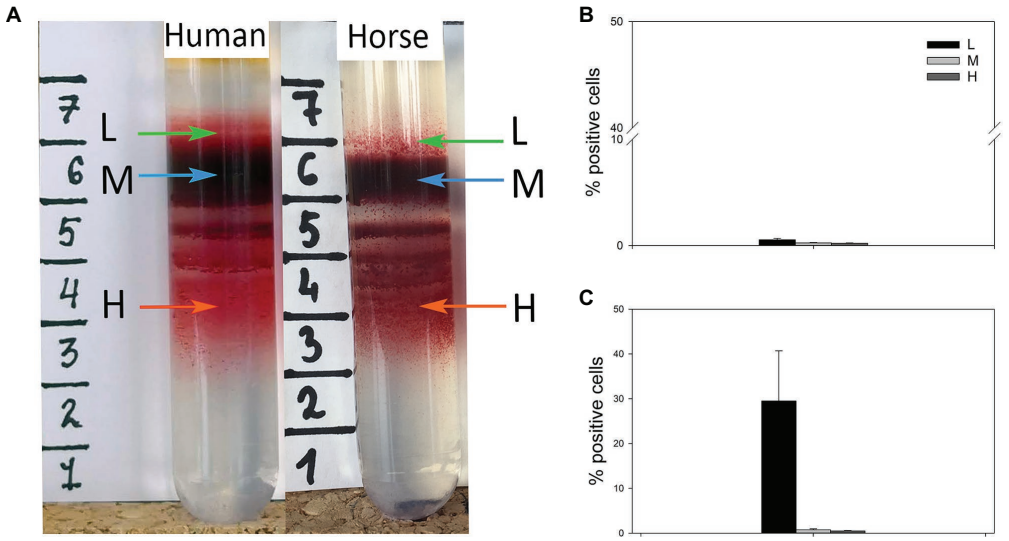

FIGURE 1 | (A) Distribution of RBCs of human and horse within Percoll density gradient and the abundance of RNA+ cells within the light (L), medium (M) and high (H) density fractions of horse **(B)** and human **(C)** blood. Data are means ± SD for four humans and four horses.

TABLE 1 | RBC indices for horses and humans.

Parameter	Horse RBCs (*T* 140–170 days) (Lording, 2008)		Human RBCs (*T* 100–120 days) (Turgeon, 2005)	
	Warm-blooded	Cold-blooded	Female	Male
Ery, 10^{12}/L	8.2–12.2	5.5–9.5	4.2–5.4	4.6–6.2
Hb, g/L	130–170	80–140	115–160	140–180
MCHC, g Hb/L	330–390	320–380	300–340	300–340
MCV, fL	36–50	40–48	80–95	80–95
Diameter, μm	5.7		6.2–8.2 (7.2)	
RDW,%	14–25		11.5–14.5	

Mild echinocytosis was seen in all fractions of several, but not all, horses (**Figure 2B**). In the L and M fractions, RBCs with a broad variety of projected areas (**Figures 2C,D**) were observed. Within the H fraction only discocytes with small projected areas were observed (**Figure 2D**). Detailed probability density analysis of the distribution of projected areas revealed that L and M fractions contain the cells of similar sizes and shapes (**Figure 2C**). A small population of cells within the L fraction with a projected area of 42–45 μm^2 was exceeding that in the M fraction (p = 0.069). The majority of RBCs forming the H fraction had significantly smaller projection areas than the cells forming or M fraction (**Figure 2D**).

RBC ellipticity (longest to shortest diameter ratio) was gradually increasing from L to H fractions making up (mean ± SD): 1.070 ± 0.018, 1.072 ± 0.028, and 1.078 ± 0.025 for L, M, and H fractions, respectively. However, the significant differences in eccentricity were only recorded between the L and H fractions, showing that the cells with lower density were also more "round" ($p < 0.05$ Mann-Whitney Rank Sum Test).

Forward (FS) and side (SS) scatter and their variances (SDs) were used as an indirect indicator of RBC shape heterogeneity and sphericity. The cells forming the H fraction differed from the cells in M and L fraction by having lower FS, whereas side scatter did not differ between the fractions (**Figures 3A,C**). In line with the data obtained from morphometry analysis (**Figure 2D**), the densest RBCs appeared more homogeneous than those from the M and L fractions, as followed from reduction in variance of FS (FS SD, **Figure 3B**). One more special feature of the cells forming the H fraction was a decrease in band 3 abundance compared to the other fractions (**Figure 3D**).

Functional test for the ability of RBCs to change their shape to more spherical in response to acute hypo-osmotic stress, expressed as a change in SS. As follows from **Figure 3E**, equine RBCs of the H fraction were less responsive to hypo-osmotic stimulation compared to the cells of L and M fractions. Similar to those of horses, RBCs forming the H fraction in humans were also limited in swelling propensity compared to those from the L and M fractions (**Figure 3F**). The ability of RBCs to respond to hypoosmotic stress (delta SS) correlated positively (p = 0.00318, Pearson Product Moment Correlation) with the band 3 abundance (**Figure 3G**).

Intracellular Free Ca^{2+} Content

Comparison the fluo-4 readouts obtained by micro fluorescence imaging of unfractionated RBCs (whole blood) of humans (**Figure 4A**) and horses (**Figure 4B**) reveals several species-specific features. The fluorescence intensity in human cells is higher than that in RBCs of horses. This observation is at least in part explained by the increased quenching of the signal by hemoglobin in equine cells due to the higher MCHC (**Table 1**), but may also reflect the higher levels of free Ca^{2+} in human cells (see also **Figure 5**). Furthermore, higher inter- and intra-cellular heterogeneity in fluo-4 fluorescence was observed in equine RBCs compared to the human ones. In human RBCs, some middle-sized vesicles

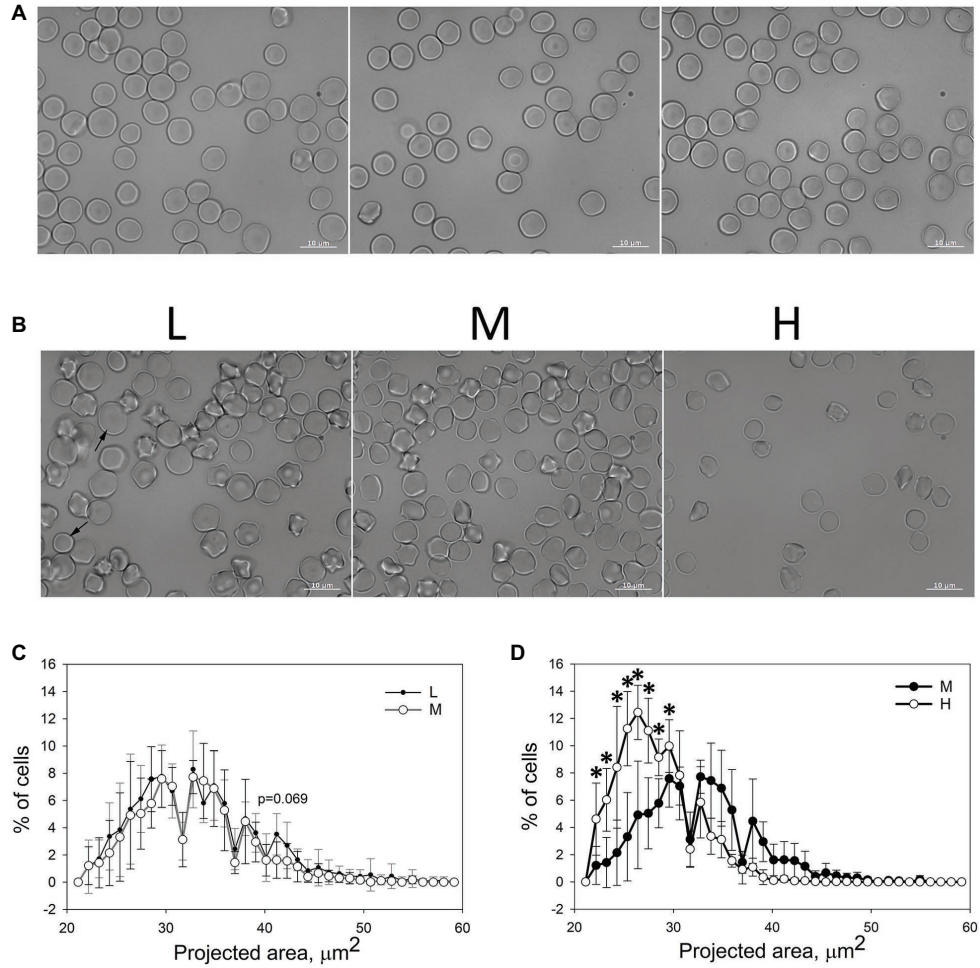

FIGURE 2 | Microscopic evaluation of equine RBC. **(A)** Morphological appearance of equine RBCs in whole blood of three different horses. **(B)** Morphology of equine RBCs forming L, M and H fractions. **(C,D)** Binned projected area assessed for RBCs forming L, M, and H fractions for six horses ±SD. Wilcoxon signed rank test was used for statistical analysis and the two-tailed *p* values are presented as stars (*signifies $p < 0.05$).

may be seen in some cells. The abundance of such cells varies between the healthy donors (compare the panels in **Figure 4A**). In non-fractionated equine RBCs (**Figure 4B**), three types of cells are always present: those with low basal fluorescence and no vesicles or one single large vesicle (highlighted with orange arrows) and the ones with high intracellular free Ca^{2+} and multiple smaller vesicles (highlighted with green arrows). Fractionation resulted in accumulation of the cells with higher Ca^{2+} and multiple small Ca^{2+}-filled vesicles in the L fraction (**Figure 4C**). Cells with a single larger Ca^{2+}-filled compartment were only found in the H fraction (**Figure 4C**).

To achieve higher throughput in quantification of the whole-cell fluorescence intensity, flow cytometry was used and the readouts for 100,000 cells per sample were maintained. As follows from the representative dot-plots, the absolute levels of fluo-4-derived fluorescence intensity for human cells (**Figure 5A**) exceeded that for equine RBCs (**Figure 5B**). Two sub-populations of RBCs were detected is each density fraction in both human and equine samples: main sub-population (gates M in **Figures 5A,B**) and a smaller sub-population with High Ca^{2+} levels (gates HC in **Figures 5A,B**). Both human and horse samples also contained Ca^{2+}-loaded Vesicles (gates V in **Figures 5A,B**). The human and equine RBCs forming the L fraction's M population were presented with the maximal fluorescence intensity of fluo-4 [**Figure 5C** (human) and **Figure 5D** (equine)]. The M and H fractions did not differ from each other and were both less fluorescent the lightest cells. Fluorescence intensity of the RBCs forming the H population decreased with an increase in density (**Figures 5E,F**).

Hypo-osmotic challenge is known to cause activation of mechano-sensitive Ca^{2+} uptake in RBCs of humans (Cahalan et al., 2015; Fermo et al., 2017). Increase in fluo-4 signal triggered by swelling (delta FI) in human RBCs was similar in L and H fractions, and lower in the M fraction (**Figure 5G**). Delta FI in equine RBCs was smaller in absolute values and maximal in the cells forming L fraction. It decreased progressively with increasing density (**Figure 5H**).

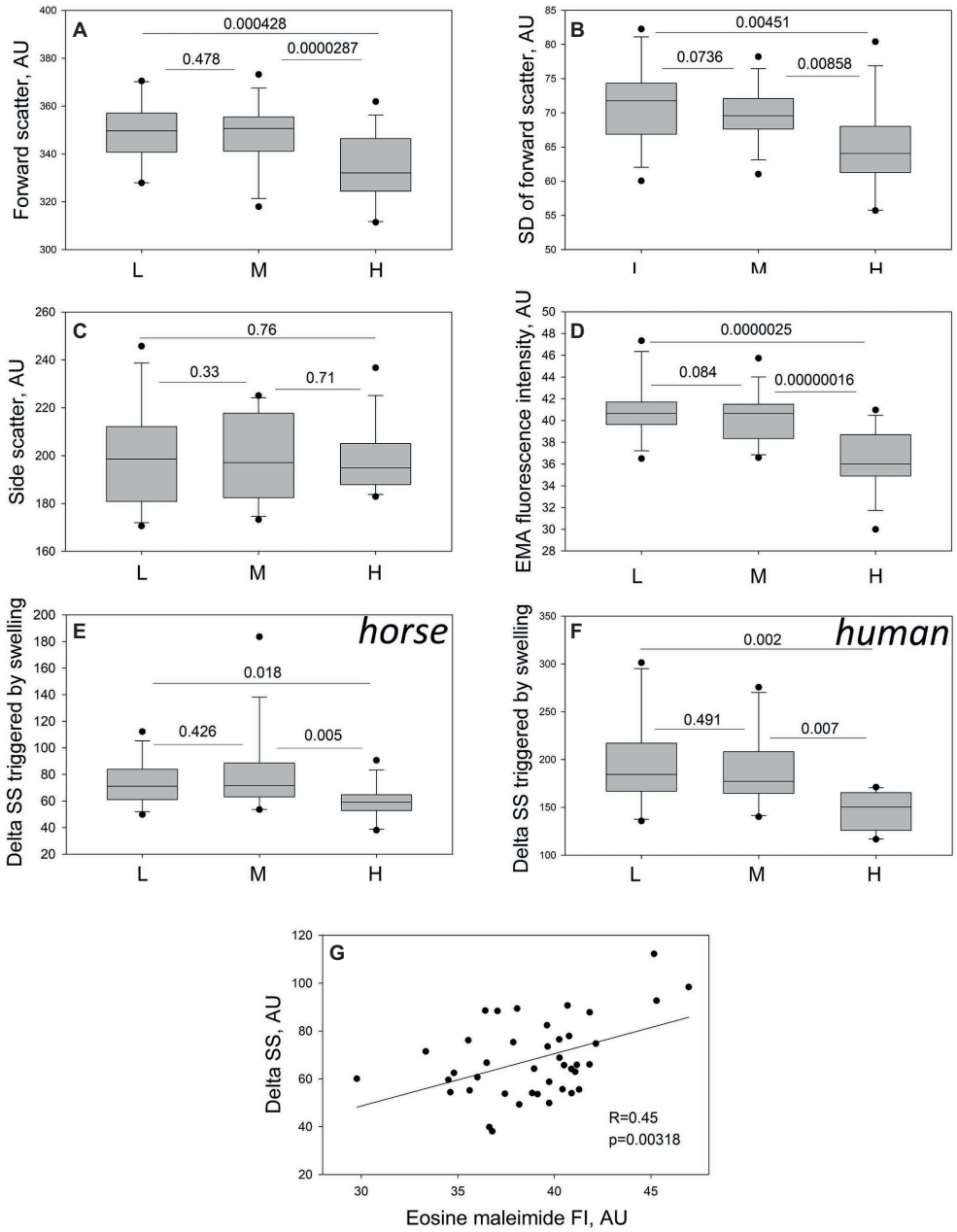

FIGURE 3 | Assessment of the RBC sphericity and membrane loss in equine RBCs by flow cytometry. Forward scatter **(A)** and its variance **(B)**, side scatter **(C)** and band 3 abundance **(D)** in equine RBCs forming L, M, and H fractions of 13 different animals. Changes in side scatter (delta SS) in horse **(E)** and human **(F)** RBCs forming L, M, and H fractions to hypo-osmotic challenge in 13 horses and 10 healthy humans. **(G)** Product Moment Correlation between the EMA staining intensity and delta SS in equine RBCs of 13 horses. For 41 data-points $R = 0.450$, and $p = 0.00318$ were calculated. Wilcoxon signed rank test was used for statistical analysis and the two-tailed "*p*" are presence.

Redox State Indicators

RBCs harvested from the L and often H fraction of one horse was not enough to use any macroscopic method of detection of reduced glutathione. So, florescence readouts (autofluorescence and monobromobimane staining) were used to assess oxidized hemoglobin products and intracellular free thiols in RBCs using flow cytometry. As follows from **Figure 6A**, equine RBCs forming the H fraction showed higher auto-fluorescence in green and red channels compared to the cells of L and M fractions. Interestingly, the highest levels of reduced thiols were observed in RBCs from the M fraction, whereas cells from the L and H fractioned were more "oxidized" (**Figure 6B**).

Band 4.1a:b Ratio

Equine membrane protein separation was performed using SDS PAGE. On the gels obtained for horse membrane proteins

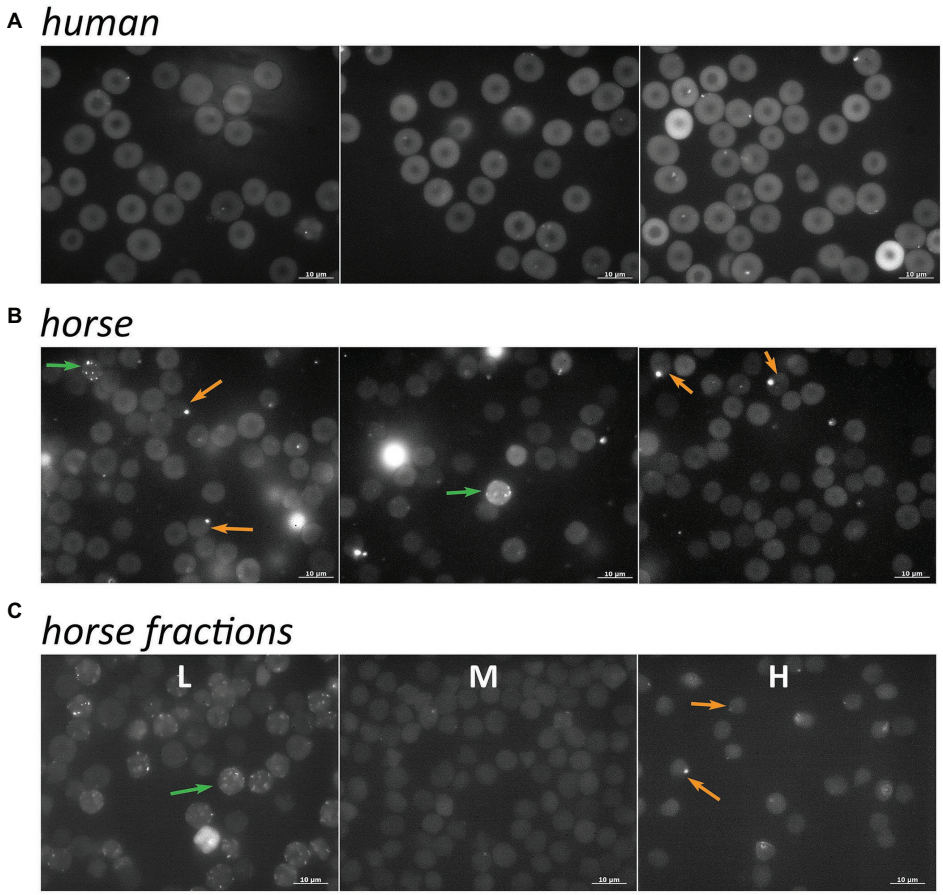

FIGURE 4 | Distribution of intracellular free Ca^{2+} in non-fractionated RBCs of humans (**A**, three different donors) and horses (**B**, three different horses) from whole blood. **(C)** Ca^{2+} distribution in equine RBCs forming L, M, and H fractions. Green arrows indicate RBCs with high basal fluorescence intensity and multiple small Ca^{2+}-filled vesicles and orange arrows show the cells with low basal fluorescence and a single large compartment filled with Ca^{2+}.

characteristic bands for spectrins, band 3 and band 4.1R-sized protein was obtained (**Figure 7A**). Densitometric ratio obtained for the "band 4.1a:b" was increasing with an increase in RBC density (**Figure 7C**) in equine RBCs. Apart of that, a faint band of about 180 kDa seen was identified as a product of ankyrin cleavage using mass spectrometry. This cleavage product could be detected in comparable amounts all fractions, L, M, and H. The presence of such band on the gels where human RBC membrane proteins were isolated (**Figure 7B**) revealed certain degree of proteolysis. If that happened (compare the left and right lanes in **Figure 7B**), an additional band, identified as ankyrin fragment was present above the band 4.1R double-band. We therefore performed mass spectrometry of the band 4.1-like duplet isolated from equine membranes and indeed found the presence of ankyrin fragment along with the band 4.1 protein. Sequence alignment of horse vs. human band 4.1 protein revealed the absence of the Asp in position corresponding to the Asn502 for all three isoforms of *EPB41* gene-related products of horse genome (**Figure 7D**). Deamidation of this Asn residue within the band 4.1R protein gives rise to the shift in electrophoretic mobility. It occurs progressively over the RBC life-span and is used as a biological clock showing age of RBCs of humans and other species (Inaba and Maede, 1988, 1992; Inaba et al., 1992). Isoforms 1 and 3 sequences for horses differ significantly from the human sequence in the vicinity of Asn502 having no Asn residues within it. Equine *EBP41* isoform 2 showing greater homology to the human *EBP41* has Asn502 replaced by Gln.

DISCUSSION

Equine RBC forming L, M, and H fractions are presented with several potentially age-related features that confirm the increase of RBC density with aging and may be used for identification of RBC longevity. These features include the differences in RBC size and morphology, membrane loss, changes in redox state and sub-cellular distribution, and of bulk levels of fluo-4 fluorescence intensity. Majority of methods used for detection of these parameters in our study require smaller volumes of blood and standard equipment that is often available in a specialized clinical laboratory such as a flow cytometer and a fluorescent microscope.

Aging of human RBCs is associated with a gradual loss of membrane, oxidation, and proteolytic cleavage of hemoglobin and cytoskeletal proteins (Lutz and Bogdanova, 2013). Younger

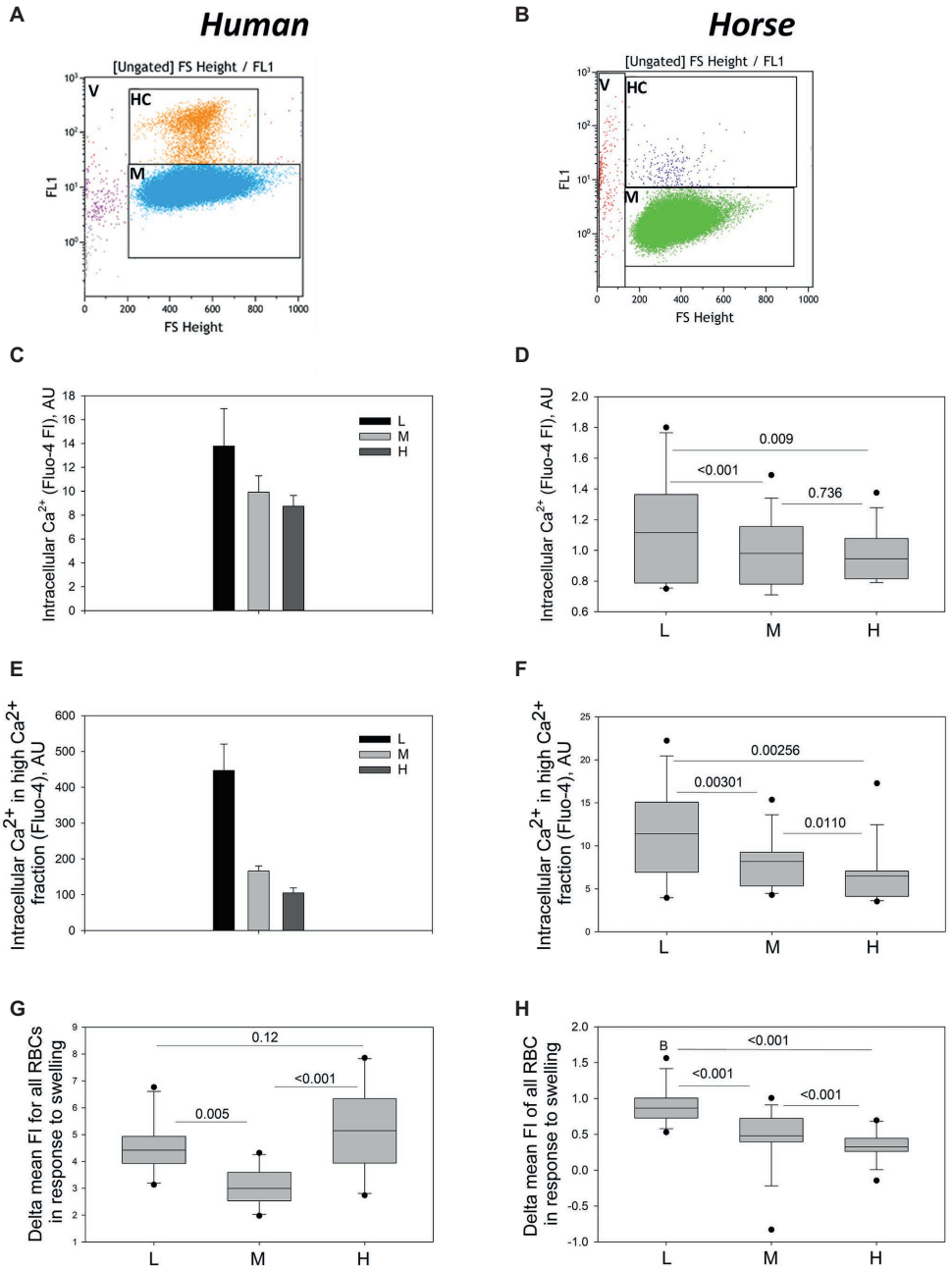

FIGURE 5 | Intracellular Ca^{2+} in L, M and H fraction monitored using flow cytometry. Gating for High Ca^{2+} (HC) and Main (M) population of human **(A)** and equine **(B)** RBCs. **(C)** Fluo-4 fluorescence intensity for the human cells forming L, M, and H fractions (M and H populations). Data are means for four humans ±SD. Fluo-4 fluorescence intensity for the M **(D)** and H **(E)** populations equine RBCs forming L, M, and H fractions (M and H populations). Data are obtained for 13 horses. Increase in fluo-4 fluorescence intensity (delta FI) in equine (panel **F**, n = 13) and human (panel **G**, n = 10). RBCs from L, M, and H fraction in response to hypoosmotic challenge.

human cells also have higher Ca^{2+} levels as recorded by fluo-4 fluorescence intensity (**Figures 5C,E**; Makhro et al., 2013). Persisting stress erythropoiesis gives rise to more immature and thus less stable RBC phenotype combining the features of young and senescent cells that have shorter life-span than the cells produced under conditions of basal erythropoiesis (Bogdanova et al., 2007). At the same time, in most studies in which erythropoiesis markers were studied in horses, stress erythropoiesis was induced by administration of pro-hemolytic compound phenylhydrazine, by phlebotomy or by recombinant human erythropoietin to increase the number of reticulocytes (Lumsden et al., 1975a,b;

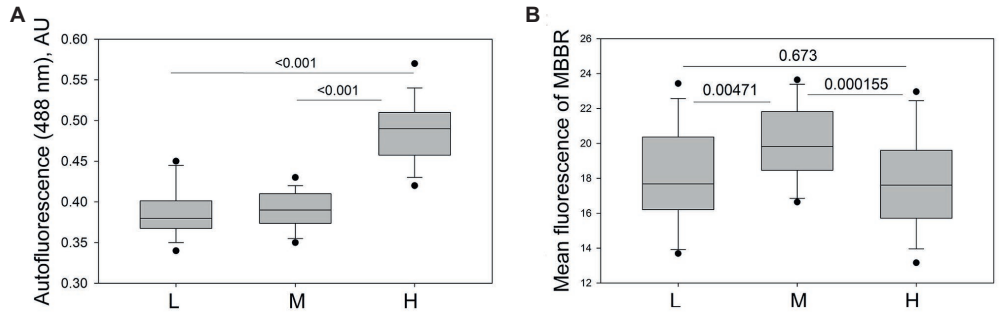

FIGURE 6 | Markers of oxidation in equine RBCs of L, M and H fractions. **(A)** Autofluorescence in green channel and **(B)** fluorescence intensity for monobromobimane (MBBR) and in L, M and H fractions of RBCs of 13 horses. Wilcoxon signed rank test was used for statistical analysis and the two-tailed "*p*" are presented as numbers.

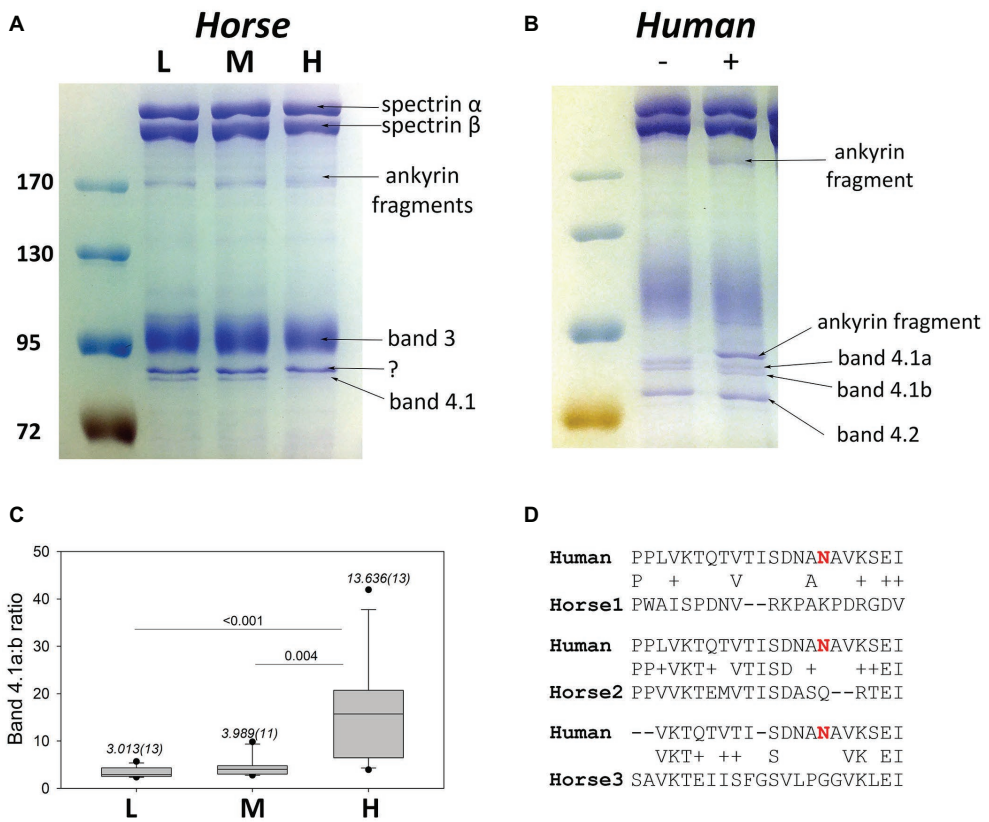

FIGURE 7 | Band 4.1Ra:b potential as an aging marker in horses. **(A)** A representative SDS PAGE gel with equine membrane proteins isolated from L, M and H fractions. **(B)** A representative gel with human membrane proteins without ("–") and with ("+") proteolytic ankyrin cleavage. **(C)** Quantitative densitometry for the band 4.1a:b ratio for 11–13 horses (numbers in brackets). Shown are medians (numbers above the bars) and variance as well and the outcome of Wilcoxon signed rank test. **(D)** Sequence alignments for human and equine 4.1 protein sequences.

Radin et al., 1986; Cooper et al., 2005; Singh et al., 2007; McKeever et al., 2016). In these studies, focused on detection of (stress?) reticulocytes, a transient increase in both MCV and heterogeneity in RBC volume (RDW and MCV SD) was reported after induction of stress erythropoiesis. The only one study that, similar to us, used Percoll density gradient to isolate fractions of cells of low, medium, and high density, were assumed to be enriched with young, mature, and presumably senescent cells, reported a density-dependent change in the intracellular creatine content of RBCs (Wu et al., 1983). We have chosen similar approach when searching for further markers of RBC aging without triggering stress erythropoiesis based on characterization of equine RBCs forming L, M, and H fractions.

How do we know that the densest RBCs are also the oldest? The only ultimate marker accepted for human RBCs as a "biological clock" is the degree of deamidation of the band 4.1 protein. Deamidation of band 4.1 protein was also reported to occur in RBC membranes of several other mammalian species, including horses (Inaba and Maede, 1988, 1992; Inaba et al., 1992; Lutz et al., 1992). In order to prove the existence of deamidation, the authors used an antibody with a broad spectrum of inter-species cross-reactivity (Inaba and Maede, 1988) However, these findings raised some caution due to the lack of homology between the horse and human *EPB41* sequence (**Figure 7C**). The question, that remains unsolved, is on the nature of the shift in electrophoretic mobility for what may be two forms of EPB41 proteins in the absence of the main deamidation site (Asn502) in horses (Inaba et al., 1992; Inaba and Maede, 1992). Non-enzymatic Gln deamidation is occurring as well, but deamidation rate is approximately 100 times slower than that for Asn residues (Robinson and Robinson, 2004). Thus, it is unlikely that Gln deamidation in the homologous position within the equine band 4.1 protein would be a reliable marker of RBC age. Mass spectrometry revealed the presence of band 4.1 protein in these bands as well as ankyrin fragments, which may contribute to the alterations in density of the upper and lower band within 80 kDa range revealing an increase in cleavage of alpha-spectrin, band 3 protein, or ankyrin rather than modification of the band 4.1protein itself. Until the nature of changes leading to an increase in "band 4.1a:b ratio" along with cell density will be solved, we cannot use it as a reliable marker of equine RBC aging.

Characterization of the other "hallmarks of RBC aging" was then performed for the RBC forming L, M, and H fractions. The presence of cells positive for RNA was a reliable clinically relevant marker showing enrichment of the human L fraction with reticulocytes (**Figure 1C**), in line with the previous reports (Cooper et al., 2005). Earlier on the traces of one more marker of reticulocytes, CD71 (transferrin receptor), were reported to be associated not with RBCs, but with vesicles in serum of horses recovering from anemia caused by phlebotomy (Rout et al., 2015). We could not confirm or disapprove of the presence of any of reticulocyte markers in vesicles originating from these cells, as fractionation on Percoll density gradient is incompatible with this approach. Single vesicles, some of which contained larger Ca^{2+}-filled compartments, similar to those seen in the H fraction, could be observed when whole blood was used for loading with fluo-4 and for life imaging (**Figure 4B**).

We could furthermore confirm that an increase in RBC density was at least in part caused by membrane loss. RBCs forming the H fractions were smaller in projected are (**Figure 2D**), deprived of band 3 protein and showed blunted response to hypoosmotic challenge (**Figures 3E,G**). Loss of CD71, ion pumps and channels and some other proteins accompany RBC membrane maturation, whereas loss of band 3 protein is a sign of aging and senescence of human RBCs (Lutz et al., 1988; Pantaleo et al., 2009; Lutz, 2012). We may therefore suggest that band 3 deprivation of equine RBCs forming the H fraction is a sign of senescence.

Oxidation was earlier on reported as a marker of RBC senescence [for review, see (Lutz and Bogdanova, 2013; Rifkind and Nagababu, 2013)]. Clusterization of oxidized band 3 protein is a marker tagging senescent RBCs for recognition by naturally occurring antibodies and clearance (Lutz, 2012). In horse blood, the densest RBCs showed signs of oxidative stress and inability to resist irreversible hemoglobin oxidation and damage (**Figure 6A**). Whereas the reduced thiol levels are comparable in cells from the L and H fraction (**Figure 6B**), increase in autofluorescence, known as a marker of hemoglobin oxidation and production of hemichromes (Kannan et al., 1988; Stoya et al., 2002) was consistent with age-related oxidation.

Finally, we have found alterations in basal intracellular free Ca^{2+} levels as well as the changes in its compartmentalization with an increase in density of equine RBCs. Aging of human RBCs is associated with the loss of activity and abundance of both Ca^{2+} pumps and Ca^{2+}-permeable channels such as NMDA receptors in human RBCs (Luthra and Kim, 1980; Bogdanova et al., 2013). As a result free Ca^{2+} levels are reduced in dense senescent cells (**Figures 4, 5**; Bogdanova et al., 2013). For the equine RBCs as well increase in density was associated with a decrease in free Ca^{2+} levels (**Figures 5D,F**). Significant number of cells within the L fraction contained high Ca^{2+} cells with the nanovesicles filled with Ca^{2+}, whereas the cells within the H fraction were presented with a single micrometer-sized compartment (**Figures 4B,C**). Earlier on production of two types of vesicles, microvesicles of ~150 nm and nanovesicles, ~50–60 nm in diameter was described in human RBCs in response to Ca^{2+} uptake (Salzer et al., 2002). Microvesicles contain low amounts of hemoglobin, Band 3 protein and glycophorins, and are enriched with acetylcholinesterase and stomatin. Nanovesicles are preferentially formed by lipid rafts and are hence enriched with stomatin as well as with proteins that are recruited to the rafts in response to Ca^{2+} uptake, synexin and sorcin (Salzer et al., 2002, 2008; Hagerstrand et al., 2006). Interestingly, mature equine RBCs are deprived of sphingomyelin (SM), compared to human, ovine, bovine, or porcine cells, although cholesterol levels are comparable (Wessels and Veerkamp, 1973). It is tempting to suggest, that SM could be lost from the membrane due to the effective maturation of equine RBCs. However, comparable or even lower SM levels have been shown for canine RBC membranes (Wessels and Veerkamp, 1973; Plasenzotti et al., 2007; Spengler et al., 2008), for which reticulocytes are easily detectible in blood (Bauer et al., 2012).

Precise control over the intracellular free Ca^{2+} and adaptations that prevent excessive Ca^{2+} accumulation in RBCs contribute to the prolongation of life expectancy of RBCs in human athletes (Bogdanova et al., 2013; Makhro et al., 2016). Majority of horses are physically active and seem to successfully cope with excess of intracellular Ca^{2+} in dense (and most likely senescent) RBCs by packaging it into the intracellular compartment. Thereby, activation of calpain and further unwanted effects related to Ca^{2+} overload are most likely prevented giving rise to an increase in life span for equine RBCs above that for humans (**Figure 5, Table 1**; Bogdanova et al., 2013).

LIMITATIONS, CONCLUSIONS, AND THE OUTLOOK

In our study we have performed detailed analysis of properties of equine RBCs as a function of the RBC density. Animals from which blood was collected were attending the Animal Hospital Zurich with various health issues not related to hematological phenotype. We furthermore did not discriminate between the warm and the coldblooded breeds, the age and gender of the animals. All these factors contributed to a larger variance, but revealed the robustness of the RBC aging markers, as they were shared by all the study participants. These markers included membrane loss, oxidation, and alterations in the intracellular free Ca^{2+} levels and its distribution pattern are robust and may be used as predictors of RBC age in horses.

The processes that contribute to maturation of young RBC in horses most likely involve very effective control over membrane loss and over the intracellular Ca^{2+} maintenance. As a result, premature damage is avoided and the longevity of RBCs is supported. Oxidative stress, as well as the growing density and stiffness of senescent horse RBC most likely trigger their clearance. More work, particularly at the level of bone marrow, has to be done to unravel the mysterious cause for of the lack of reticulocytes in peripheral blood of horses.

DATA AVAILABILITY

All datasets generated for this study are included in the manuscript and/or the supplementary files.

ETHICS STATEMENT

Equine heparinized blood samples from 19 horses were obtained from Clinical Laboratory of the Vetsuisse Faculty, University of Zurich. The samples were collected by veterinary practitioners as a part of diagnostic workup and sent to the laboratory for routine diagnostic purposes. Leftovers of the samples were used, and no additional blood volume was collected for the current study. No ethical approval was necessary for this study in compliance with the Swiss regulations. Blood samples were processed for analysis less than 12 h after blood withdrawal. Human blood samples were collected within the study on neocytolysis (DFG-SNF, # 320030E_180227) from four health male participants. The study involving human subjects was approved by the Ethics committee of the Medical Department of the University of Heidelberg (S-066/2018). Blood was collected by the medical practitioner at the Medical Department.

AUTHOR CONTRIBUTIONS

AB, AM, RH-L, and BR planned the study. AB supervised the study. SK, ES, and JB performed experiments. SK, AM, and AB analyzed the data. All the authors discussed the findings. AB and AM were writing the manuscript. All authors discussed the text and agreed with it.

FUNDING

This study was supported by the Symphasis Foundation and the D-A-CH grant (320030E_180227) to AB.

REFERENCES

Bauer, N., Nakagawa, J., Dunker, C., Failing, K., and Moritz, A. (2012). Evaluation of the automated hematology analyzer Sysmex XT-2000iV compared to the ADVIA® 2120 for its use in dogs, cats, and horses. Part II: accuracy of leukocyte differential and reticulocyte count, impact of anticoagulant and sample aging. *J. Vet. Diagn. Investig.* 24, 74–89. doi: 10.1177/1040638711436243

Bogdanova, A., Makhro, A., Wang, J., Lipp, P., and Kaestner, L. (2013). Calcium in red blood cells-a perilous balance. *Int. J. Mol. Sci.* 14, 9848–9872. doi: 10.3390/ijms14059848

Bogdanova, A., Mihov, D., Lutz, H., Saam, B., Gassmann, M., and Vogel, J. (2007). Enhanced erythro-phagocytosis in polycythemic mice overexpressing erythropoietin. *Blood* 110, 762–769. doi: 10.1182/blood-2006-12-063602

Cahalan, S. M., Lukacs, V., Ranade, S. S., Chien, S., Bandell, M., and Patapoutian, A. (2015). Piezo1 links mechanical forces to red blood cell volume. *elife* 4. doi: 10.7554/eLife.07370

Carter, E. I., Valli, V. E., McSherry, B. J., Milne, F. J., Robinson, G. A., and Lumsden, J. H. (1974). The kinetics of hematopoiesis in the light horse. I. The lifespan of peripheral blood cells in the normal horse. *Can. J. Comp. Med.* 38, 303–313.

Ciana, A., Achilli, C., Gaur, A., and Minetti, G. (2017a). Membrane remodelling and vesicle formation during ageing of human red blood cells. *Cell. Physiol. Biochem.* 42, 1127–1138. doi: 10.1159/000478768

Ciana, A., Achilli, C., and Minetti, G. (2017b). Spectrin and other membrane-skeletal components in human red blood cells of different age. *Cell. Physiol. Biochem.* 42, 1139–1152. doi: 10.1159/000478769

Cooper, C., Sears, W., and Bienzle, D. (2005). Reticulocyte changes after experimental anemia and erythropoietin treatment of horses. *J. Appl. Physiol.* 99, 915–921. doi: 10.1152/japplphysiol.00438.2005

Fermo, E., Bogdanova, A., Petkova-Kirova, P., Zaninoni, A., Marcello, A. P., Makhro, A., et al. (2017). 'Gardos Channelopathy': a variant of hereditary Stomatocytosis with complex molecular regulation. *Sci. Rep.* 7:1744. doi: 10.1038/s41598-017-01591-w

Grondin, T. M., and Dewitt, S. F. (2010). "Normal hematology of the horse and donkey" in *Schalm's veterinary hematology.* 6th Edn. eds. D. J. Weiss and K. J. Wardrop (Ames, USA: Wiley-Blackwell, A John Wiley & Sons, Ltd., Publication), 821–828.

Hagerstrand, H., Mrowczynska, L., Salzer, U., Prohaska, R., Michelsen, K. A., Kralj-Iglic, V., et al. (2006). Curvature-dependent lateral distribution of raft markers in the human erythrocyte membrane. *Mol. Membr. Biol.* 23, 277–288. doi: 10.1080/09687860600682536

Inaba, M., Gupta, K. C., Kuwabara, M., Takahashi, T., Benz, E. J. Jr., and Maede, Y. (1992). Deamidation of human erythrocyte protein 4.1: possible role in aging. *Blood* 79, 3355–3361.

Inaba, M., and Maede, Y. (1988). Correlation between protein 4.1a/4.1b ratio and erythrocyte life span. *Biochim. Biophys. Acta* 944, 256–264.

Inaba, M., and Maede, Y. (1992). The critical role of asparagine 502 in post-translational alteration of protein 4.1. *Comp. Biochem. Physiol. B* 103, 523–526.

Kannan, R., Labotka, R., and Low, P. S. (1988). Isolation and characterization of the hemichrome-stabilized membrane protein aggregates from sickle erythrocytes. Major site of autologous antibody binding. *J. Biol. Chem.* 263, 13766–13773.

Lording, P. M. (2008). Erythrocytes. *Vet. Clin. North Am. Equine Pract.* 24, 225–237. doi: 10.1016/j.cveq.2008.04.002

Lumsden, H. J., Valli, V. E., McSherry, B. J., Robinson, G. A., and Claxton, M. J. (1975a). The kinetics of hematopoiesis in the light horse III. The hematological response to hemolytic anemia. *Can. J. Comp. Med.* 39, 332–339.

Lumsden, J. H., Valli, V. E., McSherry, B. J., Robinson, G. A., and Claxton, M. J. (1975b). The kinetics of hematopoiesis in the light horse II. The hematological response to hemorrhagic anemia. *Can. J. Comp. Med.* 39, 324–331.

Luthra, M. G., and Kim, H. D. (1980). (Ca^2+ + Mg^2+)-ATPase of density-separated human red cells. Effects of calcium and a soluble cytoplasmic activator (calmodulin). *Biochim. Biophys. Acta* 600, 480–488.

Lutz, H. U. (2012). Naturally occurring anti-band 3 antibodies in clearance of senescent and oxidatively stressed human red blood cells. *Transfus. Med. Hemother.* 39, 321–327. doi: 10.1159/000342171

Lutz, H. U., and Bogdanova, A. (2013). Mechanisms tagging senescent red blood cells for clearance in healthy humans. *Front. Physiol.* 4:387. doi: 10.3389/fphys.2013.00387

Lutz, H. U., Fasler, S., Stammler, P., Bussolino, F., and Arese, P. (1988). Naturally occurring anti-band 3 antibodies and complement in phagocytosis of oxidatively-stressed and in clearance of senescent red cells. *Blood Cells* 14, 175–203.

Lutz, H. U., Stammler, P., Fasler, S., Ingold, M., and Fehr, J. (1992). Density separation of human red blood cells on self forming Percoll gradients: correlation with cell age. *Biochim. Biophys. Acta* 1116, 1–10. doi: 10.1016/0304-4165(92)90120-j

Makhro, A., Haider, T., Wang, J., Bogdanov, N., Steffen, P., Wagner, C., et al. (2016). Comparing the impact of an acute exercise bout on plasma amino acid composition, intraerythrocytic Ca(2+) handling, and red cell function in athletes and untrained subjects. *Cell Calcium* 60, 235–244. doi: 10.1016/j.ceca.2016.05.005

Makhro, A., Hanggi, P., Goede, J. S., Wang, J., Bruggemann, A., Gassmann, M., et al. (2013). N-methyl D-aspartate (NMDA) receptors in human erythroid precursor cells and in circulating red blood cells contribute to the intracellular calcium regulation. *Am. J. Physiol. Cell Physiol.* 305, C1123–C1138. doi: 10.1152/ajpcell.00031.2013

Makhro, A., Kaestner, L., and Bogdanova, A. (2017). NMDA receptor activity in circulating red blood cells: methods of detection. *Methods Mol. Biol.* 1677, 265–282. doi: 10.1007/978-1-4939-7321-7_15

McKeever, K. H., McNally, B. A., Hinchcliff, K. W., Lehnhard, R. A., and Poole, D. C. (2016). Effects of erythropoietin on systemic hematocrit and oxygen transport in the splenectomized horse. *Respir. Physiol. Neurobiol.* 225, 38–47. doi: 10.1016/j.resp.2016.02.001

Pantaleo, A., Ferru, E., Giribaldi, G., Mannu, F., Carta, F., Matte, A., et al. (2009). Oxidized and poorly glycosylated band 3 is selectively phosphorylated by Syk kinase to form large membrane clusters in normal and G6PD-deficient red blood cells. *Biochem. J.* 418, 359–367. doi: 10.1042/BJ20081557

Piccinini, G., Minetti, G., Balduini, C., and Brovelli, A. (1995). Oxidation state of glutathione and membrane proteins in human red cells of different age. *Mech. Ageing Dev.* 78, 15–26. doi: 10.1016/0047-6374(94)01511-J

Plasenzotti, R., Windberger, U., Ulberth, F., Osterode, W., and Losert, U. (2007). Influence of fatty acid composition in mammalian erythrocytes on cellular aggregation. *Clin. Hemorheol. Microcirc.* 37, 237–243.

Radin, M. J., Eubank, M. C., and Weiser, M. G. (1986). Electronic measurement of erythrocyte volume and volume heterogeneity in horses during erythrocyte regeneration associated with experimental anemias. *Vet. Pathol.* 23, 656–660.

Rifkind, J. M., and Nagababu, E. (2013). Hemoglobin redox reactions and red blood cell aging. *Antioxid. Redox Signal.* 18, 2274–2283. doi: 10.1089/ars.2012.4867

Robinson, N. E., and Robinson, A. B. (2004). *Molecular clocks. Deamisation of asparaginyl and glutaminyl residues in peptides and proteins*. Cave Junction, OR, USA: Althouse Press.

Rout, E. D., Webb, T. L., Laurence, H. M., Long, L., and Olver, C. S. (2015). Transferrin receptor expression in serum exosomes as a marker of regenerative anaemia in the horse. *Equine Vet. J.* 47, 101–106. doi: 10.1111/evj.12235

Salzer, U., Hinterdorfer, P., Hunger, U., Borken, C., and Prohaska, R. (2002). Ca(++)-dependent vesicle release from erythrocytes involves stomatin-specific lipid rafts, synexin (annexin VII), and sorcin. *Blood* 99, 2569–2577. doi: 10.1182/blood.V99.7.2569

Salzer, U., Zhu, R., Luten, M., Isobe, H., Pastushenko, V., Perkmann, T., et al. (2008). Vesicles generated during storage of red cells are rich in the lipid raft marker stomatin. *Transfusion* 48, 451–462. doi: 10.1111/j.1537-2995.2007.01549.x

Satue, K., Hernandez, A., and Munoz, A. (2012). "Physiological factors in the interpretation of equine hematological profile" in *Hematology – Science and practice*. ed. C. Lawrie (InTech), 573–596.

Schalm, O. W. (1975). Equine hematology: part IV. Erythroid marrow cytology in response to anaemia. *Calif. Vet.* 29, 8–14.

Schalm, O. W. (1981). Bone marrow cytology as an aid to diagnosis. *Vet. Clin. North Am. Small Anim. Pract.* 11, 383–404. doi: 10.1016/S0195-5616(81)50035-0

Shull, R. M. (1981). Biochemical changes in equine erythrocytes during experimental regenerative anemia. *Cornell Vet.* 71, 280–287.

Singh, A. K., Gupta, S., Barnes, A., Carlson, J. M., and Ayers, J. K. (2007). Red blood cell erythropoietin, not plasma erythropoietin, concentrations correlate with changes in hematological indices in horses receiving a single dose of recombinant human erythropoietin by subcutaneous injection. *J. Vet. Pharmacol. Ther.* 30, 175–178. doi: 10.1111/j.1365-2885.2007.00828.x

Spengler, M. I., Bertoluzzo, S. M., Catalani, G., and Rasia, M. L. (2008). Study on membrane fluidity and erythrocyte aggregation in equine, bovine and human species. *Clin. Hemorheol. Microcirc.* 38, 171–176.

Stoya, G., Klemm, A., Baumann, E., Vogelsang, H., Ott, U., Linss, W., et al. (2002). Determination of autofluorescence of red blood cells (RbCs) in uremic patients as a marker of oxidative damage. *Clin. Nephrol.* 58, 198–204. doi: 10.5414/CNP58198

Turgeon, M. L. (2005). *Clinical hematology. Theory and procedures*. Philadelphia, Baltimore, New York, London, Buenos Aeres, Hong Kong, Sydney, Tokyo: Lippincott Williams & Wilkins.

Wessels, J. M., and Veerkamp, J. H. (1973). Some aspects of the osmotic lysis of erythrocytes. 3. Comparison of glycerol permeability and lipid composition of red blood cell membranes from eight mammalian species. *Biochim. Biophys. Acta* 291, 190–196.

Wu, M. J., Feldman, B. F., Zinkl, J. G., and Jain, N. C. (1983). Using red blood cell creatine concentration to evaluate the equine erythropoietic response. *Am. J. Vet. Res.* 44, 1427–1432.

Conflict of Interest Statement: The authors declare that the research was conducted in the absence of any commercial or financial relationships that could be construed as a potential conflict of interest.

frontiers in Physiology

REVIEW
published: 31 July 2019
doi: 10.3389/fphys.2019.00945

Red Blood Cells: Chasing Interactions

Virginia Pretini[1,2], Mischa H. Koenen[3], Lars Kaestner[2,4], Marcel H. A. M. Fens[5], Raymond M. Schiffelers[1], Marije Bartels[6] and Richard Van Wijk[1]**

[1] Department of Clinical Chemistry and Haematology, University Medical Center Utrecht, Utrecht University, Utrecht, Netherlands, [2] Theoretical Medicine and Biosciences, Saarland University, Homburg, Germany, [3] Department of Laboratory of Translational Immunology and Department of Pediatric Immunology, Wilhelmina Children's Hospital, University Medical Centre Utrecht, Utrecht, Netherlands, [4] Experimental Physics, Saarland University, Saarbrücken, Germany, [5] Department of Pharmaceutics, Utrecht Institute of Pharmaceutical Sciences (UIPS), Faculty of Science, Utrecht University, Utrecht, Netherlands, [6] Paediatric Haematology Department, Wilhelmina Children's Hospital, University Medical Centre Utrecht, Utrecht, Netherlands

Human red blood cells (RBC) are highly differentiated cells that have lost all organelles and most intracellular machineries during their maturation process. RBC are fundamental for the nearly all basic physiologic dynamics and they are key cells in the body's respiratory system by being responsible for the oxygen transport to all cells and tissues, and delivery of carbon dioxide to the lungs. With their flexible structure RBC are capable to deform in order to travel through all blood vessels including very small capillaries. Throughout their in average 120 days lifespan, human RBC travel in the bloodstream and come in contact with a broad range of different cell types. In fact, RBC are able to interact and communicate with endothelial cells (ECs), platelets, macrophages, and bacteria. Additionally, they are involved in the maintenance of thrombosis and hemostasis and play an important role in the immune response against pathogens. To clarify the mechanisms of interaction of RBC and these other cells both in health and disease as well as to highlight the role of important key players, we focused our interest on RBC membrane components such as ion channels, proteins, and phospholipids.

Keywords: red blood cells, interactions, membrane proteins, phospholipids, plasma proteins, platelets, endothelial cells, pathogens

OPEN ACCESS

Edited by:
Giampaolo Minetti, University of Pavia, Italy

Reviewed by:
Robert Campbell, The University of Utah, United States
Gregory Barshtein, Hebrew University of Jerusalem, Israel

****Correspondence:***
Virginia Pretini
V.Pretini-2@umcutrecht.nl
Richard Van Wijk
R.vanWijk@umcutrecht.nl

Specialty section:
This article was submitted to Red Blood Cell Physiology, a section of the journal Frontiers in Physiology

Received: *09 May 2019*
Accepted: *09 July 2019*
Published: *31 July 2019*

Citation:
Pretini V, Koenen MH, Kaestner L, Fens MHAM, Schiffelers RM, Bartels M and Van Wijk R (2019) Red Blood Cells: Chasing Interactions. Front. Physiol. 10:945. doi: 10.3389/fphys.2019.00945

INTRODUCTION

Red blood cells (RBC) are the most abundant cell type in human blood. They are devoid of nuclei, ribosomes, mitochondria, and other organelles, which are important in other cell types to perform specific functions critical to cell survival (Adams, 2010). This unconventional cell composition has evolved in order to allow accumulation of hemoglobin, a protein that is responsible for the delivery of oxygen (O_2) to peripheral tissues. In a typical healthy adult, every second 2 million of newly formed RBC enter the circulation from the bone marrow and at the same time about the same number is cleared (Higgins, 2015). RBC production, or erythropoiesis, is a tightly regulated process in which new RBC are continuosly produced in the bone marrow niche, sitting side by side in a rich environment with different cells and other tissues like endothelial cells (ECs), osteoblasts, stromal

cells, hematopoietic cells as well as extracellular matrix proteins. In the bone marrow they are in direct contact with cell adhesion molecules, growth factors and cytokines (Dzierzak and Philipsen, 2013). During the last step of the RBC maturation process, which takes place during the first couple of days in the bloodstream, the reticulocytes or premature RBC, enter the peripheral blood. They go through a selective sorting process in which they lose 20% of the plasma membrane and the remaining RNA content. The RBC membrane in particular undergoes different morphological and structural changes from the maturation stage until the clearance stage. They undergo multiple and often tightly regulated processes, in order to remodel their structure starting with the loss of the complex organelles system and the consequent acquisition of the typical biconcave shape.

This process effectuates a selection, segregation and depletion of membrane proteins (Moras et al., 2017), like the decline of Na^+/K^+ATPase, the sodium-hydrogen antiporter 1 (NHE1), Glycophorin A (GPA), cluster of differentiation 47 (CD47) and cluster of differentiation 36 (CD36), Duffy antigen/chemokine receptor (DARC) and Kell antigen (XK) system with the loss of Transferrin Receptor (CD71) and intercellular adhesion molecule-4 (ICAM4). In contrast, other relevant membrane proteins are increased during maturation of RBC, when compared to reticulocytes, such as band 3, Glycophorin C (GPC), rhesus protein (Rh), Rh-associated glycoproteins (RhAG), XK, and GPA (Minetti et al., 2018).

After maturation RBC acquire the remarkable ability of being deformable in response to external forces (Huisjes et al., 2018) and use this in order to pass through the narrowest blood capillaries (Viallat and Abkarian, 2014). The importance of this characteristic becomes more evident when defects and abnormalities related to RBC shape and/or deformability lead to drastic and premature cell clearance. These changes can provide key information in establishing a differential diagnosis and categorizing different diseases (Ford, 2013).

Much has been reported on the complexity of the interactions between the different components of the mature RBC membrane and other cells in the last decades. However, a complete overview of these interactions is lacking. In this review, we focus on the broad and diverse types of interactions that have been described to occur between RBC and other cells present in peripheral blood, and the consequences of these interactions. Many of the interactions known to occur are mediated by RBC membrane components (**Figure 1**).

STRUCTURE OF RBC MEMBRANE AND MEMBRANE SKELETON

In RBC, the cytoskeleton and the plasma membrane are extremely and closely connected to create a fundamental and complex structure called membrane skeleton. This is essential for the shape and reversible deformability of RBC. Thanks to the membrane structural integrity maintenance; RBC are flexible and able to survive in the circulation (Lux, 2016). RBC can deform with linear extension up to an estimated 250%, whereas a 3–4% increase in surface area results in lysis of the cell. RBC owe these unique membrane properties due to interaction of the plasma membrane envelope with the cytoskeleton. The plasma membrane is composed of a lipid bilayer with embedded transmembrane proteins that form multi-protein complexes. The bilayer itself consists of equal proportions of cholesterol and phospholipids (Cooper, 2000). For structural integrity, the bilayer links to the membrane skeleton through two macroprotein complexes: the ankyrin complex and the junctional complex (also known as the 4.1R complex). The RBC skeleton is a protein meshwork in which the most important components are spectrin, actin, actin-associated proteins, protein 4.1R and ankyrin. The membrane skeleton constitutes of spectrin tetramers that bind short actin filaments that in turn form a pseudohexagonal arrangement with six triangular spectrins binding one actin filament. Each arrangement has three junction complexes and three ankyrin complexes that facilitate membrane-cytoskeleton linkages (Goodman and Shiffer, 1983; Mankelow et al., 2012; Lux, 2016). The ankyrin complex can link ankyrin to β-spectrin on one side and band 3 and RhAG in the RBC membrane, on the other side. The junction complex links membrane proteins GPC and GPD, XK, Rh and Duffy onto the actin-spectrin cytoskeleton through interaction with protein 4.1R (Mohandas and Gallagher, 2008; Burton and Bruce, 2011; Lux, 2016).

There are more than 50 types of transmembrane proteins embedded in the lipid bilayer that are involved in transport, adhesion and structural integrity (**Figure 2**). Transmembrane transport is executed by several proteins such as band 3, aquaporin-1, glucose transporter 1 (GLUT1), Kidd antigen protein, RhAG and various ion transporters, dependent on the cargo. Proteins involved in adhesion or cell-cell interactions include ICAM-4 and Lu. Generally, RBC are not considered adhesive cells but several studies have reported the expression of a large number of adhesion molecules (Altankov and Serafimov-Dimitrov, 1990; de Oliveira and Saldanha, 2010; Weisel and Litvinov, 2019). However, in a number of pathological and disease-associated circumstances, such as in sickle cell disease (SCD), malaria, polycythemia vera, hereditary spherocytosis, retinal vein occlusion and diabetes mellitus, RBC notably change their behavior and become stimulated and consequently adhesive to each other (Steffen et al., 2011) and in particular to the endothelium (Coste et al., 2001; Kaul, 2008; Grossin et al., 2009b; Colin et al., 2014).

TRANSMEMBRANE TRANSPORT-PROTEINS MEDIATED INTERACTIONS

Ion Co-transporters

A large part of the RBC membrane is occupied by anion exchanger proteins. These allow RBC to maintain the correct balance between extracellular and intracellular water and solute content, in order to preserve the regular physiological functionality and homeostasis of RBC. For example, in case sodium influx exceeds potassium efflux the RBC swell, and conversely, if the outflow of potassium exceeds sodium influx

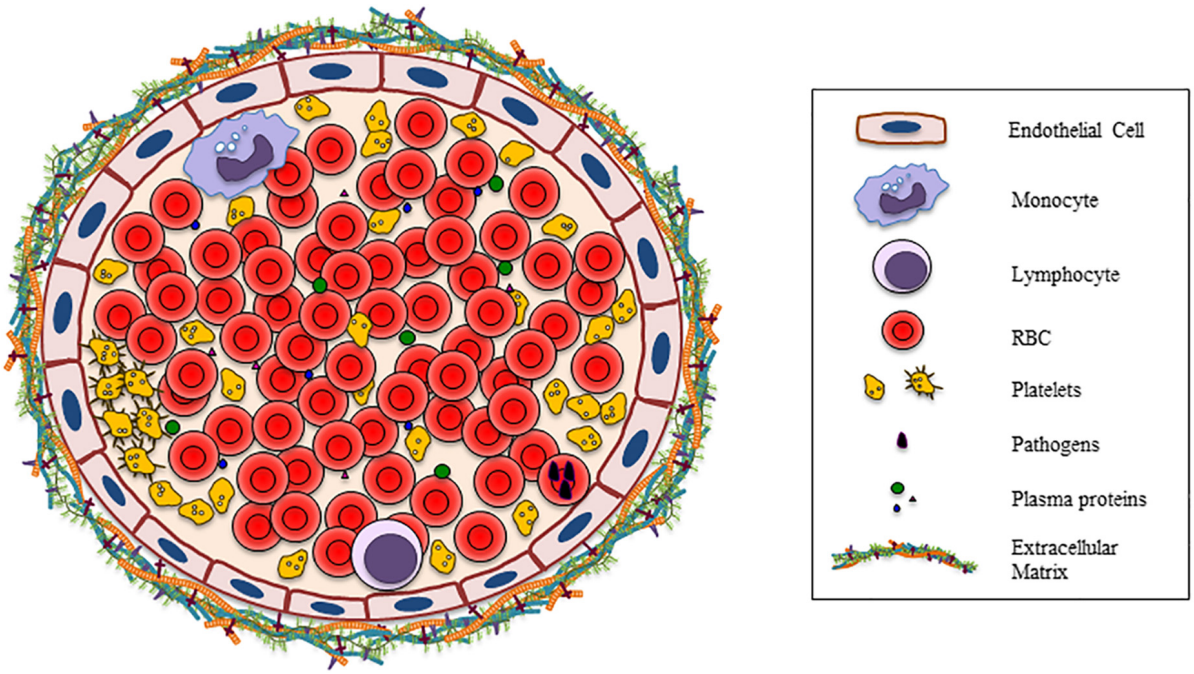

FIGURE 1 | Vessel section shows all the possible cells, plasma proteins, bacteria, and the extracellular matrix that are involved in the interaction with RBC.

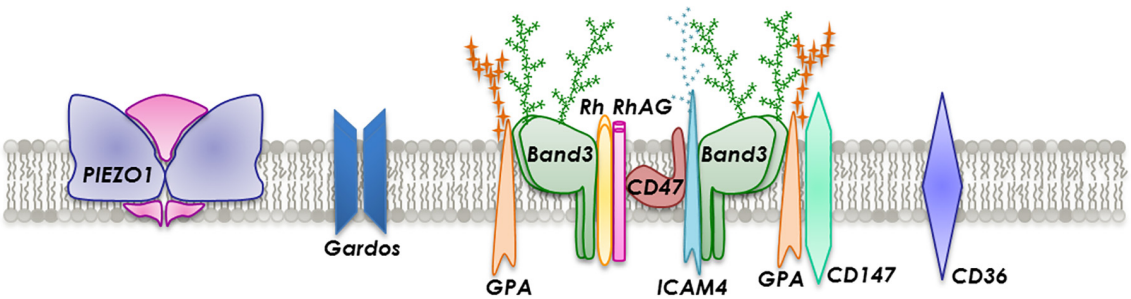

FIGURE 2 | Section of the RBC membrane with a focus on the composition of integral membrane proteins incorporated into a phospholipid bilayer.

into the RBC, the cells shrink (Gallagher, 2017). For this reason, a drastic change or a defect in the mechanism controlling the hydration balance could evolve into altered and unusual behavior of RBC (Azouzi et al., 2018).

Band 3

The major anion exchanger protein in RBC membranes is band 3. This transmembrane glycoprotein (100 kDa) provides integrity to the RBC membrane. In addition, the N-terminal cytoplasmic side is a key site for the connection to the membrane skeleton, glycolytic enzymes and deoxyhemoglobin, whereas the C-terminal integral membrane side includes the anion-exchange transporter role and supports carbon dioxide transport (Lux, 2016). Changes at the hamoglobin level can be transmitted to the membrane and this causes oxidative stress and band 3 oligomerization which plays an important role in the macrophages-mediated clearance of altered and old RBC by forming senescence-induced-antigens that are recognized by natural antibodies (NAbs; Klei et al., 2017; Azouzi et al., 2018).

The numerous binding sites connect band 3 with other membrane proteins. Hereby, a crucial network is provided allowing the transduction of signals from the membrane to the cytoskeleton, and vice versa, thereby regulating the flexibility, stability, and deformability of RBC. Rifkind and Nagababu showed that the interaction of hemoglobin (Hb) with band 3 under hypoxic conditions is critical for generation of RBC membrane changes that trigger the removal from the circulation (Rifkind and Nagababu, 2013). In patients with diabetes mellitus, band 3 is glycated (AGE) and binds to the receptor for advance glycation end products (RAGE) present on ECs and this enhances the oxidant stress in the vessel wall (Schmidt et al., 1996; Grossin et al., 2009a). The protein glycation induces a series of changes which is associated with high risk of vascular complications, which is particularly apperent in diabetes mellitus

in the microcirculation of the eyes leading to retinopathy and diabetic nephropathy (Wautier et al., 2004).

PIEZO1

The recently discovered non-selective cation channel PIEZO1, is a mechanosensor that plays an important role in maintaining RBC volume homeostasis. It is known that genetic mutations of PIEZO1 are the primary cause of hereditary xerocytosis. These genetic alterations influence channel kinetics, response to osmotic stress and membrane trafficking (Glogowska et al., 2017), thereby causing a decrease in total cellular cation, calcium and potassium content without proportional intake of sodium and water, ultimately leading to significant dehydration (Bae et al., 2013; Honoré et al., 2015; Patel et al., 2015). The nature of this channel is primarily and directly dependent on the activation by mechanical forces (i.e., poking, stretching, and shear stress) (Cahalan et al., 2015; Gottlieb, 2017; Parpaite and Coste, 2017). There are multiple hypotheses regarding PIEZO1 activation mechanisms. One sustains the "force-from-lipids" model, in which membrane tension can cause lipid reorganizations around the protein causing the channel to open. Another theory is the "force-from-filaments," which supports a model of interaction and tethering of the channel with extracellular matrix or intercellular cytoskeletal proteins (Murthy et al., 2017). Functional studies have shown that specific regions of the protein are more susceptible to mechanical perturbation than other regions. Moreover, there are many mechanical stimuli, such as shear stress, generated from the fluid flow over cells, that could interact and consequently activate PIEZO1 channels (Murthy et al., 2017). However, these mechanisms are still not completely understood and PIEZO1 is recognized as a potential candidate for the stretch-induced cation pathway and is involved in RBC aging, and circulatory shear stress (Bagriantsev et al., 2014). It has also been described to play a role in malaria parasite (*Plasmodium falciparum*) invasion (Zuccala et al., 2016; Ma et al., 2018). Interestingly, it was found that a third of the African population carry the novel variant of PIEZO1 that is associated with malaria resistance *in vitro* (Ma et al., 2018).

KCNN4-Gardos Channel

The Gardos channel, or KCNN4/IK-1, is a calcium-activated potassium channel which is present in a low copy number on the RBC membrane. In fact the estimated number of channels per RBC measured is around 10 (Grygorczyk et al., 1984; Brugnara et al., 1993; Thomas et al., 2011; Kaestner, 2015). Gardos channel-mediated interactions with other cell types are indirect and often mediated by two other membrane proteins: PIEZO1 and an other unknown receptor. An example is the ability of RBC to change their ratio shape/volume to pass through narrow capillaries and interstices (Danielczok et al., 2017). The mechanism behind this is the activation of PIEZO1 resulting in increased intracellular Ca^{2+} which in turn initiates Gardos channel activity. This also implicates that Gardos channels play a role in disorders related to the RBC hydration like in hereditary xerocytosis (Gallagher, 2017; Rapetti-Mauss et al., 2017).

Regarding the interaction between the Gardos channel and a putative associated unknown receptor on the RBC membrane, a link was found between the endothelin receptor and Gardos activity with elevated levels of cytokines such as endothelin-1, interleukin-8, and platelet activator factor (PAF) in plasma of SCD patients: this disease is characterized by the intrinsic property of hemoglobin S to sickle under deoxygenation. Sickling is enhanced under various conditions, including dehydration due to activation of Gardos channels with consequently loss of K^+ (Rivera et al., 2002). Moreover, SCD RBC have been shown to interact with vascular ECs, thereby stimulating the release of endothelin-1 and regulating the expression of the corresponding gene in culture. This mechanism could contribute to the vaso-occlusive events seen in SCD (Phelan et al., 1995).

Recently, pathological alterations were discovered correlating with mutations in the Gardos channel gene (Fermo et al., 2017): in fact, in some cases, patients with hemolytic anemia have been reported carrying exclusively these mutations responsible for this disease (Glogowska et al., 2015; Gallagher, 2017). These mutations changes the Ca^{2+} sensitivity affecting the activation threshold but also modifies functional properties making the channel more active leading to dehydrated RBC with a deficit in intracellular potassium (Archer et al., 2014; Andolfo et al., 2015; Rapetti-Mauss et al., 2015; Fermo et al., 2017).

Other Transport-Proteins

Other important RBC transport-proteins are GLUT-1, responsible for glucose trafficking, ABCB6 (adenosine triphosphate-binding cassette), linked to heme biosynthesis and porphyrin transport, urea passive transporter (Azouzi et al., 2013), to preserve the osmotic stability and deformability of the cell (Macey, 1984), aquaporin-1, key pore for water transport and fundamental for the metabolism and transport of CO_2, and volume-regulated anion channels (VRAC), a small conductand, stretch-activated channel, with the essential and recently descovered component SWELL1 (LRRC8A), located in proximity of the channel pore and responsible fort he regulation of cell volume homeostasis (Qiu et al., 2014; Syeda et al., 2016; Gallagher, 2017; Hsu et al., 2017). In addition, there are also regulatory proteins that cooperate with transport channel functionality like stomatin, which is a major protein of human RBC membranes that mainly interacts with the channels mentioned above (Rungaldier et al., 2013). It is currently unknown if these transport-proteins can induce interactions with other cells.

PHOSPHOLIPIDS MEDIATED INTERACTIONS

Red blood cells membranes are composed of a complex mixture of different kinds of phospholipid species that differ in head group and side chains (Kuypers, 2008). The lipid bilayer composition is similar to any other cell: there is an equal distribution of cholesterol and phospholipids (Cooper, 2000), while there is an asymmetrical proportion of the four major phospholipids between the two leaflets (**Figure 3**). In fact, the outer leaflet of the membrane is rich in phosphatidylcholine (PC, 27% of total membrane phospholipids) and sphingomyelin

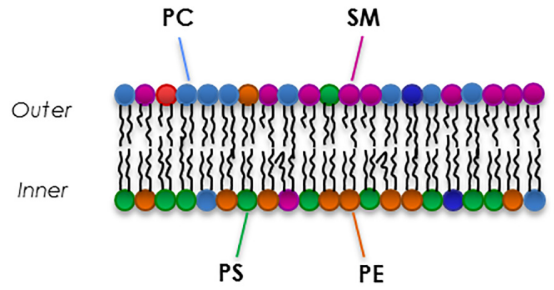

FIGURE 3 | An example of the composition of the major phospholipids of the RBC membrane.

(SM, 23%), while the inner leaflet is mostly constituted by phosphatidylethanolamine (PE, 30%) phosphatidylserine (PS, 15%) and the minor phosphoinositide (PI, 5%) (Goodman and Shiffer, 1983; Pasvol et al., 1992; Kuypers and de Jong, 2004; Mohandas and Gallagher, 2008; Fujimoto and Parmryd, 2016). The translocase proteins present in the RBC membrane, flippase, floppase, and scramblase are responsible for the movement of phospholipids. Flippase and floppase maintain and regulate the asymmetry in response to different stimuli and signals (Smith and Lambert, 2003; Hankins et al., 2015). In contrast, activation of scramblase is known to be involved in loss and disruption of the membrane phosholipids asymmetry that is essential for maintaining lipid homeostasis in RBC membranes (Pretorius et al., 2016).

The unbalance proportion and composition of the membrane lipids drives to defects that are able to influence membrane protein activation and in some cases leading to diseases such as hemolytic anemia: in fact, an increased phosphatidylcholine in the RBC have been reported in some intermediate syndromes of hereditary xerocytosis, associated with PIEZO1 defect (Clark et al., 1993; Imashuku et al., 2016; Gallagher, 2017).

Phosphatidylserine (PS)

Phosphatidylserine is an amino-phospholipid that is known to play a crucial role in mediating the recognition of senescent RBC, serving as an eat-me signal. During aging, upon injury of cells, or under certain pathologic conditions, scramblase translocates PS from the inner leaflet to the outer, leading to increased concentration on the external surface (Nguyen et al., 2011). It was shown that RBC of SCD patients expose PS upon deoxygenation and this process is mediated by Ca^{2+} influx activating the Gardos channels. In fact, scramblase requires Ca^{2+} for scrambling PS (Weiss et al., 2011; Wesseling et al., 2016). PS exposure on RBC has a second fundamental physiological function which is promoting coagulation. Generally, exposure of PS is described to increase the adhesiveness (Kaestner et al., 2012; Kaestner and Minetti, 2017). Regarding its role in coagulation, it was shown that RBC can directly bind to CD36 and PS-receptor (PSR) on ECs (Closse et al., 1999; Manodori et al., 2000; Setty et al., 2002; Heppel, 2008), as well as through CXCL16 or CD36 present on platelets after their activation (by ADP or thrombin) (Walker et al., 2013). PSR gets upregulated after activation of microvascular ECs by lipopolysaccharides (LPS), cytokines, hypoxia, and heme (Setty and Betal, 2008). CXC chemokine ligand 16 (CXCL16) is a direct ligand for PS exposed on RBC (Borst et al., 2012). CXCL16 gets strongly upregulated when stimulated with inflammatory cytokines such as IFN-γ or TNF-α (Abel et al., 2004), but also by peptidoglycans of the bacterial wall (Abed et al., 2013). Another way PS-exposure is promoted, is upon platelet interaction with FasR on RBC through FasL (Mackman, 2018). Moreover, key interaction induced by PS is the initiation of cell clearance, which involves different phagocytic cells such as macrophages, and usually takes place in liver and spleen. Various receptors have been identified to mediate direct binding via recognition of PS such as Tim1, Tim4, and Stabilin-1, leading to phagocytosis (Kobayashi et al., 2007; Park et al., 2009). Furthermore, there are several bridging molecules, or opsonins, like lactadherin, thrombospondin, Gas6, Protein S, that can facilitate macrophages recognition upon interaction with PS expose on RBC (de Back et al., 2014). Lastly, it was shown that changes in the cholesterol/phospholipid ratio in RBC had a marked effects on the PS exposure: in fact, an excess of cholesterol inhibites the PS exposure, whereas cholesterol depletion increases it (van Zwieten et al., 2012) and this could lead to increased susceptibility to the clearance of these cells.

GLYCOPROTEINS MEDIATED INTERACTIONS

Glycophorins

The glycophorin family is a group of transmembrane proteins [glycoproteins A-D (GPA-D)] that play an important role in regulating mechanical properties of RBC (Chasis and Mohandas, 1992). They comprise the most abundant integral type of proteins of the RBC membrane with around a million copies per cell (Alenghat and Golan, 2013; Aoki, 2017).

Glycophorin A is the major syaloglycoprotein responsible for the net negative surface charge of the cell membrane: for this reason the heavily glycosylated glycans on the extracellular domain are important to minimize the cell-cell interactions and RBC aggregation (Chasis and Mohandas, 1992; Poole, 2000). With this complex extracellular structure, GPA has a role into the composition of the pericellular matrix, the glycocalyx (Poole, 2000). GPA is also involved in pathogen recognition, acting as a decoy receptor in RBC. It mediates the binding of pathogens to the surface of RBC thereby preventing the invasion of these organisms into important tissues (Morera and MacKenzie, 2011). Consequently, pathogen load is reduced because pathogens bound to RBC are commonly cleared by macrophages in the spleen (Baum et al., 2002).

Additionally, it is shown that the sialoglycoproteins (GPA, GPB, and GPC) play a crucial role in the invasion of RBC by malaria parasites (i.e., *P. falciparum*). RBC deficient in any of the sialoglycophorins resist infection by merozoites to varying degrees (Pasvol, 1984). For instance, Gerbich-negative blood group (Ge-), characterized by defective GPC receptor expression, has been associated in malaria resistance with high prevalence in malaria-endemic regions (Williams, 2006).

Intercellular Adhesion Molecule 4 (ICAM-4)

Intercellular adhesion molecule 4 is a glycoprotein, which plays a crucial role in cell-cell interaction or adhesion with potential significance in a variety of physiological processes including hemostasis and thrombosis (de Oliveira and Saldanha, 2010). It binds to different members of integrin receptor families expressed on white blood cells (WBC) and ECs (Goel, 2002; Hermand et al., 2002) and can get activated in RBC under the influence of the hormone epinephrine. Upon exposure to epinephrine, ICAM-4 is able to bind directly to $\alpha_v\beta_3$ integrin on ECs (Zennadi et al., 2004; Kaul et al., 2006; Trinh-Trang-Tan et al., 2010; Zhang et al., 2017) through activation of the cAMP-PKA pathway. Epinephrine stimulates the β2-adrenergic receptors on RBC, which in turn stimulate adenylyl cyclase. Adenylyl cyclase catalyzes the production of cAMP from ATP. Finally, ATP activates protein kinase A (PKA) through the extracellular signal-regulated kinase 1/2 (ERK 1/2) cascade and phosphorylates ICAM-4 to an active state that can bind to $\alpha_v\beta_3$ integrin on activated ECs. In this process, A-kinase anchoring proteins (AKAPs) are critical since they guide PKA to specific locations in the cell, initiating phosphorylation of neighboring RBC receptors (Zennadi et al., 2012; Maciaszek et al., 2013; Zhang et al., 2017). It has also been shown that ICAM-4 has a potential physiological significance in mediating RBC-platelet interactions in hemostasis and thrombosis (Hermand et al., 2004). The platelet integrin $\alpha_{IIb}\beta_3$ (fibrinogen receptor GPIIb-IIIa) has been identified as a receptor for ICAM-4 *in vitro* (Hermand et al., 2002) and under flow conditions (Du et al., 2014). A specific ICAM-4 binding peptide could competitively block binding of fibrinogen to integrin $\alpha_{IIb}\beta_3$. Blocking the interaction via ICAM-4 and integrin $\alpha_{IIb}\beta_3$ reduced thrombin and fibrin deposition, with thicker and less fiber branches being present in the formed thrombi. This is likely to be of clinical consequence, since a significantly higher tail bleeding time was seen in mice in which the ICAM4-integrin $\alpha_{IIb}\beta_3$-pathway was blocked. The mechanism behind decreased thrombus formation could be that the ICAM-4-$\alpha_{IIb}\beta_3$ interaction causes intracellular signaling in platelets activating other platelets (Du et al., 2014). By blocking $\alpha_{IIb}\beta_3$, the binding of RBC to platelets decreased from 72 to 29% (Du et al., 2014) indicating that $\alpha_{IIb}\beta_3$ is involved in RBC-platelet interaction. In addition, it has been suggested that this interaction leading to RBC-platelets aggregates might contribute to vaso-occlusive events typically seen in SCD (Hermand et al., 2004).

Finally, other studies on adhesion of hemopoietic and non-hemopoietic cells, reported that ICAM-4 might also interact with $\alpha_v\beta_1$ and $\alpha_v\beta_5$ integrins (Hermand et al., 2004).

Cluster of Differentiation 36 (CD36)

Cluster of differentiation 36 is a highly glycosylated protein capable of binding to thrombospondin, Von Willebrand factor (vWF) and fibronectin (Lee et al., 2001). It is involved in hemostasis, thrombosis and inflammation events. CD36 is an adhesion molecule for monocytes, platelets, and ECs. Initially it was though that the expression of CD36 on erythroid progenitors declined with the maturation, but in the early 1990s van Schravendijk et al. showed that CD36 is also present on the surface of normal adult RBC. They also showed that its expression appears to be physiologically significant during infection with *P. falciparum*, when CD36 acts as a receptor for rosetting of *P. falciparum*-infected RBC with uninfected RBC: in fact, CD36 is defined as a scavenger receptor that bind numerous ligands, including the selective interaction with a specific domain of the *P. falciparum* erythrocyte membrane protein1 (PfEMP1) (Glenister et al., 2009; Cabrera et al., 2019). Moreover, low expression of this receptor may be sufficient for important and physiological interactions leading to cell adhesion, not only in malaria (Handunnetti et al., 1992). A high expression of CD36 was discovered in SCD RBC, and plays a key role in the adhesion of sickle cells to the endothelium and the consequent vaso-occlusive process (Lee et al., 2001; Sakamoto et al., 2013). Lastly, it is also shown that trauma-hemorrhagic shock induces an increase of several RBC adhesion molecules including CD36 which are responsible for the adhesiviness to the endothelial receptors like integrin $\alpha_v\beta_3$ and VCAM-1 and the development of microvascular dysfunction (Deitch et al., 2014).

Cluster of Differentiation 47 (CD47)

Cluster of differentiation 47 is an integrin-associated transmembrane protein (IAP) that has high affinity for thrombospondin (TSP) and signal-regulatory protein alpha (SIRPα) on the macrophage membrane (Lutz, 2004). CD47 is directly involved in the prevention of phagocytosis by macrophages through interaction with SIRPα on the macrophage surface inducing downstream inhibitory signaling (Klei et al., 2017). RBC that lack CD47 or express CD47 with switched conformation, are rapidly cleared from the circulation by splenic red pulp macrophages. In case of oxidative stress or aging, CD47 undergoes a conformational change, which triggers TSP binding and this altered/oxidized additionally is a recognition signal for SIRPα that indicates an intracellular damage (Burger et al., 2012). Moreover, Brittain et al. showed that CD47 mediates the adhesion of sickle RBC to immobilized TSP under both flow and static conditions. This leads to the adhesion of the RBC to the blood vessel wall contributing to vaso-occlusive crises in SCD (Brittain et al., 2001). CD47 could also play a very important and fundamental role in prevention of storage lesion of blood products and the early removal of RBC after transfusion. It has been suggested that reduction of CD47 expression on RBC, as a result of senescence or storage, is due to oxidative stress (Burger et al., 2012). It has also been shown that, since CD47 and Rh proteins are expressed as a complex on the RBC surface, in Rh_{null} individuals the expression of CD47 is less than 25% of normal levels. Consequently, those individuals show hemolytic anemia, reticulocytosis, and stomatocytosis that can be corrected by splenectomy (Oldenborg et al., 2000).

Cluster of Differentiation 147 (CD147)

Cluster of differentiation 147 is part of the immunoglobulin superfamily, highly glycosylated and associated with GPA into the band 3 complex. This protein is expressed in mature RBC as a carrier molecule for the blood group antigen Ok system (also known as BASIGIN or EMMPRIN) (Coste et al., 2001). It is also considered as an adhesion molecule in multiple circumstances:

for example it is known to be the direct receptor for PfRh5, which is a parasite ligand essential for *P. falciparum* blood stage growth (Crosnier et al., 2011). It was also demonstrated that CD147 is involved in promoting *P. falciparum* parasite invasion into RBC: this invasion can be inhibited by using the humanized monoclonal antibody HP6H8 against CD147 that blocks the interaction with a specific rhoptry-associated protein (RAP2) on the merozoites surface (Crosnier et al., 2011; Zenonos et al., 2015; Muramatsu, 2016; Zhang et al., 2018). Moreover, the group of Coste showed that CD147 plays a critical role in the re-entry of mature RBC from the spleen into the general circulation and when CD147 presence on the membrane was masked by antibody in mice, the migration out of the spleen was blocked and the RBC selectively trapped, inducing anemia and de novo erythropoiesis (Coste et al., 2001).

Complement Inhibitors CD55 and CD59, and Cellular Adhesion Molecule CD44

Three other glycoproteins that have shown to confer an important role are CD55, or decay accelerating factor (DAF), CD59, and CD44. The first two are complement inhibitors anchored to the RBC membrane by glycosylphosphatidylinositol (GPI), and responsible for the regulation of the autologous lysis system. CD55 binds the complement 3 (C3) convertase, limiting the formation of complement 5 (C5) convertase and formation of the membrane attack complex. In this way this glycoprotein protects RBC against lysis mediated by natural killers cells, and also functions also as ICAM and as a receptor for viruses, like Echoviruses and coxsackie B viruses, and microorganisms. For example, it was shown that CD55-null RBC are resistant to invasion by *P. falciparum* due to failure to attach properly to the RBC surface (Lelliott et al., 2015; Egan, 2018). In fact, polymorphisms in CD55 are more prevalent in populations endemic for malaria infection, indicating a possible selection pressure on this gene (Egan et al., 2015).

CD59 is a major inhibitor of the terminal complement pathway. It blocks complement 8 (C8) and complement 9 (C9) in the assembling membrane attack complex for the pore formation (Richaud-Patin et al., 2003). Defects in the biosynthesis of GPI causes paroxysmal nocturnal hemoglobinuria (PNH), a hematological disease characterized by increased intravascular hemolysis and complement activation due to the absence of CD55 and CD59 (Alegretti et al., 2012; Brodsky, 2015). In systemic lupus erythematosus patients, hematologic abnormalities are common and the expression of CD55 and CD59 is decreased (Alegretti et al., 2010).

CD44 is a single pass transmembrane glycoprotein involved in cell-cell communication. It is the receptor for hyaluronic acid (HA), osteopontin, and fibronectin (Telen, 2005; Xu, 2011): in fact, its glycosylation affects its affinity to HA (Aoki, 2017). Also CD44 is a host factor required for efficient invasion of RBC by *P. falciparum* (Lelliott et al., 2015).

Rh/RhAG Complex

The Rh blood group system is a complex association of membrane polypeptides composed of non-glycosylated Rh proteins and RhAG (Avent and Reid, 2000). In RBC, Rh is configured as a tetramer of two Rh and two RhAG subunits. Rh family proteins have an important clinical role in transfusion medicine due to their strong antigenic properties. The Rh complex contributes to the membrane stability and structure of RBC. In normal healthy conditions, Rh proteins are involved in the transport of NH_4^+ (Nakhoul and Hamm, 2004) and they are responsible, together with aquaporin-1, for half of normal CO_2 permeability (Endeward et al., 2008). In fact, RhAG possesses a gas channel for the passage of CO_2 in addition to NH_3 (Endeward et al., 2008). The Rh null phenotype is described as an inherited condition in which various Rh antigens deficiencies result in a clinical syndrome characterized by a hemolytic anemia of varying severity (Ripoche et al., 2004).

PLASMA PROTEINS MEDIATED INTERACTIONS

Thrombospondin (TSP)

Thrombospondin can be found as an immobilized extracellular matrix protein as well as a soluble plasma protein. It can facilitate adherence as a bridging molecule between RBC and ECs or platelets (Telen, 2005). Following concomitant expression of CD36 on both RBC and ECs, TSP can form a connection between these receptors (Trinh-Trang-Tan et al., 2010). In addition, TSP can interact with PS on RBC through the heparin-binding domain of CD36 (Betal and Setty, 2008). Other potential TSP receptors present on the RBC are CD47 and sulfated glycolipids. Conversely, TPS binds to $\alpha_v\beta_3$ integrin expressed on the EC surface (Manodori et al., 2000; Brittain et al., 2001; Setty et al., 2002; El Nemer et al., 2007; Kaul, 2008). It has been demonstrated that, upon addition of heparin, TSP binding can be inhibited (Gupta et al., 1999). Soluble TSP also induces an activation pathway via binding to RBC CD47, which in turn activates $\alpha_4\beta_1$ for extra adhesion to immobilized TSP (Brittain et al., 2004; Heppel, 2008). Activation of this signaling pathway is enhanced when RBC are exposed to shear stress (Telen, 2005). Concerning the interaction with platelets, TSP could also be a bridging molecule between RBC and platelets since it is known that TSP can also bind CD47, CD36, $\alpha_4\beta_1$, PS, and sulfated glycolipids on RBC (Betal and Setty, 2008; Heppel, 2008; Trinh-Trang-Tan et al., 2010). The CD36-TSP interaction activates the CD47-dependent pathway. CD47 can bind to platelet $\alpha_{IIb}\beta_3$ integrin, which in turn can bind ICAM-4 (Lagadec et al., 2003). TSP expression was found markedly increased in the vessel wall in multiple diseases like cardiovascular disorders, diabetes mellitus, atherosclerosis and ischemia-reperfusion injury (IRI; (Csányi et al., 2012).

Von Willebrand Factor (vWF)

Von Willebrand factor serves as a bridging molecule between the endothelial receptor $\alpha_v\beta_3$ and/or the endothelial receptor glycoprotein Ib, to a yet-unknown receptor on the RBC in a platelet-independent way (Setty et al., 2002; Smeets M. et al., 2017). Adhesion mediated by vWF seems to have a quantitatively and qualitatively different role in large vessel endothelium compared to the microvascular endothelium

(Brittain et al., 1992). In general, increased RBC stress is linked to the pathology of several diseases including SCD, sepsis, chronic kidney disease, hemolytic uremic syndrome, hepatic failure, Wilson's disease, diabetes, Alzheimer's disease, and thrombotic thrombocytopenic. In all these conditions, RBC binds to ECs through interaction with monomer vWF and long multimers vWF, organized in large insoluble fibers. This leads to microangiopathic vascular damage, impairing the blood flow with the subsequent (multiple) organ failure (Smeets M.W. et al., 2017). The adhesion molecule that has been shown to interact with vWF and therefore promotes binding to RBC is PS (Nicolay et al., 2018). This interaction exists due to Annexin V molecule, which cannot only bind to PS on the RBC surface but also to vWF and thereby anchor the PS-exposing membrane to vWF or to vessel wall (Nicolay et al., 2018). Another study demonstrated that under reduced vascular wall shear stress, RBC bind specifically to vWF, forming the aggregates structure of venous thrombi (Smeets M. et al., 2017). Upon increased levels of intracellular Ca^{2+}, which can occur in sickle cells but also normal RBC (Bogdanova et al., 2013), RBC can adhere to vWF strings which are connected to the endothelium by P-selectin or $\alpha_v\beta_3$ integrin on the luminal surface (Smeets M.W. et al., 2017) and also by the endothelial glycocalyx (Kalagara et al., 2018). The group of Sultana et al. showed that sickle cells that are incubated with ECs in presence of multimers of vWF resulted in an increase of ICAM-1, E-selectin and VCAM-1 expression in the ECs, which in turn facilitated the adhesion of the sickle cells to the ECs (Sultana et al., 1998).

Laminin Alpha 5

Laminin is an extracellular matrix glycoprotein also found in the sub-endothelium (Hillery et al., 1996; Wautier and Wautier, 2013). It has been shown that laminin alpha 5 chain can bind to Basal-cell adhesion molecule/Lutheran blood group glycoprotein (B-CAM/LU) on the RBC membrane. B-CAM/LU, or CD239, plays a crucial role in vaso-occlusion in SCD (Wautier and Wautier, 2013). On normal RBC B-CAM/LU is a relatively inactive receptor of laminin alpha 5, but it is highly expresses on sickle RBC (de Oliveira and Saldanha, 2010). The interaction of B-CAM/LU with laminin alpha 5 is inhibited when interacting in cis conformation, with GPC-derived sialic acid residues on the RBC. Upon loss of this interaction during aging, B-CAM/LU can interact, in trans, with sialic acid on laminin alpha 5 (Klei et al., 2018). In polycythemia vera, a myeloproliferative disorder characterized by a high occurrence of thrombosis, there is a correlation between the mutation of the janus kinase and phosphorylation of B-CAM/LU, which in turn initiates the interaction with endothelial laminin alpha 5 (Wautier et al., 2007; Wautier and Wautier, 2013). B-CAM/LU is directly linked to the RBC cytoskeleton via spectrin (An et al., 2008). This adhesion process is under the influence of epinephrine that activates B-CAM/LU through the cAMP-PKA pathway (Hines et al., 2003; Maciaszek et al., 2013; Wautier and Wautier, 2013; Zhang et al., 2017). It seems that the adhesion of RBC to ECs mediated by B-CAM/LU depends on its phosphorylated status and not on the amount of expressed receptors (Chaar et al., 2014). Phosphorylation of B-CAM/LU weakens the interaction with spectrin, which is accompanied by enhanced cell adhesion to laminin (An et al., 2008). The weakening of B-CAM/LU-spectrin interaction enables these molecules to aggregate and generate a larger adhesive force (Maciaszek et al., 2013). Hydroxycarbamide decreases the phosphorylation of B-CAM/LU and consequently reduces cell adhesion (Bartolucci et al., 2010; Chaar et al., 2014). It can therefore be used as a therapy in SCD patients. Interestingly, when ICAM4-$\alpha_v\beta_3$ interactions are abolished, the adhesive capacity of laminin strongly decreases, suggesting that laminin-mediated interactions might function as a secondary adhesive interaction after ICAM4 interacted with $\alpha_v\beta_3$ integrin (Ko et al., 2005; Zennadi et al., 2008).

Fibrinogen

Fibrinogen is a plasma glycoprotein. The concentration of fibrinogen can be elevated under pathological conditions, such as bleeding tendency, liver disease (Tsang et al., 1990). In cerebrovascular dysfunction, high levels of fibrinogen lead to inflammation with accumulation of plasma proteins and increased vascular permeability which promotes hypercoagulation and thrombogenesis (Muradashvili and Lominadze, 2013). It was shown that the increase of fibrinogen correlates with elevated levels of C-reactive protein (CRP), which has been connected to thrombotic events, and the erythrocyte sedimentation rate (ESR): these last two are used as diagnostic parameters (Bitik et al., 2015; Flormann et al., 2015). In addition, fibrinogen has been shown to be able to adhere to different receptors on RBC, such as CD47, and on platelets with $\alpha_{IIb}\beta_3$–like integrin (Carvalho et al., 2010; De Oliveira et al., 2012). Fibrinogen can also bind to ICAM1 on platelets (Massberg et al., 1999). Lastly, it was observed that sickle deoxygenated RBC tend to stick together and this occurs in presence of fibrinogen (Weiss et al., 2011).

Immunoglobulin G (IgG)

Immunoglobulin G is the most abundant and common type of antibody, representing 75% of all plasma antibodies (Painter, 1998). The opsonization of specific targets, in particular band 3 by IgG, is essential for recognition of senescent RBC by macrophages (Meinderts et al., 2017). IgG specifically co-localizes with membrane aggregates composed by band 3, partially denatured hemoglobin and complement factor C3 (Badior and Casey, 2017). The group of Janvier et al. described that warm IgG autoantibodies are specific for the third external loop of band 3 and this is the major target in patients with warm antibody autoimmune hemolytic anemia (AIHA) (Janvier et al., 2013). It has also been suggested that a correlation between the decrease in sialic acid content of senescent RBC and accumulation of autologous IgG on the membrane has also been suggested to play an important role in physiological erythrophagocytosis (Ensinck et al., 2006).

Lactadherin (MFG-E8)

Lactadherin or milk fat globule-EGF factor 8 (MFG-E8) is a plasma protein bridging molecule that plays a role as a cell adhesion protein. It contains an EGF-like domain at the amino terminus with the RGD sequence, a motif of Arginine,

Glycine, and Aspartate aminoacids, and two C-domains at the carboxy terminus (Raymond et al., 2009). This protein is known to participate in a wide variety of cellular interactions, including phagocytosis of apoptotic cells (de Back et al., 2014). Lactadherin promotes engulfment of PS-containing apoptotic cells by macrophages (Guchhait et al., 2007). It has been shown that the presence of lactadherin enhaces and mediates the adhesion of PS-exposing sickle RBC to the endothelium via the $\alpha_v\beta_3$ integrin (Guchhait et al., 2007). Lastly, it was shown that activated ECs are able to phagocyte PS-exposing and rigid RBC under both static and flow conditions: this mechanism could lead to ECs loss and contribute to vasopathological effects as in SCD (Fens et al., 2008, 2012).

Growth Arrest Specific 6 (Gas6) and Protein S

Growth arrest specific 6, together with Protein S, is a ligand for tyrosin-protein kinase receptors like Tyro3, Axl and Mer (TAM): these are essential for the efficient phagocytosis of apoptotic cells. The TAM signaling appears to be autocrine/paracrine: since the TAM positive cells also produce the ligands (Lemke, 2013). This ligand physically links a TAM receptor expressed on the membrane of a phagocyte to PS-exposing cells suggesting that PS-exposing RBC are cleared via macrophages recognizing these PS/ligand binding (de Back et al., 2014).

RBC-DERIVED MICROPARTICLES MEDIATED INTERACTIONS

Microparticles (MPs) derived from RBC are membranous extracellular structures shedded into the plasma under various circumstances. RBC-derived MPs size are 50–200 nm in diameter and they have an important role as key mediators of intercellular communication and consequently have an impact on various physiological processes such as blood homeostasis and modulation of immune responses (Dumaswala and Greenwalt, 1984; Willekens et al., 2008; Antonelou et al., 2010; Westerman and Porter, 2016). The reorganization of the membrane involving the lipid ratio and the disruption of the protein-protein interactions induce the microvesicles generation (Leal et al., 2018). MPs themselves expose antigens derived from the RBC membrane such as GPA, band 3, and PS on their membrane. PS can function to promote the coagulation cascade (Morel et al., 2011). By unknown mechanisms, RBC MPs contain a number of selected membrane components. For example, it was shown that MPs derived from old stored (20 days) RBC are rich in band 3, stomatin and PS (Lutz and Bogdanova, 2013). RBC-derived MPs levels are commonly elevated in *ex vivo* stored transfusion blood and during the course of some pathological conditions such as malaria, SCD, (Barteneva et al., 2013) and in hemolytic anemias (Litvinov and Weisel, 2017). Due to molecular defects, in hereditary membranophaties such as hereditary spherocytosis (HS) the instability of RBC membrane correlates with the membrane loss through vesiculation, with the outcome of less deformable RBC (Alaarg et al., 2013). Surprisingly, whereas HS RBC become more rigid, the extracellular vesicles in HS have a lower bending modulus (Vorselen et al., 2018). The role of RBC-derived MPs in different pathologies and mechanisms, such as inflammation, thrombosis and autoimmune reactions, is currently under investigation (Leal et al., 2018). The biological effects of RBC MPs comprise, for example, the regulation of coagulation mediated by binding to protein S (Koshiar et al., 2014), immune modulation, enhanced endothelial adhesion and scavenging action on nitric oxide (NO) (Said et al., 2018). RBC MPs especially appear to play a relevant role in the pathophysiology of SCD, promoting pro-inflammatory cytokine secretion, oxidative stress, endothelial apoptosis, leading to SCD vaso-occlusive crises (Said et al., 2018). The characterization of the MPs composition in specific blends of transmembrane proteins and lipids could lead to better understanding of interactions between specific cells or tissues.

DYNAMIC INTERACTIONS

The motile nature of RBC has elicited multiple studies that focused on interactions from a spatial, mechanical and fluidic point of view. These interactions focus on rheologic dynamic, based on the nonspecific forces instead of the mediation by adhesion molecules (Lowe, 1988; Cabel et al., 1997).

RBC Aggregation

Red blood cells are the most predominant blood cells and have a significant contribution to the fluidity of blood under physiological conditions (Simmonds et al., 2013). In fact, their ability to deform and aggregate contribute to blood viscosity high shear rates and low shear rates, respectively. RBC have the intrinsic tendency to form aggregates: it is possible to assist to this reversible phenomenon in which RBC assume the rouleau conformation, a specialy shaped structure composed by a linear arrays of stocked RBC, or with the 3D aggregates stasis (Baskurt and Meiselman, 2008). This mechanism occurs in health, aging and disease conditions and can be explained by two theories: the first is the bridging model, where the intercellular interaction is mediated by a protein or polymer such as fibrinogen or immunoglobulins. The second one is the depletion model, the most supported one, where protein or polymers are less concentrated near the RBC surface, creating an osmotic gradient (Wagner et al., 2013). According to the Fahraeus-Lindqvist effect, blood viscosity decreases with decreasing vessel diameters. In this way RBC migrate to the center of the vessel, leaving the plasma concentrated at the vessel wall. In various disease conditions, RBC aggregates increase blood viscosity and hydrodinamic resistence in large vessels, thereby promoting venus thrombosis (Weisel and Litvinov, 2019). Changes in plasma composition, such as during inflammatory reactions where fibrinogen level may rise fivefold, or increases in hematocrit are triggers that lead to serious hyperviscosity, intense aggregation and hydrodinamic clusters of RBC (Brust et al., 2014). This event is especially enhanced or abnormal in infections (sepsis), circulatory disorders (myocardial infarction), acute phase response, metabolic disordes, hematological disorders (polycythemia vera, SCD) and malignant diseases (Simmonds et al., 2013).

RBC and ECs

The adhesion of RBC to other cell types and surfaces has been of particular interest due to the fact that this unusual aggregation and adhesiveness to other RBC and to ECs have been linked to various vascular disorders, such as SCD, DM, and hypertension (Setty et al., 2002; Wautier and Wautier, 2004). It was recently shown that non-absorbing macromolecules can have a marked impact on mediating the adhesion efficiency of RBC to ECs in patients with type 2 diabetes mellitus (T2DM) (Kaliyaperumal et al., 2019). Studies of nonspecific forces, like attractive, repulsive electrostatic forces, have considered macromolecular depletion as an effective mechanism inducing cell-surface adhesion (Neu and Meiselman, 2006). Other flow studies found different behavior of blood flow at microvascular level compared to macrovascular vessels due to the additional resistence of the endothelial glycocalyx layer on the luminal surface of the smaller blood vessel wall (Liu and Yang, 2009). This dynamic interaction of RBC and ECs involves the status of their glycocalyx located on the surfaces of both RBC and ECs. These layers facilitate "cushion" functions because the anionic properties of endothelial glycocalyx repels the negatively charged RBC, avoiding cells from coming to close (Liu and Yang, 2009). Endothelial glycocalyx can get damaged in metabolic syndrome, inflammatory processes and excess sodium intake (Noble et al., 2008; Lipowsky et al., 2011; Oberleithner et al., 2011). RBC glycocalyx get damaged due to increased oxidative stress as well as aging of the RBC (Neu et al., 2003). It seems that damaged EC glycocalyx leads to shedding of RBC glycocalyx and vice versa after these cells dynamically interact (Oberleithner, 2013). When a defect has occurred in either the glycocalyx of the RBC or the EC, this defect further enhances itself through the interaction of these cells with one another. Since the function of glycocalyx is prevention of adhesion (Liu and Yang, 2009), it could be that adhesiveness of RBC to ECs could increase when such a defect occurs. However, this has not yet been proven *in vivo*.

RBC and Platelets

A different type of interplay that has been described between cells are hydrodynamic interactions. Platelets exhibit a phenomenon called platelet margination or lateral drift, in which the concentration of platelets is highest near the vessel wall (Namdee et al., 2013; Vahidkhahb et al., 2014). This seems to be the result of an interaction with RBC (Vahidkhah et al., 2013; Carboni, 2017). When a platelet comes across a RBC, either a crossing or a turning interaction occurs. In the crossing type of interaction the platelet rolls over the RBC, slightly deforming the flexible RBC, and moves in the same direction. In the turning type the platelet approaches the RBC, but then reverses back into the direction it came from without making direct contact with RBC. Whether crossing or turning occurs depends upon the initial lateral separation of the platelet and the RBC (Vahidkhah et al., 2013). When platelet-RBC interaction occurs in midflow of the vessel, this lateral separation is the only factor (Decuzzi et al., 2005). However, if the interaction occurs closer to the vessel wall, this affects the movement (Eckstein et al., 1988; Bächer et al., 2018). When a platelet is located farther away from the vessel wall than the RBC it is more likely to undergo a turning interaction trajectory, while when a platelet is located nearer to the vessel wall than the RBC crossing interaction is more likely (Vahidkhah et al., 2013). These events cause the platelet to be continuously driven away from the RBC-rich region in the center of the vessel into the plasma layer close to the vessel wall (Vahidkhah et al., 2013). Tokarev et al. suggested in their model that shear rate, hematocrit level and RBC size influence the mechanism in which the platelets are pushed against the vessel wall as a result of rebounding collision with an outrunning RBC or other blood cells (Tokarev et al., 2011; Fitzgibbon et al., 2015). These mechanisms could also explain why elevated hematocrit enhances platelet accumulation and binding to the vascular wall. It is also thought that an elevated hematocrit enlarges the interaction frequency of platelets with thrombi, which in turn accelerates the accumulation of platelets and thus the formation of thrombi (Yazdani and Em Karniadakis, 2016; Walton et al., 2017). Rigidity of RBC also plays a role: more rigid RBC increase platelet marginalization which increases sustainability for thrombosis (Aarts et al., 1986). In T2DM RBC and platelets exhibit abnormal biomechanical properties and biorheology which can affect blood flow dynamics and blood cell transport. In fact, less deformable T2DM RBC reduce the heterogenous collisions with the highest near-wall accumulation of T2DM platelets (Chang et al., 2018).

RBC and White Blood Cells (WBC)

In order to roll on the endothelium, circulating WBC must migrate radially to contact the vessel wall (Munn and Dupin, 2008). This phenomenon is called margination and it is attributed to the RBC's ability to aggregate and exclude WBC from the bulk solution. Munn and Dupin showed that rouleau formation of RBC is more effective in pushing WBC to the vessel wall than a loosely associated group of cells. WBC margination also depends on the local hematocrit, flow rate, RBC and WBC deformability (Fedosov and Gompper, 2014). RBC bounce the WBC against the endothelium and especially in small vessels WBC reverse the Fahraeus-Lindqvist effect and the resistant becomes greater due to the large size of the WBC (Munn and Dupin, 2008). In particular circumstances such as SCD, adherent WBC bind RBC and contribute to the microvascular pathology (Finnegan et al., 2007).

RBC and Macrophages

The interaction between RBC and macrophages has been frequently discussed. Macrophages are directly involved in the two most delicate processes of RBC: erythropoiesis and erythrophagocytosis. So on one side macrophages are important for providing signals that induce differentiation and proliferation of RBC progenitors in the bone marrow niche. On the other side defective RBC are filtered, repaired and/or ultimately removed from the circulation by splenic and liver macrophages (Klei et al., 2017). Regarding these two fundamental stages specific and detailed reviews in health (de Back et al., 2014; Klei et al., 2017; Badior and Casey, 2018) and diseases (Mohanty et al., 2014; Risso et al., 2014; Flegel, 2015) are suggested. Since the focus of this review is on interactions that occur during RBC life, interactions involved in maturation and clearance are not discussed.

RBC INTERACTION WITH PATHOGENS

Red blood cells do not only have the principal functions associated to oxygen and carbon dioxide transport and the role they play in homeostasis and blood flow distribution (Morera and MacKenzie, 2011), but RBC are also involved in the innate immune response (Minasyan, 2018). In a dynamic compartment such in the bloodstream, the clearance of bacteria is performed by oxycytosis. This means that bacteria moving with the blood flow, become triboeletrically charged and consequently attracted to RBC (Minasyan, 2016). This contact causes the release of oxygen from oxyhemoglobyn to the surface of the RBC and thereby killing the bacteria. This dimishes the triboelectric charge and the bacteria are finally washed from the RBC surface and digested in the liver or spleen (Minasyan, 2018). Although free hemoglobin may confer antimicrobial protection under homeostatic conditions, it has the opposite effect during disease, such as in severe sepsis often leading to increased mortality (Anderson et al., 2018). Many pathogens are able to bind glycophorins, such as reovirus, influenza C, sendai, mycoplasma pneumonie, *Escherichia coli* and ureaplasma urealyticum, acting as a chaperone and thereby avoiding the important tissues and facilitating the clearance of this pathogens by the spleen with macrophages (Baum et al., 2002). On the other hand it is via the same glycophorins that *P. falciparum* parasites adhere and invade the RBC (Morera and MacKenzie, 2011; Anderson et al., 2018). The malaria parasites multiply and evolve inside the RBC and are able to digest the hemoglobin converting it in crystals known as hemozoin (Parroche et al., 2007). This also happens for the HIV-1 virions and Zika virus in which they respectivly enrich the viral infectivity by binding to RBC (Beck et al., 2009) and hiding inside the RBC (Stone et al., 2017).

Thus, pathogens binding to or internalized into RBC could be both advantageous or detrimental to the host (Anderson et al., 2018).

CONCLUSION

An overview of current knowledge on the interaction of RBC with other cells, ECs and platelets, in physiological and disease conditions, is presented here. Both direct interactions through receptors on the RBC and other key players, such as ECs, platelets, WBC, macrophages, other RBC, have been discussed, as well as indirect interactions between these cells (**Supplementary Table S1**). Indirect interaction can occur through plasma ligands, proteins and released molecules or particles from these cells. Other indirect interactions described in this review are mechanical: these kind of interactions are focused on the dynamic and rheological distribution of RBC in contact with other cells in physiological flow conditions. This underlines the complexity of the global interactions in which the mature RBC are involved and, more importantly, addresses a crucial attention to the pathological circumstances. Regarding the interaction with endothelium, depletion interaction plays an important role, while in interaction with platelets and WBC the margination caused by RBC is the largest contributing factor to interaction. Finally, we also reviewed the critical interaction of RBC with pathogens.

We note that studies on RBC interactions with other cells are, in most cases, conducted under artificial conditions that may differ from physiological conditions. For example, interaction with cultured ECs could be different compared to *in vivo* vascular ECs since cultured cells do not express the same structure and amount of glycocalyx *in vitro* as *in vivo* (Weinbaum et al., 2007). Also, often cells that are present *in vivo* are excluded in experimental setups to not influence the measurements. Finally, *in vitro* studies that are conducted, often use flat cultured monolayer of ECs, so the influence of the three-dimensional vessel wall is not taken into account. The largest amount of studies conducted on adhesiveness of RBC is performed using blood of SCD patients or rodents. These cells are active and express PS and other receptors on their membranes which enable them to adhere to other cells. However, it is not known if sickle cells adhere in the same manner as other activated RBC would do. With regard to receptor-based interactions there are probably multiple receptors and interactions responsible for adhesion of RBC. It is also not necessarily so that high-affinity mechanisms shown in laboratory studies are the largest contribution factor to adhesion *in vivo*. Microvascular blood flow can be intermittent and RBC can be slowed by passing granulocytes because of their larger size. In such conditions lower affinity mechanism may also play an important role in adhesion.

It is recurrently observed that in different pathological conditions, such as SCD, T2DM, G6PD deficiency, thalassemia, chronic diseases, malaria, RBC become more adhesive and less deformable and this enhances the possible interactions with the surrounding cells. This leads to the development of microvascular obstructions with consequential impaired oxygen and nutrient delivery to organs and tissues which can cause organ failure.

To conclude, this overview goes beyond the characteristics of the RBC itself to yet expand our knowledge concerning RBC function and crucial roles. Studying the interactions between RBC and other cell types, proteins, pathogens or other cellular mediators will therefore increase our understanding of RBC homeostasis and contribute to novel insights in a variety of hematological and non-hematological disorders.

AUTHOR CONTRIBUTIONS

All authors listed have made a substantial, direct and intellectual contribution to the work, and approved it for publication.

FUNDING

This work was supported by the European Union's Horizon 2020 Research and Innovation Program under grant agreement No. 675115 – RELEVANCE – H2020-MSCA-ITN-2015/H2020-MSCA-ITN-2015.

SUPPLEMENTARY MATERIAL

The Supplementary Material for this article can be found online at: https://www.frontiersin.org/articles/10.3389/fphys.2019.00945/full#supplementary-material

TABLE S1 | Summary of the classified interactions with the key player factors and the pathologies involved. The key players of each specific interaction and pathologies correlated are connetted with the same corresponding number (ECs = endothelial cells; SCD = sickle cell disease; G6PD = glucose-6-phosphate dehydrogenase; WBC = white blood cells; PNH = paroxysmal nocturnal hemoglobinuria; MPs = microparticles).

REFERENCES

Aarts, P. A., Banga, J. D., and van Houwerlinger, H. C. (1986). Increased red blood cell deformability due to isoxsuprine administration decreases platelet adherence in a perfusion chamber: a double-blind cross-over study in patients with intermittent claudication. *Blood* 67, 1474–1481.

Abed, M., Towhid, S. T., Pakladok, T., Alesutan, I., Götz, F., Gulbins, E., et al. (2013). Effect of bacterial peptidoglycan on erythrocyte death and adhesion to endothelial cells. *Int. J. Med. Microbiol.* 303, 182–189. doi: 10.1016/j.ijmm.2013.01.004

Abel, S., Hundhausen, C., Mentlein, R., Schulte, A., Berkhout, T. A., Broadway, N., et al. (2004). The transmembrane CXC-chemokine ligand 16 is induced by IFN-gamma and TNF-alpha and shed by the activity of the disintegrin-like metalloproteinase ADAM10. *J. Immunol.* 172, 6362–6372. doi: 10.4049/jimmunol.172.10.6362

Adams, J. (2010). "Eukaryotic cells possess a nucleus and membrane-bound organelles," in *Essentials of Cell Biology*, ed. R. Becker (Cambridge, MA: NPG Education).

Alaarg, A., Schiffelers, R., van Solinge, W., and van Wijk, R. (2013). Red blood cell vesiculation in hereditary hemolytic anemia. *Front. Physiol.* 4:365. doi: 10.3389/fphys.2013.00365

Alegretti, A. P., Mucenic, T., Merzoni, J., Faulhaber, G., Silla, L., and Xavier, R. (2010). Expression of CD55 and CD59 on peripheral blood cells from systemic lupus erythematosus (SLE) patients. *Cell Immunol.* 265, 127–132. doi: 10.1016/j.cellimm.2010.07.013

Alegretti, A. P., Schneider, L., Piccoli, A., and Xavier, R. (2012). The role of complement regulatory proteins in peripheral blood cells of patients with systemic lupus erythematosus: review. *Cell Immunol.* 277, 1–7. doi: 10.1016/j.cellimm.2012.06.008

Alenghat, F. J., and Golan, D. E. (2013). Membrane protein dynamics and functional implications in mammalian cells. *Curr. Top. Membr.* 72, 89–120. doi: 10.1016/B978-0-12-417027-8.00003-9

Altankov, G., and Serafimov-Dimitrov, V. (1990). Adhesive properties of blood cells. *Haematologia* 23, 239–248.

An, X., Gauthier, E., Zhang, X., Guo, X., Anstee, D. J., Mohandas, N., et al. (2008). Adhesion activity of Lu Glycoproteins is regulated by interaction with spectrin. *Blood* 112, 5212–5218. doi: 10.1182/blood-2008-03-146068

Anderson, H. L., Brodsky, I., and Mangalmurti, N. (2018). The evolving erythrocyte: red blood cells as modulators of innate immunity. *J. Immunol.* 201, 1343–1351. doi: 10.4049/jimmunol.1800565

Andolfo, I., Russo, R., Manna, F., Shmukler, B., Gambale, A., Vitiello, G., et al. (2015). Novel Gardos channel mutations linked to dehydrated hereditary stomatocytosis (xerocytosis). *Am. J. Hematol.* 90, 921–926. doi: 10.1002/ajh.24117

Antonelou, M., Kriebardis, A., and Papassideri, I. (2010). Aging and death signalling in mature red cells: from basic science to transfusion practice. *Blood Transfus* 8(Suppl. 3), s39–s47.

Aoki, T. (2017). A comprehensive review of our current understanding of red blood cell (RBC) glycoproteins. *Membranes* 7:E56. doi: 10.3390/membranes7040056

Archer, N., Shmukler, B., Andolfo, I., Vandorpe, D., Gnanasambandam, R., Higgins, J., et al. (2014). Hereditary xerocytosis revisited. *Am. J. Hematol.* 89, 1142–1146. doi: 10.1002/ajh.23799

Avent, N. D., and Reid, M. (2000). The Rh blood group system: a review. *Blood* 95, 375–387.

Azouzi, S., Gueroult, M., Ripoche, P., Genetet, S., Aronovicz, Y. C., Le Van, et al. (2013). Energetic and molecular water permeation mechanisms of the human red blood cell urea transporter B. *PLoS One* 8:e82338. doi: 10.1371/journal.pone.0082338

Azouzi, S., Romana, M., Arashiki, N., Takakuma, Y., Nemer, W. E., Peyrard, T., et al. (2018). Band 3 phosphorylation induces irreversible alterations of stored red blood cells. *Am. J. Hematol.* 93, E110–E112.

Bächer, C., Kihm, A., Schrack, L., Kaestner, L., Laschke, M., Wagner, C., et al. (2018). Antimargination of microparticles and platelets in the vicinity of branching vessels. *Biophys. J.* 115, 411–425. doi: 10.1016/j.bpj.2018.06.013

Badior, K., and Casey, J. (2018). Molecular mechanism for the red blood cell senescence clock. *IUBMB Life* 70, 32–40. doi: 10.1002/iub.1703

Badior, K. E., and Casey, J. R. (2017). Molecular mechanism for the red blood cell senescence clock. *IUBMB Life* 70, 32–40. doi: 10.1002/iub.1703

Bae, C., Gnanasambandam, R., Nicolai, C., Sachs, F., and Gottlieb, P. A. (2013). Xerocytosis is caused by mutations that alter the kinetics of the mechanosensitive channel PIEZO1. *Proc. Natl. Acad. Sci. U.S.A.* 110, E1162–E1168. doi: 10.1073/pnas.1219777110

Bagriantsev, S. N., Gracheva, E. O., and Gallagher, P. G. (2014). Piezo proteins: regulators of mechanosensation and other cellular processes. *J. Biol. Chem.* 289, 31673–31681. doi: 10.1074/jbc.R114.612697

Barteneva, N., Fasler-Kan, E., Bernimoulin, M., Stern, J., Ponomarev, E., Duckett, L., et al. (2013). Circulating microparticles: square the circle. *BMC Cell Biol.* 14:23. doi: 10.1186/1471-2121-14-23

Bartolucci, P., Chaar, V., Picot, J., Bachir, D., Habibi, A., Fauroux, C., et al. (2010). Decreased sickle red blood cell adhesion to laminin by hydroxyurea is associated with inhibition of Lu/BCAM protein phosphorylation. *Blood* 116, 2152–2159. doi: 10.1182/blood-2009-12-257444

Baskurt, O., and Meiselman, H. (2008). RBC aggregation: more important than RBC adhesion to endothelial cells as a determinant of in vivo blood flow in health and disease. *Microcirculation* 15, 585–590. doi: 10.1080/10739680802107447

Baum, J., Ward, R., and Conway, D. (2002). Natural selection on the erythrocyte surface. *Mol. Biol. Evol.* 19, 223–229. doi: 10.1093/oxfordjournals.molbev.a004075

Beck, Z., Brown, B., Wieczorek, L., Peachman, K., Matyas, G., Polonis, V., et al. (2009). Human erythrocytes selectively bind and enrich infectious HIV-1 virions. *PLoS One* 4:e8297. doi: 10.1371/journal.pone.0008297

Betal, S. G., and Setty, Y. B. (2008). Phosphatidylserine-positive erythrocytes bind to immobilized and soluble thrombospondin-1 via its heparin binding domain. *Transl. Res.* 152, 165–177. doi: 10.1016/j.trsl.2008.07.007

Bitik, B., Mercan, R., Tufan, A., Tezcan, E., Küçük, H., İlhan, M., et al. (2015). Differential diagnosis of elevated erythrocyte sedimentation rate and C-reactive protein levels: a rheumatology perspective. *Eur. J. Rheumatol.* 2, 131–134. doi: 10.5152/eurjrheum.2015.0113

Bogdanova, A., Makhro, A., Wang, J., Lipp, P., and Kaestner, L. (2013). Calcium in red blood cells - a perilous balance. *Int. J. Mol. Sci.* 14, 9848–9872. doi: 10.3390/ijms14059848

Borst, O., Abed, M., Alesutan, I., Towhid, S. T., Qadri, S. M., Föller, M., et al. (2012). Dynamic adhesion of eryptotic erythrocytes to endothelial cells via. *Am. J. Physiol. Cell Physiol.* 302, C644–C651.

Brittain, H. A., Eckman, J. R., and Wick, T. M. (1992). Sickle erythrocyte adherence to large vessel and microvascular endothelium under physiologic flow is qualitatively different. *J. Lab. Clin. Med.* 120, 538–545.

Brittain, J. E., Han, J., Ataga, K. I., Orringer, E. P., and Parise, L. V. (2004). Mechanism of CD47-induced alpha4beta1 integrin activation and adhesion in sickle reticulocytes. *J. Biol. Chem.* 279, 42393–42402. doi: 10.1074/jbc.m407631200

Brittain, J. E., Mlinar, K. J., Anderson, C. S., Orringer, E. P., and Parise, L. V. (2001). Integrin-associated protein is an adhesion receptor on sickle red blood cells for immobilized thrombospondin. *Blood* 97, 2159–2164. doi: 10.1182/blood.v97.7.2159

Brodsky, R. (2015). Complement in hemolytic anemia. *Blood* 126, 2459–2465. doi: 10.1182/blood-2015-06-640995

Brugnara, C., De Franceschi, L., and Alper, S. (1993). Ca(2+)-activated K+ transport in erythrocytes: comparison of binding and transport inhibition by scorpion toxins. *J. Biol. Chem.* 268, 8760–8768.

Brust, M., Aouane, O., Thiébaud, M., Flormann, D., Verdier, C., Kaestner, L., et al. (2014). The plasma protein fibrinogen stabilizes clusters of red blood cells in microcapillary flows. *Sci. Rep.* 4:4348. doi: 10.1038/srep04348

Burger, P., de Korte, D., van den Berg, T., and van Bruggen, R. (2012). CD47 in erythrocyte ageing and clearance – the Dutch point of view. *Transfus. Med. Hemother.* 39, 348–352. doi: 10.1159/000342231

Burton, N. M., and Bruce, L. J. (2011). Modelling the structure of the red cell membrane. *Biochem. Cell Biol.* 89, 200–215. doi: 10.1139/o10-154

Cabel, M., Meiselman, H., Popel, A., and Johnson, P. (1997). Contribution of red blood cell aggregation to venous vascular resistance in skeletal muscle. *Am. J. Physiol.* 272(2 Pt 2), H1020–H1032.

Cabrera, A., Neculai, D., Tran, V., Lavstsen, T., Turner, L., and Kain, K. (2019). *Plasmodium falciparum*-CD36 structure-function relationships defined by ortholog scanning mutagenesis. *J. Infect. Dis.* 219, 945–954. doi: 10.1093/infdis/jiy607

Cahalan, S. M., Lukacs, V., Ranade, S. S., Chien, S., Bandell, M., and Patapoutian, A. (2015). Piezo1 links mechanical forces to red blood cell volume. *eLife* 4:e07370. doi: 10.7554/eLife.07370

Carboni, E. J. (2017). *The Margination and Transport of Particles in Blood Flow*, Vol. 1581. Doctoral Dissertations, University of Connecticut, Storrs, CT.

Carvalho, F. A., Connell, S., Miltenberger-Miltenyi, G., Pereira, S. V., Tavares, A., Ariëns, R. A., et al. (2010). Atomic force microscopy-based molecular recognition of a fibrinogen receptor on human erythrocytes. *ACS Nano* 4, 4609–4620. doi: 10.1021/nn1009648

Chaar, V., Laurance, S., Lapoumeroulie, C., Cochet, S., De Grandis, M., Colin, Y., et al. (2014). Hydroxycarbamide decreases sickle reticulocyte adhesion to resting endothelium by inhibiting endothelial lutheran. *J. Biol. Chem.* 289, 11512–11521. doi: 10.1074/jbc.M113.506121

Chang, H., Yazdani, A., Li, X., Douglas, K., Mantzoros, C., and Karniadakis, G. (2018). Quantifying platelet margination in diabetic blood flow. *Biophys. J.* 115, 1371–1382. doi: 10.1016/j.bpj.2018.08.031

Chasis, J. A., and Mohandas, N. (1992). Red blood cell glycophorins. *Blood* 80, 1869–1879.

Clark, M., Shohet, S., and Gottfried, E. (1993). Hereditary hemolytic disease with increased red blood cell phosphatidylcholine and dehydration: one, two, or many disorders? *Am. J. Hematol.* 42, 25–30. doi: 10.1002/ajh.2830420107

Closse, C., Dechary-Prigent, J., and Boisseau, M. R. (1999). Phosphatidylserine-related adhesion of human erythrocytes to vascular endothelium. *Br. J. Haematol.* 107, 300–302. doi: 10.1046/j.1365-2141.1999.01718.x

Colin, Y., Le Van, Kim, C., and El Nemer, W. (2014). Red cell adhesion in human diseases. *Curr. Opin. Hematol.* 21, 186–192. doi: 10.1097/MOH.0000000000000036

Cooper, G. M. (ed.). (2000). "Cell membranes the chemistry of cells," in *Part I; The Cell: A Molecular Approach*, 2nd Edn, (Sunderland, MA: Sinauer Associates).

Coste, I., Gauchat, J. F., Wilson, A., Izui, S., Jeannin, P., Delneste, Y., et al. (2001). Unavailability of CD147 leads to selective erythrocyte trapping in the spleen. *Blood* 97, 3984–3988. doi: 10.1182/blood.v97.12.3984

Crosnier, C., Bustamante, L., Bartholdson, S., Bei, A., Theron, M., Uchikawa, M., et al. (2011). Basigin is a receptor essential for erythrocyte invasion by *Plasmodium falciparum*. *Nature* 480, 534–537. doi: 10.1038/nature10606

Csányi, G., Yao, M., Rodríguez, A., Al Ghouleh, I., Sharifi-Sanjani, M., Frazziano, G., et al. (2012). Thrombospondin-1 regulates blood flow via CD47 receptor-mediated activation of NADPH oxidase 1. *Arterioscler. Thromb. Vasc. Biol.* 32, 2966–2973. doi: 10.1161/ATVBAHA.112.300031

Danielczok, J., Terriac, E., Hertz, L., Petkova-Kirova, P., Lautenschläger, F., Laschke, M., et al. (2017). Red blood cell passage of small capillaries is associated with transient Ca^{2+}-mediated adaptations. *Front. Physiol.* 8:979. doi: 10.3389/fphys.2017.00979

de Back, D., Kostova, E., van Kraaij, M., van den Berg, T., and van Bruggen, R. (2014). Of macrophages and red blood cells; a complex love story. *Front. Physiol.* 5:9. doi: 10.3389/fphys.2014.00009

De Oliveira, S., de Almeida, V. V., Calado, A., Rosário, H. S., and Saldanha, C. (2012). Integrin-associated protein (CD47) is a putative mediator for soluble fibrinogen interaction with human red blood cells membrane. *Biochim. Biophys. Acta* 1818, 481–490. doi: 10.1016/j.bbamem.2011.10.028

de Oliveira, S., and Saldanha, C. (2010). An overview about erythrocyte membrane. *Clin. Hemorheol. Microcirc.* 44, 63–74. doi: 10.3233/CH-2010-1253

Decuzzi, P., Lee, S., Bhushan, B., and Ferrari, M. (2005). A theoretical model for the margination of particles within blood vessels. *Ann. Biomed. Eng.* 33, 179–190. doi: 10.1007/s10439-005-8976-5

Deitch, E., Condon, M., Feketeova, E., Machiedo, G., Mason, L., Vinluan, G., et al. (2014). Trauma-hemorrhagic shock induces a CD36-dependent RBC endothelial-adhesive phenotype. *Crit. Care Med.* 42, e200–e210. doi: 10.1097/CCM.0000000000000119

Du, V. X., de Groot, P. G., van Wijk, R., Ruggeri, Z. M., and de Laat, B. (eds). (2014). "Identification of intercellular adhesion molecule 4 on erythrocytes as mediator of erythrocyte-platelet interaction in thrombus formation," in *Expanding Horizons in Thrombosis and Hemostasis*, (Utrecht: Utrecht University), 50–72.

Dumaswala, U. J., and Greenwalt, T. (1984). Human erythrocytes shed exocytic vesicles in vivo. *Transfusion* 24, 490–492. doi: 10.1046/j.1537-2995.1984.24685066807.x

Dzierzak, E., and Philipsen, S. (2013). Erythropoiesis: development and differentiation. *Cold Spring Harb. Perspect. Med.* 3:a011601. doi: 10.1101/cshperspect.a011601

Eckstein, E. C., Tilles, A., and Millero, F. J. (1988). Conditions for the occurrence of large near-wall excesses of small particles during blood flow. *Microvasc. Res.* 36, 31–39. doi: 10.1016/0026-2862(88)90036-2

Egan, E. (2018). Beyond hemoglobin: screening for malaria host factors. *Trends Genet.* 34, 133–141. doi: 10.1016/j.tig.2017.11.004

Egan, E., Jiang, R., Moechtar, M., Barteneva, N., Weekes, M., Nobre, L., et al. (2015). Malaria. A forward genetic screen identifies erythrocyte CD55 as essential for *Plasmodium falciparum* invasion. *Science* 348, 711–714. doi: 10.1126/science.aaa3526

El Nemer, W., Wautier, M. P., Rahuel, C., Gane, P., Hermand, P., Galacteros, F., et al. (2007). Endothelial Lu/BCAM glycoproteins are novel ligands for red blood cell alpha4beta1 integrin: role in adhesion of sickle red blood cells to endothelial cells. *Blood* 109, 3544–3551. doi: 10.1182/blood-2006-07-035139

Endeward, V., Cartron, J., Ripoche, P., and Gros, G. (2008). RhAG protein of the Rhesus complex is a CO_2 channel in the human red cell membrane. *FASEB J.* 22, 64–73. doi: 10.1096/fj.07-9097com

Ensinck, A., Biondi, C., Marini, A., García Borrás, S., Racca, L., Cotorruelo, C., et al. (2006). Effect of membrane-bound IgG and desialysation in the interaction of monocytes with senescent erythrocytes. *Clin. Exp. Med.* 6, 138–142. doi: 10.1007/s10238-006-0110-y

Fedosov, D. A., and Gompper, G. (2014). White blood cells margination in microcirculation. *R. Soc. Chem.* 10, 2961–2970. doi: 10.1039/c3sm52860j

Fens, M., Mastrobattista, E., de Graaff, A., Flesch, F., Ultee, A., Rasmussen, J., et al. (2008). Angiogenic endothelium shows lactadherin-dependent phagocytosis of aged erythrocytes and apoptotic cells. *Blood* 111, 4542–4550. doi: 10.1182/blood-2007-06-094763

Fens, M., van Wijk, R., Andringa, G., van Rooijen, K., Dijstelbloem, H., Rasmussen, J., et al. (2012). A role for activated endothelial cells in red blood cell clearance: implications for vasopathology. *Haematologica* 97, 500–508. doi: 10.3324/haematol.2011.048694

Fermo, E., Bogdanova, A., Petkova-Kirova, P., Zaninoni, A., Marcello, A., Makhro, A., et al. (2017). 'Gardos Channelopathy': a variant of hereditary Stomatocytosis with complex molecular regulation. *Sci. Rep.* 7:1744. doi: 10.1038/s41598-017-01591-w

Finnegan, E. M., Turhan, A., Golan, D., and Barabino, G. (2007). Adherent leukocytes capture sickle erythrocytes in an in vitro flow model of Vaso-occlusion. *Am. J. Hematol.* 82, 266–275. doi: 10.1002/ajh.20819

Fitzgibbon, S., Spann, A., Qi, Q., and Shaqfeh, E. (2015). In vitro measurement of particle margination in the microchannel flow: effect of varying hematocrit. *Biophys. J.* 108, 2601–2608. doi: 10.1016/j.bpj.2015.04.013

Flegel, W. A. (2015). Pathogenesis and mechanisms of antibody-mediated hemolysis. *Transfusion* 55, 47–58.

Flormann, D., Kuder, E., Lipp, P., Wagner, C., and Kaestner, L. (2015). Is there a role of C-reactive protein in red blood cell aggregation? *Int. J. Lab. Haematol.* 37, 474–482. doi: 10.1111/ijlh.12313

Ford, J. (2013). Red blood cell morphology. *Int. Soc. Lab. Hematol.* 35, 351–357.

Fujimoto, T., and Parmryd, I. (2016). Interleaflet coupling, pinning, and leaflet asymmetry—major players in plasma membrane nanodomain formation. *Front. Cell Dev. Biol.* 4:155. doi: 10.3389/fcell.2016.00155

Gallagher, P. (2017). Disorders of erythrocyte hydration. *Blood* 130, 2699–2708. doi: 10.1182/blood-2017-04-590810

Glenister, F., Kats, F. K., Hanssen, E., Mohandas, N., Coppel, R., and Cooke, B. (2009). Functional alteration of red blood cells by a megadalton protein of *Plasmodium falciparum*. *Blood* 113, 919–928. doi: 10.1182/blood-2008-05-157735

Glogowska, E., Lezon-Geyda, K., Maksimova, Y., Schulz, V., and Gallagher, P. (2015). Mutations in the Gardos channel (KCNN4) are associated with hereditary xerocytosis. *Blood* 126, 1281–1284. doi: 10.1182/blood-2015-07-657957

Glogowska, E., Schneider, E. R., Maksimova, Y., Schulz, V. P., Lezon-Geyda, K., Wu, J., et al. (2017). Novel mechanisms of PIEZO1 dysfunction in hereditary xerocytosis. *Blood* 130, 1845–1856. doi: 10.1182/blood-2017-05-786004

Goel, D. S. (2002). Adhesion of normal erythrocytes at depressed venous shear rates to activated neutrophils. *Blood* 100, 3797–3803. doi: 10.1182/blood-2002-03-0712

Goodman, S. R., and Shiffer, K. (1983). The spectrin membrane skeleton of normal and abnormal human erythrocytes: a review. *Am. J. Physiol.* 244, 121–141.

Gottlieb, P. A. (2017). A tour de force: the discovery, properties, and function of Piezo channels. *Curr. Top. Membr.* 79, 1–36. doi: 10.1016/bs.ctm.2016.11.007

Grossin, N., Wautier, M., Picot, J., Stern, D., and Wautier, J. (2009a). Differential effect of plasma or erythrocyte AGE-ligands 286 of RAGE on expression of transcripts for receptor isoforms. *Diabetes Metab.* 35, 410–417. doi: 10.1016/j.diabet.2009.04.009

Grossin, N., Wautier, M. P., and Wautier, J. L. (2009b). Red blood cell adhesion in diabetes mellitus is mediated by advanced glycation end product receptor and is modulated by nitric oxide. *Biorheology* 46, 63–72. doi: 10.3233/BIR-2009-0519

Grygorczyk, R., Schwarz, W., and Passow, H. (1984). Ca^{2+}-activated K^+ channels in human red cells. Comparison of single-channel currents with ion fluxes. *Biophys. J.* 45, 693–698. doi: 10.1016/s0006-3495(84)84211-3

Guchhait, P., Dasgupta, S., Le, A., Yellapragada, S., López, J., and Thiagarajan, P. (2007). Lactadherin mediates sickle cell adhesion to vascular endothelial cells in flowing blood. *Haematologica* 92, 1266–1267. doi: 10.3324/haematol.11379

Gupta, K., Gupta, P., Solovey, A., and Hebbel, R. P. (1999). Mechanism of interaction of thrombospondin with human endothelium and inhibition of sickle erythrocyte adhesion to human endothelial cells by heparin. *Biochim. Biophys. Acta* 1453, 63–73. doi: 10.1016/s0925-4439(98)00085-4

Handunnetti, S., van Schravendijk, M., Hasler, T., Barnwell, J., Greenwalt, D., and Howard, R. (1992). Involvement of CD36 on erythrocytes as a rosetting receptor for *Plasmodium falciparum*-infected erythrocytes. *Blood* 80, 2097–2104.

Hankins, M., Baldridge, R. D., Xu, P., and Graham, T. R. (2015). Role of flippases, scramblases and transfer proteins in phosphatidylserine subcellular distribution. *Traffic* 16, 35–47. doi: 10.1111/tra.12233

Heppel, R. P. (2008). Adhesion of sickle red cells to endothelium: myths and future directions. *Transfus. Clin. Biol.* 15, 14–18. doi: 10.1016/j.tracli.2008.03.011

Hermand, P., Gane, P., Callebaut, I., Kieffer, N., Cartron, J., and Bailly, P. (2004). Integrin receptor specificity for human red cell ICAM-4 ligand. Critical residues for alphaIIbeta3 binding. *Eur. J. Biochem.* 271, 3729–3740. doi: 10.1111/j.1432-1033.2004.04313.x

Hermand, P., Gane, P., Huet, M., Jallu, V., Kaplan, C., Sonneborn, H. H., et al. (2002). Red cell ICAM-4 is a novel ligand for platelet-activated αIIbβ3 integrin. *J. Biol. Chem.* 278, 4892–4898. doi: 10.1074/jbc.m211282200

Higgins, J. (2015). Red blood cell population dynamics. *Clin. Lab. Med.* 35, 43–57. doi: 10.1016/j.cll.2014.10.002

Hillery, C. A., Du, M., Montgomery, R., and Scott, J. (1996). Increased adhesion of erythrocytes to components of the extracellular matrix: isolation and characterization of a red blood cell lipid that binds thrombospondin and laminin. *Blood* 87, 4879–4886.

Hines, P. C., Zen, Q., Burney, S. N., Shea, D. A., Ataga, K. I., and Orringer, E. P. (2003). Novel epinephrine and cyclic AMP-mediated activation of B-CAM/LU-dependent sickle (SS) RBC adhesion. *Blood* 101, 3281–3287. doi: 10.1182/blood-2001-12-0289

Honoré, E., Martins, J. R., Penton, D., Patel, A., and Demolombe, S. (2015). The Piezo mechanosensitive ion channels: may the force be with you! *Rev. Physiol. Biochem. Pharmacol.* 169, 25–41. doi: 10.1007/112_2015_26

Hsu, K., Lee, T. Y., Periasamy, A., Kao, F. J., Li, L. T., Lin, C. Y., et al. (2017). Adaptable interaction between aquaporin-1 and band 3 reveals a potential role of water channel in blood CO_2 transport. *FASEB J.* 31, 4256–4264. doi: 10.1096/fj.201601282R

Huisjes, R., Bogdanova, A., van Solinge, W., Schiffelers, R., Kaestner, L., and van Wijk, R. (2018). Squeezing for life – properties of red blood cell deformability. *Front. Physiol.* 9:656. doi: 10.3389/fphys.2018.00656

Imashuku, S., Muramatsu, H., Sugihara, T., Okuno, Y., Wang, X., Yoshida, K., et al. (2016). PIEZO1 gene mutation in a Japanese family with hereditary high phosphatidylcholine hemolytic anemia and hemochromatosis-induced diabetes mellitus. *Int. J. Hematol.* 104, 125–129. doi: 10.1007/s12185-016-1970-x

Janvier, D., Lam, Y., Lopez, I., Elakredar, L., and Bierling, P. (2013). A major target for warm immunoglobulin G autoantibodies: the third external loop of Band 3. *Transfusion* 53, 1948–1955. doi: 10.1111/trf.12026

Kaestner, L. (2015). Channelizing the red blood cell: molecular biology competes with patch-clamp. *Front. Mol. Biosci.* 2:46. doi: 10.3389/fmolb.2015.00046

Kaestner, L., and Minetti, G. (2017). The potential of erythrocytes as cellular aging models. *Cell Death Differ.* 24, 1475–1477. doi: 10.1038/cdd.2017.100

Kaestner, L., Steffen, P., Nguyen, D., Wang, J., Wagner-Britz, L., Jung, A., et al. (2012). Lysophospatidic acid induced red blood cell aggregation in vitro. *Bioelectrochemistry* 87, 89–95. doi: 10.1016/j.bioelechem.2011.08.004

Kalagara, T., Moutsis, T., Yang, Y., Pappelbaum, K., Farken, A., Cladder-Micus, L., et al. (2018). The endothelial glycocalyx anchors von Willebrand factor fibers to the vascular endothelium. *Blood Adv.* 2, 2347–2357. doi: 10.1182/bloodadvances.2017013995

Kaliyaperumal, R., Deng, X., Meiselman, H., Song, H., Dalan, R., Leow, M., et al. (2019). Depletion interaction forces contribute to erythrocyte-endothelial adhesion in diabetes. *Biochem. Biophys. Res. Commun.* 516, 144–148. doi: 10.1016/j.bbrc.2019.06.018

Kaul, D. K. (2008). Sickle red cell adhesion: many issues and some answers. *Transfusion* 15, 51–55. doi: 10.1016/j.tracli.2008.03.012

Kaul, D. K., Liu, X.-D., Zhang, X., Mankelow, T., Parsons, S., Spring, F., et al. (2006). Peptides based on alphaV-binding domains of erythrocyte ICAM-4 inhibit sickle red cell-endothelial interactions and Vaso-occlusion in the microcirculation. *Am. J. Physiol. Cell Physiol.* 291, 922–930.

Klei, T., de Back, D., Asif, P., Verkuijlen, P., Veldthuis, M., Ligthart, P., et al. (2018). Glycophorin-C sialylation regulates Lu/BCAM adhesive capacity during erythrocyte aging. *Blood Adv.* 2, 14–24. doi: 10.1182/bloodadvances.2017013094

Klei, T., Meinderts, S., van den Berg, T., and van Bruggen, R. (2017). From the cradle to the grave: the role of macrophages in erythropoiesis and erythrophagocytosis. *Front. Immunol.* 8:73. doi: 10.3389/fimmu.2017.00073

Ko, M., Laura, M., Castro, D., Jonassaint, J. C., Batchvarova, M., Zennadi, R., et al. (2005). The relationship of plasma laminin levels to anemia and the effect of soluble laminin on sickle red cell adhesion in SCD. *Blood* 106:2336.

Kobayashi, N., Karisola, P., Peña-Cruz, V., Dorfman, D., Jinushi, M., Umetsu, S., et al. (2007). TIM-1 and TIM-4 glycoproteins bind phosphatidylserine and mediate uptake of apoptotic cells. *Immunity* 27, 927–940. doi: 10.1016/j.immuni.2007.11.011

Koshiar, R., Somajo, S., Norström, E., and Dahlbäck, B. (2014). Erythrocyte-derived microparticles supporting activated protein C-mediated regulation of blood coagulation. *PLoS One* 9:e104200. doi: 10.1371/journal.pone.0104200

Kuypers, F., and de Jong, K. (2004). The role of phosphatidylserine in recognition and removal of erythrocytes. *Cell. Mol. Biol.* 50, 147–158.

Kuypers, F. A. (2008). Red cell membrane lipids in hemoglobinopathies. *Curr. Mol. Med.* 8, 633–638. doi: 10.2174/156652408786241429

Lagadec, P., Dejoux, O., Ticchioni, M., Cottrez, F., Johansen, M., Brown, E. J., et al. (2003). Involvement of a CD47-dependent pathway in platelet adhesion on inflamed vascular endothelium under flow. *Blood* 101, 4836–4843. doi: 10.1182/blood-2002-11-3483

Leal, J., Adjobo-Hermans, M., and Bosman, G. (2018). Red blood cell homeostasis: mechanisms and effects of microvesicle generation in health and disease. *Front. Physiol.* 9:703. doi: 10.3389/fphys.2018.00703

Lee, K., Gane, P., Roudot-Thoraval, F., Godeau, B., Bachir, D., Bernaudin, F., et al. (2001). The nonexpression of CD36 on reticulocytes and mature red blood cells does not modify the clinical course of patients with sickle cell anemia. *Blood* 98, 966–971. doi: 10.1182/blood.v98.4.966

Lelliott, P., McMorran, B., Foote, S., and Burgio, G. (2015). The influence of host genetics on erythrocytes and malaria infection: is there therapeutic potential? *Malar. J.* 14:289. doi: 10.1186/s12936-015-0809-x

Lemke, G. (2013). Biology of the TAM receptors. *Cold Spring Harb. Perspect. Biol.* 5:a009076. doi: 10.1101/cshperspect.a009076

Lipowsky, H., Gao, L., and Lescanic, A. (2011). Shedding of the endothelial glycocalyx in arterioles, capillaries, and venules and its effect on capillary hemodynamics during inflammation. *Am. J. Physiol. Heart Circ. Physiol.* 301, 2235–2245. doi: 10.1152/ajpheart.00803.2011

Litvinov, R. I., and Weisel, J. W. (2017). Role of red blood cells in haemostasis and thrombosis. *ISBT Sci. Ser.* 12, 176–183. doi: 10.1111/voxs.12331

Liu, M., and Yang, J. (2009). Electrokinetic effect of the endothelial glycocalyx layer on two-phase blood flow in small blood vessels. *Microvasc. Res.* 78, 14–19. doi: 10.1016/j.mvr.2009.04.002

Lowe, G. D. O. (1988). *Clinical Blood Rheology*. Boca Raton, FL: CRC Press.

Lutz, H. (2004). Innate immune and non-immune mediators of erythrocyte clearance. *Cell. Mol. Biol.* 50, 107–116.

Lutz, H. U., and Bogdanova, A. (2013). Mechanisms tagging senescent red blood cells for clearance in healthy humans. *Front. Physiol.* 4:387. doi: 10.3389/fphys.2013.00387

Lux, S. D. (2016). Anatomy of the red cell membrane skeleton: unanswered questions. *Blood* 127, 187–199. doi: 10.1182/blood-2014-12-512772

Ma, S., Cahalan, S., LaMonte, G., Grubaugh, N., Zeng, W., Murthy, S., et al. (2018). Common PIEZO1 allele in African populations causes RBC dehydration and attenuates plasmodium infection. *Cell* 173, 443–455.e12. doi: 10.1016/j.cell.2018.02.047

Macey, R. (1984). Transport of water and urea in red blood cells. *Am. J. Physiol.* 246(3 Pt 1), C195–C203.

Maciaszek, J. L., Andemariam, B., Huber, G., and Lykotrafitis, G. (2013). Epinephrine modulates BCAM/Lu and ICAM-4 expression on the sickle cell trait red blood cell membrane. *Biophys. J.* 102, 1137–1143. doi: 10.1016/j.bpj.2012.01.050

Mackman, N. (2018). The red blood cell death receptor and thrombosis. *J. Clin. Investig.* 128, 3747–3749. doi: 10.1172/JCI122881

Mankelow, T. J., Satchwell, T. J., and Burton, N. M. (2012). Refined views of multi-protein complexes in the erythrocyte membrane. *Blood Cells Mol. Dis.* 49, 1–10. doi: 10.1016/j.bcmd.2012.03.001

Manodori, B., Barabino, G. A., Lubin, B. H., and Kuypers, F. A. (2000). Adherence of phosphatidylserine-exposing erythrocytes to endothelial matrix thrombospondin. *Blood* 95, 1293–1300.

Massberg, S., Enders, G., and Matos, F. C. (1999). Fibrinogen deposition at the postischemic vessel wall promotes platelet adhesion during ischemia-reperfusion in vivo. *Blood* 94, 3831–3838.

Meinderts, S., Oldenborg, P., Beuger, B., Klei, T., Johansson, J., Kuijpers, T., et al. (2017). Human and murine splenic neutrophils are potent phagocytes of IgG-opsonized red blood cells. *Blood Adv.* 1, 875–886. doi: 10.1182/bloodadvances.2017004671

Minasyan, H. (2016). Mechanisms and pathways for the clearance of bacteria from blood circulation in health and disease. *Pathophysiology* 23, 61–66. doi: 10.1016/j.pathophys.2016.03.001

Minasyan, H. (2018). Phagocytosis and oxycytosis: two arms of human innate immunity. *Immunol. Res.* 66, 271–280. doi: 10.1007/s12026-018-8988-5

Minetti, G., Achilli, C., Perotti, C., and Ciana, A. (2018). Continuous change in membrane and membrane-skeleton organization deuring development from proerythroblast to senescent red blood cell. *Front. Physiol.* 9:286. doi: 10.3389/fphys.2018.00286

Mohandas, N., and Gallagher, P. G. (2008). Red cell membrane: past, present, and future. *Blood* 112, 3939–3947. doi: 10.1182/blood-2008-07-161166

Mohanty, J., Nagababu, E., and Rifkind, J. (2014). Red blood cell oxidative stress impairs oxygen delivery and induces red blood cell aging. *Front. Physiol.* 5:84. doi: 10.3389/fphys.2014.00084

Moras, M., Lefevre, S. D., and Ostuni, M. A. (2017). From erythroblasts to mature red blood cells: organelle clearance in mammals. *Front. Physiol.* 8:1076. doi: 10.3389/fphys.2017.01076

Morel, O., Jesel, L., Freyssinet, J. M., and Toti, F. (2011). Cellular mechanisms underlying the formation of circulating microparticles. *Arterioscler. Thromb. Vasc. Biol.* 31, 15–26. doi: 10.1161/atvbaha.109.200956

Morera, D., and MacKenzie, S. A. (2011). Is there a direct role for erythrocytes in the immune response? *Vet. Res.* 42:89. doi: 10.1186/1297-9716-42-89

Munn, L. L., and Dupin, M. (2008). Blood cell interactions and segregation in flow. *Ann. Biomed. Eng.* 36, 534–544. doi: 10.1007/s10439-007-9429-0

Muradashvili, N., and Lominadze, D. (2013). Role of fibrinogen in cerebrovascular dysfunction after traumatic brain injury. *Brain Inj.* 27, 1508–1515. doi: 10.3109/02699052.2013.823562

Muramatsu, T. (2016). Basigin (CD147), a multifunctional transmembrane glycoprotein with various binding partners. *J. Biochem.* 159, 481–490. doi: 10.1093/jb/mvv127

Murthy, S., Dubin, A., and Patapoutian, A. (2017). Piezos thrive under pressure: mechanically activated ion channels in health and disease. *Nat. Rev. Mol. Cell Biol.* 18, 771–783. doi: 10.1038/nrm.2017.92

Nakhoul, N., and Hamm, L. (2004). Non-erythroid Rh glycoproteins: a putative new family of mammalian ammonium transporters. *Pflugers Arch.* 447, 807–812. doi: 10.1007/s00424-003-1142-8

Namdee, K., Thompson, A., Charoenphol, P., and Eniola-Adefeso, O. (2013). Margination propensity of vascular-targeted spheres from blood flow in a microfluidic model of human microvessels. *Langmuir* 29, 2530–2535. doi: 10.1021/la304746p

Neu, B., and Meiselman, H. (2006). Depletion interactions in polymer solutions promote red blood cell adhesion to albumin-coated surfaces. *Biochim. Biophys. Acta* 1760, 1772–1779. doi: 10.1016/j.bbagen.2006.09.005

Neu, B., Sowemimo-Coker, S. O., and Meiselman, H. J. (2003). Cell-cell affinity of senescent human erythrocytes. *Biophys. J.* 85, 75–84. doi: 10.1016/s0006-3495(03)74456-7

Nguyen, D., Wagner-Britz, L., Maia, S., Steffen, P., Wagner, C., Kaestner, L., et al. (2011). Regulation of phosphatidylserine exposure in red blood cells. *Cell. Physiol. Biochem.* 28, 847–856. doi: 10.1159/000335798

Nicolay, J., Thorn, V., Daniel, C., Amann, K., Siraskar, B., Lang, F., et al. (2018). Cellular stress induces erythrocyte assembly on intravascular von Willebrand factor strings and promotes microangiopathy. *Sci. Rep.* 8:10945. doi: 10.1038/s41598-018-28961-2

Noble, M. I., Drake-Holland, A. J., and Vink, H. (2008). Hypothesis: arterial glycocalyx dysfunction is the first step in the atherothrombotic process. *QJM* 101, 513–518. doi: 10.1093/qjmed/hcn024

Oberleithner, H. (2013). Vascular endothelium leaves fingerprints on the surface of erythrocytes. *Mol. Cell. Mech. Dis.* 465, 1451–1458. doi: 10.1007/s00424-013-1288-y

Oberleithner, H., Peters, W., Kusche-Vihrog, K., Korte, S., Schillers, H., Kliehe, K., et al. (2011). Salt overload damages the glycocalyx sodium barrier of vascular endothelium. *Pflugers Arch.* 462, 519–528. doi: 10.1007/s00424-011-0999-1

Oldenborg, P., Zheleznyak, A., Fang, Y., Lagenaur, C., Gresham, H., and Lindberg, F. (2000). Role of CD47 as a marker of self on red blood cells. *Science* 288, 2051–2054. doi: 10.1126/science.288.5473.2051

Painter, R. H. (1998). *Encyclopedia of Immunology*, ed. J. D. Peter (Oxford: Elsevier), 1208–1211.

Park, S., Jung, M., Lee, S., Kang, K., Gratchev, A., Riabov, V., et al. (2009). Stabilin-1 mediates phosphatidylserine-dependent clearance of cell corpses in alternatively activated macrophages. *J. Cell Sci.* 122, 3365–3373. doi: 10.1242/jcs.049569

Parpaite, T., and Coste, B. (2017). Piezo channels. *Curr. Biol.* 3, R243–R258.

Parroche, P., Lauw, F., Goutagny, E., Monks, B., Visitin, A., Halmen, K., et al. (2007). Malaria hemozoin is immunologically inert but radically enhances innate responses by presenting malaria DNA to Toll-like receptor 9. *Proc. Natl. Acad. Sci. U.S.A.* 104, 1919–1924. doi: 10.1073/pnas.0608745104

Pasvol, G. (1984). Receptors on red cells for *Plasmodium falciparum* and their interaction with merozoites. *Philos. Trans. R. Soc. Lond. Ser. B Biol. Sci.* 307, 189–200. doi: 10.1098/rstb.1984.0119

Pasvol, G., Clough, B., and Carlsson, J. (1992). Malaria and the red cell membrane. *Blood Rev.* 6, 183–192. doi: 10.1016/0268-960x(92)90014-h

Patel, A., Demolombe, S., and Honore, E. (2015). Piezo1 Ion Channels: an alternative to force. *eLife* 4:e08659.

Phelan, M., Perrine, S. P., Brauer, M., and Faller, D. V. (1995). Sickle erythrocytes, after sickling, regulate the expression of the endothelin-1 gene and protein in human endothelial cells in culture. *J. Clin. Investig.* 96, 1145–1151. doi: 10.1172/jci118102

Poole, J. (2000). Red cell antigens on band 3 and glycophorin A. *Blood Rev.* 14, 31–43. doi: 10.1054/blre.1999.0124

Pretorius, E., du Plooy, J. N., and Bester, J. (2016). A comprehensive review on eryptosis. *Cell. Physiol. Biochem.* 39, 1977–2000. doi: 10.1159/000447895

Qiu, Z., Dubin, A., Mathur, J., Tu, B., Reddy, K., Miraglia, L., et al. (2014). SWELL1, a plasma membrane protein, is an essential component of volume-regulated anion channel. *Cell* 157, 447–458. doi: 10.1016/j.cell.2014.03.024

Rapetti-Mauss, R., Lacoste, C., Picard, V., Guitton, C., Lombard, E., Loosveld, M., et al. (2015). A mutation in the Gardos channel is associated with hereditary xerocytosis. *Blood* 126, 1273–1280. doi: 10.1182/blood-2015-04-642496

Rapetti-Mauss, R., Picard, V., Guitton, C., Ghazal, K., Proulle, V., Badens, C., et al. (2017). Red blood cell Gardos channel (KCNN4): the essential determinant of erythrocyte dehydration in hereditary xerocytosis. *Haematologica* 102, e415–e418. doi: 10.3324/haematol.2017.171389

Raymond, A., Ensslin, M., and Shur, B. (2009). SED1/MFG-E8: a bi-motif protein that orchestrates diverse cellular interactions. *J. Cell. Biochem.* 106, 957–966. doi: 10.1002/jcb.22076

Richaud-Patin, Y., Pérez-Romano, B., Carrillo-Maravilla, E., Rodriguez, A., Simon, A., Cabiedes, J., et al. (2003). Deficiency of red cell bound CD55 and CD59 in patients with systemic lupus erythematosus. *Immunol. Lett.* 88, 95–99. doi: 10.1016/s0165-2478(03)00066-x

Rifkind, J., and Nagababu, E. (2013). Hemoglobin redox reactions and red blood cell aging. *Antioxid. Redox Signal.* 18, 2274–2283. doi: 10.1089/ars.2012.4867

Ripoche, P., Bertrand, O., Gane, P., Birkenmeier, C., Colin, Y., and Cartron, Y. (2004). Human Rhesus-associated glycoprotein mediates facilitated transport of NH3 into red blood cells. *Proc. Natl. Acad. Sci. U.S.A.* 101, 17222–17227. doi: 10.1073/pnas.0403704101

Risso, A., Ciana, A., Achilli, C., Antonutto, G., and Minetti, G. (2014). Neocytolysis: none, one or many? A reappraisal and future perspectives. *Front. Physiol.* 5:54. doi: 10.3389/fphys.2014.00054

Rivera, A., Jarolim, P., and Brugnara, C. (2002). Modulation of Gardos channel activity by cytokines in sickle erythrocytes. *Blood* 99, 357–603.

Rungaldier, S., Oberwagner, W., Salzer, U., Csaszar, E., and Prohaska, R. (2013). Stomatin interacts with GLUT1/SLC2A1, band 3/SLC4A1, and aquaporin-1 in human erythrocyte membrane domains. *Biochim. Biophys. Acta* 1828, 956–966. doi: 10.1016/j.bbamem.2012.11.030

Said, A. S., Rogers, S., and Doctor, A. (2018). Physiologic impact of circulating RBC microparticles upon blood-vascular interactions. *Front. Physiol.* 8:1120. doi: 10.3389/fphys.2017.01120

Sakamoto, T., Canalli, A., Traina, F., Franco-Penteado, C., Gambero, S., Saad, S., et al. (2013). Altered red cell and platelet adhesion in hemolytic diseases: hereditary spherocytosis, paroxysmal nocturnal hemoglobinuria and sickle cell disease. *Clin. Biochem.* 46, 1798–1803. doi: 10.1016/j.clinbiochem.2013.09.011

Schmidt, A. M., Hori, O., Cao, R., Yan, S., Brett, J., Wautier, J., et al. (1996). RAGE: a novel cellular receptor for advanced glycation end products. *Diabetes* 45(Suppl. 3), S77–S80.

Setty, Y., and Betal, S. G. (2008). Microvascular endothelial cells expresss a phosphatidylserine receptor: a functionally active receptor for phosphatidylserine-positive erythrocytes. *Blood* 111, 905–914. doi: 10.1182/blood-2007-07-099465

Setty, Y., Kulkarni, S., and Stuart, M. J. (2002). Role of erythrocyte phosphatidylserine in sickle red cell-endothelial adhesion. *Blood* 99, 1564–1571. doi: 10.1182/blood.v99.5.1564

Simmonds, M., Meiselman, H., and Baskurt, O. (2013). Blood rheology and aging. *J. Geriatr. Cardiol.* 10, 291–301.

Smeets, M., Mourik, M., Niessen, H., and Hordijk, P. (2017). Stasis promotes erythrocyte adhesion to von willebrand factor. *Arterioscler. Thromb. Vasc. Biol.* 37, 1618–1627. doi: 10.1161/ATVBAHA.117.309885

Smeets, M. W., Bierings, R., Meems, H., Mul, F. P., Geerts, D., Vlaar, A. P., et al. (2017). Platelet-independent adhesion of calcium-loaded erythrocytes to von Willebrand factor. *PLoS One* 12:e0173077. doi: 10.1371/journal.pone.0173077

Smith, B. D., and Lambert, T. N. (2003). Molecular ferries: membrane carriers that promote phospholipid flip-flop and chloride transport. *Chem. Commun.* 21, 2261–2268.

Steffen, P., Jung, A., Nguyen, D., Müller, T., Bernhardt, I., Kaestner, L., et al. (2011). Stimulation of human red blood cells leads to Ca^{2+} mediated intercellular adhesion. *Cell Calcium* 50, 54–61. doi: 10.1016/j.ceca.2011.05.002

Stone, M., Bakkour, S., Lee, H. T., Lanteri, M., Simmons, G., Brambilla, D., et al. (2017). Zika RNA persistence in blood and body fluids and clinical outcomes in infected blood donors. *Transfusion* 57:4A.

Sultana, C., Shen, Y., Rattan, V., Johnson, C., and Kalra, V. (1998). Interaction of sickle erythrocytes with endothelial cells in the presence of endothelial cell conditioned medium induces oxidant stress leading to transendothelial migration of monocytes. *Blood* 92, 3924–3935.

Syeda, R., Qiu, Z., Dubin, A., Murthy, S., Florendo, M., Mason, D., et al. (2016). LRRC8 proteins form volume-regulated anion channels that sense ionic strength. *Cell* 164, 499–511. doi: 10.1016/j.cell.2015.12.031

Telen, M. J. (2005). Erythrocyte adhesion receptors: blood group antigens and related molecules. *Transfus. Med. Rev.* 19, 32–44. doi: 10.1016/j.tmrv.2004.09.006

Thomas, S., Bouyer, G., Cueff, A., Egée, S., Glogowska, E., and Ollivaux, C. (2011). Ion channels in human red blood cell membrane: actors or relics? *Blood Cells Mol. Dis.* 46, 261–265. doi: 10.1016/j.bcmd.2011.02.007

Tokarev, A. A., Butylin, A. A., and Ataullakhanov, F. I. (2011). Platelet adhesion from shear blood flow is controlled by near-wall rebounding collisions with erythrocytes. *Biophys. J.* 100, 799–808. doi: 10.1016/j.bpj.2010.12.3740

Trinh-Trang-Tan, M.-M., Villela-Lamego, C., Picot, J., Wautier, M.-P., and Cartron, J.-P. (2010). Intercellular adhesion molecule-4 and CD36 are implicated in the abnormal adhesiveness of sickle cell SAD mouse erythrocytes to endothelium. *Haematologica* 95, 730–737. doi: 10.3324/haematol.2009.017392

Tsang, S. S., Szeto, R., and Feng, C. (1990). Fibrinogen level in health and disease. *Singapore Med. J.* 31, 51–52.

Vahidkhah, K., Diamond, S. L., and Bagchi, P. (2013). Hydrodynamic interaction between a platelet and an erythrocyte: effect of erythrocyte deformability, dynamics, and wall proximity. *J. Biomech. Eng.* 135:51002. doi: 10.1115/1.4023522

Vahidkhahb, K., Diamond, S., and Bagchi, P. (2014). Platelet dynamics in three-dimensional simulation of whole blood. *Biophys. J.* 106, 2529–2540. doi: 10.1016/j.bpj.2014.04.028

van Zwieten, R., Bochem, A., Hilarius, P., van Bruggen, R., Bergkamp, F., Hovingh, G., et al. (2012). The cholesterol content of the erythrocyte membrane is an important determinant of phosphatidylserine exposure. *Biochim. Biophys. Acta* 1821, 1493–1500. doi: 10.1016/j.bbalip.2012.08.008

Viallat, A., and Abkarian, M. (2014). Red blood cell: from its mechanics to its motion in shear flow. *Int. Soc. Lab. Hematol.* 36, 237–243. doi: 10.1111/ijlh.12233

Vorselen, D., van Dommelen, S., Sorkin, R., Piontek, M., Schiller, J., Döpp, S., et al. (2018). The fluid membrane determines mechanics of erythrocyte extracellular vesicles and is softened in hereditary spherocytosis. *Nat. Commun.* 9:4960. doi: 10.1038/s41467-018-07445-x

Wagner, C., Steffen, P., and Svetina, S. (2013). Aggregation of red blood cells: from rouleaux to clot formation. *C. R. Phys.* 14, 459–469. doi: 10.1016/j.crhy.2013.04.004

Walker, B., Towhid, S. T., Schmid, E., Hoffmann, S. M., Abed, M., Munzer, P., et al. (2013). Dynamic adhesion of eryptotic erythrocytes to immobilized platelets via platelet phosphatidylserine receptors. *Am. J. Physiol. Cell Physiol.* 306, C291–C297. doi: 10.1152/ajpcell.00318.2013

Walton, L., Lehmann, M., Wkorczewski, T., Holle, L. A., Beckman, J. D., Cribb, J. A., et al. (2017). Elevated hematocrit enhances platelet accumulation following vascular injury. *Blood* 129, 2537–2546. doi: 10.1182/blood-2016-10-746479

Wautier, J. L., and Wautier, M. P. (2004). Erythrocytes and platelet adhesion to endothelium are mediated by specialized molecules. *Clin. Hemorheol. Microcirc.* 30, 181–184.

Wautier, J.-L., and Wautier, P. M. (2013). Molecular basis of erythrocyte adhesion to endothelial cells in diseases. *Clin. Hemorheol. Microcirc.* 53, 11–21. doi: 10.3233/CH-2012-1572

Wautier, M., Boulanger, E., Guillausseau, P., Massin, P., and Wautier, J. L. (2004). AGEs, macrophage colony stimulating factor and vascular adhesion molecule blood levels are increased in patients with diabetic microangiopathy. *Throm. Haemost.* 91, 879–885. doi: 10.1160/th03-07-0486

Wautier, M., El Nemer, W., Gane, P., Rain, J., Cartron, J., Colin, Y., et al. (2007). Increased adhesion to endothelial cells of erythrocytes from patients with polycythemia vera is mediated by laminin alpha5 chain and Lu/BCAM. *Blood* 110, 894–901. doi: 10.1182/blood-2006-10-048298

Weinbaum, S., Tarbell, J., and Damiano, E. (2007). The structure and function of the endothelial glycocalyx layer. *Annu. Rev. Biomed. Eng.* 9, 121–167. doi: 10.1146/annurev.bioeng.9.060906.151959

Weisel, J., and Litvinov, R. (2019). Red blood cells: the forgotten player in hemostasis and thrombosis. *J. Thromb. Haemost.* 17, 271–282. doi: 10.1111/jth.14360

Weiss, E., Rees, D. C., and Gibson, J. S. (2011). Role of calcium in phosphatidylserine externalisation in red blood cells from sickle cell patients. *Anemia* 2011:379894. doi: 10.1155/2011/379894

Wesseling, M., Wagner-Britz, L., Nguyen, D., Asanidze, S., Mutua, J., Mohamed, N., et al. (2016). Novel insights in the regulation of phosphatidylserine exposure in human red blood cells. *Cell. Physiol. Biochem.* 39, 1941–1954. doi: 10.1159/000447891

Westerman, M., and Porter, J. (2016). Red blood cell-derived microparticles: an overview. *Blood Cells Mol. Dis.* 59, 134–139. doi: 10.1016/j.bcmd.2016.04.003

Willekens, F. L., Werre, J., Groenen-Döpp, Y., Roerdinkholder-Stoelwinder, B., de Pauw, B., and Bosman, G. (2008). Erythrocyte vesiculation: a self-protective mechanism? *Br. J. Haematol.* 141, 549–556. doi: 10.1111/j.1365-2141.2008.07055.x

Williams, T. (2006). Red blood cell defects and malaria. *Mol. Biochem. Parasitol.* 149, 121–127. doi: 10.1016/j.molbiopara.2006.05.007

Xu, Q. (2011). The Indian blood group system. *Immunohematology* 27, 89–93.

Yazdani, A., and Em Karniadakis, G. (2016). Sub-cellular modeling of platelet transport in blood flow through microchannels with constriction. *R. Soc. Chem.* 12, 4339–4351. doi: 10.1039/c6sm00154h

Zennadi, L., Castro, D., Eyler, C., Xu, K., Ko, M., and Telen, M. J. (2008). Role and regulation of sickle red cell interactions with other cells: ICAM-4 and other adhesion receptors. *Transfusion* 15, 23–28. doi: 10.1016/j.tracli.2008.04.009

Zennadi, R., Hines, P. C., de Castro, L. M., Cartron, J. P., Parise, L. V., and Telen, M. J. (2004). Epinephrine acts through erythroid signaling pathways to activate sickle cell adhesion to endothelium via LW-alphavbeta3 interactions. *Blood* 104, 3774–3781. doi: 10.1182/blood-2004-01-0042

Zennadi, R., Whalen, E. J., Soderblom, E. J., Alexander, S. C., Thompson, J. W., Dubois, L. G., et al. (2012). Erythrocyte plasma membrane-bound ERK1/2 activation promotes ICAM-4-mediated sickle red cell adhesion to endothelium. *Blood* 119, 1217–1227. doi: 10.1182/blood-2011-03-344440

Zenonos, Z., Dummler, S., Müller-Sienerth, N., Chen, J., Preiser, P., Rayner, J., et al. (2015). Basigin is a druggable target for host-oriented antimalarial interventions. *J. Exp. Med.* 212, 1145–1151. doi: 10.1084/jem.20150032

Zhang, J., Abiraman, K., Jones, M. S., Lykotrafitis, G., and Andemariam, B. (2017). Regulation of active ICAM-4 on normal and sickle cell disease RBCs via AKAPs is revealed by AFM. *Biophys. J.* 112, 143–152. doi: 10.1016/j.bpj.2016.11.3204

Zhang, M. Y., Zhang, Y., Wu, X., Zhang, K., Lin, P., Bian, H., et al. (2018). Disrupting CD147-RAP2 interaction abrogates erythrocyte invasion by *Plasmodium falciparum*. *Blood* 131, 1111–1121. doi: 10.1182/blood-2017-08-802918

Zuccala, E., Satchwell, T., Angrisano, F., Tan, Y., Wilson, M., Heesom, K., et al. (2016). Quantitative phospho-proteomics reveals the Plasmodium merozoite triggers pre-invasion host kinase modification of the red cell cytoskeleton. *Sci. Rep.* 6:19766. doi: 10.1038/srep19766

Conflict of Interest Statement: The authors declare that the research was conducted in the absence of any commercial or financial relationships that could be construed as a potential conflict of interest.

frontiers in Physiology

REVIEW
published: 20 August 2019
doi: 10.3389/fphys.2019.01070

Red Blood Cell Membrane Processing for Biomedical Applications

*Luigia Rossi[1,2], Alessandra Fraternale[1], Marzia Bianchi[1] and Mauro Magnani[1,2]**

[1] Department of Biomolecular Sciences, University of Urbino "Carlo Bo", Urbino, Italy, [2] EryDel SpA, Bresso, Italy

Red blood cells (RBC) are actually exploited as innovative drug delivery systems with unconventional and convenient properties. Because of a long *in vivo* survival and a non-random removal from circulation, RBC can be loaded with drugs and/or contrasting agents without affecting these properties and maintaining the original immune competence. However, native or drug-loaded RBC, can be modified decorating the membrane with peptides, antibodies or small chemical entities so favoring the targeting of the processed RBC to specific cells or organs. Convenient modifications have been exploited to induce immune tolerance or immunogenicity, to deliver antibodies capable of targeting other cells, and to deliver a number of constructs that can recognize circulating pathogens or toxins. The methods used to induce membrane processing useful for biomedical applications include the use of crosslinking agents and bifunctional antibodies, biotinylation and membrane insertion. Another approach includes the expression of engineered membrane proteins upon *ex vivo* transfection of immature erythroid precursors with lentiviral vectors, followed by *in vitro* expansion and differentiation into mature erythrocytes before administration to a patient in need. Several applications have now reached the clinic and a couple of companies that take advantage from these properties of RBC are already in Phase 3 with selected applications. The peculiar properties of the RBC and the active research in this field by a number of qualified investigators, have opened new exciting perspectives on the use of RBC as carriers of drugs or as cellular therapeutics.

Keywords: RBC targeting, RBC carriers, RBC membrane modifications, RBC circulation, drug targeting

OPEN ACCESS

Edited by:
Giampaolo Minetti, University of Pavia, Italy

Reviewed by:
James Palis, University of Rochester, United States
Emile Van Den Akker, Sanquin Diagnostic Services, Netherlands

***Correspondence:**
Mauro Magnani
mauro.magnani@uniurb.it

Specialty section:
This article was submitted to Red Blood Cell Physiology, a section of the journal Frontiers in Physiology

Received: *24 May 2019*
Accepted: *05 August 2019*
Published: *20 August 2019*

Citation:
Rossi L, Fraternale A, Bianchi M and Magnani M (2019) Red Blood Cell Membrane Processing for Biomedical Applications. Front. Physiol. 10:1070. doi: 10.3389/fphys.2019.01070

INTRODUCTION

For many years, drug-loaded red blood cells (RBC) have been exploited as delivery systems for the release in circulation of active agents, for the increase in the life-span in circulation of therapeutic agents, for the protection by immune inactivation of therapeutic enzymes, and for a prolonged circulation of contrasting agents useful in diagnostic applications (reviewed in Rossi et al., 2016; Villa et al., 2016; Pierigè et al., 2017). In addition, native or drug-loaded RBC could be conveniently modified by membrane decoration with peptides, antibodies, receptors, nanoparticles and other constructs expanding the use and scope in processing RBC for therapeutic applications. This review

will summarize these approaches providing information on the potential use of these engineered RBC and highlighting the limits of each of the methods developed.

RED BLOOD CELL MEMBRANE AND OSMOTIC LOADING PROCEDURE FOR THERAPEUTIC APPLICATIONS

The possibility of using RBC as carriers takes advantage from the discovery performed many years ago (Ihler et al., 1973) that these non-nucleate cells could swell under hypotonic conditions and that pores could open on the RBC membrane. Once the pores are open, these can be easily crossed by extracellular agents (drugs, enzymes, nanoparticles, etc.), which are later entrapped into the RBC simply restoring the physiological osmolarity followed by pore closing. Several variants of this process have been described during the years (Pierigè et al., 2008; Rossi et al., 2016) but only with the development of specific medical devices capable of processing blood under sterile and non-pyrogenic conditions, the use of RBC as carriers entered into the clinic (Ropars et al., 1987; Hunault-Berger et al., 2015; Mambrini et al., 2017). Nowadays several trials are ongoing and the most advanced are in Phase 3 (ClinicalTrials.gov Identifier: NCT02770807; NCT03563053; NCT01518517). Several biomedical applications of RBC as carriers of therapeutic or contrasting agents require the resealing of the membrane pores produced during the loading procedure and the annealing of the RBC membrane to the cytoskeleton. These requirements are mandatory to prevent the release of the encapsulated drugs, to preserve the RBC immunogenicity avoiding the induction of anti-carrier immune responses and to maintain native phospholipid asymmetry preventing RBC clearance by macrophages. In fact, the lipid composition of the RBC membrane is mainly represented by equal weight of cholesterol and phospholipids. The latter are asymmetrically distributed with the prevalence of phosphatidylcholine and sphingomyelin in the outer monolayer and phosphatidylethanolamine and phosphatidylserine in the inner monolayer (Mohandas and Gallagher, 2008). This phospholipid asymmetry is not spontaneous but maintained by energy dependent and independent enzymes. This asymmetry prevents the adhesion of RBC to vascular endothelial cells and the recognition as well as the removal of phosphatidylserine-exposing RBC by liver and spleen macrophages (McEvoy et al., 1986). Thus, it is responsible for RBC survival in circulation. The phospholipid bilayer is also associated directly and indirectly to the RBC cytoskeleton. The 2-dimensional spectrin based cytoskeleton together with ankyrin, actin and protein 4.1R are connected with selected membrane proteins including but not limited to band 3, glycophorin C and others. The cohesion of the membrane proteins with the cytoskeleton enables the RBC to maintain their favorable membrane surface area preventing vesiculation and preserving the cell integrity (Diez-Silva et al., 2010). Thus, all osmotic-based procedures used to encapsulate agents into RBC should carefully consider not only restoring the physiological osmolarity of the cell but also the annealing of the lipid bilayer with the cell cytoskeleton to preserve the cell integrity, the normal biconcave shape of RBC, and the membrane surface area in excess to permit RBC deformability. In addition, cell-volume regulation by several membrane proteins with transport functions regulates cytoplasmic viscosity and ultimately RBC deformability (Milanick and Hoffman, 1986). All these processes are energy demanding. Thus, annealing of the lipid bilayer with the cytoskeleton, normalization of cytosol viscosity and cell deformability, require the addition, during the resealing of RBC submitted to the osmotic encapsulation of therapeutic agents, of compounds useful to produce ATP, and other relevant metabolic intermediates in the RBC, in adequate amounts and for an adequate time at 37°C (Magnani and DeLoach, 1992). An alternative approach to produce RBC as carriers of therapeutic agents is based on the *in vitro* generation of engineered erythrocytes to express therapeutic molecules inside the cells starting from hematopoietic precursor cells. For example, this strategy has been used to generate erythrocytes containing an enzyme able to metabolize phenylalanine that are entering a phase I clinical trial for the treatment of patients with phenylketonuria[1].

THE RED BLOOD CELL MEMBRANE CAN BE CONVENIENTLY MODIFIED TO IMPROVE THE DELIVERY OF THERAPEUTIC AGENTS

Early methods for coupling therapeutic agents on the RBC membrane were based on the use of crosslinking agents including tannic acid and chromium chloride (Muzykantov et al., 1987, 1993; Chiarantini et al., 1992) with limited specificity and orientation. More than 35 years ago Samokhin et al. (1983) showed that the RBC membrane can be modified by biotinylation in order to couple selected antibodies by way of an avidin bridge. The system was very efficient and up to 80,000–100,000 molecules per cell could be easily coupled on the RBC membrane. Unfortunately, Muzykantov et al. (1991) showed that avidin causes complement activation via alternative pathway and leads to RBC lysis. This problem was subsequently solved by reducing the number of biotin molecules per cell or by reducing the amount of bound streptavidin molecules per cell (Muzykantov et al., 1996). The same system was also used to deliver therapeutic enzymes (Magnani et al., 1992a). Optimization of RBC biotinylation depends on a series of factors, i.e., the number of biotin molecules coupled, the selected biotinylation chemistry and the biotin spacer length (Magnani et al., 1994). Other approaches have explored the possibility of targeting complement receptor 1 (CR1) which is present almost exclusively on RBC membrane.

Taylor et al. (1991) have prepared bispecific cross-linked antibodies to target antigens or ligands to the human RBC membrane via CR1. Spitzer et al. (2004) produced instead a fusion protein by linking a murine red blood cell restricted surface antigen (a scFv specific for TER-119) to the amino-terminus of the human complement regulatory protein (CRP)

[1]https://www.rubiustx.com

decay-accelerating factor (DAF). This construct was safe without affecting the circulation and stability of the RBC in mice.

However, a significant improvement was obtained by coupling the drug of interest, i.e., tissue type plasminogen activator (tPA) to an antibody able to recognize human CR1 (Zaitsev et al., 2006). RBC modified by the monoclonal antibody coupled to tPA had a normal viability in a proper preclinical animal model and were effective in preventing occlusive clots (Danielyan et al., 2008). The major expert in the field (Muzykantov, 2010) demonstrated that RBC carrying up to 10^5 tPA molecules do not induce complement activation, hemolysis, phagocytosis and accelerated clearance in preclinical animal models. Furthermore, normal hemostasis is not affected and tPA is protected from plasma inhibitors by the RBC glycocalyx. The estimated therapeutic window of RBC/PA in humans may vary from hours to days or even weeks depending on the dose. The approach was found to be effective especially in thromboprophylaxis of brain ischemia and stroke (Danielyan et al., 2008). More recently the use of cross-linked antibody-tPA conjugate has been substituted by an antigen binding single chain variable fragment (scFv) fused with a mutated recombinant tPA. The RBC target was also changed using glycophorin A (GPA) instead of CR1 (Zaitsev et al., 2010). Subsequently Zaitsev et al. (2012) studied the function and efficacy of an antibody fragment against Ter-119 fused to the extracellular domain of mouse trombomodulin (TM). They demonstrated that murine RBC receiving this construct were stable and capable of preventing platelet activation and vascular occlusion by clots. Of interest, it became later evident that the target selection on the RBC membrane was also relevant. In fact, binding fusions to RBC on band 3/GPA and RhCE (Rh17) similarly endowed RBC with hTM activity, but differed in their effects on RBC physiology. hTM-scFv targeted to band 3/GPA increased membrane rigidity and sensitized RBC to hemolysis induced by mechanical stress; in contrast, binding of hTM-scFv to RhCE did not alter deformability or sensitivity to mechanical and osmotic stress (Villa et al., 2018). Thus, RBC can be conveniently modified, covalently or non-covalently, to deliver membrane bound therapeutic agents but target specificity, number of target sites on the RBC membrane, and the resulting effect of coupling the therapeutic agent must be carefully investigated to prevent RBC damage and ultimately hemolysis and/or fast removal from circulation. The historical experience about crosslinking agents and the recent data from Muzykantov laboratory (Villa et al., 2016) have clearly documented the limits and the potential solutions to the problem.

Other approaches have been developed during the years. In the nineties, proteins carrying a transmembrane domain were successfully electro-inserted into the RBC membrane providing stable constructs with near normal *in vivo* survival (Mouneimne et al., 1990; Mouneimne et al., 1991; Zeira et al., 1991). Others (Müller et al., 2000) have used coupling to non-specific NH_2 groups on the RBC membrane apparently without damaging the same (only *in vitro* data are available). Proteins, in particular Decay accelerating factor (DAF) or CD59 insertion, were coupled via a lipid anchor, glycosylphosphatidylinositol (GPI), on the RBC membrane (Civenni et al., 1998). This approach resulted in the formation of functional constructs but released more easily the inserted proteins than native RBC.

The methods for coupling therapeutic agents on the RBC membrane herein described are schematized in **Figures 1a–g**.

IMMUNOGENICITY OR IMMUNE TOLERANCE?

One key question arisen during the years on the experimental use of agents coupled to the RBC membrane is related to the potential immunogenicity of the modified cells. Smith et al. (2012) showed that mice receiving transfusions of RBC expressing human GPA did not produce anti hGPA antibodies and became tolerant to further immunizations with the same antigen. Ryder et al. (2014) observed that RBC antigens trigger immune responses in mice depending on antigen properties as well as on donor and recipient features. This conclusion apparently describes also the situation in humans although the mechanisms for alloimmunization are not completely clear (Hendrickson and Tormey, 2016). Others and we have reported that RBC can perform as antigen delivery systems inducing an immunological response that overcomes also the use of adjuvants (Magnani et al., 1992b; Chiarantini et al., 1997). This response was also partially protective in a feline model of retroviral infection (Chiarantini et al., 1998). Furthermore, these constructs were able to induce CTL responses and neutralizing antibodies (Corinti et al., 2002; Dominici et al., 2003). Richards et al. (2016) showed that inflammation should be considered a key factor in the induction of erythrophagocytosis or tolerance involving different antigen presenting cells. In particular, macrophages in the spleen and liver appear to induce a tollerogenic phenotype while plasmacytoid dendritic cells and monocytes may be associated with humoral alloimmunization. Cremel et al. (2013) provided evidence that macrophages in the liver and spleen represent "tollerogenic" antigen-presenting cells and that the ability to target RBC-loaded with an antigen to these districts can be used conveniently to induce immune tolerance. Murray et al. (2006) instead demonstrated that humoral immune responses can be evoked by using antigen-loaded carrier erythrocytes without adjuvants. The main difference among these experimental approaches was based on the stability of the antigen-loaded RBC. Cremel et al. (2013) intentionally modified the carrier RBC to be quickly removed in the liver and spleen while Murray et al. (2006) produced antigen-loaded RBC with near-normal survival in circulation. Apparently, antigen-carrier RBC induce an immune response if the constructs have a near-normal survival while they induce immune tolerance if they are rapidly removed from bloodstream by the antigen-presenting cells of liver and spleen. Taking into consideration also previous data cited above, it is possible to conclude that antigens taken up by antigen presenting cells in the absence of an inflammatory context induce anergy or immune tolerance (Baekkeskov et al., 2017). Hubbell and colleagues (Kontos et al., 2013) developed a strategy of antigen coupling to mouse RBC by decorating the immunogenic selected protein with the peptide sequence WMVLPWLPGTLD (ERY1) with high specificity for GPA. An antigen specific deletion of

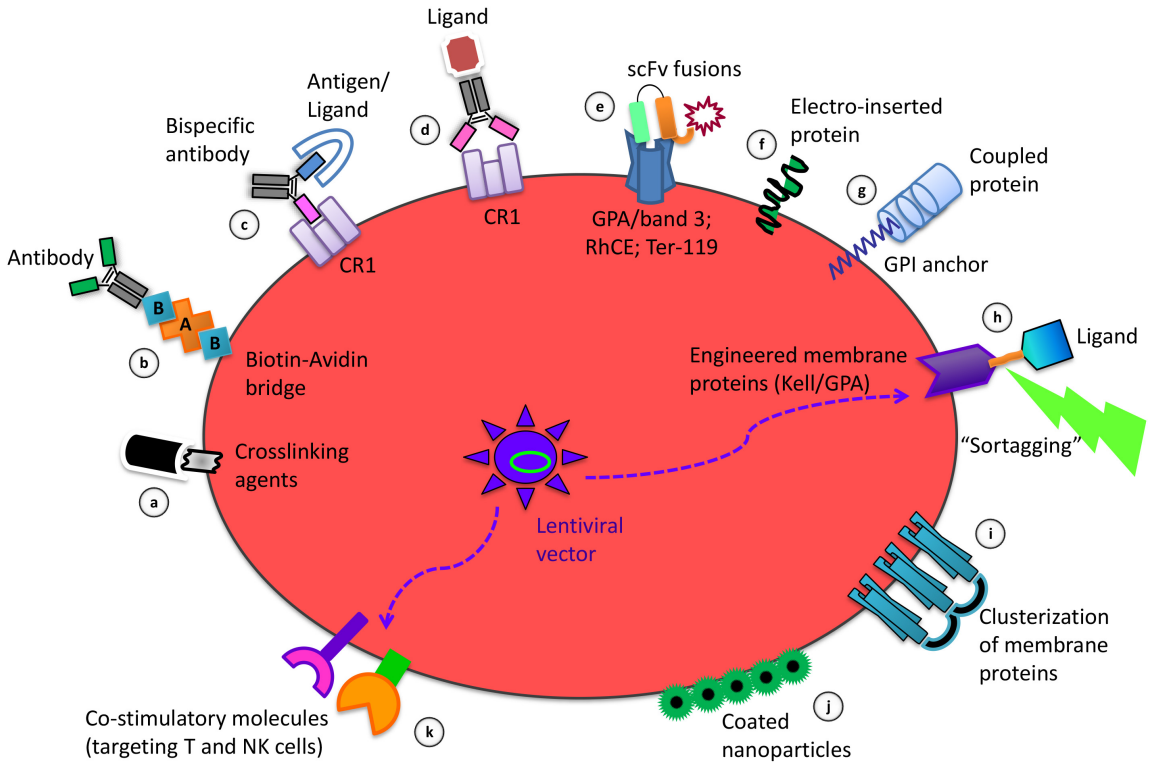

FIGURE 1 | Strategies of RBC membrane processing to obtain the delivery and targeting of therapeutic agents and to induce immune tolerance or immunogenicity. Among the coupling modalities for binding of molecules to the RBC surface there are: the use of crosslinking agents for chemical coupling of ligands **(a)**; the biotinylation to couple selected antibodies by an avidin bridge **(b)**; the use of bispecific antibodies targeting antigens/ligands to the RBC specific protein target CR1 **(c)**; the crosslinking of antibodies carrying a specific ligand to Complement Receptor 1 (CR1) **(d)**; the use of scFv-based fusion constructs targeting GPA/band 3, RhCE, Ter-119, on the RBC surface **(e)**; the electro-insertion of transmembrane proteins into the RBC membrane **(f)**; the coupling of proteins using the GPI lipid anchor **(g)**; the Sortase A-mediated tagging ("sortagging") of molecules to genetically engineered membrane proteins, expressed upon *ex vivo* transfection of erythroid precursors with lentiviral vectors, followed by their differentiation into enucleated RBC **(h)**; the clusterization of RBC membrane proteins for selective targeting **(i)**; the non-covalent attachment of coated nanoparticles to the RBC surface **(j)**; the lentivirus-driven co-expression of combinations of co-stimulatory molecules on engineered RBC **(k)**.

reactive CD4 and CD8 T cells was induced when these constructs were administered to mice. Antigens targeted by RBC but not in soluble form were able to activate Tregs. Moreover, Grimm et al. (2015) observed that one antigenic epitope could modulate responses to other epitopes in the same protein antigen. Of interest Lorentz et al. (2015) demonstrated that binding of E. coli L-Asparaginase (a therapeutic enzyme) to erythrocytes abrogated development of antibody titer by >1,000-fold and extended the pharmacodynamic (PD) effect of the drug 10-fold in mice.

Lodish and coworkers (Shi et al., 2014) developed a further innovative approach based on the possibility to attach payloads to selected RBC surface proteins by exploiting sortase-mediated site-specific cut. However, the transpeptidase Sortase A recognizes the LPXTG motif near the C-terminus of the substrate. Thus, the RBC membrane proteins must be first modified to express this target motif that is not naturally present on RBC membrane proteins. Starting from tissue culture of erythrocyte progenitors, normal murine and human red cells can be obtained; Lodish et al. introduced genes into the progenitor cells encoding membrane surface proteins that can be modified by sortases. Two sortase-modifiable membrane proteins, the blood group antigen Kell and GPA, were expressed in erythroid progenitors (**Figure 1h**). The Kell is a type II membrane protein with the C-terminus exposed to the extracellular milieu while GPA is a type I membrane protein with the N-terminus extracellularly disposed. Of interest, to target the RBC to a specific cell type, the red cells were modified by linking on their surface a single domain antibody with full retention of binding specificity. These constructs show near normal circulation in mice and mature *in vitro* to enucleated reticulocytes up to 50–60% of retroviral transduced precursor cells. Later on, Pishesha et al. (2017) demonstrated that modified RBC expressing specific antigens blunt the immune response of the main immune effector cells (B, CD4 T cells, and CD8 T cells). The encouraging results obtained in different mouse models of autoimmune diseases led to conclude that this strategy may be applied in therapeutic approaches and prophylactic measures.

Overall, the apparent discrepancy arisen from the results of the above mentioned studies about the different immune responses evoked by the engineered RBC, maybe be due to several reasons: a) membrane proteins used to bind the antigens; b) half-life in bloodstream of the engineered RBC;

c) experimental protocol characteristics, e.g., number of RBC administrations, experiment duration, time-interval between RBC administrations. Therefore, these observations suggest that a number of variants could be responsible for the final immunological outcome and that a unique protocol to mount either immunogenicity or immune tolerance versus an antigen delivered by RBC is not yet available.

THE RED BLOOD CELL MEMBRANE CAN BE CONVENIENTLY MODIFIED TO FACILITATE DRUG TARGETING

The possibility of coupling proteins and different types of ligands on the RBC external membrane without compromising RBC survival in circulation, prompted investigators to target RBC to selected target cells or circulating compounds. Several examples have already been illustrated above but other relevant considerations and approaches are summarized here. Chiarantini et al. (1992) demonstrated the possibility of selective targeting of T cells by coupling a specific antibody on the RBC membrane. In, Chiarantini et al. (1995) showed that controlled modification of RBC membrane proteins can conveniently target the RBC to liver and spleen macrophages. In case the RBC have been previously loaded with molecules of interest, the same will also be selectively transferred to these phagocytic cells (Magnani et al., 1992c, 1996; Rossi et al., 1998). The mechanism identified was based on the use of agents (Zn, BS^3 or both) able to induce clusterization of RBC membrane associated proteins (**Figure 1i**). The extension of the clusterization was responsible for the observed removal of processed RBC from circulation. Many years later Cremel et al. (2013) used only BS^3 for a fast and efficient method to target RBC to liver and spleen phagocytic cells confirming the

TABLE 1 | Coupling modalities for the binding of molecules of interest to the RBC membrane.

Coupling modality	Advantages	Limits	References
Chromium Chloride	High efficiency	Limited specificity/orientation	Muzykantov et al., 1987, 1993; Chiarantini et al., 1992
Biotin-Avidin	High efficiency	Complement activation and cell lysis at high copy number	Muzykantov et al., 1991; Magnani et al., 1994
Crosslinking of antibodies to Complement Receptor 1 (CR1)	No complement activation, no hemolysis, no phagocytosis, no accelerated clearance	Significant variation in CR1 expression levels among individuals and limited dosing CR1 conjugates	Taylor et al., 1991; Birmingham and Herbert, 2001; Zaitsev et al., 2006; Danielyan et al., 2008; Muzykantov, 2010
Crosslinking of antibody fragments (scFv) to glycophorin A (GPA)/band 3	Stability, high efficiency, no RBC aggregation, no hemolysis, no uptake by RES	Membrane rigidity and hemolysis induced by mechanical stress	Zaitsev et al., 2010; Villa et al., 2018
Crosslinking of antibody fragments (scFv) to Ter-119	High efficiency, no RBC damage, no survival RBC alteration	Unknown	Zaitsev et al., 2012
Crosslinking of antibody fragments (scFv) to RhCE	No deformability or sensitivity to mechanical and osmotic stress, no impact on RBC physiology, presence on the RBC of 100% of the human population	Unknown	Villa et al., 2018
Electro-insertion of transmembrane proteins into the RBC membrane	Almost normal *in vivo* survival of RBC	Unknown	Mouneimne et al., 1990, 1991; Zeira et al., 1991
Coupling of proteins via a glycosylphosphatidylinositol (GPI)-anchor on the RBC membrane	Formation of functional constructs	Early release of the inserted proteins respect to the endogenous GPI-anchored proteins	Civenni et al., 1998
Coupling of antigens to RBC upon conjugation to the linear peptide sequence (ERY1) with high specificity for GPA	Antigen specific deletion of reactive CD4 and CD8 T cells	Unknown	Kontos et al., 2013
Sortase-mediated site-specific covalent attachment of "cargo" to engineered surface proteins (Kell, GPA) in erythroid precursors	Acceptable *in vitro* maturation of retroviral transduced precursor cells to enucleated reticulocytes Near normal circulation	Expensive and time-consuming	Shi et al., 2014; Pishesha et al., 2017
Clusterization of RBC surface membrane proteins by crosslinking agents (Zn, BS3)	Targeting of RBC (loaded or not with agents) to liver and spleen macrophages	Unknown	Magnani et al., 1992c; Chiarantini et al., 1995; Magnani et al., 1996; Rossi et al., 1998; Cremel et al., 2013
Non-covalent attachment of nanoparticles (NPs), coated with the agents of interest, to RBC	Increased blood levels of NPs. Lung targeting and retention. Reduced uptake by liver and spleen	Unknown	Anselmo et al., 2013 Brenner et al., 2018
RBC precursors engineered to co-express combinations of co-stimulatory molecules	Targeting of T and NK cells	Unknown	https://www.rubiustx.com/

previous observations. Thus, RBC targeting to spleen and liver phagocytic cells is feasible, can be modulated in the rate of processed cells removed from circulation, and can be adopted also for the targeting of RBC previously loaded with drugs or agents of interest. Huang et al. (2017) demonstrated that, by using RBC expressing chimeric proteins that consisted of single-domain camelid antibodies (VHHs) against botulinum neurotoxin A fused with GPA or Kell, a prolonged protection against bacterial toxins was attainable. The system was very efficient in mice conferring resistance to a lethal dose in the order of 10,000-times the effect observed using free antibodies. Anselmo et al. (2013) showed that it is possible to increase the amount of nanoparticles (NPs) in circulation and their persistence in the lungs over 24 h by a non-covalent attachment of NPs to RBC, while reducing their removal by liver and spleen phagocytic cells. A further increase in lung targeting and retention of NPs is achievable by linking anti-ICAM-1 antibody to the exposed surface of NPs attached to RBC. Thus, a new, indirect, drug targeting system was developed by using NPs coated with specific antibodies and non-covalently bound on the RBC membrane (**Figure 1j**). More recently, Brenner et al. (2018) have reported clear evidences for a general targeting platform based on nanocarrier hitching onto RBC for a selective targeting to different organs according to the site of injection. This platform is of general interest since it works with a large variety of nanocarriers. Actually, https://www.rubiustx.com/ is developing engineered RBC obtained from precursor erythroid cells transfected with lentiviral vectors to co-express combination of co-stimulatory molecules on the RBC membrane to target T cells and NK cells aiming at killing tumor cells (**Figure 1k**).

CONCLUSION

For several years, RBC have not only been exploited as oxygen carriers but also as drug delivery and targeting agents. The RBC have unique properties that outperform conventional and new drug delivery systems. These interesting properties permit: to load the RBC with agents of interest without affecting the *in vivo* RBC circulation and the RBC immunological properties; to couple or decorate the RBC membrane by agents useful to target the cells to selected cells and/or organs; to express antibodies able to inactivate toxins; to carry antigens for the induction of immune tolerance or induce immunogenicity. This review focuses on these last properties and considers different modalities for coupling or inserting peptides, proteins or antibodies on the RBC membrane. Having shown that different modalities illustrated by many groups listed in this review produce RBC with different properties, the researchers can be guided in selecting the most appropriate approach for the intended application (**Table 1**). For example, we know now that chemical linking of proteins or peptides on the RBC membrane is rarely the modality to be preferred if survival in circulation is the necessary requirement. In addition, the engagement of selected cell determinants during the coupling procedure could affect some important physiological functions of the RBC. Finally, when ligands or proteins are inserted into the membrane, their membrane distribution and the stability of the constructs should be considered. Of interest, recent observations that describe the possibility of RBC-hitching of nanocarriers open additional perspectives. Finally, the isolation of RBC precursors, their transfection with lentiviral vectors, the expansion and *in vitro* maturation of enucleated reticulocytes and mature RBC, will also open new unexplored possibilities for the expression on the human RBC membrane of new therapeutic agents. These possibilities should be exploited case-by-case since they could also be associated with unwanted secondary effects. Similarly, some limitations can also arise when therapeutic molecules are administered confined inside RBC such as: (a) premature uptake of drug-loaded erythrocytes from bloodstream when a prolonged permanence in circulation is required; (b) limited kinetics of erythrocyte transmembrane transport of substrates or products when therapeutic enzymes are loaded inside; (c) drug leaking across cell membranes; (d) possible alterations operated by some drugs on RBC structure (Leuzzi et al., 2016). Considering the peculiarity of human RBC versus other animal species, the experimental evidences should not be limited to animal models but derived also from clinical trials. In conclusion, the use of RBC is continuing to open new possibilities for realizing carriers endowed with enormous potential for the benefit of patients in need and for the improvement of therapeutic agents with limited or poor pharmacokinetic (PK)/PD properties. These approaches have reached the clinic and at least two companies are already in Phase 3 for selected applications[2,3]. The activities in place, and the excellent amount of publications in this field, make the scientific community optimistic about the possibility of a fast clinical development and approval of the use of RBC as carriers and delivery systems in many conditions with unmet medical needs.

AUTHOR CONTRIBUTIONS

All authors have provided substantial contributions to the concept of the work, analysis and interpretation of the data for the work, drafting the work and revising it critically, approval for publication, and agreed to be accountable for all aspects of the work.

FUNDING

This work was partially supported by the University of Urbino and FanoAteneo, Italy.

ACKNOWLEDGMENTS

We greatly acknowledge the colleagues and the students who during the years have contributed to these developments. Furthermore, we thank the agencies that supported our work.

[2]http://www.erydel.com/

[3]https://erytech.com/

REFERENCES

Anselmo, A. C., Gupta, V., Zern, B. J., Pan, D., Zakrewsky, M., Muzykantov, V., et al. (2013). Delivering nanoparticles to lungs while avoiding liver and spleen through adsorption on red blood cells. *ACS Nano* 7, 11129–11137. doi: 10.1021/nn404853z

Baekkeskov, S., Hubbell, J. A., and Phelps, E. A. (2017). Bioengineering strategies for inducing tolerance in autoimmune diabetes. *Adv. Drug Deliv. Rev.* 114, 256–265. doi: 10.1016/j.addr.2017.06.007

Birmingham, D. J., and Herbert, L. A. (2001). CR1 and CR1-like: the primate immune adherence receptors. *Immunol. Rev.* 180, 100–111.

Brenner, J. S., Pan, D. C., Myerson, J. W., Marcos-Contreras, O. A., Villa, C. H., Patel, P., et al. (2018). Red blood cell-hitchhiking boosts delivery of nanocarriers to chosen organs by orders of magnitude. *Nat. Commun.* 9:2684. doi: 10.1038/s41467-018-05079-7

Chiarantini, L., Argnani, R., Zucchini, S., Stevanato, L., Zabardi, P., Grossi, M. P., et al. (1997). Red blood cells as delivery system for recombinant HSV-1 glycoprotein B: immunogenicity and protection in mice. *Vaccine* 15, 276–280.

Chiarantini, L., Droleskey, R., Magnani, M., and DeLoach, J. R. (1992). In vitro targeting of erythrocytes to cytotoxic T-cells by coupling of Thy-1.2 monoclonal antibody. *Biotechnol. Appl. Biochem.* 15, 171–184.

Chiarantini, L., Matteucci, D., Pistello, M., Mancini, U., Mazzetti, P., Massi, C., et al. (1998). AIDS vaccination studies using an ex vivo feline immunodeficiency virus model: homologous erythrocytes as a delivery system for preferential immunization with putative protective antigens. *Clin. Diagn. Lab. Immunol.* 5, 235–241.

Chiarantini, L., Rossi, L., Fraternale, A., and Magnani, M. (1995). Modulated red blood cell survival by membrane protein clustering. *Mol. Cell. Biochem.* 144, 53–59.

Civenni, G., Test, S. T., Brodbeck, U., and Bütikofer, P. (1998). In vitro incorporation of GPI-anchored proteins into human erythrocytes and their fate in the membrane. *Blood* 91, 1784–1792.

Corinti, S., Chiarantini, L., Dominici, S., Laguardia, M. E., Magnani, M., and Girolomoni, G. (2002). Erythrocytes deliver Tat to interferon-gamma-treated human dendritic cells for efficient initiation of specific type 1 immune responses in vitro. *J. Leukoc. Biol.* 71, 652–658.

Cremel, M., Guérin, N., Horand, F., Banz, A., and Godfrin, Y. (2013). Red blood cells as innovative antigen carrier to induce specific immune tolerance. *Int. J. Pharm.* 443, 39–49. doi: 10.1016/j.ijpharm.2012.12.044

Danielyan, K., Ganguly, K., Ding, B. S., Atochin, D., Zaitsev, S., Murciano, J. C., et al. (2008). Cerebrovascular thromboprophylaxis in mice by erythrocyte-coupled tissue-type plasminogen activator. *Circulation* 118, 1442–1449. doi: 10.1161/CIRCULATIONAHA.107.750257

Diez-Silva, M., Dao, M., Han, J., Lim, C. T., and Suresh, S. (2010). Shape and biomechanical characteristics of human red blood cells in health and disease. *MRS Bull.* 35, 382–388.

Dominici, S., Laguardia, M. E., Serafini, G., Chiarantini, L., Fortini, C., Tripiciano, A., et al. (2003). Red blood cell-mediated delivery of recombinant HIV-1 Tat protein in mice induces anti-Tat neutralizing antibodies and CTL. *Vaccine* 21, 2073–2081.

Grimm, A. J., Kontos, S., Diaceri, G., Quaglia-Thermes, X., and Hubbell, J. A. (2015). Memory of tolerance and induction of regulatory T cells by erythrocyte-targeted antigens. *Sci. Rep.* 5:15907. doi: 10.1038/srep15907

Hendrickson, J. E., and Tormey, C. A. (2016). Understanding red blood cell alloimmunization triggers. *Hematology Am. Soc. Hematol. Educ. Program.* 2016, 446–451. doi: 10.1182/asheducation-2016.1.446

Huang, N. J., Pishesha, N., Mukherjee, J., Zhang, S., Deshycka, R., Sudaryo, V., et al. (2017). Genetically engineered red cells expressing single domain camelid antibodies confer long-term protection against botulinum neurotoxin. *Nat. Commun.* 8:423. doi: 10.1038/s41467-017-00448-0

Hunault-Berger, M., Leguay, T., Huguet, F., Leprêtre, S., Deconinck, E., Ojeda-Uribe, M., et al. (2015). A phase 2 study of L-asparaginase encapsulated in erythrocytes in elderly patients with Philadelphia chromosome negative acute lymphoblastic leukemia: the GRASPALL/GRAALL-SA2-2008 study. *Am. J. Hematol.* 90, 811–818. doi: 10.1002/ajh.24093

Ihler, G. M., Glew, R. H., and Schnure, F. W. (1973). Enzyme loading of erythrocytes. *Proc. Natl. Acad. Sci. U.S.A.* 70, 2663–2666. doi: 10.1073/pnas.70.9.2663

Kontos, S., Kourtis, I. C., Dane, K. Y., and Hubbell, J. A. (2013). Engineering antigens for in situ erythrocyte binding induces T-cell deletion. *Proc. Natl. Acad. Sci. U.S.A.* 110, E60–E68. doi: 10.1073/pnas.1216353110

Leuzzi, V., Rossi, L., Gabucci, C., Nardecchia, F., and Magnani, M. (2016). Erythrocyte-mediated delivery of recombinant enzymes. *J. Inherit. Metab. Dis.* 39, 519–530. doi: 10.1007/s10545-016-9926-0

Lorentz, K. M., Kontos, S., Diaceri, G., Henry, H., and Hubbell, J. A. (2015). Engineered binding to erythrocytes induces immunological tolerance to *E. coli* asparaginase. *Sci. Adv.* 1:e1500112. doi: 10.1126/sciadv.1500112

Magnani, M., Casabianca, A., Fraternale, A., Brandi, G., Gessani, S., Williams, R., et al. (1996). Synthesis and targeted delivery of an azidothymidine homodinucleotide conferring protection to macrophages against retroviral infection. *Proc. Natl. Acad. Sci. U.S.A.* 93, 4403–4408. doi: 10.1073/pnas.93.9.4403

Magnani, M., Chiarantini, L., and Mancini, U. (1994). Preparation and characterization of biotinylated red blood cells. *Biotechnol. Appl. Biochem.* 20, 335–345.

Magnani, M., and DeLoach, J. R. (1992). *The Use of Resealed Erythrocytes as Carriers and Bioreactors*. New York, NY: Plenum Press.

Magnani, M., Chiarantini, L., Vittoria, E., Mancini, U., Rossi, L., and Fazi, A. (1992b). Red blood cells as an antigen-delivery system. *Biotechnol. Appl. Biochem.* 16, 188–194.

Magnani, M., Mancini, U., Bianchi, M., and Fazi, A. (1992a). Comparison of uricase-bound and uricase-loaded erythrocytes as bioreactors for uric acid degradation. *Adv. Exp. Med. Biol.* 326, 189–194.

Magnani, M., Rossi, L., Brandi, G., Schiavano, G. F., Montroni, M., and Piedimonte, G. (1992c). Targeting antiretroviral nucleoside analogues in phosphorylated form to macrophages: in vitro and in vivo studies. *Proc. Natl. Acad. Sci. U.S.A.* 89, 6477–6481. doi: 10.1073/pnas.89.14.6477

Mambrini, G., Mandolini, M., Rossi, L., Pierigè, F., Capogrossi, G., Salvati, P., et al. (2017). *Ex vivo* encapsulation of dexamethasone sodium phosphate into human autologous erythrocytes using fully automated biomedical equipment. *Int. J. Pharm.* 517, 175–184. doi: 10.1016/j.ijpharm.2016.12.011

McEvoy, L., Williamson, P., and Schlegel, R. A. (1986). Membrane phospholipid asymmetry as adeterminant of erythrocyte recognition by macrophages. *Proc. Natl. Acad. Sci. U.S.A.* 83, 3311–3315. doi: 10.1073/pnas.83.10.3311

Milanick, M. A., and Hoffman, J. F. (1986). Ion transport and volume regulation in red blood cells. *Ann. N. Y. Acad. Sci.* 488, 174–186.

Mohandas, N., and Gallagher, P. G. (2008). Red cell membrane: past, present, and future. *Blood* 112, 3939–3948. doi: 10.1182/blood-2008-07-161166

Mouneimne, Y., Tosi, P. F., Barhoumi, R., and Nicolau, C. (1990). Electroinsertion of full length recombinant CD4 into red blood cell membrane. *Biochim. Biophys. Acta* 1027, 53–58.

Mouneimne, Y., Tosi, P. F., Barhoumi, R., and Nicolau, C. (1991). Electroinsertion of xeno proteins in red blood cell membranes yields a long lived protein carrier in circulation. *Biochim. Biophys. Acta* 1066, 83–89. doi: 10.1016/0005-2736(91)90254-6

Müller, M., Büchi, L., Woodtli, K., Haeberli, A., and Beer, J. H. (2000). Preparation and characterization of 'heparinocytes': erythrocytes with covalently bound low molecular weight heparin. *FEBS Lett.* 468, 115–119. doi: 10.1016/s0014-5793(00)01204-7

Murray, A. M., Pearson, I. F., Fairbanks, L. D., Chalmers, R. A., Bain, M. D., and Bax, B. E. (2006). The mouse immune response to carrier erythrocyte entrapped antigens. *Vaccine* 24, 6129–6139. doi: 10.1016/j.vaccine.2006.05.013

Muzykantov, V. R. (2010). Drug delivery by red blood cells: vascular carriers designed by mother nature. *Expert Opin. Drug Deliv.* 7, 403–427. doi: 10.1517/17425241003610633

Muzykantov, V. R., Murciano, J. C., Taylor, R. P., Atochina, E. N., and Herraez, A. (1996). Regulation of the complement-mediated elimination of red blood cells modified with biotin and streptavidin. *Anal. Biochem.* 241, 109–119. doi: 10.1006/abio.1996.0384

Muzykantov, V. R., Sakharov, D. V., Domogatsky, S. P., Goncharov, N. V., and Danilov, S. M. (1987). Directed targeting of immunoerythrocytes provides local protection of endothelial cells from damage by hydrogen peroxide. *Am. J. Pathol.* 128, 276–285.

Muzykantov, V. R., Smirnov, M. D., and Samokhin, G. P. (1991). Avidin attachment to biotinylated erythrocytes induces homologous lysis via the alternative pathway of complement. *Blood* 78, 2611–2618.

Muzykantov, V. R., Smirnov, M. D., Zaltzman, A. B., and Samokhin, G. P. (1993). Tannin-mediated attachment of avidin provides complement-resistant immunoerythrocytes that can be lysed in the presence of activator of complement. *Anal. Biochem.* 208, 338–342. doi: 10.1006/abio.1993.1057

Pierigè, F., Bigini, N., Rossi, L., and Magnani, M. (2017). Reengineering red blood cells for cellular therapeutics and diagnostics. *Wiley Interdiscip. Rev. Nanomed. Nanobiotechnol.* 9, e1454. doi: 10.1002/wnan.1454

Pierigè, F., Serafini, S., Rossi, L., and Magnani, M. (2008). Cell-based drug delivery. *Adv. Drug Deliv. Rev.* 60, 286–295. doi: 10.1016/j.addr.2007.08.029

Pishesha, N., Bilate, A. M., Wibowo, M. C., Huang, N. J., Li, Z., Deshycka, R., et al. (2017). Engineered erythrocytes covalently linked to antigenic peptides can protect against autoimmune disease. *Proc. Natl. Acad. Sci. U.S.A.* 114, 3157–3162. doi: 10.1073/pnas.1701746114

Richards, A. L., Hendrickson, J. E., Zimring, J. C., and Hudson, K. E. (2016). Erythrophagocytosis by plasmacytoid dendritic cells and monocytes is enhanced during inflammation. *Transfusion* 56, 905–916. doi: 10.1111/trf.13497

Ropars, C., Avenard, G., and Chassaigne, M. (1987). Large-scale entrapment of drugs into resealed red blood cells using a continuous-flow dialysis system. *Methods Enzymol.* 149, 242–248.

Rossi, L., Brandi, G., Schiavano, G. F., Balestra, E., Millo, E., Scarfì, S., et al. (1998). Macrophage protection against human immunodeficiency virus or herpes simplex virus by red blood cell-mediated delivery of a heterodinucleotide of azidothymidine and acyclovir. *AIDS Res. Hum. Retroviruses* 14, 435–444. doi: 10.1089/aid.1998.14.435

Rossi, L., Pierigè, F., Antonelli, A., Bigini, N., Gabucci, C., Peiretti, E., et al. (2016). Engineering erythrocytes for the modulation of drugs' and contrasting agents' pharmacokinetics and biodistribution. *Adv. Drug Deliv. Rev.* 106, 73–87. doi: 10.1016/j.addr.2016.05.008

Ryder, A. B., Zimring, J. C., and Hendrickson, J. E. (2014). Factors influencing RBC alloimmunization: lessons learned from murine models. *Transfus. Med. Hemother.* 41, 406–419. doi: 10.1159/000368995

Samokhin, G. P., Smirnov, M. D., Muzykantov, V. R., Domogatsky, S. P., and Smirnov, V. N. (1983). Red blood cell targeting to collagen-coated surfaces. *FEBS Lett.* 154, 257–261.

Shi, J., Kundrat, L., Pishesha, N., Bilate, A., Theile, C., Maruyama, T., et al. (2014). Engineered red blood cells as carriers for systemic delivery of a wide array of functional probes. *Proc. Natl. Acad. Sci. U.S.A.* 111, 10131–10136. doi: 10.1073/pnas.1409861111

Smith, N. H., Hod, E. A., Spitalnik, S. L., Zimring, J. C., and Hendrickson, J. E. (2012). Transfusion in the absence of inflammation induces antigen-specific tolerance to murine RBCs. *Blood* 119, 1566–1569. doi: 10.1182/blood-2011-09-382655

Spitzer, D., Unsinger, J., Bessler, M., and Atkinson, J. P. (2004). ScFv-mediated in vivo targeting of DAF to erythrocytes inhibits lysis by complement. *Mol. Immunol.* 40, 911–919.

Taylor, R. P., Sutherland, W. M., Reist, C. J., Webb, D. J., Wright, E. L., and Labuguen, R. H. (1991). Use of heteropolymeric monoclonal antibodies to attach antigens to the C3b receptor of human erythrocytes: a potential therapeutic treatment. *Proc. Natl. Acad. Sci. U.S.A.* 88, 3305–3309. doi: 10.1073/pnas.88.8.3305

Villa, C. H., Anselmo, A. C., Mitragotri, S., and Muzykantov, V. (2016). Red blood cells: supercarriers for drugs, biologicals, and nanoparticles and inspiration for advanced delivery systems. *Adv. Drug Deliv. Rev.* 106, 88–103. doi: 10.1016/j.addr.2016.02.007

Villa, C. H., Pan, D. C., Johnston, I. H., Greineder, C. F., Walsh, L. R., Hood, E. D., et al. (2018). Biocompatible coupling of therapeutic fusion proteins to human erythrocytes. *Blood Adv.* 2, 165–176. doi: 10.1182/bloodadvances.2017011734

Zaitsev, S., Danielyan, K., Murciano, J. C., Ganguly, K., Krasik, T., Taylor, R. P., et al. (2006). Human complement receptor type 1-directed loading of tissue plasminogen activator on circulating erythrocytes for prophylactic fibrinolysis. *Blood* 108, 1895–1902. doi: 10.1182/blood-2005-11-012336

Zaitsev, S., Kowalska, M. A., Neyman, M., Carnemolla, R., Tliba, S., Ding, B. S., et al. (2012). Targeting recombinant thrombomodulin fusion protein to red blood cells provides multifaceted thromboprophylaxis. *Blood* 119, 4779–4785. doi: 10.1182/blood-2011-12-398149

Zaitsev, S., Spitzer, D., Murciano, J. C., Ding, B. S., Tliba, S., Kowalska, M. A., et al. (2010). Targeting of a mutant plasminogen activator to circulating red blood cells for prophylactic fibrinolysis. *J. Pharmacol. Exp. Ther.* 332, 1022–1031. doi: 10.1124/jpet.109.159194

Zeira, M., Tosi, P. F., Mouneimne, Y., Lazarte, J., Sneed, L., Volsky, D. J., et al. (1991). Full-length CD4 electroinserted in the erythrocyte membrane as a long-lived inhibitor of infection by human immunodeficiency virus. *Proc. Natl. Acad. Sci. U.S.A.* 88, 4409–4413. doi: 10.1073/pnas.88.10.4409

Conflict of Interest Statement: MM and LR hold shares in EryDel SpA a company with interests in the technology of RBC-based drug delivery.

The remaining authors declare that the research was conducted in the absence of any commercial or financial relationships that could be construed as a potential conflict of interest.

frontiers in Physiology

ORIGINAL RESEARCH
published: 20 December 2019
doi: 10.3389/fphys.2019.01529

Cholesterol Deficiency Causes Impaired Osmotic Stability of Cultured Red Blood Cells

*Claudia Bernecker[1], Harald Köfeler[2], Georg Pabst[3], Martin Trötzmüller[2], Dagmar Kolb[2,4], Karl Strohmayer[5], Slave Trajanoski[2], Gerhard A. Holzapfel[5,6], Peter Schlenke[1] and Isabel Dorn[1]**

[1] Department for Blood Group Serology and Transfusion Medicine, Medical University of Graz, Graz, Austria, [2] Center for Medical Research, Medical University of Graz, Graz, Austria, [3] Institute of Molecular Biosciences, University of Graz, Biophysics Division, BioTechMed Graz, Graz, Austria, [4] Division of Cell Biology, Histology and Embryology, Gottfried Schatz Research Center, Medical University of Graz, Graz, Austria, [5] Institute of Biomechanics, Graz University of Technology, Graz, Austria, [6] Department of Structural Engineering, Norwegian University of Science and Technology, Trondheim, Norway

OPEN ACCESS

Edited by:
Giampaolo Minetti, University of Pavia, Italy

Reviewed by:
Maria Luisa Genova, University of Bologna, Italy
Emile Van Den Akker, Sanquin Diagnostic Services, Netherlands

***Correspondence:**
Isabel Dorn
isabel.dorn@medunigraz.at

Specialty section:
This article was submitted to Red Blood Cell Physiology, a section of the journal Frontiers in Physiology

Received: *13 September 2019*
Accepted: *04 December 2019*
Published: *20 December 2019*

Citation:
Bernecker C, Köfeler H, Pabst G, Trötzmüller M, Kolb D, Strohmayer K, Trajanoski S, Holzapfel GA, Schlenke P and Dorn I (2019) Cholesterol Deficiency Causes Impaired Osmotic Stability of Cultured Red Blood Cells. Front. Physiol. 10:1529. doi: 10.3389/fphys.2019.01529

Ex vivo generation of red blood cells (cRBCs) is an attractive tool in basic research and for replacing blood components donated by volunteers. As a prerequisite for the survival of cRBCs during storage as well as in the circulation, the quality of the membrane is of utmost importance. Besides the cytoskeleton and embedded proteins, the lipid bilayer is critical for membrane integrity. Although cRBCs suffer from increased fragility, studies investigating the lipid content of their membrane are still lacking. We investigated the membrane lipid profile of cRBCs from $CD34^+$ human stem and progenitor cells compared to native red blood cells (nRBCs) and native reticulocytes (nRETs). *Ex vivo* erythropoiesis was performed in a well-established liquid assay. cRBCs showed a maturation grade between nRETs and nRBCs. High-resolution mass spectrometry analysis for cholesterol and the major phospholipid classes, phosphatidylcholine, phosphatidylethanolamine, phosphatidylinositol, phosphatidylserine, sphingomyelin and lysophosphatidylcholin, demonstrated severe cholesterol deficiency in cRBCs. Although cRBCs showed normal deformability capacity, they suffered from increased hemolysis due to minimal changes in the osmotic conditions. After additional lipid supplementation, especially cholesterol during culturing, the cholesterol content of cRBCs increased to a subnormal amount. Concurrently, the osmotic resistance recovered completely and became comparable to that of nRETs. Minor differences in the amount of phospholipids in cRBCs compared to native cells could mainly be attributed to the ongoing membrane remodeling process from the reticulocyte to the erythrocyte stage. Obtained results demonstrate severe cholesterol deficiency as a reason for enhanced fragility of cRBCs. Therefore, the supplementation of lipids, especially cholesterol during *ex vivo* erythropoiesis may overcome this limitation and strengthens the survival of cRBCs *ex vivo* and *in vivo*.

Keywords: *ex vivo* erythropoiesis, red cell, phospholipids, cholesterol, mass spectrometry

INTRODUCTION

Ex vivo generation of red blood cells (RBCs) is a common tool in basic and translational research investigating RBC physiology, RBC affecting disorders and developmental biology. Furthermore, in agreement with overall technical and medical progress, personalized medicine with cultured red blood cells (cRBCs) might become a realistic option for severely alloimmunized patients with chronic blood demand. Current technologies enable the generation of up to 10^6 cRBCs from a single hematopoietic stem and progenitor cell (HSPC) with homogenous lineage-restricted differentiation and near 100% enucleation (Zeuner et al., 2012; Shah et al., 2014). As an important milestone, the Douays group in 2011 performed the first autologous proof-of-principle transfusion of cRBCs into a human recipient (Giarratana et al., 2011). However, a prerequisite for broader clinical application of cRBCs is the rigorous biological and immunological characterization of these cells. Functional analyses investigating the enzyme content, oxygen uptake and release capacity, and deformability of cRBCs have already been performed (Giarratana et al., 2011). Furthermore, the expression pattern of the most relevant blood group antigens (Fujimi et al., 2008; Giarratana et al., 2011; Hawksworth et al., 2018) and proteome profiles have been reported (Gautier et al., 2016; Wilson et al., 2016). In contrast, little attention has been given to the lipid composition of cRBCs, although changes in membrane lipid organization are critical for the biomechanical stability and longevity of RBCs. Impaired lipid composition might cause the obvious fragility of cRBCs and their limited life span.

The flexible and robust membrane of native red blood cells (nRBCs) consists of a lipid bilayer with embedded proteins attached to the underlying membrane skeleton. In RBCs, cholesterol and a variety of phospholipid species form the core structure of this membrane (Mohandas and Gallagher, 2008). Cholesterol is the most abundant membrane lipid, and due to its single polar hydroxyl group, it is a mainly hydrophobic molecule. Cholesterol is well known to increase hydrocarbon chain order by laterally condensing membrane lipids (Silvius, 2003). This process increases overall membrane rigidity. At the same time, however, cholesterol maintains membrane fluidity. In addition to its lipid-ordering effect, cholesterol is considered to be involved in various processes, including raft formation (Simons and Ikonen, 2000) and specific lipid/protein interactions (Fantini and Barrantes, 2013). Another major membrane lipid is phosphatidylcholine (PC), a glycerophospholipid that creates fluid bilayers when unsaturated. Additional phospholipids in the membrane are phosphatidylethanolamine (PE); phosphatidylinositol (PI), the foundation for phosphoinositides with signaling function; phosphatidylserine (PS); and sphingomyelin (SM), which is the most abundant sphingolipid (van Meer, 2005; Carquin et al., 2014). The various phospholipids differ in their polar head groups and in their esterified non-polar fatty acyl chains.

Interestingly, nRBCs show a high level of specificity with only a few hundred different lipid molecules, although there are thousands of possible combinations. Even interindividual differences in humans are only marginal. Lipids are distributed asymmetrically across the bilayer, which is strictly orchestrated by integral proteins (flippases, floppases, and scramblases). In the RBC steady state, PC and SM are located almost exclusively in the outer leaflet, whereas the inner monolayer contains mostly the amino phospholipids PE and PS with mainly polyunsaturated hydrocarbon chains (Marquardt et al., 2015). In general, the lipid composition is preserved in a narrow range throughout the life span of an erythrocyte. Massive alterations lead to dysfunction and ultimately to cell death. The externalization of internal PS functions as a signal for macrophages to eliminate these cells (Penberthy and Ravichandran, 2016).

The regulation of lipid metabolism during erythropoiesis is poorly understood. Most studies have focused on the lipid content of nRBCs under pathophysiological conditions (Quinn et al., 2009; Wang et al., 2011). In *ex vivo* culture systems, erythroblasts may synthetize their lipids from fatty acids carried by proteins such as albumin or take up lipids from the medium (Migliaccio and Migliaccio, 1987; Huang et al., 2018). Consequently, the lipid pattern of the cells depends on the efficacy of their lipid biosynthesis and the content of the surrounding culture medium (Huang et al., 2018). Some *ex vivo* erythropoiesis models already use different lipid supplementations at various concentrations, while others do not use any (**Supplementary Table S1**). Currently, a commonly accepted scientific rationale for additional lipid supplementation is still missing. For a comparison of cRBCs and nRBCs, it must be considered that all erythropoiesis models generate mainly reticulocytes (RETs), lacking the final differentiation into biconcave-shaped erythrocytes (Shah et al., 2014). Native reticulocytes (nRETs) released from the bone marrow are irregularly shaped and less flexible than erythrocytes (Malleret et al., 2013). After transendothelial migration into the blood stream, nRETs become functional erythrocytes within 3 days (Chasis et al., 1989). This maturation process includes extensive membrane remodeling, cytoskeletal rearrangement, loss of organelles and RNA and a reduction of the cell volume. Ultimately, the mature erythrocytes are optimized for gas transport and are very flexible and persistent. nRBCs require a high deformation capacity for their frequent passages through the microvasculature and "quality check" in the spleen sinusoids.

To the best of our knowledge, this is the first study to investigate the lipid composition of cRBCs and compare it to that of their native counterparts. The lipid patterns of nRETs, nRBCs and cRBCs were analyzed by high-resolution mass spectrometry. In addition to the seven main lipid classes, 59 phospholipid subtypes were investigated. This quantitative analysis was completed by functional investigation of the membrane deformability and osmotic resistance. Our results demonstrate the importance of lipid, especially cholesterol supplementation during *ex vivo* erythropoiesis and its influence on the functionality of cRBCs.

MATERIALS AND METHODS

Human Specimens and Cell Preparation

$CD34^+$ HSPCs were isolated from peripheral blood (PB), (purity 97.8 ± 0.7%) and cord blood (CB) (purity 93.7 ± 2.6%) with magnetic beads as described by the manufacturer (CD34

Microbead Kit Ultrapure, Miltenyi Biotec). nRBCs were obtained from fresh RBC units within 24 h after donation, and nRETs were isolated from CB with magnetic beads within 12 h post-partum (CD71 Microbead Kit; Miltenyi Biotec). Written informed consent was given prior to sampling. The study was approved by the local ethics committee in line with the Declaration of Helsinki (EK 27 165ex 14/15).

Erythroid Differentiation

$CD34^+$ HSPCs from PB and CB were cultured in an established three-step differentiation model in Iscove's liquid medium (Biochrom) with 5% human plasma (Octapharma) (Giarratana et al., 2011; Betz et al., 2016). This culture medium was used for the generation of cRBC from PB-derived HSPCs ($cRBC^{pb}$) and from CB-derived HSPCs ($cRBC^{cb}$). For lipid-enrichment experiments (generation of $cRBC^{pb+lipids}$ from PB-derived HSPCs), the medium was additionally supplemented with 4 mg/dl cholesterol-rich lipids (Sigma-Aldrich) from day 0 onwards. The lipid content of used media and supplements was measured quantitatively by a clinical chemistry Analyzer AU680 (Beckman Coulter). To obtain the pure enucleated fraction of cRBCs from PB and CB, day 18 cells were filtered through a syringe filter (Acrodisc® WBC Pall). The maturation stage of filtered cells was determined microscopically after New Methylene Blue staining (Reticulocyte Stain, Sigma-Aldrich). Cells were further characterized by flow cytometry on the basis of Thiazole Orange staining (Retic Count™, Becton Dickinson) and expression of CD71. Additionally, the cells were assessed by an ADVIA 212 analyzer (Siemens) for their volume and hemoglobin content. Details are given in the **Supplementary Material**.

Lipid Analysis

Lipids were quantitatively measured by mass spectrometry. We analyzed cholesterol, PC (13 subtypes), PE (17 subtypes), PS (2 subtypes), SM (14 subtypes), LPC (7 subtypes), and PI (6 subtypes). Lipids were extracted from cell pellets (10^7 cells) according to Matyash et al. (2008). Data were acquired according to Triebl et al. (2017) by Orbitrap-MS (LTQ-Orbitrap, Thermo Fisher Scientific). Full-scan spectra from m/z 450 to 1050 for positive ion mode and from m/z 400 to 1000 for negative ion mode were acquired in the Orbitrap mass analyzer at a resolution of 100 k at m/z 400 and <2 ppm mass accuracy. Every sample was measured once in positive polarity and once in negative polarity. For MS/MS experiments, the 10 most abundant ions of the full-scan spectrum were sequentially fragmented in the ion trap using He as the collision gas (CID, normalized collision energy: 50; isolation width: 1.5; activation Q: 0.2; and activation time: 10), and centroided product spectra at a normal scan rate (33 kDa/s) were collected. The exclusion time was set to 10 s. Data analysis was performed by Lipid Data Analyzer (Hartler et al., 2011; Hartler et al., 2017). Details are given in the **Supplementary Material**.

Deformability Testing

Filtered cells (4×10^8/ml) were examined on a laser optical rotational cell analyzer (Lorrca®; RR Mechatronics Hoorn) according to an established protocol (Plasenzotti et al., 2004; Baskurt et al., 2009). The elongation index (EI) was calculated, describing the deformation of the cells in relation to the applied shear stress.

Osmotic Resistance

Filtered cells (1×10^6/tube) were incubated in decreasing NaCl concentrations (0.9–0%). To detect free hemoglobin, 50 µl of supernatant was analyzed in 500 µl of Harboe buffer (Bioanalytic) with the Harboe 3-wavelength-absorption method (380, 415, 450 nm) using a Shimadzu-1800 spectrophotometer (Harboe, 1959).

Cholesterol Depletion

Cholesterol depletion was performed using Methyl-β-cyclodextrin (MBCD, Sigma-Aldrich) as previously described (Domingues et al., 2010). nRBCs were obtained from fresh RBC units and suspended up to 20% hematocrit in 5 and 6.5 mM MBCD in PBS buffer. Cells were incubated 30 min at 37°C and then washed three times with PBS by centrifugation at 500 *g* for 10 min to remove the MBCD-cholesterol complexes. Cholesterol-depleted cells were analyzed for osmotic resistance as described above. Non-treated RBCs were used as controls.

Statistics

The non-parametric Mann–Whitney *U* test and Kruskal–Wallis test with subsequent Bonferroni correction were performed to test for differences between groups. $p < 0.05$ was considered statistically significant.

RESULTS

Erythroid Differentiation

For extensive lipid analysis of cRBCs, *ex vivo* erythropoiesis from $CD34^+$ PB HSPCs ($cRBC^{pb}$) and $CD34^+$ CB HSPCs ($cRBC^{cb}$) was performed in a well-established three-phase erythropoiesis assay (Giarratana et al., 2011; Betz et al., 2016). An overview of the study is given in **Figure 1**. The used culture medium for the generation of $cRBC^{pb}$ and $cRBC^{cb}$ contained 5% human plasma as the only lipid source. The complete culture medium contained 3 mg/dl cholesterol, 5 mg/dl triglycerides and 13 mg/dl phospholipids. Lipid concentrations of used media and supplements are summarized in **Supplementary Table S2**. The homogeneous differentiation of $CD34^+$ HSPCs into terminally mature erythroid cells was confirmed by morphology and flow cytometry (**Supplementary Figure S1**) (Giarratana et al., 2011; Betz et al., 2016). The cumulative expansion averaged $0.5 \times 10^5 \pm 0.2 \times 10^5$-fold and $1.1 \times 10^5 \pm 0.1 \times 10^5$-fold in PB-/CB-derived cultures. Compared to $cRBC^{pb}$, $cRBC^{cb}$ showed a slightly delayed maturation as indicated by a lower percentage of $hemoglobin^+$ cells on days 8 and 11 followed by a delay in further enucleation (**Supplementary Figures S1D,H**). This observation was also reflected by cell surface marker expression. Although already on day 8 >95% of cells from both sources expressed the early erythroid marker CD36, in $cRBC^{cb}$, higher percentages of $CD45^+$ erythroblasts and lower percentages of

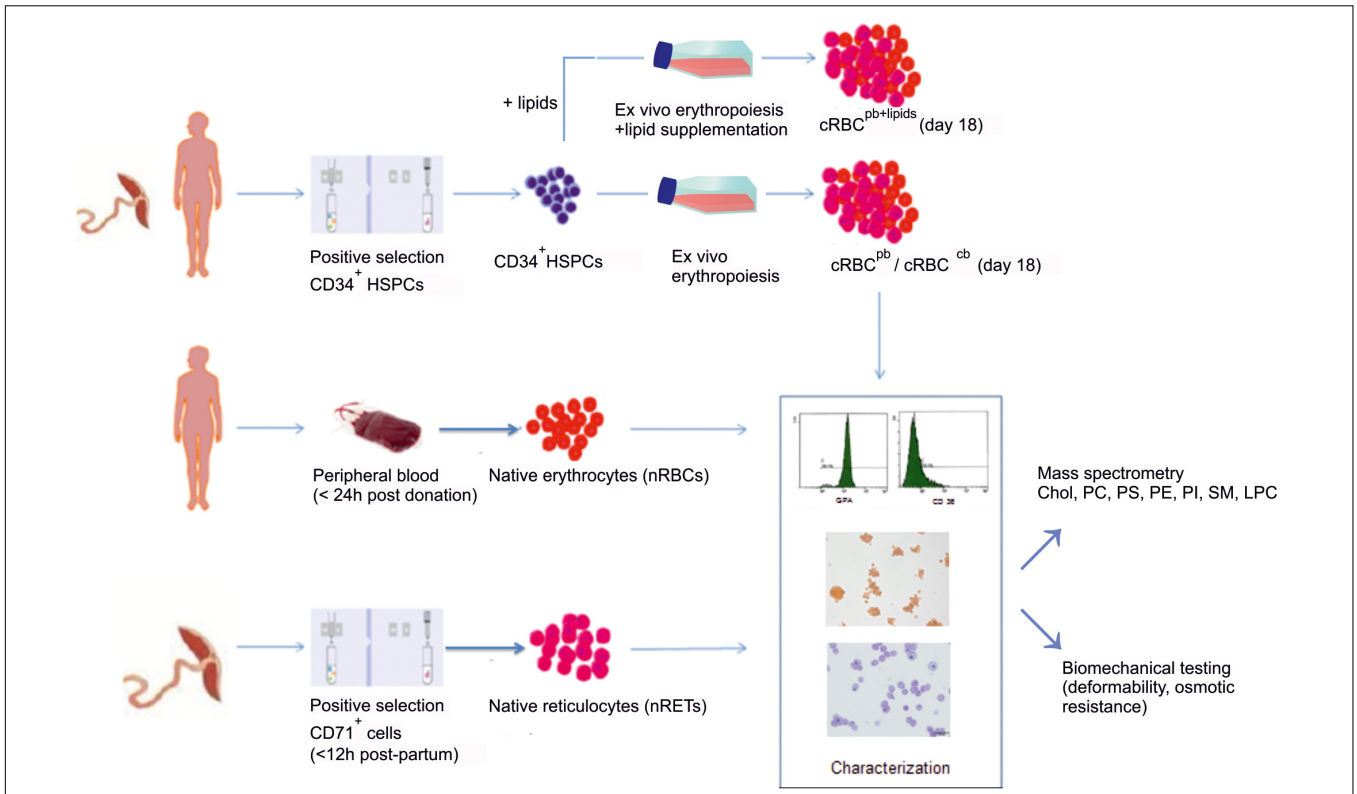

FIGURE 1 | Overall scheme of the study. In an initial set of experiments, *ex vivo* erythropoiesis was performed from CD34$^+$HSPCs derived from PB (cRBC^{pb}) and CB (cRBC^{cb}) in an established liquid culture system. Filtered, enucleated day 18 cells were compared to PB-derived nRBCs and CB-derived nRETs. Cells from all sources were characterized by flow cytometry and immunohistochemistry regarding their maturation stage. The cellular cholesterol and phospholipid contents were measured by mass spectrometry. In addition, the deformability and osmotic resistance of cells were analyzed. Based on results from initial experiments, we performed additional experiments from CD34$^+$ HSPCs by adding cholesterol rich lipids to the culture medium (cRBC$^{pb+lipids}$).

already glycophorin A$^+$ (GPA$^+$) cells were observed on days 8 and 11 (**Supplementary Figures S1C,G**). On final culture days >99% of cells from both sources expressed the erythroid marker GPA. In line with terminal maturation, the percentage of CD36$^+$ cells decreased to 21.4 ± 7.0% in cRBC^{pb} and 59.2 ± 12.5% in cRBC^{cb} (Kieffer et al., 1989; Hu et al., 2013). The enucleation reached 83.0 ± 7.0% and 70.0 ± 6.0% for cRBC^{pb} and cRBC^{cb}, respectively. To eliminate the remaining nucleated normoblasts and extruded nuclei, on day 18 a filtration step was performed. The obtained purity of enucleated cells was >98% for both sources, ensuring comparability for subsequent lipid profiling.

Maturation Stage of cRBCs

The maturation stage of filtered cRBCs was determined by New Methylene Blue staining. Depending on the content of remaining ribosomal organelles, maturation stages were classified between 0 (dense chromatin residues) and V (no chromatin residues) (**Figure 2**; Koepke and Koepke, 1986; Houwen, 1992). nRETs isolated from CB samples by CD71 purification (purity >98%) showed an almost homogeneous maturation stage of young nRETs with typical dark blue mesh-like ribosomal RNA residuals, corresponding to stage 0-II. nRBCs lacked chromatin spots, corresponding to stage V. In comparison to these controls, cRBCs showed a mixture of all five stages, displaying an intermediate maturation between nRETs and nRBCs. A comparable maturation pattern of cRBC^{pb} was obtained by flow cytometry after Thiazole Orange staining for the detection of remaining nucleic acids together with CD71 (**Supplementary Figure S2**). 74.4 ± 6.9% of the cRBC^{pb} stained positive for Thiazole Orange, compared to 88.0 ± 4.2% of nRETs and only 2.6 ± 0.6% of nRBCs. In line with an intermediate maturation stage of cRBCs, they also differed from nRETs and nRBCs in the expression of the Transferrin receptor CD71, which is known to be downregulated during terminal reticulocyte maturation (**Supplementary Figures S1, S2**) (Hu et al., 2013; Malleret et al., 2013). Based on New methylene Blue staining, cRBC^{pb} reached a slightly higher maturation grade than did cRBC^{cb}. This slight difference between cRBC^{pb} and cRBC^{cb} became also evident by higher cell surface expression of CD71 and CD36 in cRBC^{cb} (**Supplementary Figures S1C,G**). Additionally, the mean corpuscular volume (MCV), mean corpuscular hemoglobin content (CHm) and mean corpuscular hemoglobin concentration (CHCm) of cRBC^{pb} were analyzed by ADVIA analyzer (**Supplementary Table S3**). Under *ex vivo* conditions, cRBC^{pb} had an increased MCV (141.5 ± 9.7 fl) compared to that of nRET^{pb} (103.5 ± 3.0 fl), which is in line with stress-induced erythropoiesis, as previously reported (Giarratana et al., 2011). CHCm was reduced (25.5 ± 6.0 g/dl)

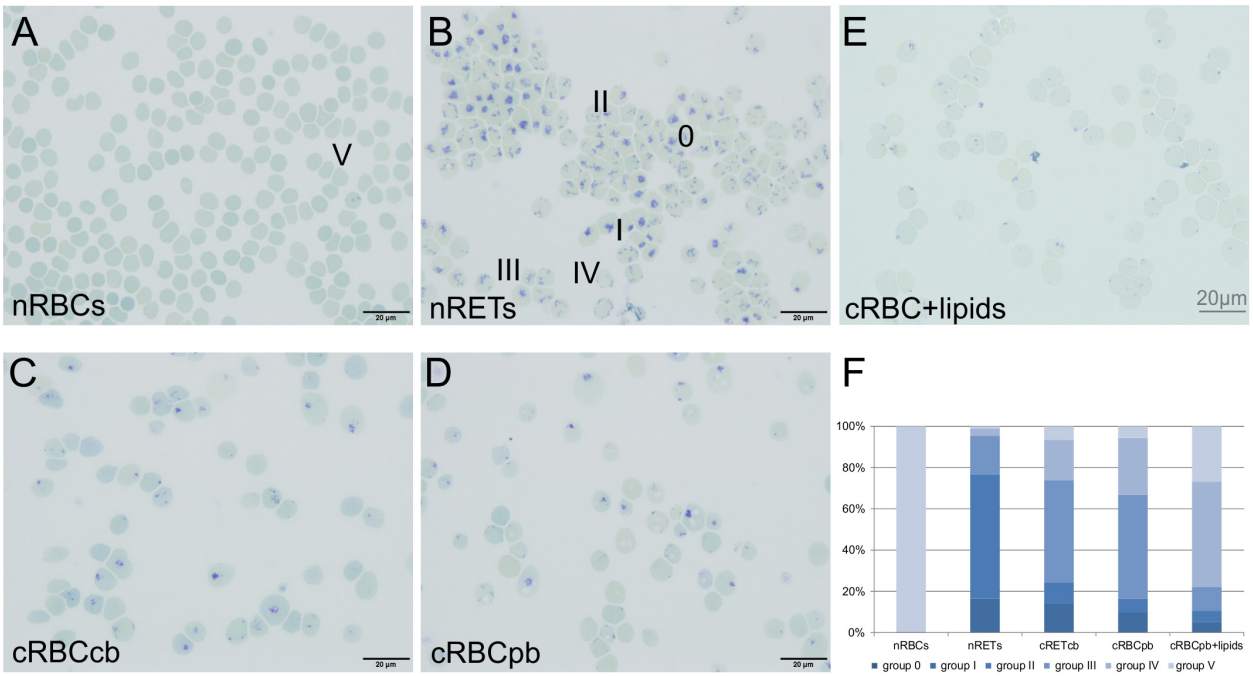

FIGURE 2 | Maturation stage of nRBCs, nRETs, cRBC^{cb}, cRBC^{pb} and cRBC$^{pb+lipids}$ (filtered day 18 cells) determined by microscopic evaluation after New Methylene Blue staining. **(A–E)** Representative pictures of cells from all sources. Bright field, oil, 100 × magnification (scale bar: 20 µm). Dependent on the remaining RNA network, cells are classified into stages 0 to V. Stage 0 shows the typical reticular mesh-like structures of immature cells stained in dark blue, while stage V represents fully mature erythrocytes without any dark blue reticular staining. **(F)** Diagram showing the affiliation of cells for the different maturation stages in nRBCs, nRETs, cRBC^{cb},cRBC^{pb} and cRBC$^{pb+lipids}$ (n = 4, each) displayed in%.

compared to our own data for nRET^{pb} (31.7 ± 1.1 g/dl), although near the normal range published for PB-derived reticulocytes measured by ADVIA analyzer (27–33 g/dl) (Nebe et al., 2011).

Lipid Composition of cRBCs

Quantitative comparison of the lipid content of RBCs (cholesterol, PC, PS, SM, PE, PI and lysophosphatidylcholine (LPC) was performed by high-resolution mass spectrometry. In nRBCs, cholesterol represented the largest fraction, with 49.2 ± 9.9% of the total lipid content, followed by PC (20.7 ± 4.3%) and SM (16.6 ± 3.1%). The sum of all the other lipids constituted the remaining 13.5 ± 3.1% (**Figure 3A** and **Supplementary Figure S3**). Interestingly, exactly the same pattern was found in nRETs, although the absolute content of lipids (17.2 ± 5.4 nmol/10^7 cells) was significantly higher than that in nRBCs (7.3 ± 0.4 nmol/10^7 cells), in line with the larger cell size and membrane surface (**Figure 3B**). In more detail, in nRETs higher absolute amounts were observed for each individual lipid type with the exception of LPC, reaching statistical significance for PC and PE (**Figure 4**).

With a mean total lipid content of 10.2 ± 0.5 nmol/10^7 cells, the lipid content of cRBCs was between that of the native sources. In comparison to native cells, the cholesterol content was obviously impaired in cRBCs, indicating a severe culture artifact. This phenomenon was reflected by both the absolute (2.3 ± 0.9 nmol/10^7 cells) and relative (23.7 ± 8.1%) cholesterol contents (**Figures 3**, **4** and **Supplementary Figure S3**). Despite some minor variations, we did not observe any significant differences in phospholipids between cRBCs derived from CB and PB. These minor variations might reflect differences of the biological replicates or the slightly lower maturation stage of cRBC^{cb} as described above. However, only cRBC^{cb} differed in their higher absolute amount of PI from nRBCs and only cRBC^{pb} in their higher absolute amount of SM from nRBCs (**Figure 4**). Observed minor variations between both sources might be the reason for these different significance levels compared to nRBCs. In general, the content of PI and SM was comparable between cRBC^{pb} and cRBC^{cb} and like in nRETs higher than in nRBCs. Interestingly, only in nRBCs was the total amount of LPC higher than that of PI, while in nRETs and cRBCs, the PI content was higher. The highest LPC content was observed in cRBC^{pb}. Additional calculations of the average chain lengths and double bonds of the phospholipid classes are given in the **Supplementary Material** and **Supplementary Figures S4**, **S5**. While a longer lipid chain causes lower flexibility, a higher number of double bonds accounts for higher flexibility of the molecule.

Lipid Subtype Distribution in cRBCs

Next, we performed a detailed analysis of a total number of 59 phospholipid subtypes. The statistical evaluation of lipidomics data showed a distinct clustering of cRBC^{cb}/cRBC^{pb} versus nRETs and nRBCs in principal component analysis (PCoA) (**Figure 5A**). In addition to the PCoA analysis, phospholipid

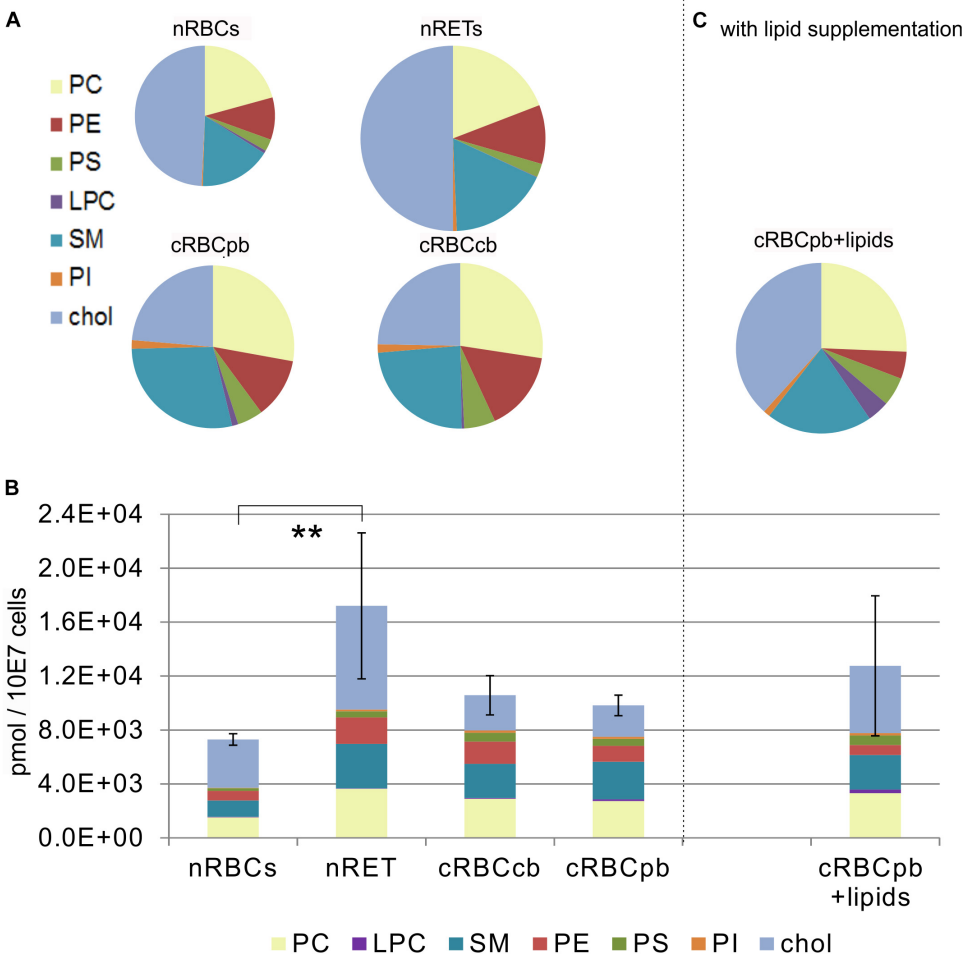

FIGURE 3 | Lipid content measured by high-resolution mass spectrometry in nRBCs, nRETs, cRBC^{pb}, cRBC^{cb} and cRBC after lipid supplementation (cRBC$^{pb+lipids}$) (n = 4 each) **(A)** Proportional lipid content including PE, PC, PS, PI, SM, LPC and cholesterol of nRBCs, nRETs, cRBC^{pb}, cRBC^{cb} and **(C)** cRBC$^{pb+lipids}$ displayed as pie charts. The magnitudes of the circles correspond to the absolute lipid content of the cell type. **(B)** Absolute lipid content of nRBCs, nRETs, cRBC^{pb} and cRBC^{cb} and cRBC$^{pb+lipids}$ (n = 4 each) regarding the phospholipid groups PC, PE, PS, PI, SM, LPC, and cholesterol. Values are depicted as pmol/10^7 cells (**$p < 0.01$).

subtype profiles are presented in a heatmap, where the contents of individual lipid subclasses according to the standardized Z-score values are represented by different colors (**Figure 5B**). Hierarchical clustering was performed to group the samples according to their phospholipid profiles. The nRBCs (red label) show a homogenous pattern in the heat map and close relatedness in the hierarchical clustering tree above, revealing a homogenous group of samples. nRETs (green label) are clustering apart from the nRBCs and show some inhomogeneity among their group. This might be caused by their different biological origins and maturity levels. The two cRBC groups (light blue and dark blue labels) are clustering as one group closely related to nRETs. Only one exception (cRBC^{pb} dark blue) is clustering with nRBCs. The reason for this outlier remains elusive so far. These findings were strengthened by the correlation analysis, as shown in **Supplementary Figure S6**.

To elucidate the statistical significance of the shown differences, subsequent Kruskal–Wallis tests with Bonferroni adjustment were performed. Phospholipid subtype analysis revealed the most significant differences between nRBCs and nRETs, with 33% reduced, 1.5% elevated and 65.5% evenly distributed lipids in nRBCs (**Figure 6**). Differences (>5-fold change and $p < 0.05$) were observed particularly with respect to the absolute levels of PC (PC 32:0; PC 32:1), PI (PI 38:5; PI 40:4), PE (PE 34:2; PE 40:3; PE 40:4; PE 40:5), and SM (SM 26:0; SM 26:1; SM 26:2). Interestingly, only PE 34:2 levels were significantly lower in nRETs than in nRBCs, whereas all other lipid species were significantly more abundant. **Supplementary Table S4** summarizes differences between groups.

Between cRBC^{pb} and cRBC^{cb}, we observed minor variations but did not find any significant differences (**Figure 6**). PI (PI 38:3), PE (PE 38:3; PE 40:3; PE 40:4; PE 40:5), and PC (PC 38:3) levels were significantly higher in cRBC^{cb} than in nRBCs. Furthermore, cRBC^{pb} had significantly higher levels of PI (PI 38:4) than did nRBCs (**Supplementary Table S4**). These higher levels may be due to the lower maturity level of cRBCs compared

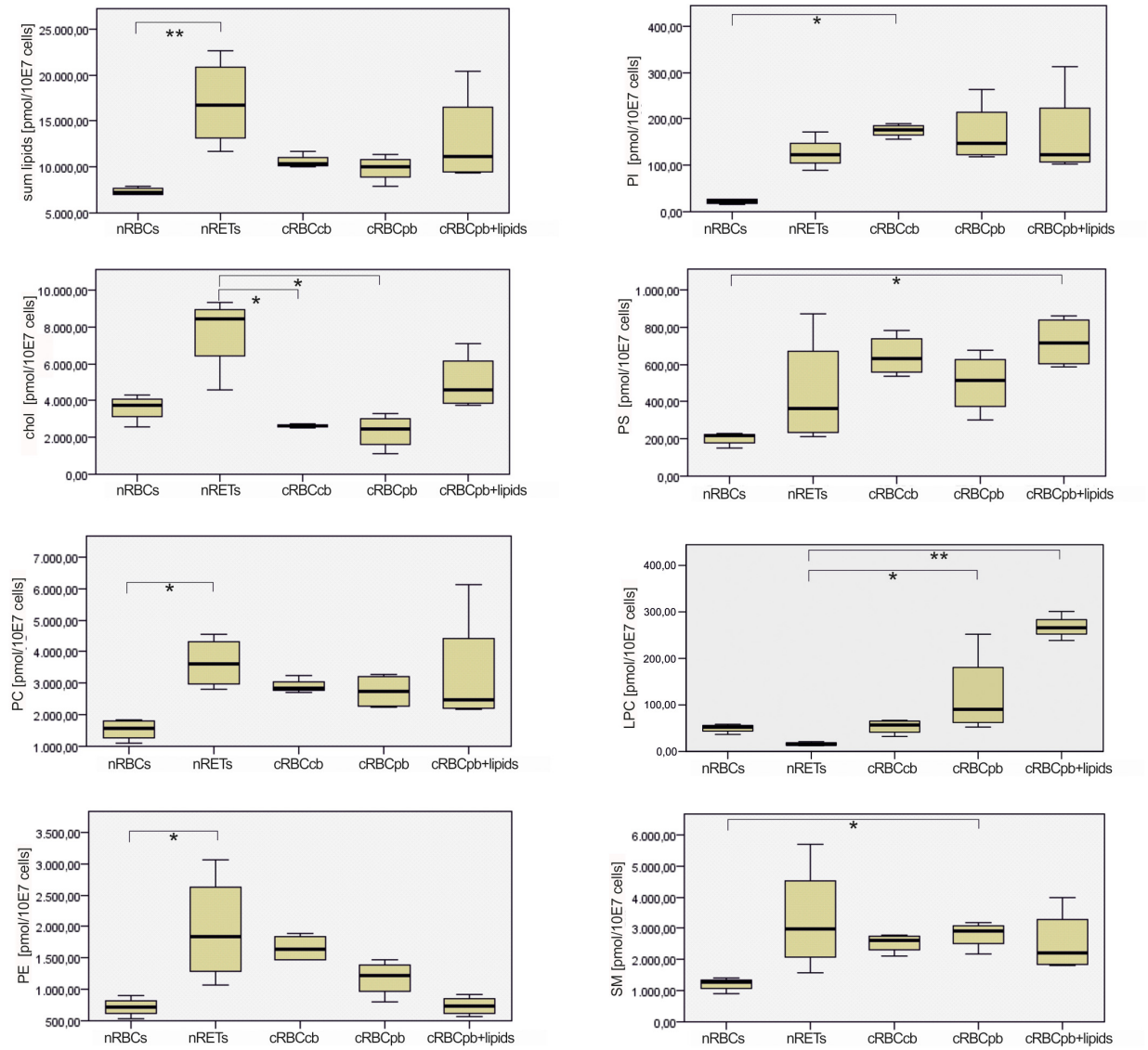

FIGURE 4 | Box and Whisker Blots showing differences in absolute contents of cholesterol and measured phospholipid species between nRBCs, nRETs, $cRBC^{cb}$, $cRBC^{pb}$, and $cRBC^{pb+lipids}$ ($n = 4$, each). Samples were analyzed with Kruskal–Wallis Test for independent samples. Significance values were adjusted with Bonferroni correction (*$p < 0.05$; **$p < 0.01$).

to nRBCs. Similar to in nRETs, PE34:2 was the only PE subclass that was lower in $cRBC^{pb}$ than in nRBCs.

cRBCs were specifically distinct from nRETs in LPC, PE, SM and PS contents. $cRBC^{pb}$ had significantly elevated LPC (LPC16:0; LPC 18:0; LPC 18:1) and SM (SM 20:0) values, while PS (PS 40:6) and PE (PE 34:1; PE 38:6; PE 40:7) values were much lower in $cRBC^{pb}$ than in nRETs. $cRBC^{cb}$ differed significantly from nRETs mainly in LPC (LPC 21:0; LPC 22:0), PE (PE 22:0; PE 36:3), and SM (SM 18:0) levels. In detail, PE 36:3 and SM 18:0 were significantly higher in $cRBC^{cb}$ than in nRETs, while the other parameters were considerably lower (**Supplementary Table S4**).

Again, observed non-significant variations between $cRBC^{pb}$ and $cRBC^{cb}$ might explain their different significance values compared to nRBCs and nRETs. When compared to nRBCs and nRETs, above mentioned lipid subtypes showed a similar pattern of enhancement or reduction in both cRBC sources, although reaching significance only in $cRBC^{cb}$ or $cRBC^{pb}$.

Biomechanical Properties of cRBCs

The deformability of cRBCs was measured using a laser optical rotational cell analyzer (Lorrca®) (**Figures 7A,B**). The Elongation Index (EI) was calculated to describe the deformation of the cell in relation to the applied shear stress. Compared to the deformability curve of nRBCs (EImax 0.584), the maximum EI was lower in nRETs (EImax 0.428). The EImax of the cRBCs was positioned between these two physiological sources (EImax 0.489). Especially, in the lower range (0–10 Pa),

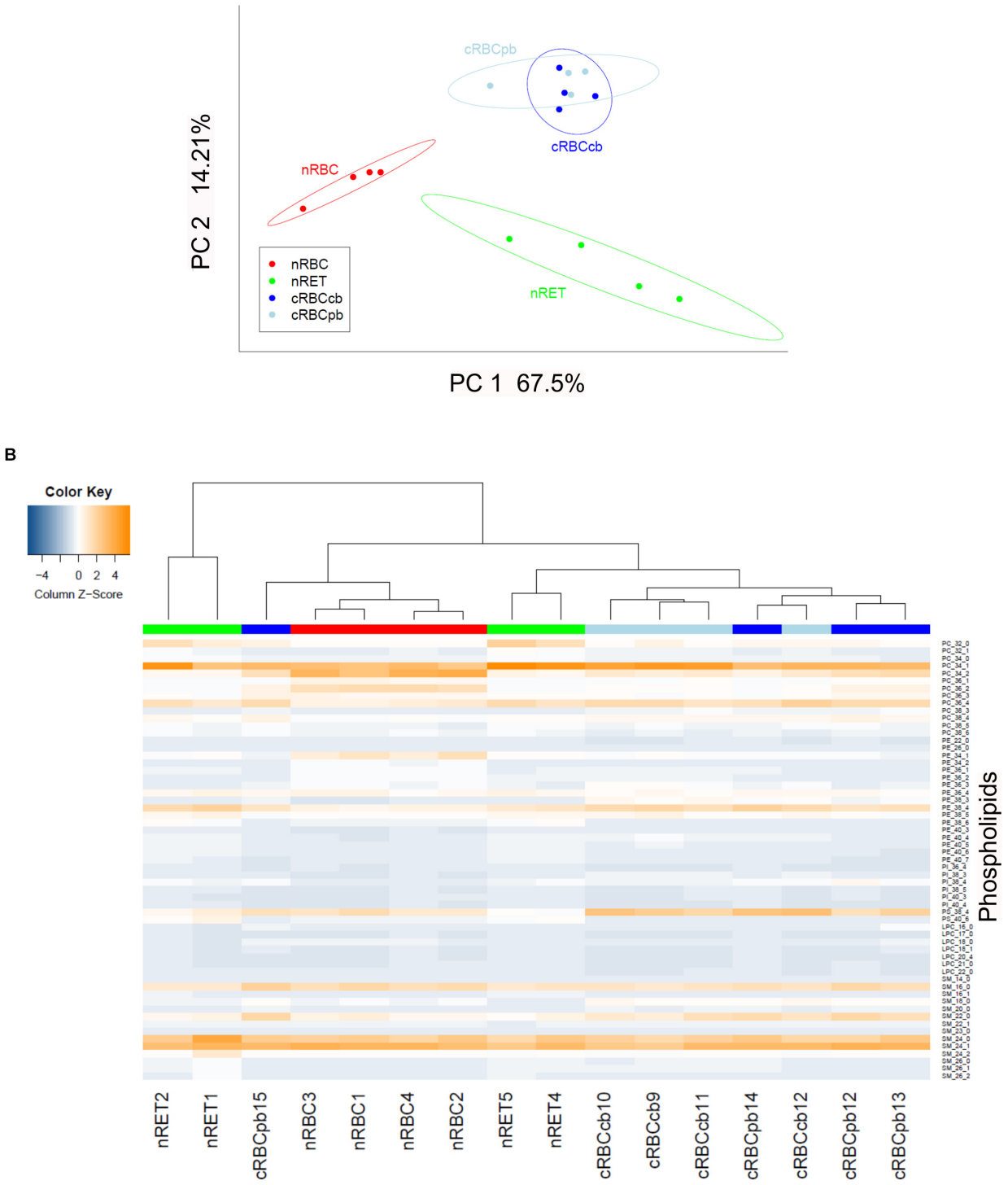

FIGURE 5 | Statistical evaluation of lipidomics data after lipid subtype analysis. **(A)** Principle component analysis showing clustering of nRETs, nRBCs, cRBC^{pb}, and cRBC^{cb} (n = 4 each). The ellipses show the 95% confidence interval. The first two principal components (PC1 and PC2) covered 81.71% of the data variability. **(B)** Heat map with hierarchical clustering analysis. Color bars mark the different sources (red: nRBCs, green: nRETs, dark blue: cRBC^{pb}, light blue: cRBC^{cb}). To standardize the data for the heatmap, z-scores over the samples were calculated by subtracting the sample mean and dividing over its standard deviation. Coloring is helping to easily visualize whole data, where blue tones show lower values and orange tones higher values. The reader can immediately recognize data patterns as well as similarities/differences between samples. The color key of the heat map shows the column z-scores. Cell types were clustered with the complete linkage agglomerative hierarchical clustering method on Euclidean distances. We used this statistical method to group the samples according to their phospholipid profiles.

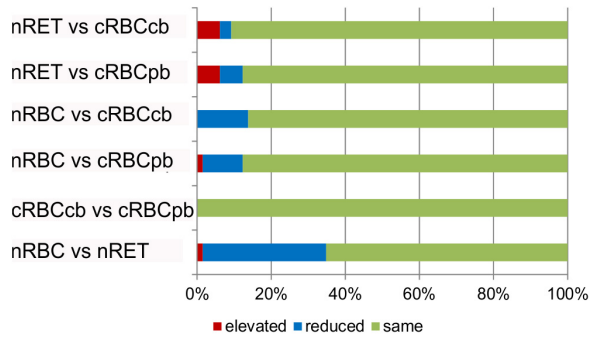

FIGURE 6 | Lipid subtype analysis. Absolute amounts of phospholipid subtypes (n = 59) were compared between nRBCs, nRETs and cRBC^{pb} and cRBC^{cb} (n = 4 each). Bars show% of significantly elevated (red), reduced (blue), and unaltered (green) lipids among indicated groups.

mimicking physiological conditions, the cultured cells performed similarly to the native cells (**Figure 7B**). Additionally, osmotic stability assays were performed, measuring the free hemoglobin concentration after incubation of RBCs with decreasing NaCl concentrations. Evaluation of nRBCs resulted in an s-shaped curve with 50% hemolysis between 0.45 and 0.4% NaCl and a steep transition point. In contrast, analysis of nRETs revealed an s-shaped curve with 50% hemolysis between 0.35 and 0.3% NaCl (**Figure 8A**). The first assessment of the cRBC^{pb} resulted in a tilted s-shaped curve with increased hemolysis already at higher NaCl concentrations, while 50% hemolysis occurred between 0.45 and 0.4% NaCl. In conclusion, nRETs showed the highest stability against osmotic changes, whereas cRBCpb suffered from significantly increased hemolysis due to minimal changes in osmolality.

Lipid Enrichment Experiments

Driven by the obvious differences in the cholesterol content of cRBCs and their impaired osmotic resistance, we performed additional *ex vivo* erythropoiesis experiments from PB-derived HSCs using culture medium supplemented with cholesterol-rich lipids from d0 onward. This supplementation corresponds with concentrations of 7 mg/dl cholesterol, 5 mg/dl triglycerides and 16 mg/dl phospholipids (**Supplementary Table S2**). Growth

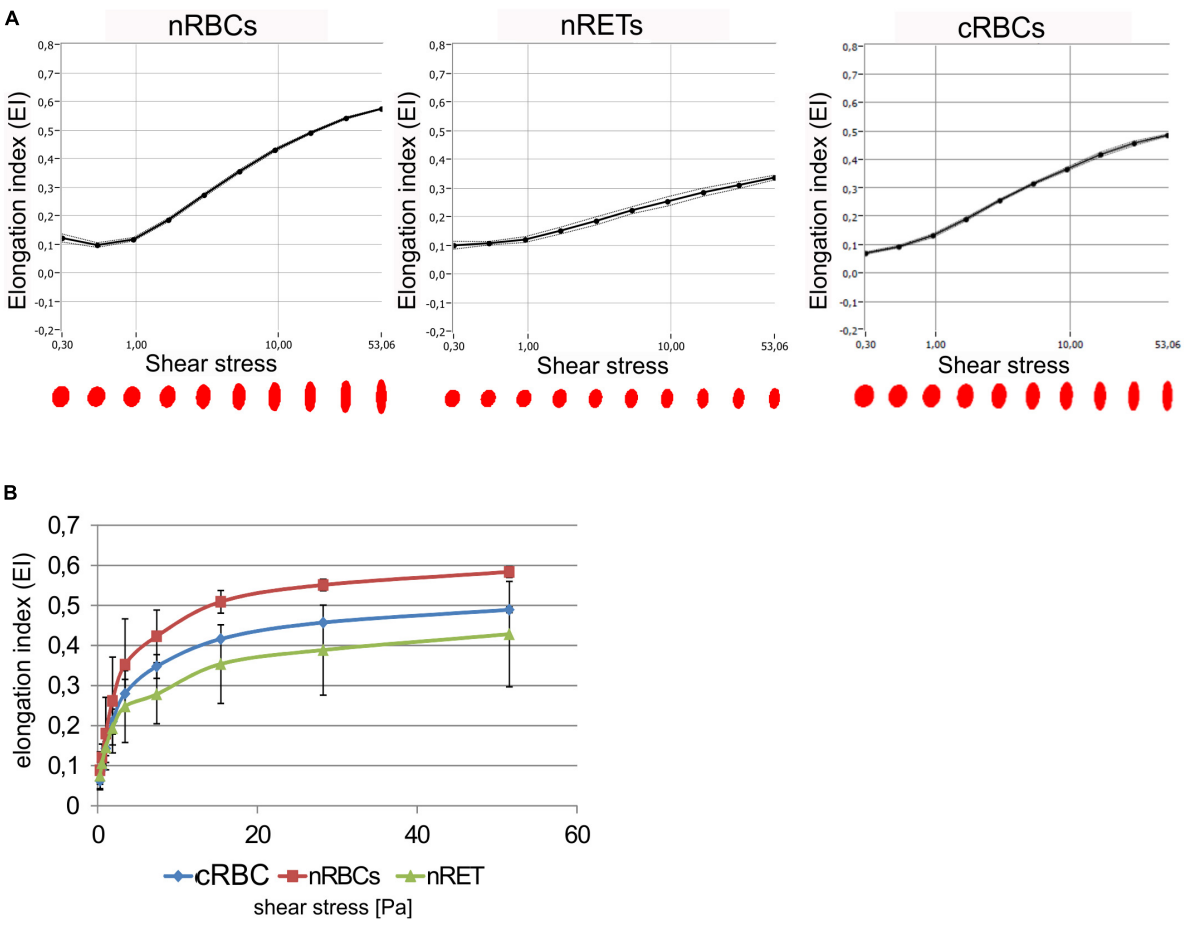

FIGURE 7 | Biomechanical analysis of cRBCs. **(A)** Deformability was measured using Lorrca®. Deformability of cells is given as the elongation index (EI) measured under increasing shear stress. Shown are deformability curves for one representative experiment with nRBCs, cRBCs and nRETs **(B)** Deformability curves calculated from Lorrca analysis for cRBC^{pb} (n = 5), nRBCs (n = 2), and nRETs (n = 2) (mean ± SD). No significant differences were observed between different sources.

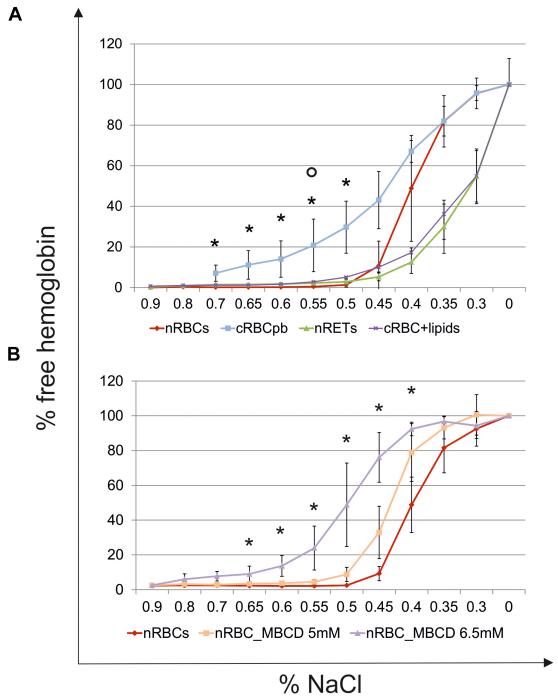

FIGURE 8 | Osmotic resistance analyses. **(A)** Osmotic resistance analyses of nRBCs ($n = 6$), cRBC^{pb} ($n = 5$), nRETs ($n = 2$) and cRBC^{pb} with lipid supplementation (cRBC$^{pb+lipids}$) ($n = 4$, mean ± SD). Osmotic resistance was calculated based on the amount of free hemoglobin after incubation of cells with decreasing NaCl concentrations (*$p < 0.05$ cRBC^{pb} versus nRBCs and $p < 0.05$ cRBC$^{pb+lipids}$ versus nRBCs). **(B)** Osmotic resistance of nRBCs after cholesterol depletion using 5 and 6.5 mM Methyl-β-cyclodextrin (MBCD). Non-treated nRBCs were used as controls (*$p < 0.05$ nRBC_6.5 mM MBCD versus nRBCs).

and differentiation kinetics are summarized in **Supplementary Figure S7**. Compared to our initial experiments without lipid supplementation (**Supplementary Figure S1**), the differentiation of cells was slightly accelerated. Enucleated cells on day 18 showed a higher maturation grade, as indicated by New Methylene Blue staining (**Figure 2**) and flow cytometry analysis after Thiazole Orange and CD71 staining (**Supplementary Figure S2**). Compared to cRBC^{pb} the MCV was reduced (129 fl) and became more comparable to that of nRETs (**Supplementary Table S3**) (Nebe et al., 2011). Subsequent lipidomics analysis of enucleated day 18 cells revealed that the phospholipid composition showed marginal differences but did not change significantly compared to that of previous cultures (**Figures 3**, **4** and **Supplementary Figure S3**). However, the absolute cholesterol content of cRBC^{pb} increased from 2.3 ± 0.9 nmol/10^7 cells to 5.0 ± 1.5 nmol/10^7 cells after lipid supplementation (cRBC$^{pb+lipids}$), ($p < 0.05$). Likewise, the relative cholesterol content increased from 23.7 ± 8.1% without to 40.8 ± 0.8% after lipid supplementation (**Figure 3A** and **Supplementary Figure S3**). In conclusion, the cholesterol content of cRBC$^{pb+lipids}$ became more comparable to that of the native counterparts. Absolute cellular lipid contents with and without lipid supplementation are summarized in **Figures 3B**, **4**.

Subsequent osmotic stability analysis revealed a sigmoid curve for cRBC$^{pb+lipids}$, analogous to that of nRETs. Consequently, the measured osmotic resistance of cRBC$^{pb+lipids}$ with 50% hemolysis at 0.35–0.3% NaCl (**Figure 8A**) was similar to that of nRETs and indicates cholesterol as one crucial factor in membrane stability. To further confirm this hypothesis, we performed osmotic resistance measurements of nRBCs after cholesterol depletion by Methyl-β-cyclodextrin (**Figure 8B**; Domingues et al., 2010). Cholesterol depletion resulted in a dose dependent increase in hemolysis rates already at higher NaCl concentrations, comparable to cRBC^{pb}. Scanning electron microscopy of cRBC^{pb} and cRBC$^{pb+lipids}$ also indicated that lipid supplementation resulted in improved membrane stability, as cRBC$^{pb+lipids}$ resembled the shape of nRETs (**Figure 9A**), whereas cRBC^{pb} showed mainly characteristics of echinocytes (**Figure 9B**). The higher resistance of cRBC$^{pb+lipids}$ became further evident calculating the recovery of reticulocytes after filtration of cultured cells on days 18. Recovery significantly increased from a relatively low level (40.1 ± 9.7%) in cRBC^{pb} to 84.3 ± 12.5% in cRBC$^{pb+lipids}$ ($p < 0.01$, $n = 10$).

DISCUSSION

Ex vivo culturing of RBCs is an attractive and common tool in various fields of RBC research. In addition, it is a promising approach in replacing classical blood components in clinical transfusion medicine. As a prerequisite for these applications, the integrity of the RBC membrane is of utmost importance. Otherwise, cRBCs will suffer from impaired membrane function, which results in reduced expansion and differentiation, altered biomechanical properties and finally reduced survival *ex vivo* and *in vivo*. In addition to the cytoskeleton and embedded proteins, the lipid bilayer is critical for membrane integrity. Current knowledge about lipid synthesis and the changes in membrane lipid composition during erythropoiesis is scarce. Although cRBCs suffer from increased fragility and reduced survival, studies investigating the lipid content of cRBCs are still lacking.

The present study compared the lipid composition of cRBCs with that of their native counterparts, nRETs and nRBCs. In line with published data, the *ex vivo* erythropoiesis protocol (Giarratana et al., 2011; Betz et al., 2016) allowed for the homogenous maturation of HSCs into terminally differentiated erythroid cells. Nucleic acid staining and analysis of cell surface marker expression showed that the cRBCs were in a transient maturation stage between spheroid nRETs and biconcave-shaped mature erythrocytes, accounting for their still high plasma membrane content. Likewise, lipidomics data revealed a total lipid content of cRBCs between that of the two native counterparts. In nRETs, similar to their higher membrane amount, the lipid content was higher than in nRBCs. In our study, the source of human HSPCs (PB or CB) did not make any difference in the lipid content and composition of cRBCs. Comparable observations were made by Wilson et al. (2016) for proteomics data.

High-resolution mass spectrometry analysis revealed most disparities in lipid composition between nRBCs and nRETs,

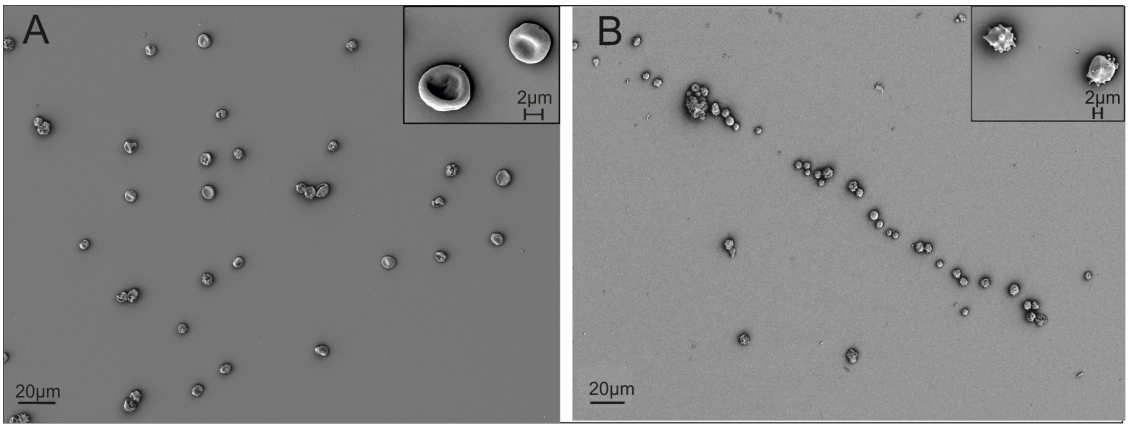

FIGURE 9 | Scanning electron microscopy of cRBCs after filtration on day 18 (scale bars: 20 µm and 2 µm). **(A)** Representative picture of $cRBC^{pb+lipids}$. **(B)** Representative picture of $cRBC^{pb}$.

mostly reflecting the membrane remodeling process during RBC maturation, resulting in reorganization and loss of 20% of the membrane area (Liu et al., 2010; Minetti et al., 2018). Although lower in absolute amount, we found exactly the same proportional distribution of cholesterol and phospholipids in nRBCs and nRETs. In both sources, cholesterol represented the largest fraction, with 50% of the lipid content. In cRBCs, the most obvious discrepancy with the native counterparts was observed in the percentage of cellular cholesterol, which turned out to be due to culture-based malnutrition. In contrast, observed minor differences in the amount of various phospholipids might be explained by their intermediate stage of maturation, associated with ongoing changes in the plasma membrane content.

With respect to the results of Buchwald et al. (2000) that with increasing cholesterol content, membrane flexibility decreases, the membrane characteristics of nRBCs and nRETs were expected to be similar in stiffness, with clear differences from less rigid cRBCs. This was not found for Lorrca® testing, where cRBCs performed comparably to nRBCs and nRETs. In contrast, cRBCs suffered from reduced osmotic resistance by showing enhanced hemolysis due to minimal osmotic changes. The osmotic resistance is known to be affected by membrane integrity as well as by the surface-area-to-volume ratio (Fischbach and Dunning, 2009). To investigate these likely culture-related effects, further *ex vivo* erythropoiesis experiments were performed. By adding cholesterol-rich lipids to the standard culture medium, the concentration of cholesterol was enhanced from 3 mg/dl to a relatively high level of 7 mg/dl. As expected, cRBCs from lipid-enriched cultures showed higher relative cholesterol content, near the content of native cells, whereas no significant changes in phospholipid content were observed compared to those of previous cRBCs. Consequently, cRBCs with lipid supplementation recovered and showed osmotic resistance comparable to that of the nRETs. Likewise, cholesterol depletion of nRBCs by Methyl-β-cyclodextrin treatment resulted in reduced osmotic resistance comparable to $cRBC^{pb}$ without supplementation. These results demonstrate that lipid uptake, especially of cholesterol, from the medium is crucial for the membrane functionality of cRBCs, and therefore sufficient lipid supplementation is mandatory during *ex vivo* erythropoiesis.

The necessity of cholesterol for membrane biosynthesis and survival of RBCs is also evidenced *in vivo*, where mutations in genes of cholesterol synthesis lead to anemias (Jira et al., 2003; Wang et al., 2014). Our findings are further in line with those of Leberbauer et al. (2005) who reported enhanced erythroid expansion due to the addition of cholesterol-rich lipids to the culture medium and a more recent publication by the group of Migliaccio, who stated that *ex vivo* expansion of immature erythroblasts is highly dependent on plasma lipoproteins (Zingariello et al., 2019). Both groups examined the impact of steroids like dexamethasone and lipid supplementation on the *ex vivo* expansion and maturation of cRBCs without investigating the final lipid composition of cRBCs (Zingariello et al., 2019). In our study, expansion rates were not massively affected by lipid supplementation, while a tendency toward faster differentiation was noticed.

Despite statistical significance, the differences found in phospholipid subtype analysis were rather marginal and might primarily be explained by the intermediate maturity level of cRBCs. This is further in line with the observation that RBCs are able to undergo *de novo* lipid synthesis, deacetylation and reacetylation, as well as exchange with other membranes and the environment during their maturation from nRETs to nRBCs (Soupene et al., 2008; Soupene and Kuypers, 2012; Wu et al., 2016). Phospholipids are mostly synthesized by the Kennedy pathway, a *de novo* pathway in the Golgi and endoplasmic reticulum (ER), and repaired by a remodeling pathway called Lands' cycle (Moessinger et al., 2014). The final organization of phospholipids occurs after the enucleation and release of the nRETs into the blood stream for terminal maturation. Due to a lack of Golgi apparatus and ER, mature nRBCs do not have *de novo* synthesis of phospholipids (Wu et al., 2016).

Investigating the phospholipids and their subtypes in more detail, we found in the immature nRETs and cRBCs the most prominent increases in PC, SM, PE, PI, and LPC compared to these levels in nRBCs. First, we focused on components of the

outer leaflet. The diacyl PC content, particularly PC 32:0, was found to be the lowest in nRBCs. This result might explain the higher deformability of erythrocytes, as these molecules have a cylinder-like molecular shape and can consequently pack neatly in a planar bilayer. In a simplified view, the rigidity of membranes results from the packing gradient of its constituent molecules (proteins and lipids) at different depths within the bilayer. Lipids yield different molecular shapes (cylinders, cones, inverted-cones) depending on the composition of their hydrophilic heads and hydrophobic tails; when forced into a planar membrane environment, these shapes experience varying lateral packing densities, which may either increase or decrease the membrane's resistance to deformation (Frolov et al., 2011). Furthermore, SM subclasses were decreased in nRBCs compared to those in cRBCs and nRETs. SM also has a cylinder-like molecular shape but packs even more tightly than PC due to strong intermolecular hydrogen bonding (Slotte, 2016). Thus, the higher the SM content is, the stiffer the membrane. Taken together, our results obtained for the outer membrane lipids are in line with the literature, stating the highest deformability for nRBCs.

In the inner leaflet, we found a decrease in PE content in nRBCs compared to that in nRETs. A high PE content is known to augment membrane stiffness by both intermolecular hydrogen bonding (Boggs, 1980) and significant hydrocarbon splay compared to the small head group (Kollmitzer et al., 2013). Consequently, the lower PE content of the more flexible nRBCs is plausible. Interestingly, PE 34:2 was significantly lower in cRBCs and nRETs, whereas the levels of PE subclasses with longer and more unsaturated hydrocarbons were increased. The resulting membrane bending resistance may be compensated for by the decrease in PC and SM in nRBCs. Alternatively, the observed increase in the number of double bonds, as shown in the **Supplementary Material** in PE, may increase the overall membrane fluidity and hence contribute to increased cell flexibility. Furthermore, nRBCs showed a proportional decrease in the PI content compared to all of the less-mature cell types. Only the more unsaturated species, such as PI 38:4 and PI 38:5, remained elevated, speculatively to maintain necessary cellular function and PIP/PLC signaling. Phosphoinositides are important regulators of autophagy by controlling the cytosol-membrane interface (Schink et al., 2013). These findings are in line with ongoing autophagic and membrane restructuring processes during terminal transition from the reticulocyte to the erythrocyte (Mankelow et al., 2015).

In summary, the obtained results demonstrate the importance of the lipid bilayer composition on the functionality on cRBCs. Cholesterol-deficient cRBCs suffer from impaired osmotic resistance. This observation might be the main reason for the observed fragility of cRBCs and their reduced survival rates *ex vivo* and *in vivo*. *Ex vivo* culturing of RBCs is a common tool in all fields of RBC research. In the absence of a scientifically based rationale, current lipid supplementation underlies a high variability and is generally below the concentrations reported in the present study. The maintenance of RBC membrane integrity by lipid supplementation will improve results obtained from *ex vivo*-generated RBCs due to a decrease in hemolysis and an improvement of biomechanical properties. In our study this was demonstrated by improved shape of cultured cells as well as higher recovery after filtration. This further strengthens the efforts to make *ex vivo*-generated RBCs clinically applicable in terms of their storability and *in vivo* survival, especially for the blood supply of patients with rare blood groups or alloimmunization against multiple blood group antigens. To further elucidate the role of lipids membrane stability of cRBCs, detailed analyses of the impact of single lipoprotein fractions for lipid supplementation as well as their optimal source, concentration and administration time are necessary.

DATA AVAILABILITY STATEMENT

The datasets generated for this study are available on request to the corresponding author.

ETHICS STATEMENT

The study was reviewed and approved by the Ethics Committee of the Medical University of Graz, Graz, Austria. The patients/participants provided their written informed consent to participate in this study.

AUTHOR CONTRIBUTIONS

CB, PS, and ID conceptualized and designed the study. CB, ID, and KS were involved in collection and assembly of the data. MT did mass spectrometry analyses. DK contributed the scanning electron microscopy. CB, HK, GP, ST, GH, PS, and ID contributed to the data analysis and interpretation. CB, ID, HK, and GP wrote the manuscript. PS edited the manuscript. All authors edited and revised the manuscript and gave final approval for publication.

FUNDING

This study was supported by research funding from the Österreichische Nationalbank (#17932) to CB and the German Society for Transfusion Medicine and Immunohematology to ID and PS.

ACKNOWLEDGMENTS

We greatly acknowledge the excellent technical assistance of Marie-Therese Frisch and Lisa Rohrhofer. We thank Verena Siebarth for support with red blood cell generation and characterization. Furthermore, we thank Max R. Hardeman and Ursula Windberger for support with the Lorrca® analyses.

SUPPLEMENTARY MATERIAL

The Supplementary Material for this article can be found online at: https://www.frontiersin.org/articles/10.3389/fphys.2019.01529/full#supplementary-material

REFERENCES

Baskurt, O. K., Hardeman, M. R., Uyuklu, M., Ulker, P., Cengiz, M., Nemeth, N., et al. (2009). Parameterization of red blood cell elongation index–shear stress curves obtained by ektacytometry. *Scand. J. Clin. Lab. Invest.* 69, 777–788. doi: 10.3109/00365510903266069

Betz, J., Dorn, I., Kouzel, I. U., Bauwens, A., Meisen, I., Kemper, B., et al. (2016). Shiga toxin of enterohaemorrhagic *Escherichia coli* directly injures developing human erythrocytes. *Cell Microbiol.* 18, 1339–1348. doi: 10.1111/cmi.12592

Boggs, J. M. (1980). Intermolecular hydrogen boning between lipids: influence on organization and function of lipids in membranes. *Can. J. Biochem.* 58, 755–770. doi: 10.1139/o80-107

Buchwald, H., O'dea, T. J., Menchaca, H. J., Michalek, V. N., and Rohde, T. D. (2000). Effect of plasma cholesterol on red blood cell oxygen transport. *Clin. Exp. Pharmacol. Physiol.* 27, 951–955. doi: 10.1046/j.1440-1681.2000.03383.x

Carquin, M., Pollet, H., Veiga-Da-Cunha, M., Cominelli, A., Van Der Smissen, P., N'kuli, F., et al. (2014). Endogenous sphingomyelin segregates into submicrometric domains in the living erythrocyte membrane. *J. Lipid Res.* 55, 1331–1342. doi: 10.1194/jlr.M048538

Chasis, J. A., Prenant, M., Leung, A., and Mohandas, N. (1989). Membrane assembly and remodeling during reticulocyte maturation. *Blood* 74, 1112–1120. doi: 10.1182/blood.v74.3.1112.1112

Domingues, C. C., Ciana, A., Buttafava, A., Casadei, B. R., Balduini, C., De Paula, E., et al. (2010). Effect of cholesterol depletion and temperature on the isolation of detergent-resistant membranes from human erythrocytes. *J. Membr. Biol.* 234, 195–205. doi: 10.1007/s00232-010-9246-5

Fantini, J., and Barrantes, F. J. (2013). How cholesterol interacts with membrane proteins: an exploration of cholesterol-binding sites including CRAC, CARC, and tilted domains. *Front. Physiol.* 4:31. doi: 10.3389/fphys.2013.00031

Fischbach, F. F. T., and Dunning, M. B. (2009). *A Manual of Laboratory and Diagnostic Tests*. Alphen aan den Rijn: Wolters Kluwer Health.

Frolov, V. A., Shnyrova, A. V., and Zimmerberg, J. (2011). Lipid polymorphisms and membrane shape. *Cold Spring Harb. Perspect. Biol.* 3:a004747. doi: 10.1101/cshperspect.a004747

Fujimi, A., Matsunaga, T., Kobune, M., Kawano, Y., Nagaya, T., Tanaka, I., et al. (2008). Ex vivo large-scale generation of human red blood cells from cord blood CD34+ cells by co-culturing with macrophages. *Int. J. Hematol.* 87, 339–350. doi: 10.1007/s12185-008-0062-y

Gautier, E. F., Ducamp, S., Leduc, M., Salnot, V., Guillonneau, F., Dussiot, M., et al. (2016). Comprehensive proteomic analysis of human erythropoiesis. *Cell Rep.* 16, 1470–1484. doi: 10.1016/j.celrep.2016.06.085

Giarratana, M. C., Rouard, H., Dumont, A., Kiger, L., Safeukui, I., Le Pennec, P. Y., et al. (2011). Proof of principle for transfusion of in vitro-generated red blood cells. *Blood* 118, 5071–5079. doi: 10.1182/blood-2011-06-362038

Harboe, M. (1959). A method for determination of hemoglobin in plasma by near-ultraviolet spectrophotometry. *Scand. J. Clin. Lab. Invest.* 11, 66–70. doi: 10.3109/00365515909060410

Hartler, J., Triebl, A., Ziegl, A., Trotzmuller, M., Rechberger, G. N., Zeleznik, O. A., et al. (2017). Deciphering lipid structures based on platform-independent decision rules. *Nat. Methods* 14, 1171–1174. doi: 10.1038/nmeth.4470

Hartler, J., Trotzmuller, M., Chitraju, C., Spener, F., Kofeler, H. C., and Thallinger, G. G. (2011). Lipid data analyzer: unattended identification and quantitation of lipids in LC-MS data. *Bioinformatics* 27, 572–577. doi: 10.1093/bioinformatics/btq699

Hawksworth, J., Satchwell, T. J., Meinders, M., Daniels, D. E., Regan, F., Thornton, N. M., et al. (2018). Enhancement of red blood cell transfusion compatibility using CRISPR-mediated erythroblast gene editing. *EMBO Mol. Med.* 10:e8454.

Houwen, B. (1992). Reticulocyte maturation. *Blood Cells* 18, 167–186.

Hu, J., Liu, J., Xue, F., Halverson, G., Reid, M., Guo, A., et al. (2013). Isolation and functional characterization of human erythroblasts at distinct stages: implications for understanding of normal and disordered erythropoiesis in vivo. *Blood* 121, 3246–3253. doi: 10.1182/blood-2013-01-476390

Huang, N. J., Lin, Y. C., Lin, C. Y., Pishesha, N., Lewis, C. A., Freinkman, E., et al. (2018). Enhanced phosphocholine metabolism is essential for terminal erythropoiesis. *Blood* 131, 2955–2966. doi: 10.1182/blood-2018-03-838516

Jira, P. E., Waterham, H. R., Wanders, R. J., Smeitink, J. A., Sengers, R. C., and Wevers, R. A. (2003). Smith-lemli-opitz syndrome and the DHCR7 gene. *Ann. Hum. Genet.* 67, 269–280.

Kieffer, N., Bettaieb, A., Legrand, C., Coulombel, L., Vainchenker, W., Edelman, L., et al. (1989). Developmentally regulated expression of a 78 kDa erythroblast membrane glycoprotein immunologically related to the platelet thrombospondin receptor. *Biochem. J.* 262, 835–842. doi: 10.1042/bj2620835

Koepke, J. F., and Koepke, J. A. (1986). Reticulocytes. *Clin. Lab. Haematol.* 8, 169–179.

Kollmitzer, B., Heftberger, P., Rappolt, M., and Pabst, G. (2013). Monolayer spontaneous curvature of raft-forming membrane lipids. *Soft Matter* 9, 10877–10884.

Leberbauer, C., Boulme, F., Unfried, G., Huber, J., Beug, H., and Mullner, E. W. (2005). Different steroids co-regulate long-term expansion versus terminal differentiation in primary human erythroid progenitors. *Blood* 105, 85–94. doi: 10.1182/blood-2004-03-1002

Liu, J., Guo, X., Mohandas, N., Chasis, J. A., and An, X. (2010). Membrane remodeling during reticulocyte maturation. *Blood* 115, 2021–2027. doi: 10.1182/blood-2009-08-241182

Malleret, B., Xu, F., Mohandas, N., Suwanarusk, R., Chu, C., Leite, J. A., et al. (2013). Significant biochemical, biophysical and metabolic diversity in circulating human cord blood reticulocytes. *PLoS One* 8:e76062. doi: 10.1371/journal.pone.0076062

Mankelow, T. J., Griffiths, R. E., Trompeter, S., Flatt, J. F., Cogan, N. M., Massey, E. J., et al. (2015). Autophagic vesicles on mature human reticulocytes explain phosphatidylserine-positive red cells in sickle cell disease. *Blood* 126, 1831–1834. doi: 10.1182/blood-2015-04-637702

Marquardt, D., Geier, B., and Pabst, G. (2015). Asymmetric lipid membranes: towards more realistic model systems. *Membranes* 5, 180–196. doi: 10.3390/membranes5020180

Matyash, V., Liebisch, G., Kurzchalia, T. V., Shevchenko, A., and Schwudke, D. (2008). Lipid extraction by methyl-tert-butyl ether for high-throughput lipidomics. *J. Lipid Res.* 49, 1137–1146. doi: 10.1194/jlr.D700041-JLR200

Migliaccio, G., and Migliaccio, A. R. (1987). Cloning of human erythroid progenitors (BFU-E) in the absence of fetal bovine serum. *Br. J. Haematol.* 67, 129–133. doi: 10.1111/j.1365-2141.1987.tb02315.x

Minetti, G., Achilli, C., Perotti, C., and Ciana, A. (2018). Continuous change in membrane and membrane-skeleton organization during development from proerythroblast to senescent red blood cell. *Front. Physiol.* 9:286. doi: 10.3389/fphys.2018.00286

Moessinger, C., Klizaite, K., Steinhagen, A., Philippou-Massier, J., Shevchenko, A., Hoch, M., et al. (2014). Two different pathways of phosphatidylcholine synthesis, the kennedy pathway and the lands cycle, differentially regulate cellular triacylglycerol storage. *BMC Cell Biol.* 15:43. doi: 10.1186/s12860-014-0043-3

Mohandas, N., and Gallagher, P. G. (2008). Red cell membrane: past, present, and future. *Blood* 112, 3939–3948. doi: 10.1182/blood-2008-07-161166

Nebe, T. B. F., Bruegel, M., Fiedler, G. M., Gutensohn, K., Heimpel, H., Krebs, N., et al. (2011). Multicentric determination of reference ranges for automated blood counts. *J. Lab. Med.* 35, 1–25.

Penberthy, K. K., and Ravichandran, K. S. (2016). Apoptotic cell recognition receptors and scavenger receptors. *Immunol. Rev.* 269, 44–59. doi: 10.1111/imr.12376

Plasenzotti, R., Stoiber, B., Posch, M., and Windberger, U. (2004). Red blood cell deformability and aggregation behaviour in different animal species. *Clin. Hemorheol. Microcirc.* 31, 105–111.

Quinn, P. J., Rainteau, D., and Wolf, C. (2009). Lipidomics of the red cell in diagnosis of human disorders. *Methods Mol. Biol.* 579, 127–159. doi: 10.1007/978-1-60761-322-0_7

Schink, K. O., Raiborg, C., and Stenmark, H. (2013). Phosphatidylinositol 3-phosphate, a lipid that regulates membrane dynamics, protein sorting and cell signalling. *Bioessays* 35, 900–912. doi: 10.1002/bies.201300064

Shah, S., Huang, X., and Cheng, L. (2014). Concise review: stem cell-based approaches to red blood cell production for transfusion. *Stem Cells Transl. Med.* 3, 346–355. doi: 10.5966/sctm.2013-0054

Silvius, J. R. (2003). Role of cholesterol in lipid raft formation: lessons from lipid model systems. *Biochim. Biophys. Acta* 1610, 174–183. doi: 10.1016/s0005-2736(03)00016-6

Simons, K., and Ikonen, E. (2000). How cells handle cholesterol. *Science* 290, 1721–1726. doi: 10.1126/science.290.5497.1721

Slotte, J. P. (2016). The importance of hydrogen bonding in sphingomyelin's membrane interactions with co-lipids. *Biochim. Biophys. Acta* 1858, 304–310. doi: 10.1016/j.bbamem.2015.12.008

Soupene, E., Kemaladewi, D. U., and Kuypers, F. A. (2008). ATP8A1 activity and phosphatidylserine transbilayer movement. *J. Receptor Ligand. Channel Res.* 1, 1–10. doi: 10.2147/jrlcr.s3773

Soupene, E., and Kuypers, F. A. (2012). Phosphatidylcholine formation by LPCAT1 is regulated by Ca(2+) and the redox status of the cell. *BMC Biochem.* 13:8. doi: 10.1186/1471-2091-13-8

Triebl, A., Trotzmuller, M., Hartler, J., Stojakovic, T., and Kofeler, H. C. (2017). Lipidomics by ultrahigh performance liquid chromatography-high resolution mass spectrometry and its application to complex biological samples. *J. Chromatogr. B Analyt. Technol. Biomed. Life Sci* 1053, 72–80. doi: 10.1016/j.jchromb.2017.03.027

van Meer, G. (2005). Cellular lipidomics. *EMBO J.* 24, 3159–3165. doi: 10.1038/sj.emboj.7600798

Wang, L., Tsai, M., Manson, J. E., Djousse, L., Gaziano, J. M., Buring, J. E., et al. (2011). Erythrocyte fatty acid composition is associated with the risk of hypertension in middle-aged and older women. *J. Nutr.* 141, 1691–1697. doi: 10.3945/jn.111.138867

Wang, Z., Cao, L., Su, Y., Wang, G., Wang, R., Yu, Z., et al. (2014). Specific macrothrombocytopenia/hemolytic anemia associated with sitosterolemia. *Am. J. Hematol.* 89, 320–324. doi: 10.1002/ajh.23619

Wilson, M. C., Trakarnsanga, K., Heesom, K. J., Cogan, N., Green, C., Toye, A. M., et al. (2016). Comparison of the proteome of adult and cord erythroid cells, and changes in the proteome following Reticulocyte maturation. *Mol. Cell Proteom.* 15, 1938–1946. doi: 10.1074/mcp.M115.057315

Wu, H., Bogdanov, M., Zhang, Y., Sun, K., Zhao, S., Song, A., et al. (2016). Hypoxia-mediated impaired erythrocyte lands' cycle is pathogenic for sickle cell disease. *Sci. Rep.* 6:29637. doi: 10.1038/srep29637

Zeuner, A., Martelli, F., Vaglio, S., Federici, G., Whitsett, C., and Migliaccio, A. R. (2012). Concise review: stem cell-derived erythrocytes as upcoming players in blood transfusion. *Stem Cells* 30, 1587–1596. doi: 10.1002/stem.1136

Zingariello, M., Bardelli, C., Sancillo, L., Ciaffoni, F., Genova, M. L., Girelli, G., et al. (2019). Dexamethasone predisposes human erythroblasts toward impaired lipid metabolism and renders their ex vivo expansion highly dependent on plasma lipoproteins. *Front. Physiol.* 10:281. doi: 10.3389/fphys.2019.00281

Conflict of Interest: The authors declare that the research was conducted in the absence of any commercial or financial relationships that could be construed as a potential conflict of interest.

frontiers in Physiology

MINI REVIEW
published: 10 January 2020
doi: 10.3389/fphys.2019.01629

Intracellular Ca^{2+} Concentration and Phosphatidylserine Exposure in Healthy Human Erythrocytes in Dependence on *in vivo* Cell Age

*Ingolf Bernhardt[1], Duc Bach Nguyen[1], Mauro C. Wesseling[1] and Lars Kaestner[2,3]**

[1]*Laboratory of Biophysics, Faculty of Natural Science and Technology, Saarland University, Saarbrücken, Germany,* [2]*Experimental Physics, Faculty of Natural Science and Technology, Saarland University, Saarbrücken, Germany,* [3]*Theoretical Medicine and Biosciences, Medical Faculty, Saarland University, Homburg, Germany*

After about 120 days of circulation in the blood stream, erythrocytes are cleared by macrophages in the spleen and the liver. The "eat me" signal of this event is thought to be the translocation of phosphatidylserine from the inner to the outer membrane leaflet due to activation of the scramblase, while the flippase is inactivated. Both processes are triggered by an increased intracellular Ca^{2+} concentration. Although this is not the only mechanism involved in erythrocyte clearance, in this minireview, we focus on the following questions: Is the intracellular-free Ca^{2+} concentration and hence phosphatidylserine exposure dependent on the erythrocyte age, i.e. is the Ca^{2+} concentration, progressively raising during the erythrocyte aging *in vivo*? Can putative differences in intracellular Ca^{2+} and exposure of phosphatidylserine to the outer membrane leaflet be measured in age separated cell populations? Literature research revealed less than dozen of such publications with vastly contradicting results for the Ca^{2+} concentrations but consistency for a lack of change for the phosphatidylserine exposure. Additionally, we performed reanalysis of published data resulting in an ostensive illustration of the situation described above. Relating these results to erythrocyte physiology and biochemistry, we can conclude that the variation of the intracellular free Ca^{2+} concentration is limited with 10 μM as the upper level of the concentration. Furthermore, we propose the hypothesis that variations in measured Ca^{2+} concentrations may to a large extent depend on the experimental conditions applied but reflect a putatively changed Ca^{2+} susceptibility of erythrocytes in dependence of *in vivo* cell age.

Keywords: red blood cells, aging, Ca^{2+} content, phosphatidylserine exposure, lysophosphatidic acid, flow cytometry

OPEN ACCESS

Edited by:
Anna Rita Migliaccio, Icahn School of Medicine at Mount Sinai, United States

Reviewed by:
Anneke Brand, Leiden University Medical Center, Netherlands
Donatienne Tyteca, de Duve Institute and Université catholique de Louvain, Belgium

****Correspondence:***
Lars Kaestner
lars_kaestner@me.com

Specialty section:
This article was submitted to Red Blood Cell Physiology, a section of the journal Frontiers in Physiology

Received: *29 August 2019*
Accepted: *24 December 2019*
Published: *10 January 2020*

Citation:
Bernhardt I, Nguyen DB, Wesseling MC and Kaestner L (2020) Intracellular Ca^{2+} Concentration and Phosphatidylserine Exposure in Healthy Human Erythrocytes in Dependence on in vivo Cell Age. Front. Physiol. 10:1629. doi: 10.3389/fphys.2019.01629

INTRODUCTION

The formation of erythrocytes named erythropoiesis takes about 7 days (Silbernagel and Despopoulus, 2007). It happens before birth in the yolk sac, liver, spleen, and bone marrow and after birth only in the red marrow of the plates and short bones (Dzierzak and Philipsen, 2013). From multipotent stem cells, erythroblasts first emerge, which still have a nucleus. After

erythroblasts have lost their nucleus and organelles, they are called reticulocytes and migrate into the blood stream. The normal lifespan of an erythrocyte is about 120 days. One of the first data analysis giving a result of about 120 days was published by Callender et al. (1945).

In a drop of human blood one can obviously find a composition of cells in all different ages. There is an age-dependent variation in their density. Young cells have a significantly lower density in comparison to old cells (Piomelli and Seaman, 1993). Based on this, it is possible to separate the erythrocytes into at least five fractions by density gradient centrifugation making use of, e.g., stractan (Ballas et al., 1986; Waugh et al., 1992) or Percoll (Lutz et al., 1992; Makhro et al., 2016). Although there are exceptions (Lew and Tiffert, 2013), this difference in density makes it possible to investigate cell physiological parameters of cell populations in dependence on the age of the cells.

It has been reported that physiological erythrocyte aging results in a decreased cell volume, size, and mean corpuscular volume (Nash and Wyard, 1980; Linderkamp and Meiselman, 1982; van Oss, 1982; Bosch et al., 1992). In addition, the 2,3-diphosphoglycerate/hemoglobin ratio (Samaja et al., 1990) and the deformability (Clark et al., 1983; Gifford et al., 2006) are reduced in aged erythrocytes. Further parameters are increased, such as mean corpuscular hemoglobin concentration (Bosch et al., 1992), glycated hemoglobin (Bunn et al., 1976), osmotic fragility (Rifkind et al., 1983), and creatine levels (Syllm-Rapoport et al., 1981). Seppi et al. (1991) showed that band 3 protein and membrane skeleton proteins undergo conformational changes and/or oxidation with increasing cell age. This was confirmed by Castellana et al. (1992). In contrast, Piccinini et al. (1995) reported that the oxidation state of membrane proteins does not seem to change during the erythrocyte life span. A decrease of the anti-oxidant defense-related activity when erythrocytes increase their age was reported by D'Alessandro et al. (2013). Ciana et al. (2004) described an increased Tyr-phosphorylation level of band 3 protein of old erythrocytes compared to younger ones under hypertonic conditions. Furthermore, it is well known that there is an age-dependent increase of the protein ratio of band 4.1a:4.1b proteins, which is regarded as a molecular clock. Measurements of the 4.1a:4.1b ratio make it possible to determine differences in cell age of erythrocytes separated in fractions (Mueller et al., 1987; Inaba and Maede, 1988; Kaestner and Minetti, 2017).

The factors, crucial for the aging process and the mechanisms for the removal of damaged or old erythrocytes from the circulation are not yet fully understood. However, once erythrocytes reach a threshold for intracellular free Ca^{2+}, the associated phosphatidylserine exposure leads to erythrocyte clearance (Kuypers and de Jong, 2004; Bosman et al., 2005; Bogdanova et al., 2013; de Back et al., 2014). However, it is unclear if the way to the increased Ca^{2+} concentration is a continuous process accompanying the erythrocyte aging or a rather rapid process directly triggering the removal.

Here, we provide the context and a literature review about reports investigating if there is an *in vivo* age dependence of the intracellular Ca^{2+} concentration and phosphatidylserine exposure in healthy human erythrocytes. The focus on these parameters is by no means a statement that this process is regarded as the most important in erythrocyte clearance. We focus on healthy human erythrocytes and refer to primarily *in vivo* conditions, explicitly excluding processes occurring during erythrocyte storage in particular storage lesions (Flatt et al., 2014; Petkova-Kirova et al., 2018).

THE INTRACELLULAR Ca^{2+} CONCENTRATION, PHOSPHATIDYLSERINE EXPOSURE, AND THEIR DEPENDENCE OF ERYTHROCYTE AGE

Historically, first investigations described an increase of the total intracellular Ca^{2+} concentration in the process of human erythrocyte aging. La Celle et al. (1973) reported an increase from 60 μM in young erythrocytes to 100 μM in old ones, whereas Shiga et al. (1985) found only an increase from 15 to 33 μM Ca^{2+}. However, physiologically important is the free cytosolic Ca^{2+} concentration, which is the portion of Ca^{2+} freely available to the cytosolic and membrane proteins (Tiffert et al., 2002), i.e., the portion of Ca^{2+} acting as messenger in cellular signaling. In all following statements, the Ca^{2+} concentration refers to the free intracellular Ca^{2+} concentration.

The intracellular Ca^{2+} concentration of erythrocytes can be determined under physiological conditions by different methods such as Ca^{2+} chelators and atomic absorption spectroscopy. Fluorescent indicators for Ca^{2+} such as Fura-2, Fluo-3, and Fluo-4 have been commonly applied (for Fura-2 see, e.g., Romero et al., 1997). However, Kaestner et al. (2006) pointed out that the application of Fura-2 is problematic in human erythrocytes because its excitation and emission properties are distorted by the absorption of hemoglobin. Additionally, ultraviolet light as required for the excitation of Fura-2 may photo-convert hemoglobin into fluorescent photoproducts (Kaestner et al., 2006). Therefore, the quantitative measurement of the free intracellular Ca^{2+} concentration of individual erythrocytes is not possible with the ratiometric Ca^{2+} fluorophores Fura-2 or Indo-1 (Kaestner et al., 2006). However, it appears reasonable to determine the average physiological intracellular Ca^{2+} concentration in human erythrocytes to be below 100 nM (Tiffert et al., 1993; Tiffert and Lew, 1997). Although the single-cell measurements based on the fluorescent dyes Fluo-3 and Fluo-4 do not allow a quantitative measurement of the Ca^{2+} concentration (Kaestner et al., 2006), they reveal a high intercellular variation (Wang et al., 2014). A cell is typically regarded to show an increased intracellular Ca^{2+} concentration, when fluorescence intensity increase exceeds three times the standard deviation of the fluorescence recorded during control conditions (Wang et al., 2013).

The in principle low intracellular Ca^{2+} concentration represents the balance between the passive Ca^{2+} influx and the active Ca^{2+} extrusion (Ca^{2+} efflux) realized by the Ca^{2+} pump. The passive Ca^{2+} influx is mediated through low capacity transport pathways with carrier properties (Ferreira and Lew, 1977; Desai et al., 1991), ion channels (Kaestner et al., 2020) and a putative "leak." Interestingly, Lew et al. (2007) found that the plasma membrane Ca^{2+} pump activity declines with erythrocyte age. In a variety of reports, we have described possible mechanisms leading to an increased intracellular Ca^{2+} content of erythrocytes, mainly based on the activity of ion channels (Kaestner et al., 2000; Kaestner and Bernhardt, 2002; Wagner-Britz et al., 2013; Fermo et al., 2017; Danielczok et al., 2017; Rotordam et al., 2019; for a recent review see Kaestner et al., 2020).

Increase in free intracellular Ca^{2+} activates the lipid scramblase (see e.g. Woon et al., 1999; Lang et al., 2004, 2005; Nguyen et al., 2011). This lipid translocator in turn mediates a significant exposure of phosphatidylserine on the outer membrane leaflet (Woon et al., 1999). At the same time the flippase, which actively (ATP-dependent) transports phophatidylserine from the outer membrane leaflet to the inner one is inhibited (Devaux et al., 2008). Although the flippase shows an almost complete inactivation at a Ca^{2+} concentration of 400 nM (Bitbol et al., 1987), for physiological Ca^{2+} concentrations, total suppression of flippase activity leaves the membrane asymmetry undisturbed (Arashiki et al., 2016). In contrast, for scramblase, the values for half maximal activation were determined by different studies with varying methodologies and slightly different results. Values varied between approximately 30 μM determined in liposomes (Stout et al., 1989) and 70 μM measured in erythrocyte ghosts (Woon et al., 1999). Considering the Hill coefficient describing the steepness of the slope for the activation and the predominant role of the scramblase shown by the application of the specific scramblase inhibitor R5421 (Wesseling et al., 2016a), an enhanced free Ca^{2+} content above 10 μM in erythrocytes will result in an increase in phosphatidylserine on the outer membrane leaflet (Bogdanova et al., 2013). An increase in phosphatidylserine of the outer membrane leaflet of the erythrocyte we regard as any Annexin-V-fluorophore signal above zero, practically this is regarded to be the case when the signal exceeds the average background value by two times the noise amplitude.

After this methodological and molecular-mechanistical view on the intracellular Ca^{2+} concentration and phosphatidylserine exposure, we want to take a closer look on the cell age dependence of these parameters. Therefore, we searched the literature for investigations of intracellular-free Ca^{2+} and phosphatidylserine exposure measurements but excluded *in vitro* and artificial aging and focused exclusively on healthy human erythrocytes.

Concerning the free intracellular Ca^{2+}, it has been reported that older erythrocytes contain an increased free intracellular Ca^{2+} concentration (Aiken et al., 1992; Romero et al., 1997). Combining a fluorinated calcium chelator probe (5,5'-difluoroBAPTA) and fluorine magnetic resonance (^{19}F-NMR) technique Aiken et al. (1992) found for the young and old cell fraction of erythrocytes a mean intracellular-free Ca^{2+}concentration of 62 and 221 nM, respectively.

In contrast, for the very young red blood cells, the reticulocytes de Haro et al. (1985) reported an increased intracellular Ca^{2+} concentration compared with mature erythrocytes, whereas Wiley and Shaller (1977) measured that reticulocytes are more permeable to Ca^{2+} than mature cells but their intracellular Ca^{2+} concentration is not increased.

Wesseling et al. (2016b) reported a lack of difference in the intracellular Ca^{2+} concentration and in the phosphatidylserine exposure in dependence on erythrocyte age (based on density separated erythrocytes).

Taken all these reports together, we have a very controversial situation. To further illustrate this conflicting situation, we present a reanalysis of previously published data (Wesseling et al., 2016b). The percentage of erythrocytes showing an enhanced Ca^{2+} concentration as well as phosphatidylserine exposure present a linear relation relative to the density centrifugation fractions representing erythrocyte age. The regression values R^2 for Ca^{2+} and phosphatidylserine of 0.94 and 0.92, respectively, speak for themselves (**Figure 1A**). Surprisingly, in a different set of experiments under conditions with similar characteristics (**Figure 1B**), the intracellular Ca^{2+} was linear decreasing (R^2 of 0.92), while the phosphatidylserine exposure was increasing (R^2 of 0.80). The only differences between the two separate measurements (A and B) were the donors (but all healthy) and the composition of the solutions (see legend of **Figure 1**). However, the major point is that the slope of the linear regressions in both conditions (A and B) failed to be significantly different from zero, i.e., albeit we have very nice (high R^2) regression lines for different conditions, the data from Wesseling et al. (2016b) show no dependence of intracellular Ca^{2+} concentration and phosphatidylserine exposure from erythrocyte age. In other words: Although the panels of **Figure 1** seem contradicting, from a statistical point of view they are consistent.

For phosphatidylserine exposure in erythrocytes, Franco et al. (2013) reported independence on cell age. Only after extended storage of erythrocytes for 2 days in Ringer solution (cp. **Figure 1B**), a significant enhancement in the intracellular Ca^{2+} concentration and also an increase in the phosphatidylserine translocation with cell age could be observed (Ghashghaeinia et al., 2012). The latter result was confirmed by Wesseling et al. (2016b). As this resembles storage conditions it cannot be regarded as reflecting *in vivo* conditions. In contrast, short-time (30 min) incubation experiments showed that there was neither significant difference of the Ca^{2+} content (see above) nor a phosphatidylserine translocation depending on cell age when comparing age populations in pairs (Wesseling et al., 2016b).

Summarizing this section, it is still elusive if there is an alteration of intracellular Ca^{2+} in dependence of erythrocyte age (several conflicting reports). However, since there is

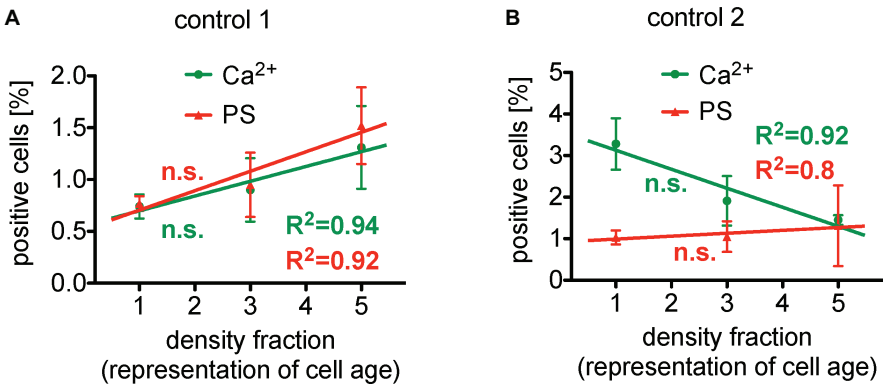

FIGURE 1 | Reanalysis of data initially presented in Wesseling et al. (2016b). In the original publication, all fractions were only compared in pairs, while here we followed the approach to plot (and analyze) the measured effect in dependence of the cell age. Both panels present the situation under control conditions (without pharmalogical stimulation). **(A)** The percentage of erythrocytes showing increased Ca^{2+} content as well as phosphatidylserine exposure depicts a linear behavior in dependence of cell age with a very good regression, R^2 given in the figure. However, the slope of these linear regressions failed to be significantly different from zero, i.e., failed to show a significant change. **(B)** The percentage of erythrocytes showing decreased Ca^{2+} content, while phosphatidylserine exposure depicts a linear increase in dependence of cell age, again, with a very good regression, R^2 given in the figure. The slope of both linear regressions also failed to be significantly different from zero, i.e., failed to show a significant change. Furthermore, comparing the particular fractions between the two measurements **(A,B)** applying an unpaired *t*-test with Welch's correction (unequal SD values), none of the fractions showed a significant difference ($p > 0.05$). Both measurements **(A,B)** were performed in the same laboratory. Blood samples were given from healthy sportsmen (Department of Sports Medicine) with an age between 18 and 36 years. Each data point consists of three donors (not identical between **A** and **B**) and for each donor and condition, 90,000 cells were analyzed by flow cytometry. The only obvious difference is the composition of the solutions. [**(A)** in mM]: 145 NaCl, 7.5 KCl, 2 $CaCl_2$, 10 glucose, 10 HEPES, pH 7.4 (Tyrode solution); [**(B)** in mM]: 125 NaCl, 5 KCl, 1 $CaCl_2$, 1 $MgCl_2$, 5 glucose, 32 HEPES, pH 7.4 (Ringer solution). **(A)** A reprint from Bernhardt et al. (2019).

consistence in the reports concerning phosphatidylserine exposure (no change with cell age), we can conclude that the variation of the free intracellular Ca^{2+} concentration does not exceed 10 μM, which resembles the onset of the scramblase activation while the flippase is inactivated (Bogdanova et al., 2013).

STIMULATION OF Ca^{2+} ENTRY AND INCREASED PHOSPHATIDYLSERINE EXPOSURE IN DEPENDENCE ON ERYTHROCYTE AGE

Pharmacologically, the Ca^{2+} entry into erythrocytes can be stimulated by lysophosphatidic acid or prostaglandin E_2 (Li et al., 1996; Yang et al., 2000; Kaestner et al., 2004). Although the process itself is well known, the molecular signaling leading to the Ca^{2+} entry is still controversial (Yang et al., 2000; Kaestner et al., 2004; Wagner-Britz et al., 2013). Both substances (lysophosphatidic acid and prostaglandin E_2) are released from activated platelets and therefore resemble a physiological stimulation occurring *in vivo* (in healthy humans). Under mechanical stress, prostaglandin E_2 can even be released by the erythrocytes themselves (Oonishi et al., 1998). However, we were able to demonstrate that after activation of erythrocytes (e.g., by lysophosphatidic acid) most erythrocytes with increased Ca^{2+} content also responded with phosphatidylserine exposure (Nguyen et al., 2011).

There is a debate in the literature whether erythrocytes depict a cell age dependency in the response of lysophosphatidic acid stimulated (see also above). To this end, we present a reanalysis of data by Wesseling et al. (2016b) as a plot depicting age dependence. After stimulation of the erythrocytes with lysophosphatidic acid, the cellular behavior is quite complex. **Figure 2A** shows the response after 15 min of 2.5 μM lysophosphatidic acid stimulation. While the Ca^{2+} content relate inversely proportional to erythrocyte age (slope significantly different from zero), phosphatidylserine positive erythrocytes depict a rather quadratic dependence on cell age.

Interestingly, in reticulocytes lysophosphatidic acid could not activate any measurable Ca^{2+} signals (Wang et al., 2013). To judge the quadratic age dependence of the phosphatidylserine exposure, we reanalyzed a more direct stimulation also published by Wesseling et al. (2016b). **Figure 2B** shows the percentage of phosphatidylserine exposing cells upon massive Ca^{2+} increase in all erythrocytes by use of the Ca^{2+} ionophore A23187 (dark red circles in **Figure 2B**) and by stimulation of protein kinase Cα (orange triangles in **Figure 2B**) by phorbol-12 myristate-13 acetate (for details, see **Figure 2**). Although different in amplitude, both stimulations also result in a quadratic response relative to the erythrocyte age (meaning the medium fraction always displays the lowest number in phosphatidylserine positive erythrocytes). For a thorough discussion of the relationship between intracellular Ca^{2+} increase and phosphatidylserine exposure upon phorbol-12 myristate-13 acetate stimulation of erythrocytes, we refer to Nguyen et al. (2011) and Bernhardt et al. (2019).

Although we have no mechanistic hypothesis for this quadratic response, the consistency along the various types of physiological [lysophosphatidic acid; concentrations of 1–5 μM when platelets

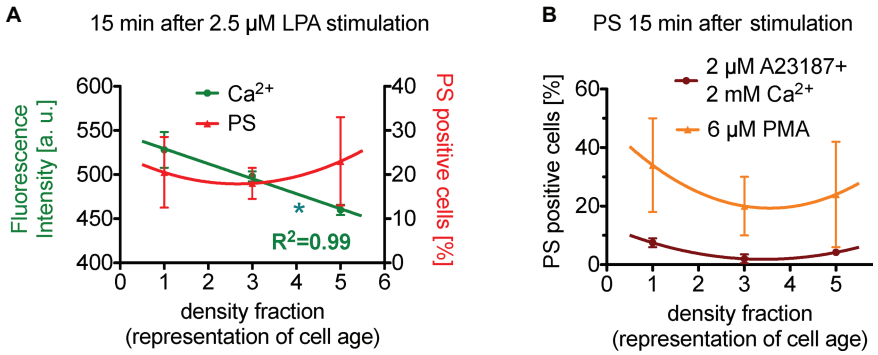

FIGURE 2 | Reanalysis of data initially presented in Wesseling et al. (2016b). In the original publication, all fractions were only compared in pairs, while here we followed the approach to plot (and analyze) the measured effect in dependence of the cell age. **(A)** Presents the situation after 15 min of stimulation with lysophosphatidic acid (LPA). While the Ca^{2+} concentration seems to relate inversely proportional to erythrocyte age (slope is significant different from zero, $p < 0.05$ is marked with *), phosphatidylserine positive cells show a rather quadratic dependence on cell age. **(B)** Presents exclusively the phosphatidylserine exposure under more direct stimulations (15 min), namely the direct increase in intracellular Ca^{2+} in all cells by application of the Ca^{2+} ionophore A23187 in 2 mM Ca^{2+} containing solutions (dark red circles) and by a direct Ca^{2+}-independent activation of protein kinase Cα (PKCα, orange triangles) by phorbol-12 myristate-13 acetate (PMA, an unspecific activator of conventional and novel PKCs but PKCα is the sole PKC of these 2 groups found in erythrocytes). Although different in amplitude, both stimulations result in a quadratic dependence on cell age. Blood samples were given from healthy sportsmen (Department of Sports Medicine) with an age between 18 and 36 years. Each data point consists of three donors and for each donor and condition 90,000 cells were analyzed by flow cytometry. For a complete dataset on the different stimulation modes, see Wesseling et al. (2016b). **(A)** A reprint from Bernhardt et al. (2019).

are activated (Eichholtz et al., 1993)] and artificial (Ca^{2+} ionophore, phorbol-12 myristate-13 acetate) stimulation indicates such a dependence as a general property.

INTERPRETATIONS, CONCLUSIONS, AND OUTLOOK

We cannot solve the question whether the Ca^{2+} content of human erythrocytes is related to cellular aging at all. Nevertheless, intracellular Ca^{2+} is very likely be increased immediately prior erythrocyte clearance but since phosphatidylserine exposing erythrocytes are quickly cleared (Kuypers and de Jong, 2004; Bosman et al., 2005; Bogdanova et al., 2013; de Back et al., 2014) it is experimentally challenging to detect/measure the cells with increased phosphatidylserine exposure (see below for detailed discussion).

An initial explanation for varying and contradicting results might be caused by the measurement technique: While microscopy examines erythrocytes settled on a coverslip in a measurement chamber, the cells do not experience a serious mechanical challenge and therefore microscopy can be regarded as a rather gentle technique. In contrast, in flow cytometry measurements, the erythrocytes experience severe mechanical forces, like high pressure and significant shear forces (Minetti et al., 2013). As a result, a decent number of erythrocytes with enhanced Ca^{2+}, which are more fragile, simply may lyse when passing the flow cytometer. This means the number of cells with increased intracellular Ca^{2+} might by systematically decreased in flow cytometry experiments. The variety in specifications of flow cytometers may even add to the heterogeneity in measurements throughout different laboratories.

Another more conceptual interpretation is based on the above described findings that (1) increase in the intracellular Ca^{2+} concentration and phosphatidylserine exposure of erythrocytes increases with storage time in physiological (Ca^{2+} containing) solutions in an age-dependent manner (Ghashghaeinia et al., 2012) and (2) *in vivo*, phosphatidylserine exposing cells are cleared by macrophages in the liver and the spleen (Kuypers and de Jong, 2004; Bosman et al., 2005; de Back et al., 2014). Therefore, *in vivo,* these cells are filtered out, making putative age differences invisible. Older cells may have a higher susceptibility for Ca^{2+} (maybe just by a decreased Ca^{2+} pump activity) and not necessarily an increased Ca^{2+} concentration. The measurements *in vitro* may then reflect the experimental conditions addressing this susceptibility (cp. **Figure 1**), which is likely to be modulated by a plethora of conditions and parameters, such as type of anticoagulant, temperature and temperature changes, modulations in gravity (extend and time of centrifugation), pH value, mechanical stimulation (vortexing), composition of solution (salts, additives, solvents), and other metabolic conditions, just to name a few.

The Ca^{2+} concentration we measure might thus be the product of an (*in vivo*) susceptibility for Ca^{2+} and the (*in vitro*) experimental conditions. Our measurements may therefore reflect the erythrocyte susceptibility for Ca^{2+} if we manage to keep the experimental conditions constant, which can be achieved in a laboratory but makes direct comparison of independent studies of different laboratories almost impossible. Furthermore, there might be conditions (in addition to the absence of external Ca^{2+}) that do not act on the susceptibility for Ca^{2+} (factor zero in the above-mentioned product).

This hypothesis has the potential to explain the greatly variable and partly contradicting experimental results concerning the dependence of intracellular Ca^{2+} in erythrocytes in dependence on cell age. Previous observations of highly variable Ca^{2+} concentrations after blood sample shipments (Hertz et al., 2017) support this hypothesis. However, further investigations are required to substantiate the hypothesis and continue to explore the phenomenon of the variability of intracellular Ca^{2+} measurements.

Finally, the conflicting reports reveal once more the need for intralaboratory and interlaboratory validation of protocols by quality controls in particular for the measurement of intracellular Ca^{2+} as we previously proposed for erythrocyte research in general (Minetti et al., 2013).

AUTHOR CONTRIBUTIONS

All authors listed have made a substantial, direct and intellectual contribution to the work, and approved it for publication.

FUNDING

The research leading to these results has received funding from the European Framework "Horizon 2020" under grant agreement number 675115 (RELEVANCE). Additionally, we acknowledge support by the Deutsche Forschungsgemeinschaft (DFG, German Research Foundation) and Saarland University within the funding programme Open Access Publishing.

REFERENCES

Aiken, N. R., Satterlee, J. D., and Galey, W. R. (1992). Measurement of intracellular Ca^{2+} in young and old human erythrocytes using F-NMR spectroscopy. *Biochim. Biophys. Acta* 1136, 155–160.

Arashiki, N., Saito, M., Koshino, I., Kamata, K., Hale, J., Mohandas, N., et al. (2016). An unrecognized function of cholesterol: regulating the mechanism controlling membrane phospholipid asymmetry. *Biochemistry* 55, 3504–3513. doi: 10.1021/acs.biochem.6b00407

Ballas, S. K., Flynn, J. C., Pauline, L. A., and Murphy, D. L. (1986). Erythrocyte Rh antigens increase with red cell age. *Am. J. Hematol.* 23, 19–24. doi: 10.1002/ajh.2830230104

Bernhardt, I., Wesseling, M. C., Nguyen, D. B., and Kaestner, L. (2019). "Red blood cells actively contribute to blood coagulation and thrombus formation" in *Erythrocyte*. ed. A. Tombak (London: IntechOpen).

Bitbol, M., Fellmann, P., Zachowski, A., and Devaux, P. F. (1987). Ion regulation of phosphatidylserine and phosphatidylethanolamine outside-inside translocation in human erythrocytes. *Biochim. Biophys. Acta* 904, 268–282.

Bogdanova, A., Makhro, A., Wang, J., Lipp, P., and Kaestner, L. (2013). Calcium in red blood cells - a perilous balance. *Int. J. Mol. Sci.* 14, 9848–9872. doi: 10.3390/ijms14059848

Bosch, F. H., Werre, J. M., Roerdinkholder-Stoelwinder, B., Huls, T. H., Willekens, F. L., and Halle, M. R. (1992). Characteristics of red blood cell populations fractionated with a combination of counterflow centrifugation and Percoll separation. *Blood* 79, 254–260. doi: 10.1182/blood.V79.1.254.254

Bosman, G. J. C. G. M., Willekens, F. L. A., and Werre, J. M. (2005). Erythrocyte aging: a more than superficial resemblance to apoptosis? *Cell. Physiol. Biochem.* 16, 1–8. doi: 10.1159/000087725

Bunn, H. F., Haney, D. N., Kamin, S., Gabbay, K. H., and Gallop, P. M. (1976). The biosynthesis of human haemoglobin A1c. Slow glycosylation of haemoglobin *in vivo*. *J. Clin. Invest.* 57, 1652–1659. doi: 10.1172/JCI108436

Callender, S. T., Powell, E. O., and Witts, J. C. (1945). The life-span of the red cell in man. *J. Pathol. Bacteriol.* 57, 129–139. doi: 10.1002/path.1700570116

Castellana, M. A., Piccini, G., Minetti, G., Seppi, C., Balduini, C., and Brovelli, A. (1992). Oxidation of membrane proteins and functional activity of band 3 in human red cell senescence. *Arch. Gerontol. Geriatr.* 1, 101–110.

Ciana, A., Minetti, G., and Balduini, C. (2004). Phosphotyrosine phosphatases acting on band 3 in human erythrocytes of different age: PTP1B processing during cell ageing. *Bioelectrochemistry* 62, 169–173. doi: 10.1016/j.bioelechem.2003.07.004

Clark, M. R., Mohandas, N., and Shohet, S. B. (1983). Osmotic gradient ektacytometry: comprehensive characterization of red cell volume and surface maintenance. *Blood* 61, 899–910. doi: 10.1182/blood.V61.5.899.899

D'Alessandro, A., Blasi, B., D'Amici, G. M., Marrocco, C., and Zolla, L. (2013). Red blood cell subpopulations in freshly drawn blood: application of proteomics and metabolomics to a decades-long biological issue. *Blood Transfus.* 11, 75–87. doi: 10.2450/2012.0164-11

Danielczok, J., Hertz, L., Ruppenthal, S., Kaiser, E., Petkova-Kirova, P., Bogdanova, A., et al. (2017). Does erythropoietin regulate TRPC channels in red blood cells? *Cell. Physiol. Biochem.* 41, 1219–1228. doi: 10.1159/000464384

de Back, D., Kostova, E., van Kraaij, M., van den Berg, T., and van Bruggen, R. (2014). Of macrophages and red blood cells; a complex love story. *Front. Physiol.* 5:9. doi: 10.3389/fphys.2014.00009

de Haro, C., de Herreros, A. G., and Ochoa, S. (1985). Protein phosphorylation and translational control in reticulocytes: activation of the heme-controlled translational inhibitor by calcium ions and phospholipid. *Curr. Top. Cell. Regul.* 27, 63–81.

Desai, S. A., Schlesinger, P. H., and Krogstad, D. J. (1991). Physiologic rate of carrier-mediated Ca^{2+} entry matches active extrusion in human erythrocytes. *J. Gen. Physiol.* 98, 349–364. doi: 10.1085/jgp.98.2.349

Devaux, P. F., Herrmann, A., Ohlwein, N., and Kozlov, M. M. (2008). How lipid flippases can modulate membrane structure. *Biochim. Biophys. Acta* 1778, 1591–1600. doi: 10.1016/j.bbamem.2008.03.007

Dzierzak, E., and Philipsen, S. (2013). Erythropoiesis: development and differentiation. *Cold Spring Harb. Perspect. Med.* 3:a011601. doi: 10.1101/cshperspect.a011601

Eichholtz, T., Jalink, K., Fahrenfort, I., and Moolenaar, W. H. (1993). The bioactive phospholipid lysophosphatidic acid is released from activated platelets. *Biochem. J.* 291, 677–680. doi: 10.1042/bj2910677

Fermo, E., Bogdanova, A. Y., Petkova-Kirova, P., Zaninoni, A., Marcello, A. P., Makhro, A., et al. (2017). 'Gardos Channelopathy': a variant of hereditary stomatocytosis with complex molecular regulation. *Sci. Rep.* 7:1744. doi: 10.1038/s41598-017-01591-w

Ferreira, H. G., and Lew, V. L. (1977). "Passive Ca transport and cytoplasmic Ca buffering in intact red cells" in *Membrane transport in red cells*. eds. J. C. Ellory and V. L. Lew (London: Academic Press), 53–91.

Flatt, J. F., Bawazir, W. M., and Bruce, L. J. (2014). The involvement of cation leaks in the storage lesion of red blood cells. *Front. Physiol.* 5:214. doi: 10.3389/fphys.2014.00214

Franco, R. S., Puchulu-Campanella, M. E., Barber, L. A., Palascak, M. B., Joiner, C. H., Low, P. S., et al. (2013). Changes in the properties of normal human red blood cells during *in vivo* aging. *Am. J. Hematol.* 88, 44–51. doi: 10.1002/ajh.23344

Ghashghaeinia, M., Cluitmans, J. C., Akel, A., Dreischer, D., Toulany, M., Köberle, M., et al. (2012). The impact of erythrocyte age on eryptosis. *Br. J. Haematol.* 157, 606–614. doi: 10.1111/j.1365-2141.2012.09100.x

Gifford, S. C., Derganc, J., Shevkoplyas, S. S., Yoshida, T., and Bitensky, M. W. (2006). A detailed study of time-dependent changes in human red blood cells: from reticulocyte maturation to erythrocyte senescence. *Br. J. Haematol.* 135, 395–404. doi: 10.1111/j.1365-2141.2006.06279.x

Hertz, L., Huisjes, R., Llaudet-Planas, E., Petkova-Kirova, P., Makhro, A., Danielczok, J., et al. (2017). Is increased intracellular calcium in red blood cells a common component in the molecular mechanism causing anemia? *Front. Physiol.* 8:673. doi: 10.3389/fphys.2017.00673

Inaba, M., and Maede, Y. (1988). Correlation between protein 4.1a/4.1b ratio and erythrocyte life span. *Biochim. Biophys. Acta* 944, 256–264.

Kaestner, L., and Bernhardt, I. (2002). Ion channels in the human red blood cell membrane: their further investigation and physiological relevance. *Bioelectrochemistry* 55, 71–74. doi: 10.1016/S1567-5394(01)00164-5

Kaestner, L., Bogdanova, A., and Egee, S. (2020). Calcium channels and calcium-regulated channels in human red blood cells. *Adv. Exp. Med. Biol.* 2020, 625–648. doi: 10.1007/978-3-030-12457-1_25

Kaestner, L., Christophersen, P., Bernhardt, I., and Bennekou, P. (2000). Properties of the non-selective voltage-activated cation channel in the human red blood cell membrane. *Bioelectrochemistry* 52, 117–125. doi: 10.1016/S0302-4598(00)00110-0

Kaestner, L., and Minetti, G. (2017). The potential of erythrocytes as cellular aging models. *Cell Death Differ.* 24, 1475–1477. doi: 10.1038/cdd.2017.100

Kaestner, L., Tabellion, W., Lipp, P., and Bernhardt, I. (2004). Prostaglandin E2 activates channel-mediated calcium entry in human erythrocytes: an indicator for a blood clot formation supporting process. *Thromb. Haemost.* 92, 1269–1272. doi: 10.1160/TH04-06-0338

Kaestner, L., Tabellion, W., Weiss, E., Bernhardt, I., and Lipp, P. (2006). Calcium imaging of individual erythrocytes: problems and approaches. *Cell Calcium* 39, 13–19. doi: 10.1016/j.ceca.2005.09.004

Kuypers, F. A., and de Jong, K. (2004). The role of phosphatidylserine in recognition and removal of erythrocytes. *Cell. Mol. Biol.* 50, 147–158.

La Celle, P. L., Kirkpatrick, F. H., and Udkow, M. P. (1973). "Relation of altered deformability, ATP, DPG and Ca^{++} concentration in senescent erythrocytes" in *Recent advances in membrane and metabolic research*. eds. E. Gerlach, K. Meser, E. Deutsch, and W. Wilmann (Stuttgart: Thieme), 49–52.

Lang, F., Gulbins, E., Szabo, I., Leppel-Wienhues, A., Huber, S. M., Duranton, C., et al. (2004). Cell volume and the regulation of apoptotic cell death. *J. Mol. Recognit.* 17, 473–480. doi: 10.1002/jmr.705

Lang, K. S., Lang, P. A., Bauer, C., Duranton, C., Wieder, T., Huber, S. M., et al. (2005). Mechanisms of suicidal erythrocyte death. *Cell. Physiol. Biochem.* 15, 195–202. doi: 10.1159/000086406

Lew, V. L., Daw, N., Etzion, Z., Tiffert, T., Muoma, A., Vanagas, L., et al. (2007). Effects of age-dependent membrane transport changes on the homeostasis of senescent human red blood cells. *Blood* 110, 1334–1342. doi: 10.1182/blood-2006-11-057232

Lew, V. L., and Tiffert, T. (2013). The terminal density reversal phenomenon of aging human red blood cells. *Front. Physiol.* 4:171. doi: 10.3389/fphys.2013.00171

Li, Q., Jungmann, V., Kiyatkin, A., and Low, P. S. (1996). Prostaglandin E2 stimulates a Ca^{2+}-dependent K+ channel in human erythrocytes and alters cell volume and filterability. *J. Biol. Chem.* 271, 18651–18656. doi: 10.1074/jbc.271.31.18651

Linderkamp, O., and Meiselman, H. J. (1982). Geometric, osmotic, and membrane mechanical properties of density-separated human red cells. *Blood* 59, 1121–1127. doi: 10.1182/blood.V59.6.1121.1121

Lutz, H. U., Stammler, P., Fasler, S., Ingold, M., and Fehr, J. (1992). Density separation of human red blood cells on self-forming Percoll gradients: correlation with cell age. *Biochim. Biophys. Acta* 1116, 1–10. doi: 10.1016/0304-4165(92)90120-j

Makhro, A., Huisjes, R., Verhagen, L. P., Mañú-Pereira, M. M., Llaudet-Planas, E., Petkova-Kirova, P., et al. (2016). Red cell properties after different modes of blood transportation. *Front. Physiol.* 7:288. doi: 10.3389/fphys.2016.00288

Minetti, G., Egee, S., Mörsdorf, D., Steffen, P., Makhro, A., Achilli, C., et al. (2013). Red cell investigations: art and artefacts. *Blood Rev.* 27, 91–101. doi: 10.1016/j.blre.2013.02.002

Mueller, T. J., Jackson, C. W., Dockter, M. E., and Morrison, M. (1987). Membrane skeletal alterations *in vivo* mouse red cell aging. Increase in the band 4.1a:4.1b ratio. *J. Clin. Invest.* 79, 492–499. doi: 10.1172/JCI112839

Nash, G. B., and Wyard, S. J. (1980). Changes in surface area and volume measured by micropipette aspiration of erythrocytes aging *in vivo*. *Biorheology* 17, 478–484.

Nguyen, D. B., Wagner-Britz, L., Maia, S., Steffen, P., Wagner, C., Kaestner, L., et al. (2011). Regulation of phosphatidylserine exposure in red blood cells. *Cell. Physiol. Biochem.* 28, 847–856. doi: 10.1159/000335798

Oonishi, T., Sakashita, K., Ishioka, N., Suematsu, N., Shio, H., and Uyesaka, N. (1998). Production of prostaglandins E1 and E2 by adult human red blood cells. *Prostaglandins Other Lipid Mediat.* 56, 89–101. doi: 10.1016/S0090-6980(98)00045-8

Petkova-Kirova, P., Hertz, L., Makhro, A., Danielczok, J., Huisjes, R., Llaudet-Planas, E., et al. (2018). A previously unrecognized Ca^{2+}-inhibited non-selective cation channel in red blood cells. *HemaSphere* 2:e146. doi: 10.1097/HS9.0000000000000146

Piccinini, G., Minetti, G., Balduini, C., and Brovelli, A. (1995). Oxidation state of glutathione and membrane proteins in human red cells of different age. *Mech. Ageing Dev.* 78, 15–26. doi: 10.1016/0047-6374(94)01511-J

Piomelli, S., and Seaman, C. (1993). Mechanism of red blood cell aging: relationship of cell density and cell age. *Am. J. Hematol.* 42, 46–52. doi: 10.1002/ajh.2830420110

Rifkind, J. M., Araki, K., and Hadley, E. C. (1983). The relationship between the osmotic fragility of human erythrocytes and cell age. *Arch. Biochem. Biophys.* 222, 582–589. doi: 10.1016/0003-9861(83)90556-8

Romero, P. J., Romero, E. A., and Winkler, M. D. (1997). Ionic calcium content of light dense human red cells separated by Percoll density gradients. *Biochim. Biophys. Acta* 1323, 23–28.

Rotordam, G. M., Fermo, E., Becker, N., Barcellini, W., Brüggemann, A., Fertig, N., et al. (2019). A novel gain-of-function mutation of Piezo1 is functionally affirmed in red blood cells by high-throughput patch clamp. *Haematologica* 104:e181. doi: 10.3324/haematol.2018.201160

Samaja, M., Rovida, E., Motterlini, R., Tarantola, M., Rubinacci, A., and di Prampero, P. E. (1990). Human red cell age, oxygen affinity and oxygen transport. *Respir. Physiol.* 79, 69–79. doi: 10.1016/0034-5687(90)90061-3

Seppi, C., Castellana, M. A., Minetti, G., Piccinini, G., Balduini, C., and Brovelli, A. (1991). Evidence for membrane protein oxidation during *in vivo* aging of human erythrocytes. *Mech. Ageing Dev.* 57, 247–258. doi: 10.1016/0047-6374(91)90050-A

Shiga, T., Sekiya, M., Maeda, N., Kon, K., and Okazaki, M. (1985). Cell age-dependent changes in deformability and calcium accumulation of human erythrocytes. *Biochim. Biophys. Acta* 814, 289–299.

Silbernagel, S., and Despopoulus, A. (2007). *Taschenatlas physiology*. Stuttgart: Thieme.

Stout, J. G., Zhou, Q., Wiedmer, T., and Sims, P. J. (1989). Change in conformation of plasma membrane phospholipid scramblase induced by occupancy of its Ca^{2+} binding site. *Biochemistry* 37, 14860–14866.

Syllm-Rapoport, I., Daniel, A., Starck, H., Hartwig, A., and Gross, J. (1981). Creatine in density-fractionated red cells, a useful indicator of erythropoietic dynamics and of hypoxia past and present. *Acta Haematol.* 66, 86–95.

Tiffert, T., Bookchin, R. M., and Lew, V. L. (2002). "Calcium homeostasis in Normal and abnormal human red cells" in *Red cell membrane transport in health and disease*. eds. I. Bernhardt and J. C. Ellory (Berlin: Springer), 373–405.

Tiffert, T., Etzion, Z., Bookchin, R. M., and Lew, V. L. (1993). Effects of deoxygenation on active and passive Ca^{2+} transport and cytoplasmic Ca^{2+} buffering in normal human red cells. *J. Physiol.* 464, 529–544. doi: 10.1113/jphysiol.1993.sp019649

Tiffert, T., and Lew, V. L. (1997). Apparent Ca^{2+} dissociation constant of Ca^{2+} chelators incorporated non-disruptively into intact human red cells. *J. Physiol.* 505, 403–410. doi: 10.1111/j.1469-7793.1997.403bb.x

van Oss, C. J. (1982). Shape of aging erythrocytes. *Biorheology* 19:725.

Wagner-Britz, L., Wang, J., Kaestner, L., and Bernhardt, I. (2013). Protein kinase Cα and P-type Ca^{2+} channel $Ca_V2.1$ in red blood cell calcium signalling. *Cell. Physiol. Biochem.* 31, 883–891. doi: 10.1159/000350106

Wang, J., van Bentum, K., Sester, U., and Kaestner, L. (2014). Calcium homeostasis in red blood cells of dialysis patients in dependence of erythropoietin treatment. *Front. Physiol.* 5:16. doi: 10.3389/fphys.2014.00016

Wang, J., Wagner-Britz, L., Bogdanova, A., Ruppenthal, S., Wiesen, K., Kaiser, E., et al. (2013). Morphologically homogeneous red blood cells present a heterogeneous response to hormonal stimulation. *PLoS One* 8:e67697. doi: 10.1371/journal.pone.0085650

Waugh, R. E., Narla, M., Jackson, C. W., Mueller, T. J., Suzuki, T., and Dale, G. L. (1992). Rheologic properties of senescent erythrocytes: loss of surface area and volume with red blood cell age. *Blood* 79, 1351–1358. doi: 10.1182/blood.V79.5.1351.1351

Wesseling, M. C., Wagner-Britz, L., Huppert, H., Hanf, B., Hertz, L., Nguyen, D. B., et al. (2016b). Phosphatidylserine exposure in human red blood cells depending on cell age. *Cell. Physiol. Biochem.* 38, 1376–1390. doi: 10.1159/000443081

Wesseling, M. C., Wagner-Britz, L., Nguyen, D. B., Asanidze, S., Mutua, J., Mohamed, N., et al. (2016a). Novel insights in the regulation of

Phosphatidylserine exposure in human red blood cells. *Cell. Physiol. Biochem.* 39, 1941–1954. doi: 10.1159/000447891

Wiley, J. S., and Shaller, C. C. (1977). Selective loss of calcium permeability on maturation of reticulocytes. *J. Clin. Invest.* 59, 1113–1119. doi: 10.1172/JCI108735

Woon, L. A., Holland, J. W., Kable, E. P., and Roufogalis, B. D. (1999). Ca^{2+} sensitivity of phospholipid scrambling in human red cell ghosts. *Cell Calcium* 25, 313–320. doi: 10.1054/ceca.1999.0029

Yang, L., Andrews, D. A., and Low, P. S. (2000). Lysophosphatidic acid opens a Ca(++) channel in human erythrocytes. *Blood* 95, 2420–2425. doi: 10.1182/blood.V95.7.2420

Conflict of Interest: The authors declare that the research was conducted in the absence of any commercial or financial relationships that could be construed as a potential conflict of interest.

frontiers in Physiology

ORIGINAL RESEARCH
published: 17 March 2020
doi: 10.3389/fphys.2020.00215

Membrane Rearrangements in the Maturation of Circulating Human Reticulocytes

Giampaolo Minetti[1], Claudia Bernecker[2], Isabel Dorn[2], Cesare Achilli[1], Stefano Bernuzzi[3], Cesare Perotti[3] and Annarita Ciana[1]*

[1] Laboratories of Biochemistry, Department of Biology and Biotechnology "L. Spallanzani", University of Pavia, Pavia, Italy, [2] Department of Blood Group Serology and Transfusion Medicine, Medical University of Graz, Graz, Austria, [3] Servizio Immunoematologia e Medicina Trasfusionale, Fondazione Istituto di Ricovero e Cura a Carattere Scientifico Policlinico San Matteo, Pavia, Italy

Red blood cells (RBCs) begin their circulatory life as reticulocytes (Retics) after their egress from the bone marrow where, as R1 Retics, they undergo significant rearrangements in their membrane and intracellular components, via autophagic, proteolytic, and vesicle-based mechanisms. Circulating, R2 Retics must complete this maturational process, which involves additional loss of significant amounts of membrane and selected membrane proteins. Little is known about the mechanism(s) at the basis of this terminal differentiation in the circulation, which culminates with the production of a stable biconcave discocyte. The membrane of R1 Retics undergoes a selective remodeling through the release of exosomes that are enriched in transferrin receptor and membrane raft proteins and lipids, but are devoid of Band 3, glycophorin A, and membrane skeletal proteins. We wondered whether a similar selective remodeling occurred also in the maturation of R2 Retics. Peripheral blood R2 Retics, isolated by an immunomagnetic method, were compared with mature circulating RBCs from the same donor and their membrane protein and lipid content was analyzed. Results show that both Band 3 and spectrin decrease from R2 Retics to RBCs on a "per cell" basis. Looking at membrane proteins that are considered as markers of membrane rafts, flotillin-2 appears to decrease in a disproportionate manner with respect to Band 3. Stomatin also decreases but in a more proportionate manner with respect to Band 3, hinting at a heterogeneous nature of membrane rafts. High resolution lipidomics analysis, on the contrary, revealed that those lipids that are typically representative of the membrane raft phase, sphingomyelin and cholesterol, are enriched in mature RBCs with respct to Retics, relative to total cell lipids, strongly arguing in favor of the selective retention of at least certain subclasses of membrane rafts in RBCs as they mature from Retics. Our hypothesis that rafts serve as additional anchoring sites for the lipid bilayer to the underlying membrane-skeleton is corroborated by the present results. It is becoming ever more clear that a proper lipid composition of the reticulocyte is necessary for the production of a normal mature RBC.

Keywords: membrane rafts, membrane skeleton, Band 3, flotillin, stomatin, cultured red blood cells, lipidomics, Western blotting

Abbreviations: Chol, cholesterol; DRM, detergent-resistant-membrane; ILV, intraluminal vesicle; LPC, lysophosphatidylcholine; MVB, multivesicular body; PC, phosphatidylcholine; PI, phosphatidylinositol, PS, phosphatidylserine; SM, sphingomyeline.

OPEN ACCESS

Edited by:
Lucia De Franceschi, University of Verona, Italy

Reviewed by:
Velia M. Fowler, The Scripps Research Institute, United States
Mauro Magnani, University of Urbino Carlo Bo, Italy

****Correspondence:***
Giampaolo Minetti
minetti@unipv.it

Specialty section:
This article was submitted to Red Blood Cell Physiology, a section of the journal Frontiers in Physiology

Received: *12 October 2019*
Accepted: *24 February 2020*
Published: *17 March 2020*

Citation:
Minetti G, Bernecker C, Dorn I, Achilli C, Bernuzzi S, Perotti C and Ciana A (2020) Membrane Rearrangements in the Maturation of Circulating Human Reticulocytes. Front. Physiol. 11:215. doi: 10.3389/fphys.2020.00215

INTRODUCTION

Reticulocytes (Retics) are the result of the enucleation in the bone marrow of their immediate nucleated precursor, the orthochromatic erythroblast, and still retain several components in their membrane and cytoplasm with an excess of approximately 20% of plasma membrane that must be removed. Part of the maturation occurs in the bone marrow, where the cells are defined as R1 Retics, part in the circulation (R2 Retics) where they will lose additional components and residual excess membrane before they attain the final structure of a fully functional and stable biconcave discocytic red blood cell (RBC) (Chasis et al., 1989; Moras et al., 2017; Ovchynnikova et al., 2018). In turn, RBCs lose membrane surface area and cell volume as they age in the circulation. It is common belief that surface area is lost through the release of vesicles. Vast literature is available on the characterization of vesicles released *in vitro* under a variety of treatments: nutrient deprivation, increased intracellular Ca^{2+}, pH changes, intercalation of amphiphilic compounds in the membrane, etc. The vast majority of types of *in vitro*-released vesicles are defined as being spectrin-free (devoid of membrane skeleton). If the vesicles that are supposedly released *in vivo* were also spectrin-free, young and old RBCs should contain the same amount of spectrin. We have recently shown that this is not the case, as the membrane skeleton is apparently lost in parallel with the lipid bilayer during RBC aging (Ciana et al., 2017a,b), suggesting that the membrane is lost by/removed from aging RBCs in a form that is different from the well-known and characterized spectrin-free vesicles obtained *in vitro*. A recent model proposes that, in the peculiar environment of the oscillatory splenic flow, conditions may arise whereby RBCs can spontaneously release vesicles through a novel deformation mode, called "infolding" (Asaro et al., 2018). Support to this theoretical model from experimental evidence obtained *in vivo* is still lacking. Also unknown is the mechanism by which the membrane and the membrane skeleton are removed, but probably require the active intervention of other tissues/organs (spleen, liver, endothelium).

When looking at the membrane of young and old circulating RBCs, we have found that flotillin-2, a membrane raft component, is lost disproportionately with respect to the loss of membrane that takes place during RBC aging (more flotillin is lost than surface area extension). This suggests that selected portions of the membrane, enriched in flotillins are shed/removed during the physiological aging of the cell. Interestingly, when looking at the partitioning of flotillin-2 between the membrane of the cell and that of the vesicles released *in vitro* by Ca^{2+}-treatment, the protein is found to be depleted in the vesicles, again pointing to a different mechanism of membrane shedding *in vivo* and *in vitro* (Ciana et al., 2017a,b). This evidence suggested that membrane rafts are involved in the selective processing of the plasma membrane as RBCs age *in vivo*.

Membrane rafts are already known to be involved in the maturation of R1 Retics in the bone marrow after enucleation of the orthochromatic erythroblast. Recent advances in the field of erythropoiesis and the production of cultured RBCs, have clearly shown that an important role is played by membrane lipids, in particular cholesterol, in the differentiation and maturation process (Bernecker et al., 2019; Gu et al., 2019; Zingariello et al., 2019). With the discovery of the multivesicular body (MVB), it became clear that certain proteins are retained in the membrane (Band 3, glycophorin A, all membrane-skeletal proteins), while others (transferrin receptor, TfR or CD71) are lost in exosomes that result from membrane trafficking that starts at the plasma membrane, leads to the endosomal compartment, then to the multivesicular body [(containing intraluminal-vesicles (ILV)] and finally to the extracellular space (Pan and Johnstone, 1983; Harding et al., 1984). Only in more recent years, and after the notion of membrane rafts became popular, it was observed that exosomes are also enriched in membrane raft components (de Gassart et al., 2003). Despite the much advancement in this field, it could be said that the study of Retic maturation is still in its infancy. In fact, many questions concerning the major pathways of erythroblast maturation and their overlapping, especially around the terminal maturation of the Retic, are still unanswered (Ney, 2011). For instance, it is still unclear: (i) why the TfR, that is endocytosed in clathrin-coated vesicles (that do not contain membrane rafts) is then found in the exosomes together with membrane raft components; (ii) to what extent cultured Retics can mature *in vitro*: although the erythroblasts spontaneously enucleate *in vitro*, do the resulting Retics also traffic membrane via the MVB and release exosomes?; (iii) how R2 Retics lose an extra amount of membrane and the residual TfR to become mature discocytes; (iv) how selective is the loss of membrane components from R2 Retics?; (v) is there any loss of membrane-skeleton from R2 Retics? and (vi) how the lipid composition of the membrane bilayer changes all along erythroid differentiation and in particular in the maturation of Retics (both R1 and R2) (Minetti et al., 2018).

We reasoned that, if membrane rafts are important in the two above-described steps (aging of mature RBCs in the circulation and maturation of R1 Retics in the marrow), they could also be involved in the terminal maturation of circulating (R2) Retics. We therefore approached the characterization of the membrane of circulating Retics and RBCs from the same donor. Thus, we focused on flotillins and stomatin as selected protein markers of rafts, aiming at evaluating whether a selective sorting of these raft components in Retics and RBCs could be detected. Membrane rafts are defined as being enriched in cholesterol and sphingolipids (Sonnino et al., 2006). If a rearrangement of the membrane rafts phase occurred in the terminal maturation of Retics *in vivo*, this should be reflected by changes in the lipid composition of the plasma membrane. Because of this, and in the light of the ever increasing importance that lipids appear to have in erythropoiesis (Bernecker et al., 2019; Zingariello et al., 2019), lipidomics analysis of R2 Retics and mature RBCs was carried out. Answering these basic questions could help expand our knowledge of erythropoiesis and the mechanism(s) of clearance of normal and pathological RBCs, and to find new solutions for

the production of fully mature and functional cultured RBCs (Anstee et al., 2012).

MATERIALS AND METHODS

Human blood samples were collected in standard 6 ml vials containing lithium heparin as the anticoagulant by the local Transfusion center (Servizio di Immunoematologia e Medicina Trasfusionale of the IRCCS Policlinico San Matteo, Pavia, Italy) from regular donors after informed consent was obtained, according to the protocol approved on 2017/04/10, by the local ethics committee (Comitato Etico Area Pavia, IRCCS Policlinico San Matteo, Pavia, Italy). Processing of blood and blood cells was terminated within the day of withdrawal.

Blood Filtration, RBC, and Retic Recovery

The blood was filtered to separate RBCs from white blood cells and platelets (Beutler et al., 1976; Achilli et al., 2011). Whole blood (8–10 ml) was centrifuged at 1000 × *g* for 5 min to sediment the cells. One milliliter of plasma was collected and diluted with 9 ml of PBSG [5 mM sodium phosphate pH 7.4, 154 mM NaCl, 4.5 mM KCl, 305–310 mosmol/kg H_2O (osmolality was measured with a freezing point depression osmometer Micro-Osmometer Type 13/13 DR Roebling, Berlin, Germany) supplemented with 10 mM glucose before use]. The remaining plasma was collected and set aside. The diluted plasma was used to condition the cellulose filter through which blood was filtered. The filter was contained in a plastic Buchner funnel (d = 5.2 cm internal) and was formed by a cellulose bed. Six gram of a mixture of equal parts, by weight, of α-cellulose (Merck Sigma-Aldrich code C8002) and microcrystalline cellulose (Merck Sigma-Aldrich code S5504) were suspended in about 60 ml of PBSG and poured into the Buchner funnel whose bottom was lined with a disc of Whatman grade 4 filter paper (that holds particles larger than 20–25 μm). The cellulose bed was washed with 100 ml of PBSG to ensure the washing out of finer cellulose particles (<20–25 μm) that would co-elute with, and contaminate RBCs during filtration. The packed RBCs left in the tube after removal of the plasma were resuspended to approximately 50% hematocrit (Ht) with PBSG and the suspension was uniformly distributed on the cellulose filter. Once the RBCs entered the cellulose, PBSG was added and the eluate, containing the filtered RBCs was collected in 50 ml polypropylene centrifuge tubes until no more RBCs emerged from the filter. Through two washes with PBSG and centrifugation for 5 min at 1000 × g at 20°C, the contents of all the tubes was combined into a single tube, which was again centrifuged. Sufficient PBSG was removed to bring the Ht to approximately 20% and the volume of the resulting suspension and its Ht were measured. Some experiments were dedicated to evaluate the yield of Retics after filtration. Aliquots of whole blood and of filtered RBCs as suspensions of approximately 20% Ht, were counted for Retic number with an Advia 2120 Automated Hematology analyzer (Siemens, Munich, Germany) at the "Laboratory of Analysis," IRCCS Foundation, Policlinico San Matteo, Pavia.

Immuno-Magnetic Separation of Retics

This method was used for the positive selection and purification of Retics using "CD71 MicroBeads" (conjugated to monoclonal anti-human CD71 antibodies, isotype: mouse IgG2a; clone AC108.1, MACS Miltenyi Biotec, United States). The procedure was carried out at 4°C. Filtered RBCs (3.2 ml packed cells) were brought to 20% Ht with PBSG containing 0.5% (w/v) BSA for a final volume of 16 ml. To this suspension, 600 μl of "CD71 MicroBeads" were added and the mixture was rotated end-over-end for 45 min. Extension of incubation time from the 15 min suggested by the manufacturer to 45 min proved to be essential to increase Retic recovery. One magnetic column of the type MS (Medium size, Miltenyi Biotec, code 130-042-201) or, in later experiments LS (Large size, Miltenyi Biotec, code 130-042-401) was inserted into the permanent magnet of a MiniMACS^{TM} or MidiMACS^{TM} separator (Miltenyi Biotec). Four such columns were used per experiment, with blood from a single donor, expecting to recover from 10^7 to 10^8 Retics in total from each experiment. Three milliliter of PBSG + BSA were passed through each column to condition it. Then, 4 ml of RBC suspension + "CD71 Microbeads" were loaded on each column and the eluate was collected and saved. Three milliliter PBSG + BSA were then added to wash out the remaining RBCs. Retic recovery was also increased by reducing the flow rate during both loading of the cell suspension on the column and washing of the column before eluting the Retics. Reduction of flow rate was obtained by attaching a small-gauge needle to the Luer-slip fitting of the column. The column was then extracted from the magnet and 1.5 ml of PBSG were added to elute, with the aid of a plunger, the Retics in a 2 ml Eppendorf tube. Retics were sedimented for 4 min at 1000 × g. The supernatant was discarded and the Retics were resuspended with PBSG (final volume approximately 55–60 μl). Five microliter of this suspension were set aside for Retic staining and counting. The remaining suspension was destined for Western blotting or lipid analysis and processed as follows.

Sample Preparation for Western Blotting

Fifty microliter of Retic suspension were mixed with 450 μl of "Diluted SDS-PAGE sample Buffer" [prepared by mixing 1 volume of 3X SDS-PAGE sample buffer (50 mM Tris/HCl, pH 6.8, 5% SDS (w/v), 35% sucrose (w/v), 5 mM EDTA, 0.01% bromophenol blue, 200 mM dithiotreitol) with 1.7 volumes of 5% SDS (w/v) in MilliQ water] and the samples were incubated at 60°C for 15 min. Samples were stored frozen at −80°C in 100 μl aliquots until analysis by SDS-PAGE and Western Blotting.

Sample Preparation for Lipid Analysis

Five, out of a 50 μl of Retic suspension were mixed with 45 μl of "Diluted SDS-PAGE sample Buffer" (see above), treated at 60°C for 15 min and stored frozen for Western blotting analysis. To the remaining 45 μl of Retic suspension, 1 ml of ice-cold, HPLC-grade methanol was added, the sample transferred into Pyrex® glass tubes (Code: 1636726MP, capacity 11 ml, SciLabware Ltd., United Kingdom) and stored frozen at −80°C until analysis.

Cell Count

In some experiments Retics and RBCs were manually counted in Neubauer chamber after suitable dilution of the stock cell suspensions with PBSG + BSA.

Lipid Analysis

The quantitative lipid measurement was done by high resolution mass spectrometry (LTQ-Orbitrap, Thermo Scientific) (Triebl et al., 2017). Lipids were extracted from cell pellets (10^7–10^8 cells) with an established MTBE (Methyl-tert-butylether) protocol (Matyash et al., 2008). The Orbitrap Velos Pro hybrid mass spectrometer was operated in Data Dependent Acquisition mode using a HESI II ion source. Full scan profile spectra from m/z 450 to 1050 for positive ion mode and from m/z 400 to 1000 for negative ion mode were acquired in the Orbitrap mass analyzer at a resolution of 100k at m/z 400 and <2 ppm mass accuracy. Samples were measured once in positive polarity and once in negative polarity. For MS/MS experiments, the ten most abundant ions of the full scan spectrum were sequentially fragmented in the ion trap using He as collision gas (CID, Normalized Collision Energy: 50; Isolation Width: 1.5; Activation Q: 0.2; and Activation Time: 10). Centroided product spectra at a normal scan rate (33 kDa/s) were collected. The custom developed software tool Lipid Data Analyzer was used for data analysis (Hartler et al., 2011; Hartler et al., 2017). Seven classes of lipids were quantified, together with their subclasses according to the length and number of double bonds of the acyl chains linked to the glycerol or sphingosine moiety: phosphatidylcholine (PC), lysophosphatidylcholine (LPC), sphingomyeline (SM), phosphatidylethanolamine (PE), phosphatidylserine (PS), phosphatidylinositol (PI), and cholesterol (Chol).

SDS-PAGE and Western Blotting

RBC and Retic proteins were separated by Polyacrylamide Gel Electrophoresis in Sodium DodecylSulfate (SDS-PAGE), following the Laemmli method (Laemmli, 1970), in 10% acrylamide isocratic (or, for analysis of spectrin, 5–15% acrylamide linear gradients) mini-gels (80 × 60 × 1.5 mm) in a Mini Protean 3 system (Bio-Rad Laboratories, United States). Sample loading is indicated in the Results section or in figure legends.

Proteins separated by the SDS-PAGE were electro-transferred to a PVDF membrane (0.2 μm pores) using a Trans Blot Turbo system (Bio-Rad Laboratories, United States) according to manufacturer's instructions. Membranes were blocked with a blocking solution [5% skimmed milk in 20 mM Tris, pH 7.4, 150 mM NaCl, 0.05% Tween 20 (v/v)] and then incubated overnight at 4°C with the primary antibody directed to the protein of interest (**Table 1**).

Antibodies were diluted in a washing buffer [50 mM Tris/HCl pH 7.5, 0.2 M NaCl, 0.5 ml/l Tween 20, 1 g/l polyethylene glycol (PEG) 20000, 1 g/l BSA] that was also used for washing the membranes. The secondary horseradish-peroxidase-(HRP)-conjugated antibodies were used at the dilution indicated in **Table 1**. Membranes were developed with the chemiluminescence kit Prime Western Blotting Detection Reagent (GE Healthcare, United States) and the signal was acquired with a Molecular Imager ChemiDoc XRS + (Bio-Rad Laboratories, United States). Densitometry of the bands was performed using the software Scion Image (Scion Corporation, United States).

TABLE 1 | Primary and secondary antibodies used (at the dilution indicated in parentheses) for Western blotting in the present study.

Primary antibodies	Secondary antibodies
Anti human flotillin-2, mouse polyclonal, Abnova H00002319-B02P (1:3000).	HRP-conjugated goat anti-mouse IgGs, ENZO Life Sciences BML-SA204 (1:5000)
Anti human stomatin, goat polyclonal (M-14), SCBT sc-48308 (1:3000)	HRP-conjugated donkey anti-goat IgGs, SCBT sc-2020 (1:15000)
Anti human Band 3, mouse monoclonal (BIII-136), Merck Sigma-Aldrich B9277 (1:15000)	HRP-conjugated goat anti-mouse IgGs, ENZO Life Sciences BML-SA204 (1:15000)
Anti human β-spectrin, mouse monoclonal (VD4), SCBT sc-53901 (1:2000)	HRP-conjugated goat anti-mouse IgGs, ENZO Life Sciences BML-SA204 (1:10000)
Anti human CD71, mouse monoclonal (H68.4), SCBT sc-51829 (1:200)	HRP-conjugated goat anti-mouse IgGs, Bio-Rad 170-6516 (1:4000)

Antibodies Used

Mouse polyclonal anti human flotillin-2, H00002319-B02, Abnova, Taipei, Taiwan. Mouse monoclonal (BIII-136) anti human Band 3, B9277, Merck Sigma-Aldrich, Darmstadt, Germany. Mouse monoclonal (H68.4) anti human CD71, sc-51829; goat polyclonal anti human stomatin (M-14), sc-48308; mouse monoclonal anti human β-spectrin (VD4), sc-53901; HRP conjugated donkey anti-goat IgGs, sc-2020, Santa Cruz Biotechnology (SCBT), Dallas, TX, United States. HRP-conjugated goat anti-mouse IgGs, BML-SA204, ENZO Life Sciences, Lausanne, Switzerland. HRP-conjugated goat anti-mouse IgGs, 170-6516 Bio-Rad Laboratories, Milan, Italy. Antibodies were used at the dilutions given in **Table 1**.

Membrane Raft Isolation as Detergent-Resistant Membrane

Membrane rafts were isolated from Retics and RBCs as detergent-resistant-membrane (DRM) according to our previously described protocol (Ciana et al., 2011). Due to the limited quantity of Retics available, a mini-preparation was performed. Briefly, the Retics obtained as described above by immunomagnetic sorting and a corresponding amount of RBCs from the same donor, were resuspended in HKM buffer (10 mM HEPES, 150 mM KCl, 4.5 mM NaCl, 1 mM $MgCl_2$, pH 7.4, 300–315 mOsm/kg H_2O) to a final volume of 30 μl. Five microliter were treated with SDS-PAGE sample buffer for Western blotting as described above. To 22.5 μl of Retic suspension in HKM, and 22.5 μl of RBC suspension in HKM (containing the equivalent of approximately 12.5 μl of packed RBCs), 37.5 μl of HKM, containing 1.67% (v/v) Triton X-100, were added at 4°C. The mixture was allowed to stand for 15 min on ice. Then, 62.5 μl of an 80% sucrose solution in 0.3 M K_2CO_3 were added to each sample for a total of 125 μl, and the mixtures

transferred to the bottom of miniature ultracentrifuge tubes (Cod. 344090 Polyallomer Ultra-Clear, total volume 800 µl, 5 mm × 41 mm, Beckman Coulter, Milano, Italia). On top of the sample mixture, 350 µl of 30% sucrose in HKM were added, followed by a layer of 150 µl of 5% sucrose solution in HKM. The tubes were inserted into an adaptor to fit the rotor buckets used here (Delrin adapters, Cod. 356860 Beckman Coulter, Milano, Italia) and spun for 14 h at 225,000 × g_{max} at 4°C in a bench-top ultracentrifuge (Optima-Max, equipped with a swinging-arm MLS50 rotor, Beckman Coulter, Milan, Italy). At the end, six fractions of 100 µl each were collected from the top of the tube. The first five fractions were mixed each with 50 µl of 3X SDS-PAGE sample buffer, while the last fraction was mixed with 400 µl of "Diluted SDS-PAGE sample Buffer" (see above). All fractions were incubated at 60°C for 15 min, aliquoted and stored frozen.

RESULTS

Filtration of Blood and Its Impact on Retic Yield

Given the importance of working with purified RBC suspensions, free of contaminating leukocytes and platelets (Minetti et al., 2013) blood was leukodepleted by filtration through cellulose filters, as described in Materials and Methods section. The current protocol of filtration also includes a treatment of the filtered RBCs with diisopropylfluorophosphate (DFP) to inhibit the proteases from possible residual neutrophils. However, in preliminary experiments we observed that DFP impacts on the TfR of the Retic membrane, partially impairing the binding of anti CD71 antibodies and thus reducing the yield of the immuno-magnetic isolation of Retics (not shown). Therefore, in these experiments DFP treatment was omitted. Although the original article (Beutler et al., 1976) excluded loss of Retics during filtration through cellulose, we decided to confirm this observation in our setup. The results shown in **Figure 1** revealed that only approximately 10% of Retics remained trapped in the filter.

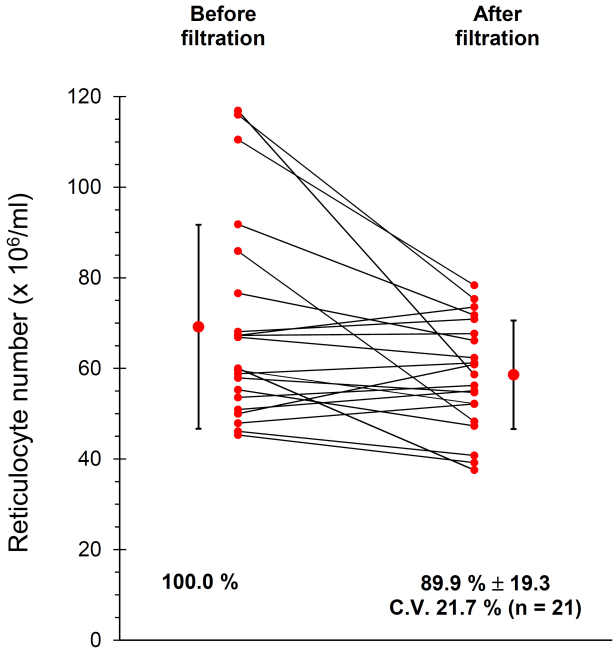

FIGURE 1 | Recovery of Retics after filtration of whole blood through cellulose. Samples of cells as suspensions of approximately 20% Ht, before and after filtration through cellulose were analyzed in 21 independent experiments as described in Materials and Methods section. An average of approximately 10% of Retics was lost during filtration (n = 21, p = 0.014 at the paired Student's t-test; CV, coefficient of variation).

Quantification of Flotillin-2 and Stomatin Relative to Band 3 in Retics and RBCs

Peripheral blood R2 Retics were isolate in pure form with the immunomagnetic method described in Materials and Methods section and processed as such while still attached to the "CD71 Microbeads" (**Figure 2**). Membrane rafts are known to be involved in the sorting of proteins that occurs during the maturation of R1 Retics, which is reflected in the release of exosomes enriched in proteins and lipids that are typical constituents of rafts (Skotland et al., 2017). Flotillins and stomatin are highly enriched in membrane rafts (de Gassart et al., 2003; Ciana et al., 2014). We have previously observed that especially flotillin-2 is lost in a disproportionate manner with respect to the loss of membrane surface area that takes place during the physiological aging of RBCs, suggesting an involvement of membrane rafts also in this physiological age-related remodeling of the RBC membrane (Ciana et al., 2017a). We therefore wondered whether membrane rafts are also in some way selected for removal from the membrane of R2 Retics. An analysis of the relative abundance of flotillin-2 and stomatin with respect to Band 3 in pure Retics and RBCs from the same donor was therefore conducted. This quantification was approached by Western blotting. Quantification of a given protein by densitometric analysis of a Western blotting membrane cannot be considered reliable in the absence of a calibration standard with known amounts of the protein of interest. To circumvent this problem and reduce the error, quantification was performed by loading in the same electrophoretic gel increasing amounts of each of the two samples to be compared (RBCs and Retics). Two identical gels were loaded in this way and electro-transferred to two PVDF membranes. One membrane was probed for Band 3 and the other for flotillin-2 or stomatin. Preliminary tests were conducted to ensure a proper sample loading so that the detected signal never reached saturation. Digital images from the Western blotting were subjected to densitometric analysis to measure the integrated density of each band. The normalization of flotillin-2 and stomatin levels over Band 3 levels was conducted as shown in **Figures 3**, **4**, respectively, and described in the legend to **Figure 3**. For flotillin-2, the results obtained in 11 independent experiments were averaged and are reported in **Table 2**. It can be observed that flotillin-2 levers are on average 2.5 times higher in Retics than in RBCs when normalized over Band 3 levels.

For stomatin, the results collected in six independent experiments are reported in **Table 2**. Stomatin levels are on

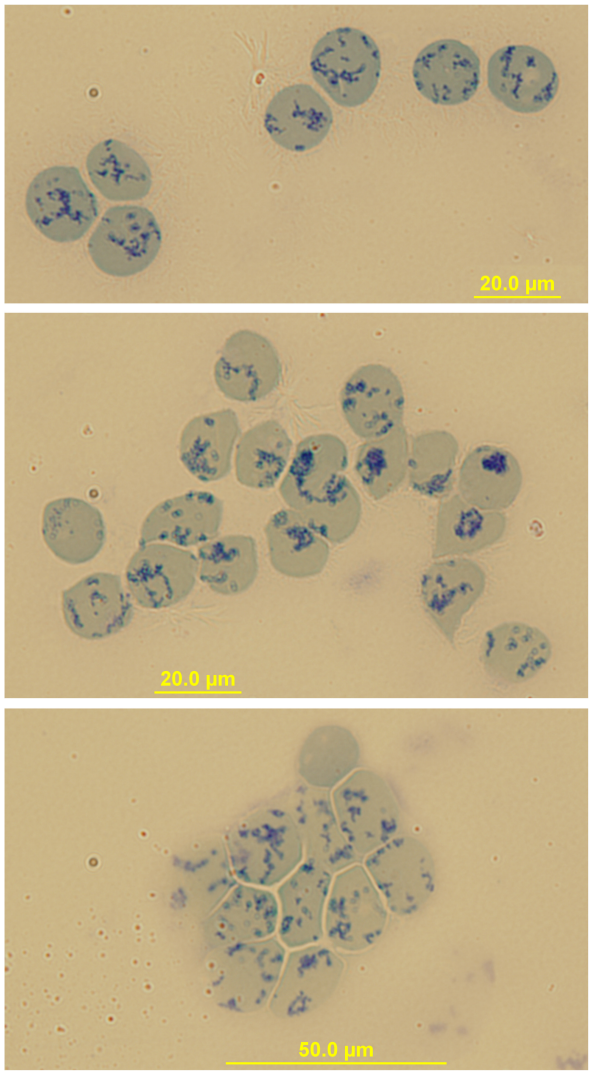

FIGURE 2 | Immunomagnetical isolation of peripheral blood Retics. Images of Retics after isolation with "CD71-microbeads" and staining with New Methylene Blue. Sometimes clumps of Retics are visible (bottom image) probably due to a crosslinking effect of the microbeads.

average 1.5 times higher in Retics than in RBCs when normalized over Band 3. After statistical analysis, it emerged that, whereas flotillin-2 levels are significantly higher in Retics than in RBCs relative to the same amounts of Band 3 from each cell type, those of stomatin are not significantly different between RBCs and Retics (not different from a ratio of 1:1). Moreover, flotillin-2 and stomatin values are significantly different from each other (for details see also **Supplementary Material, Sheet "SUMMARY"**).

Estimation of the Relative Levels of Band 3 per Cell in Retics and RBCs

We initially assumed that the number of copies of Band 3 per cell remains constant also in the maturation of R2 Retics to RBCs, as it does in the maturation of R1 Retics (exosomes don't contain Band 3). We reasoned that even if the assumption was incorrect, and Band 3 was to some extent lost with the membrane of maturing R2 Retics, a decrease in flotillin-2 or stomatin relative to Band 3 from Retics to RBCs would be at most underestimated. We wanted, however, to gain more insight on this issue and performed a new Western blotting quantification by loading the same number of RBCs and Retics and evaluating the levels of Band 3 and β-spectrin, as representative of the most abundant membrane-skeletal proteins. Results obtained in two independent experiments showed that Band 3 levels in Retics are 2.48 times higher than in the same number of RBCs (individual measurements deviated from the mean by 0.7%). When β-spectrin was analyzed by the same method, it turned out that Retics have 2.19 times more than RBCs (individual measurements deviated from the mean by 21%) (see **Supplementary Material, Sheet "EXP09-10-B3-Sp"**).

Partition of TfR in Membrane Rafts in Retics and RBCs

It is known that, although TfR and membrane raft components are together present in exosomes, the TfR itself does not co-localize with other membrane raft proteins in the plasma membrane. Therefore, diverse endocytic pathways that lead to the formation of a late endosomal compartment (then becoming a MVB from which the ILV/exosomes originate) must exist, carrying, on the one hand the TfR and, on the other, raft components to the MVB (see Minetti et al., 2018 for a discussion of this issue). To the best of our knowledge, the partitioning of TfR between the membrane and rafts phase in human R2 Retics has not been investigated before. It could be that due to the profound rearrangements in the architecture of the membrane that occur in the maturation of R1 Retics, some constraints are relieved that excluded the TfR from the rafts, allowing it to partition into these membrane domains in more mature Retics. We addressed this issue by isolating membrane rafts as DRM according to the correct procedure in the absence of

TABLE 2 | Western blotting quantification of the ratio between flotillin-2 and stomatin in Retics and in RBCs normalized over identical amounts of Band 3, as determined by the procedure described in the text.

	Retics/RBCs (n = 11)	Retics/RBCs (n = 6)	UNPAIRED t-test		
	FLOT-2	STOM	FLOT-2 vs. STOM	FLOT-2 vs. 1	STOM vs. 1
MEAN	2.55	1.49	$p < 0.05$	$p < 0.0001$	$p > 0.05$
SD	0.93	0.63			
CV%	36.5	42.6			

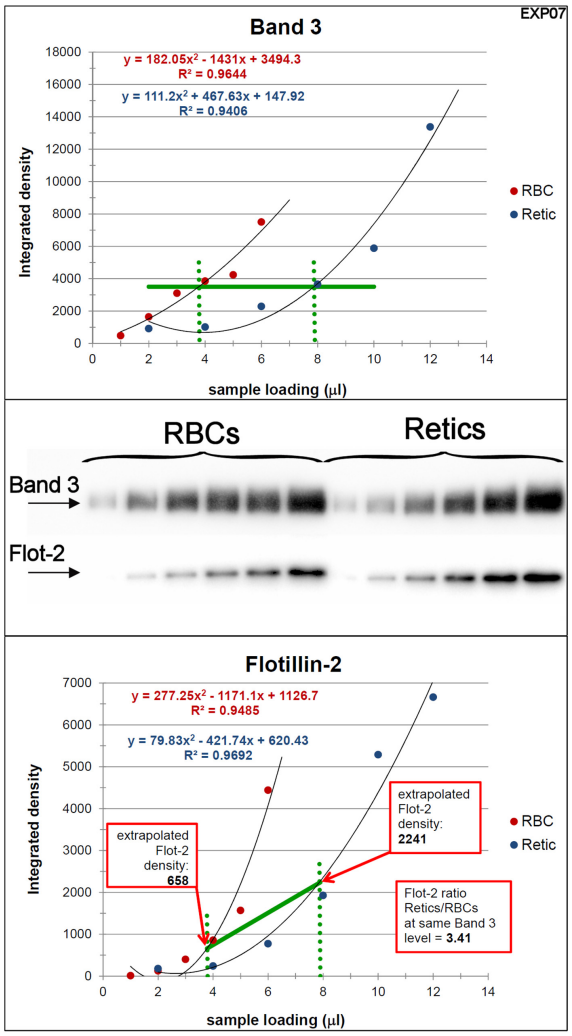

FIGURE 3 | Quantification of the relative amounts of flotillin-2 with respect to Band 3 in Retics and RBCs. The integrated densities of Band 3 obtained by densitometry of the Western blotting membrane shown in the figure (the two series of RBC and Retic samples were loaded in the same gel) were fitted with a polynomial curve (2nd order), one for the RBC and one for the Retic series (Band 3 graph). The two curves were intersected with a horizontal line at a Y value taken approximately mid-way on the polynomial curves (horizontal green line in the Band 3 graph). From the intercepts between the polynomials and the horizontal green line, vertical lines (dotted green lines) were projected on the X axis. The intercepts on the X axis were taken as the loading values (in µl) that would give the same intensity (amount) of Band 3 for RBCs and Retics. These values were used to extrapolate, from the graph where flotillin-2 integrated densities were similarly interpolated by a parabolic function (flotillin-2 graph), the flotillin-2 densities expected for an equal amount of Band 3 in RBCs and Retics. The ratio between the flotillin-2 density extrapolated on the Retic curve and that extrapolated on the RBC curve gave the ratio of flotillin-2 between Retics and RBCs at the same level of Band 3. This procedure was repeated in 11 independent experiments (see detailed data in **Supplementary Material**).

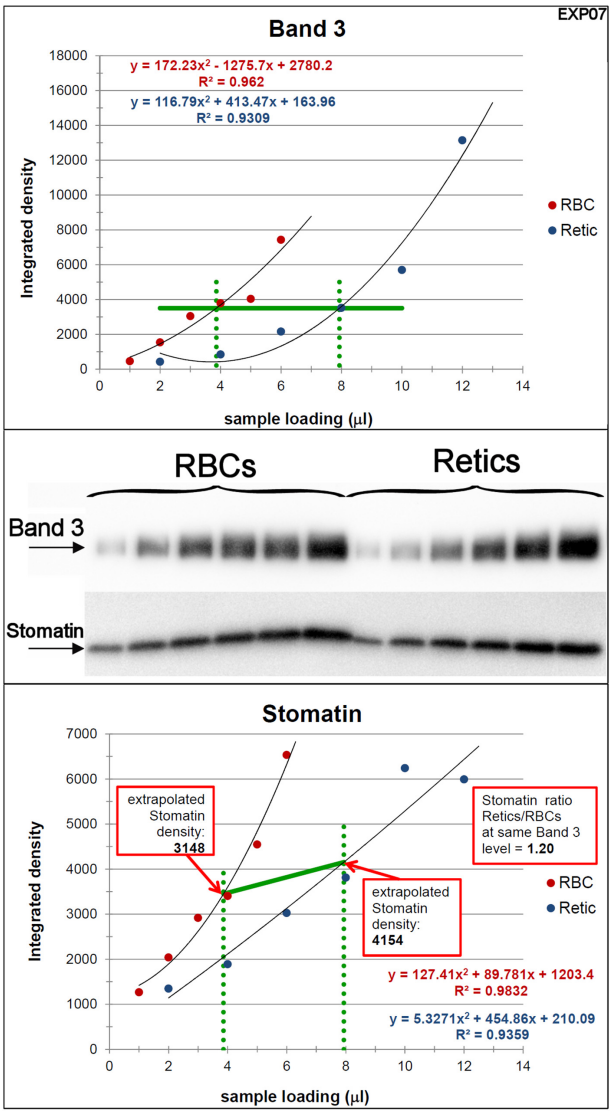

FIGURE 4 | Quantification of the relative amounts of stomatin with respect to Band 3 in Retics and RBCs. The same procedure adopted for flotillin-2 was performed to quantify the levels of stomatin in Retics and RBCs from the same donor. See legend to **Figure 3** for details.

proteolysis and with the use of carbonate (Ciana et al., 2011). A miniaturized protocol for DRM isolation was adopted due to the scarce quantity of Retics available. In **Figure 5** the results of the Western blotting for flotillin-2, stomatin and CD71 (TfR) of DRM fractions from RBCs and Retics are shown. It can be concluded that, unlike flotillin-2 and stomatin, which partition almost exclusively in the DRM region in both Retics and RBCs, TfR is totally absent from the DRM in Retics (in mature RBCs no TfR could be expected to be detected).

Lipidomics of Retics and RBCs

Proceeding from the evidence of a selective decrease in flotillin-2 and, although to a lesser extent, stomatin relative to Band 3 in the maturation from Retics to RBCs, and being flotillins and stomatin established membrane raft markers (Salzer and Prohaska, 2001), we hypothesized that the analysis of

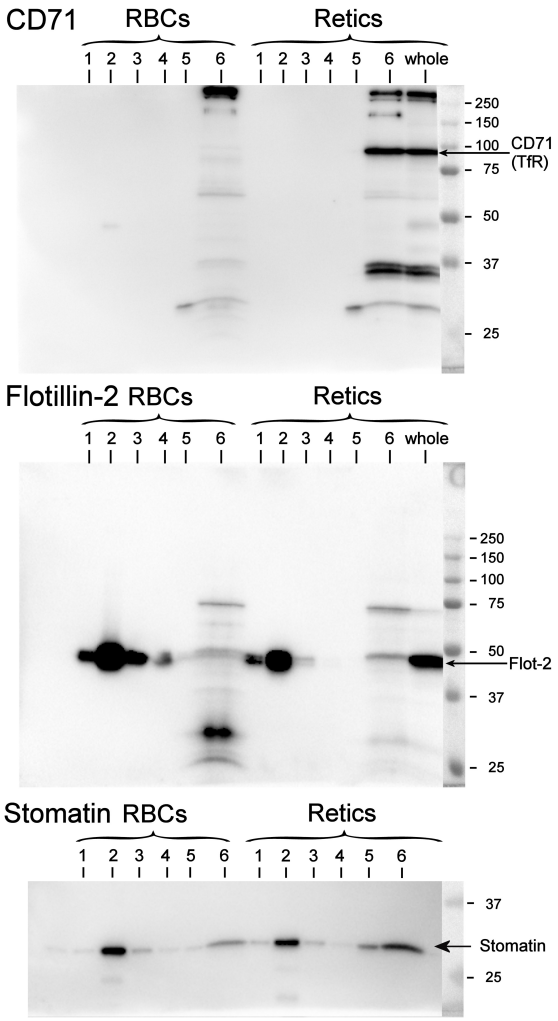

FIGURE 5 | Partitioning of TfR, flotillin-2 and stomatin between the raft and non-raft phase in RBCs and Retics. Six fractions of a sucrose gradient from a mini-preparation of membrane rafts as DRM from Retics and RBCs were probed by Western blotting for CD71, flotillin-2 and stomatin. Membrane rafts partition in fraction 2 from the top of the gradient, as shown by the presence of flotillin-2 and stomatin in this fraction for both Retic and RBC samples. In the Retic sample the TfR is only detected in the non-raft fraction at the bottom of the gradient (fraction 6). "Whole" is a sample of whole Retics. See text for details.

membrane lipids in Retics and RBCs could reveal a similar decrease of those lipids that are described as being enriched in membrane rafts, namely sphingolipids and cholesterol, and the ratio (sphingolipids + Chol)/phospholipids would decrease accordingly. Lipids from pure Retics and RBCs were therefore analyzed in five independent experiments, the results are shown in **Table 3**. It can be observed that, contrary to what hypothesized, sphingolipids and Chol actually increased relative to total lipids, in a statistically significant way, from Retics to RBCs. Conversely, PC and PS decreased. The ratio (SM + Chol)/phospholipids changed from 1.69 ± 0.10 in Retics to 2.00 ± 0.09 in RBCs ($n = 5$; $p = 0.003$).

TABLE 3 | Quantification of lipids in the membrane of Retics and RBCs in five independent experiments with five different donors.

		RETIC	RBC	*p*-value
−	PC	24.0 ± 1.3	20.5 ± 1.1	0.007*
	LPC	1.2 ± 0.2	1.2 ± 0.2	0.910
+	SM	17.2 ± 0.8	19.8 ± 1.0	0.015*
	PE	7.1 ± 2.1	7.5 ± 0.9	0.539
−	PS	4.2 ± 0.5	3.5 ± 0.5	0.010*
	PI	0.7 ± 0.2	0.7 ± 0.2	0.559
+	Chol	45.6 ± 1.2	46.8 ± 0.8	0.041*

Values are mean ± standard deviation and are expressed as mol% over the total lipids analyzed in each sample of Retics or RBCs. The symbols in the left column indicate whether the quantity of a given lipid increases (minus) or decreases (plus) from Retic to RBC. To the right, the p values obtained from the statistical elaboration of the data with the Student's t-test are shown. An asterisk indicates where $p < 0.05$.

Tables 4–6 report the relative abundance of the subclasses for those lipids that changed most in the maturation of Retics: PC, SM, and PS. It is worth mentioning, in particular, that the subclasses of SM are represented differently in Retics and RBCs, whereby SM with saturated acyl chains are more abundant in RBCs than in Retics. In Retics, unsaturated acyl chains prevail in SM (**Table 4**).

For PC, which in total decreased from Retics to RBCs, the opposite is true, with saturated and mono-unsaturated species contributing more to the decrease and poly-unsaturated species prevailing in RBCs over total PC forms (**Table 5**).

Finally, although a statistically significant overall decrease of PS over total lipids was observed in the maturation to RBCs, the minor differences that were observed in the relative abundance of the two major species of PS were not statistically significant (**Table 6**).

DISCUSSION

The series of maturational processes that RBCs and Retics undergo *in vivo* cannot be studied by analyzing the material that is lost in the circulation, because this is cleared before it could be recovered from plasma (Ciana et al., 2017a). Therefore, the only hints could be obtained from the comparison of the membrane at the beginning and end of the process, be this the maturation of R2 Retics to RBCs or the aging of the circulating RBCs, with all the inaccuracy and lack of sensitivity associated with the quantification of differences between large numbers. Yet, by applying this method differences could be detected, and we have recently proposed that a continuous process of maturation that involves the progressive loss of membrane raft components characterizes the life of RBCs from the stage of young cells in the circulation to clearance (Minetti et al., 2018). The selective loss of membrane rafts and selected membrane proteins (i.a. the TfR) with exosomes and the complete retention of the membrane-skeleton and the main integral membrane proteins (Band 3, glycophorins) was already amply demonstrated in the maturation of R1 Retics (de Gassart et al., 2003). The available results of lipid analysis are less consistent in clearly showing the

TABLE 4 | SM subclasses in Retics and RBCs subjected to lipidomics analysis.

		RETIC	RBC	*p*-value
+	SM 14:0	1.9 ± 0.2	2.0 ± 0.3	0.014*
+	SM 15:0	1.3 ± 0.1	1.4 ± 0.1	0.002*
+	SM 16:0	22.6 ± 1.8	24.4 ± 2.5	0.020*
+	SM 16:1	1.8 ± 0.3	2.0 ± 0.3	0.002*
+	SM 17:0	0.5 ± 0.1	0.7 ± 0.1	0.003*
+	SM 18:0	2.1 ± 0.2	3.7 ± 0.3	0.000*
+	SM 18:1	0.8 ± 0.1	1.3 ± 0.1	0.000*
+	SM 20:0	1.1 ± 0.2	1.2 ± 0.2	0.030*
−	SM 22:0	8.6 ± 0.9	8.1 ± 0.9	0.074
−	SM 22:1	3.1 ± 0.5	2.7 ± 0.4	0.004*
−	SM 23:0	2.0 ± 0.3	2.0 ± 0.3	0.318
−	SM 24:0	18.1 ± 1.5	17.8 ± 1.7	0.636
−	SM 24:1	28.1 ± 2.5	26.0 ± 2.1	0.005*
−	SM 24:2	7.0 ± 0.6	5.5 ± 0.4	0.001*
+	SM 26:0	1.0 ± 0.1	1.1 ± 0.1	0.035*
+	SATURATED	59.1 ± 2.2	62.5 ± 2.1	0.003*
−	MONO	33.8 ± 2.5	32.1 ± 2.1	0.014*
−	PUFA	7.0 ± 0.6	5.5 ± 0.4	0.001*
−	UNSATURATED	40.9 ± 2.2	37.5 ± 2.1	0.003*

Values of each lipid subclass are expressed as mol% over the total SM. Numbers in the name of each SM species indicate the length and the number of unsaturations in the acyl chain N-amidated to the sphingosine moiety. The four rows at the bottom group, respectively, all the subclasses of SM with saturated acyl chains (SATURATED), those with a mono-unsaturated acyl chain (MONO), those with an acyl chain with more than one double bond (PUFA) and the total of unsaturated species (MONO + PUFA) (UNSATURATED). The symbols in the left column indicate whether the quantity of a given lipid increases (minus) or decreases (plus) from Retic to RBC. To the right, the p values obtained from the statistical elaboration of the data with the Student's t-test are shown. An asterisk indicates where $p < 0.05$.

TABLE 5 | PC subclasses in Retics and RBCs subjected to lipidomics analysis.

		RETIC	RBC	*p*-value
−	PC 32:0	13.6 ± 3.8	6.6 ± 1.2	0.005*
+	PC 32:1	1.4 ± 0.5	1.5 ± 1.0	0.698
−	PC 33:0	1.4 ± 0.2	1.0 ± 0.1	0.012*
−	PC 34:0	2.8 ± 0.2	2.4 ± 0.3	0.030*
−	PC 34:1	33.6 ± 3.4	25.7 ± 2.2	0.001*
+	PC 34:2	13.1 ± 1.9	23.3 ± 1.3	0.000*
−	PC 35:0	1.4 ± 0.3	1.0 ± 0.0	0.069
−	PC 35:1	1.1 ± 0.2	0.9 ±0.1	0.015*
+	PC 35:2	0.5 ± 0.1	0.5 ± 0.0	0.242
−	PC 35:3	0.5 ± 0.2	0.3 ± 0.0	0.093
−	PC 35:4	0.5 ± 0.2	0.3 ± 0.0	0.066
+	PC 36:1	3.9 ± 0.6	6.1 ± 1.0	0.001*
+	PC 36:2	6.3 ± 1.1	10.9 ± 1.8	0.000*
+	PC 36:3	4.3 ± 0.7	5.8 ± 0.4	0.001*
−	PC 36:4	6.4 ± 0.9	5.8 ± 1.0	0.375
−	PC 37:3	4.9 ± 1.7	3.1 ± 0.2	0.069
−	PC 37:5	0.6 ± 0.3	0.3 ± 0.0	0.079
+	PC 38:3	0.4 ± 0.1	0.8 ± 0.2	0.019*
−	PC 38:4	2.4 ± 0.5	2.4 ± 0.4	0.914
+	PC 38:6	1.0 ± 0.1	1.2 ± 0.6	0.275
−	SATURATED	19.1 ± 3.6	11.0 ± 1.3	0.002*
−	MONO	40.1 ± 3.2	34.3 ± 1.6	0.004*
+	PUFA	40.8 ± 6.3	54.8 ± 2.4	0.002*

*Values of each lipid subclass are expressed as mol% over the total PC. Numbers in the name of each PC species indicate the length and the number of unsaturations in the acyl chains esterified to the glycerol backbone. Please refer to the legend of **Table 4** for additional details.*

TABLE 6 | PS subclasses in Retics and RBCs subjected to lipidomics analysis.

		RETIC	RBC	*p*-value
+	PS 38:3	2.0 ± 0.5	2.9 ± 2.2	0.453
−	PS 38:4	75.4 ± 11.5	74.0 ± 10.0	0.793
+	PS 40:6	22.6 ± 11.7	23.1 ± 9.2	0.906

*Values of each lipid subclass are expressed as mol% over the total PS. Numbers in the name of each PS species indicate the length and the number of unsaturations in the acyl chains esterified to the glycerol backbone. Please refer to the legend of **Table 4** for additional details.*

paradigmatic enrichment of raft lipids in the released exosomes, in particular from Retics. This could be also due to the paucity of studies that have addressed this issue. In one study, only a minor enrichment in SM in the exosomes released *in vitro* by maturing guinea pig Retics was reported (Vidal et al., 1989). A more recent high-resolution lipidomics study conducted on rat "stress" Retics revealed a more complex scenario, whereby the lipid composition of exosomes varied at various stages of maturation of the Retics (Carayon et al., 2011). Therefore it is still unclear whether the lipid composition of exosomes really reflects, as the protein components apparently does, the enrichment in membrane rafts in this type of microvesicles, at least for the Retic (Skotland et al., 2017). Independently from what happens to the lipid component in the maturation of R1 Retics, we have observed here a profound rearrangement of membrane lipids with the significant increase in SM and Chol and the decrease in PC and PS in the maturation of circulating R2 Retics, that translated into a highly significant increase in the ratio (SM + Chol)/phospholipids. We initially hypothesized that this ratio should decrease in the maturation of R2 Retics. In fact, our recent study of young and old RBCs revealed that a disproportionate loss of flotillin-2 and stomatin takes place during the aging *in vivo* of RBCs (Ciana et al., 2017a). We inferred from this that all membrane raft components could be selectively lost, pointing to a possible involvement of membrane rafts in the age-related remodeling of the RBC membrane in the circulation.

By examining here the disproportionate loss of flotillin-2 and, to a lesser extent, of stomatin relative to Band-3 from Retics to RBCs, we initially recognized the hypothesized continuum of selective decrease in membrane raft components. When challenged with the analysis of lipids, however, this tenet could no longer be sustained because of the actual increase, instead of the expected decrease in the relative abundance of membrane raft lipids in the mature RBC with respect to the R2 Retic, as if RBCs were enriched in membrane rafts with respect to Retics. The two results are clearly conflicting and their interpretation is challenging (see below for additional comments).

The literature abounds with report of protein quantification carried out by Western blotting. In the light of results obtained

here, we caution against the fallacious assumption that is at the basis of such quantifications, i.e., that the chemiluminescence signal obtained by Western blotting is linearly proportional to the quantity of protein. To at least partially solve this problem, we have here adopted a different approach in which signal response curves were fitted with parabolic functions. In our particular setup, the best fitting curve was used on the Band 3 blots to determine the sample volume where identical quantities of Band 3 were present for RBCs and Retics. These values were then used to extrapolate the intensity signal of flotillin-2 (or stomatin) for Retics and RBCs on parabolic curves that fitted the flotillin-2 (or stomatin) signal obtained from the series of loaded samples. The ratio between these two signal values was then calculated and trusted as the real quantitative relation of the protein of interest between Retics and RBCs. However, it must be remarked that these two values of intensity signal lie on a curve which is in itself non-linear, and therefore their ratio is an overestimation of the real value. In other words, with this method the differences between samples are amplified to an extent proportional to the deviation from linearity of the "dose-response" curve. A value of 2.5 times more flotillin-2 in Retics than RBCs relative to Band 3 (or a value of 1.5 for stomatin) is therefore most likely over-estimated because of this distortion.

Quantification of Band 3 in experiments where the same number of cells (Retics and RBCs) were loaded (see **Supplementary Material, Sheet "EXP09-10-B3-Sp"**) revealed a decrease that, according to the Western blotting results, also appeared to be disproportionate to the difference in surface area between Retics and RBCs. Band 3 levels appear to be 2.5 higher in Retics than in RBCs from the same donor. As it is unlikely that R2 Retics lose more than half of their membrane in maturing to RBCs, the Band 3 difference is probably overestimated, due to the non-linearity of Western blotting quantification. Yet, as the differences in flotillin-2 and stomatin between Retics and RBCs were evaluated relative to Band 3, they must reflect a real selective loss of the two proteins (higher for flotillin-2, lower for stomatin), disproportionate with respect to the loss of membrane surface area and of Band 3.

Another comment on Band 3 quantification, is that a difference of approximately 30% in the levels of Band 3 between two donors when the same numbers of cells were loaded in the gels was observed, both for RBCs and Retics. The mean cell volume (MCV) difference of RBCs from the two donors was in the same direction as the Band 3 difference (higher MCV for the donor with more Band 3), but it amounted to no more than 1%. As it is unlikely that copy numbers of Band 3 molecules per RBC in the general population differ by as much as 30%, this value must have been again amplified because of the non-linear bias intrinsic in the Western blotting quantification.

Concerning the observed decrease relative to Band 3, in the raft marker protein flotillin-2 (and, to a lesser extent in stomatin), and the conflicting result of an apparent relative increase in raft lipids from Retics to RBCs, additional comments are in order. Considering the never settled debate as to whether DRM are a valid representation of membrane rafts, it could be questioned whether flotillins are indeed a component of membrane rafts, because, from our results, they seem to be lost independently from the typical raft lipids. Although the literature on the localization of flotillins in cell membranes provides evidence of a selective partitioning of these proteins in the liquid ordered phase, this notion is largely derived from studies conducted on DRM that assume the identity of DRM and membrane rafts with all the limitations associated with this questioned protocol. Flotillin-1 defines a form of clathrin-independent endocytosis, different form the fluid phase endocytosis dependent on caveolae (Glebov et al., 2006). Consistent with this, it is found localized in different rafts from those where caveolins are found. Whether flotillins are also capable of driving these forms of endocytosis, and if they exist in RBCs is unknown. It was earlier hypothesized that membrane rafts are heterogeneous entities (Pike, 2004). It could be therefore that different raft families exist, some in which flotillins and stomatin are absent, and some with variable and different amounts of each of these two proteins. This different distribution could be driven by a different lipid composition of the rafts, perhaps also in terms of different phospholipid subclasses. Whereas, all the raft classes could be isolated as DRM with the non-ionic detergent; only one or more subclasses are indeed lost with the maturation of Retics, taking with them a significant portion of flotillin-2 and stomatin. The larger difference in flotillin-2 content than in stomatin content between Retics and RBCs that we have documented here seems to support this view. It is always possible, on the other hand, that flotillins decrease through mechanisms independent from the loss of membrane extension (e.g., proteolysis, aggregation). That flotillins behave differently from other membrane raft proteins is suggested by our own results on the above-mentioned disproportionate decrease in flotillin-2 with RBC aging. In the same study, the decrease in stomatin from young to old RBCs was much less pronounced than that of flotillin-2, and almost entirely justifiable by the loss of membrane surface area from young to old RBCs (Ciana et al., 2017a). Future investigations into this aspect will require the analysis of a wider range of raft proteins and lipids in Retics and RBCs. Also, lipidomics analysis of RBCs of different age is in order to ascertain whether there is a remodeling of the lipid components with the aging of RBCs.

Results of the lipidomics analysis of the different lipid subclasses revealed significant differences between Retics and RBCs. In front of an increase of total SM and also of all the SM subclasses with respect to total membrane lipids (about 2.7% of total lipids) from Retics to RBCs, the relative abundance of the various subclasses changed significantly in this maturation process. The species with a shorter and saturated N–amidated acyl chain increased more than the unsaturated species so that the ratio saturated/unsaturated became higher in RBCs. Scarce are literature data on the different lipid subclasses in membrane rafts. In one study, DRMs from human RBC ghosts were shown to be enriched in the saturated species of SM and depleted in the unsaturated ones (Koumanov et al., 2005). Our results would therefore corroborate the view of the retention of membrane rafts in the maturation of Retics to RBCs. Less clear are the changes in PC content. Here, an overall decrease of PC of about 3.5% from Retics to RBCs would still be compatible with the retention of membrane rafts in the transition Retic to RBC, because the percentage of PC over total lipids is lower in rafts than

in the parent cell membrane. Therefore a preferential loss of non-raft material from Retics would be compatible with the overall decrease in PC observed here. Looking at the reorganization of PC subclasses in our data set, more subtle and interesting differences emerge. The saturated and mono-unsaturated PC species decrease more in RBCs than the polyunsaturated species. Assuming that the PC content in rafts is represented more by saturated and monounsaturated species, as could be inferred from data obtained in other cell types (Ogiso et al., 2015), our data shows an enrichment in RBCs of the polyunsaturated PC classes which go against the above hypothesized retention of rafts in the maturation of Retics to RBCs. However, the composition of rafts varies widely in different cell types, the distribution of PC subclasses in raft and non-raft human RBC samples was not documented in the mentioned article (Koumanov et al., 2005) and we could not find a source for this information in the literature. Therefore, this interpretation is not final. It could be also conceived that with the preferential decrease in saturated PC species, the unsaturated ones would contribute to an overall fluidification of the membrane in mature RBCs.

From the reassortment of lipids between R2 Retics and RBCs it could be concluded that membrane rafts are relatively enriched in RBCs. It remains to be established whether the same enrichment occurs during the aging of RBCs in the circulation, and future work will fill this gap. In our previous research on membrane rafts, isolated as DRM from human RBC ghosts (Ciana et al., 2005; Crepaldi Domingues et al., 2009) or whole RBCs (Domingues et al., 2010; Ciana et al., 2011, 2013) we have amply demonstrated that for the extraction of DRM, an increase in pH and ionic strength of the medium containing the non-ionic detergent (Triton X-100) must be also provided. This requirement was interpreted as if electrostatic interactions existed, determining the association between membrane rafts and the membrane-skeleton (Ciana et al., 2014). This pointed to the existence of proteolipid interactions between the bilayer and the spectrin network that contribute, beside the conventional protein-mediated anchorages, to the stabilization of the membrane. Such high-salt-sensitive association between raft proteins and the membrane skeleton was recently confirmed in a proteomic analysis of triton-insoluble membrane skeletons from human RBCs (Basu et al., 2015). Maturing Retics are highly unstable, because the lipid bilayer is not yet completely anchored to the skeleton, and an excess membrane must be eliminated. The selective retention of membrane rafts in mature RBCs may find an explanation in the role of the rafts as additional anchoring sites that associate the bilayer with the skeleton. After the rafts, or at least those raft subclasses that have this ability, become associated with the spectrin network, the excess of plasma membrane that is not linked with the skeleton could be lost. Because this extra membrane is relatively depleted in rafts, the lipid composition of the bilayer in the mature RBC will reflect this selective rearrangement with the increase in the relative content of SM and Chol, as we have shown here. A graphical conceptualization of the model of Retic maturation proposed here is shown in **Figure 6**.

Other aspects have emerged from this study that are connected with the relative quantification of Band 3 and spectrin in Retics vs. RBCs. With all the limitations associated with the non-linearity of Western blotting quantification, results showed nonetheless that Band 3 and spectrin seem to be partially lost with the membrane of maturing R2 Retics. With this approach we could not assess whether β-spectrin is lost together with portions of the membrane skeleton, or as isolated heterodimers with α-spectrin or tetramers. From results on the maturation of R1 Retics, where, despite the significant loss of plasma membrane, all membrane-skeletal proteins are retained together with Band 3, it was expected that also for the maturation of R2 retics an efficient method was selected to salvage important and precious macromolecules that could all contribute to defining the final architecture of the mature RBCs. This loss of membrane skeleton

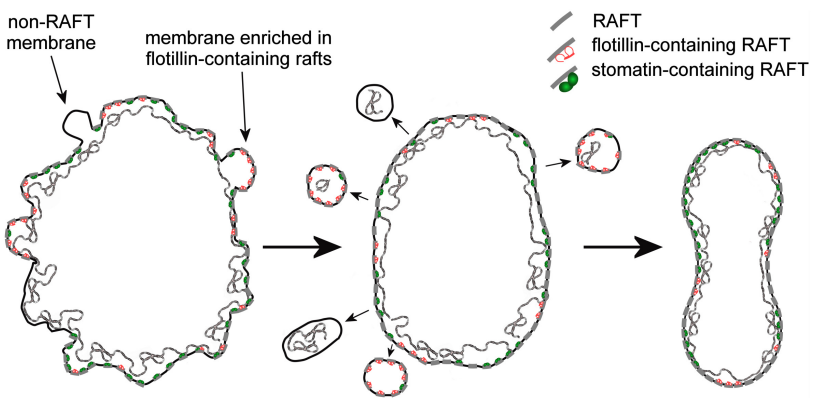

FIGURE 6 | Graphical conceptualization of the process of membrane raft enrichment in the maturation of R2 Retics. From a large and irregularly shaped R2 Retic (left) selected portions of non-raft membrane, or membrane selectively enriched in flotillin-2-containing rafts, together with some membrane skeleton are lost or, more likely, pinched off in the splenic milieu by the action of macrophages. The now resized lipid bilayer (middle) completes the anchoring to the membrane skeleton also thanks to the contribution of membrane raft interaction with the spectrin network, resulting in a mature and stable discocytic shape (right). The anchoring complexes based on band 3-ankyrin and the actin-based junctional complexes have been omitted for clarity. Membrane rafts are shown as short segments crossing the lipid bilayer. The various components are not drawn in scale.

was therefore somewhat unexpected, and if confirmed, it will thicken the mystery surrounding the mechanism(s) of terminal Retic maturation. In fact, it is still unclear if, and to what extent Retics can complete maturation *in vitro* (Gronowicz et al., 1984; Koury et al., 2005). In our opinion it is unlikely that membrane loss is a process that R2 Retics can perform spontaneously. In support to this concept there are two major observations: in splenectomized subjects, maturation of Retics is delayed and altered and RBCs display morphological and biochemical alterations (Holroyde and Gardner, 1970; Shattil and Cooper, 1972; Crosby, 1977; De Haan et al., 1988) *in vitro* cultured RBCs fail to achieve complete maturation to biconcave discocytes (Giarratana et al., 2005; Shah et al., 2014). In an early report it was described that Retics contain a high molecular weight complex, composed of spectrin and other not better characterized membrane proteins, that is lost with maturation only in normal subjects, whereas it is still present in circulating RBCs in splenectomized patients (Lux and John, 1977). This membrane remodeling was interpreted as the result of a "culling" action of the spleen. This organ would be continuously processing the cells and be responsible for generating those changes that R2 Retics and RBCs sustain throughout their circulatory life, simply because these cell types are no longer able to remodel their structure spontaneously. Shedding light on basic mechanisms of membrane remodeling, on the role of lipids in erythropoiesis, and on the interplay between RBCs and other components of the vascular system may also contribute to improve the conditions for the cultivation and full maturation *in vitro* of RBCs for transfusion purposes.

DATA AVAILABILITY STATEMENT

The datasets generated for this study are available on request to the corresponding author.

ETHICS STATEMENT

The studies involving human participants were reviewed and approved on 2017/04/10, by the local ethics committee: Comitato Etico Area Pavia, IRCCS Policlinico San Matteo, Pavia, Italy. The patients/participants provided their written informed consent to participate in this study.

AUTHOR CONTRIBUTIONS

GM, AC, and CA contributed to the conception and design of the work. GM, CA, AC, CB, and ID contributed to the experimental work. CB and ID contributed to the lipid analyses. GM, AC, CA, CB, ID, SB, and CP contributed to the data analysis and interpretation. GM and AC contributed to the writing of the manuscript. CB, ID, SB, and CP contributed to the editing of the manuscript. All authors edited and revised the manuscript, and gave final approval for publication.

FUNDING

This work was supported by the EU Commission Horizon 2020 Marie Skłodowska-Curie Actions Innovative Training Networks project RELEVANCE Grant Agreement N. 675115. Research conducted within the "Dipartimenti di Eccellenza" program (2018–2022) of the Italian Ministry of Education, University and Research (MIUR) – Dept. of Biology and Biotechnology "L. Spallanzani," University of Pavia (to CA, AC, GM).

ACKNOWLEDGMENTS

We would like to thank the following contributors: the personnel of the "Servizio di Immunoematologia e Medicina Trasfusionale" of the IRCCS Policlinico San Matteo, Pavia, and all the blood donors who accepted to provide samples for the conduction of this research; the personnel of the "Laboratorio Analisi Chimico Cliniche, Dipartimento Medicina Diagnostica," IRCCS Policlinico San Matteo, Pavia, for performing reticulocyte counts; Harald Köfeler and Martin Trötzmüller at the core facility mass spectrometry, Center for Medical Research, Medical University of Graz, Graz, Austria for the analyses of lipids.

SUPPLEMENTARY MATERIAL

The Supplementary Material for this article can be found online at: https://www.frontiersin.org/articles/10.3389/fphys.2020.00215/full#supplementary-material

REFERENCES

Achilli, C., Ciana, A., Balduini, C., Risso, A., and Minetti, G. (2011). Application of gelatin zymography for evaluating low levels of contaminating neutrophils in red blood cell samples. *Anal. Biochem.* 409, 296–297. doi: 10.1016/j.ab.2010.10.019

Anstee, D. J., Gampel, A., and Toye, A. M. (2012). Ex-vivo generation of human red cells for transfusion. *Curr. Opin. Hematol.* 19, 163–169. doi: 10.1097/MOH.0b013e328352240a

Asaro, R. J., Zhu, Q., and Cabrales, P. (2018). Erythrocyte aging, protection via vesiculation: an analysis methodology via oscillatory flow. *Front. Physiol.* 9:1607. doi: 10.3389/fphys.2018.01607

Basu, A., Harper, S., Pesciotta, E. N., Speicher, K. D., Chakrabarti, A., and Speicher, D. W. (2015). Proteome analysis of the triton-insoluble erythrocyte membrane skeleton. *J. Proteomics* 128, 298–305. doi: 10.1016/j.jprot.2015.08.004

Bernecker, C. M., Köfeler, H., Pabst, G., Trötzmüller, M., Kolb, D., Strohmayer, K., et al. (2019). Cholesterol deficiency causes impaired osmotic stability of cultured red blood cells. *Front. Physiol.* 10:1529. doi: 10.3389/fphys.2019.01529

Beutler, E., West, C., and Blume, K. G. (1976). The removal of leukocytes and platelets from whole blood. *J. Lab. Clin. Med.* 88, 328–333.

Carayon, K., Chaoui, K., Ronzier, E., Lazar, I., Bertrand-Michel, J., Roques, V., et al. (2011). Proteolipidic composition of exosomes changes during reticulocyte maturation. *J. Biol. Chem.* 286, 34426–34439. doi: 10.1074/jbc.M111.257444

Chasis, J. A., Prenant, M., Leung, A., and Mohandas, N. (1989). Membrane assembly and remodeling during reticulocyte maturation. *Blood* 74, 1112–1120. doi: 10.1182/blood.v74.3.1112.1112

Ciana, A., Achilli, C., Balduini, C., and Minetti, G. (2011). On the association of lipid rafts to the spectrin skeleton in human erythrocytes. *Biochim. Biophys. Acta* 1808, 183–190. doi: 10.1016/j.bbamem.2010.08.019

Ciana, A., Achilli, C., Gaur, A., and Minetti, G. (2017a). Membrane remodelling and vesicle formation during ageing of human red blood cells. *Cell. Physiol. Biochem.* 42, 1127–1138. doi: 10.1159/000478768

Ciana, A., Achilli, C., and Minetti, G. (2017b). Spectrin and other membrane-skeletal components in human red blood cells of different age. *Cell. Physiol. Biochem.* 42, 1139–1152. doi: 10.1159/000478769

Ciana, A., Achilli, C., Hannoush, R. N., Risso, A., Balduini, C., and Minetti, G. (2013). Freely turning over palmitate in erythrocyte membrane proteins is not responsible for the anchoring of lipid rafts to the spectrin skeleton: a study with bio-orthogonal chemical probes. *Biochim. Biophys. Acta* 1828, 924–931. doi: 10.1016/j.bbamem.2012.11.029

Ciana, A., Achilli, C., and Minetti, G. (2014). Membrane rafts of the human red blood cell. *Mol. Membr. Biol.* 31, 47–57. doi: 10.3109/09687688.2014.896485

Ciana, A., Balduini, C., and Minetti, G. (2005). Detergent-resistant membranes in human erythrocytes and their connection to the membrane-skeleton. *J. Biosci.* 30, 317–328. doi: 10.1007/BF02703669

Crepaldi Domingues, C., Ciana, A., Buttafava, A., Balduini, C., de Paula, E., and Minetti, G. (2009). Resistance of human erythrocyte membranes to Triton X-100 and C12E8. *J. Membr. Biol.* 227, 39–48. doi: 10.1007/s00232-008-9142-4

Crosby, W. H. (1977). Splenic remodeling of red cell surfaces. *Blood.* 50, 643–645. doi: 10.1182/blood.V50.4.643.643

de Gassart, A., Geminard, C., Fevrier, B., Raposo, G., and Vidal, M. (2003). Lipid raft-associated protein sorting in exosomes. *Blood* 102, 4336–4344. doi: 10.1182/blood-2003-03-0871

De Haan, L. D., Werre, J. M., Ruben, A. M., Huls, A. H., de Gier, J., and Staal, G. E. (1988). Reticulocyte crisis after splenectomy: evidence for delayed red cell maturation? *Eur. J. Haematol.* 41, 74–79. doi: 10.1111/j.1600-0609.1988.tb00872.x

Domingues, C. C., Ciana, A., Buttafava, A., Casadei, B. R., Balduini, C., de Paula, E., et al. (2010). Effect of cholesterol depletion and temperature on the isolation of detergent-resistant membranes from human erythrocytes. *J. Membr. Biol.* 234, 195–205. doi: 10.1007/s00232-010-9246-5

Giarratana, M. C., Kobari, L., Lapillonne, H., Chalmers, D., Kiger, L., Cynober, T., et al. (2005). Ex vivo generation of fully mature human red blood cells from hematopoietic stem cells. *Nat. Biotechnol.* 23, 69–74. doi: 10.1038/nbt1047

Glebov, O. O., Bright, N. A., and Nichols, B. J. (2006). Flotillin-1 defines a clathrin-independent endocytic pathway in mammalian cells. *Nat. Cell Biol.* 8, 46–54. doi: 10.1038/ncb1342

Gronowicz, G., Swift, H., and Steck, T. L. (1984). Maturation of the reticulocyte in vitro. *J. Cell Sci.* 71, 177–197.

Gu, Q., Yang, X., Lv, J., Zhang, J., Xia, B., Kim, J. D., et al. (2019). AIBP-mediated cholesterol efflux instructs hematopoietic stem and progenitor cell fate. *Science* 363, 1085–1088. doi: 10.1126/science.aav1749

Harding, C., Heuser, J., and Stahl, P. (1984). Endocytosis and intracellular processing of transferrin and colloidal-gold transferrin in rat reticulocytes: demonstration of a pathway for receptor shedding. *Eur. J. Cell Biol.* 35, 256–263.

Hartler, J., Triebl, A., Ziegl, A., Trotzmuller, M., Rechberger, G. N., Zeleznik, O. A., et al. (2017). Deciphering lipid structures based on platform-independent decision rules. *Nat. Methods* 14, 1171–1174. doi: 10.1038/nmeth.4470

Hartler, J., Trotzmuller, M., Chitraju, C., Spener, F., Kofeler, H. C., and Thallinger, G. G. (2011). Lipid data analyzer: unattended identification and quantitation of lipids in LC-MS data. *Bioinformatics* 27, 572–577. doi: 10.1093/bioinformatics/btq699

Holroyde, C. P., and Gardner, F. H. (1970). Acquisition of autophagic vacuoles by human erythrocytes. Physiological role of the spleen. *Blood* 36, 566–575. doi: 10.1182/blood.v36.5.566.566

Koumanov, K. S., Tessier, C., Momchilova, A. B., Rainteau, D., Wolf, C., and Quinn, P. J. (2005). Comparative lipid analysis and structure of detergent-resistant membrane raft fractions isolated from human and ruminant erythrocytes. *Arch. Biochem. Biophys.* 434, 150–158. doi: 10.1016/j.abb.2004.10.025

Koury, M. J., Koury, S. T., Kopsombut, P., and Bondurant, M. C. (2005). In vitro maturation of nascent reticulocytes to erythrocytes. *Blood* 105, 2168–2174. doi: 10.1182/blood-2004-02-0616

Laemmli, U. K. (1970). Cleavage of structural proteins during the assembly of the head of bacteriophage T4. *Nature* 227, 680–685. doi: 10.1038/227680a0

Lux, S. E., and John, K. M. (1977). Isolation and partial characterization of a high molecular weight red cell membrane protein complex normally removed by the spleen. *Blood* 50, 625–641. doi: 10.1182/blood.V50.4.625.625

Matyash, V., Liebisch, G., Kurzchalia, T. V., Shevchenko, A., and Schwudke, D. (2008). Lipid extraction by methyl-tert-butyl ether for high-throughput lipidomics. *J. Lipid. Res.* 49, 1137–1146. doi: 10.1194/jlr.D700041-JLR200

Minetti, G., Achilli, C., Perotti, C., and Ciana, A. (2018). Continuous change in membrane and membrane-skeleton organization during development from proerythroblast to senescent red blood cell. *Front. Physiol.* 9:286. doi: 10.3389/fphys.2018.00286

Minetti, G., Egée, S., Mörsdorf, D., Steffen, P., Makhro, A., Achilli, C., et al. (2013). Red cell investigations: art and artefacts. *Blood Rev.* 27, 91–101. doi: 10.1016/j.blre.2013.02.002

Moras, M., Lefevre, S. D., and Ostuni, M. A. (2017). From erythroblasts to mature red blood cells: organelle clearance in mammals. *Front Physiol.* 8:1076. doi: 10.3389/fphys.2017.01076

Ney, P. A. (2011). Normal and disordered reticulocyte maturation. *Curr. Opin. Hematol.* 18, 152–157. doi: 10.1097/MOH.0b013e328345213e

Ogiso, H., Taniguchi, M., and Okazaki, T. (2015). Analysis of lipid-composition changes in plasma membrane microdomains. *J. Lipid Res.* 56, 1594–1605. doi: 10.1194/jlr.M059972

Ovchynnikova, E., Aglialoro, F., Von Lindern, M., and van den Akker, E. (2018). The shape shifting story of reticulocyte maturation. *Front. Physiol.* 9:829. doi: 10.3389/fphys.2018.00829

Pan, B. T., and Johnstone, R. M. (1983). Fate of the transferrin receptor during maturation of sheep reticulocytes in vitro: selective externalization of the receptor. *Cell* 33, 967–978. doi: 10.1016/0092-8674(83)90040-5

Pike, L. J. (2004). Lipid rafts: heterogeneity on the high seas. *Biochem. J.* 378, 281–292. doi: 10.1042/BJ20031672

Salzer, U., and Prohaska, R. (2001). Stomatin, flotillin-1, and flotillin-2 are major integral proteins of erythrocyte lipid rafts. *Blood* 97, 1141–1143. doi: 10.1182/blood.v97.4.1141

Shah, S., Huang, X., and Cheng, L. (2014). Concise review: stem cell-based approaches to red blood cell production for transfusion. *Stem Cells Transl. Med.* 3, 346–355. doi: 10.5966/sctm.2013-0054

Shattil, S. J., and Cooper, R. A. (1972). Maturation of macroreticulocyte membranes in vivo. *J. Lab. Clin. Med.* 79, 215–227.

Skotland, T., Sandvig, K., and Llorente, A. (2017). Lipids in exosomes: current knowledge and the way forward. *Prog. Lipid Res.* 66, 30–41. doi: 10.1016/j.plipres.2017.03.001

Sonnino, S., Prinetti, A., Mauri, L., Chigorno, V., and Tettamanti, G. (2006). Dynamic and structural properties of sphingolipids as driving forces for the formation of membrane domains. *Chem. Rev.* 106, 2111–2125. doi: 10.1021/cr0100446

Triebl, A., Trotzmuller, M., Hartler, J., Stojakovic, T., and Kofeler, H. C. (2017). Lipidomics by ultrahigh performance liquid chromatography-high resolution mass spectrometry and its application to complex biological samples. *J. Chromatogr. B Analyt. Technol. Biomed. Life Sci.* 1053, 72–80. doi: 10.1016/j.jchromb.2017.03.027

Vidal, M., Sainte-Marie, J., Philippot, J. R., and Bienvenue, A. (1989). Asymmetric distribution of phospholipids in the membrane of vesicles released during in vitro maturation of guinea pig reticulocytes: evidence precluding a role for "aminophospholipid translocase. *J. Cell Physiol.* 140, 455–462. doi: 10.1002/jcp.1041400308

Zingariello, M., Bardelli, C., Sancillo, L., Ciaffoni, F., Genova, M. L., Girelli, G., et al. (2019). Dexamethasone predisposes human erythroblasts toward impaired lipid metabolism and renders their ex vivo expansion highly dependent on plasma lipoproteins. *Front Physiol.* 10:281. doi: 10.3389/fphys.2019.00281

Conflict of Interest: The authors declare that the research was conducted in the absence of any commercial or financial relationships that could be construed as a potential conflict of interest.

frontiers in Physiology

ORIGINAL RESEARCH
published: 28 April 2020
doi: 10.3389/fphys.2020.00357

Expression of South East Asian Ovalocytic Band 3 Disrupts Erythroblast Cytokinesis and Reticulocyte Maturation

*Joanna F. Flatt[1], Christian J. Stevens-Hernandez[1,2], Nicola M. Cogan[1], Daniel J. Eggleston[1], Nicole M. Haines[1], Kate J. Heesom[2], Veronique Picard[3,4], Caroline Thomas[5] and Lesley J. Bruce[1]**

[1] Bristol Institute for Transfusion Sciences, National Health Service (NHS) Blood and Transplant, Bristol, United Kingdom, [2] School of Biochemistry, University of Bristol, Bristol, United Kingdom, [3] Assistance Publique-Hôpitaux de Paris, Service d'Hématologie Biologique, Hôpital Bicêtre, Paris, France, [4] Faculté de Pharmacie, Université Paris-Saclay, Chatenay Malabry, France, [5] Hématologie et Immunologie Pédiatrique, Hôpital Mère Enfants, Nantes, France

OPEN ACCESS

Edited by:
Giampaolo Minetti, University of Pavia, Italy

Reviewed by:
Seth Leo Alper, Beth Israel Deaconess Medical Center, United States
Elisa Fermo, IRCCS Ca 'Granda Foundation Maggiore Policlinico Hospital, Italy
Reinhart Reithmeier, University of Toronto, Canada

***Correspondence:**
Lesley J. Bruce
Lesley.Bruce@nhsbt.nhs.uk

Specialty section:
This article was submitted to Red Blood Cell Physiology, a section of the journal Frontiers in Physiology

Received: *31 January 2020*
Accepted: *27 March 2020*
Published: *28 April 2020*

Citation:
Flatt JF, Stevens-Hernandez CJ, Cogan NM, Eggleston DJ, Haines NM, Heesom KJ, Picard V, Thomas C and Bruce LJ (2020) Expression of South East Asian Ovalocytic Band 3 Disrupts Erythroblast Cytokinesis and Reticulocyte Maturation. Front. Physiol. 11:357. doi: 10.3389/fphys.2020.00357

Southeast Asian Ovalocytosis results from a heterozygous deletion of 9 amino acids in the erythrocyte anion exchange protein AE1 (band 3). The report of the first successful birth of an individual homozygous for this mutation showed an association with severe dyserythropoietic anemia. Imaging of the proband's erythrocytes revealed the presence of band 3 at their surface, a reduction in Wr(b) antigen expression, and increases in glycophorin C, CD44, and CD147 immunoreactivity. Immunoblotting of membranes from heterozygous Southeast Asian Ovalocytosis red cells showed a quantitative increase in CD44, CD147, and calreticulin suggesting a defect in reticulocyte maturation, as well as an increase in phosphorylation at residue Tyr359 of band 3, and peroxiredoxin-2 at the membrane, suggesting altered band 3 trafficking and oxidative stress, respectively. *In vitro* culture of homozygous and heterozygous Southeast Asian Ovalocytosis erythroid progenitor cells produced bi- and multi-nucleated cells. Enucleation was severely impaired in the homozygous cells and reduced in the heterozygous cells. Large internal vesicular accumulations of band 3 formed, which co-localized with other plasma membrane proteins and with the autophagosome marker, LC3, but not with ER, Golgi or recycling endosome markers. Immunoprecipitation of band 3 from erythroblast cell lysates at the orthochromatic stage showed increased interaction of the mutant band 3 with heat shock proteins, ubiquitin and cytoskeleton proteins, ankyrin, spectrin and actin. We also found that the mutant band 3 forms a strong interaction with non-muscle myosins IIA and IIB, while this interaction could not be detected in wild type erythroblasts. Consistent with this, the localization of non-muscle myosin IIA and actin was perturbed in some Southeast Asian Ovalocytosis erythroblasts. These findings provide new insights toward understanding *in vivo* dyserythropoiesis caused by the expression of mutant membrane proteins.

Keywords: Southeast Asian ovalocytosis, Band 3, SLC4A1, dyserythropoiesis, hereditary stomatocytosis, congenital dyserythropoiesis type II, cytokinesis, reticulocyte maturation

INTRODUCTION

We previously reported on the only known case of homozygous Southeast Asian Ovalocytosis (SAO) (Picard et al., 2014), a condition caused by a mutation in *SLC4A1* the gene encoding erythrocyte anion exchanger 1 (AE1, band 3). The affected child was born prematurely with hydrops and severe anemia and developed distal renal tubular acidosis (dRTA) at 3 months. Bone marrow aspiration showed dyserythropoiesis. Unexpectedly, we found that some mature red blood cells (RBCs), containing SAO band 3 alone, were produced by the child's bone marrow and survived in the circulation. These cells were very large, cigar-shaped and had an altered affinity for certain anti-band 3 antibodies. We were interested to further characterize these cells and examine the effect that the expression of SAO band 3 had on erythropoiesis.

SAO is caused by the heterozygous deletion of codons 400–408 in *SLC4A1*. The translated protein carries the corresponding deletion of 9 amino acid residues (Jarolim et al., 1991; Tanner et al., 1991). The deletion occurs at the boundary between the cytoplasmic N-terminal domain and the transport-active transmembrane domain. This mutation abolishes the anion exchange activity of band 3, and is associated with significant structural changes, nonetheless the mutant protein is successfully expressed at the plasma membrane (Tanner et al., 1991; Schofield et al., 1992). Studies have shown that SAO band 3 is able to interact with and modify normal band 3 expressed in the same cell (Kuma et al., 2002). Band 3 exists as dimers and tetramers in the red cell membrane, but SAO band 3 is believed to form higher oligomers and associate with the underlying erythrocyte cytoskeleton more readily than wild type band 3, offering an explanation for the observed increase in membrane rigidity in these cells (Mohandas et al., 1992; Sarabia et al., 1993; Liu et al., 1995).

SAO has a distinctive geographical distribution, with cases predominantly in Malaysia, The Philippines and Papua New Guinea, and has thus far only ever been described in the heterozygous state (Liu et al., 1994). This is despite a relatively high allele frequency of 5–20% in certain populations (Amato and Booth, 1977). SAO has been the subject of much interest, because the mutation confers some protection from cerebral malaria, a severe complication of *Plasmodium falciparum* infection (Allen et al., 1999) and also protects against infection by *Plasmodium* vivax (Rosanas-Urgell et al., 2012). It had previously been thought that *P. falciparum* cannot invade SAO cells as easily as control cells, but there is no clinical data to support this (Lin et al., 2010). Experiments have shown that reduced invasion by *P. falciparum* is at least partly explained by accelerated depletion of ATP levels in SAO cells *in vitro* (Dluzewski et al., 1992). The depletion of ATP is secondary to a cation leak caused by the mutant band 3 protein, and in this respect SAO is similar to another cation-leaky disorder, cryohydrocytosis (CHC; Guizouarn et al., 2011). The SAO mutation is unusual in the context of the currently known band 3 mutations producing a cation leak, since these are invariably point mutations leading to single amino acid substitutions occurring around the transport domain, transmembrane spans 9 and 10 (Bruce et al., 2005).

In the present study, we have studied blood and bone marrow samples from the affected child, homozygous for the SAO mutation, and blood samples from their heterozygous parents. Analysis of the mature red cells and of erythroid progenitor cells grown in culture revealed multiple changes in both homozygous and heterozygous SAO cells, including altered band 3 protein interactions and trafficking. Notably, the expression of SAO band 3 results in multinucleated erythroblasts, and reduced proliferation and enucleation, producing a dyserythropoietic phenotype.

MATERIALS AND METHODS

Patients

The homozygous SAO patient and heterozygous SAO parents have been described (Picard et al., 2014). In brief, the child was born prematurely with hydrops, and severe anemia which was treated with monthly transfusions. Distal renal tubular acidosis (dRTA) developed at 3 months and was treated with sodium bicarbonate and potassium gluconate. The severe anemia was caused in part by hemolysis (perhaps aggravated by the co-inherited hemoglobin defects) but also from deficient red cell production. Genetic analyses indicated that the child inherited a heterozygous 3.7 kb alpha-globin deletion (HBA1 HBA2-3.7 kb del) from the mother, a heterozygous beta-globin variant "La Desirade" (resulting from HBB c.389 C > T) from the father, and homozygous SAO. He did not inherit his mother's sickle cell trait (HBB c.20 C > T). Hb "La Desirade" is asymptomatic in heterozygotes and could not account for the early severe anemia because beta-globin is not significantly expressed at 22 weeks gestation. The heterozygous -3.7 alpha thalassemia trait has usually very mild consequences on erythropoiesis and is totally asymptomatic, except for minor microcytosis, even when homozygous. Indeed, the mother has a homozygous -3.7 alpha thalassemia trait (plus a beta globin S variant) with no anemia. Bone marrow aspirate from the child showed binuclearity, karyorrhexis and macrocytosis, features typical of dyserythropoiesis. The child is now 10 years old and quite well, with regular transfusions, iron chelation and acidosis treatment. Written informed consent was obtained from both parents for themselves and the child. This study is part of a larger study approved by the National Health Service National Research Ethics Service South West entitled "*In Vitro* Studies of Erythropoiesis in Health and Disease."

Erythrocyte Membrane Protein Analysis

Preparation of erythrocyte membranes, SDS-PAGE and Western blotting analysis of heterozygous SAO membranes were carried out as previously described (Bruce et al., 2003). Antibodies are listed in **Table 1**. Blots were analyzed using semi-quantitative

TABLE 1 | Antibodies used in the study.

Protein/antigen	Antibody/clone	Company	Product no.	Species	Technique
Band 3	BRIC170	IBGRL		Mouse	IF/WB
Band 3	BRIC155	IBGRL		Mouse	IF
Band 3	BRIC132	IBGRL		Mouse	IF
Band 3	BRAC17	IBGRL		Rat	IF
Band 3	BRAC66	IBGRL		Rat	IP
Phospho-B3 Y8	polyclonal	In-house		Rabbit	WB
Phospho-B3 Y359	polyclonal	In-house		Rabbit	IF/WB
Phospho- B3 Y904	polyclonal	In-house		Rabbit	WB
Protein 4.2	polyclonal	In-house		Rabbit	WB
GPA	BRIC256	IBGRL		Mouse	IF
GPA	polyclonal	In-house		Rabbit	IF/WB
Wr(b)	BIRMA84b	IBGRL		Mouse	IF
Wr(b)	BRIC13	IBGRL		Mouse	IF
Wr(b)	BRAC13	IBGRL		Rat	IF
GPB (and to a lesser extent GPA)	R1.3	IBGRL		Mouse	IF/WB
RhAG	LA1818	IBGRL		Mouse	IF
RhAG	polyclonal	In-house		Rabbit	WB
Rh	polyclonal	In-house		Rabbit	WB
Rh	BRIC69	IBGRL		Mouse	IF
CD47	BRIC211	IBGRL		Mouse	IF
CD47	polyclonal	In-house		Rabbit	WB
ICAM-4	BS46/BS56	IBGRL		Mouse	WB
GPC	BRIC10	IBGRL		Mouse	IF
GPC	polyclonal	In-house		Rabbit	IF/WB
CD44	BRIC235	IBGRL		Mouse	IF/WB
CD44	polyclonal	In-house		Rabbit	IF
Ankyrin	BRIC274	IBGRL		Mouse	IF
Alpha-spectrin	BRIC174	IBGRL		Mouse	IF/WB
Beta-spectrin	BRAC65	IBGRL		Rat	WB
NMMIIA	polyclonal	Abcam	ab24762	Rabbit	IF/WB
NMMIIB	polyclonal	Abcam	ab24761	Rabbit	WB
Glut1	polyclonal	Gift from S. Baldwin		Rabbit	IF
Stomatin	GARP50	Gift from R. Prohaska		Mouse	IF
Stomatin	polyclonal	In-house		Rabbit	IF/WB
SLP-2	polyclonal	In-house		Rabbit	WB
Aquaporin-1	polyclonal	In-house		Rabbit	IF/WB
CD147	MEM-M6/1	AbD Serotec	MCA1876	Mouse	IF
CD147	EPR4053	Abcam	ab108308	Rabbit	WB
Lutheran	BRIC221	IBGRL		Mouse	WB
LFA-3 (CD58)	BRIC5	IBGRL		Mouse	WB
DAF (CD55)	BRIC128	IBGRL		Mouse	WB
Transferrin receptor	polyclonal	Abcam	ab84036	Rabbit	IF/WB
Calreticulin	polyclonal	Abcam	ab2907	Rabbit	IF/WB
Giantin	polyclonal	Covance	PRB-114C	Rabbit	IF
LAMP1	polyclonal	Abcam	ab24170	Rabbit	IF
LAMP2	monoclonal	Abcam	ab25631	Mouse	WB
LC3	polyclonal	MBL	PM036	Rabbit	IF
Pericentrin	polyclonal	Abcam	ab4448	Rabbit	IF
CD63	H5C6	BD Biosciences	556019	Mouse	IF
VDAC1	polyclonal	Abcam	ab15895	Rabbit	IF/WB
Peroxiredoxin 2	EPR5154	Abcam	ab109367	Rabbit	WB
Beta-actin	AC-15	Abcam	ab6276	Mouse	WB

IF, immunofluorescence; IP, immunoprecipitation; WB, Western blotting.

scanning densitometry with the use of ImageJ software[1] and ImageStudio (LI-COR Biosciences).

Culture of CD34$^+$ Cells

CD34$^+$ cells were isolated from a 3 ml sample of bone marrow from the proband and 50 ml peripheral blood samples from the parents and controls by positive selection using paramagnetic microbeads (Miltenyi Biotec, Germany) according to the manufacturer's instructions and cultured as described (Flatt et al., 2011). Briefly, cells were cultured at 37°C in a humidified atmosphere of 5% CO_2 in air. The base culture medium used throughout comprised IMDM (Biochrom, Germany) supplemented with 3% AB serum, 10 μg/ml insulin, 3 IU/ml heparin (all from Sigma-Aldrich, Poole, United Kingdom), 2% FCS (Hyclone, Fisher Scientific, Ltd., United Kingdom) 3 U/ml EPO (Roche, Basel, Switzerland) and 200 μg/ml holotransferrin (R&D Systems Minneapolis, MN, United States). On days 0–8 cells were cultured in base medium with 40 ng/ml SCF and 1 ng/ml IL3 (R&D systems). From days 9 to 12, in base medium with 10 ng/ml SCF and from day 13 onward in base medium with an increased holotransferrin concentration of 500 μg/ml. Cytomicrographs were prepared by cytocentrifugation (Shandon) of 2–4 $\times$ 10^4 cells onto slides at 1350 rpm for 5 min and stained with Leishman's (VWR) according to the manufacturer's instructions.

Confocal Microscopy

Peripheral blood samples from the homozygous SAO proband were obtained immediately before transfusion. Confocal imaging was carried out as described (Flatt et al., 2011). Briefly, erythrocytes (5 $\times$ 10^5 cells/slide) were fixed using 1% formaldehyde, 0.0075% glutaraldehyde and permeabilized with 0.1% Triton-X100. Reticulocytes and late stage erythroblasts (5 $\times$ 10^5 cells/slide) were fixed using 1% formaldehyde and permeabilized using 0.01% saponin. Early stage erythroblasts (5 $\times$ 10^5 cells/slide) were fixed using 3% formaldehyde and permeabilized with 0.01% digitonin. Antibodies are listed in **Table 1**.

Cultured Cell Lysate Analysis

At selected time points 2 $\times$ 10^6 cells were removed from the culture, washed once in PBS, then solubilized in 200 μl erythroblast lysis buffer (20 mM Tris-HCl, pH 7.5, 10% glycerol, 150 mM NaCl, 1% Triton-X100, 0.1% SDS, 2 mM PMSF, 1× protease inhibitor cocktail). Protein concentration was estimated using Bradford's reagent. Lysates were separated by SDS-PAGE on a 10% acrylamide gel. Equal amounts of protein (usually 10 μg) were loaded per gel track. Gels were immunoblotted as described (Bruce et al., 2003).

Immunoprecipitation of Proteins

Cultured homozygous SAO cells (4 $\times$ 10^6) at day 27, and cultured control cells (4 $\times$ 10^6) at day 14 matching the stage of the SAO cells as closely as possible (predominantly orthochromatic erythroblasts, ∼10% enucleated) were solubilized in NP40-IP buffer (1% Non-idet-P40, 150 mM KCl, 10 mM Tris-HCl, pH 7.4) and immunoprecipitated using protein G sepharose beads preloaded with rat monoclonal anti-band 3 (BRAC66) as described (Bruce et al., 2003). Immunoprecipitated proteins, using anti-band 3 (BRAC66) were separated by SDS-PAGE and analyzed by LC-MS/MS.

Protein Identification for Immunoprecipitates

Immunoprecipitated proteins, using anti-band 3 (BRAC66) antibody, were separated by SDS-PAGE. The gel lane was cut into 3 slices and each slice subjected to in-gel tryptic digestion using a ProGest automated digestion unit (Digilab United Kingdom). The resulting peptides were fractionated using a Dionex Ultimate 3000 nanoHPLC system in line with an LTQ-Orbitrap Velos mass spectrometer (Thermo Fisher Scientific). In brief, peptides in 1% (vol/vol) formic acid were injected onto an Acclaim PepMap C18 nano-trap column (Dionex). After washing with 0.5% (vol/vol) acetonitrile 0.1% (vol/vol) formic acid peptides were resolved on a 250 mm $\times$ 75 μm Acclaim PepMap C18 reverse phase analytical column (Dionex) over a 150 min organic gradient, using 7 gradient segments (1–6% solvent B over 1 min, 6–15% B over 58 min., 15–32%B over 58 min, 32–40%B over 3 min, 40–90%B over 1 min., held at 90%B for 6 min and then reduced to 1%B over 1 min.) with a flow rate of 300 nl min^{-1}. Solvent A was 0.1% formic acid and Solvent B was aqueous 80% acetonitrile in 0.1% formic acid. Peptides were ionized by nano-electrospray ionization at 2.1 kV using a stainless steel emitter with an internal diameter of 30 μm (Thermo Fisher Scientific) and a capillary temperature of 250°C. Tandem mass spectra were acquired using an LTQ- Orbitrap Velos mass spectrometer controlled by Xcalibur 2.1 software (Thermo Fisher Scientific) and operated in data-dependent acquisition mode. The Orbitrap was set to analyze the survey scans at 60,000 resolution (at m/z 400) in the mass range m/z 300–2000 and the top twenty multiply charged ions in each duty cycle selected for MS/MS in the LTQ linear ion trap. Charge state filtering, where unassigned precursor ions were not selected for fragmentation, and dynamic exclusion (repeat count, 1; repeat duration, 30 s; exclusion list size, 500) were used. Fragmentation conditions in the LTQ were as follows: normalized collision energy, 40%; activation q, 0.25; activation time 10 ms; and minimum ion selection intensity, 500 counts.

The raw data files were processed and quantified using Proteome Discoverer software v1.2 (Thermo Fisher Scientific) and searched against the SwissProt Human database (122604 entries) using the SEQUEST algorithm. Peptide precursor mass tolerance was set at 10 ppm, and MS/MS tolerance was set at 0.8 Da. Search criteria included carbamidomethylation of cysteine (+57.0214) as a fixed modification and oxidation of methionine (+15.9949) as a variable modification. Searches were performed with full tryptic digestion and a maximum of 1 missed cleavage was

[1] http://imagej.nih.gov/ij/

allowed. The reverse database search option was enabled and all peptide data was filtered to satisfy false discovery rate (FDR) of 5%.

RESULTS

Homozygous SAO Erythrocytes Are Large and Aberrantly-Shaped With Altered Membrane Protein Expression

In the clinical report of this patient we showed that homozygous SAO cells were clearly identifiable amongst the normal transfused donor red cells based on morphology and reduced reactivity with anti-band 3 monoclonal antibody BRIC6 (Smythe et al., 1995). The homozygous SAO cells can be very large (11–13 μm in length) and have grossly abnormal morphology. Cells are predominantly cigar-shaped, and some show a central cleft (**Figure 1**). These morphological changes probably result in cytoskeletal stretching, and affect protein packing, modifying the accessibility and presentation of epitopes. Indeed, apparent altered antigen expression in heterozygous SAO cells has been reported (Booth et al., 1977).

In order to investigate further changes in the SAO membrane, intact cells were incubated with various antibodies to extracellular epitopes of erythrocyte membrane proteins. The band 3 monoclonal antibody BRAC17 showed reduced binding compared to the donor cells (**Figure 1A**), as reported (Smythe et al., 1995; Picard et al., 2014). Similarly, anti-Rh-associated glycoprotein (RhAG) and anti-glycophorin A (GPA) showed slightly reduced immunoreactivity (**Figure 1A**), and reduced reactivity occurred with antibodies directed against the Wr(b) antigen which is formed by an interaction between GPA and band 3 (Bruce et al., 1995). Anti-glycophorin B (GPB) and anti-CD47 showed similar staining between the SAO and donor RBCs (**Figure 1A**). Anti-CD147, anti-CD44 and anti-glycophorin C (GPC) showed increased staining (**Figure 1A**). Increased CD147 staining was of interest because this protein has been identified as a universal receptor for *P. falciparum* invasion of red cells (Crosnier et al., 2011).

Nucleated erythroid cells were also detected in the homozygous SAO circulating red cell population, indicating their premature egress from the bone marrow (**Figure 1B**).

These changes in antibody staining in the confocal imaging analysis of SAO RBCs may reflect a quantitative change in protein expression, or a change in epitope presentation. Homozygous SAO RBC membranes were not available (as the patient was regularly transfused) so heterozygous SAO RBC membranes were analyzed by immunoblotting. Relative to control membranes, band 3, protein 4.2, GPA, RhAG, CD47 and Rh proteins were present in normal amounts, whereas GPB and aquaporin 1 (AQP1) were slightly reduced (**Figure 2**). Heterozygous SAO RBC membranes showed a 3-fold increase in the amount of Lutheran protein by immunoblotting but no difference in glycophorin C (GPC) (**Figure 2**). Strikingly, the membrane-associated anti-oxidant enzyme peroxiredoxin-2 (PRDX2) was 20-fold increased (**Figure 2**).

Examination of intracellular epitopes using α-spectrin and ankyrin antibodies and confocal imaging showed increased staining in homozygous SAO cells (**Figure 3**), but no quantitative increase was seen in α-spectrin in the heterozygous SAO immunoblots (**Figure 2**). Similarly, staining with intracellular band 3 antibodies (BRIC170, BRIC155, BRIC132) and intracellular antibodies to GPC and stomatin showed increased staining in homozygous SAO cells (**Figure 3**), but no quantitative increase was seen in the corresponding heterozygous SAO immunoblots (**Figure 2**), suggesting that the increased staining in the confocal imaging analysis of many of the intracellular epitopes may be due to an increased permeability of the SAO membrane.

In contrast, staining produced by an antibody specific to tyrosine phosphorylation of band 3 at residue 359 was increased in SAO homozygote erythrocytes (**Figure 3**) and immunoblotting confirmed the increased band 3 tyrosine phosphorylation at residue 359 in heterozygous SAO membranes (**Figure 2**). Phosphorylation at tyrosine residue 904 was absent in both SAO and control cells (data not shown).

Of note, a number of proteins migrated more slowly than wild type in SDS-PAGE, consistent with hyperglycosylation and suggestive of altered trafficking (**Figure 2**). These proteins included band 3, CD47, ICAM-4, and LFA-3, some of which are known to associate with band 3 in RBC membrane complexes (Bruce et al., 2003) and may be trafficked together with band 3 in the internal membranes.

Cultured SAO Cells Show a Dyserythropoietic Phenotype

$CD34^+$ cells from the bone marrow of the homozygous SAO proband were cultured alongside control $CD34^+$ cells from peripheral blood of a healthy volunteer. Control cells showed normal proliferation and differentiation (**Figures 4A–C**). In contrast, proliferation of homozygous SAO cells was normal at early stages of the culture, but reduced once band 3 started to be expressed around day 7 (**Figure 4A**). This reduction in the rate of proliferation of homozygous SAO cells had a number of causes but cannot be attributed to a difference in stem cell source (**Figure 4C**). Numerous dead cells and debris were noted in the homozygous SAO culture post day 11. Homozygous SAO cells also exhibited high numbers of multinucleated cells, coinciding with the time that band 3 is expressed (**Figure 4D**). The multiple nuclei in these cells suggest a defect in cytokinesis, the final stage of cell division. Although in the later stages of the culture, the percentage of multinucleated cells was observed to decrease slightly (**Figures 4D**, **5**). In later stages of the culture the low cell numbers may have been caused in part by the instability of the very large reticulocytes formed. It was also noted that the homozygous SAO cells failed to enucleate efficiently, reaching only 7% enucleation after 20 days in culture compared to 68% in controls (**Figure 4E**).

In a separate experiment $CD34^+$ cells from the peripheral blood of the heterozygous SAO parents of the proband were cultured alongside control $CD34^+$ cells from peripheral blood of a healthy volunteer. The heterozygous SAO cells from the father

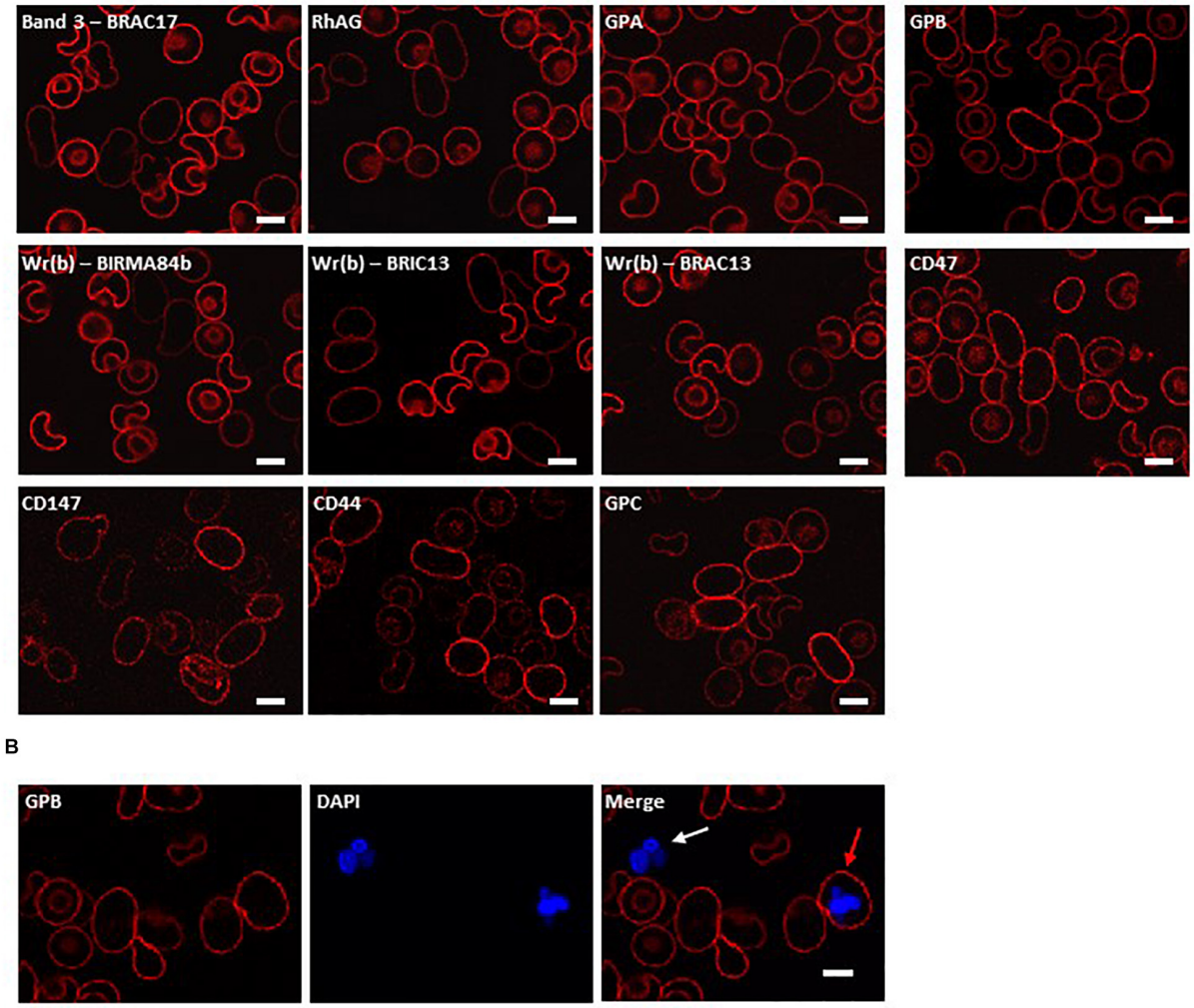

FIGURE 1 | Immunocytochemistry of homozygous SAO erythrocytes. Circulating erythrocytes from the homozygous SAO individual, containing both large, aberrantly-shaped homozygous SAO cells and normal biconcave donor cells, were imaged using immunofluorescent labeling and confocal microscopy. **(A)** Red cells were reacted with monoclonal antibodies directed to extracellular epitopes of membrane proteins of interest: Band 3 (BRAC17), RhAG (LA1818), GPA (BRIC256), GPB (and to a lesser extent GPA) (R1.3), Wr(b) (BIRMA 84b, BRIC13 and BRAC13), CD47 (BRIC211), CD147 (MEM6-6), CD44 (BRIC235), and GPC (BRIC10). **(B)** Red cells were co-stained with erythroid marker anti-GPB (and to a lesser extent GPA, R1.3; red) and DNA dye DAPI (blue). The white arrow indicates a leukocyte, the red arrow indicates an erythroid cell that has retained nuclear material. Numbers of nucleated erythroid cells were not sufficient to quantify accurately but were seen occasionally in the confocal slides of homozygous SAO peripheral blood whereas they are very rare in control slides. Images are representative of at least 5 different fields from one experiment. Scale bars represent 5 μm.

showed normal proliferation, whereas the cells from the mother grew less well (**Figure 4B**). Unexpectedly, the heterozygous SAO erythroblasts from both parents also displayed multinuclearity, although to a lesser extent (**Figures 4D**, **5**). Heterozygous SAO cells achieved 40–45% enucleation, compared to 60% in the control, at day 20 (**Figure 4E**).

Internal Vesicles of SAO Band 3 Co-stain With Other Membrane Proteins

In both heterozygous and homozygous RBCs SAO band 3 was successfully expressed at the erythroblast cell membrane throughout erythropoiesis (**Figure 6A**). However, at later stages of erythropoiesis it was present in large areas of dense staining in some SAO erythroblasts, but not in controls (**Figure 6A**). These were often located in the region between nuclei in bi-nuclear cells, and across the midbody area where the cytokinesis furrow is expected to form. Higher magnification imaging of heterozygous SAO cells revealed that these areas are composed of numerous clustered band 3-positive vesicles (**Figure 6B**). Immunoblots of cultured cell lysates showed reduced levels of band 3 and the presence of higher and lower molecular weight bands that probably represent aggregated band 3 and proteolytic fragments in homozygous SAO respectively. Again,

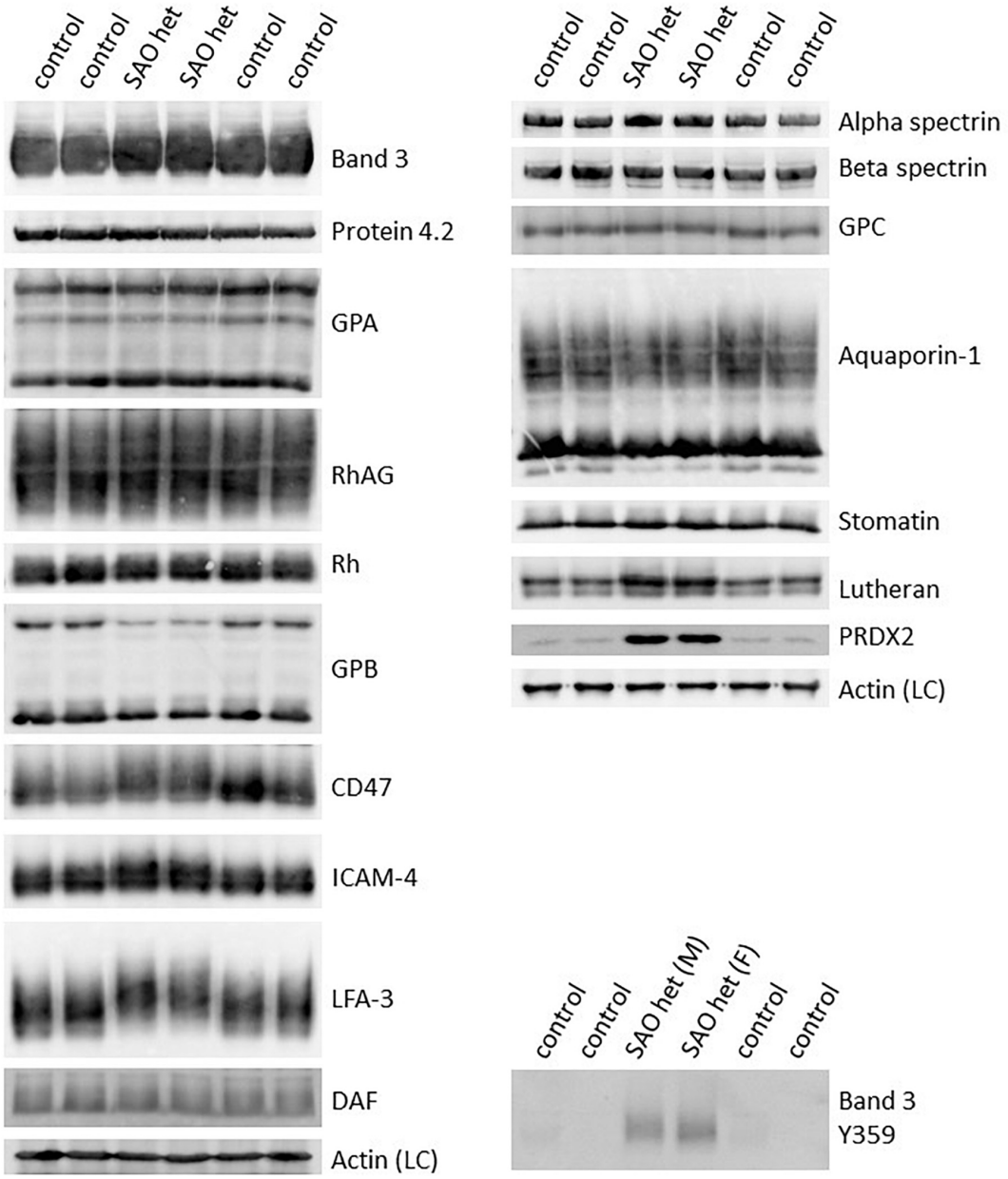

FIGURE 2 | Altered expression of membrane proteins in heterozygous SAO red cells. Red cell membranes from SAO and control peripheral blood samples were prepared, separated by SDS-PAGE and immunoblotted. The antibodies directed against protein 4.2, GPA, RhAG, Rh polypeptides, CD47, aquaporin-1, GPC, stomatin and phospho-Tyr359 band 3 were in-house rabbit polyclonal antibodies. Commercial antibodies were used to detect actin (ab6276) and peroxiredoxin-2 (PRDX2; ab109367) both from Abcam, Cambridge, United Kingdom. Monoclonal antibodies were used to detect band 3 (BRIC170), alpha-spectrin (BRIC174), beta-spectrin (BRAC65), GPB (and to a lesser extent GPA, R1.3), ICAM-4 (BS46/BS56), LFA-3 (BRIC5), DAF (BRIC128) and Lutheran (BRIC221). SAO het and SAO het (F): Membranes prepared from the heterozygous father of the homozygous SAO child. SAO het (M): Membranes prepared from the heterozygous mother of the homozygous SAO child. LC, Loading control.

it was noted that SAO band 3 migrated more slowly than wild type in SDS-PAGE, consistent with hyperglycosylation and suggestive of altered trafficking (**Figure 6C**). CD147 levels were found to be increased in homozygous SAO lysates relative to control in the early stages of culture (days 7 and 11) and total PRDX2 levels only began to increase relative to control in late culture (day 17).

Dual staining of band 3 with compartmental markers showed strong colocalization with the autophagosome marker LC3, but not with secretory pathway markers (**Figure 7**). Aquaporin-1 acted as a marker for the plasma membrane and showed strong colocalization with the band 3 aggregates (**Figure 7**). Other membrane proteins (CD44, GPA, GPC, stomatin, CD47, RhAG) also showed positive staining in the areas of aggregated band 3

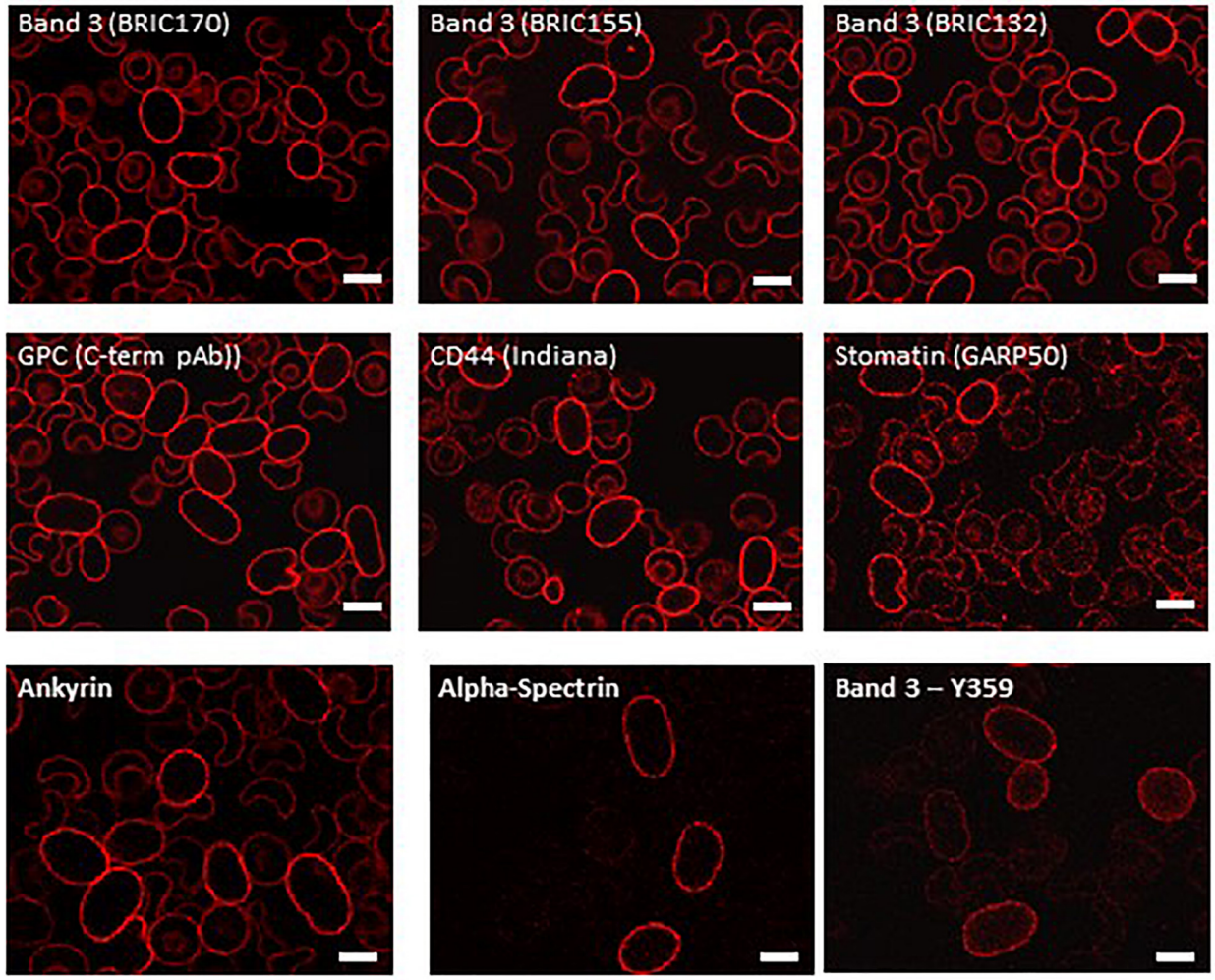

FIGURE 3 | Immunocytochemistry of permeabilized homozygous SAO erythrocytes. Circulating erythrocytes from the homozygous SAO individual were fixed, permeabilized and imaged using immunofluorescent labeling and confocal microscopy. Antibodies directed against intracellular epitopes of plasma membrane proteins. Mouse monoclonal antibodies were used to detect band 3 (BRIC170, BRIC155, BRIC132), stomatin (GARP50), ankyrin (BRIC274) and alpha-spectrin (BRIC174). In-house rabbit polyclonal antibodies were used to detect GPC, CD44 and phospho-Tyr359 band 3. Scale bars represent 5 μm.

(**Figure 8**), although the glucose transporter 1 (Glut1) formed aggregates that did not appear to colocalize with aggregated band 3. Membrane proteins that colocalized included proteins not known to associate directly with band 3 (CD44, GPC) suggesting that the origin of some of these vesicles may be endocytosis from the plasma membrane, although it is more probable that the vesicles arise from a problem in trafficking of membrane from Golgi to surface.

Analysis of Proteins Associated With Band 3

To identify which proteins were associating with band 3, band 3 immunoprecipitates (IP) from lysates of cultured homozygous SAO cells and control cells that were as closely stage-matched as possible were analyzed by Mass Spectrometry. The spectral count obtained for certain proteins were compared between control and SAO (**Figure 9A**). Band 3 appeared more strongly in the control [1239 peptide spectral matches (PSMs) vs. 573 PSMs in SAO]. In contrast, many of the known binding partners of band 3 showed an increase in the SAO IP, including RhAG and GLUT1 (Bruce et al., 2003). Of interest, SAO band 3 pulled down four times as much alpha and beta globin than did WT band 3 (**Figure 9A**). More PSMs were also identified for ankyrin, spectrin and actin, consistent with an increased association of SAO band 3 with cytoskeletal proteins (Mohandas et al., 1992; Sarabia et al., 1993; Liu et al., 1995).

Significant levels of non-muscle myosin proteins IIA and IIB were identified in the SAO IP but none in the control (**Figure 9A**). Heterozygous SAO red cell membranes contained an increased amount of both proteins (**Figure 9B**). Non-muscle myosin II (NMMII) is involved in contractile ring formation in cytokinesis, and non-muscle myosin IIB plays a crucial role in erythroblast enucleation (Ubukawa et al., 2012;

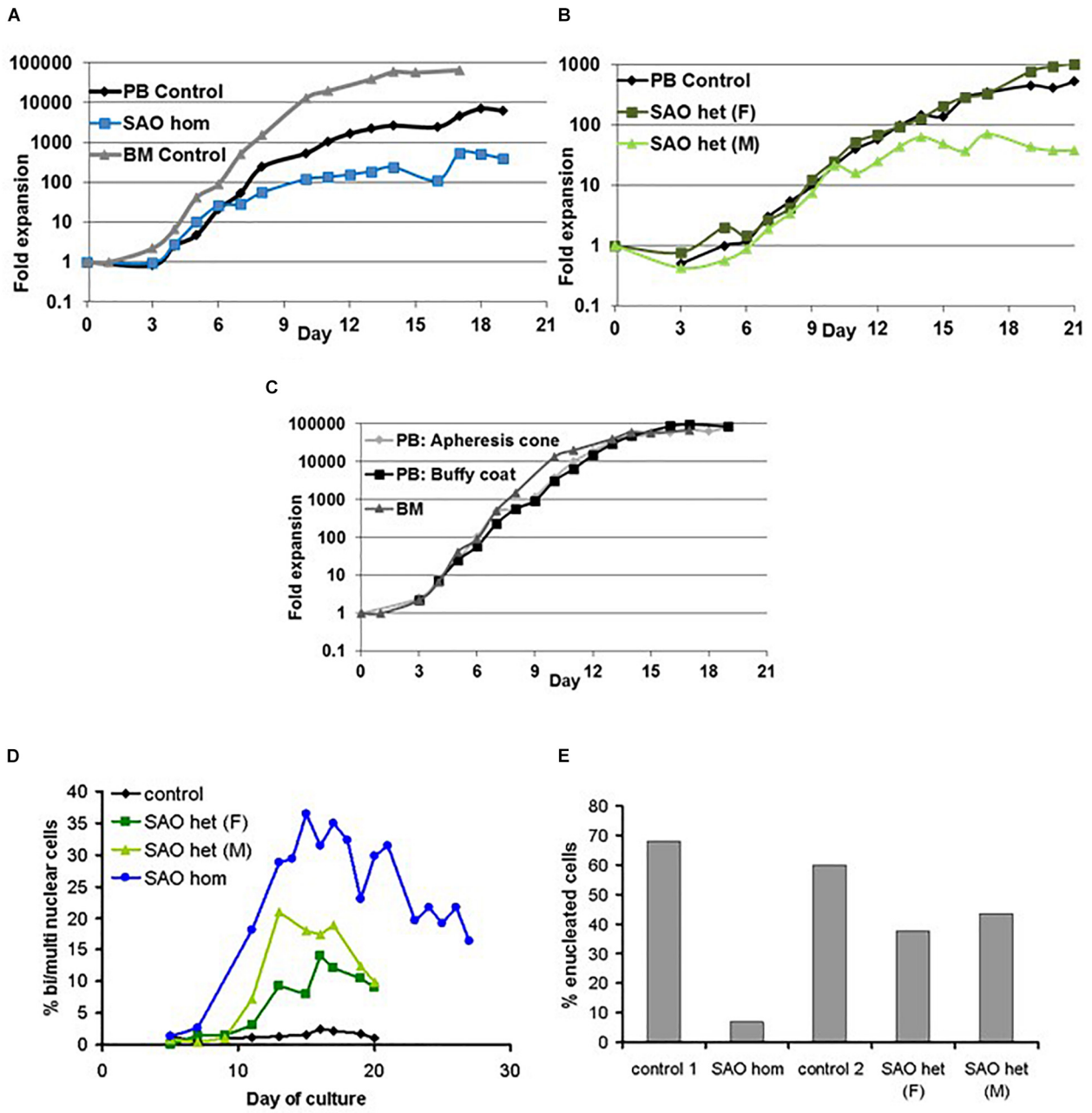

FIGURE 4 | Proliferation of cultured CD34$^+$ cells. Control, heterozygous SAO and homozygous SAO CD34$^+$ cells were cultured, and their fold-increase in cell number is shown, plotted against the day of culture. **(A)** Expansion of homozygous SAO (blue line) and control (black line) CD34$^+$ cells in culture. The SAO CD34$^+$ cells were isolated from 3 ml of bone marrow (BM), the control CD34$^+$ cells from peripheral blood (PB; 50 ml). A further control CD34$^+$ culture grown from frozen BM CD34$^+$ cells, but at a different time and therefore not directly comparable, is shown (gray line). **(B)** Expansion of heterozygous SAO (SAO [father (F) dark green line]; SAO [mother (M) pale green line]) and control (black line) CD34$^+$ cells in culture. All three cultures were grown from CD34$^+$ cells isolated from peripheral blood (PB; 50 ml). **(C)** Comparison of the typical rate of expansion of three controls where the CD34$^+$ cells were isolated from different sources. Expansion of adult derived CD34$^+$ cells in culture from a fresh apheresis cone (pale gray line), fresh buffy coat (black line) or from frozen bone marrow (gray line). **(D)** Graph showing the percentage of cells with two or more nuclei over the course of the cultures. Cells were counted from cytomicrographs, and counts were averaged from 3 different fields. Numbers of cells counted per field were 125 ± 48 (s.d.). **(E)** Graph showing the percentage of cells that had successfully enucleated at day 20 in culture. Cells were counted from cytomicrographs, and counts were averaged from 5 different fields. Numbers of cells counted per field were 136 ± 45 (s.d.).

Moura et al., 2018). It is possible that in healthy erythroid cells band 3 and NMMII do interact during cell division, but that the transient nature of the interaction is not detectable by co-immunoprecipitation. SAO band 3 may form stronger interactions with NMMII, as it does with other cytoskeletal components, and disrupt the normal localization and function

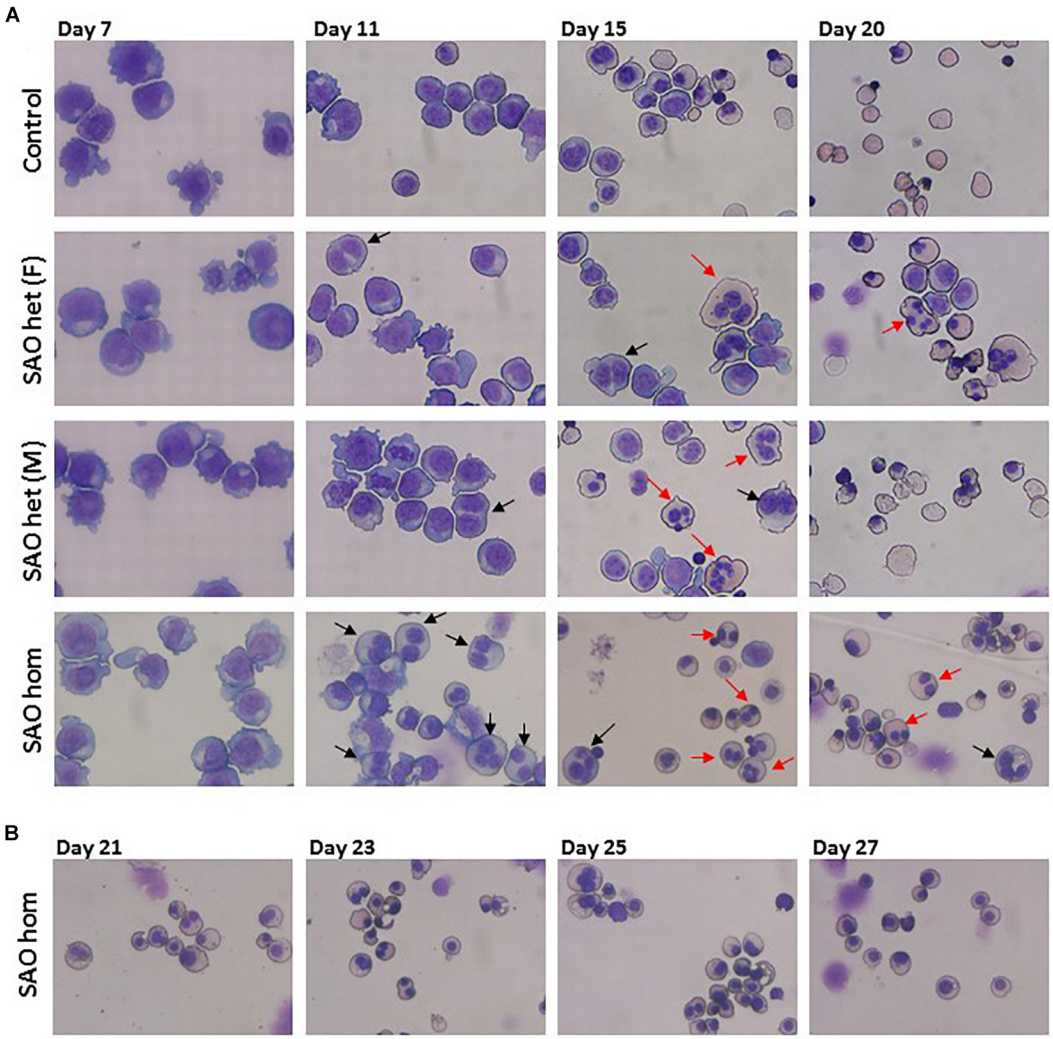

FIGURE 5 | Cytomicrographs of cultured control and SAO CD34^{+} cells. **(A)** Comparison of control with heterozygous SAO [(F) = father, (M) = mother] and homozygous SAO cells over 20 days of culture. Bi-nuclear proerythroblasts and basophilic erythroblasts are indicated with black arrows. Multi-nuclear polychromatophilic and orthochromatic erythroblasts are indicated with red arrows. **(B)** Homozygous SAO cells cultured for a further 7 days did not achieve a significant level of enucleation.

of myosin during the final stage of cell division. This hypothesis was examined by immunofluorescence of cultured control and heterozygous SAO cells. In normal nucleated cells NMMIIA shows a diffuse cytoplasmic staining pattern, which later also localizes at the plasma membrane (**Figure 9C**). NMMIIA staining was condensed and punctate in some of the nucleated heterozygous SAO erythroblasts containing band 3 aggregates (**Figure 9C**). Although colocalization between the two proteins was not observed, they frequently appeared immediately adjacent to each other (**Figure 9C**). Similarly, the cytoskeletal protein actin is important for both cytokinesis and enucleation (Konstantinidis et al., 2012). The increased association with band 3 implied by our proteomic data and the dyserythropoietic phenotype prompted us to study its localization in late stage homozygous SAO erythroblasts. In healthy cells F-actin staining is restricted to the periphery of the cell, at the plasma membrane (**Figure 9D**). However, in some SAO cells the staining pattern was internal and punctate, often located within regions of aggregated band 3 staining (**Figure 9D**).

The proteomics data also suggested that more Heat Shock 70 Proteins (HSP70) are associated with band 3 in homozygous SAO cells, in particular HSP70-5 (HSPA5; also known as GRP78 and/or BiP). In healthy cells, when misfolded proteins are produced, they are initially dealt with by these chaperone proteins that aid in the correct folding or refolding of the protein in the endoplasmic reticulum. HSP70-5 plays an important role in regulating the unfolded protein response (Brodsky and Skach, 2011). If chaperone-mediated refolding is unsuccessful the cell destroys the

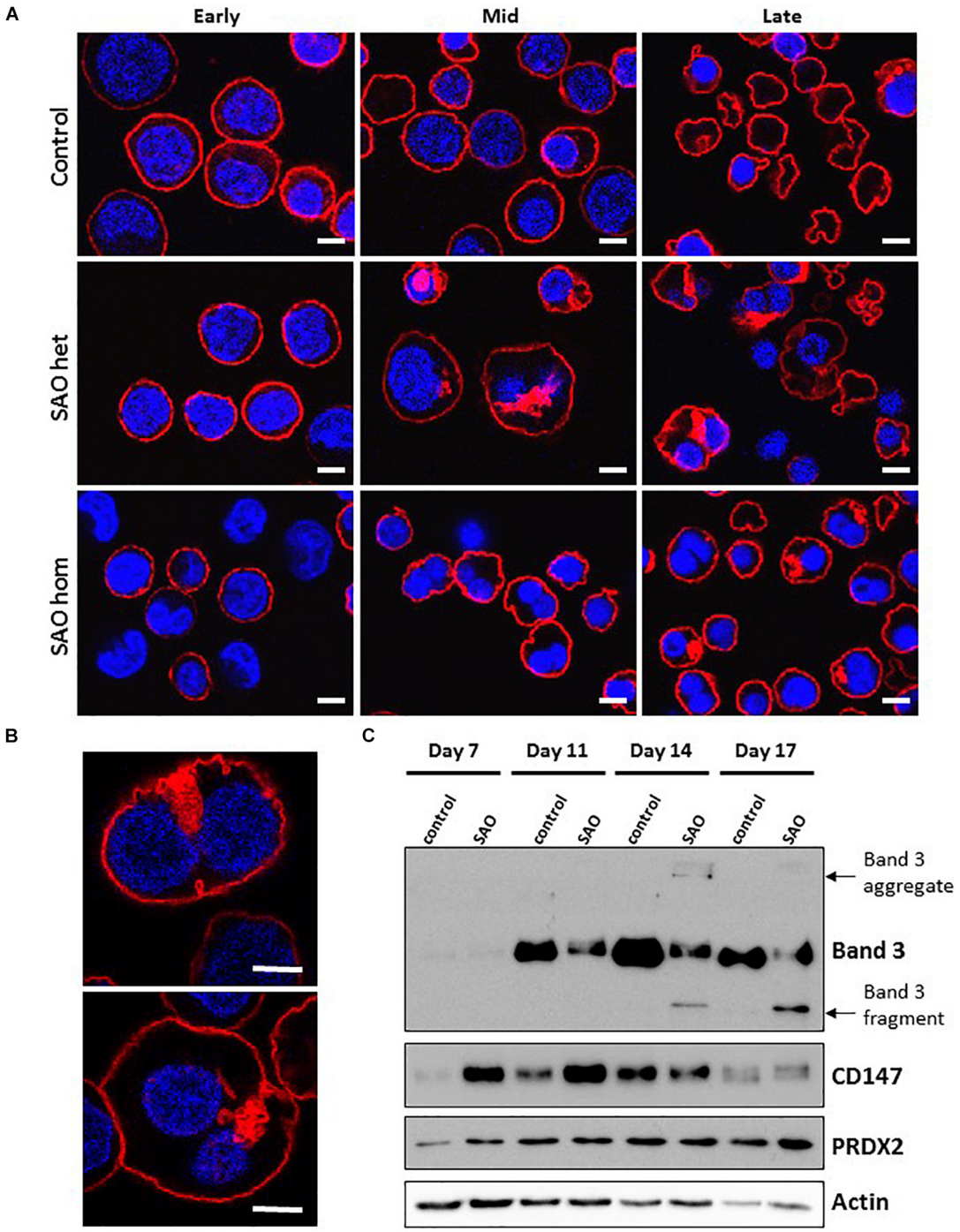

FIGURE 6 | Expression of SAO band 3 throughout erythropoiesis. Control, heterozygous (father of proband) and homozygous SAO CD34^{+} cells were cultured for 21 days and their band 3 expression was monitored by the use of monoclonal anti-band 3 antibody after fixation and permeabilization. Confocal microscope images are shown from 3 different time-points: Early (day 10), Mid (day 14) and Late (day 21). **(A)** Comparison of control, heterozygous and homozygous SAO cells using BRAC17 (red) and DAPI (blue). Early homozygous SAO erythroblasts express very little band 3 probably because SAO band 3 is mis-folded and has problems trafficking to the red cell membrane. The difference in size and morphology of cells, especially notable in heterozygous SAO cells mid-culture is due to the formation of the large aberrantly-shaped SAO cells that eventually become SAO red cells. Scale bars represent 5 μm. **(B)** Higher magnification images of day 17 heterozygous SAO cells exhibiting internal clusters of band 3 vesicles. Staining shows Band 3 (BRAC17; red) and nuclei (DAPI; blue). Images are representative of at least 5 different fields from one experiment. Scale bars represent 5 μm. **(C)** Immunoblot of cultured homozygous SAO and control cell lysates probed with anti-band 3 (BRIC170); anti-CD147 (rabbit monoclonal antibody; ab108308); anti-PRDX2 (ab109367) and loading control anti-actin (ab6276).

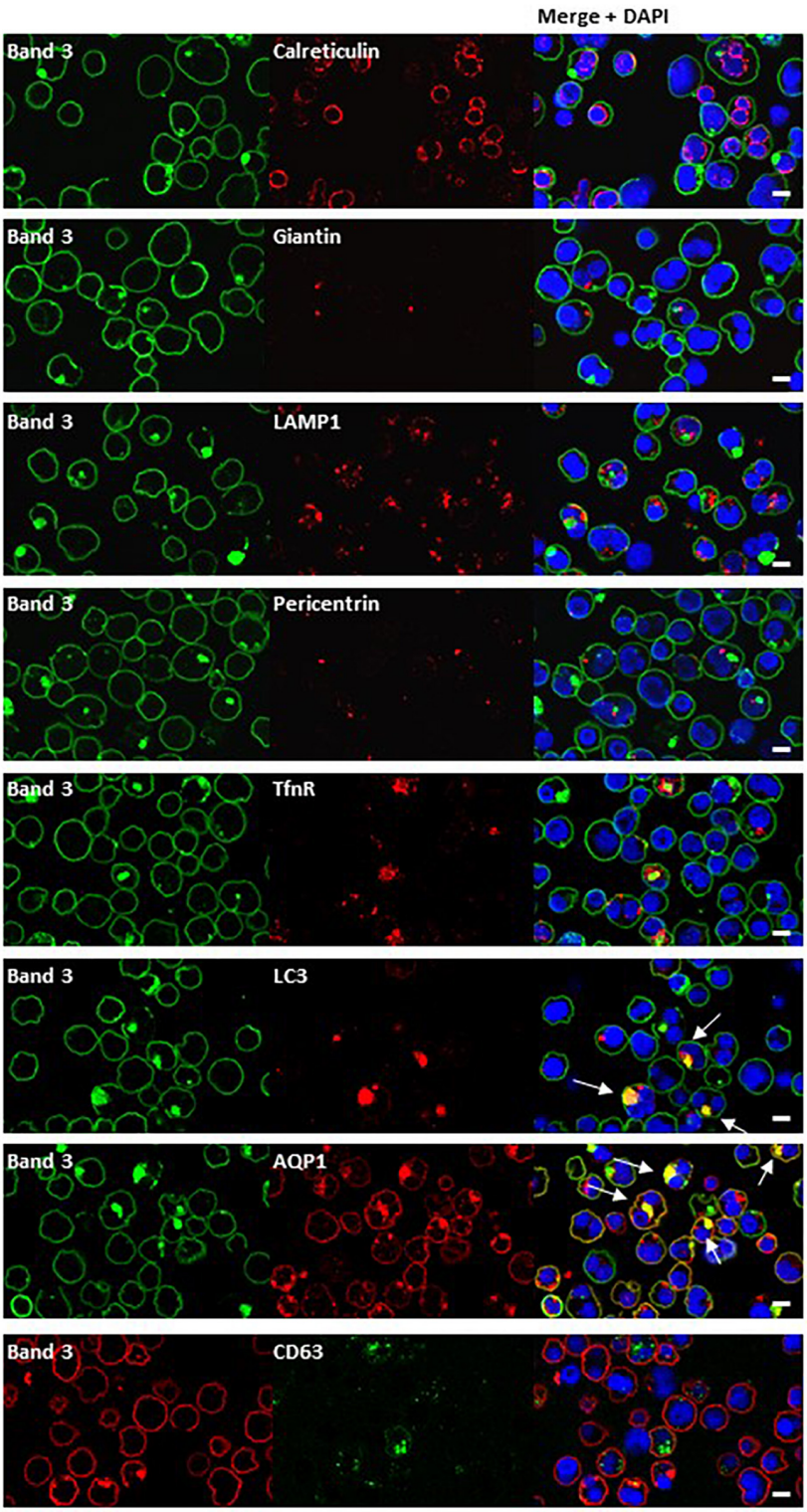

FIGURE 7 | Immunocytochemistry of homozygous SAO erythroblasts. Late stage homozygous SAO cells were dual stained using antibodies against band 3 (BRIC170, green; or BRAC17, red) and markers for plasma membrane, internal compartments or organelles. Markers used were: Calreticulin (endoplasmic reticulum; ab2907), Giantin [Golgi; PRB-114C (Covance)], LAMP1 (lysosome associated membrane protein 1; lysosome; ab24170), Pericentrin (microtubule organizing center; ab4448), TfnR (Transferrin receptor/CD71; ab84036), LC3 [microtubule-associated proteins 1A/1B light chain 3A; autophagosome; PM036 (MBL)], AQP1 (Aquaporin-1; plasma membrane), and CD63 [recycling endosome; 556019 (BD Biosciences)]. Colocalization is indicated with white arrows (yellow areas in merged images). Images are representative of at least 5 different fields from one experiment. Scale bars represent 5 μm.

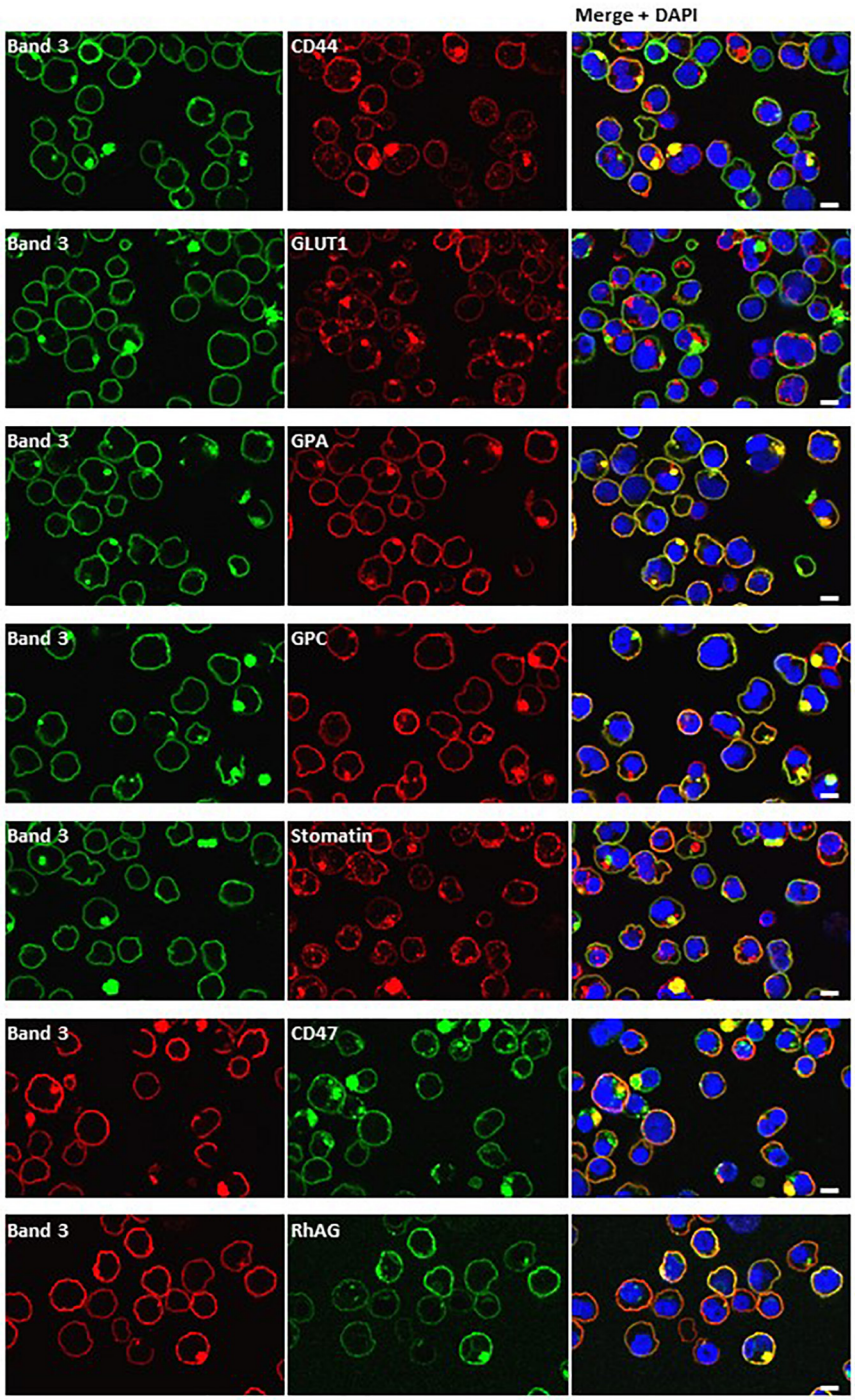

FIGURE 8 | Dual staining with plasma membrane markers. Late stage homozygous SAO cells were fixed, permeabilized and dual stained with anti-band 3 (BRIC170, green; or BRAC17, red) and antibodies against plasma membrane proteins. Antibodies used were rabbit polyclonals against CD44, GLUT1 (gift from Prof. S. Baldwin), GPA, GPC and mouse monoclonals against stomatin (gift from Prof. R. Prohaska; GARP50), CD47 (BRIC211) and RhAG (LA1818). Yellow areas in merged images indicate colocalization. Scale bars represent 5 μm.

misfolded protein, primarily via ubiquitination and proteasomal degradation. Our data showed a 6-fold increase in amounts of ubiquitin associated with SAO band 3, or one of the other co-immunoprecipitated proteins within the SAO band 3 IP (**Figure 9A**), consistent with its targeting for degradation by the proteasome. Ubiquitination is also implicated in tagging proteins for internalization from the plasma membrane (Barriere et al., 2006).

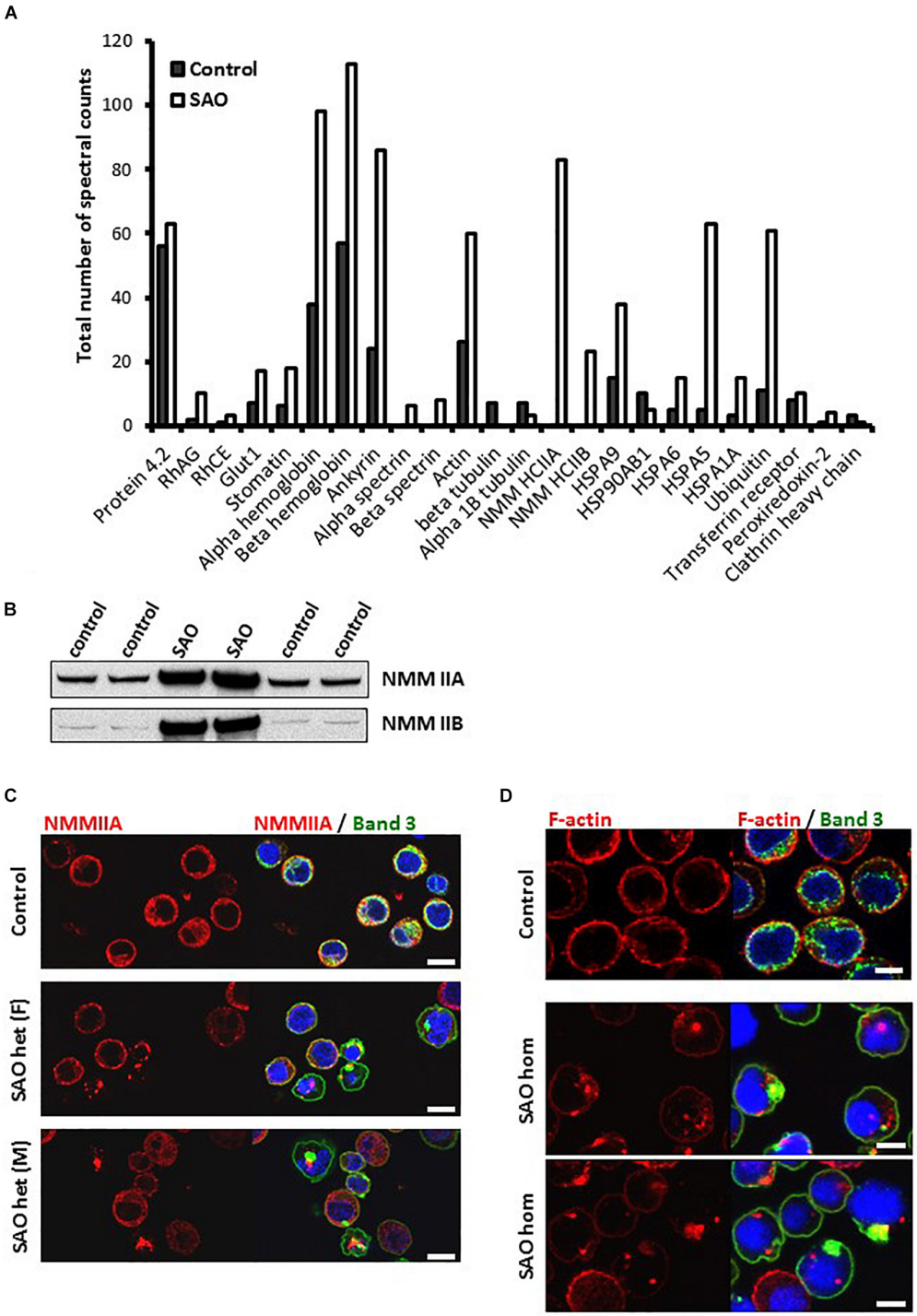

FIGURE 9 | SAO band 3 immunoprecipitation. **(A)** Band 3 was immunoprecipitated from control (day 14) and homozygous SAO (day 27) cultured $CD34^+$ cell lysates. These stages were not ideal but were chosen in order to match both cell types as closely as possible (predominantly orthochromic erythroblasts and 10% enucleated as shown in **Figure 4**). The immunoprecipitate was analyzed by mass spectrometry. The number of spectral counts obtained for the co-immunoprecipitated proteins from each culture are shown. **(B)** Immunoblots of control and heterozygous SAO mature erythrocyte membranes. Antibodies used were anti-NMMIIA (ab24762) and anti-NMMIIB (ab24761). **(C)** Day 14 control and heterozygous SAO cells were stained with anti-NMMIIA antibody (red) and anti-band 3 antibody (BRIC170; green). DNA was stained with DAPI (blue). Scale bars represent 10 μm. **(D)** Day 14 cells imaged using anti-band 3 antibody (BRIC170; green) and AlexaFluor 546-conjugated phalloidin, which binds F-actin (red). DNA was stained with DAPI (blue). Images are representative of at least 5 different fields from one experiment. Scale bars represent 5 μm.

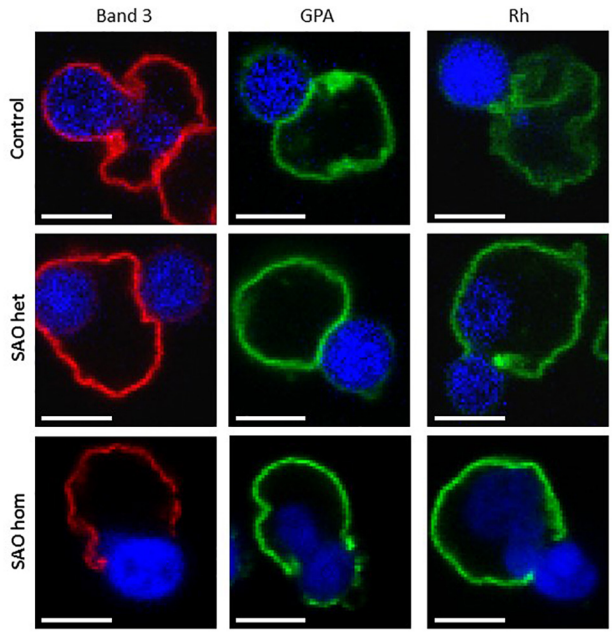

FIGURE 10 | Immunocytochemistry of enucleating cultured CD34^{+} cells. Late stage control, heterozygous SAO and homozygous SAO cells were fixed, permeabilized and imaged using antibodies directed against band 3 (BRAC17), GPA (BRIC256) and Rh (BRIC69). Images are representative of at least 23 (band 3), 10 (GPA) or 5 (Rh) similar cells observed. Scale bars represent 5 μm.

Sorting of Membrane Proteins at Enucleation

Mutations in membrane proteins can give rise to mis-sorting of partner proteins during enucleation (Salomao et al., 2010; Satchwell et al., 2015). We used immunofluorescence to determine whether this occurs in cells expressing SAO band 3. In control cells band 3 was seen around both the reticulocyte and the extruding nucleus. This is consistent with previous observations using human cells (Lee et al., 2004; Bell et al., 2013). In contrast, very little was seen around the extruding nucleus in heterozygous SAO cells and none whatsoever in homozygous SAO cells (**Figure 10**). This suggests that all the band 3 in these cells is cytoskeletally-attached, as it is entirely restricted to the nascent reticulocyte.

Rh polypeptide sorting was unaffected in SAO cells, however homozygous SAO cells showed increased GPA staining around the nucleus compared to heterozygote and control cells (**Figure 10**). This is consistent with a weakened band 3-GPA interaction, as suggested by the depression in Wr(b) antigen.

Reticulocyte Maturation

Both CD44 and CD147, proteins that would normally be reduced in the mature RBC membrane following enucleation and reticulocyte maturation, were found to be increased in the heterozygote SAO mature RBC membranes (**Figure 11**). CD147 also migrated more slowly than wild type in SDS-PAGE. The increase in these proteins, together with the size of mature

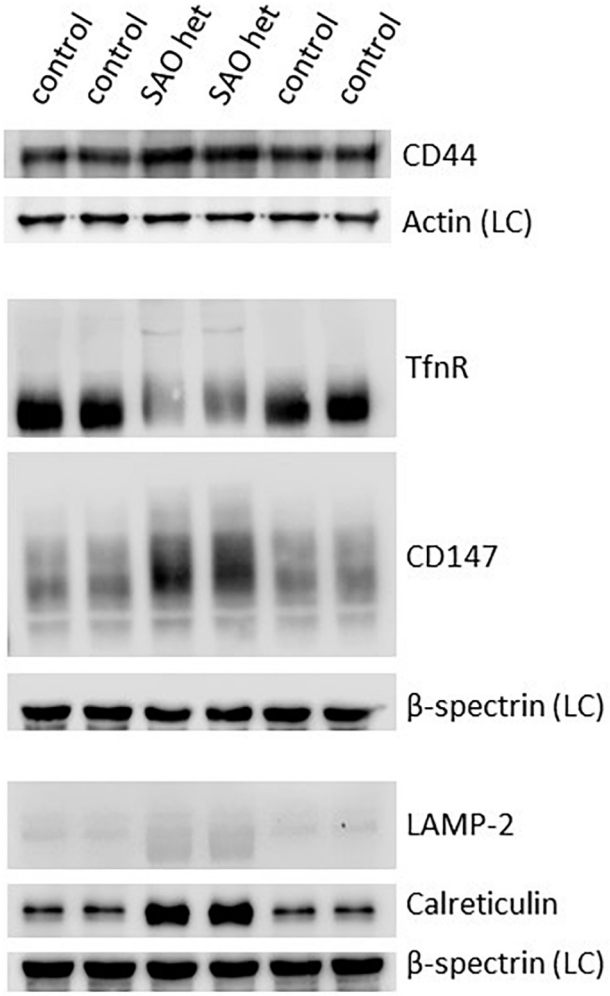

FIGURE 11 | Expression of membrane proteins involved in reticulocyte maturation. Red cell membranes from heterozygous SAO and control peripheral blood samples were prepared, separated by SDS-PAGE and immunoblotted. The antibody directed against CD44 was an in-house rabbit polyclonal antibody. Commercial antibodies were used to detect actin (ab6276), calreticulin (ab2907); CD147 (ab108308), LAMP-2 (ab25631) and transferrin receptor (TfnR) (ab84036); all from Abcam, Cambridge, United Kingdom. An in-house monoclonal antibody was used to detect beta-spectrin (BRAC65). SAO het: Membranes prepared from the heterozygous father of the homozygous SAO child. LC: Loading control.

SAO RBCs, suggested a reticulocyte maturation defect. Other proteins that would normally be depleted during reticulocyte maturation were also assessed (**Figure 11**). Stomatin-like protein 2 (SLP-2) and voltage dependent anion channel 1 (VDAC1), both mitochondrial proteins, were absent suggesting mitochondria are correctly cleared from SAO cells (data not shown). There was a slight increase in the level of lysosome-associated membrane protein 2 (LAMP-2) in the heterozygous SAO RBC membranes suggesting retention of some lysosomal membranes (**Figure 11**) and LAMP-2 had an accelerated mobility in SDS-PAGE. Levels of calreticulin, an endoplasmic reticulum (ER) protein, were much higher in the heterozygous SAO RBC membranes than

in controls (**Figure 11**) suggesting significant retention of ER membranes. Unexpectedly transferrin receptor was substantially decreased (**Figure 11**). It is usual for the transferrin receptor (TfnR, CD71) to be partially lost during reticulocyte maturation. If there was a maturation defect, TfnR would be expected to remain high. However, it can be seen that the migration of TfnR in the SDS-PAGE gel was slower suggesting a trafficking defect (**Figure 11**) and TfnR formed internal aggregates in erythroblasts partially overlapping with the band 3 aggregates (**Figure 7**). So it is likely that some TfnR is degraded in the erythroblast before enucleation and reticulocyte maturation, explaining the reduced amount found in the mature SAO RBC.

DISCUSSION

Dyserythropoiesis in Homozygous SAO

It is of great interest that the SAO mutation in band 3 results in a cytokinesis defect. There are two possible mechanisms; that the large amount of misfolded protein congests the system, or the intriguing possibility that SAO band 3 disrupts cytokinesis specifically. It has previously been observed that a deficiency of band 3 causes dyserythropoiesis in zebrafish (27% binuclear erythroblasts), which could be rescued by wild type band 3. Ablating the protein 4.1 binding site on band 3 prevented rescue, suggesting that the band 3-protein 4.1 interaction is critical for completion of mitosis (Paw et al., 2003). However, 2 different strains of band 3 deficient mouse models exhibited 4 and 14% erythroblast binuclearity, suggesting that other factors have a modifying effect (Bell et al., 2013). In humans, total band 3 deficiency is almost unknown and results in severe Hereditary Spherocytosis (HS). In one study of total band 3 deficiency, erythroid progenitor cells from the individual reported by Ribeiro et al. (2000) were cultured to reticulocytes without manifestation of a dyserythropoietic phenotype (Satchwell et al., 2015), although a later study of total band 3 deficiency did show a mild dyserythropoiesis (Kager et al., 2017). Therefore, the current data suggest that absence of functional band 3 does not result in a cytokinetic defect *per se*.

Consequently, the more likely explanation for the dyserythropoiesis in SAO RBCs is that the expression of large amounts of misfolded band 3 protein overwhelm the internal trafficking system of the cell. However, if this is the case then it begs the question of why dyserythropoiesis is not observed in other membrane RBC conditions where large amounts of misfolded proteins are produced. Two hereditary cation-leaky conditions, overhydrated stomatocytosis (OHSt) and stomatin-deficient cryohydrocytosis (sdCHC), are caused by mutations in non-band 3 erythrocyte membrane proteins and produce large amounts of misfolded protein but have not been associated with dyserythropoiesis (Bruce et al., 2009; Flatt et al., 2011; Bawazir et al., 2012). It has been shown that the most leaky of these, OHSt, is caused by misfolded RhAG (Bruce et al., 2009), which, like band 3, is synthesized in large quantities during erythropoiesis ($\sim 2 \times 10^5$ copies per mature RBC). A secondary effect in OHSt is the mis-trafficking of stomatin, which is retained in perinuclear vesicles, but no cytokinesis defect was seen in cultured primary erythroblasts (Fricke et al., 2005). The second most-leaky hereditary stomatocytosis condition, sdCHC, is caused by misfolded Glut1 (Flatt et al., 2011). Again, Glut1 is synthesized in large quantities during erythropoiesis (~ 2–8×10^5 copies per mature RBC) and stomatin is severely depleted in sdCHC RBCs (Flatt et al., 2011) but to our knowledge dyserythropoiesis has not been reported in sdCHC patients (Fricke et al., 2004; Bawazir et al., 2012).

It is notable that stomatin is absent or reduced in the above two RBC phenotypes. Stomatin is a lipid raft protein involved in RBC vesiculation (Salzer et al., 2007, 2008). There is evidence to suggest that these vesicles often contain misfolded proteins (Coleman and Hill, 2015; Leal et al., 2018) and may be a mechanism for prolonging the life span of circulating RBCs, or of stored RBCs, by removal of oxidized or damaged membrane protein. It is tempting to speculate that, during erythropoiesis stomatin may play a similar role, removing misfolded proteins by vesiculation, and that in OHSt or sdCHC erythroblasts stomatin is lost in vesicles along with the misfolded RhAG or Glut1. This would prevent accumulation of misfolded protein within the cell and congestion of the trafficking system and thus prevent dyserythropoiesis. It would also result in the depletion of stomatin. In SAO RBCs it is unlikely that the SAO band 3 can be extracted from the membrane, due to its entanglement with the cytoskeleton and other proteins, and therefore this clearance mechanism would not be available.

Overall, the evidence suggests that dyserythropoiesis in SAO RBCs is a specific effect of the expression of misfolded band 3. This conclusion is supported by a report which described another mutation in human band 3 that has been linked with dyserythropoiesis (G796R; Band 3 Ceinge; Iolascon et al., 2009). Interestingly, in this case there was also a red cell cation leak and the patient had the cryohydrocytosis (CHC) phenotype, implying the presence of misfolded band 3 at the membrane. There are numerous other band 3 mutations that give rise to CHC and where the misfolded band 3 protein is expressed, but no others have been investigated for dyserythropoiesis (Bruce et al., 2005). The CHC phenotype is very similar to the SAO phenotype, characterized by cation leaky RBCs that express a misfolded band 3 that does not transport anions or bind anion transport inhibitors (Guizouarn et al., 2011). It would be of great interest to culture $CD34^+$ cells from other patients with CHC *SLC4A1* SNPs and investigate whether they too have a similar dyserythropoietic phenotype.

Endocytic Vesicle Trafficking in SAO

It is thought that vesicle trafficking during mitosis is necessary to provide additional membrane at the site of division. Endocytosis of the plasma membrane occurs at the polar regions during anaphase and early telophase and these vesicles are then trafficked to the site of the cleavage furrow, where further endocytosis occurs during cytokinesis (Schweitzer et al., 2005). We looked for colocalization of the band 3-positive vesicles with some of the proteins implicated in this process (Arf6, clathrin) but none was observed. However, the internal band 3 vesicles colocalized with other plasma membrane proteins (**Figure 8**), and not with secretory pathway markers (**Figure 7**), suggesting endocytosis.

There was also evidence consistent with the hypothesis that large amounts of misfolded SAO band 3, trafficking from the Golgi to the plasma membrane, had overwhelmed the proteasomal degradation pathway. Such proteins can form aggregates and can be sequestered in "aggresomes," which are subsequently subject to macroautophagy (Johnston et al., 1998). The autophagy marker, LC3, colocalized with the aggregated band 3 (**Figure 7**) and numerous other proteins appeared to become entangled in the aggresomes (**Figures 8**). Many of these proteins appeared to have been through multiple recycling loops through the ER increasing their glycan structures and apparent molecular weight (**Figure 2**).

In homozygous SAO cells with large aggregates it appeared that internal staining for CD71 (transferrin receptor) was increased, and was located around the aggregate (**Figure 7**), perhaps hinting at wider-spread disruption to vesicle trafficking in these cells. Further evidence of the wide disruption to protein movement within the SAO cells came from the analysis of proteins associating with band 3 (**Figure 9**). SAO band 3 had unusually strong associations with cytoskeletal proteins, spectrin, ankyrin, myosin and actin. Previous reports have shown that SAO band 3 interacts more strongly with the cytoskeleton (Mohandas et al., 1992; Sarabia et al., 1993; Liu et al., 1995). Cytoskeletal rearrangement within the erythroblast of myosin and actin was also disrupted with evidence that these proteins aggregated in clusters rather than dispersing throughout the cytoplasm as in control cells (**Figure 9**).

Vesicle trafficking has been shown to be important in erythroblast enucleation (Keerthivasan et al., 2010), so it is possible that disrupted vesicle trafficking contributes to the enucleation defect observed in homozygous SAO. Equally, the enucleation defect may occur because of altered band 3 associations. In WT erythroblast enucleation, a proportion of the band 3 (the mobile fraction not associated with cytoskeleton-linked complexes) distributes evenly between the pyrenocyte and the emerging reticulocyte (Lee et al., 2004). However, confocal imaging analysis of enucleation in SAO RBCs seemed to suggest that all the SAO band 3 was associated with the cytoskeleton, either through the major protein complexes, in association with ankyrin or adducin, or through simple entanglement in the cytoskeleton. The association of band 3 with GPA was also weakened, causing the loss of GPA from the reticulocyte at least in the homozygous SAO cells (**Figure 10**).

Band 3 Trafficking and the Effect of SAO

Erythrocyte band 3 can be phosphorylated at tyrosine residues at positions 8, 21, 359, and 904. The phosphorylation of Tyr8 and Tyr21 is carried out by kinase Syk, which allows the phosphorylation of Tyr359 and Tyr904 by kinase Lyn (Brunati et al., 2000). It has been shown in kidney cells that phosphorylation of Tyr359 is a critical factor in band 3 trafficking (Williamson et al., 2008). In red cells, the study of a rare band 3 mutant revealed that phosphorylation of the entire protein is dependent on the presence of the first 11 amino acids (Perrotta et al., 2005). We found an increase in Tyr359 band 3 phosphorylation in homozygous SAO cells, and also saw an increase in phospho-Tyr359 in heterozygous SAO. This was striking as wild-type band 3 is only transiently tyrosine phosphorylated and longer-term tyrosine phosphorylation may only be achieved by inhibition of the highly active phosphatase using pervanadate or another protein-tyrosine phosphatase inhibitor. The SAO cells had not been treated with any phosphatase inhibitor, suggesting that band 3 Tyr359 is phosphorylated in the homeostatic state in these cells. This elevated steady-state phosphorylation of Tyr359 in SAO band 3 is another compelling indication of altered trafficking in SAO cells.

Evidence for Oxidative Damage Caused by Misfolded SAO Band 3

PRDX2 (peroxiredoxin-2) is a cytoprotective anti-oxidant enzyme, which is upregulated in response to oxidative stress (Lee et al., 2003; De Franceschi et al., 2011). It is thought that PRDX2 associates with the membrane via binding to band 3 (Matte et al., 2013), and its membrane association is increased in cases of hereditary spherocytosis in response to oxidative stress (Rocha et al., 2008). We did not observe a significant upregulation of total PRDX2 expression during homozygous SAO erythropoiesis (**Figure 6C**). However, we found that PRDX2 is present at significantly higher levels in heterozygous SAO ghost membranes compared to controls (**Figure 2**), which is suggestive of oxidative stress in these cells. The presence of aggresomes has been linked to oxidative damage and inflammation (Luciani et al., 2010), with the consequence of further cellular damage if they are not successfully cleared. The large amounts of accumulated misfolded band 3 in SAO may therefore be the cause of oxidative damage in these cells.

Incomplete Reticulocyte Maturation in SAO

The homozygous SAO red cells found in the circulation are large and stomatocytic. They have failed to lose their excess membrane and remodel their cytoskeleton to form a biconcave disc. In healthy cells proteins and membrane are lost at enucleation and during reticulocyte maturation (Johnston et al., 1998; Griffiths et al., 2012; Mankelow et al., 2016). The increased cytoskeletal attachment of SAO band 3 may inhibit cytoskeletal reorganization, endocytosis and vesicle expulsion required for reticulocyte maturation (Griffiths et al., 2012). We have found an altered distribution of proteins at enucleation and the presence of nuclei, organelles and proteins that should have been cleared from the cells (**Figures 1B**, **2**, **9B**, **10**). CD147 is one such protein, in that the majority partitions with the extruded nucleus during enucleation and then is further depleted by removal in vesicles during reticulocyte maturation (Griffiths et al., 2012). In homozygous SAO late erythroblasts there are normal levels of CD147 but increased amounts in mature red cells (and in heterozygote red cells), suggestive of a defect in reticulocyte maturation. CD44 is usually quantitatively reduced during the late stages of erythropoiesis, but also remains high in cells expressing SAO band 3. Incomplete clearance of organelles from SAO cells was shown by the increased amounts of LAMP-2 (lysosome)

and calreticulin (ER), although clearance of mitochondria appeared to be normal.

Similarities Between Dyserythropoiesis in SAO and CDAII Cells

In both SAO and CDAII erythroblasts there is a cytokinesis defect, the cells fail to separate and there are numerous binuclear cells. Immunogold electron microscopy of CDAII cells detects a dense discontinuous ring of ER-derived membrane beneath the plasma membrane (Alloisio et al., 1996). In fact, the authors suggest that increased levels of glucose-regulated protein GRP78, calreticulin or protein disulfide isomerase (PDI), all major protein of the ER, could be used as markers for CDAII (Alloisio et al., 1996). A similar analysis of SAO membranes, using electron microscopy, has not been done but we have shown a massive increase in calreticulin in heterozygous SAO membranes (**Figure 2**) suggesting that the SAO cells still contain significant amounts of ER membranes, although it is also possible that calreticulin is expressed in the plasma membrane of SAO cells. The immunoprecipitation of homozygous erythroblast lysates also showed a strong association between band 3 and HSP70, otherwise known as GRP78, an ER-associated heat shock protein (**Figure 9**). Another protein that has been suggested as a marker for CDAII is CD44 (Singleton et al., 2018) and we found that CD44 protein is high in SAO RBCs. One difference between SAO and CDAII is the apparent molecular weight of the band 3 protein when separated by SDS-PAGE. SAO band 3 migrates slower than normal whereas CDAII band 3 has a faster mobility (Denecke et al., 2008). Nonetheless, it would be of interest to investigate the expression of band 3 through erythropoiesis in CDAII cells. As band 3 is the major membrane protein expressed in RBC, with 10^6 copies per RBC, the Sec23b mutation in CDAII cells that causes a trafficking defect is quite likely to result in the accumulation of band 3 aggregates similar to those seen in SAO cells.

Clinical Significance of the Heterozygous SAO Mutation

Homozygous SAO is an extremely rare condition as it is usually lethal (Mgone et al., 1996), however, heterozygous SAO is relatively common in certain parts of SE Asia and Papua New Guinea or other regions of the world where malaria is rife (Amato and Booth, 1977; Mgone et al., 1996; Paquette et al., 2015). A greater understanding of the SAO phenotype is useful for the clinical care of individuals with SAO. One study showed that babies with heterozygous SAO often have a significant anemia at birth due to hemolysis, and 16 of the 31 babies studied developed neonatal hyperbilirubinemia, but this reverts to normal in the first few months of life (Laosombat et al., 2010). Although heterozygous SAO is apparently asymptomatic in adults, we observed a multinuclear phenotype in cultured heterozygous SAO erythroblasts (albeit to a lesser degree than homozygous erythroblasts), altered protein trafficking and impaired reticulocyte maturation and changes in the membrane protein composition of mature heterozygous SAO RBCs including oxidative damage. So it is possible that individuals with heterozygous SAO could experience complications when presenting with other conditions. For example, as band 3 SAO does not transport anions, inheritance of band 3 SAO *in trans* to another mutant band 3 allele such as one causing the loss of band 3 and hereditary spherocytosis can result in severe hemolytic anemia and dRTA (Alexander et al., 2019).

CONCLUDING REMARKS

In this study we examined in greater depth the phenotype of the first known case of homozygous SAO. Despite the absence of wild type band 3, SAO band 3 is expressed at the red cell surface. During *in vitro* culture, erythroid progenitors from the proband exhibited a defect in the late phase of cell division, cytokinesis, resulting in multinucleated cells, which occurred along with a clear reduction in enucleation. Culture of the parents' heterozygous SAO erythroid progenitor cells produced a milder version of this dyserythropoietic phenotype. This study has shown that the production of misfolded SAO band 3 overwhelms the usual protein quality control mechanisms and results in the formation of large areas of aggregated protein in some cells. These colocalized with the autophagosomal marker LC3.

The misfolded SAO band 3 was altered in its reactivity with monoclonal anti-band 3 antibodies, and immunoprecipitation experiments supported previous findings that SAO band 3 associates more strongly with cytoskeletal proteins. A strong interaction between SAO band 3 and non-muscle myosins IIA and IIB was detected, along with perturbed cellular localization of myosin IIA and actin, supporting the hypothesis that the important role of myosin in cytokinesis is blocked and results in the dyserythropoietic phenotype.

DATA AVAILABILITY STATEMENT

All datasets generated for this study are freely available from the corresponding author.

ETHICS STATEMENT

The studies involving human participants were reviewed and approved by National Health Service National Research Ethics Service South West. Written informed consent to participate in this study was provided by the participants' legal guardian/next of kin.

AUTHOR CONTRIBUTIONS

JF designed and performed experiments, analyzed data, and wrote the manuscript. NC performed culture experiments. CS-H, DE, and NH performed immunoblotting experiments. KH conducted mass spectrometry experiments. VP and CT provided patient samples and edited the manuscript. LB designed the study, analyzed data, and edited the manuscript.

FUNDING

This study was supported by the National Institute for Health Research Blood and Transplant Research Unit (NIHR BTRU) in Red Cell Products (IS-BTU-1214-10032) and by the UK National Health Service R&D Directorate (JF, CH-S, NC, DE, NH, and LB). The views expressed are those of the authors and not necessarily those of the National Health Service, NIHR, or the Department of Health and Social Care.

ACKNOWLEDGMENTS

We thank the family for their interest and support.

REFERENCES

Alexander, R. T., Law, L., Gil-Peña, H., Greenbaum, L. A., and Santos, F. (2019). "Hereditary distal renal tubular acidosis," in *GeneReviews®* , eds M. P. Adam, H. H. Ardinger, R. A. Pagon, S. E. Wallace, L. J. H. Bean, K. Stephens, et al. (Seattle (WA: University of Washington), 1993–2020.

Allen, S. J., O'Donnell, A., Alexander, N. D., Mgone, C. S., Peto, T. E., Clegg, J. B., et al. (1999). Prevention of cerebral malaria in children in Papua New Guinea by southeast Asian ovalocytosis band 3. *Am. J. Trop. Med. Hyg.* 60, 1056–1060.

Alloisio, N., Texier, P., Denoroy, L., Berger, C., Miraglia del Giudice, E, Perrotta, S., et al. (1996). The cisternae decorating the red blood cell membrane in congenital dyserythropoietic anemia (type II) originate from the endoplasmic reticulum. *Blood* 87, 4433–4439.

Amato, D., and Booth, P. B. (1977). Hereditary ovalocytosis in melanesians. *P N G Med J.* 20, 26–32.

Barriere, H., Nemes, C., Lechardeur, D., Khan-Mohammad, M., Fruh, K., and Lukacs, G. L. (2006). Molecular basis of oligoubiquitin-dependent internalization of membrane proteins in Mammalian cells. *Traffic* 7, 282–297.

Bawazir, W. M., Gevers, E. F., Flatt, J. F., Ang, A. L., Jacobs, B., Oren, C., et al. (2012). An infant with pseudohyperkalemia, hemolysis, and seizures: cation-leaky GLUT1-deficiency syndrome due to a SLC2A1 mutation. *J. Clin. Endocrinol. Metab.* 97, E987–E993. doi: 10.1210/jc.2012-1399

Bell, A. J., Satchwell, T. J., Heesom, K. J., Hawley, B. R., Kupzig, S., Hazell, M., et al. (2013). Protein distribution during human erythroblast enucleation in vitro. *PLoS One* 8:e60300. doi: 10.1371/journal.pone.0060300

Booth, P. B., Serjeantson, S., Woodfield, D. G., and Amato, D. (1977). Selective depression of blood group antigens associated with hereditary ovalocytosis among melanesians. *Vox Sang.* 32, 99–110.

Brodsky, J. L., and Skach, W. R. (2011). Protein folding and quality control in the endoplasmic reticulum: recent lessons from yeast and mammalian cell systems. *Curr. Opin. Cell Biol.* 23, 464–475.

Bruce, L. J., Beckmann, R., Ribeiro, M. L., Peters, L. L., Chasis, J. A., Delaunay, J., et al. (2003). A band 3-based macrocomplex of integral and peripheral proteins in the RBC membrane. *Blood* 101, 4180–4188.

Bruce, L. J., Guizouarn, H., Burton, N. M., Gabillat, N., Poole, J., Flatt, J. F., et al. (2009). The monovalent cation leak in overhydrated stomatocytic red blood cells results from amino acid substitutions in the Rh-associated glycoprotein. *Blood* 113, 1350–1357.

Bruce, L. J., Ring, S. M., Anstee, D. J., Reid, M. E., Wilkinson, S., and Tanner, M. J. (1995). Changes in the blood group Wright antigens are associated with a mutation at amino acid 658 in human erythrocyte band 3: a site of interaction between band 3 and glycophorin A under certain conditions. *Blood* 85, 541–547.

Bruce, L. J., Robinson, H. C., Guizouarn, H., Borgese, F., Harrison, P., King, M. J., et al. (2005). Monovalent cation leaks in human red cells caused by single amino-acid substitutions in the transport domain of the band 3 chloride-bicarbonate exchanger. AE1. *Nat. Genet.* 37, 1258–1263.

Brunati, A. M., Bordin, L., Clari, G., James, P., Quadroni, M., Baritono, E., et al. (2000). Sequential phosphorylation of protein band 3 by Syk and Lyn tyrosine kinases in intact human erythrocytes: identification of primary and secondary phosphorylation sites. *Blood* 96, 1550–1557.

Coleman, B. M., and Hill, A. F. (2015). Extracellular vesicles – their role in the packaging and spread of misfolded proteins associated with neurodegenerative diseases. *Semin. Cell Dev. Biol.* 40, 89–96.

Crosnier, C., Bustamante, L. Y., Bartholdson, S. J., Bei, A. K., Theron, M., Uchikawa, M., et al. (2011). Basigin is a receptor essential for erythrocyte invasion by Plasmodium falciparum. *Nature* 480, 534–537.

De Franceschi, L., Bertoldi, M., De Falco, L., Santos Franco, S., Ronzoni, L., Turrini, F., et al. (2011). Oxidative stress modulates heme synthesis and induces peroxiredoxin-2 as a novel cytoprotective response in β-thalassemic erythropoiesis. *Haematologica* 96, 1595–1604.

Denecke, J., Kranz, C., Nimtz, M., Conradt, H. S., Brune, T., Heimpel, H., et al. (2008). Characterization of the N-glycosylation phenotype of erythrocyte membrane proteins in congenital dyserythropoietic anemia type II (CDA II/HEMPAS). *Glycoconj J.* 25, 375–382. doi: 10.1007/s10719-007-9089-1

Dluzewski, A. R., Nash, G. B., Wilson, R. J., Reardon, D. M., and Gratzer, W. B. (1992). Invasion of hereditary ovalocytes by Plasmodium falciparum in vitro and its relation to intracellular ATP concentration. *Mol. Biochem. Parasitol.* 55, 1–7.

Flatt, J. F., Guizouarn, H., Burton, N. M., Borgese, F., Tomlinson, R. J., Forsyth, R. J., et al. (2011). Stomatin-deficient cryohydrocytosis results from mutations in SLC2A1: a novel form of GLUT1 deficiency syndrome. *Blood* 118, 5267–5277.

Fricke, B., Jarvis, H. G., Reid, C. D., Aguilar-Martinez, P., Robert, A., Quittet, P., et al. (2004). Four new cases of stomatin-deficient hereditary stomatocytosis syndrome: association of the stomatin-deficient cryohydrocytosis variant with neurological dysfunction. *Br. J. Haematol.* 125, 796–803.

Fricke, B., Parsons, S. F., Knöpfle, G., von Düring, M., and Stewart, G. W. (2005). Stomatin is mis-trafficked in the erythrocytes of overhydrated hereditary stomatocytosis, and is absent from normal primitive yolk sac-derived erythrocytes. *Br. J. Haematol.* 131, 265–277.

Griffiths, R. E., Kupzig, S., Cogan, N., Mankelow, T. J., Betin, V. M., Trakarnsanga, K., et al. (2012). Maturing reticulocytes internalize plasma membrane in glycophorin A—containing vesicles that fuse with autophagosomes before exocytosis. *Blood* 119, 6296–6306. doi: 10.1182/blood-2011-09-376475

Guizouarn, H., Borgese, F., Gabillat, N., Harrison, P., Goede, J. S., McMahon, C., et al. (2011). South-east Asian ovalocytosis and the cryohydrocytosis form of hereditary stomatocytosis show virtually indistinguishable cation permeability defects. *Br. J. Haematol.* 152, 655–664.

Iolascon, A., De Falco, L., Borgese, F., Esposito, M. R., Avvisati, R. A., Izzo, P., et al. (2009). novel erythroid anion exchange variant (Gly796Arg) of hereditary stomatocytosis associated with dyserythropoiesis. *Haematologica* 94, 1049–1059.

Jarolim, P., Palek, J., Amato, D., Hassan, K., Sapak, P., Nurse, G. T., et al. (1991). Deletion in erythrocyte band 3 gene in malaria-resistant Southeast Asian ovalocytosis. *Proc. Natl. Acad. Sci. U.SA.* 88, 11022–11026.

Johnston, J. A., Ward, C. L., and Kopito, R. R. (1998). Aggresomes: a cellular response to misfolded proteins. *J. Cell Biol.* 143, 1883–1898.

Kager, L., Bruce, L. J., Zeitlhofer, P., Flatt, J. F., Maia, T. M., Ribeiro, M. L., et al. (2017). Band 3 null^{VIENNA}, a novel homozygous SLC4A1 p.Ser477X variant causing severe hemolytic anemia, dyserythropoiesis and complete distal renal tubular acidosis. *Pediatr. Blood Cancer* 64:10.1002/bc.26227. doi: 10.1002/pbc.26227

Keerthivasan, G., Small, S., Liu, H., Wickrema, A., and Crispino, J. D. (2010). Vesicle trafficking plays a novel role in erythroblast enucleation. *Blood* 116, 3331–3340.

Konstantinidis, D. G., Pushkaran, S., Johnson, J. F., Cancelas, J. A., Manganaris, S., Harris, C. E., et al. (2012). Signaling and cytoskeletal requirements in erythroblast enucleation. *Blood* 119, 6118–6127.

Kuma, H., Abe, Y., Askin, D., Bruce, L. J., Hamasaki, T., Tanner, M. J., et al. (2002). Molecular basis and functional consequences of the dominant effects

of the mutant band 3 on the structure of normal band 3 in Southeast Asian ovalocytosis. *Biochemistry* 41, 3311–3320.

Laosombat, V., Viprakasit, V., Dissaneevate, S., Leetanaporn, R., Chotsampancharoen, T., Wongchanchailert, M., et al. (2010). Natural history of Southeast Asian Ovalocytosis during the first 3 years of life. *Blood Cells Mol. Dis.* 45, 29–32. doi: 10.1016/j.bcmd.2010.03.010

Leal, J. K. F., Adjobo-Hermans, M. J. W., and Bosman, G. J. C. G. M. (2018). Red blood cell homeostasis: mechanisms and effects of microvesicle generation in health and disease. *Front. Physiol.* 9:703. doi: 10.3389/fphys.2018.00703

Lee, J. C., Gimm, J. A., Lo, A. J., Koury, M. J., Krauss, S. W., Mohandas, N., et al. (2004). Mechanism of protein sorting during erythroblast enucleation: role of cytoskeletal connectivity. *Blood* 103, 1912–1919. doi: 10.1182/blood-2003-03-0928

Lee, T. H., Kim, S. U., Yu, S. L., Kim, S. H., Park, D. S., Moon, H. B., et al. (2003). Peroxiredoxin II is essential for sustaining life span of erythrocytes in mice. *Blood* 101, 5033–5038.

Lin, E., Tavul, L., Michon, P., Richards, J. S., Dabod, E., Beeson, J. G., et al. (2010). Minimal association of common red blood cell polymorphisms with plasmodium falciparum infection and uncomplicated malaria in papua new guinean school children. *Am. J. Trop. Med. Hyg.* 83, 828–833.

Liu, S. C., Jarolim, P., Rubin, H. L., Palek, J., Amato, D., Hassan, K., et al. (1994). The homozygous state for the band 3 protein mutation in Southeast Asian Ovalocytosis may be lethal. *Blood* 84, 3590–3501.

Liu, S. C., Palek, J., Yi, S. J., Nichols, P. E., Derick, L. H., Chiou, S. S., et al. (1995). Molecular basis of altered red blood cell membrane properties in Southeast Asian ovalocytosis: role of the mutant band 3 protein in band 3 oligomerization and retention by the membrane skeleton. *Blood* 86, 349–358.

Luciani, A., Villella, V. R., Esposito, S., Brunetti-Pierri, N., Medina, D., Settembre, C., et al. (2010). Defective CFTR induces aggresome formation and lung inflammation in cystic fibrosis through ROS-mediated autophagy inhibition. *Nat. Cell Biol.* 12, 863–875.

Mankelow, T. J., Griffiths, R. E., Trompeter, S., Flatt, J. F., Cogan, N. M., Massey, E. J., et al. (2016). The ins and outs of reticulocyte maturation revisited: the role of autophagy in sickle cell disease. *Autophagy* 12, 590–591. doi: 10.1080/15548627.2015.1125072

Matte, A., Bertoldi, M., Mohandas, N., An, X., Bugatti, A., Brunati, A. M., et al. (2013). Membrane association of peroxiredoxin-2 in red cells is mediated by the N-terminal cytoplasmic domain of band 3. *Free Radic. Biol. Med.* 55, 27–35.

Mgone, C. S., Koki, G., Paniu, M. M., Kono, J., Bhatia, K. K., Genton, B., et al. (1996). Occurrence of the erythrocyte band 3 (AE1) gene deletion in relation to malaria endemicity in Papua New Guinea. *Trans. R. Soc. Trop. Med. Hyg.* 90, 228–231. doi: 10.1016/s0035-9203(96)90223-0

Mohandas, N., Winardi, R., Knowles, D., Leung, A., Parra, M., George, E., et al. (1992). Molecular basis for membrane rigidity of hereditary ovalocytosis. A novel mechanism involving the cytoplasmic domain of band 3. *J. Clin. Invest.* 89, 686–692. doi: 10.1172/JCI115636

Moura, P. L., Hawley, B. R., Mankelow, T. J., Griffiths, R. E., Dobbe, J. G. G., Streekstra, G. J., et al. (2018). Non-muscle myosin II drives vesicle loss during human reticulocyte maturation. *Haematologica* 103, 1997–2007. doi: 10.3324/haematol.2018.199083

Paquette, A. M., Harahap, A., Laosombat, V., Patnode, J. M., Satyagraha, A., Sudoyo, H., et al. (2015). The evolutionary origins of Southeast Asian Ovalocytosis. *Infect. Genet. Evol.* 34, 153–159. doi: 10.1016/j.meegid.2015.06.002

Paw, B. H., Davidson, A. J., Zhou, Y., Li, R., Pratt, S. J., Lee, C., et al. (2003). Cell-specific mitotic defect and dyserythropoiesis associated with erythroid band 3 deficiency. *Nat. Genet.* 34, 59–64.

Perrotta, S., Borriello, A., Scaloni, A., De Franceschi, L., Brunati, A. M., Turrini, F. et al. (2005). The N-terminal 11 amino acids of human erythrocyte band 3 are critical for aldolase binding and protein phosphorylation: implications for band 3 function. *Blood* 106, 4359–4366. doi: 10.1182/blood-2005-07-2806

Picard, V., Proust, A., Eveillard, M., Flatt, J. F., Couec, M. L., Caillaux, G., et al. (2014). Homozygous Southeast Asian ovalocytosis is a severe dyserythropoietic anemia associated with distal renal tubular acidosis. *Blood* 123, 1963–1965.

Ribeiro, M. L., Alloisio, N., Almeida, H., Gomes, C., Texier, P., Lemos, C., et al. (2000). Severe hereditary spherocytosis and distal renal tubular acidosis associated with the total absence of band 3. *Blood* 96, 1602–1604.

Rocha, S., Vitorino, R. M., Lemos-Amado, F. M., Castro, E. B., Rocha-Pereira, P., Barbot, J., et al. (2008). Presence of cytosolic peroxiredoxin 2 in the erythrocyte membrane of patients with hereditary spherocytosis. *Blood Cells Mol. Dis.* 41, 5–9.

Rosanas-Urgell, A., Lin, E., Manning, L., Rarau, P., Laman, M., Senn, N., et al. (2012). Reduced risk of plasmodium vivax malaria in papua new guinean children with southeast asian ovalocytosis in two cohorts and a case-control study. *PLoS Med.* 9:e1001305. doi: 0.1371/journal.pmed.1001305

Salomao, M., Chen, K., Villalobos, J., Mohandas, N., An, X., and Chasis, J. A. (2010). Hereditary spherocytosis and hereditary elliptocytosis: aberrant protein sorting during erythroblast enucleation. *Blood* 116, 267–269.

Salzer, U., Mairhofer, M., and Prohaska, R. (2007). Stomatin: a new paradigm of membrane organization emerges. *Dyn. Cell Biol.* 1, 20–33.

Salzer, U., Zhu, R., Luten, M., Isobe, H., Pastushenko, V., Perkmann, T., et al. (2008). Vesicles generated during storage of red cells are rich in the lipid raft marker stomatin. *Transfusion* 48, 451–462.

Sarabia, V. E., Casey, J. R., and Reithmeier, R. A. (1993). Molecular characterization of the band 3 protein from Southeast Asian ovalocytes. *J. Biol. Chem.* 268, 10676–10680.

Satchwell, T. J., Hawley, B. R., Bell, A. J., Ribeiro, M. L., and Toye, A. M. (2015). The cytoskeletal binding domain of band 3 is required for multiprotein complex formation and retention during erythropoiesis. *Haematologica* 100, 133–142.

Schofield, A. E., Reardon, D. M., and Tanner, M. J. (1992). Defective anion transport activity of the abnormal band 3 in hereditary ovalocytic red blood cells. *Nature* 355, 836–838.

Schweitzer, J. K., Burke, E. E., Goodson, H. V., and D'Souza-Schorey, C. (2005). Endocytosis resumes during late mitosis and is required for cytokinesis. *J. Biol. Chem.* 280, 41628–41635.

Singleton, B. K., Ahmed, M., Green, C. A., Heimpel, H., Woźniak, M. J., Ranjha, L., et al. (2018). CD44 as a potential screening marker for preliminary differentiation between congenital dyserythropoietic anemia Type II and hereditary spherocytosis. *Cytometry B Clin. Cytom.* 94, 312–326. doi: 10.1002/cyto.b.21488

Smythe, J. S., Spring, F. A., Gardner, B., Parsons, S. F., Judson, P. A., and Anstee, D. J. (1995). Monoclonal antibodies recognizing epitopes on the extracellular face and intracellular N-terminus of the human erythrocyte anion transporter (band 3) and their application to the analysis of South East Asian ovalocytes. *Blood* 85, 2929–2936.

Tanner, M. J., Bruce, L., Martin, P. G., Rearden, D. M., and Jones, G. L. (1991). Melanesian hereditary ovalocytes have a deletion in red cell band 3. *Blood* 78, 2785–2786.

Ubukawa, K., Guo, Y. M., Takahashi, M., Hirokawa, M., Michishita, Y., Nara, M., et al. (2012). Enucleation of human erythroblasts involves non-muscle myosin IIB. *Blood* 119, 1036–1044.

Williamson, R. C., Brown, A. C., Mawby, W. J., and Toye, A. M. (2008). Human kidney anion exchanger 1 localisation in MDCK cells is controlled by the phosphorylation status of two critical tyrosines. *J. Cell Sci.* 121(Pt 20), 3422–3432.

Conflict of Interest: The authors declare that the research was conducted in the absence of any commercial or financial relationships that could be construed as a potential conflict of interest.

frontiers in Physiology

REVIEW
published: 16 February 2021
doi: 10.3389/fphys.2021.604738

The Redox Balance and Membrane Shedding in RBC Production, Maturation, and Senescence

*Eitan Fibach**

Department of Hematology, Hadassah University Hospital, Jerusalem, Israel

Membrane shedding in the form of extracellular vesicles plays a key role in normal physiology and pathology. Partial disturbance of the membrane–cytoskeleton linkage and increased in the intracellular Ca content are considered to be mechanisms underlying the process, but it is questionable whether they constitute the primary initiating steps. Homeostasis of the redox system, which depends on the equilibrium between oxidants and antioxidants, is crucial for many cellular processes. Excess oxidative power results in oxidative stress, which affects many cellular components, including the membrane. Accumulating evidence suggests that oxidative stress indirectly affects membrane shedding most probably by affecting the membrane–cytoskeleton and the Ca content. In red blood cells (RBCs), changes in both the redox system and membrane shedding occur throughout their life—from birth—their production in the bone marrow, to death—aging in the peripheral blood and removal by macrophages in sites of the reticuloendothelial system. Both oxidative stress and membrane shedding are disturbed in diseases affecting the RBC, such as the hereditary and acquired hemolytic anemias (i.e., thalassemia, sickle cell anemia, and autoimmune hemolytic anemia). Herein, I review some data-based and hypothetical possibilities that await experimental confirmation regarding some aspects of the interaction between the redox system and membrane shedding and its role in the normal physiology and pathology of RBCs.

Keywords: red blood cell, microvesicles, membrane, aging, oxidation stress

OPEN ACCESS

Edited by:
Philippe Connes, Université Claude Bernard Lyon 1, France

Reviewed by:
Nicola Conran, State University of Campinas, Brazil
Elie Nader, Université Claude Bernard Lyon 1, France

***Correspondence:**
Eitan Fibach
Fibach@yahoo.com

Specialty section:
This article was submitted to Red Blood Cell Physiology, a section of the journal Frontiers in Physiology

Received: *10 September 2020*
Accepted: *18 January 2021*
Published: *16 February 2021*

Citation:
Fibach E (2021) The Redox Balance and Membrane Shedding in RBC Production, Maturation, and Senescence. Front. Physiol. 12:604738. doi: 10.3389/fphys.2021.604738

INTRODUCTION

Most, if not all, cells shed part of their plasma membrane as extracellular vesicles, the role of which in physiological and pathophysiological processes is increasingly appreciated (Raposo and Stoorvogel, 2013). These vesicles differ in their mechanisms of production, composition, and function. In red blood cells (RBCs), membrane shedding (vesiculation) continues throughout their entire life, from birth to death, serving multiple roles at different phases: production and maturation in the bone marrow, circulation, functioning, and aging (senescence) in the peripheral blood, and removal (clearance) in sites of the reticuloendothelial system, such as the spleen (Leal et al., 2018).

Oxidative stress is one of the mechanisms that have been suggested to contribute to vesiculation (Willms et al., 2016, 2018).

The redox status of cells depends on the equilibrium between oxidants and antioxidants. Its homeostasis is crucial for the functioning of many systems of the body, including the normal physiology of RBCs and their ability to produce and shed membrane-bound vesicles (Margolis and Sadovsky, 2019). Oxidative stress, which presents an imbalance in the redox state, is considered to be involved in many diseases, including those intimately concerned with the erythroid cell system, such as the hemolytic anemias (Fibach and Rachmilewitz, 2008).

Herein, I review the interdependence of oxidative stress and membrane shedding throughout the life of the RBCs and their involvement in normal and pathological physiology.

MEMBRANE SHEDDING

Membrane shedding in the form of membrane-bound particles is common to all cells. It occurs as exosomes (50–150 nm in diameter)—released upon exocytosis; microvesicles (MVs) or microparticles, and apoptotic bodies (1–5 μm)—generated by blebbing of the plasma membranes of cells undergoing programmed cell death (Raposo and Stoorvogel, 2013).

The RBC, like any other cell, produces MVs, which are shed from the plasma membrane (Willekens et al., 2008; Leal et al., 2018). This process occurs at all stages of the RBC life: its production, maturation, aging (senescence), and removal, and it constitutes an intrinsic part of homeostasis in terms of the quantity and quality of the RBC. It also occurs during the storage of RBC in banks. Normal blood plasma contains approximately 1,000 RBC-derived MVs per milliliter; however, as they contain immunological recognition and removal signals, they are rapidly eliminated (probably within minutes) from the circulation by the spleen macrophages (Willekens et al., 2008).

Microvesicles are surrounded by a lipid-bilayered membrane that is different in its composition from the plasma membrane from which they are derived, suggesting that their formation (vesiculation) involves a regulated sorting process, leading to enrichment or depletion of various components. MVs are enriched in cellular constituents characterizing the oldest RBC—the glycated hemoglobins (Hb), HbA1c and HbA1e2 (Leal et al., 2018), and redox enzymes, such as glutathione S-transferase, thioredoxin and peroxiredoxins 1 and 2, and the protein-degrading ubiquitin. They contain senescence signals such as phosphatidylserine (PS), and band-3 epitopes (Westerman and Porter, 2016). In addition, MVs contain the glycosylphosphatidyl-inositol (GPI)–anchored, complement-inhibiting proteins, the decay-accelerating factor (CD55), and the membrane inhibitor of reactive lysis (CD59), although probably not in a functional form, as demonstrated for the GPI-anchored enzyme acetylcholinesterase (Leal et al., 2017).

Membrane shedding affects the production of RBCs, their functionality and their clearance. In the circulation, the process leads to the removal of damaged cell constituents. This is exemplified by the loss of 20% of the Hb and the cell membrane during RBC aging (Leal et al., 2018).

MECHANISMS OF MEMBRANE SHEDDING

Two mechanisms have been suggested as the main driving forces of membrane shedding and extracellular MV production:

Partial Cytoskeleton:Membrane Uncoupling

The RBC membrane comprised a cytoskeleton and a lipid bilayer. The latter includes various phospholipids and sphingolipids, cholesterol, and integral membrane proteins such as Band-3 and glycophorin. The cytoskeleton is tethered to the lipid bilayer via "immobile" Band-3 proteins at the spectrin–ankyrin binding sites and via glycophorin at the actin junctional complexes. One mechanism of vesiculation occurs as a result of phosphorylation of the membrane proteins, mostly Band-3, leading to a weakening of the link between the lipid bilayer and the cytoskeleton [for detailed review, see Leal et al. (2018)]. This hypothesis is supported by the finding of accumulated amounts of Band-3 and actin, but the absence of spectrin, in MVs.

Calcium Accumulation

Calcium is a potent, specific, and tightly controlled cellular regulator including in RBC [for detailed review, see Bogdanova et al. (2013)]. Increased intracellular Ca^{2+} concentration could be triggered by various cytotoxic stimuli such as hyperosmolarity, exposure to xenobiotics, and oxidative stress (Kass et al., 1990; Cameron et al., 1993) that occurs during normal RBC senescence and eryptosis (apoptosis-like pathological destruction of mature enucleated RBCs) (Lang et al., 2005). The increase in Ca^{2+} triggers biochemical and structural changes that result in vesiculation, such as activation of the apoptosis mediator caspase-3, which can trigger vesiculation, and enhancing Floppase and scramblase and inhibiting Flippase—the enzymes that control the externalization of PS (Allan and Thomas, 1981). Vesicles collected under experimental treatment with Ca^{2+} ionophores, such as A23187, are of two sizes (∼200 and ∼120 nm in diameter) that contain Hb and are enriched in GPI-anchored proteins (e.g., acetylcholinesterase and CD55) and raft lipids, but are free of cytoskeleton components (Leal et al., 2018).

These two mechanisms may not be mutually exclusive. For example, increased Ca^{2+} level may activate proteolytic enzymes such as calpains (Guerini et al., 2005) that decrease the cytoskeleton:membrane interaction, leading to vesiculation.

Although these mechanisms are most probably involved in vesiculation, they may not be the primary events of the process. For example, cytoskeleton modifications may be the consequence, rather than the cause, of the vesiculation (Guerini et al., 2005). It was suggested that, in the blood bank, only after 35 days of storage RBCs exhibit clustered Band-3 MVs (Azouzi et al., 2018), which could imply that another mechanism is involved in vesiculation before that. Based on the difference in the protein composition of MVs generated upon senescence and storage to those induced experimentally by Ca^{2+} ionophores, Bosman et al. proposed that the latter is not the initiating event of the generation of RBC-MVs (Bosman, 2013).

OXIDATIVE STRESS

The redox status represents the balance between oxidants, such as reactive oxygen species (ROS), and antioxidants [for review, see Halliwell and Gutteridge (1999)]. Imbalance due to excess oxidants or insufficient antioxidants results in oxidative stress. Although oxidants have important roles in normal physiology, e.g., in signal transduction, excess oxidants may interact with, and damage, various cellular components (e.g., proteins, lipids, and nucleic acids). Aging of the organism; senescence of cells, such as the RBCs; and many environmental and pathological situation are related to oxidative stress. Oxidative stress is involved in many pathologies such as neurodegenerative, cardiovascular, metabolic, and malignant diseases. In some diseases, the RBCs are the prime target of oxidative stress; this includes the hemolytic anemias (Fibach and Rachmilewitz, 2008).

In most cells, ROS is generated during oxidative energy production in the mitochondria. Approximately 2% of the total O_2 consumption results in the superoxide anion radical ($O_2^{\bullet}$) (Halliwell and Gutteridge, 1999). In the mitochondria-deficient RBC, Hb is the primary source of ROS generation, when heme iron interacts with oxygen. Normally, approximately 3% of the Hb is auto-oxidized to form metHb and superoxide that in turn produces hydrogen peroxide (H_2O_2) and oxygen by dismutation (Scott et al., 1989).

Many pathological conditions are associated with oxidative stress in various cell types (Liguori et al., 2018). We have studied particularly the hereditary and acquired hemolytic anemias, where oxidative stress involves mainly, but not exclusively, the erythroid cells (Fibach and Rachmilewitz, 2008). In these diseases, the destruction of mature RBCs and their precursors (hemolysis) is accelerated—over the capacity to produce new ones, resulting subsequently in chronic anemia. Among the hemolytic anemias are the following diseases:

The Hemoglobinopathies—Thalassemia (Thal) and Sickle Cell Disease (SCD)

Are caused by hereditary mutations in the globin genes. The major adult Hb, HbA, is a tetramer of two α-globin and two β-globin chains ($\alpha_2\beta_2$). In α-thal or β-thal, the respective genes are mutated, leading to reduced or no production of their polypeptides (Rund and Rachmilewitz, 2005). In SCD, a mutation in the β-globin gene leads to the production of abnormal globin chains (β^S) that form the abnormal sickle Hb (HbS). The latter polymerizes under the deoxygenated conditions of the narrow capillaries, altering the physical and chemical properties of the RBCs. They acquire a sickle-like morphology and an increased tendency to hemolyze and to adhere to the vasculature walls (Steinberg, 1998; Cisneros and Thein, 2020).

Glucose-6-phosphate Dehydrogenase Deficiency

An RBC enzymopathy caused by mutations in the Glucose-6-Phosphate Dehydrogenase (G6PD) gene. The latter encodes a key enzyme of the pentose pathway (hexose monophosphate shunt), which in RBCs is the major supplier of the reducing agent nicotinamide adenine dinucleotide phosphate (NADPH) that is essential for several biosynthetic pathways (Luzzatto and Battistuzzi, 1985) and the redox homeostasis (Tian et al., 1998). The G6PD- and NADPH-deficient RBCs are under oxidative stress, especially after oxidative insult induced by certain foods (fava beans) and oxidative drugs, oxidant drugs, or chemicals (Arese et al., 2012).

Hereditary Spherocytosis

An RBC membranopathy due to mutations in various genes encoding for membrane proteins. Deficiency in spectrin is the most prevalent abnormality (Panizo Morgado et al., 2020), but sometimes it is secondary to a deficiency or dysfunction of the spectrin-binding protein–ankyrin (Hanspal et al., 1991; Panizo Morgado et al., 2020). The disease is characterized by RBCs with sphere shape (instead of biconcave disks), with reduced surface-to-volume ratio and increased osmotic fragility—properties that make them inclined to hemolysis (Perrotta et al., 2008; Chagula et al., 2020). Elliptocytosis is another RBC membranopathy with spectrin tetramer self-association, leading to RBCs with an elliptical or elongated shape (Pollet et al., 2020).

Paroxysmal Nocturnal Hemoglobinuria

A clonal stem cell disorder due to acquired somatic mutations predominantly in the phosphatidylinositol glycan complementation class A gene. The gene encodes an enzyme that participates in the production of the GPI anchor, by which some proteins are linked to the plasma membrane. Lack of this anchor leads to a partial or complete deficiency in these proteins on the hematopoietic stem cells and their differentiated progeny. The decay-accelerating factor (CD55) and the membrane inhibitor of reactive lysis (CD59) (Walport, 2001) belong to this family, making the affected RBCs prone to hemolysis by complement fixation and activation (Parker, 2007).

Autoimmune Hemolytic Anemia

An acquired disease caused by autoantibodies to surface RBC antigens. Binding of these antibodies marks them for complement-mediated and/or Fc-mediated lysis—intravascular and extravascular hemolysis, respectively. This can occur alone or with other conditions such as autoimmunity, malignancy, pharmacological treatment, blood transfusion, and pregnancy (Sawitsky and Ozaeta, 1970).

Myelodysplastic Syndromes

These conditions, affecting mostly elderly people, are characterized by ineffective production (dysplasia) of several blood cell lineages and bone marrow failure, leading to severe anemia that may require blood transfusion. One-third of the patients develop fatal acute myelogenous leukemia (Cazzola, 2012).

These, and other hemolytic anemias, vary in their etiology, but they all share damage to erythroid cells by oxidative stress [for review, see Fibach and Rachmilewitz (2008)]. Using flow cytometry methodology, we have documented oxidative

stress in their RBCs that included high production of ROS and membrane lipid peroxides and low content of reduced glutathione (Freikman et al., 2008), their primary antioxidant. ^{1}H–nuclear magnetic resonance (NMR) analysis demonstrated their oxidative stress by an elevated lactate-to-pyruvate ratio (Freikman et al., 2008).

Oxidative stress in RBCs in these anemias is due mainly, but not exclusively, to the following reasons:

Hemoglobin Instability

In thal, because of the shortage of one globin chain, there is an excess of other globins α in β-thal and γ and β in α-thal. These unmatched globins form homotetramers that dissociate into monomers that are oxidized; first to meHb and then to hemichromes (Rachmilewitz, 1974). Heme, iron, and the degraded protein moiety accumulate in the cytosol and on the plasma membrane. This leads to increased generation of ROS, catalyzed by free iron (see below), which damage membrane lipids and proteins, e.g., Band 4.1 and Band-3 (Rachmilewitz and Harari, 1972; Advani et al., 1992). In SCD, the metHbS is more unstable than metHbA, resulting in increased production of hemichromes that precipitate as Heinz bodies (Winterbourn and Carrell, 1974).

Iron Excess (Iron Overload)

In most hemolytic anemias, iron accumulates as a result of excess acquisition due to RBC transfusions and increased absorption from the diet (Fibach and Rachmilewitz, 2008). In addition, the release of iron-containing compounds (Hb or hemin) during hemolysis adds to the iron load. Normally, iron circulates complexed to transferrin and is taken up by cells through the membrane transferrin receptor (TfR) (Wang and Pantopoulos, 2011). Most of the intracellular iron is bound in a redox-inactive form to proteins such as in Hb and myoglobin; excess iron is stored in ferritin (Konijn et al., 1979). When extra iron is acquired, it saturates the transferrin; excess iron exists in the plasma as non–transferrin-bound iron (Breuer et al., 2000). This iron is taken up by cells through transferrin-independent pathways and forms the "labile iron pool" (Fibach and Rachmilewitz, 2010; Prus and Fibach, 2011)—a transitory intermediate between the cellular iron pools (Jacobs, 1977). Labile iron is redox-active—it takes part in the Fenton and Haber–Weiss reactions that generate ROS (Fibach and Rachmilewitz, 2010).

Complement Activation

Serum complement and oxidative stress are associated with paroxysmal nocturnal hemoglobinuria (Amer et al., 2008) and autoimmune hemolytic anemia (Fibach and Rachmilewitz, 2008). The affected RBCs are hypersensitive to oxidative insults (e.g., by hydrogen peroxide), and their oxidative status increases by interaction with activated complement before hemolysis. Antioxidants, such as N-acetyl cysteine and ascorbic acid (vitamin C), were found to reduce excess hemolysis *in vitro* (Amer et al., 2008), and the antioxidant food supplement, fermented papaya preparation, *in vivo* (Ghoti et al., 2010).

OXIDATIVE STRESS AND MEMBRANE SHEDDING

Several findings favor the primary involvement of oxidative stress in vesiculation (Szigyarto et al., 2018; Nader et al., 2020): (I) MVs are enriched in antioxidant enzymes and irreversibly oxidized Hb (Sudnitsyna et al., 2020); (II) some studies have indicated that treatment with oxidants decreased vesiculation, whereas antioxidants have an opposite effect (Stowell et al., 2013; Nader et al., 2020). Oxidative stress, through the effects of ROS, may trigger both mechanisms of vesiculation—the clustering of Band-3 and the accumulation of intracellular Ca^{2+}. The effect on Band-3 involves (I) activation of Src tyrosine kinases that phosphorylates Band-3; (II) oxidation of Hb into hemichromes that interact with the Band-3 cytoplasmic tail. In both cases, these results in clustering and mobility of Band-3 by detachment from the membrane skeleton, likely by release from ankyrin (Azouzi et al., 2018). As for Ca^{2+}, virtually every cellular Ca control mechanism is both affected by oxidative stress and is able to affect it (Leal et al., 2017). The cytosolic content of Ca^{2+} is increased by oxidative stress through the effects on Ca pumps, exchangers, channels, and binding proteins (Leal et al., 2017).

EXTERNALIZATION AND SHEDDING OF PHOSPHATIDYLSERINE

Membrane shedding and its modulation by oxidative stress are intimately related to the externalization and shedding of PS. The distribution of phospholipids across the plasma membrane of all cells, including the RBCs, is asymmetrical (Zwaal et al., 2005); aminophospholipids, e.g., PS, are preferentially present in the inner leaflet, whereas lipids with a choline head, e.g., phosphatidylcholine (PC), are mainly present in the outer leaflet of the membrane (Op den Kamp, 1979). The PS distribution across the membrane is under a dynamic equilibrium. Inward movement is catalyzed by the enzyme aminophospholipid translocase, whereas the outward movement, by the scramblase. Some of the external PS is shed to the extracellular environment. One mechanism of oxidative stress–mediated effect on PS externalization and shedding is by inhibition of the aminophospholipid translocase, causing the PS to "flip-flop" from the inner to the outer leaflet of the membrane (Pattanapanyasat et al., 2004).

We studied the interrelationship between oxidative stress on PS externalization and shedding in RBCs and their precursors by two methodologies: flow cytometry and NMR spectroscopy. Parameters studied by flow cytometry included the generation of ROS and membrane lipid peroxides and the contents of reduced glutathione (Amer and Fibach, 2004; Amer et al., 2004), labile iron pool (Prus and Fibach, 2008), and Ca^{2+} (Freikman et al., 2011). To measure the cellular distribution and shedding of PS, we designed a two-step fluorescence inhibition procedure (Freikman et al., 2009). Commonly, PS is measured by a fluorochrome-conjugated, PS-specific, protein–annexin V. In most studies, the method refers to the percentage of cells expressing a high level of PS (Alaarg et al., 2013;

Ferru et al., 2014), neglecting cells with less bound annexin V, giving the impression that PS externalization is an "all or none" process. This measurement is mainly applicable to populations with a significant percentage of highly positive cells (e.g., following induction of apoptosis). However, *in vivo*, because of their short survival, very few such cells exist, making their determination unreliable. Additionally, this procedure does not measure the inner PS (unless the cell plasma membrane is permeabilized), nor the shed PS. Most importantly, the procedure yields a relative (in mean fluorescence channel) rather than absolute quantitative values. To overcome these shortcomings, we devised a protocol that entails two steps. First, the PS on the surface of intact cells, or in cell lysates, supernatants, or blood plasma is bound to an excess amount of annexin V. Then, the residual, non-bound annexin V is quantified by binding to PS exposed on apoptotic cells (e.g., 6-day old HL-60 cells), serving as an indicator reagent, the fluorescence of which is inversely related to the PS in the tested sample (Zwaal et al., 2005).

Using this methodology, we confirmed that mature RBCs and their precursors in thal, as in other hemolytic anemia (see below), are under oxidative stress. The results also demonstrated that oxidatively stressed RBCs (old vs. young, thal vs. normal) have a lower content of total cellular PS but more exposed and shed PS. This was reflected by a moderate increase in the proportion of highly annexin V–positive cells and by a significant increase in the average (mean fluorescence channel) cellular PS exposure of the entire population. The increased PS shedding by thal RBCs was also reflected in the higher PS concentration found in sera from patients versus normal donors. Interestingly, in addition to PS in MVs (Pattanapanyasat et al., 2004), we found significant amounts of PS shed in a membrane-free form (Freikman et al., 2008, 2009).

The interrelationship of the oxidative status, Ca flux, and PS shedding was demonstrated by measuring PS and Ca^{+2} in stressed and non-stressed RBCs (Freikman et al., 2011). Treating of thal RBCs with antioxidants (e.g., ascorbic acid or N-acetyl cysteine) led to decreased external and shed PS (Freikman et al., 2009), while treating normal RBCs with oxidants, the Ca ionophore A23187, or increasing the Ca concentration of the medium concomitantly increased the oxidative state, the Ca flux, and the PS shedding (Freikman et al., 2009).

These results were confirmed by NMR spectroscopy (Freikman et al., 2008). ^{1}H-NMR showed a higher ratio of lactate/pyruvate, reflecting oxidative stress, in normal RBCs treated with oxidants. ^{31}P-NMR showed more PC and less PS in the thal RBCs that were reversed by antioxidants. When RBCs were incubated in phosphate-buffered saline, more PS was found in the supernatant of thal cells than of normal cells. Antioxidants reduced shedding of PS, whereas oxidants increased it. The plasma of thal patients contained more PS and less PC than normal plasma. These results confirmed the results obtained by flow cytometry, indicating that the decreased PS on the membrane of oxidatively stressed RBCs resulted from increased shedding. The shed PS was further analyzed in MVs from purified from the plasma and from RBC supernatants. The results indicated more PS in thal MVs than in their normal counterparts.

These changes in the membrane composition increase the osmotic resistance and the susceptibility of RBCs to undergo phagocytosis. Using an *in vitro* system, we have shown that inducing PS externalization by treatment with an oxidant increased erythrophagocytosis by macrophages, whereas adding PS prevented it. The latter effect was most probably due to a competitive binding to PS receptors on the macrophages (Freikman et al., 2009).

MEMBRANE SHEDDING IN RBC DISEASES ASSOCIATED WITH OXIDATIVE STRESS

In addition to oxidative stress, hemolytic anemias are characterized by increased MVs derived from RBCs and their precursors as well as in other blood cell types and platelets (Westerman and Porter, 2016). Oxidative stress might be the driving force of their increased production, in addition to other disease-specific mechanisms [for review, see Leal et al. (2018)].

In α- and β-thal, the hemichromes produced in the mature RBCs and their Hb-containing precursors due to the production of unbalanced globin chains and homo-tetramers bind to Band-3 and induce their dimerization. Band-3 is subsequently phosphorylated by tyrosine kinases, weakening the cytoskeleton/membrane interaction, resulting in vesiculation.

In SCD, RBCs, platelets, and polymorphonuclear neutrophils exhibit oxidative stress (Amer et al., 2006), which in RBCs is due to the deoxygenated HbS polymers and other factors (e.g., the chronic inflammatory state) (Fibach and Rachmilewitz, 2008). It damages the RBC membrane proteins and lipids and contributes to increased intracellular Ca^{2+} and tyrosine phosphorylation of Band-3 (Evans et al., 1984). These changes lead to dehydration and membrane rigidity, poor deformability, and destabilization, leading to the increased vesiculation (Westerman and Porter, 2016). The MVs are related to the pathogenesis; they are high during both steady-state and painful crisis conditions (Margolis and Sadovsky, 2019).

In hereditary spherocytosis, although oxidative stress is common to RBCs (as well as other blood cell types) (Ghoti et al., 2011), the underlying defect, i.e., changes in ankyrin, spectrin, or Band-3, might affect the vesiculation process, producing MVs of different compositions. For instance, Band-3 has been found in MVs from ankyrin- or spectrin-defective RBCs, but not from those defective in Band-3 (Reliene et al., 2002).

Paroxysmal nocturnal hemoglobinuria and autoimmune hemolytic anemia, which are associated with oxidatively stressed RBCs (Amer et al., 2008; Fibach and Rachmilewitz, 2008), also demonstrated changes in vesiculation (Pan et al., 1991; Leal et al., 2019).

In summary, membrane shedding is elevated in oxidatively stressed RBC–centered diseases. Defects caused by oxidative stress in the cytoskeleton/membrane association are most likely the main underlying mechanisms, although other disease-related changes may contribute to vesiculation as well. RBC-derived MVs may have beneficial effects, such as preventing the untimely removal of functional RBCs. On the other hand, they may

be actively involved in pathology, e.g., by their effects on inflammation, thrombosis, and autoimmune reactions (Fibach and Rachmilewitz, 2008). This double-edged effect emphasizes the need for a better understanding of their mechanisms of generation, their pathophysiological consequences, and modes of prevention.

THE REDOX BALANCE AND MEMBRANE SHEDDING DURING RBC LIFE

Changes in the redox state and the membrane shedding characterize the RBCs at different stages of their life from birth to death, serving specific roles at each stage. The redox state depends on the rate of ROS production and scavenging (Halliwell and Gutteridge, 1999). In erythroid progenitors and precursors, ROS are produced at a high rate mainly as a byproduct of energy production in the mitochondria. They are reduced considerably in the mitochondria-free mature RBCs where they are produced mainly as a result of oxygenation of Hb. Upon senescence, RBCs undergo oxidative stress mainly due to a decrease in the antioxidative defense effects of the enzymes superoxide dismutase, catalase, G6PD, and aspartate aminotransferase (Kumar and Rizvi, 2014). The latter two enzymes are involved in the formation of antioxidant reduced glutathione and NADPH (Fornaini et al., 1985).

We have studied membrane shedding during RBC generation and senescence with respect to the externalization and shedding of PS (Freikman and Fibach, 2011).

MEMBRANE SHEDDING IN THE BONE MARROW

In humans, RBC production (erythropoiesis) takes place in the bone marrow by a physiologically regulated process that entails the proliferation and maturation of erythroid progenitors and precursors. Membrane shedding may participate in the following processes:

Erythropoiesis

The extent of erythropoiesis depends on the relative rates of generation of erythroid-committed progenitors from the pluripotent hematopoietic stem cells, their proliferation, and maturation to morphologically identified precursors and eventually to reticulocytes. These processes are taking place mainly in the bone marrow and are regulated by the hematopoietic environment and various glycoprotein cytokines. The latter induce signal transduction pathways initiated by interaction with specific surface receptors. Among the cytokines, the erythroid hormone, erythropoietin (Epo), serves a particularly important role. It stimulates the proliferation and maturation (Palis, 2014) and suppresses the death of erythroid precursors, serving as an antiapoptotic agent (Testa, 2004). The extent of the effect of cytokines is proportional to their concentration in the bone marrow environment and the abundance (number/concentration) of the surface receptors on the affected cells. Epo is produced mainly in the kidneys in response to the oxygen tension of its tissue; hypoxic conditions, such as at high altitudes or anemia, stimulate Epo production, leading to its high levels in the bone marrow. Its surface receptors (EpoR) are modulated during erythroid maturation, in a biphasic mode. Their abundance peaks in the late erythroid progenitors (colony-forming units—erythroid) and then gradually decreases to disappear altogether from mature RBCs (Wickrema et al., 1991). This modulation may explain the increasing effect of Epo during progenitor maturation and its diminishing effect on the more mature precursors. Several groups suggest that some RBCs do carry low levels of EpoR, which may explain the effect of Epo on mature RBCs (Amer et al., 2010). It could be hypothesized that membrane shedding decreases the number of surface receptors during maturation, in addition to reduced synthesis and internalization, thus contributing to the developmental modulation of the effects of Epo and other cytokines.

Apoptosis is known to involve PS externalization (Leventis and Grinstein, 2010). Using cultures of erythroid precursors, we have found that depletion of Epo during their maturation results in apoptosis that is preceded by increased externalization of PS (Freikman and Fibach, 2011). These results suggest that the PS externalization is involved in the apoptosis of erythroid precursors under physiological conditions and that increased PS externalization due to oxidative stress may be responsible to pathologically increased apoptosis leading to ineffective erythropoiesis such as in the myelodysplastic syndrome or thal. Thus, membrane shedding may confer on erythroid precursors two opposing effects concerning apoptosis, acceleration, and inhibition by removing of EpoR and exposed PS, respectively.

Iron Uptake

Erythroid maturation involves Hb production that requires iron uptake and heme and globin synthesis. Iron uptake is mostly

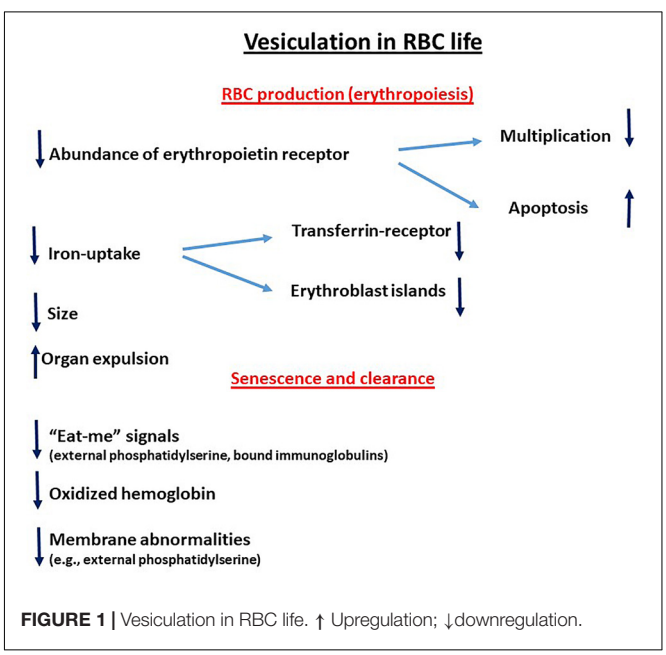

FIGURE 1 | Vesiculation in RBC life. ↑ Upregulation; ↓downregulation.

carried out by binding of the serum iron-carrying (holo-) transferrin with its surface receptor (TfR). These receptors too undergo a biphasic modulation during maturation: they peak on erythroblasts (Moura et al., 2015) and decrease afterward to disappear altogether from the mature RBCs. This TfR modulation correlates with the extent of iron uptake and Hb production. It should be mentioned, however, that other mechanisms, such as non–TfR-route, receptor-mediated, uptake of ferritin (Leimberg et al., 2003) and iron (Prus and Fibach, 2011), may complement the main, TfR, route. Membrane shedding may play a role in the disappearance of TfR (Pan et al., 1985), as well as the alternative pathways of iron uptake.

Erythroblastic Islands

Macrophages are essential for erythropoiesis (de Back et al., 2014; Moura et al., 2015). During their early development, erythroid precursors surround a central macrophage, forming the erythroblastic island (Bessis and Breton-Gorius, 1962; Chasis and Mohandas, 2008). Developmental significance of this structure is not entirely clear; one possibility is that it facilitates iron uptake by direct contact and non-TfR route, at early stages of erythroid precursors. Indeed, we have shown that cocultures of erythroid progenitors and macrophages develop Hb-containing precursors in the absence of holo-transferrin (Leimberg et al., 2008). This is probably a transient phenomenon, characterizing specific stages in the erythroid precursor maturation, prior to the peak of TfR exposure, after which this interaction is dissociated. It has been suggested that surface adhesion proteins on erythroid precursors might link them to macrophages and their extracellular matrix (Chasis and Mohandas, 2008; Soni et al., 2008). This could be hypothesized that the external PS might have a similar effect by binding to macrophages carrying PS receptors. Membrane shedding, in addition to reduced synthesis and internalization, may reduce the exposure of the adhesion proteins and PS moieties and thus lessens the binding and facilitates the release of erythroid cells from the island as they mature. This possibility awaits experimental confirmation.

Size Reduction

This process characterizes erythroid maturation in the bone marrow, as well as RBC senescence in the circulation (Jandl, 1996). It serves a functional adaptation generating mature RBCs that are small enough to pass through narrow capillaries. Size reduction also leads to a high surface-to-volume ratio (Renoux et al., 2019), promoting gas exchange between the RBCs and tissue cells. Membrane shedding might be either the cause or the outcome of size reduction. We reported that inhibition of PS externalization and shedding prevented size reduction in differentiating erythroid cells (Freikman and Fibach, 2011), favoring the first possibility.

Organelle Expulsion

At the end of their terminal maturation, erythroid precursors lose all their organelles—the nucleus (in most mammals), mitochondria, ribosomes, Golgi apparatus, and endoplasmic reticulum. Some of these processes involve membrane shedding. Nuclear expulsion (enucleation) requires preliminary changes taking place during differentiation, such as cell cycle arrest, chromatin condensation, and nuclear polarization (pyknosis). Enucleation is preceded by rearrangement of the cytoskeleton and clathrin-dependent generation of vacuoles at the nuclear–cytoplasmic border. This process, which occurs

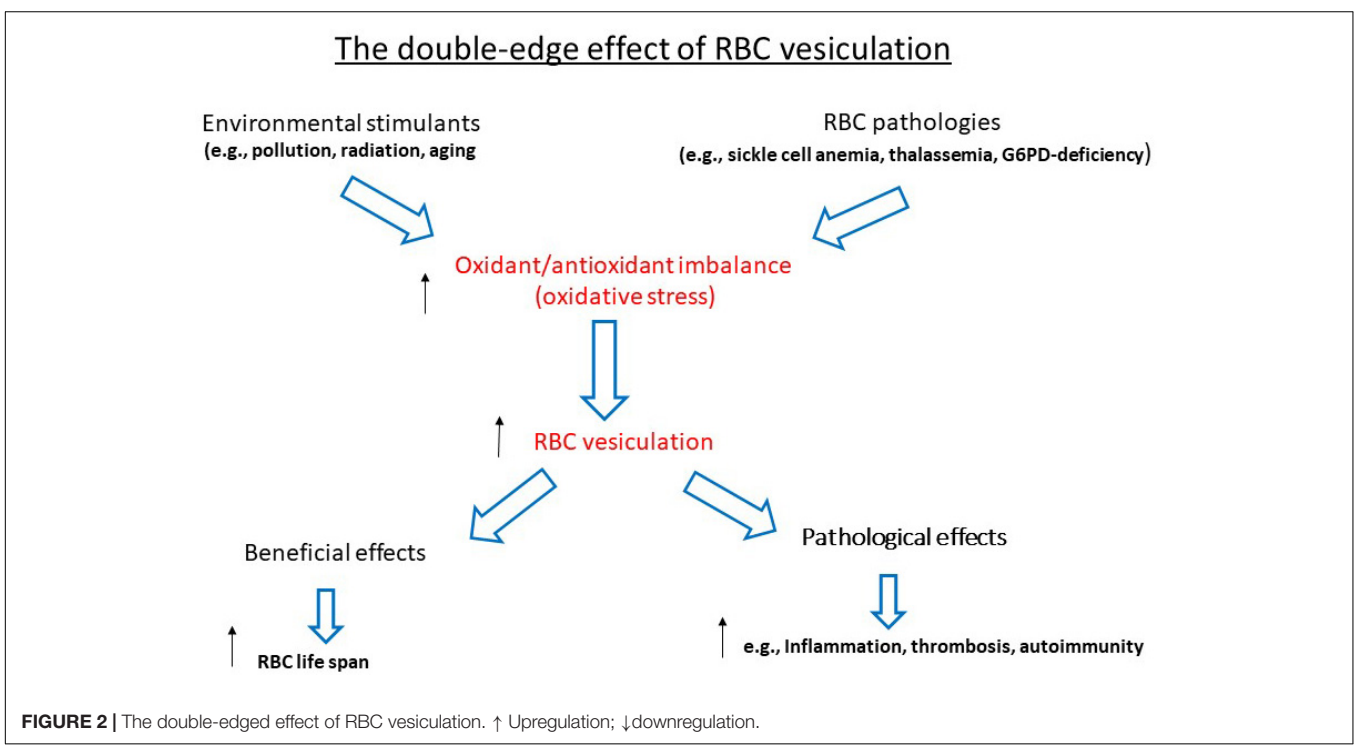

FIGURE 2 | The double-edged effect of RBC vesiculation. ↑ Upregulation; ↓downregulation.

in orthochromatic erythroblasts, produces two uneven cells: a reticulocyte and a pyrenocyte. The latter, which contains the expelled nucleus surrounded by a thin layer of cytoplasm and the plasma membrane, is rapidly engulfed by the macrophages of the erythroblastic islands. The exposed PS serves as an "eat me" signal for their elimination (Yoshida et al., 2005). Enucleated reticulocyte continues to mature, losing approximately 20% of its surface (Willekens et al., 2008) and any remaining membrane-bound cytosolic organelle by an autophagy/exosome-combined pathway (Blanc et al., 2005). This subject was reviewed in (Moras et al., 2017).

Another mechanism of removing cellular components is the clathrin-dependent invagination of the plasma membrane to form early endosomes that eventually fuse with the plasma membrane and are released as exosomes. This process was first observed in reticulocytes with respect to TfR shedding (Harding et al., 1983; Davis et al., 1986).

THE ROLES OF MEMBRANE SHEDDING IN THE CIRCULATION

RBC Senescence and Clearance

During their circulation, RBCs are exposed to stress conditions: physical, upon squeezing through small capillaries; hyperosmotic, upon passing through the kidney medulla; and oxidative, in the lungs. These stress conditions affect the RBC composition and characteristics, leading to senescence and eventually clearance by phagocytosis by macrophages in the reticuloendothelial system (Bratosin et al., 1998). Normally, the average RBC life span in the circulation is 120 days, but under pathological conditions, the life is shortened considerably, causing hemolytic anemia. Senescence is associated with exposure of various membrane signals (senescence signals), which includes externalization of PS and reduced sialic acid and CD47, and binding of immunoglobulins and opsonins [for detailed review, see Bosman et al. (2008)]. These changes are recognized by macrophages as "eat me" signals; however, the relative importance of each signal to clearance under normal and pathological conditions is not known.

Membrane shedding might affect RBC senescence and clearance by opposing mechanisms: (I) delaying clearance by removing intracellular oxidizing compounds such as oxidized Hb and aggregated Band-3 and (II) enhancing clearance by removing CD47, a surface compound that prevents recognition by macrophages (Stewart et al., 2005).

SUMMARY

The reciprocal relationship between the redox state and membrane shedding is essential for the normal physiological functioning of cells and the abnormality during various pathologies. This review summarizes some aspects of this issue during the life of the RBC—their production, maturation, circulation, senescence, and, finally, clearance—to be replaced by new ones (graphically summarized in **Figure 1**). This relationship is ablated in the hemolytic anemias that involve the RBCs and their precursors as the major targets (graphically summarized in **Figure 2**). As the redox state and oxidative stress can be modulated by oxidants and antioxidants, treatment with such drugs might have potential benefits on membrane shedding. For example, L-glutamine supplementation by the oral powder Endari has recently been approved for use in SCA based on its antioxidant effects in RBCs (Kassa et al., 2019). The understanding of the multitude of effects of membrane shedding on different cellular functions and the therapeutic potentials of treatment of redox-modifying agents at present is highly hypothetical and awaits sound and detailed studies.

AUTHOR CONTRIBUTIONS

The author confirms being the sole contributor of this work and has approved it for publication.

REFERENCES

Advani, R., Sorenson, S., Shinar, E., Lande, W., Rachmilewitz, E., and Schrier, S. L. (1992). Characterization and comparison of the red blood cell membrane damage in severe human alpha- and beta-thalassemia. *Blood* 79, 1058–1063.

Alaarg, A., Schiffelers, R. M., van Solinge, W. W., and van Wijk, R. (2013). Red blood cell vesiculation in hereditary hemolytic anemia. *Front. Physiol.* 4:365. doi: 10.3389/fphys.2013.00365

Allan, D., and Thomas, P. (1981). Ca2+-induced biochemical changes in human erythrocytes and their relation to microvesiculation. *Biochem. J.* 198, 433–440. doi: 10.1042/bj1980433

Amer, J., Dana, M., and Fibach, E. (2010). The antioxidant effect of erythropoietin on thalassemic blood cells. *Anemia* 2010:978710. doi: 10.1155/2010/978710

Amer, J., and Fibach, E. (2004). Oxidative status of platelets in normal and thalassemic blood. *Thromb. Haemost.* 92, 1052–1059.

Amer, J., Ghoti, H., Rachmilewitz, E., Koren, A., Levin, C., and Fibach, E. (2006). Red blood cells, platelets and polymorphonuclear neutrophils of patients with sickle cell disease exhibit oxidative stress that can be ameliorated by antioxidants. *Br. J. Haematol.* 132, 108–113. doi: 10.1111/j.1365-2141.2005.05834.x

Amer, J., Goldfarb, A., and Fibach, E. (2004). Flow cytometric analysis of the oxidative status of normal and thalassemic red blood cells. *Cytometry A.* 60, 73–80. doi: 10.1002/cyto.a.20017

Amer, J., Zelig, O., and Fibach, E. (2008). Oxidative status of red blood cells, neutrophils, and platelets in paroxysmal nocturnal hemoglobinuria. *Exp. Hematol.* 36, 369–377.

Arese, P., Gallo, V., Pantaleo, A., and Turrini, F. (2012). Life and death of glucose-6-phosphate dehydrogenase (G6PD) deficient erythrocytes - role of redox stress and band 3 modifications. *Transfus. Med. Hemother.* 39, 328–334. doi: 10.1159/000343123

Azouzi, S., Romana, M., Arashiki, N., Takakuwa, Y., El Nemer, W., Peyrard, T., et al. (2018). Band 3 phosphorylation induces irreversible alterations of stored red blood cells. *Am. J. Hematol.* 93, E110–E112. doi: 10.1002/ajh.25044

Bessis, M. C., and Breton-Gorius, J. (1962). Iron metabolism in the bone marrow as seen by electron microscopy: a critical review. *Blood* 19, 635–663.

Blanc, L., De Gassart, A., Geminard, C., Bette-Bobillo, P., and Vidal, M. (2005). Exosome release by reticulocytes–an integral part of the red blood cell differentiation system. *Blood Cells Mol. Dis.* 35, 21–26. doi: 10.1016/j.bcmd.2005.04.008

Bogdanova, A., Makhro, A., Wang, J., Lipp, P., and Kaestner, L. (2013). Calcium in red blood cells-a perilous balance. *Int. J. Mol. Sci.* 14, 9848–9872. doi: 10.3390/ijms14059848

Bosman, G. J. (2013). Survival of red blood cells after transfusion: processes and consequences. *Front. Physiol.* 4:376. doi: 10.3389/fphys.2013.00376

Bosman, G. J., Werre, J. M., Willekens, F. L., and Novotny, V. M. (2008). Erythrocyte ageing in vivo and in vitro: structural aspects and implications for transfusion. *Transfus. Med.* 18, 335–347. doi: 10.1111/j.1365-3148.2008.00892.x

Bratosin, D., Mazurier, J., Tissier, J. P., Estaquier, J., Huart, J. J., Ameisen, J. C., et al. (1998). Cellular and molecular mechanisms of senescent erythrocyte phagocytosis by macrophages. A review. *Biochimie* 80, 173–195. doi: 10.1016/s0300-9084(98)80024-2

Breuer, W., Hershko, C., and Cabantchik, Z. I. (2000). The importance of non-transferrin bound iron in disorders of iron metabolism. *Transfus. Sci.* 23, 185–192.

Cameron, I. L., Hardman, W. E., Smith, N. K., Fullerton, G. D., and Miseta, A. (1993). Changes in the concentration of ions during senescence of the human erythrocyte. *Cell Biol. Int.* 17, 93–98. doi: 10.1006/cbir.1993.1009

Cazzola, M. (2012). Molecular basis of myelodysplastic syndromes. *Leuk Suppl.* 1(Suppl. 2), S35–S36. doi: 10.1038/leusup.2012.20

Chagula, D. B., Rechcinski, T., Rudnicka, K., and Chmiela, M. (2020). Ankyrins in human health and disease - an update of recent experimental findings. *Arch. Med. Sci.* 16, 715–726. doi: 10.5114/aoms.2019.89836

Chasis, J. A., and Mohandas, N. (2008). Erythroblastic islands: niches for erythropoiesis. *Blood* 112, 470–478. doi: 10.1182/blood-2008-03-077883

Cisneros, G. S., and Thein, S. L. (2020). Recent advances in the treatment of sickle cell disease. *Front. Physiol.* 11:435. doi: 10.3389/fphys.2020.00435

Davis, J. Q., Dansereau, D., Johnstone, R. M., and Bennett, V. (1986). Selective externalization of an ATP-binding protein structurally related to the clathrin-uncoating ATPase/heat shock protein in vesicles containing terminal transferrin receptors during reticulocyte maturation. *J. Biol. Chem.* 261, 15368–15371.

de Back, D. Z., Kostova, E. B., van Kraaij, M., van den Berg, T. K., and van Bruggen, R. (2014). Of macrophages and red blood cells; a complex love story. *Front. Physiol.* 5:9. doi: 10.3389/fphys.2014.00009

Evans, E., Mohandas, N., and Leung, A. (1984). Static and dynamic rigidities of normal and sickle erythrocytes. Major influence of cell hemoglobin concentration. *J. Clin. Invest.* 73, 477–488. doi: 10.1172/JCI111234

Ferru, E., Pantaleo, A., Carta, F., Mannu, F., Khadjavi, A., Gallo, V., et al. (2014). Thalassemic erythrocytes release microparticles loaded with hemichromes by redox activation of p72Syk kinase. *Haematologica* 99, 570–578. doi: 10.3324/haematol.2013.084533

Fibach, E., and Rachmilewitz, E. (2008). The role of oxidative stress in hemolytic anemia. *Curr. Mol. Med.* 8, 609–619. doi: 10.2174/156652408786241384

Fibach, E., and Rachmilewitz, E. A. (2010). The role of antioxidants and iron chelators in the treatment of oxidative stress in thalassemia. *Ann. N. Y. Acad. Sci.* 1202, 10–16. doi: 10.1111/j.1749-6632.2010.05577.x

Fornaini, G., Magnani, M., Fazi, A., Accorsi, A., Stocchi, V., and Dacha, M. (1985). Regulatory properties of human erythrocyte hexokinase during cell ageing. *Arch. Biochem. Biophys.* 239, 352–358. doi: 10.1016/0003-9861(85)90698-8

Freikman, I., Amer, J., Cohen, J. S., Ringel, I., and Fibach, E. (2008). Oxidative stress causes membrane phospholipid rearrangement and shedding from RBC membranes–an NMR study. *Biochim. Biophys. Acta* 1778, 2388–2394.

Freikman, I., Amer, J., Ringel, I., and Fibach, E. (2009). A flow cytometry approach for quantitative analysis of cellular phosphatidylserine distribution and shedding. *Anal. Biochem.* 393, 111–116.

Freikman, I., and Fibach, E. (2011). Distribution and shedding of the membrane phosphatidylserine during maturation and aging of erythroid cells. *Biochim. Biophys. Acta* 1808, 2773–2780. doi: 10.1016/j.bbamem.2011.08.014

Freikman, I., Ringel, I., and Fibach, E. (2011). Oxidative stress-induced membrane shedding from RBCs is Ca flux-mediated and affects membrane lipid composition. *J. Membr. Biol.* 240, 73–82. doi: 10.1007/s00232-011-9345-y

Ghoti, H., Fibach, E., Dana, M., Abu Shaban, M., Jeadi, H., Braester, A., et al. (2011). Oxidative stress contributes to hemolysis in patients with hereditary spherocytosis and can be ameliorated by fermented papaya preparation. *Ann. Hematol.* 90, 509–513. doi: 10.1007/s00277-010-1110-2

Ghoti, H., Rosenbaum, H., Fibach, E., and Rachmilewitz, E. A. (2010). Decreased hemolysis following administration of antioxidant-fermented papaya preparation (FPP) to a patient with PNH. *Ann. Hematol.* 89, 429–430.

Guerini, D., Coletto, L., and Carafoli, E. (2005). Exporting calcium from cells. *Cell Calc.* 38, 281–289. doi: 10.1016/j.ceca.2005.06.032

Halliwell, B., and Gutteridge, J. (1999). *Free Radicals in Biology and Medicine*, 3rd Edn. Midsomer Norton: Oxford University Press.

Hanspal, M., Yoon, S. H., Yu, H., Hanspal, J. S., Lambert, S., Palek, J., et al. (1991). Molecular basis of spectrin and ankyrin deficiencies in severe hereditary spherocytosis: evidence implicating a primary defect of ankyrin. *Blood* 77, 165–173.

Harding, C., Heuser, J., and Stahl, P. (1983). Receptor-mediated endocytosis of transferrin and recycling of the transferrin receptor in rat reticulocytes. *J. Cell Biol.* 97, 329–339. doi: 10.1083/jcb.97.2.329

Jacobs, A. (1977). Low molecular weight intracellular iron transport compounds. *Blood* 50, 433–439.

Jandl, J. (1996). *Textbook of Hematology: Little*. Boston, MA: Brown and Co.

Kass, G. E., Nicotera, P., and Orrenius, S. (1990). Effects of xenobiotics on signal transduction and Ca2+ mediated processes in mammalian cells. *Princess Takamatsu Symp.* 21, 213–226.

Kassa, T., Wood, F., Strader, M. B., and Alayash, A. L. (2019). Antisickling drugs targeting betaCys93 reduce iron oxidation and oxidative changes in sickle cell hemoglobin. *Front. Physiol.* 10:931. doi: 10.3389/fphys.2019.00931

Konijn, A. M., Hershko, C., and Izak, G. (1979). Ferritin synthesis and iron uptake in developing erythroid cells. *Am. J. Hematol.* 6, 373–379. doi: 10.1002/ajh.2830060409

Kumar, D., and Rizvi, S. I. (2014). Markers of oxidative stress in senescent erythrocytes obtained from young and old age rats. *Rejuvenation Res.* 17, 446–452. doi: 10.1089/rej.2014.1573

Lang, K. S., Lang, P. A., Bauer, C., Duranton, C., Wieder, T., Huber, S. M., et al. (2005). Mechanisms of suicidal erythrocyte death. *Cell Physiol. Biochem.* 15, 195–202. doi: 10.1159/000086406

Leal, F. J. K., Adjobo-Hermans, M. J. W., Brock, R., and Bosman, G. (2017). Acetylcholinesterase provides new insights into red blood cell ageing in vivo and in vitro. *Blood Transfus.* 15, 232–238. doi: 10.2450/2017.0370-16

Leal, F. J. K., Preijers, F., Brock, R., Adjobo-Hermans, M., and Bosman, G. (2019). Red blood cell homeostasis and altered vesicle formation in patients with paroxysmal nocturnal hemoglobinuria. *Front. Physiol.* 10:578. doi: 10.3389/fphys.2019.00578

Leal, J. K. F., Adjobo-Hermans, M. J. W., and Bosman, G. (2018). Red blood cell homeostasis: mechanisms and effects of microvesicle generation in health and disease. *Front. Physiol.* 9:703. doi: 10.3389/fphys.2018.00703

Leimberg, J. M., Konijn, A. M., and Fibach, E. (2003). Developing human erythroid cells grown in transferrin-free medium utilize iron originating from extracellular ferritin. *Am. J. Hematol.* 73, 211–212. doi: 10.1002/ajh.10355

Leimberg, M. J., Prus, E., Konijn, A. M., and Fibach, E. (2008). Macrophages function as a ferritin iron source for cultured human erythroid precursors. *J. Cell Biochem.* 103, 1211–1218. doi: 10.1002/jcb.21499

Leventis, P. A., and Grinstein, S. (2010). The distribution and function of phosphatidylserine in cellular membranes. *Annu. Rev. Biophys.* 39, 407–427. doi: 10.1146/annurev.biophys.093008.131234

Liguori, I., Russo, G., Curcio, F., Bulli, G., Aran, L., Della-Morte, D., et al. (2018). Oxidative stress, aging, and diseases. *Clin. Interv. Aging* 13, 757–772. doi: 10.2147/CIA.S158513

Luzzatto, L., and Battistuzzi, G. (1985). Glucose-6-phosphate dehydrogenase. *Adv. Hum. Genet.* 14, 86–88.

Margolis, L., and Sadovsky, Y. (2019). The biology of extracellular vesicles: the known unknowns. *PLoS Biol.* 17:e3000363. doi: 10.1371/journal.pbio.3000363

Moras, M., Lefevre, S. D., and Ostuni, M. A. (2017). From erythroblasts to mature red blood cells: organelle clearance in mammals. *Front. Physiol.* 8:1076. doi: 10.3389/fphys.2017.01076

Moura, I. C., Hermine, O., Lacombe, C., and Mayeux, P. (2015). Erythropoiesis and transferrin receptors. *Curr. Opin. Hematol.* 22, 193–198. doi: 10.1097/MOH.0000000000000133

Nader, E., Romana, M., Guillot, N., Fort, R., Stauffer, E., Lemonne, N., et al. (2020). Association between nitric oxide, oxidative stress, eryptosis, red blood

cell microparticles, and vascular function in sickle cell anemia. *Front. Immunol.* 11:551441. doi: 10.3389/fimmu.2020.551441

Op den Kamp, J. A. (1979). Lipid asymmetry in membranes. *Annu. Rev. Biochem.* 48, 47–71.

Palis, J. (2014). Primitive and definitive erythropoiesis in mammals. *Front. Physiol.* 5:3. doi: 10.3389/fphys.2014.00003

Pan, B. T., Teng, K., Wu, C., Adam, M., and Johnstone, R. M. (1985). Electron microscopic evidence for externalization of the transferrin receptor in vesicular form in sheep reticulocytes. *J. Cell Biol.* 101, 942–948. doi: 10.1083/jcb.101.3.942

Pan, H., Ji, Z., Liu, E., and Zhang, Z. (1991). Erythrocyte vesiculation in paroxysmal nocturnal hemoglobinuria. *Chin. Med. Sci. J.* 6, 84–86.

Panizo Morgado, E., Darnaude, M. T., Torres Mohedas, J., Benedit, M., and Cervera Bravo, A. (2020). Beta-spectrin deletion responsible for hereditary spherocytosis: when new technologies are not the key to success. *J. Pediatr. Hematol. Oncol.* 42, e686–e688. doi: 10.1097/MPH.0000000000001742

Parker, C. J. (2007). The pathophysiology of paroxysmal nocturnal hemoglobinuria. *Exp. Hematol.* 35, 523–533.

Pattanapanyasat, K., Noulsri, E., Fucharoen, S., Lerdwana, S., Lamchiagdhase, P., Siritanaratkul, N., et al. (2004). Flow cytometric quantitation of red blood cell vesicles in thalassemia. *Cytometry B Clin. Cytom.* 57, 23–31.

Perrotta, S., Gallagher, P. G., and Mohandas, N. (2008). Hereditary spherocytosis. *Lancet* 372, 1411–1426. doi: 10.1016/S0140-6736(08)61588-3

Pollet, H., Cloos, A. S., Stommen, A., Vanderroost, J., Conrard, L., Paquot, A., et al. (2020). Aberrant membrane composition and biophysical properties impair erythrocyte morphology and functionality in elliptocytosis. *Biomolecules* 10:1120. doi: 10.3390/biom10081120

Prus, E., and Fibach, E. (2008). The labile iron pool in human erythroid cells. *Br. J. Haematol.* 142, 301–307.

Prus, E., and Fibach, E. (2011). Uptake of non-transferrin iron by erythroid cells. *Anemia* 2011:945289. doi: 10.1155/2011/945289

Rachmilewitz, E. A. (1974). Denaturation of the normal and abnormal hemoglobin molecule. *Semin. Hematol.* 11, 441–462.

Rachmilewitz, E. A., and Harari, E. (1972). Intermediate hemichrome formation after oxidation of three unstable hemoglobins (Freiburg, Riverdale-Bronx and Koln). *Hamatol. Bluttransfus.* 10, 241–250.

Raposo, G., and Stoorvogel, W. (2013). Extracellular vesicles: exosomes, microvesicles, and friends. *J. Cell Biol.* 200, 373–383. doi: 10.1083/jcb.201211138

Reliene, R., Mariani, M., Zanella, A., Reinhart, W. H., Ribeiro, M. L., del Giudice, E. M., et al. (2002). Splenectomy prolongs in vivo survival of erythrocytes differently in spectrin/ankyrin- and band 3-deficient hereditary spherocytosis. *Blood* 100, 2208–2215.

Renoux, C., Faivre, M., Bessaa, A., Da Costa, L., Joly, P., Gauthier, A., et al. (2019). Impact of surface-area-to-volume ratio, internal viscosity and membrane viscoelasticity on red blood cell deformability measured in isotonic condition. *Sci. Rep.* 9:6771. doi: 10.1038/s41598-019-43200-y

Rund, D., and Rachmilewitz, E. (2005). Beta-thalassemia. *N. Engl. J. Med.* 353, 1135–1146.

Sawitsky, A., and Ozaeta, P. B. Jr. (1970). Disease-associated autoimmune hemolytic anemia. *Bull. N. Y. Acad. Med.* 46, 411–426.

Scott, M. D., Eaton, J. W., Kuypers, F. A., Chiu, D. T., and Lubin, B. H. (1989). Enhancement of erythrocyte superoxide dismutase activity: effects on cellular oxidant defense. *Blood* 74, 2542–2549.

Soni, S., Bala, S., and Hanspal, M. (2008). Requirement for erythroblast-macrophage protein (Emp) in definitive erythropoiesis. *Blood Cells Mol. Dis.* 41, 141–147. doi: 10.1016/j.bcmd.2008.03.008

Steinberg, M. H. (1998). Pathophysiology of sickle cell disease. *Baillieres Clin. Haematol.* 11, 163–184.

Stewart, A., Urbaniak, S., Turner, M., and Bessos, H. (2005). The application of a new quantitative assay for the monitoring of integrin-associated protein CD47 on red blood cells during storage and comparison with the expression of CD47 and phosphatidylserine with flow cytometry. *Transfusion* 45, 1496–1503. doi: 10.1111/j.1537-2995.2005.00564.x

Stowell, S. R., Smith, N. H., Zimring, J. C., Fu, X., Palmer, A. F., Fontes, J., et al. (2013). Addition of ascorbic acid solution to stored murine red blood cells increases posttransfusion recovery and decreases microparticles and alloimmunization. *Transfusion* 53, 2248–2257. doi: 10.1111/trf.12106

Sudnitsyna, J., Skverchinskaya, E., Dobrylko, I., Nikitina, E., Gambaryan, S., and Mindukshev, I. (2020). Microvesicle formation induced by oxidative stress in human erythrocytes. *Antioxidants (Basel)* 9:929. doi: 10.3390/antiox9100929

Szigyarto, I. C., Deak, R., Mihaly, J., Rocha, S., Zsila, F., Varga, Z., et al. (2018). Flow alignment of extracellular vesicles: structure and orientation of membrane-associated bio-macromolecules studied with polarized light. *Chembiochem* 19, 545–551. doi: 10.1002/cbic.201700378

Testa, U. (2004). Apoptotic mechanisms in the control of erythropoiesis. *Leukemia* 18, 1176–1199. doi: 10.1038/sj.leu.2403383

Tian, W. N., Braunstein, L. D., Pang, J., Stuhlmeier, K. M., Xi, Q. C., Tian, X., et al. (1998). Importance of glucose-6-phosphate dehydrogenase activity for cell growth. *J. Biol. Chem.* 273, 10609–10617. doi: 10.1074/jbc.273.17.10609

Walport, M. J. (2001). Complement, first of two parts. *N. Engl. J. Med.* 344, 1058–1066.

Wang, J., and Pantopoulos, K. (2011). Regulation of cellular iron metabolism. *Biochem. J.* 434, 365–381. doi: 10.1042/BJ20101825

Westerman, M., and Porter, J. B. (2016). Red blood cell-derived microparticles: an overview. *Blood Cells Mol. Dis.* 59, 134–139. doi: 10.1016/j.bcmd.2016.04.003

Wickrema, A., Bondurant, M. C., and Krantz, S. B. (1991). Abundance and stability of erythropoietin receptor mRNA in mouse erythroid progenitor cells. *Blood* 78, 2269–2275.

Willekens, F. L., Werre, J. M., Groenen-Dopp, Y. A., Roerdinkholder-Stoelwinder, B., de Pauw, B., and Bosman, G. J. (2008). Erythrocyte vesiculation: a self-protective mechanism? *Br. J. Haematol.* 141, 549–556. doi: 10.1111/j.1365-2141.2008.07055.x

Willms, E., Cabanas, C., Mager, I., Wood, M. J. A., and Vader, P. (2018). Extracellular vesicle heterogeneity: subpopulations, isolation techniques, and diverse functions in cancer progression. *Front. Immunol.* 9:738. doi: 10.3389/fimmu.2018.00738

Willms, E., Johansson, H. J., Mager, I., Lee, Y., Blomberg, K. E., Sadik, M., et al. (2016). Cells release subpopulations of exosomes with distinct molecular and biological properties. *Sci. Rep.* 6:22519. doi: 10.1038/srep22519

Winterbourn, C. C., and Carrell, R. W. (1974). Studies of hemoglobin denaturation and Heinz body formation in the unstable hemoglobins. *J. Clin. Invest.* 54, 678–689.

Yoshida, H., Kawane, K., Koike, M., Mori, Y., Uchiyama, Y., and Nagata, S. (2005). Phosphatidylserine-dependent engulfment by macrophages of nuclei from erythroid precursor cells. *Nature* 437, 754–758. doi: 10.1038/nature03964

Zwaal, R. F., Comfurius, P., and Bevers, E. M. (2005). Surface exposure of phosphatidylserine in pathological cells. *Cell Mol. Life Sci.* 62, 971–988.

Conflict of Interest: The authors declare that the research was conducted in the absence of any commercial or financial relationships that could be construed as a potential conflict of interest.

Advantages of publishing in Frontiers

OPEN ACCESS
Articles are free to read for greatest visibility and readership

FAST PUBLICATION
Around 90 days from submission to decision

HIGH QUALITY PEER-REVIEW
Rigorous, collaborative, and constructive peer-review

TRANSPARENT PEER-REVIEW
Editors and reviewers acknowledged by name on published articles

Frontiers
Avenue du Tribunal-Fédéral 34
1005 Lausanne | Switzerland

Visit us: www.frontiersin.org
Contact us: frontiersin.org/about/contact

REPRODUCIBILITY OF RESEARCH
Support open data and methods to enhance research reproducibility

DIGITAL PUBLISHING
Articles designed for optimal readership across devices

FOLLOW US
@frontiersin

IMPACT METRICS
Advanced article metrics track visibility across digital media

EXTENSIVE PROMOTION
Marketing and promotion of impactful research

LOOP RESEARCH NETWORK
Our network increases your article's readership